BROAD-BAND MICROWAVE AMPLIFIER DESIGN CONSIDERATIONS

by

Gordon John Temple

A thesis submitted for the degree of Doctor of Philosophy at the

University of Warwick

ENGLAND

April

1985

I also acknowledge the Hewlett-Packard Co., South Queensferry for the provision of a number of metallized sapphire substrates

Finally, but by no means least, I thank my wife, and my children, two of whom were born during the period of my research and preparation of this thesis, for their longsuffering support and encouragement.

To Patricia, Jonathan, Stephen and Rachel.

DECLARATION

The work described in this Thesis has not been submitted to any other university for a degree. Some of the material presented has been published or may be published in the future.

Use has been made of relevant publications and references to such cases have been given appropriately. Unless explicitly stated to the contrary, all other work and conclusions are due solely to the author.

CONTENTS

C H A P T E R 1

I N T R O D U C T I O N

1. INTRODUCTION

Since their role in the initial development of radar, microwave techniques have found many other applications is the fields of communications, counter-measures, heating, remote sensing, instrumentation and even agriculture (!). Originally the domain of the vacuum physicist and the metalsmith, the emphasis has changed in favour of the solid-state technologist and the hybrid circuit engineer. Early applications required inconsequential bandwidth such that, for design purposes, only a single operating frequency need be considered and simple tuning structures could compensate discrepancies in the achieved performance. Modern systems, notably in the counter-measures and instrumentation areas, demand substantial spectral coverage, with bandwidths of an octave or more becoming common-place in current circuit specifications. Broad-band operation multiplies the complexity of the design problem. H.W. Bode's observation that no design process can be reduced entirely to a set of rules is most apt. Nevertheless it is highly desirable that coherent design methodologies for broad-band circuits should be developed, not least because it allows the increased involvement of the computer in a design automation role. The growing importance of computer-aided design (CAD) is related not to the obsessive application of computer to all human pursuits, but rather to the need to increase the productivity of all too scarce microwave engineers. This need arises as a result of the growing complexity of microwave sub-systems and the trend towards shorter product lives.

Until relatively recently microwave solid-state active devices have been predominantly of the two terminal variety (e.g. tunnel, Gunn and IMPATT diodes). By virtue of the negative real part of impedance produced by these devices under certain conditions they can be used to

sustain oscillation and to amplify. In the amplifier application they suffer the major disadvantage that, since the device provides no inherent isolation, additional structures to separate input and output waves are necessary. Recent technological advances have made available to the microwave engineer the class of three terminal devices generally known as transistors. Silicon bipolar transistors with useful performance to ~6GHz are now readily available and Gallium-Arsenide MESFETs with gain at low millimetre-wave frequencies are being reported.

Just as transistors have largely supplanted two terminal active devices (except in millimetre-wave region) so hybrid circuit technology has displaced waveguide and coax as the dominant medium for the realisation of many classes of circuits. Except in applications involving high power, or demanding the lowest losses, hybrid or printed circuit techniques offer substantial saving in cost, size and weight, and consequently permit more elaborate sub-systems to be constructed.

Using photolithographic techniques to define the metalisation pattern, complex combinations of distributed structures employing stripline, microstrip, co-planer waveguide and slotline with a wide range of electrical parameters can be realised. In addition, the pattern resolution achievable permits the use of lumped elements up to ~10GHz. Microwave circuits constructed in this manner have become known as Microwave Integrated Circuits (MICs) since they allow a multiplicity of elements to be incorporated in a single, integrated structure.

Among the most complex applications of MIC techniques is the microwave broad-band amplifier. The inclusion of active devices and discrete components on a photolithographically defined circuit with an elaborate combination of lumped and distributed elements represents the culmination of these developments. In addressing the design of such an amplifier, practically all the electrical and mechanical considerations

associated with MIC technology are encountered. For this reason, as well as the author's awareness of imminent instrument applications for such circuits, the topic of broad-band MIC amplifier design was chosen for this work.

The objectives of the programme of research were:-

i) that a coherent methodology for the design of broad-band amplifiers should be developed,

ii) that the accuracy of the design techniques and the accommodation of tolerances should be sufficient to obviate the need for circuit trimming,

iii) that an amplifier having a bandwidth in excess of an octave should be developed by the proposed methodology and meet the "no trim" objective.

In line with current device technology trends GaAs MESFETs were chosen as the active elements. The additional discipline of using packaged devices was imposed to permit correlation of amplifier performance with device characteristics as well as to minimise fabrication difficulty and to obviate the need for hermetic packaging of the amplifier.

Throughout the research programme cost was an essential and evident ingredient in many of the choices concerning both the design methodology and the realisation of the representative amplifier.

In the development of the design methodology, emphasis is given to synthesis techniques. Synthesis is the essence of the design process. It is the rational process by which a specification can be translated into a design. Conversely, analysis is regressive: relating the behaviour of a proposed circuit back to the specification. As such it performs a role in an interactive process by which the specification can ultimately be achieved. Computer optimisation packages represent the automation of this iterative process, replacing an engineer's judgement

with a cost function; removing tedium and confusion by providing a systematic scheme for the handling of the complex multi-variable problem. Nevertheless the engineer still has to generate an initial solution to which to apply computer optimisation. The starting point frequently has a substantial effect on the outcome and the engineer is often forced to try a number of initial solutions. Computer aided synthesis techniques offer the possibility of eliminating this indirect procedure and of supporting truly automated design. Figure 1.1 illustrates these relationships.

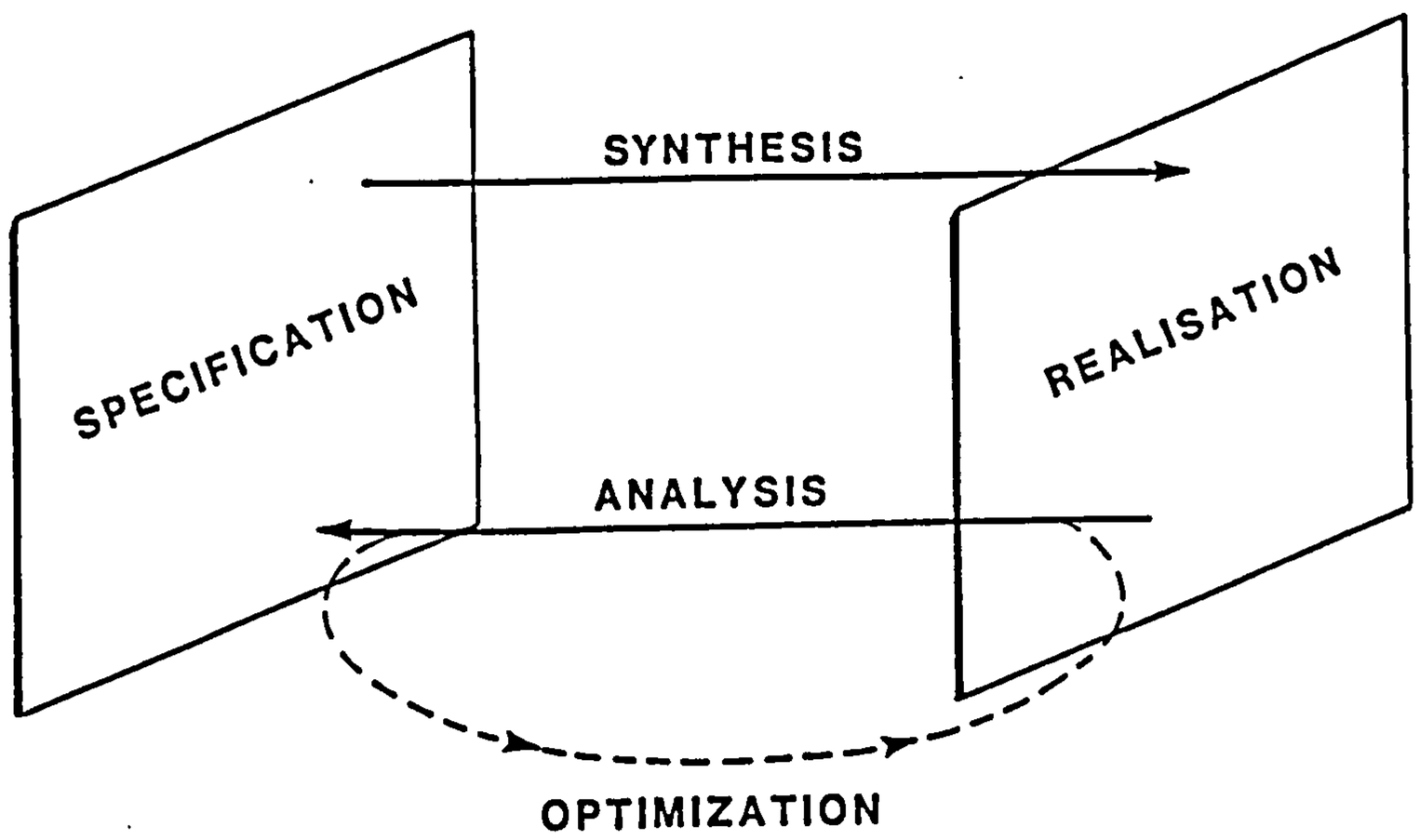

Figure 1.1 The roles of Synthesis and Analysis

This thesis covers topics involved at all stages in the design of broadband MIC amplifier. Some may be regarded as somewhat incidental to the main thrust of the research. Their inclusion was permitted on the justification that their consideration was necessary to the successful operation of the methodology and realisation of the culminating demonstration amplifier.

The material presented can be grouped under three major headings: Analysis and measurement of microstrip and related structures on

anisotropic substrates, accurate measurement of microstrip mounted devices and components, and microwave broad-band amplifier design.

1.1 ANALYSIS AND MEASUREMENT OF MICROSTRIP AND RELATED STRUCTURES

Fundamental to MIC design is the ability to accurately specify the characteristic impedance and electrical length of the transmission line elements. Errors in the electrical length can be particularly devastating when tuned stubs are employed in the circuit. Much work on the subject has been published but the vast majority of it is confined to cases where an isotropic substrate is employed. Some popular MIC substrates are prepared from single crystal materials (e.g. sapphire, quartz) and are therefore significantly anisotropic.

The author was introduced to the problem of substrate dielectric anisotropy by experience with a proprietry soft substrate known as "Epsilam-10". This ceramic loaded laminate was claimed by the manufacturers to display anisotropic properties. Early experiments proved inconclusive since the material was insufficiently consistent for meaningful measurements to be obtained. It was observed that the behaviour of microstrip on this substrate would also accord with that on an isotropic but inhomogenous (graded permittivity through the sheet) material, an explanation more consistent with the methods of laminate manufacture than dielectric anisotropy.

Against this background the work on anisotropic microstrip focused on sapphire substrates. The stable, well characterised dielectric properties of sapphire permitted measurements of microstrip propagation velocity to be made with sufficient integrity to assess the results of analysis.

Chapter 2 covers the selection of analysis techniques for the

anisotropic case. A novel method for the accurate measurement of propagation is developed in Chapter 3. The results from analysis and measurement, for a range of strip widths on sapphire substrates, are compared at the conclusion of this chapter. Chapter 4 addresses the behaviour of commonly encountered discontinuities in an approximate but efficacious manner that can be applied to both isotropic and anisotropic situations.

1.2 MEASUREMENT OF MICROSTRIP MOUNTED COMPONENTS AND DEVICES

An essential foundation for the accurate design of microwave active circuits is the ability to obtain high integrity network measurements. Before design can commence, characterisation of the components and devices to be employed is necessary. When the design is complete, and the prototype fabricated, its performance must be assessed against the design specification. If appropriate, a comparison with the behaviour predicted by CAD simulation can be a valuable starting point for re- medial, corrective design activity. Thus the design process can be illustrated by the "wheel of fortune" of figure 2.1. Measurement is the keystone of the whole activity. The number of cycles of the design process necessary to produce a satisfactory prototype is highly dependent on the quality of the measurements.

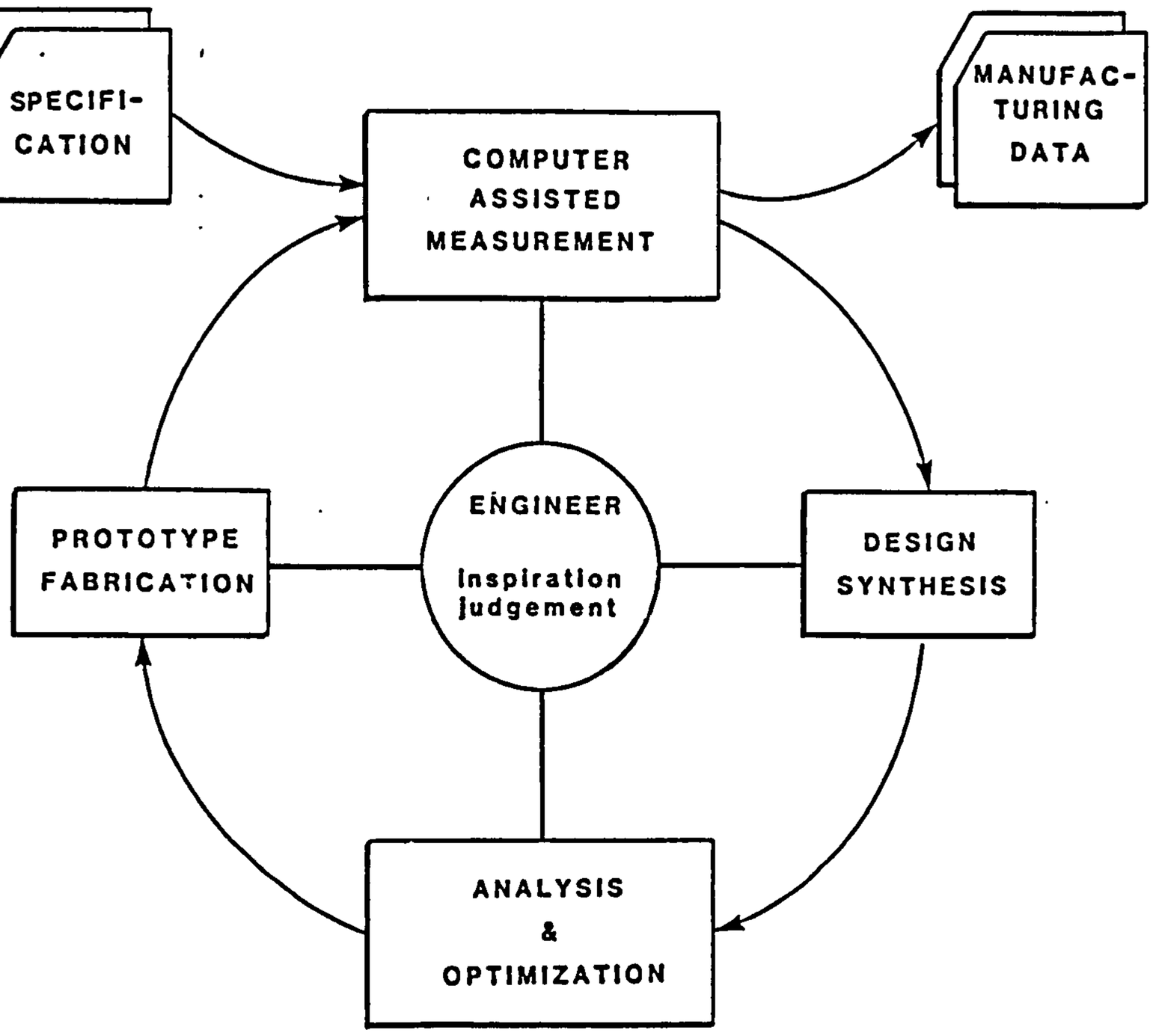

Figure 1.2 The Design Process

Since the design methodology presented here is concerned almost entirely with small signal behaviour the most important qualities to be measured are the small signal scattering (s-)parameters. The instrument involved, the microwave vector network analyser is, in its basic form, notoriously inaccurate. These errors are compounded by the imperfections of adaptors and transitions necessary to interface the Device Under Test (DUT) to the measurement system.

With the aid of the digital computer, enhanced accuracy and speed of measurement, together with versatile presentation of results, have been obtained. There are two situations where the use of a vector network analyser is necessitated. Error correction techniques require vector measurements to be made on both the DUT and a number of calibration standards. Therefore, even if scalar results only are demanded, the vector network analyser has to be employed whenever accuracy is important. Such is usually the case when complete circuits are to be

tested to specification or when measurements on sub-systems are made. Generally, the DUT will be fitted with industry standard connectors and its port impedances will approximate the characteristic impedance of the measurement system. High integrity standards for the calibration of Computer Corrected Network Analysers (CCNAs) are readily available in all common connector systems. Chapter 5 reviews CCNA principles and calibration schemes appropriate to this situation. A modified error model for 2-port measurement is described.

On the other hand, the vector network analyser is obviously essential when phase, as well as magnitude information, is required from the measurement. Design depends on the availability of vector data for the devices and components to be employed in a circuit. In this case the DUT does not carry convenient connector interfaces but rather is constructed to facilitate its ultimate inclusion in the circuit. Establishing calibration standards of suitable quality in the circuit medium, usually microstrip, presents severe problems. In Chapter 6, microstrip 1- and 2-port calibration schemes appropriate to components and devices for MIC applications, in which the standards are partially self-verifying, are described. Results obtained for GaAs MESFETs are presented.

1.3 MICROWAVE BROAD-BAND AMPLIFIER DESIGN

With the infrastructure established, attention is directed to the focus of this work; the development of a design methodology for MIC broad-band amplifiers and its application to a typical example. The representative specification, selected from real instrumentation requirements, was for an amplifier covering the frequency range 4 to 9 GHz. As packaged 1μm GaAs MESFETs were to be used, this specification represents a significant challenge.

In chapter 7 the approaches to broad-band amplifier design are reviewed. The structure of the amplifier is discussed in the light of the proposed specifications. Although the design is conducted on a small-signal basis, considerations relating to the output power are taken into account in the definition of the architecture. Other factors influencing the structure of the amplifier are cost, the stringent reverse isolation stipulation and the sensitivity to circuit and component tolerances. The concepts of the gain-bandwidth limitations for the matching of arbitrary port impedances and reactive network synthesis are introduced.

The benefits that accrue from the use of frequency dependent dissipative networks to compensate the device gain slope are discussed in Chapter 8. The method by which circuit modules having frequency independent maximum available gain, incorporating such networks, may be synthesised is developed. This process is supported by a computer program which also embodies other facilities useful to the amplifier designer. The method by which an amplifier can be designed in a straightforward and relatively exact manner using these modules, is described.

In conclusion, results from the analysis of the computer design and measurement on the constructed amplifier are compared. The efficiency of the methodology is discussed in the light of the performance of the circuit and the experience gained during the design process.

1.4 CONTRIBUTIONS

The following is a list of notable contributions made by the author that are believed to be original. In some cases similar contributions have appeared in the literature since the author completed his research on the material now presented.

* Analysis of microstrip on an anisotropic substrate using extended partial images and anisotropic Green's function.
* Assessment of microstrip parameter computation accuracy by observing the behaviour of the fringing field.
* An accurate method for the measurement of microstrip velocity of propagation using corrected measurements of short circuit resonators.
* A simple technique for the approximate calculation of the capacitive component of microstrip discontinuities.
* The definition of an anisotropic adjustment factor and its application to the calculation of discontinuity capacitances where an anisotropic substrate is employed.
* A unified set of correction equations for network analysers with alternative test set configurations.
* A mathematical description of "quadrature error" occurring in network analysers, suggesting new efficient methods for its correction.
* A microstrip calibration scheme for 2-port measurements on a computer corrected network analyser using readily fabricated and partially self calibrating standards.
* A modular approach to the design of single-ended multi-stage amplifiers based on device maximum available gain slope compensation.
* A technique for the synthesis of dissipative gain slope compensation networks to meet specified maximum available gain behaviour.

1.5 PUBLICATIONS & PRESENTATIONS

Publications and presentations of material arising from this work are as follows:

[1] ABBOTT, D.A., SHURMER, H.V. & TEMPLE, G.J.: "Automatic characterisation of 2-port components and devices in microstrip", IEE Colloquium on "Computer Controlled Microwave Measurements ", London, 7/4/1979.

[2] TEMPLE, G.J.: "Computer aided design of broad-band dissipatively compensated microwave amplifiers", IEE Colloquium on "GaAs FET Microwave Devices & Applications", London, 9/12/1982, Digest No.: 1982/89.

[3] TEMPLE, G.J.: "Quadrature Error Correction in an ANA", Automatic RF & Microwave Measurements Society (ARMMS), Inaugural meeting, University of Leeds, 12/1/1983.

[4] TEMPLE, G.J. & DA SILVA, E.: Chapter on "Error Models" and "Calibration Schemes" of book: "Microwave Network Analysers" (Ed.: H.V. Shurmer), submitted for publication.

[5] TEMPLE, G.J.: "Computer aided microwave measurements - A foundation or design", Workshop on "Microwave Computer Aided Design", European Microwave Conference, Liege, Belgium, 14/9/1984, Digest to be published by Microwave Exhibitions and Publishers Limited.

CHAPTER 2

ANALYSIS OF MICROSTRIP ON ANISOTROPIC SUBSTRATES

2. ANALYSIS OF MICROSTRIP ON ANISOTROPIC SUBSTRATES

The most common Microwave Integrated Circuit (MIC) transmission line structure is undoubtedly microstrip (figure 2.1).

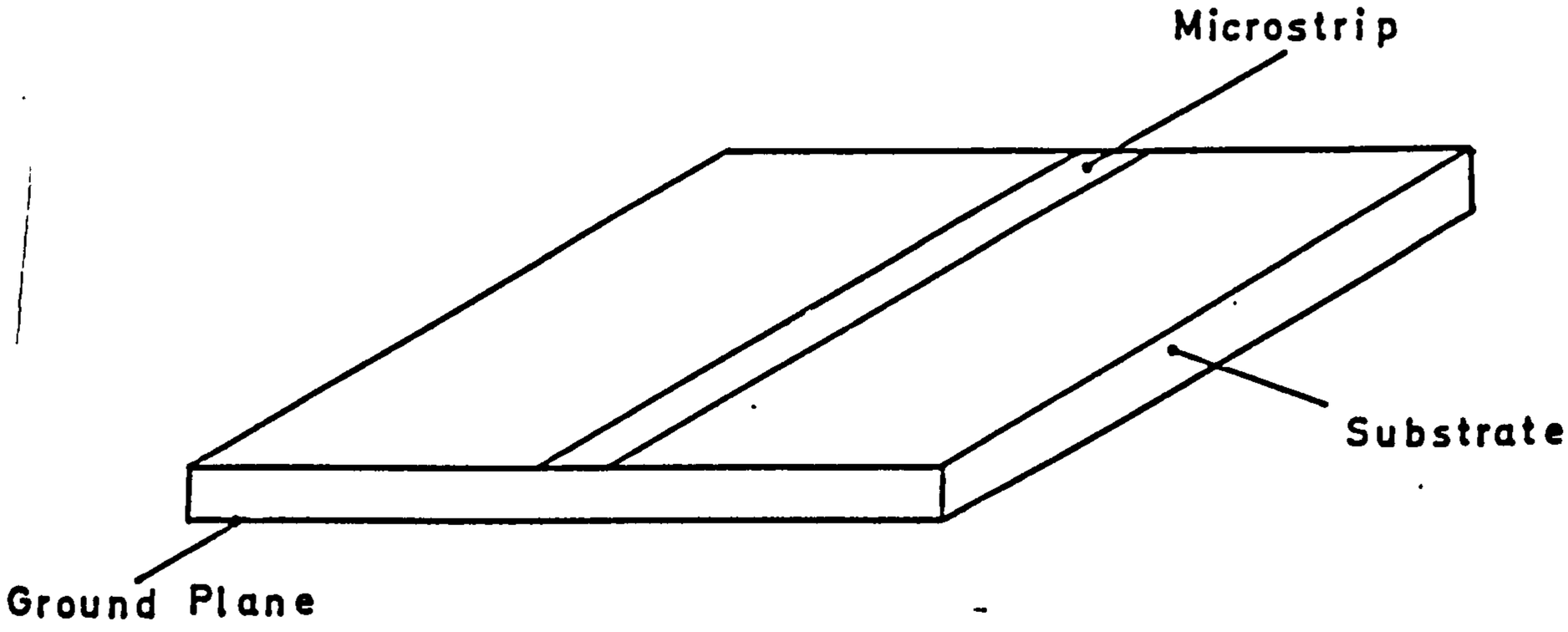

Figure 2.1 Microstrip

It evolved from stripline in which the centre conductor is embedded in a dielectric midway between two parallel conducting surfaces referred to as ground planes. The benefits of the homogeneous dielectric are sacrificed in exchange for the obvious relative ease with which components and devices can be mounted on the open structure of microstrip.

The dielectric sheet or substrate has two principle functions: it supports the thin conducting strip a constant distance, h, above the ground plane and it helps concentrate the field in the region between the two conductors. Several factors affect the choice of dielectric material. The effect of the permittivity on the size of the circuit is often a primary consideration. Hard substrates are necessary when thin or thick film technology is to be employed and are desirable when thermo-compression bonding is to be used for component attachment. Soft substrates, particularly copper clad laminates have advantages of reduced cost, simplicity of processing and versatility in shape and size. Other considerations are loss, dielectric (breakdown) strength, requirement for film resistors and consistancy of dielectric constant.

Generally soft substrates have been associated with low permittivity dielectrics being principally formed by PTFE (e_r = 2.1). Although frequently loaded with glass fibres for mechanical strength and stability, the dielectric constant of a laminate for microwave use is seldom higher than 2.4. Relatively recently a proprietory product known as "Epsilam-10"[1], having a dielectric constant similar to that of alumina ceramic has become available. Loaded with a high permittivity, low microwave loss ceramic, this PTFE based copper clad laminate can be handled and processed like the established PTFE/glass laminates. Whilst the benefits offered by this material are evident there is a drawback. The manufacturers own measurements of the material properties [1] suggest a significant degree of dielectric anisotropy. In an anisotropic dielectric the permittivity is dependant upon the direction of the electric field. The data supplied specifies the dielectric constants as 10.3 in the plane of the laminate and 13.0 perpendicular to it.

The desire to design MICs employing "Epsilam-10" as the substrate material accurately prompted this investigation of the analysis of anisotropic microstrip, or more correctly; microstrip on an anisotropic substrate. At the time of commencement negligible relevant material [7,9] was available and although other work has since appeared [10,18,19] the subject has received scant attention. This is somewhat surprising as a number of important monocrystalline substrates (sapphire, quartz, gallium-arsenide, etc.) exhibit dielectric anisotropy.

This chapter commences with a review of established microstrip analysis techniques applied to isotropic substrates. Results for alumina, having a dielectric constant in the range 9.6 - 10.0 have presented as a reference for the subsequent work. The analysis techniques are assessed for applicability to the anisotropic situation. Various proposed transformations that allow the anisotropic problem to be

treated like isotropic microstrip are evaluated. Only one is shown to be rigorously justifiable. An existing microstrip analysis computer program [11] is modified to implement this transform and is demonstrated for a substrate with the dielectric properties of "Epsilam-10".

It transpires that the dielectric consistency of "Epsilam-10" is inadequate for a useful experimental verification of the analysis. The best available results for this material [14] show broad agreement but the confidence level is low. For this reason an alternative anisotropic substrate material was selected for the measurements of Chapter 3.

Sapphire was chosen because of its well established and highly consistent dielectric properties, its mechanical stability and its relatively wide use as an MIC substrate. The dielectric properties of sapphire are discussed in Chapter 3. Both of the orientations of the crystal that result in a cross-sectional anisotropy of the microstrip structure are considered and the results are presented along with the measurements in section 3.6.

2.1 MICROSTRIP ANALYSIS

The principle parameters of an transmission line are the characteristic impedance and the velocity of propagation. If the line is non-ideal other parameters will be of consequence. Losses due to imperfections in the conductors and dielectric, and loss of microwave energy due to radiation from the open structure of microstrip give rise to line attenuation. Any transmission line structure will, when the lateral dimensions become an appreciable portion of a wavelength, support higher order TE or TM modes which modify the impedance and propagation velocity. In the case of microstrip this dispersive behaviour is accentuated by the mixed (inhomogeneous) dielectric filling

of the region in which the field is contained.

In the applications relevant to this work these second order effects are likely to be of little consequence. Some attention is, however, given to both issues in Chapter 3. For this analysis it is assumed that the microstrip is essentially lossless and that only the TEM (Transverse Electric and Magnetic) mode is supported. A consequence of this quasi-static assumption is that, for an infinite uniform microstrip line, the general 3-dimensional problem is reduced to 2 dimensions, there being no components of field in the direction of propagation. One further assumption deserves comment. The perfectly conducting strip is regarded as infinitesimally thin. This is recognised as giving rise to significant error in the analysis of narrow microstrip lines, but the additional complexity involved in the accommodation of finite conductor thickness is not considered worthwhile. A method by which the results may be corrected for metallization thickness effect is described in section 3.5.3.

2.1.1 Quasi-Static Analysis

Based on the TEM assumption the properties of the (microstrip) transmission line can be described in terms of the capacitance (C) and inductance (L) per unit length of the structure.

$$\text{Characteristic Impedance: } Z_o = \sqrt{L/C} \qquad \langle 2.1 \rangle$$

$$\text{Velocity of Propagation : } v = 1/\sqrt{LC} \qquad \langle 2.2 \rangle$$

In a homogeneous dielectric the velocity of propagation is simply related to the velocity of light in free space (v_o) thus:

$$v = v_o/\sqrt{\epsilon_r} \qquad \langle 2.3 \rangle$$

So, Z_o can be determined from a calculation of line capacitance only:

$$Z_o = 1/vC = \sqrt{\epsilon_r}/v_oC \qquad \langle 2.4 \rangle$$

As already mentioned, microstrip has an inhomogeneous dielectric, so

this simple method cannot be directly applied. The advantages of restricting the problem to the calculation of capacitance alone are, however, clear and so the following approach is adopted.

The dielectric constant is the factor that relates the capacitance of the structure with the region filled with dielectric to that when a vacuum exists. An effective dielectric constant can therefore be defined for the mixed dielectric situation of microstrip, thus:

$$\epsilon_{eff} = C_D/C_0 \qquad \langle 2.5 \rangle$$

where C_D is the capacitance/unit length with partial dielectric filling

and C_0 is the capacitance/unit length without any dielectric present (i.e. in vacuo)

then

$$v = v_o/\sqrt{\epsilon_{eff}} \qquad \langle 2.6 \rangle$$

Now, since the inductance of the structure is unchanged by the presence of the dielectric, the primary parameters of the microstrip line may be expressed entirely in terms of capacitance:

$$Z_o = 1/v_o\sqrt{C_0C_D} \qquad \langle 2.7 \rangle$$

$$v = v_o\sqrt{C_0/C_D} \qquad \langle 2.8 \rangle$$

The capacitance is simply related to the charge on either conductor and the potential difference between them:

$$C = Q/\Phi \qquad \langle 2.9 \rangle$$

If, for convenience the potential difference is set to a 1 volt the capacitance becomes numerically equal to the charge on the strip. Charge is not evenly distributed on the strip but is arranged such that the tangential component of electric field on the surface of the strip is always zero (i.e. no potential difference exists across the perfectly conducting surface) in the context of the surrounding dielectric and conductor configuration. For a region containing charges the

relationship between the potential and charge distributions may be found by solving the Poisson equation, taking into account the boundary conditions:

Poisson equation: $$\nabla^2 \phi = - \rho/\epsilon \qquad \text{<2.10>}$$

where ϕ is the potential at a point

and ρ is the charge distribution in the region.

Expressed in rectangular coordinates and where the charge distribution is non-uniform

$$\frac{\partial^2 \phi}{\partial x^2} + \frac{\partial^2 \phi}{\partial y^2} + \frac{\partial^2 \phi}{\partial z^2} = - \frac{\rho(x_o, y_o, z_o)}{\epsilon} \qquad \text{<2.11>}$$

assuming an isotropic homogeneous dielectric throughout the region.

Given the 2-dimensional nature of the quasi-static analysis on a structure with an uniform cross-section, the longditudinal electric field is zero everywhere. Since

$$\mathbf{E} = - \nabla \phi = \frac{\partial \phi}{\partial x} \mathbf{i} + \frac{\partial \phi}{\partial y} \mathbf{j} + \frac{\partial \phi}{\partial z} \mathbf{k} \qquad \text{<2.12>}$$

then $\frac{\partial \phi}{\partial z} = 0$ for all z

therefore $\frac{\partial^2 \phi}{\partial z^2} = 0$ also.

Remembering the mixed dielectric situation the 2-dimensional Poisson equation is:

$$\frac{\partial^2 \phi}{\partial x^2} + \frac{\partial^2 \phi}{\partial y^2} = \rho_o(x_o, y_o)/\epsilon(y) \qquad \text{<2.13>}$$

For this equation to be solved the boundary condition must be defined. With reference to figure 2.2 they are as follows.

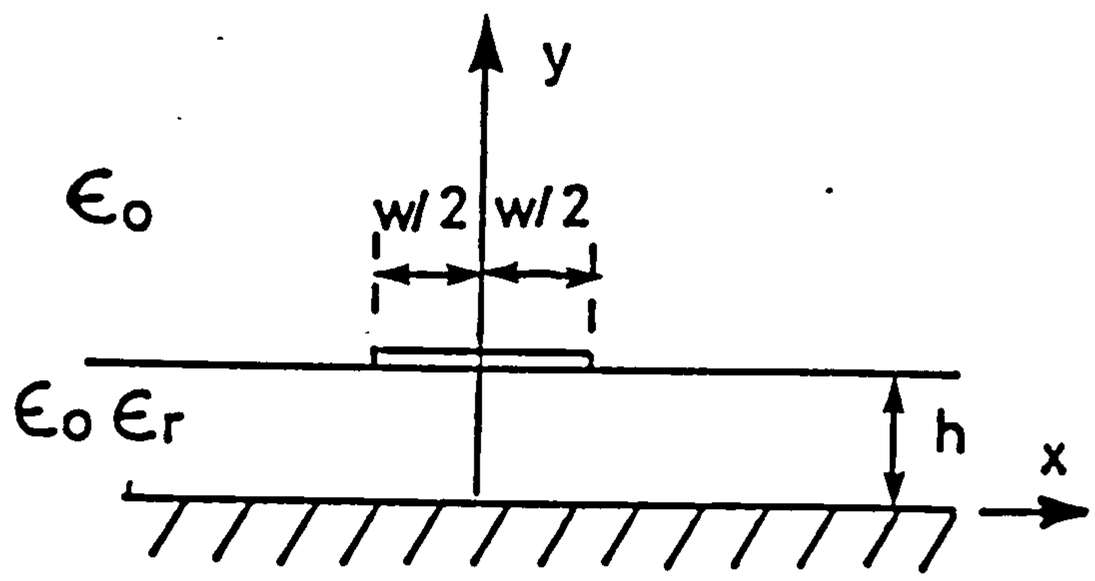

Figure 2.2 Microstrip cross-section

Conducting boundaries formed by the strip and ground plane demand that

$$E_x = 0;\ y = h,\ -w/2 \leqslant x \leqslant w/2 \qquad \langle 2.14 \rangle$$

with Φ = 1 Volt

and $E_x = 0;\ y = 0$ with $\Phi = 0$ $\langle 2.15 \rangle$

respectively. At the dielectric interface (y=h, -w/2>x>w/2) the tangential electric field is continuous across the boundary:

$$E_x(y=0_+) = E_x(y=0_-) \qquad \langle 2.16 \rangle$$

and the normal component of electric flux density ($D = \epsilon E$) is also continuous:

$$D_y(y=0_+) = D_y(y=0_-) \qquad \langle 2.17 \rangle$$

Furthermore, the solution must have the potential (Ø) which is defined on the conductors, reducing as 1/r as r (the radial distance) tends to infinity.

The foregoing represents a complete statement of the electrostatic problem.

2.1.2 Techniques for Analysis

Many techniques to the solution of non-trivial electrostatic problems are available. The major generic methods are discussed below.

2.1.2.1 Conformal Mapping

The spatial domain is mapped to transform domain, according to the

rules of conformal mapping, in which the solution to the problem becomes trivial (e.g. as for an ideal parallel plate capacitor). For a reasonable range of isotropic dielectric situations an exact analytic solution, in terms of elliptic integrals for rectangular geometries, can be found. The mixed dielectric structure of microstrip poses a problem, but nevertheless useful solutions have been developed. [3,12]

2.1.2.2 Finite Differences

The region is divided into a mesh or grid in which the potential at a node is related to that at those adjacent to it by linear expressions. With the potentials defined on the boundaries, the solution is approached iteratively using the relaxation method [2]. For the technique to be accurate the mesh size must be small enough for the field to be substantially uniform between adjacent nodes. In the vicinity of the abrupt edges of the strip the field is intense and divergent. Therefore using a regular grid can be rather inefficient; since the pitch of the mesh must be small everywhere to accommodate the local feature. Non-uniform meshes can be introduced but at the expense of complexity in this otherwise attractively direct and highly versatile technique [16].

2.1.2.3 Separation of Variables

The classical technique by which a partial differential equation (the Poisson´s Equation in this case) may be split into a set of ordinary differential equations, is known as the separation of variables or product solution technique [15]. Using the principle of superposition the solution for the latter is composed of a series of co-ordinate functions. Dependant on the symmetries of the problem and consequently the co-ordinate system employed, these functions will typically be trigonometric, exponential, hyperbolic or Bessel functions.

Unfortunately this elegant approach is really only practicable when the boundaries correspond to complete simple surfaces in the appropriate co-ordinate system. It is not therefore useful for the microstrip problem.

2.1.2.4 Integral Equation Method

The problem can be reformulated as the solution of an integral equation. The essential benefit obtained is that one attempts to find the charge distribution, which exists only on the surfaces, as compared to the potential field throughout the region; the objective of solving the differential equation directly. Thus, in the analysis of microstrip, the charge distribution is a function of one variable (x) only, where as the potential is dependant on both co-ordinates [17]. This also implies computational efficiency; for when the solution is inevitably quantitised for implementation on a digital computer, the number of points involved in the calculation by the integral equation method, will be approximately the square root of that required for the differential equation solution.

Equation <2.18> is a statement of Green's identity in the plane:

$$\int_{\xi}(f\nabla^2 g - g\nabla^2 f)ds = \oint_{L}(g\frac{\partial f}{\partial n} - f\frac{\partial g}{\partial n})dl \qquad \langle 2.18 \rangle$$

where $\int_{\xi}$ is the surface integral over the region

$\oint_{L}$ is the closed line integral over the boundary enclosing the region.

$\frac{\partial}{\partial n}$ is the derivative normal to the boundary

and f,g are scalar fields

Letting f be the potential field ϕ and g be a function G, such that

$$\nabla^2 G(r|r_o) = -\delta(r - r_o) \qquad \langle 2.19 \rangle$$

where r, r_o are position vectors

and $\delta(r-r_o)$ is the Dirac delta function in 2-dimensions

(i.e. $\delta(r-r_o) = 1$; $r = r_o$ and 0; $r \neq r_o$),

then $\int_S \{\phi\nabla^2 G - G\nabla^2\phi\}ds = \int_S \{-\phi(r)\delta(r-r_o) + G(r|r_o)\rho(r_o)/e(r')\}ds$ <2.20>

Since, if $\phi(r)$ and $\partial\phi(r)/\partial n \to 0$ as $|r| \to \infty$, conducting the integration of the right hand side of equation <2.18> over a distant boundary yields zero, and taking into account the properties of the Dirac function in equation <2.20>, the following result is obtained:

$$\phi(r) = \int_S G(r|r_o)\rho(r_o)ds_o \qquad <2.21>$$

where the effect of permittivity is absorbed into the function G. This expression is known as the Fredholm integral equation and the function G is called the Green's function.

The significance of this result can be demonstrated by observing that the equation <2.19> defining the properties of the Green's function is a Poisson equation. The Green's function is therefore the solution for the potential distribution for a unit value, infinitisimal line charge at r_o with the boundary conditions identical to those of the original problem. Assuming linearity, superposition applies and the total potential distribution is found by integration over the conducting boundaries (for which $\rho \neq 0$). This perspective does indicate that the problem of defining the Green's function can be nearly as difficult as finding the solution of the original partial differential equation, although the need to consider only a line (or point) charge does offer useful advantages.

2.1.2.5 Other Techniques

There are numerous variations of, and alternatives to these techniques for the solution of static field problems.

Some alternatives are the graphical field mapping [15], and lumped equivalent circuit network analysis [21]. Variations of the integral equation based method include the use of Fourier Transforms to find the

Green's function [23] in the spectral domain and variational calculus to determine arbitrarily close bounds on the capacitance [4]. The transverse transmission line method has been applied to the slightly more complex problem of microstrip with multilayered dieletric [22].

2.1.3 Applying the Integral Equation Method

From the foregoing assessment it seems that the integral equation method is an attractive option; being relatively efficient, reasonably straightforward and direct but adequately versatile for microstrip and related problems.

The application of this approach hinges on the derivation of the Green's function for the problem domain. Since, given the 2-dimensional nature of the problem, the Green's function describes the potential distribution for an elementary line charge it embodies all the information relating to the physical structure, including the disposition of dielectrics. The simplest Green's function is that for free space (recognisable as the solution to the Poisson's equation for a unit line charge in a boundary free region, viz:

$$G(x,y|x_o,y_o) = -\ln[(x-x_o)^2+(y-y_o)^2] \,/2\pi\epsilon \qquad \langle 2.22 \rangle$$

in rectangular co-ordinates.

For a system of conducting boundaries the method of images is a powerful technique. The boundaries are simulated by the introduction of other charges so that using the principle of superposition the potential distribution is found for a boundary free equivalent problem. Silvester [5] has extended this technique to deal with dielectric boundaries. Using the method of partial images dielectric boundaries can be substituted by additional sources of magnitude and position such that the potential distribution is maintained equivalent.

2.1.3.1 Partial Images

The first step is to find the image coefficient, K. In figure 2.3 the region is divided by a dielectric interface at y=0 and a line charge q resides at (0,d) with a postulated image of magnitude q′ at (0,-d)

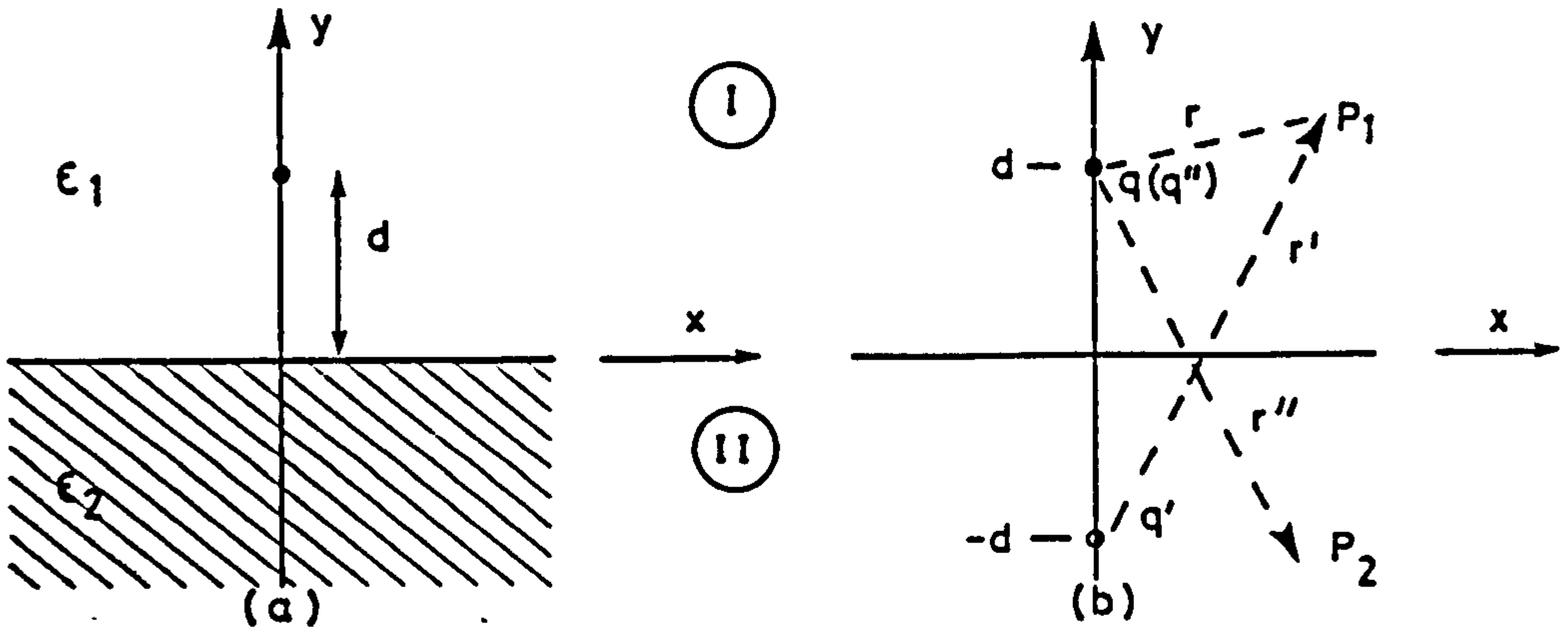

Figure 2.3 Partial images for a dielectric boundary

The image line charge must produce, in a uniform dielectric, a potential distribution identical to that with the mixed dielectric and the single source. The fields in the two half spaces of the partial image model (figure 2.3b) are considered separately:

CASE 1: Consider a point P_1 in region I; (y>0)

The potential due to charges q @ (0,d)

and q′ @ (0,-d)

$$\phi_{P1} = -q\ln(r)/2\pi\varepsilon_1 - q'\ln(r')/2\pi\varepsilon_1 \qquad \langle 2.23 \rangle$$

CASE 2: Consider a point P_2 in region II; (y<0)

The potential due to charge q" @ (0,d) (i.e. coincident with the source line charge)

$$\phi_{P2} = -q''\ln(r'')/2\pi\varepsilon_1 \qquad \langle 2.24 \rangle$$

At the interface between the regions (y=0):

$$\phi_{P1} = \phi_{P2} \qquad \langle 2.25 \rangle$$

and r = r′ = r"

therefore $q + q' = q''$ <2.26>

For the situation of figure 2.3a, the continuity conditions of <2.17> apply at this boundary. As a consequence

$$D_y = \epsilon_1 E_{y+} = \epsilon_2 E_{y-} \qquad (y=0) \qquad \text{<2.27>}$$

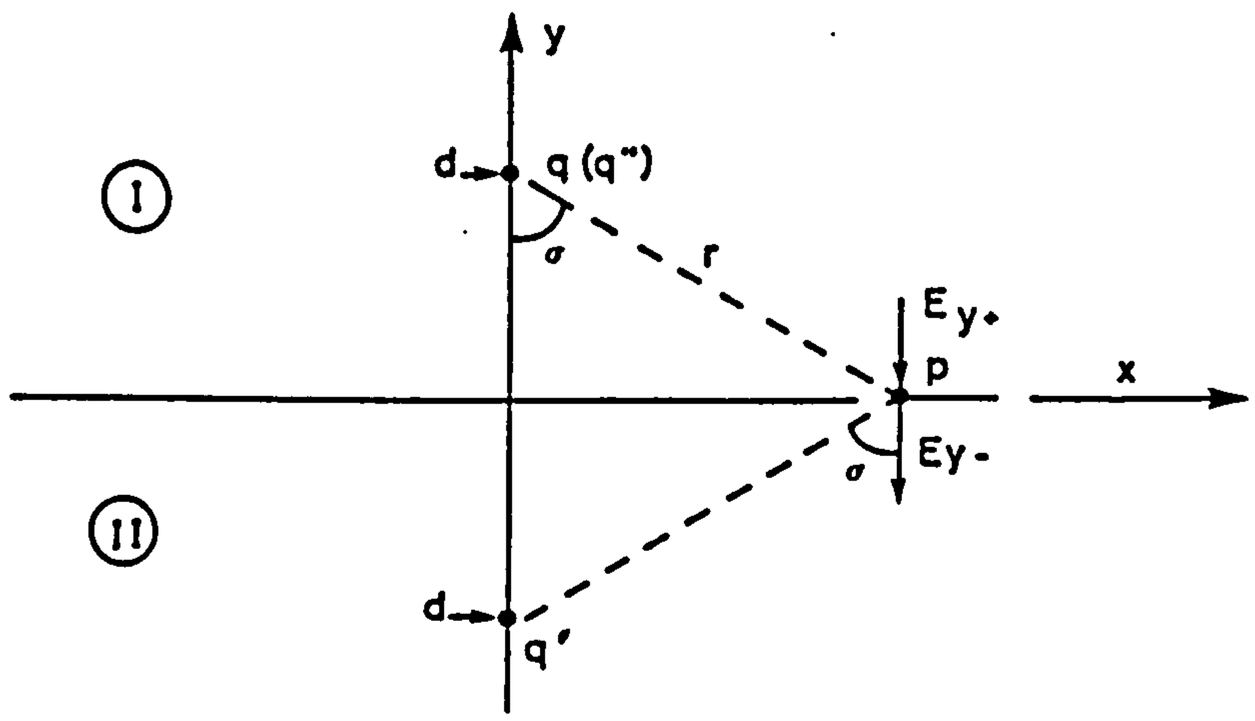

Figure 2.4 Geometry for the derivation of the image coefficient.

In figure 2.4 the field at point P due to line charge q is

$$\mathbf{E} = (q/2\ \epsilon_1 r).\mathbf{a}_r \qquad \text{<2.28>}$$

therefore, in the equivalent homogeneous model:

$$E_{y1} = (q \cos\theta - q' \cos\theta)/2\pi\epsilon_1 r \qquad \text{<2.29>}$$

$$\text{and } E_{y2} = q''\cos\theta/2\pi\epsilon_1 r$$

Substituting in <2.27> produces a second relationship between the line charge and its images:

$$q'' = (q-q')\epsilon_1/\epsilon_2 \qquad \text{<2.30>}$$

from which, in combination with the result of <2.26>

$$q' = Kq \quad \& \quad q'' = (1 + K)q \qquad \text{<2.31>}$$

$$\text{where } K = (\epsilon_1 - \epsilon_2)/(\epsilon_1 + \epsilon_2) \qquad \text{<2.32>}$$

the image coefficient, which has a negative value when region I is free space (or $\epsilon_2 > \epsilon_1$).

To summarise: a field distribution in region I, equivalent to that for the mixed dielectric situation, can be produced in a homogeneous dielectric (ϵ_1) by two line charges, the source, q, and its image, Kq. Similarly, in region II the equivalent homogeneous situation (also with the permittivity, ϵ_1) is produced by a single line charge of (1 + K)q situated coincident with the source. Note that this is slightly different to the approach taken in the literature [5,11] where the homogeneous dielectric assumed for observations in region II of has permittivity ϵ_2. This follows a preference of the author for the consistency of using one value of permittivity ($\epsilon_1 = \epsilon_o$ for microstrip) for all regions. The difference is trivial since $(1 + K)/(1 - K) = \epsilon_1/\epsilon_2$ and, in the conventional approach the image for region II has value (1 - K)q.

2.1.3.2 Microstrip Green's Function

Now that a method by which the mixed dielectric problem can be translated into an equivalent homogeneous one has been established, it is possible to define a Green's function for the microstrip structure.

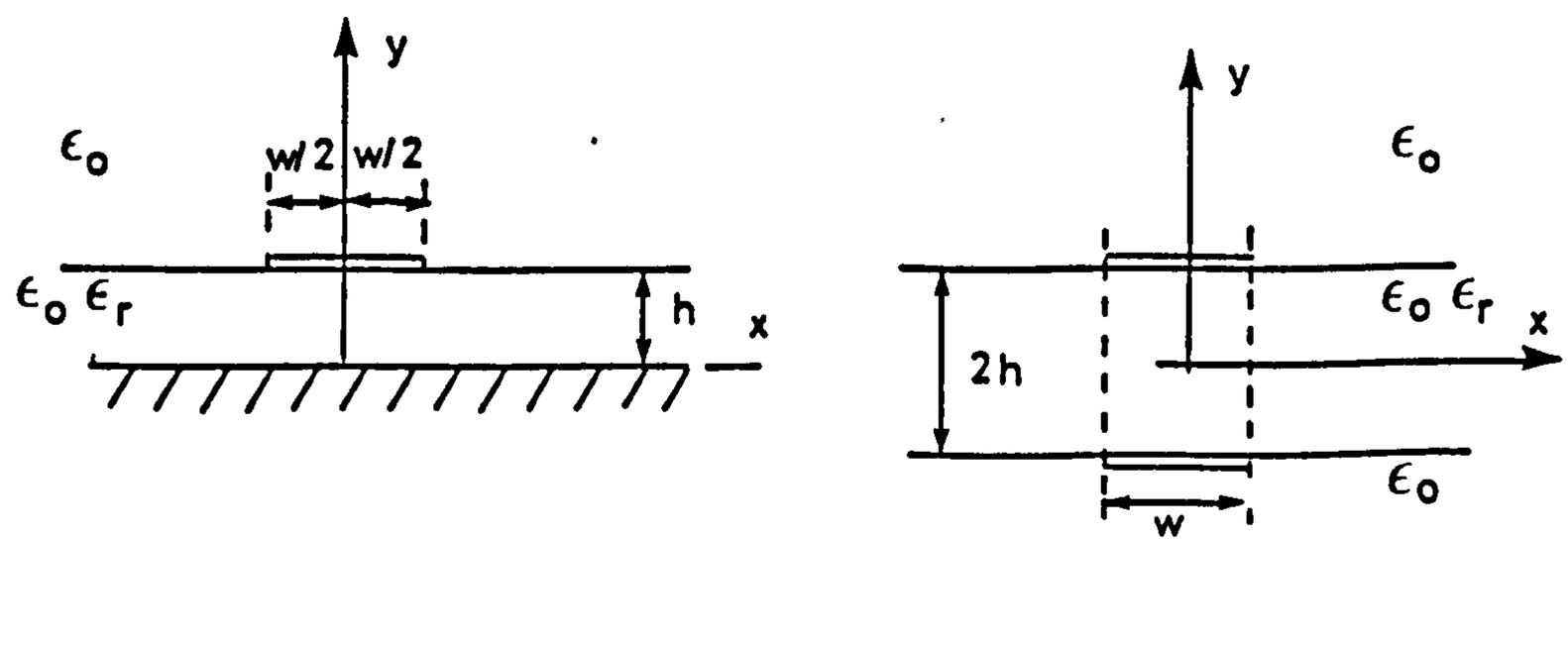

(a) (b)

Figure 2.5 Microstrip(a) and an electrically equivalent bilateral strip-line(b).

The symmetry of the structure can be increased by dealing with an

equivalent bilateral line (figure 2.5b) in which the potential on the strips is equal and opposite. Thus an electric wall exists where the microstrip ground plane would be. There are now, however, two dielectric interfaces to accommodate. This is achieved considering multiple partial images in the three regions. Using the definitions of the previous section and given that the image coefficient of the additional interface is -K; the multiple images observed in the three regions are as illustrated in figure 2.6. From this figure expressions for the potential in the three regions can be deduced. Clearly there are an infinite set of diminishing terms (K < 1).

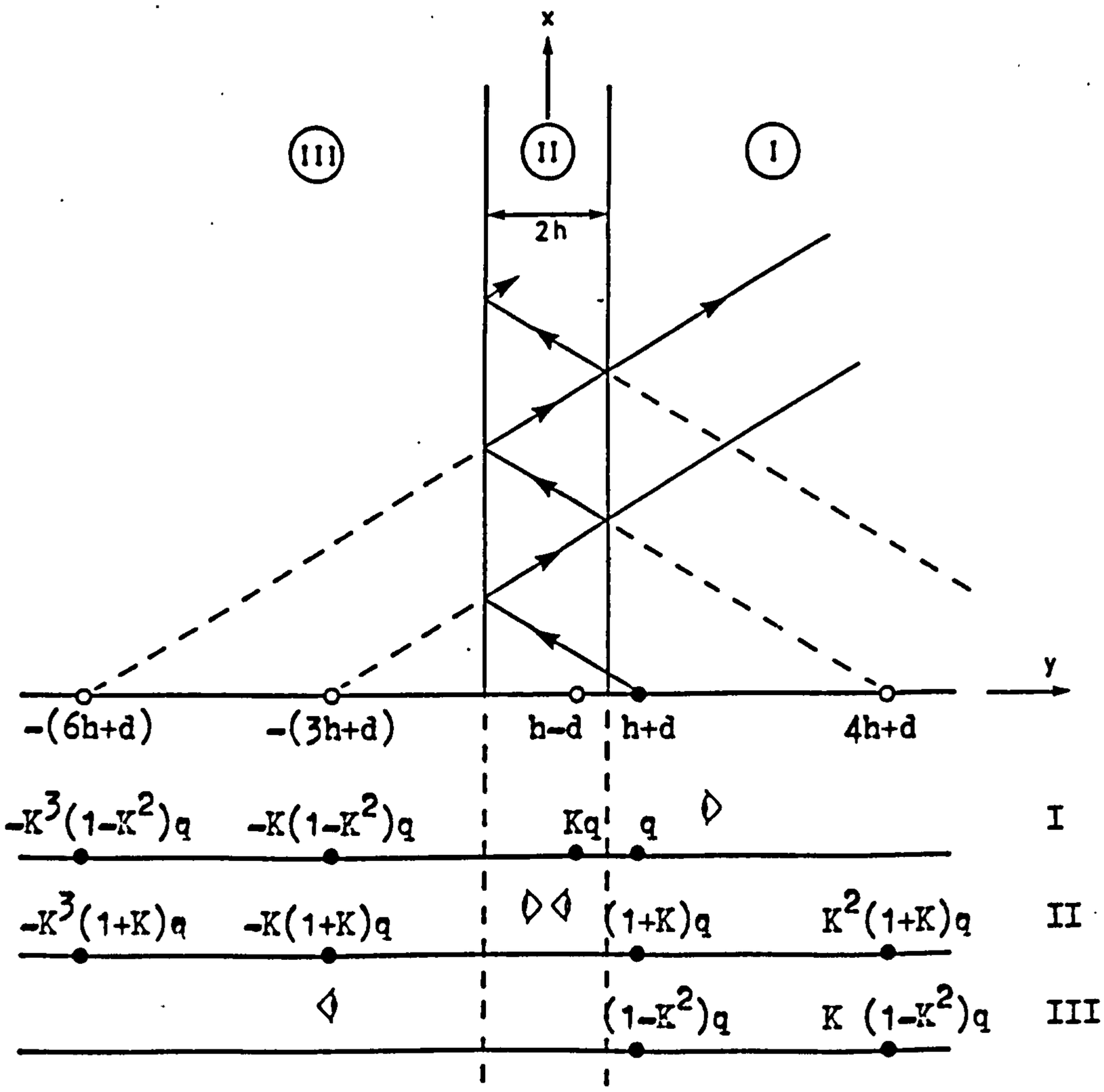

Figure 2.6 Multiple image homogeneous dielectric representation for the electric field in the region of a dielectric sheet, showing typical flux lines.

REGION I $-h < y < h,\ x_o = 0,\ y_o \geqslant h$

$$\phi(x,y) = -(q/4\pi\epsilon_o)(\ln[(x-x_o)^2+(y-y_o)^2] + K.\ln[(x-x_o)^2+(y-y_o-2h)^2]$$

$$+(1-K^2)\sum_{n=o}^{\infty}K^{2n+1}\ln[(x-x_o)^2+(y+y_o+2(2n+1)h)^2]) \qquad \langle 2.33 \rangle$$

REGION II $y < -h,\ x_o = 0,\ y_o \geqslant h$

$$\phi(x,y) = -([1+K]q/4\pi\epsilon_o)\sum_{n=o}^{\infty}K^{2n}\ln[(x-x_o)^2+(y-y_o-2nh)^2] \qquad \langle 2.34 \rangle$$

REGION III $y < -h,\ x_o = 0,\ y_o \geqslant h$

$$\phi(x,y) = -([1-K]^2/4\pi\epsilon_o)\sum_{n=1}^{\infty}K^{2n}\ln[(x-x_o)^2+(y-y_o-4nh)^2] \qquad \langle 2.35 \rangle$$

Note that only one potential singularity occurs, that due to the source in <2.33>; all the images occur outside the range of validity of the appropriate relationship. These expressions form the basis of the microstrip Green's function.

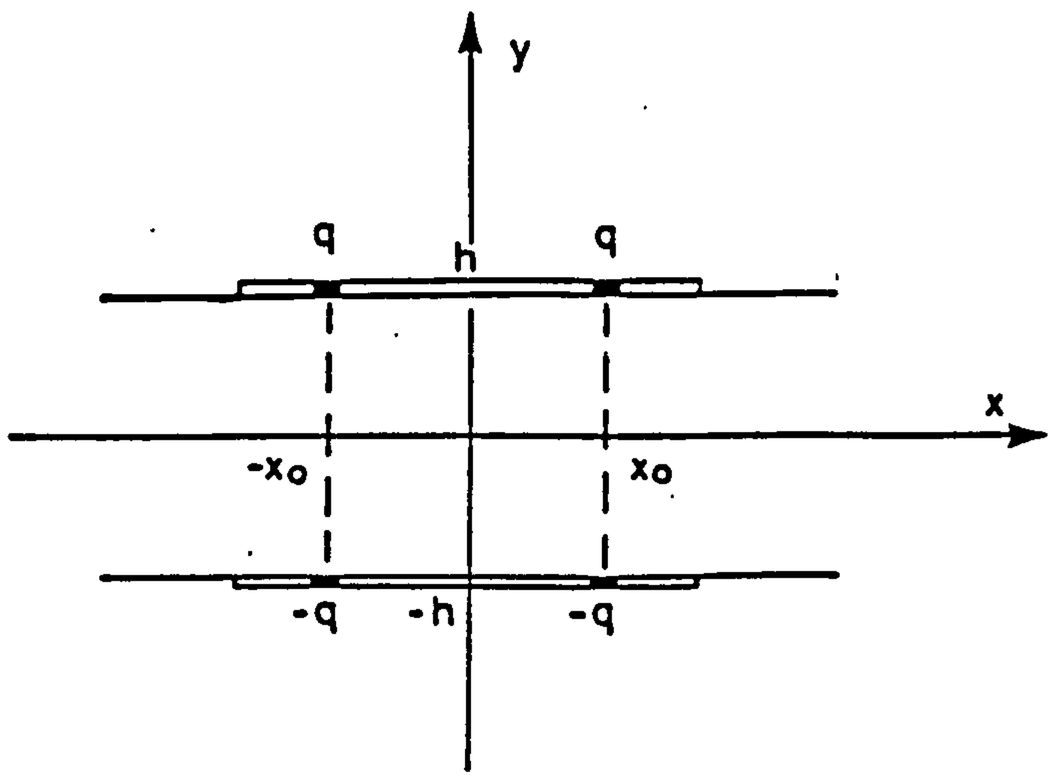

Figure 2.7 Symmetrical charge disposition for microstrip Green's function

The symmetry of the problem is utilised by considering four evenly disposed line charges of equal strength as shown in figure 2.7. For an infinitesimally thin conducting strip the potential anywhere on the dielectric surface, including the strip, can be defined by the Green's

function developed from <2.34>, approaching the surface from within the dielectric.

$$G(x,h_-|x_o,h_+) = ([1+K]/4\pi\epsilon_o)$$

$$\sum_{n=o}^{\infty} K^n \ln[([x-x_o]^2+[y-y_o+2nh]^2)/([x-x_o]^2+[y-y_o-2nh]^2)] \quad \text{<2.36>}$$

2.1.3.3 The Moment Method

For the purpose of evaluating the Fredholm integral equation <2.21> the strip conductor is divided into a number of sub-strips. Thus the potential at a point due to the contributions from all charged sub-strips is:

$$\phi(x,y) = \sum_{j=1}^{N} \rho_j(x_o,y_o) \int_{w_j} G(x,y|x_o,y_o)dl_o \quad \text{<2.37>}$$

where w_j signifies the line integral taken across substrip j, width w_j. The average potential on the ith strip is then:

$$\phi_i(x,y) = \sum_j \{(q_j/w_j)(1/w_i) \int_{w_i} \int_{w_j} G(x,y|x_o,y_o)dl_o dl\} \quad \text{<2.38>}$$

where the strips are narrow enough for the charge distribution to be regarded as substantially uniform and $q_j=\rho_j w_j$.

Rewriting this result as

$$\phi_i = D_{ij}\, q_j \quad \text{<2.40>}$$

where D_{ij} denotes the evaluation of the integral for the indicated sub-strips. Given that the potential on the strip has a defined constant value, it is the intention to evaluate the charge densities, q_j. Using matrix notation the solution is:

$$Q = D^{-1}.\Phi \quad \text{<2.41>}$$

which from <2.9> yields the capacitance of the microstrip line as

$$C = \sum_{i=1}^{M} q_i = \sum_{i}^{M} \sum_{j}^{N} [D_{ij}]^{-1} \qquad \text{<2.42>}$$

with an excitation of 1 Volt assumed. This technique for numerical solution of an integral equation is an application of the moment method [20]. For an evaluation of the integral of <2.38> the reader is referred to the work of Hosseini [11].

2.2 ANISOTROPIC DIELECTRIC MEDIA

When an anisotropic dielectric substrate is used the analysis is significantly more complex. The anisotropic property of a dielectric is the variation of its permittivity with direction or orientation. Recalling that **D**, the electric flux density vector is independent of the dielectric properties, its relationship to the electric field is now defined by a permittivity tensor, $[\epsilon]$:

$$\mathbf{D} = [\epsilon].\mathbf{E} \qquad \text{<2.44>}$$

In 3-dimensions tensor is of rank 3 and has 9 elements, which are denoted thus:

$$[\epsilon] = \begin{bmatrix} \epsilon_{11} & \epsilon_{12} & \epsilon_{13} \\ \epsilon_{21} & \epsilon_{22} & \epsilon_{23} \\ \epsilon_{31} & \epsilon_{32} & \epsilon_{33} \end{bmatrix} \qquad \text{<2.45>}$$

If the principle axes of the dielectric (usually a single crystal) are aligned to the co-ordinate system, the off-diagonal terms vanish:

$$[\epsilon] = \begin{bmatrix} \epsilon_1 & 0 & 0 \\ 0 & \epsilon_2 & 0 \\ 0 & 0 & \epsilon_3 \end{bmatrix} \qquad \text{<2.46>}$$

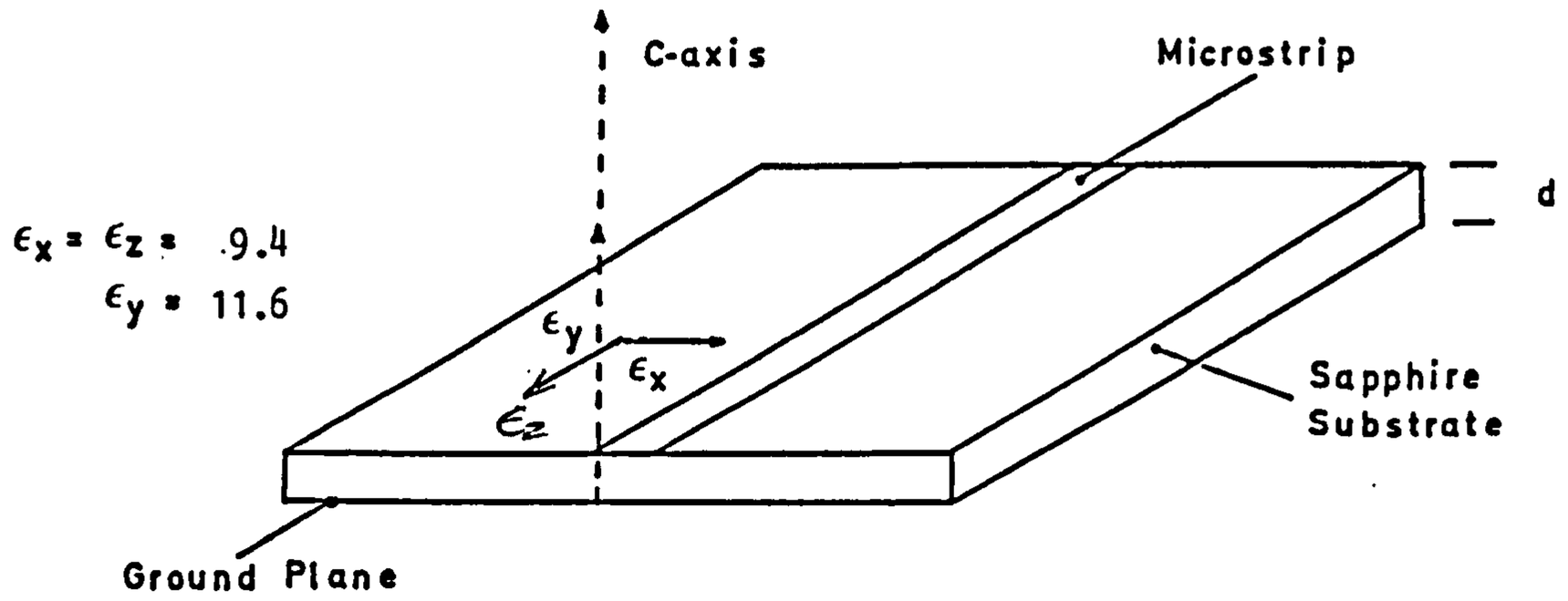

Figure 2.8 Microstrip on a simply orientated anistropic substrate

With the co-ordinates defined as in figure 2.8 and assuring TEM propagation it is clear that further simplification to a tensor of rank 2 is possible, viz:

$$\mathbf{D} = \begin{bmatrix} \epsilon_o\epsilon_x & 0 \\ 0 & \epsilon_o\epsilon_y \end{bmatrix} . \mathbf{E} \qquad \langle 2.47 \rangle$$

where, depending on orientation, ϵ_x and ϵ_y map any combination of ϵ_1, ϵ_2 and ϵ_3. Indeed, since two of the principle axis permittivities are often similar ($\epsilon_2 = \epsilon_3$, say) one choice of orientation results in a reversion to the isotropic situation. This trivial case is ignored and, for the following work, $\epsilon_x \neq \epsilon_y$ is assumed throughout.

2.2.1 Two-dimensional Fields in Amisotropic Dielectrics

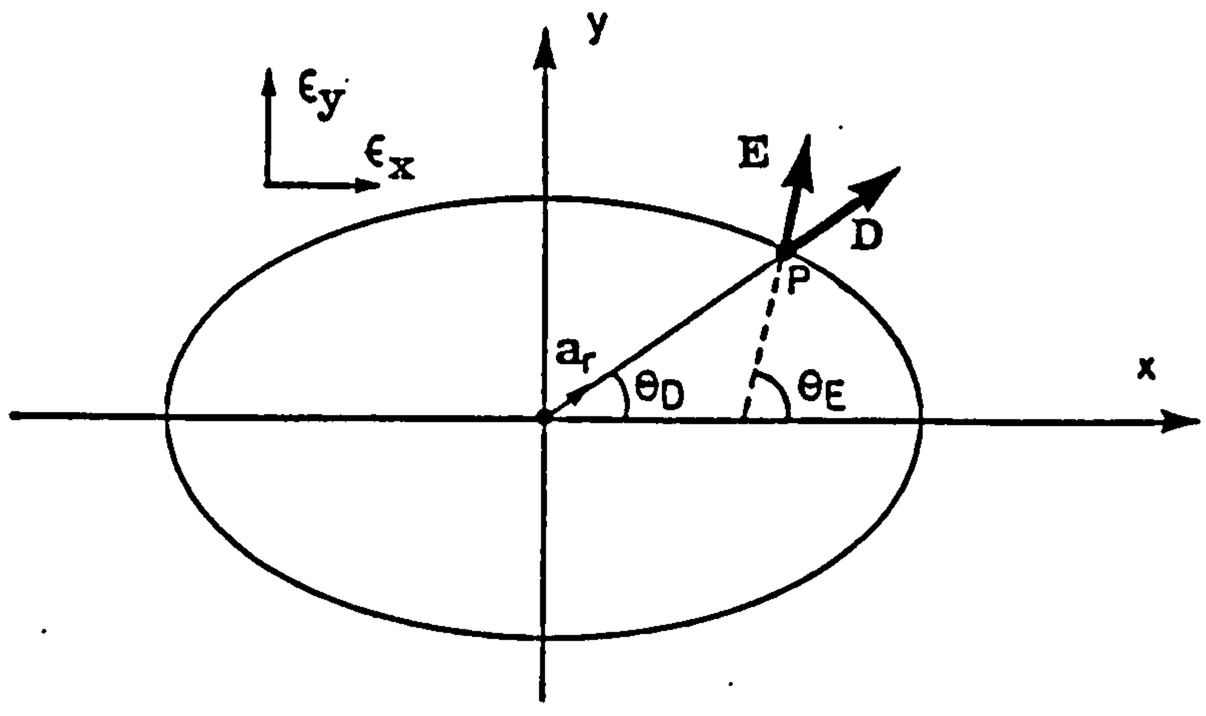

Figure 2.9 Electric field, flux density vector and equipotentials in anisotropic materials

From <2.47>

$$\mathbf{E} = (D_x/\epsilon_o\epsilon_x).\mathbf{i} + (D_y/\epsilon_o\epsilon_y).\mathbf{j} \qquad \text{<2.48>}$$

Considering a line charge at (0,0) in figure 2.9 the electric flux density at a point P(x,y) is:

$$\mathbf{D} = (q/2\pi r).\mathbf{a_r} \qquad \text{<2.49>}$$

having components resolved with rectangular co-ordinates

$$D_x = (x/r)(q/2\pi r) \quad , \quad D_y = (y/r)(q/2\pi r) \qquad \text{<2.50>}$$

If $\mathbf{a_r}$ is aligned with the x-axis then the magnitude of electric field is

$$E = q/2\pi r\epsilon_o\epsilon_x \qquad \text{<2.51a>}$$

and, similarly, with $\mathbf{a_r}$ aligned to the y-axis:

$$E = q/2\pi r\epsilon_o\epsilon_y \qquad \text{<2.51b>}$$

Thus, at a constant distance from the source, the electric field intensity is a function of the direction in anisotropic media. This distortion is reflected in the elliptical shape of the equipotentials ($\phi = -\int \mathbf{E}.\mathbf{a_r}dr$), as illustrated in figure 2.9 where $\epsilon_y > \epsilon_x$.

For any position of D

$$E_x = (x/r\epsilon_x)E_o \quad , \quad E_y = (y/r\epsilon_y)E_o \qquad \langle 2.52 \rangle$$

where $E_o = q/2\pi r\epsilon_o$ (the magnitude of a free space electric field).

So the angle of the electric field vector is:

$$\theta_E = \tan^{-1}(y\epsilon_x/x\epsilon_y)$$

$$= \tan^{-1}(\tan\theta_D . \epsilon_x/\epsilon_y) \qquad \langle 2.53 \rangle$$

where θ_D is the angle of the flux density vector. It is evident that the directions of flux density and electric field differ in an anisotropic dielectric. Nevertheless, angle of the electric field vector is still such that it is orthagonal to the equivpotentials.

From the nature of these distortions it is apparent that some sort of geometric transformation would be useful : translating electrostatic problems into an equivalent isotropic form.

2.2.2 The Anisotropic Poisson's Equation

In isotropic media electrostatic problems are addressed by finding solutions to the Poisson's equation with the particular boundary conditions applied. It is therefore desirable to obtain an anisotropic varient of Poisson's equation before attempting the solution of problems in anisotropic media.

The Poisson's equation is a consequence of the properties of the divergence of electric field:

$$\nabla . \mathbf{D} = \rho \qquad \langle 2.54 \rangle$$

Substituting from <2.47>

$$\epsilon_x \frac{\partial E_x}{\partial x} + \epsilon_y \frac{\partial E_y}{\partial y} = -\rho(x_o, y_o)/\epsilon_o$$

And, since $\mathbf{E} = \nabla\phi$;

$$\epsilon_x \frac{\partial^2 \phi}{\partial x^2} + \epsilon_y \frac{\partial^2 \phi}{\partial y^2} = -\rho(x_o, y_o)/\epsilon_o \qquad \langle 2.55 \rangle$$

the anisotropic Poisson's equation.

2.3 MICROSTRIP ON ANISOTROPIC SUBTRATES

The techniques for the solution of the quasi-static microstrip problem outlined in section 2.1.2 are reviewed in the light of the properties of the anisotropic dielectric substrate.

2.3.1 Techniques for Analysis

2.3.1.1 Conformal Mapping

Since the orientation of the dielectric is not preserved in the conformal transformation this technique has no application to the anisotropic situation.

2.3.1.2 Finite Differences

This approach has been successfully adopted by Owens, et al. [9] whose results are presented in chapter 3 (figure 3.23). Nevertheless it is still a numerically inefficient technique.

2.3.1.3 Separation of Variables

Clearly the partial differential equation <2.55> is susceptible to solution by classical techniques. Since, however this approach appears intractable with the particular boundary conditions of the microstrip problem it is no more useful for the anisotropic situation than for the isotropic.

2.3.1.4 Integral Equation Method.

This technique appears entirely appropriate and retains the advantages evidenced in its application to microstrip on an isotropic

substrate. The anisotropic Green's function is the solution of the anisotropic Poisson equation, <2.55>, viz

$$\epsilon_x \frac{\partial^2 G}{\partial x^2} + \epsilon_y \frac{\partial^2 G}{\partial y^2} = \delta(x-x_o)\delta(y-y_o)/\epsilon_o \qquad \text{<2.56>}$$

Having found an appropriate Green's function the established numerical techniques for the solution of the Fredholm equation, <2.21> can be applied.

2.3.1.5 Transform Techniques

As indicated in the discussion of the properties of anisotropic dielectrics (section 2.2.1) it would appear that an isotropic structure, electrically equivalent to the anisotropic one, could be obtained by a simple geometric transformation. If such a transform could be defined it would have the obvious benefit that it could be applied with all existing isotropic microstrip solutions.

2.3.2 Transform Methods

At the commencement of this work the author had three alternative proposed transform techniques [6-8] to assess. An existing microstrip calculation program [11] was adapted so that the results could be compared (cf. figure 2.15). Also, each method was critically examined from a theoretical standpoint. Throughout the following discussions transform variables are identified by an asterisk (*).

2.3.2.1 Spencer's Transform

This ingenious method [8] accommodates the dielectric anisotropy by introducing an effective substrate permeability; producing a transmission line structure which is, in turn, analysed using a transform

technique [13] to apply standard microstrip solutions (e.g. [12] & [24]) to solve for characteristic impedance and velocity of propagation. To this end two "pseudo" permittivities relating these quantities to their free space values are defined:

$$Z = Z_o/\sqrt{K_1} \quad \& \quad v = v_o/\sqrt{K_2} \qquad \langle 2.57 \rangle$$

where $K_1 = \epsilon_{eff}/\mu_{eff}$ & $K_2 = \epsilon_{eff}\cdot\mu_{eff}$

The effective permittivity and permeability can be found from the following eexpressions:

$$_{eff} = 1 + q_e(\epsilon^* - 1) \qquad \langle 2.58 \rangle$$

$$\mu_{eff} = 1/(1 + q_m[(1/\mu^*) - 1]) \qquad \langle 2.59 \rangle$$

where the electric and magnetic filling fractions are:

$$q_e = q_m = (1 + 1/\sqrt{1 + 10h/w})/2 \qquad \langle 2.60 \rangle$$

and μ^* is the 'pseudo permeability', which, together with an equivalent isotropic permittivity, ϵ^*, is defined in terms of the anisotropic permittivity below.

$$\epsilon^* = \sqrt{\epsilon_y\cdot\epsilon_x} \quad \& \quad \mu^* = \sqrt{\epsilon_y/\epsilon_x} \qquad \langle 2.61 \rangle$$

Results seem fair but the rational behind the method is a little obscure and it is difficult to justify rigorously. It will be noted that, in the following discussion, relationships analogeous to <2.61> appear frequently.

2.3.2.2 Weale's Transform

Initially results from this method were most disappointing. This gross error was attributable to the fact that Weale [6] had mistakenly applied his geometrical transform to the calculation of both the free space and dielectrically loaded capacitances; C_o and C_d respectively (cf. equations <2.5>-<2.7>), whereas the geometry should only have been adjusted for the calculation of the latter. Correcting this trivial error produced a marked improvement in the results obtained which

are included on the graph of figures 2.15. Nevertheless the results still deviate significantly from the measured data. Weale's method involves a scaling of the substrate thickness which results in the formation of the familiar isotropic Poisson's equation when the y-coordinate is transformed accordingly. The transform is stated as:

$$x^* = x \ , \quad y^* = y\sqrt{\epsilon_x/\epsilon_y} \quad \& \quad \epsilon^* = \epsilon_y \qquad \text{<2.61>}$$

This transform is, very similar to that due to Szentkuti [7] and therefore its justification is not discussed in isolation. It is apparent from the following analysis that the discrepancies in the results are due to a subtle error in Weale's analysis.

2.3.2.3 Szentkuti's Transform

The transform proposed by Szentkuti [7] is quoted here with the variables defined as figure 2.10.

$$x^* = x \ , \quad y^* = y\sqrt{\epsilon_x/\epsilon_y} \qquad \text{<2.62a>}$$

and $$\epsilon^* = \sqrt{\epsilon_x \cdot \epsilon_y} \qquad \text{<2.62b>}$$

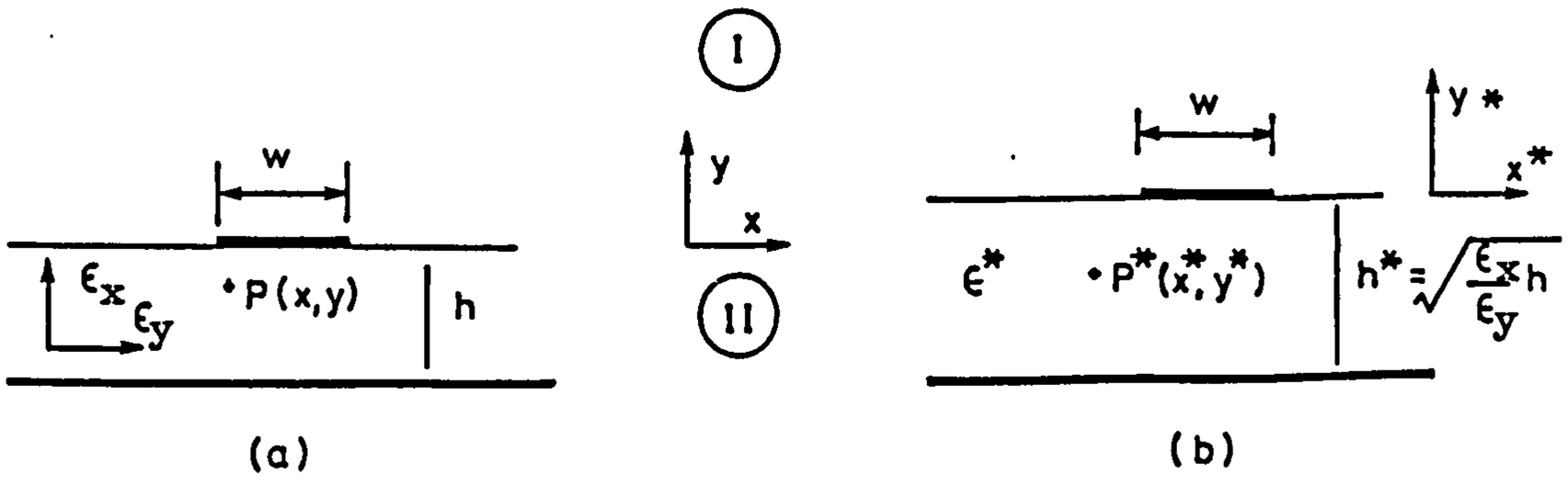

Figure 2.10 Transformation of anisotropic(a) to isotropic(b) dielectric microstrip

A proof of the validity of this transform follows:

Let the transform potentials at the points P and P^* in the original and transformed domains be related thus:

$$\phi_p = \phi_p^* \qquad \langle 2.63 \rangle$$

and similarly their spatial derivatives thus

$$\frac{\partial \phi_P}{\partial x} = \frac{\partial \phi_P^*}{\partial x^*} \cdot \frac{\partial x^*}{\partial x} , \qquad \frac{\partial \phi_P}{\partial y} = \frac{\partial \phi_P^*}{\partial y^*} \cdot \frac{\partial y^*}{\partial y} \qquad \langle 2.64 \rangle$$

or, since the transformations of the x and y axes are independent"

$$\frac{\partial \phi_P}{\partial x} = \frac{\partial \phi_P^*}{\partial x^*} \cdot \frac{dx^*}{dx} , \qquad \frac{\partial \phi_P}{\partial y} = \frac{\partial \phi_P^*}{\partial y^*} \cdot \frac{dy^*}{dy} \qquad \langle 2.65 \rangle$$

and similarly for second derivatives

$$\frac{\partial^2 \phi_P}{\partial x^2} = \frac{\partial^2 \phi_P^*}{\partial x^{*2}} \left(\frac{dx^*}{dx}\right)^2 , \qquad \frac{\partial^2 \phi_P}{\partial y^2} = \frac{\partial^2 \phi_P^*}{\partial y^{*2}} \left(\frac{dy^*}{dy}\right)^2 \qquad \langle 2.66 \rangle$$

From the geometrical transform of <2.62a>

$$\frac{dx^*}{dx} = 1 , \qquad \frac{dy^*}{dy} = \sqrt{\epsilon_x/\epsilon_y} \qquad \langle 2.67 \rangle$$

Since this transformation is relevant to the dielectric substrate only (Region II), and there are no charges within this region, the Poisson's equation degenerates to the Laplace equation. With the appropriate substitutions from <2.66> and <2.67> the anisotropic Laplace equation of <2.55> becomes:

$$\epsilon_x \frac{\partial^2 \phi^*}{\partial x^{*2}} + \epsilon_x \frac{\partial^2 \phi^*}{\partial y^{*2}} (\epsilon_x/\epsilon_y) = 0$$

or

$$\frac{\partial^2 \phi^*}{\partial x^{*2}} + \frac{\partial^2 \phi^*}{\partial y^{*2}} = 0 \qquad \langle 2.68 \rangle$$

the isotropic Laplace equation with transformed variables; demonstrating that the geometric transformation has generated an equivalent isotropic domain.

It is at this point that an error can easily be made, as has occurred [6], by using the Poisson's equation and thereby inferring the

transformed structure can be treated as isotropic with a permittivity: e_x. The implication of this move is that the whole space is subject to the transformation which, as region I is isotropic, would be fallacious. The significance of the right hand side of this Poisson's equation under transformation is both obscure and irrelevant.

In order to proceed with the microstrip problem it is necessary to re-examine the boundary conditions at the dielectric interface. From the tangential electric field:

$$E_{x+} = E_{x-} = -\frac{\partial \phi}{\partial x} = -\frac{\partial \phi^*}{\partial x^*}\left(\frac{dx^*}{dx}\right) = -\frac{\partial \phi^*}{\partial x^*} = E_{x-}^* \qquad \langle 2.69 \rangle$$

it is evident that there is no change to the boundary conditions in this respect. Considering the continuity of the normal component of flux:

$$D_{y+} = D_{y-} = -e_o e_y \frac{\partial \phi}{\partial y} = -e_o e_y \frac{\partial \phi^*}{\partial y^*}\left(\frac{dy^*}{dy}\right) \qquad \langle 2.70 \rangle$$

which under transformation becomes:

$$D_{y-} = -e_o e^* \frac{\partial \phi^*}{\partial y^*} \qquad \langle 2.71 \rangle$$

Equating the expressions of <2.70> and <2.71> the equivalent isotropic permittivity takes the value of the geometric mean of the anisotropic permittivities as proposed in <2.62b>. Q.E.D.

2.3.3 Application of the Transform to Microstrip Parameter Determination

The transform of the previous section enables the capacitance (per unit length) of the microstrip on an anisotropic substrate, C_A, to be calculated using techniques devised for the isotropic situation. There are two ways in which it is possible to apply the transform to the determination of microstrip propagation parameters.

When the microstrip parameters are calculated from capacitance computations, as in computer program implementation of any of the

techniques discussed in section 2.1.2, the transform can be applied to the computation for the dielectric filled case alone. The equations <2.7> and <2.8> then become:

$$Z = 1/v_o\sqrt{C_o.C_A} \quad \& \quad v = v_o\sqrt{C_o/C_A} \qquad \text{<2.72>}$$

If, however, explicit formulae (as in [12] and [24]) or tables (as in [25]) are used then the transform must be applied, in effect, retrospectively. In the following analysis subscripts, I and A signify isotropic and anisotropic quantities respectively and asterisks identify the variable associated with the transformed case. Impedance and velocity obtained from the formulae/tables with $h^* = h\sqrt{\epsilon_x/\epsilon_y}$ and $^* = \sqrt{\epsilon_x\epsilon_y}$ relate to the capacitances thus:

$$Z_I^* = 1/v_o\sqrt{C_o^* C_d^*} \quad \& \quad v_I^* = v_o\sqrt{C_o^*/C_d^*} \qquad \text{<2.73>}$$

but
$$C_d^* = C_A = 1/Z_I^* v_I^* \qquad \text{<2.74>}$$

and from <2.72>:

$$Z_A = \sqrt{Z_I Z_I^* v_I^*/v_I} \qquad \text{<2.75a>}$$

$$v_A = \sqrt{v_I v_I^* Z_I^*/Z_I} \qquad \text{<2.75b>}$$

Thus, by using the formulae/tables twice; first with the actual geometry and then with the transformed values for h and ϵ, values for the principle parameters of microstrip on an anisotropic substrate can be determined. Note that as the value C_I is irrelevant the former operation can be conducted with any value of substrate permittivity, most conveniently $\epsilon_r=1$ or $\epsilon_r=\epsilon^*$.

The expressions of Schneider [12], being rational function approximations to the results of a conformal mapping analysis, are included for convenience:

$$Z_o = 60\ \ln(8h/w + w/4h)\ ; \quad w/h \leq 1 \qquad \text{<2.76a>}$$

$$Z_o = 120\pi/(w/h + 2.42 - 0.44h/w + [1 - h/w]^6)\ ; \quad w/h \geq 1 \qquad \text{<2.76b>}$$

and,
$$\epsilon_{eff} = \{(\epsilon_r + 1) + (\epsilon_r - 1)\ /[1 + 10h/w]\}/2 \qquad \text{<2.77>}$$

from which;
$$Z_I = Z_o/\sqrt{\epsilon_{eff}} \quad , \quad v_I = v_o/\sqrt{\epsilon_{eff}}$$

2.3.4 Direct Solution using Green's Function

The suitability of an integral equation method was discussed in section 2.3.1.4 where the defining equation for the anisotropic situation was stated: <2.56>. Applying the co-ordinate transform of <2.62a>; $x^*=x$, $y= y\sqrt{\epsilon_x/\epsilon_y}$, the Green's function is the solution of the following equation:

$$\frac{\partial^2 G^*}{\partial x^{*2}} + \frac{\partial^2 G^*}{\partial y^{*2}} = - \delta(x-x_o)\delta(\sqrt{\epsilon_y/\epsilon_x}[y^*-y_o^*]/\epsilon_o\epsilon_x \qquad \text{<2.78>}$$

Introducing a rather curious property of the Dirac delta function [26]:

$$\delta(cy) = \delta(y)/c \qquad \text{<2.79>}$$

then

$$\frac{\partial^2 G^*}{\partial x^2} + \frac{\partial^2 G^*}{\partial y^{*2}} = - \delta(x-x_o)\delta(y^*-y_o^*)/\epsilon_o\sqrt{\epsilon_x\epsilon_y} \qquad \text{<2.80>}$$

In a boundary free region the Green's function, expressed in the original coordinates is then:

$$G(x,y|x_o,y_o) = -(1/4\pi\epsilon_o\sqrt{\epsilon_x\epsilon_y}).\ln[(x-x_o)^2 + \sqrt{\epsilon_x/\epsilon_y}(y-y_o)^2] \qquad \text{<2.81>}$$

Note the appearance of the geometric mean permittivity; confirming transformation of <2.62b>. Using this relationship systems of line charges can be studied. In particular, the theory of partial images at a dielectric boundary (cf. Section 2.1.3.1), with one medium exhibiting dielectric anisotropy, will be re-examined.

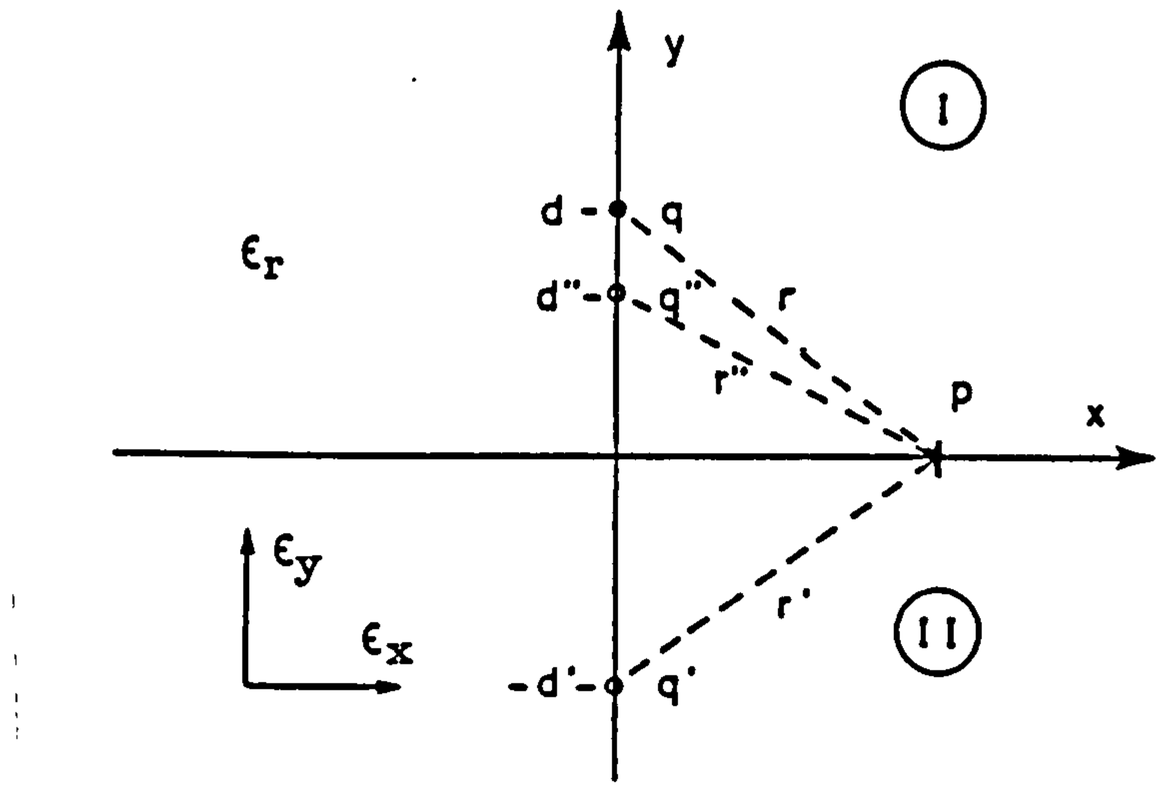

Figure 2.11 Partial Images with dielectric anisotropy

Given the dielectric anisotropy in region II, the positions of the images are made variable, as well as the image coefficient. The potential due to the charges q and q", viewed by an observer in region I, at a point P in figure 2.11, is:

$$\phi_p = -q \ln(x^2 + d^2)/4\pi\epsilon_r\epsilon_o - q'\ln(x^2 - d^2)/4\pi\epsilon_r\epsilon_o \qquad \langle 2.82 \rangle$$

But the potential due q", viewed from the anisotropic region II is:

$$\phi_p = -q"\ln(x^2 - \sqrt{\epsilon_x/\epsilon_y}\, d"^2)/4\pi\epsilon_r\epsilon_o \qquad \langle 2.83 \rangle$$

assuming a permittivity consistant with region I. Equating these expressions from continuity considerations:

$$q" = q + q' \qquad \langle 2.84 \rangle$$

where $$d' = d \quad \text{and} \quad d" = d\sqrt{\epsilon_y/\epsilon_x} \qquad \langle 2.85 \rangle$$

Considering the continuity of the normal component of flux density at the interface, firstly from region I (isotropic).

$$\begin{aligned} D_{y+} &= \epsilon_r\epsilon_o E_{y+} \\ &= (qd/r - q'd/r)/2\pi r \end{aligned} \qquad \langle 2.86 \rangle$$

And from region II (anisotropic)

$$\begin{aligned} D_{y-} &= \epsilon_y\epsilon_o E_{y-} \\ &= (q"\sqrt{\epsilon_y/\epsilon_x}\, d/r')/2\pi r" \end{aligned} \qquad \langle 2.87 \rangle$$

Equating, after the manner of <2.31>, where all observations are referred to a uniform dielectric of relative permittivity, $_r$:

$$\epsilon_r/\epsilon_y(q - q')d/(x^2 + d^2) = q''\sqrt{\epsilon_y/\epsilon_x}.d/(x^2 + \sqrt{\epsilon_y/\epsilon_x}.d^2) \qquad \text{<2.88>}$$

Substituting in the image relationships

$$q' + Kq \quad \text{and} \quad q'' = (1 + K)q$$

$$(1 - K)/(1 + K) = (\epsilon_y/\epsilon_r)\sqrt{\epsilon_y/\epsilon_x}(x^2 + d^2)/(x^2 + \sqrt{\epsilon_y/\epsilon_x}.d^2) \qquad \text{<2.89>}$$

To solve for the trivial case x = 0

$$(1 - K)/(1 + K) = \sqrt{\epsilon_x\epsilon_y}/\epsilon_r \qquad \text{<2.90>}$$

Thus:

$$K = (\epsilon_r - \epsilon^*)/(\epsilon_r + \epsilon^*) \qquad \text{<2.91>}$$

where $\epsilon^* = \sqrt{\epsilon_x\epsilon_y}$

Since a method of partial images for a boundary between isotropic and anisotropic dielectric media has been developed, previous work on multiple images and the derivation of the Green's function for microstrip can be employed. It is simple necessary to offset images observed from region II by the scale factor

$$d''/d = \sqrt{\epsilon_y/\epsilon_x}$$

or, equivalently, transform the y co-ordinate

$$y^*/y = \sqrt{\epsilon_x/\epsilon_y} \qquad \text{(cp. <2.62b>)}$$

and substitute the geometric mean permittivity for the anisotropic region in the calculation of the image co-efficient, <2.89>.

This outcome is corroborated by the work of Kobayashi [19], which although initiated with a transformation slightly different to <2.62a>, results in similar expressions for the partial image relationship. The only discrepancy is accounted for by this author's preference to refer all the fields to a uniform (isotropic) dielectric medium filling the whole space (cf. section 2.1.3.1).

'Finally the Green's function for microstrip on an anisotropic substrate is:

$$G(x,h_-|x_o,h_+) = ([1 + K]/4\pi\varepsilon_o)$$

$$\sum_{n=0}^{\infty} K^n \ln[([x-x_o]^2 + \sqrt{\epsilon_x/\epsilon_y}[y-y_o+2nh]^2)$$

$$/([x-x_o]^2 + \sqrt{\epsilon_x/\epsilon_y}[y-y_o-2nh]^2)] \qquad \langle 2.92 \rangle$$

where $K = (1 - \sqrt{\epsilon_x\epsilon_y})/(1 + \sqrt{\epsilon_x\epsilon_y})$

2.4 RESULTS

2.4.1 Computer Programs

The author had access to two computer programs for the calculation of (isotropic) microstrip parameters: named COMIC [27] and GREEN [11]. Both are implementations of the integral equation method of section 2.1. For narrow strips both programs gave near identical results but for wide strips there was some, albeit small, discrepancy. The programs were tested by subtracting, from the capacitance per unit length calculated, the fringing free (parallel plate) capacitance of the structure (cf. chapter 4). The result then represents the contribution of the fringing field to the microstrip capacitance. For wide strips (w/h > 1) the fringing fields at the opposing edges of the strip should be substantially uncoupled from each other and therefore take on value independent of the strip width. The results of these tests are presented in figure 2.12 along with values of the fringing capacitance from James & Tse [28].

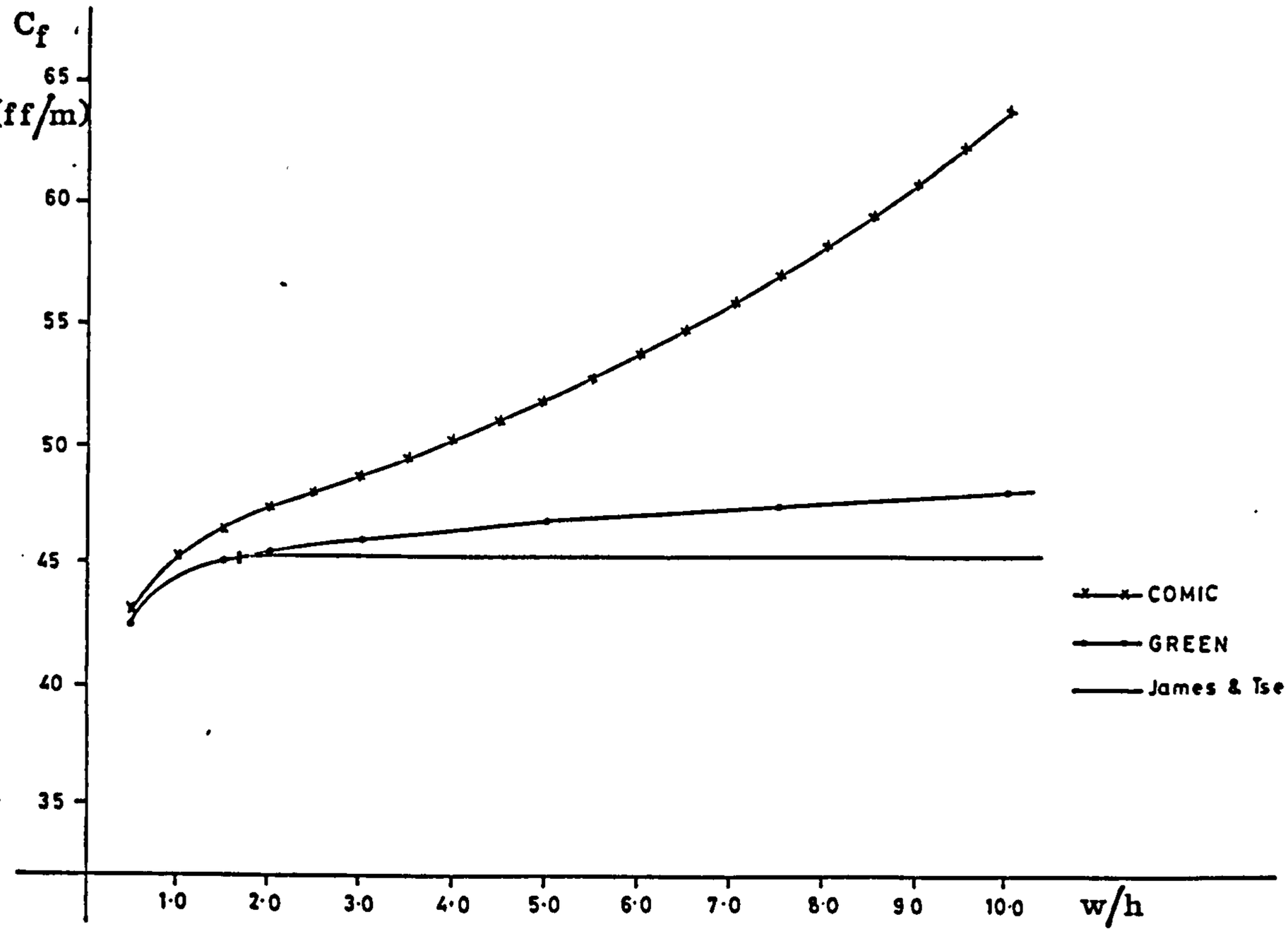

Figure 2.12 Results from the "fringing field test" of microstrip analysis programs.

The results from program GREEN were obtained after a modification to the number of sub-strips used in the computation. Previously the microstrip was divided into a maximum of 20 sub-strips. The actual number of sub-strips (n) used is specified in the input data file, but the program increased the supplied value for wide strips thus:

$$n' = n + 2(0.5 + 2.5[w/h - 1]) \ , \quad w/h > 1 \qquad \langle 2.93 \rangle$$

to a maximum of 20. The program was modified to increase the number of sub-strips allowed to 35 and to override the user supplied value of n according to this expression:

$$n' = 2(10.5 + 2.5[w/h - 1]), w/h > 1 \qquad \langle 2.94 \rangle$$

With the modification in force GREEN has a clear advantage and consequently it was adopted for all subsequent activity. Figure 2.13 presents the results from a further test on program GREEN. Using unity width to height ratio (the greatest strip width for which the automatic override for the number of sub-strips does not operate), the values of

the transmission line parameters, calculated with various numbers of sub-strips, were obtained. This does indicate that the original maximum of 20 sub-strips was barely adequate. Since the charge on the strip increases markedly towards the edge, the efficiency could be substantially improved by sub-dividing the strip non-uniformly. The complexity involved in grading the sub-strip width does not, however, seem merited; the run times being only a few seconds per point, even with 35 sub-strips.

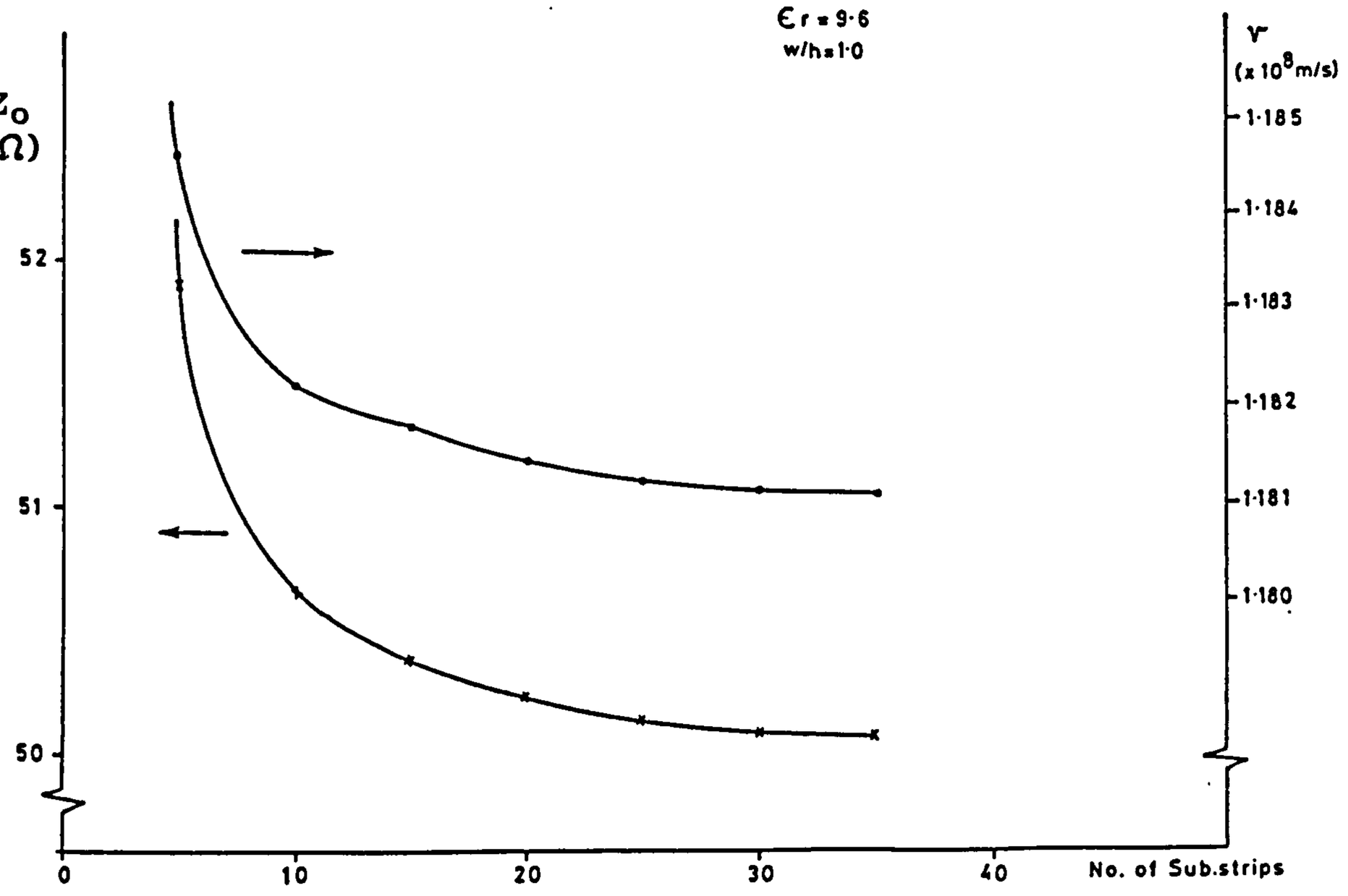

Figure 2.13 Variation in microstrip parameters (alumina substate) with number of sub-strips used in computation (GREEN)

For the calculation of the transmission line parameters of microstrip on anisotropic substrates, the program GREEN was adopted to implement the Szentkuti transform (section 2.3.2.3). The direct method of solution using the anisotropic Green's function (section 2.3.4) was not adopted as it has been shown to be analytically equivalent to the transform technique employed and therefore offers no advantage. A listing of program GREEN, including all the modifications, is included as Appendix A.

2.4.2 Results for Isotropic Microstrip

Transmission line parameters of microstrip on an alumina substrate were calculated using GREEN (modified version). The characteristic impedance is presented below whilst the velocity of propagation is plotted, along with some measured results, in figure 3.2.1.

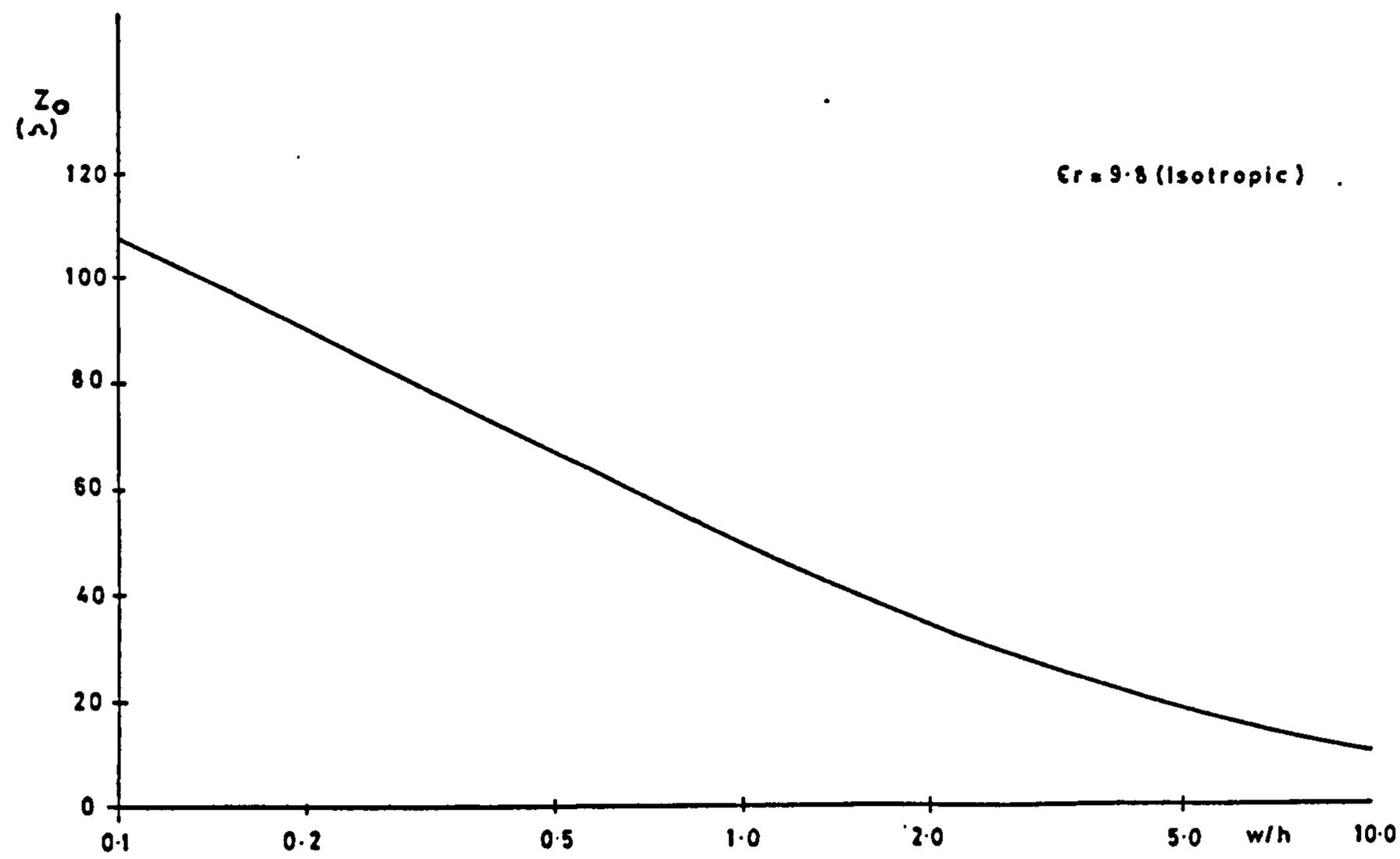

Figure 2.14 Microstrip characteristic impedance on alumina substrate

2.4.3 Results for Anisotropic Microstrip

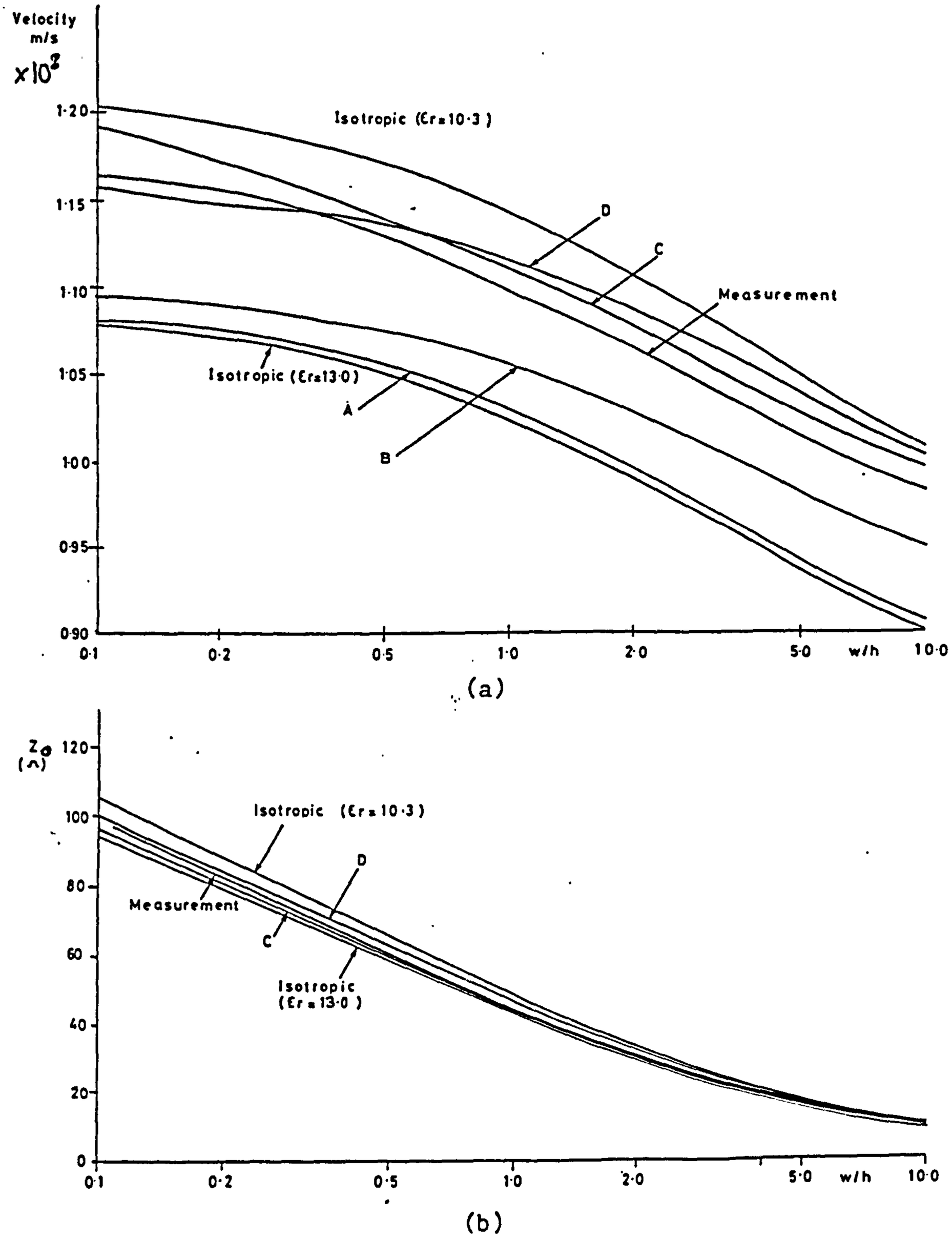

Figure 2.15 Velocity of propagation (a) and characteristic impedance (b) of microstrip on Epsilam-10 (ϵ_y = 10.3, ϵ_x = 13.0).

Key
- A - Weale's Transform (original) [6] (section 2.3.2.2)
- B - Weale's Transform (corrected) (section 2.3.2.2)
- C - Spencer's Transform [8] (section 2.3.2.1)
- D - Szentkuti's Transform [7] (section 2.3.2.3)

In the graphs of figure 2.15 the results from each of the transforms discussed are presented. Also plotted are two "boundary" curves for isotropic sustrates having permittivities equal to each of the anisotropic substrate permittivities and the results of "long line" measurements [14] (cf. chapter 3). Qualitatively, one expects the anisotropic microstrip properties to approach those of the isotropic case with $\epsilon_r = \epsilon_y$ for the widest strips, and progressively diverge towards the $\epsilon_r = \epsilon_x$ curve as the width decreases and the fringing field becomes more significant. This effect is clearly evidenced in the curves produced using the preferred (Szentkuti) transform for a sapphire substrate (figure 2.16 and 3.23).

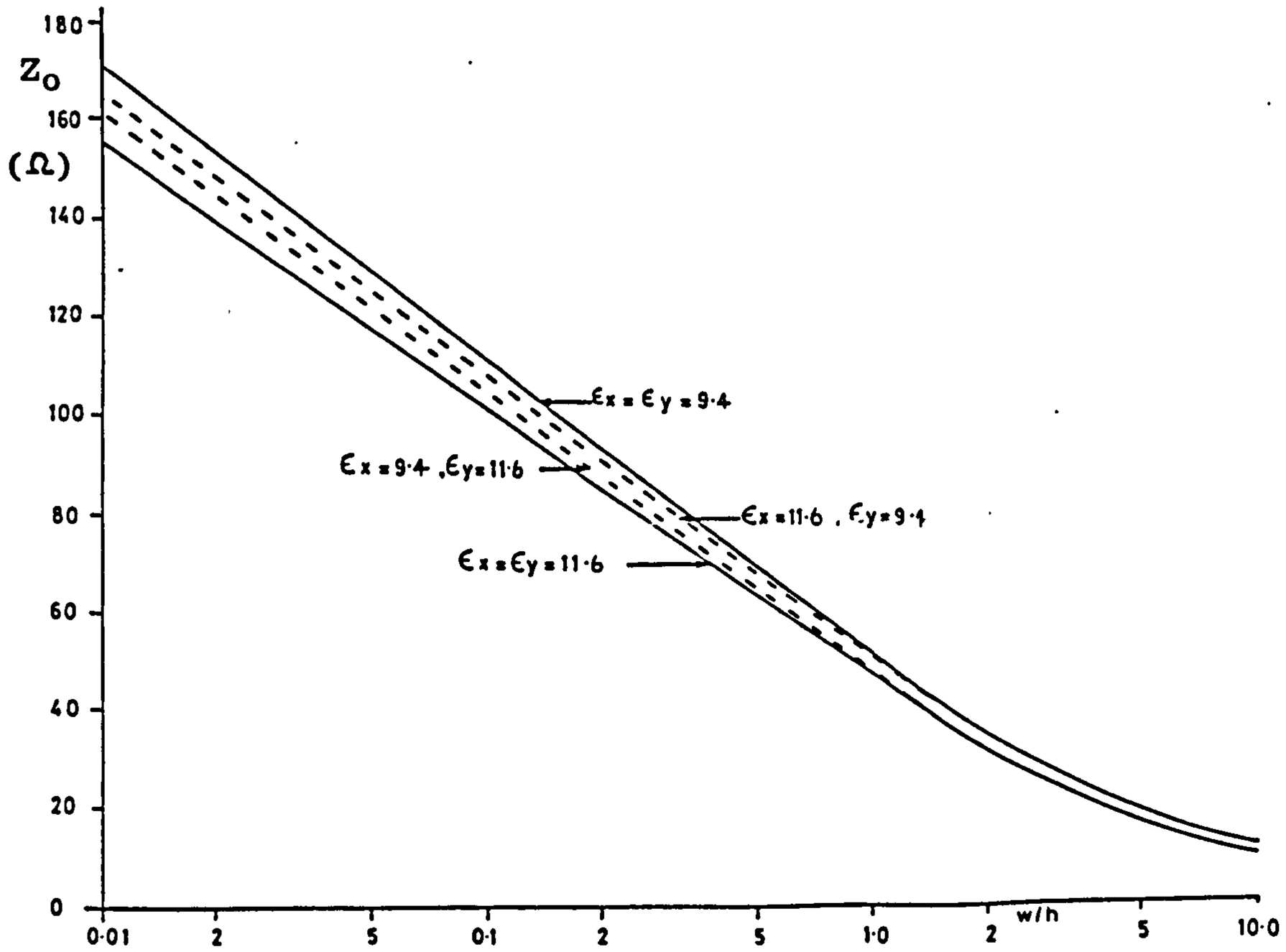

Figure 2.16 Characteristic impedance of microstrip on a sapphire substrate.

Three of the curves represent the behaviour of microstrip with the three possible orientations of sapphire: C-axis perpendicular to the substrate face (ϵ_y = 11.6, ϵ_x = 9.4), C-axis in the plane of the

substrate, both orthogonal to the direction of propagation (ϵ_x = 11.6, ϵ_y = 9.4) and aligned with the strip ($\epsilon_x = \epsilon_y$ = 9.4). The curves for velocity (figure 3.23) are shown with results from resonator measurements and data from the finite differences method of Owens et al. [9]. Assessment of the results for a sapphire substrate indicates creditable agreement between the analysis and measurement.

2.5 REFERENCES

[1] OLYPHANT, M.: "EPSILAM 10 - A new high dielectric constant conformable copper-clad laminate", Product Information, 3M.

[2] STINEHELFER, H.E.: "An accurate calculation of uniform microstrip transmission Lines", IEEE Trans., 1968, MTT-16, pp.439-444.

[3] WHEELER, H.A.: 'Transmission-line properties of parallel strips separated by a dielectric sheet", IEEE Trans., 1965, MTT-13, pp.172-85.

[4] YAMASHITA, E & MITTRA, R. "Variational method for the analysis of microstrip lines". IEEE Trans., 1968, MTT-16, pp.251-6.

[5] SILVESTER, P.: "TEM Wave Properties of Microstrip Transmission lines", Proc. IEE, 1968, Vol. 115, pp.43-48.

[6] WEALE, J., (Marconi Research Labs., Great Baddow), Private Communication, 8/6/1976.

[7] SZENTKUTI, B.T.: "Simple analysis of anisotropic microstrip lines by a transform method", Electron. Lett. Vol.12, 1976, pp.672-3.

[8] SPENCER, D.G., (Marconi Communications Systems Limited, Billericay), Private Communication, 21/3/1977.

[9] OWENS, R.P., AITKEN, J.E. & EDWARDS, T.S.: "Quasi-static characteristics of microstrip lines on an anisotropic sapphire substrate", IEEE Trans., 1976, MTT-24, pp.499-505.

[10] ALEXOPOULOS, N.G. & UZUNOGLU, N.K.: "Characteristics of microstrip on anisotropic substrates", Proc. 7th Eubropean Microwave Conference, Copenhagen, 1977, pp.140-143.

[11] HOSSEINI, N.M.: "Application of computer-aided design to microstrip circuits", Ph.D. Thesis, University of Warwick, 1977.

[12] SCHNEIDER, M.V.: "Microstrip lines for microwave integrated circuits', Bell Syst. Tech. Jnl. 1969, Vol.48, pp.1421-44.

[13] ROONE, G.T. & HAIN, H.A.: " - ",IEEE Trans., ED-?, 1968, pp.479-482.

[14] DAWE, C. & MIDDLETON, J.D.: "Measured characteristics of microstrip on Epsilam-10 substrate", Private Communication (Marconi Instruments Limited), 1976.

[15] RAMO, S., WHINNERY, J.R. & VAN DUZER, T.: "Fields and waves in communication electronics" Wiley, New York, 1965.

[16] GREEN, H.E.: "The numerical solution of some important transmission line problems", IEEE Trans. MTT-13, 1965, pp.676-92

[17] KAMMLER D.W.: "Calculation of characteristic admittances and coupling co-efficient for strip transmission lines", IEEE Trans. MTT-16, 1968, pp.925-37.

[18] ALEXOPOULOS, N.G.: "Characteristics of single and coupled microstrips on anisotropic substrates", IEEE Trans. MTT-26, 1978, pp.387-93.

[19] KOBAYASHI, M.: "Analysis of the microstrip and the electro-optic light modulator", IEEE Trans. MTT-26, 1978, pp.119-26.

[20] HARRINGTON, R.F.: "Field computation by moment methods", Macmillan Co., New York, 1968, pp.1-41.

[21] PREMOLI, A.: "A new fast and accurate algorithm for the computation of microstrip capacitances", IEEE Trans. MTT-23, 1975, pp.642-60.

[22] CRAMPAGNE, R. et al.: "A simple method for determining the Green's function for a large class of MIC lines having multi-layered dielectric structures", IEEE Trans. MTT-26, 1978, pp.82-87.

[23] BRYANT, T.G. & WEISS, J.A.: "Parameters of microstrip transmission lines and of coupled pairs of microstrip lines", IEEE Trans. MTT-16, 1968, pp.1021-7.

[24] KWON, A.H.: "Design of microstrip transmission line". Microwave Journal, Jan. 1976, pp.61-63.

[25] GUNSTON, M.A.R.: "Microwave transmission line data", Van Nostrand Reinhold Co., London, 1972, pp.48-49.

[26] LIGHTHILL, M.J.: "Introduction to Fourier Analysis and generalised functions". Cambridge University Press, 1959.

[27] WEALE, J.R.: "Numerical calculation of transmission lines parameters of microstrip transmission line", Marconi Research Labs. Report ITM-3241, 1969.

[28] JAMES, D.S. & TSE, S.H.: "Microstrip end effects", IEE Electron Lett., Vol.8, 1972, pp.46-7.

CHAPTER 3

MEASUREMENT OF MICROSTRIP PARAMETERS

3. MEASUREMENT OF MICROSTRIP PARAMETERS

In order to verify the theoretical assessment of the propagation parameters of microstrip on an anisotropic substrate it is necessary to establish a suitable measurement technique. The method must deliver sufficient precision to permit unambiguous discrimination between the results from the alternative analyses. An examination of figure 2.15b reveals that the measurement of characteristic impedance should be accurate to a small fraction , say 0.1, of an ohm. Similarly, from figure 2.15a the determination of the velocity of propagation should have an accuracy of rather better than 1%, preferably around 0.2% - equivalently discriminating to the 0.1 ohm uncertainty for impedance. (Both properties are proportionally related to $\sqrt{C_D}$, the square root of the capacitance with dielectric present, in equations <2.1> and <2.2.>.

3.1 CHOICE OF SUBSTRATE AND METALISATION

Since the purpose of the measurements is the verification of the theory the anisotropic material used for the substrate should have sufficiently well known dielectric properties to make the results significant. The square root relationship indicates that a tolerance of 0.4% on dielectric constants would be desirable although this requirement may be slightly eased, to say, 0.5%, because the region is only partially filled by dielectric. This effectively eliminates Epsilam-10 for the purpose [1] and suggests that a high purity single crystal material is required. Two examples, having good dielectric properties at microwave frequencies, are sapphire and quartz. Sapphire's two dielectric constants are known to 5 significant figures and remain invariant throughout the microwave band right up to infra-red. Since, as already

commented, the microstrip structure involves a mixed dielectric environment where the air (or free space) region "dilutes" the effect of the substrate region it is desirable, in this experiment, for the anisotropic substrate to have as high a dielectric constant as possible. Sapphire, with dielectric constants of 9.4 and 11.6 [2&3] , is therefore more suitable than quartz with constants of ~4.5. Low loss at microwave frequencies is another desirable property for the measurement of both characteristic impedance and velocity of propagation. This is particularly so if the velocity of propagation is to be determined from measurements of resonators. It is self evident that if the Q (quality factor) of the resonator is low the precision of the determination of the resonant frequency will be correspondingly poor. Furthermore, a general analysis of long transmission lines [4] reveals that the characteristic impedance is not a simple real constant. In lumped equivalent circuit form:

$$Z_{\mu} = \sqrt{(R + j\omega L)/(G + j\omega C)} \qquad \langle 3.1 \rangle$$

where R is the series resistance per unit length

L is the series inductance per unit length

G is the shunt conductance per unit length

C is the shunt capacitance per unit length.

The shunt conductance represents the dielectric loss whilst the conductor loss can be identified with the series resistance. Thus the quality of the metallization system employed is also important. Viewed as an electromagnetic waveguiding structure, one of the conditions for TEM propagation along the microstrip transmission line is that the metal boundaries should be highly conductive. It is also desirable that the metallization should be thin since the analysis took no account of the finite thickness of the strip. Thin film gold (Au) metalisation was used in the following experiments. Unfortunately it is necessary to introduce

a layer of chromium (Cr) or nichrome (NiCr) to ensure the adhesion of the gold to the substrate. As most of the lines of electric field terminate on the surface of the conductor that is in contact with the substrate the introduction of a resistive interface layer is potentially detrimental. The skin depth in resistive materials is, however, deeper than that in good conductors (equation <3.2>) and the nichrome layer is made much thinner than the skin depth.

$$\delta = 1/\sqrt{\pi f \mu \sigma} \qquad \text{<3.2>}$$

where μ is the permeability

and σ the conductivity of the metalisation

The gold metalisation is made rather thicker than a skin depth whilst maintaining its thickness small compared to all other dimensions of the microstrip structure. Throughout these experiments the metallization system was ~500Å nichrome followed by ~1000Å gold, both deposited by sputtering and selectively gold plated to a final thickness of 3 - 5μm (the narrowest track width used is ~100μm), except for a few substrates where an additional layer of 500Å of tantalum nitride (TaN_n) was included between a chromium seed layer and the gold.

The conductor loss can be anomalously exaggerated by the surface roughness of the substrate. Here again sapphire is a good choice of material as the substrate available is usually polished to optical flatness on the critical "A" face to which the strip conductor is attached. The "B" face on which the ground plane metallization is deposited has a fine ground, matt finish for identification, but the effect on loss is believed to be slight.

Clearly, the orientation of the substrate surfaces with respect to the crystallographic structure of the sapphire must be defined. Sapphire has a zincblende crystal structure and the two dielectric constants are defined for the directions parallel to ($\epsilon_{||} = 11.6$) and perpendicular to

($\epsilon_\perp$= 9.4) the C-axis otherwise known as the optical axis of the crystal. Since it is desirable for the microstrip properties to be independant of the orientation of the strip on the surface of the slice of the sapphire, it is most appropriate for the substrate to be cut with its surfaces perpendicular to the C-axis.

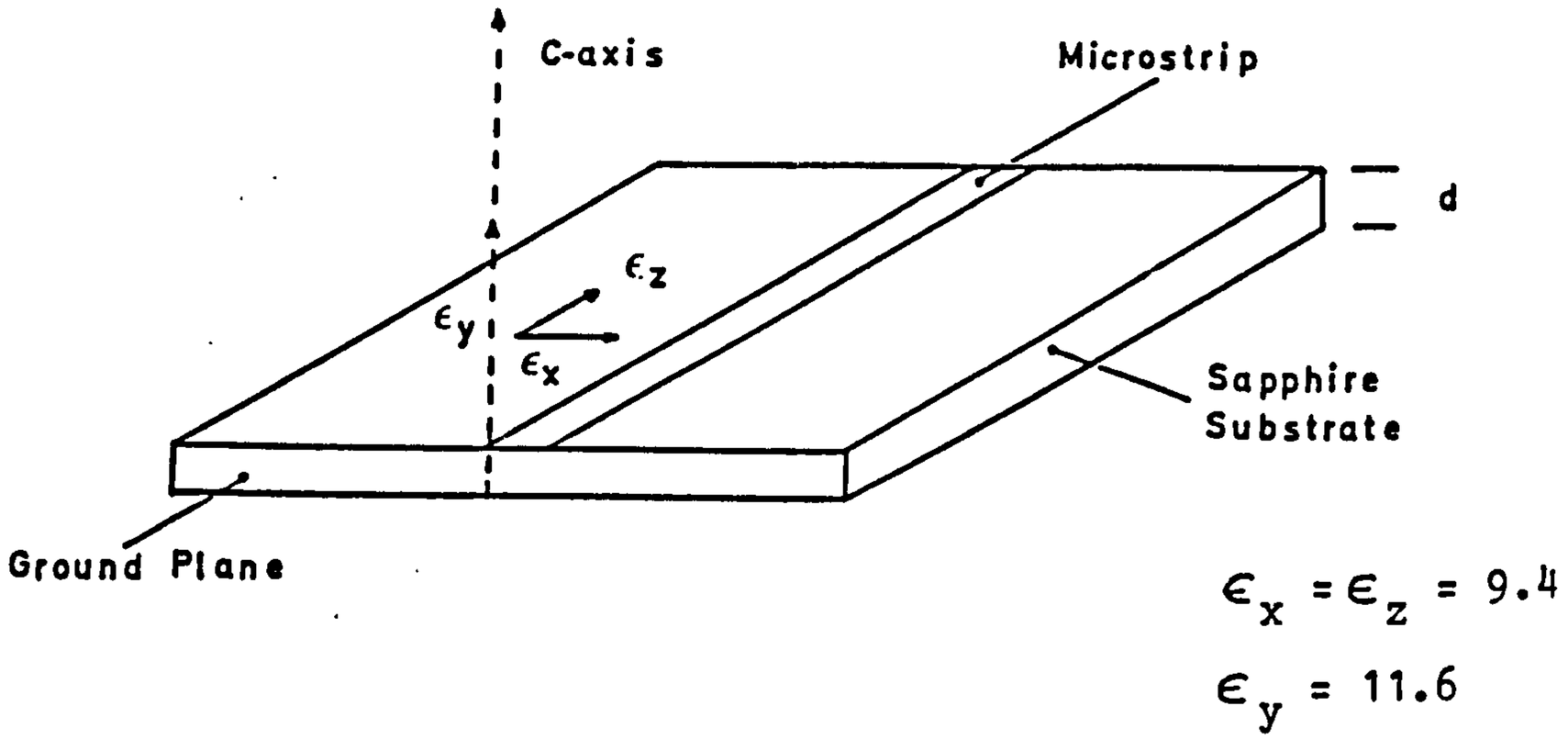

Figure 3.1 Orientation of Sapphire Substrate

Single crystal sapphire is an expensive material and the cost of substrates increases disproportionately with the size required. Generally the measurement techniques employed will require the greatest possible microstrip length especially as the measurement frequency should be minimised to comply with the conditions for non-dispersive propagation, necessary for the applicability quasi-static analysis adopted. Most of the substrates used were nominally 23.35mm (0.9193in) x 11.70mm (0.4606mm). Two nominal thicknesses were used, 0.635mm (0.025in) and 0.254 mm (0.010in).

3.2 MEASUREMENT TECHNIQUES

Two pertinent quantities can be measured, the characteristic impedance and the velocity of propagation. Methods for the measurement of both will be examined.

3.2.1 Characteristic Impedance Measurement

The simplest method involves the use of a Time Domain Reflectometer (TDR). The microstrip line is connected to the instrument via a length of close tolerance air-line and is terminated in a precision resistive load. Either the air-line or the load can be used as an impedance standard. The characteristic impedance of the airline is calculable from its cross-sectional geometry and the resistance of the load may be determined by d.c. ohmmeter measurement. The TDR applies fast rise time steps to the assembly and, employing sampling slope techniques, monitors the perturbations caused by reflection of the step input at mismatches. Since the delay is proportional to the displacement of the mismatches or discontinuities, a plot of reflection coefficient versus distance is produced.

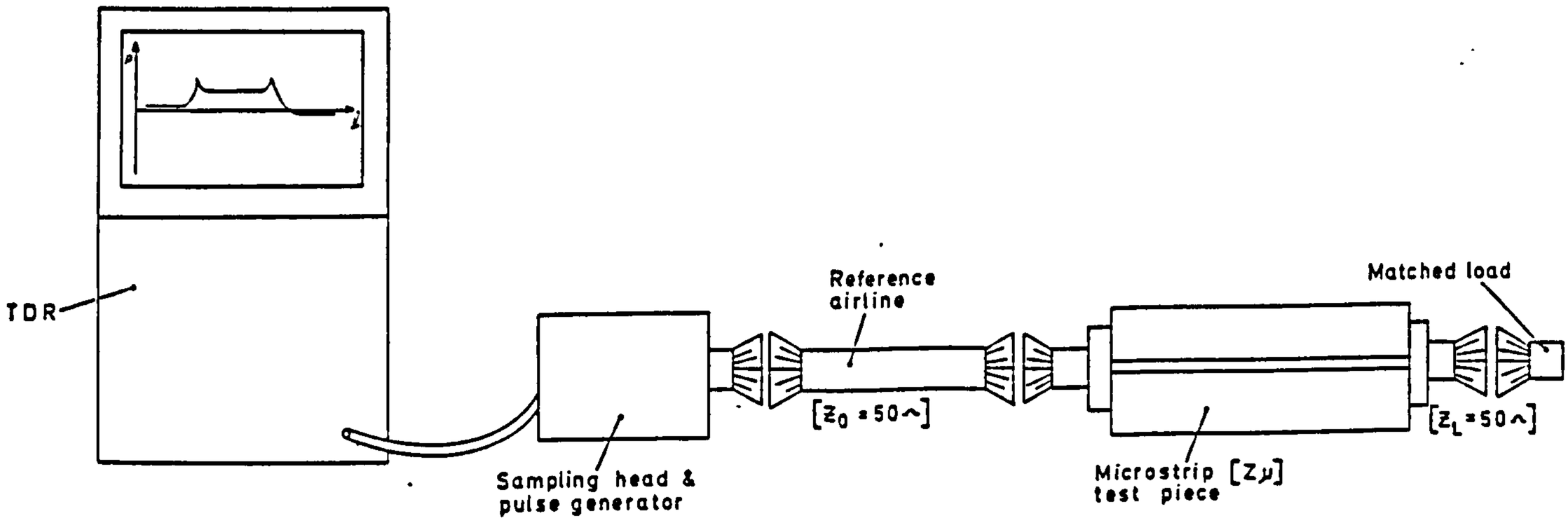

Figure 3.2 TDR Measurement of Characteristic Impedance

The method has the advantage that is provides spatial separation of mismatches and discontinuities, principally associated with the connectors and transitions, and that it is direct reading. It can be tolerably accurate providing the losses are low, the microstrip impedance is similar to that of the standards and the propagation delay of the microstrip sample is long compared to the rise time of the step.

Concerning this last condition the best TDR available has a system rise time of 35psecs; equivalent to propagation over 10mm in air or approximately 3.5mm along microstrip. Thus the available length of ~20mm would be just adequate. Even so, an overall accuracy for measurement of characteristic impedance close to that of the standards is unlikely to be established to be better than 0.5 Ohm. The most common standard impedance would be 50 Ohm and any significant deviation of the microstrip impedance from this value would result in a substantial loss of accuracy. Additionally two or more large discontinuities can interact to further reduce the precision.

An alternative method uses the conventional (sinusoidal) reflectometer to measure the reflection coefficient of the microstrip sample terminated in a load of known impedance. The locus, with changing frequency, of reflection coefficient at the reflectometer measurement port will be a circle (a consequence of the bilinear transformation involved) as illustrated in figure 3.3b for the case of a 70.7 Ohm line terminated by a 50 Ohm load

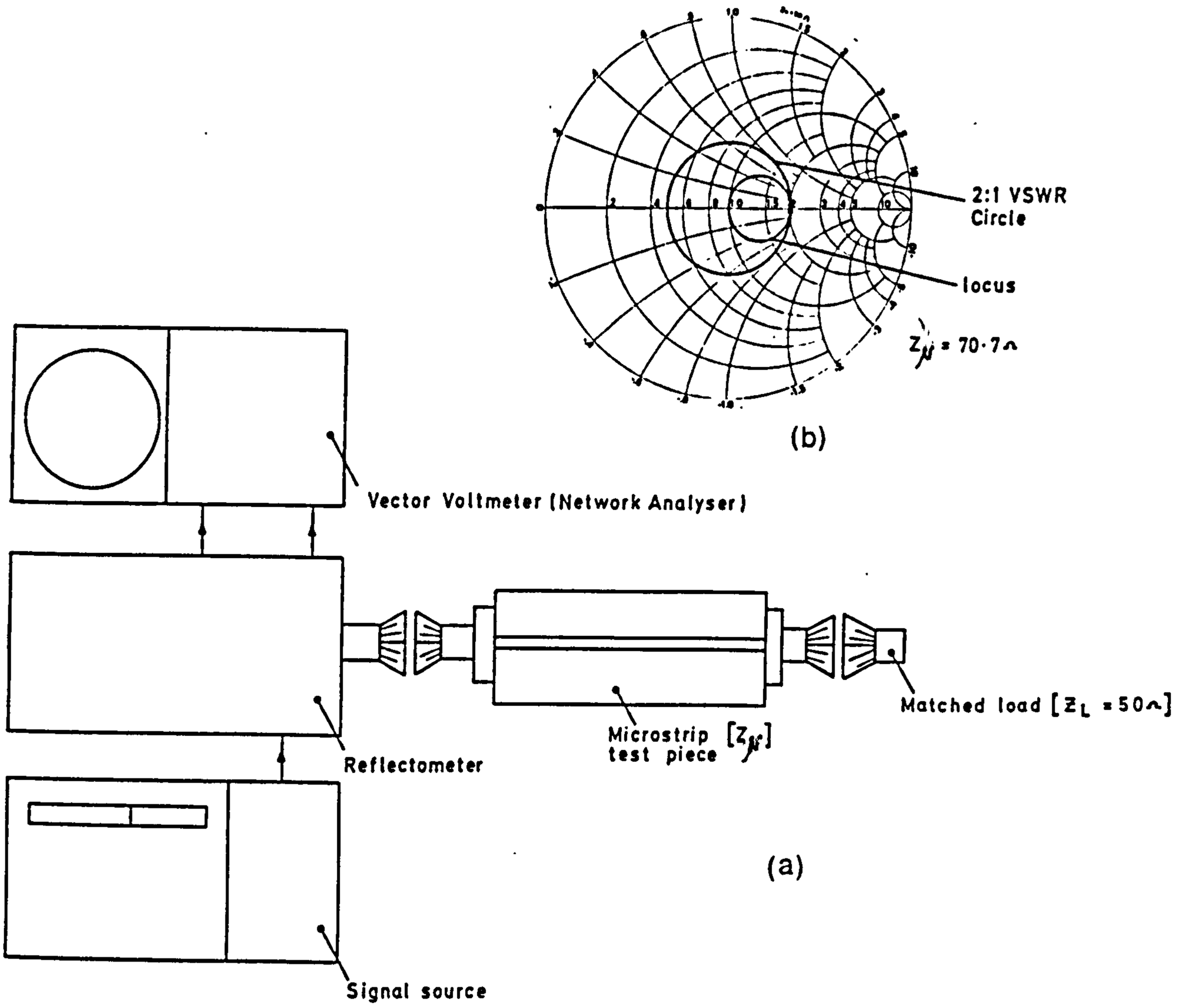

Figure 3.3 Reflectometer measurement of characteristic impedance (a) and a typical locus of reflection coefficient with frequency (b)

At a frequency for which the microstrip line is an odd integer multiple of a quarter-wavelength long, the impedance at the measurement plane is given by the expression:

$$Z_{meas} = Z_\mu^{\,2}/Z_L \quad [= 100 \text{ Ohm, in the example}] \qquad \langle 3.3 \rangle$$

where all the impedances are assumed to be purely resistive. This is related to the reflection coefficient measured by the standard equation:

$$\Gamma_{meas} = (Z_{meas}-Z_{norm})/(Z_{meas}+Z_{meas}) \quad [= 0.33] \qquad \langle 3.4 \rangle$$

and the VSWR can be obtained thus:

$$S = (1+\rho)/(1-\rho) \quad [= 0.20] \text{ where } \rho = |\Gamma| \qquad \langle 3.5 \rangle$$

Thus it is, in principle, adequate to employ a scalar reflectometer system taking a reading of reflection coefficient or VSWR having adjusted the frequency to obtain a peak value. In practice a vector system using the computer correction techniques described in chapter 5 is necessary to obtain the required precision. For microstrip lines having a characteristic impedance close to 50 Ohms a 0.1 Ohm accuracy implies an effective directivity of 60dB; a demanding stipulation for even a fully corrected network analyser system. Where the impedance of the microstrip differs greatly from the system impedance (50 Ohm) the accuracy would be predominantly limited by test point mismatch as illustrated in figure 5.4 (a chart of uncertainty versus ρ for given directivity or test port mismatch).

The problem is further aggravated by the transitions from coax to microstrip and by the discontinuities at the junction between the nominally 50 Ohm interconnecting microstrip line and the unknown line. The former can be dealt with by employing the microstrip calibration techniques of chapter 6 providing the characteristic impedance of the calibration line is precisely known. Since the load will be connected through a second transition, the 2-port scheme would be appropriate. The remaining problem of the discontinuities, albeit a second order effect, can be solved by extending the analysis to include suitable models from the literature (cf. chapter 4). Finally the accuracy is compromised by microstrip loss, which can be corrected for, but does present a problem for high impedance lines.

In summary, there is little prospect of either method yielding results of the required precision. Nevertheless commendable results for microstrip on "Epsilam-10" (available in large sheets) have been obtained by painstaking measurements on 100mm lines, using a slotted line [5].

3.2.2 Propagation Velocity Measurement

Both the methods described for the determination of characteristic impedance could be applied to the measurement of propagation velocity. The time delay between two discontinuities can be read directly from the TDR display but, since the precision of positional determination is limited by the rise time, the 0.2% accuracy demanded would necessitate a line at least 1.5m long! A further limitation is imposed by the timebase of the TDR that is unlikely to be better than 1% accurate.

The locii obtained from the vector reflectometer clearly embody velocity information. If the magnitude of the reflection coefficient (VSWR) only were to be measured the frequencies at which the line was an integer multiple of a half-wavelength long could be established more precisely than the quarter-wavelength frequencies. This is due to the fact that the first derivative of the magnitude versus frequency curve is large (and discontinuously changing sign) under the former condition but zero under the latter; a situation analagous to the slotted line measurement problem and from which the methods for handling deep nulls can be carried over. On the contrary, if the phase data were to be collected, the frequency for the quarter-wavelength condition can be more readily determined since the phase is indeterminate at the half-wavelength points. Results from this method applied to 100mm long microstrip lines on "Epsilam-10" were presented in figure 2.15a Nevertheless, neither method would be capable of delivering the desired accuracy unless an excessive length of microstrip were to be available.

A method capable of delivering results which approach the desired degree of accuracy has been demonstrated by Bianco and Parodi [6]. It involves conventional vector reflectometer measurement of four microstrip

lines of differing length terminated in open circuits. Using the principle of invariance of the complex cross-ratio under bilinear transformation the velocity of propagation can be extracted in a manner giving independence from open end effect, transition discontinuities and reflectometer error. This method, which has been fully described in connection with the microstrip network analyser calibration scheme of Chapter 6, does, however, require sufficient substrate area to accommodate the four lines. For this application an alternative was sought.

A structure providing a high rate of change of phase and/or magnitude with frequency will minimise the demands on the instrumentation. Lightly coupled resonators meet this stipulation.

3.2.3 Resonator Measurements

Resonant elements can be formed by transmission lines having lengths of integer multiples of a quarter-wavelength. The terminations of the ends of the resonant line should be purely reactive and are generally open or short circuits. The termination conditions for resonance depend on whether the multiple is odd or even. In the case of an even multiple i.e (a multiple of a half-wavelength) the terminations should be of the same kind (figure 3.4a). Conversely, for a line an odd multiple of a quarter-wavelength long, the terminations should be of opposite types (figure 3.4b). One further configuration is worthy of mention; the resonant ring. The ends of the transmission line are connected together and resonance occurs when the ring is a multiple of half-wavelength in circumference.

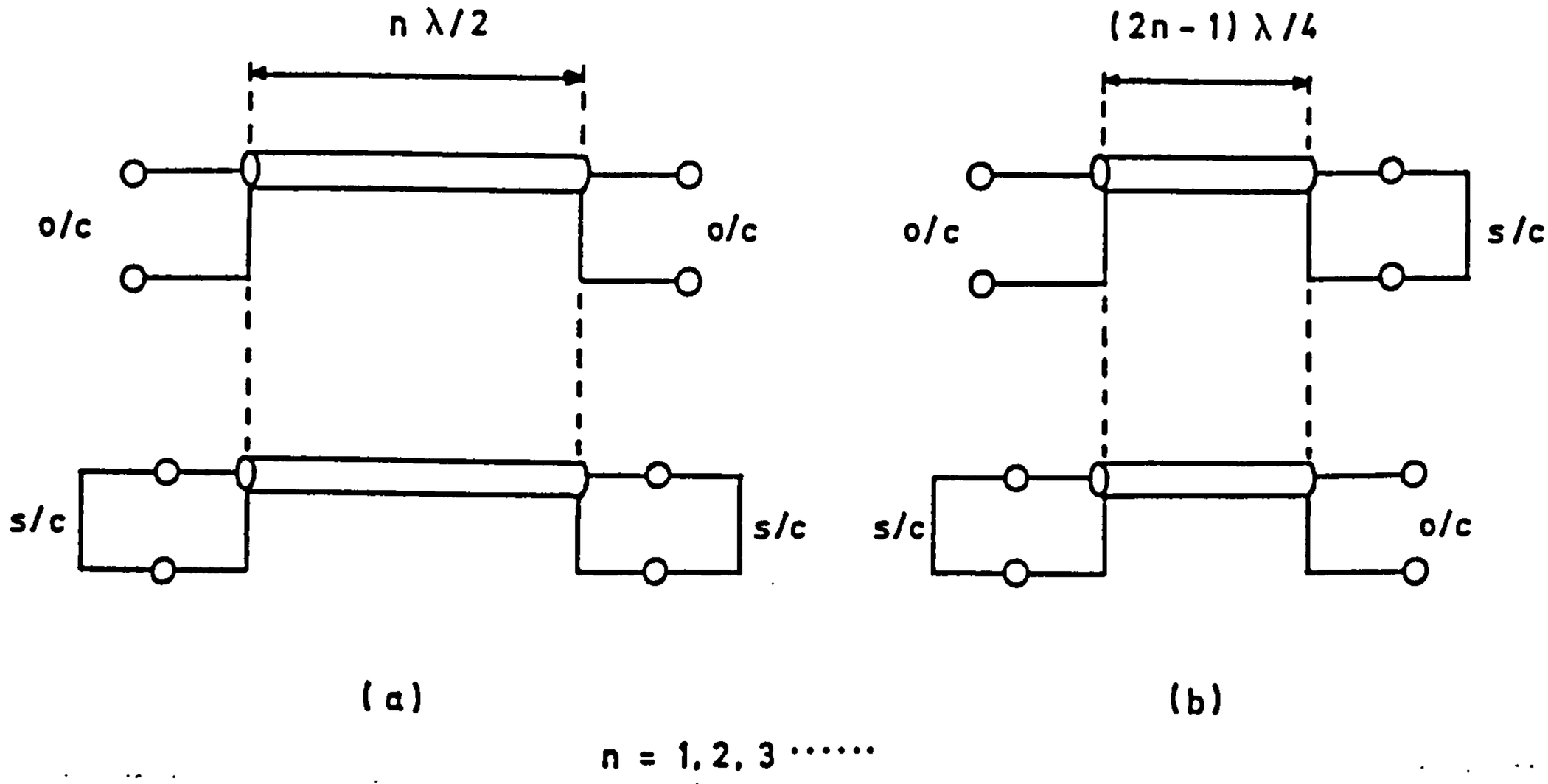

Figure 3.4 Resonant transmission line configurations for (a) half-wavelength resonators and (b) quarter-wavelength resonators

There are two lumped coupling mechanisms that are appropriate to these transmission line structures: magnetic field coupling at a point of low impedance and electric field coupling at a high impedance point. In either case the coupling can be modelled by an equivalent circuit comprising a transformer defining the coupling coefficient and a length of transmission line to account for the phase shift. Clearly any resonant structure can be accurately represented, close to resonance, by a parallel or series R,L,C equivalent circuit and, at resonance, will appear purely resistive (figure 3a and b). The coupling factor, k, can be defined, for the case of a singly coupled resonator, thus:

$$k_p = g/G \qquad \langle 3.6 \rangle$$

for the parallel resonant circuit of figure 3.5c or equivalently:

$$k_s = r/R \qquad \langle 3.7 \rangle$$

for the series resonant circuit of figure 3.5d

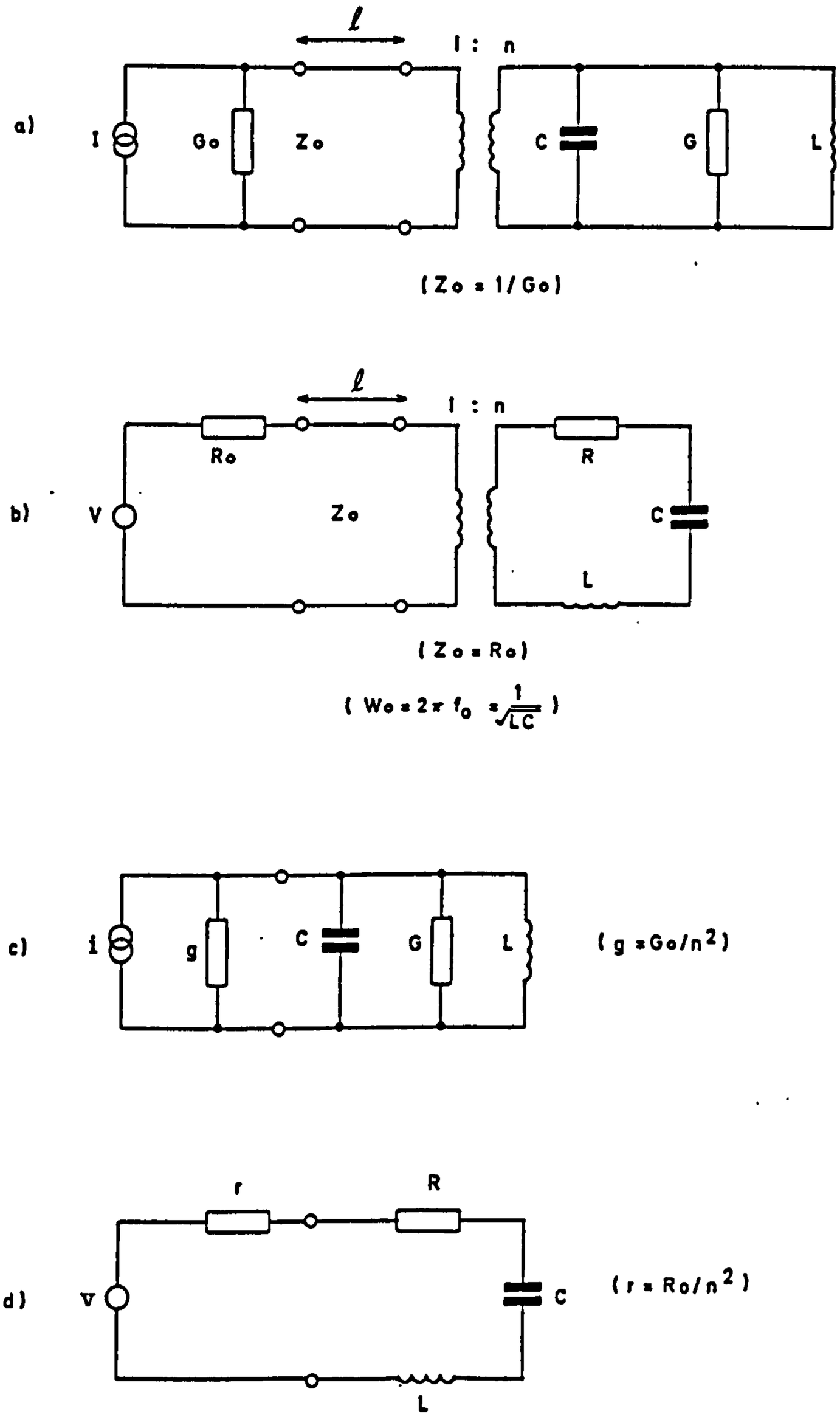

Figure 3.5 Equivalent circuits for singly coupled transmission line resonators

In the simple equivalent circuits of figure 3.5c and d the transmission line elements have been removed by making a reference plane shift. Observed with a reflectometer the behaviour close to resonance is characterised by the locii of figure 3.6. The three cases illustrated represent the under-coupled (k<1) critically coupled (k=1) and

overcoupled (k>1) situations.

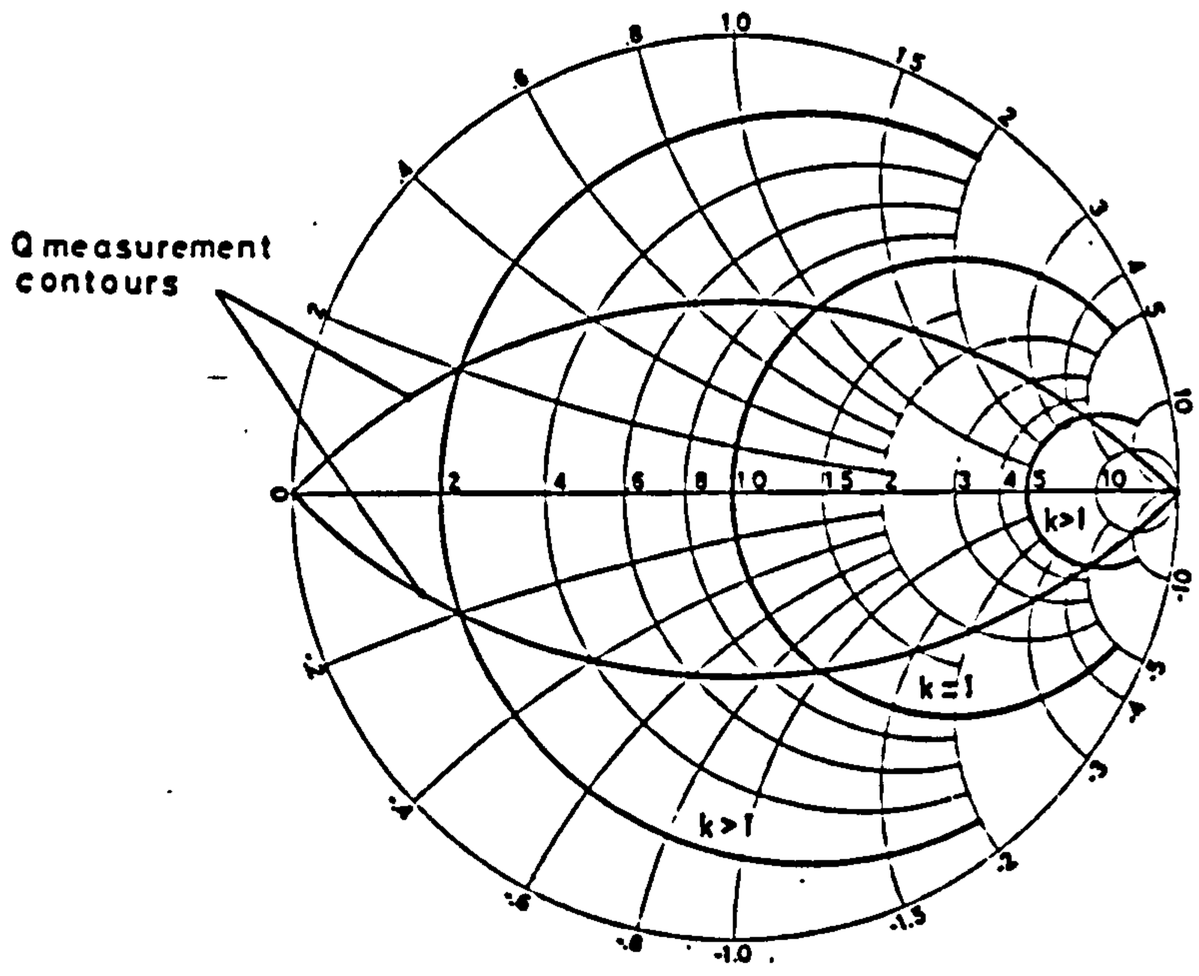

Figure 3.6 Reflection coefficient locii for resonant circuits with various coupling factors.

For the most precise determination of resonant frequency the coupling should be as 'light' as possible (k<<1) commensurate with capability of the reflectometer to detect the response. The VSWR at resonance is simply reciprocal of the coupling factor and thus the relationship of the coupling factor to the minimum reflection coefficient $\check{\rho}$ is given by the equation:

$$k = (1 - \check{\rho})/(1 + \check{\rho}) \qquad \langle 3.7 \rangle$$

The quality factor, Q, of a resonator can be defined in terms of the equivalent circuit as:

$$Q_p = \omega_o C/G = 1/\omega_o LG \qquad \langle 3.8 \rangle$$

for the parallel resonant circuit, and

$$Q_s = \omega_o L/R = 1/\omega_o CR \qquad \langle 3.9 \rangle$$

for the series resonant circuit.

Alternatively, and equivalently, the Q may be expressed in terms of the response as the separation between the frequencies at which the resistance and reactance (f_1 and f_2) are equal, normalised to the

resonant frequency, so:

$$Q = (f_2 - f_1)/f_o \qquad \langle 3.10 \rangle$$

Q measurement contours, corresponding to the above condition, are illustrated in figure 3.6. The unloaded Q (Q_U) can never be directly measured as the measurement must necessarily involve some loading, reducing the Q to a lower loaded Q (Q_L) value. The effect of loading by the measurement instrument can be expressed as an external Q, Q_E, relating the loaded and unloaded Q's thus:

$$1/Q_L = 1/Q_U + 1/Q_E \qquad \langle 3.11 \rangle$$

The unloaded Q_L can also be related to the coupling factor:

$$Q_L = Q_U/(1+k) \qquad \langle 3.12 \rangle$$

Reactive coupling, although convenient introduces a further perturbing effect; detuning of the resonator. Both the capacitive coupling used for the parallel resonant circuit and the inductive coupling appropriate to the series resonant circuit cause the resonant frequency to be reduced from the unloaded value. The higher the Q_U of the resonator the smaller the value of the coupling element for a given detectable coupling factor and thus the smaller the deviation of the observed resonance from the true resonant frequency.

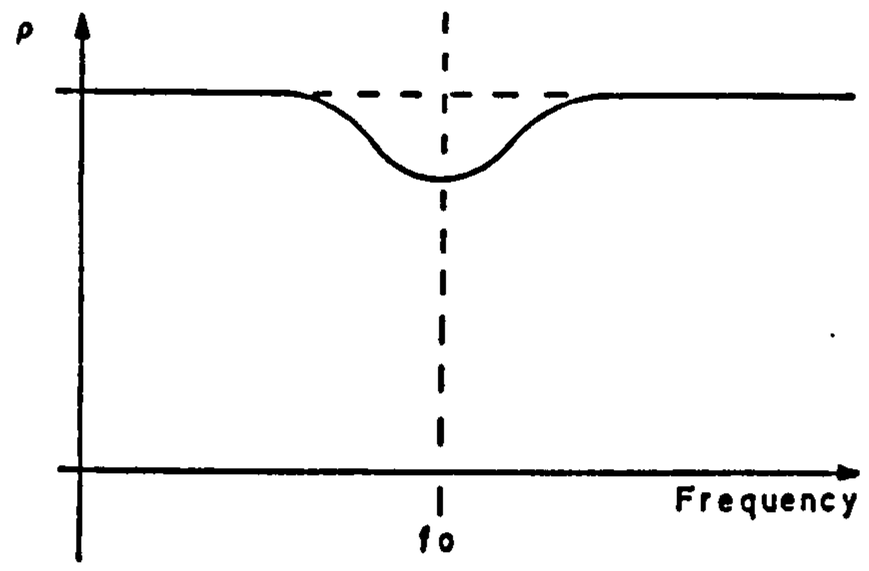

$\Gamma = \rho \angle \theta$

Figure 3.7 Representative behaviour of reflection coefficient for an under-coupled resonator.

An examination of the curves of figure 3.7 indicates that phase measurement is preferable to amplitude for the reliable determination of resonant frequency. But, although the phase versus frequency function has a peak value of first derivative at resonance, the establishing of the datum value, unnecessary for the amplitude measurement, can present a problem.

The most frequently employed resonant structure in the microstrip medium is the open circuit half-wavelength line capacitively coupled at one end [8]. The open and the coupled ends form non-ideal open circuits. Microstrip open circuit end effect is discussed in Chapter 4. The end effect can either be viewed as a lumped capacitor or an equivalent extension of the microstrip line. In either case the values are insufficiently well known to permit the accuracy required from a

half-wavelength long resonant line. Richings [8] has adopted a method involving (at least) two resonators of differing length but with identical coupling gaps. Simple simultaneous equations can be used to solve for the velocity of propagation independently from the common open and coupled end effects. Clearly this method has the disadvantage that more substrate area is required in order to accommodate the second resonator. A further consideration is that since there is some small additional loss by radiation at the open circuit ends the Q of resonators is reduced; degrading the measurement accuracy.

This latter problem can be overcome, but at some further penalty in substrate area required, by using a capacitively coupled ring resonator. For the length of the ring to be well defined the radius must be large compared to the track width. Since the intention is to explore the behaviour of propagation velocity with width to height ratio over the widest possible range of values this would involve outrageously large substrates.

An alternative solution depends on the realisation of good quality short-circuits. Short-circuits can form highly practicable, low loss, reflective terminations. Irrespective of the guided mode (TEM or otherwise), an ideal short is produced by placing a perfectly conducting surface perpendicular to the direction of propagation. At the boundary no tangential electrical field can exist. No energy can, therefore, be transferred through the surface. Thus a reverse propagating wave must be established; equal in magnitude and opposite in sense at the surface, in order to meet the boundary conditions and conservation of energy constraints. Clearly, the reflection coefficient of an ideal short-circuit is -1. The commonly used conducting materials have sufficiently low resistivities to allow this ideal to be closely approached. The principle consideration for an open structure like

microstrip is that the conducting plane should extend sufficiently far from the transmission line conductors to effectively terminate all the field. McPhun, et al. [9] have demonstrated that, in the case of microstrip on a 0.635mm (0.025in) alumina substrate the shorting conductor should extend at least 6mm from the centre conductor in all directions above the ground plane surface.

Given that effectively ideal microstrip short-circuits can be realised it is possible to consider the use of a single half-wavelength short-circuit terminated resonator as a vehicle for propagation velocity determination. This represents the most compact configuration considered as the single resonator track extends right to the edges of the substrate. Alternatively for a given maximum substrate dimension the lowest frequency resonator can be made ensuring that the TEM propagation for which the quasi static analysis holds is most closely approached. A short additional track (figure 3.8) approaching the resonator at its centre, a high impedance point, is the only other item on the substrate. An additional advantage for this arrangement is that it represents the lowest loss configuration; there being no radiation loss at the ends and rather less physical length than necessary for the ring resonator

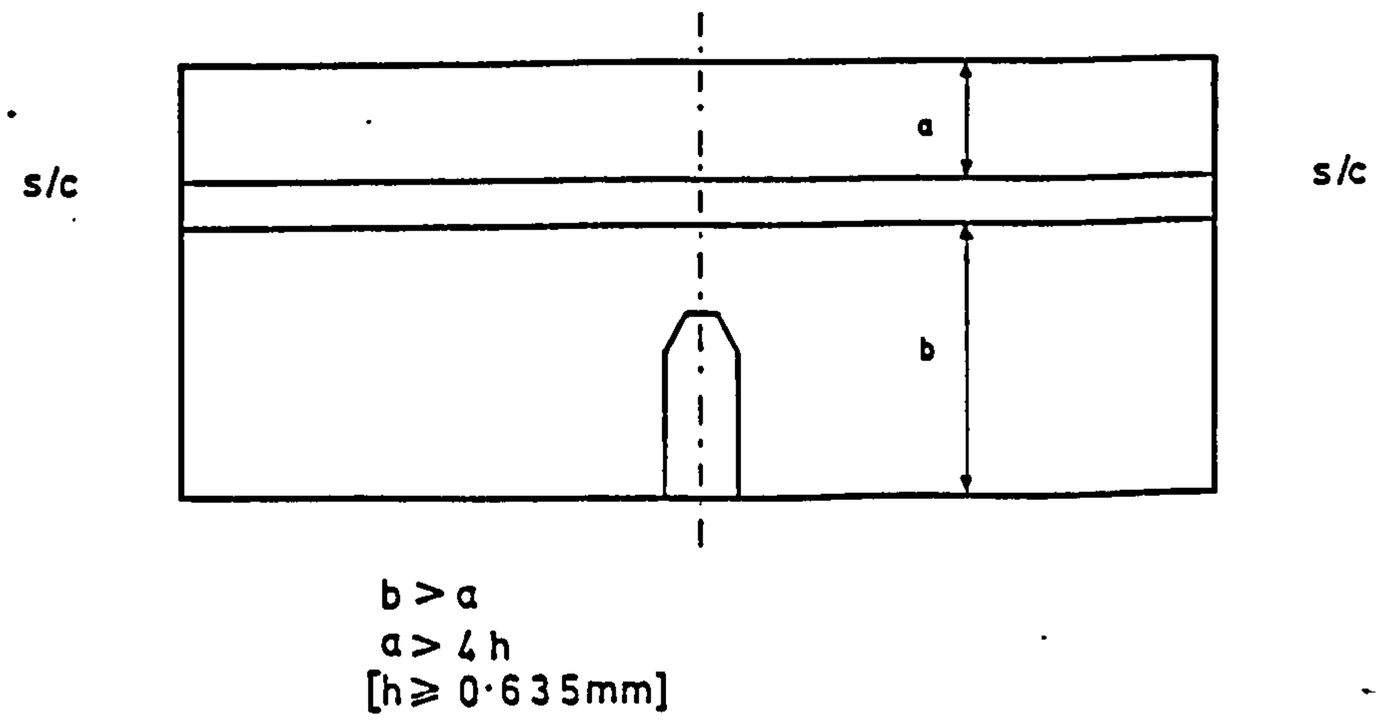

Figure 3.8 Substrate layout for the short-circuit half-wavelength resonator method.

In order to avoid the resonator properties being influenced by the

limited lateral extent of the substrate the layout was constrained by the condition that the parallel edge of the substrate should be removed from the edge of the resonator track by at least four times the greatest substrate thickness employed in the experiment. Even so, the available sapphire substrate samples permitted properties of microstrip lines to be measured for an extensive range of width to height ratios.

Any of the resonator configurations discussed above can be doubly coupled to form transmission mode structures. Figure 3.9 illustrates some possible microstrip realisations:

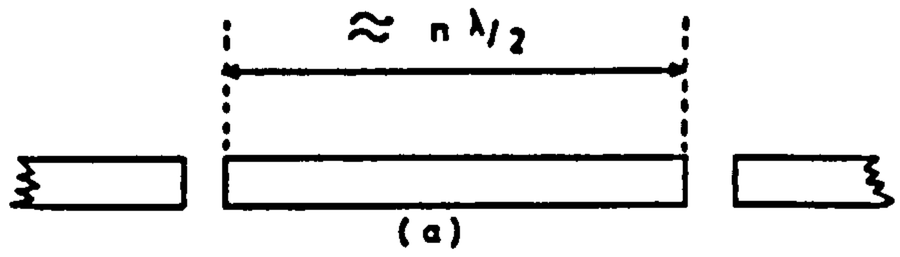

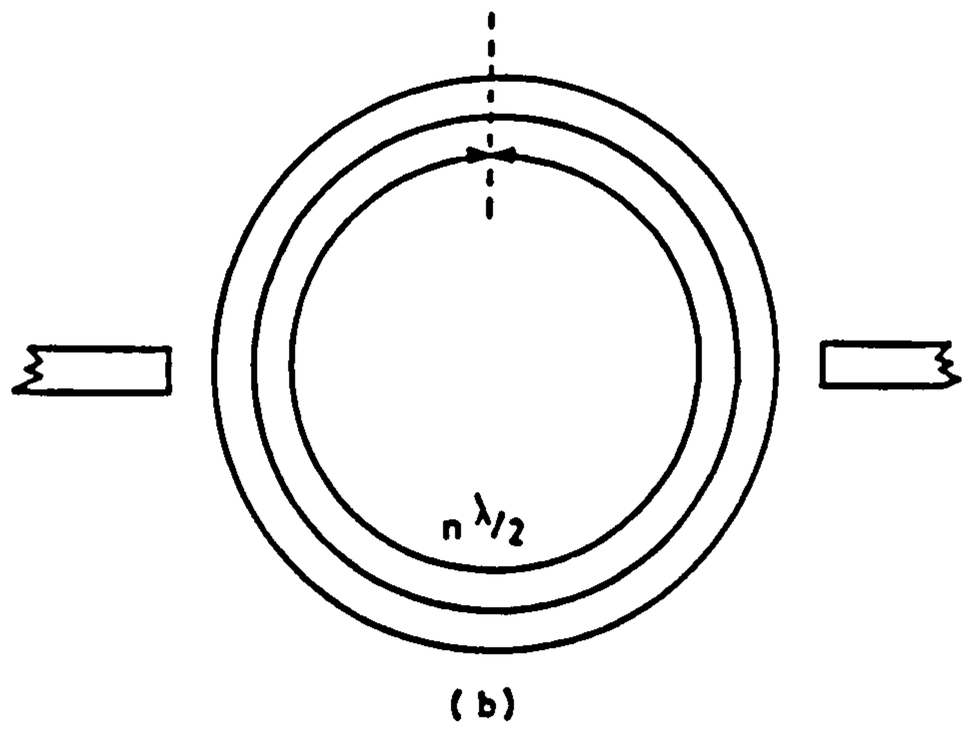

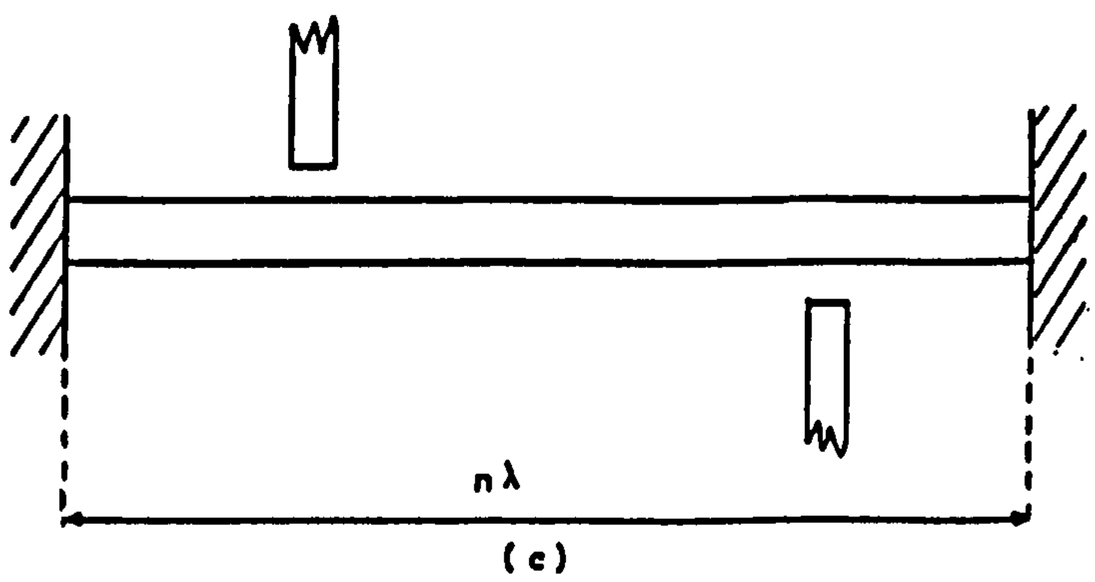

Figure 3.9 Microstrip doubly coupled transmission mode resonator configurations: open-circuit (a), ring (b), and short-circuit (c).

Since it is possible to make transmission measurements with great

sensitivity, permitting the use of lower coupling coefficients than possible for reflection mode resonator measurements, the loading and perturbing effects can be reduced. Nevertheless, the difficulties associated with coupling gap parasitics for open-circuit resonators and curvature for ring resonators still render these structures unattractive for high accuracy measurement on small substrates. Thus the short-circuit resonator is still the most attractive configuration. Although, in principle, the two coupling lines could be situated opposite, or near opposite, at the centre of a half-wavelength resonator direct coupling between them would limit the measurement sensitivity. A minimum resonator length of one wavelength is therefore necessary if benefit is to be obtained. Thus, for a given substrate dimension the measurement frequency is doubled; calling into question the validity of the TEM assumption. Some simulation experiments using the computer circuit analysis package MICRO3 [13] indicated that, in practice, using modest measurement equipment, the required accuracy of resonant frequency determination would still be difficult to obtain.

Hence the favoured option; the singly coupled, short-circuit, half-wavelength structure has been pursued, and attention has been given to the problem of correcting the results to allow for the perturbing effects of the coupling.

3.3 SHORT-CIRCUIT HALF-WAVELENGTH RESONATORS

Having decided upon the capacitively coupled short-circuit resonator as the vehicle for the measurement of microstrip propagation parameters, some theoretical analysis of the structure is appropriate. The relationship between the measured quantities and the microstrip parameters must be ascertained. The effect of the loading of the

coupling circuit must also be determined along with a method for correcting the results to allow for this effect.

3.3.1 Analysis of the Resonant Behaviour

Since the half-wavelength resonator is to be "viewed" at its centre it may be considered as two shunt connected short-circuit terminated quarter wavelength transmission lines (figure 3.10)

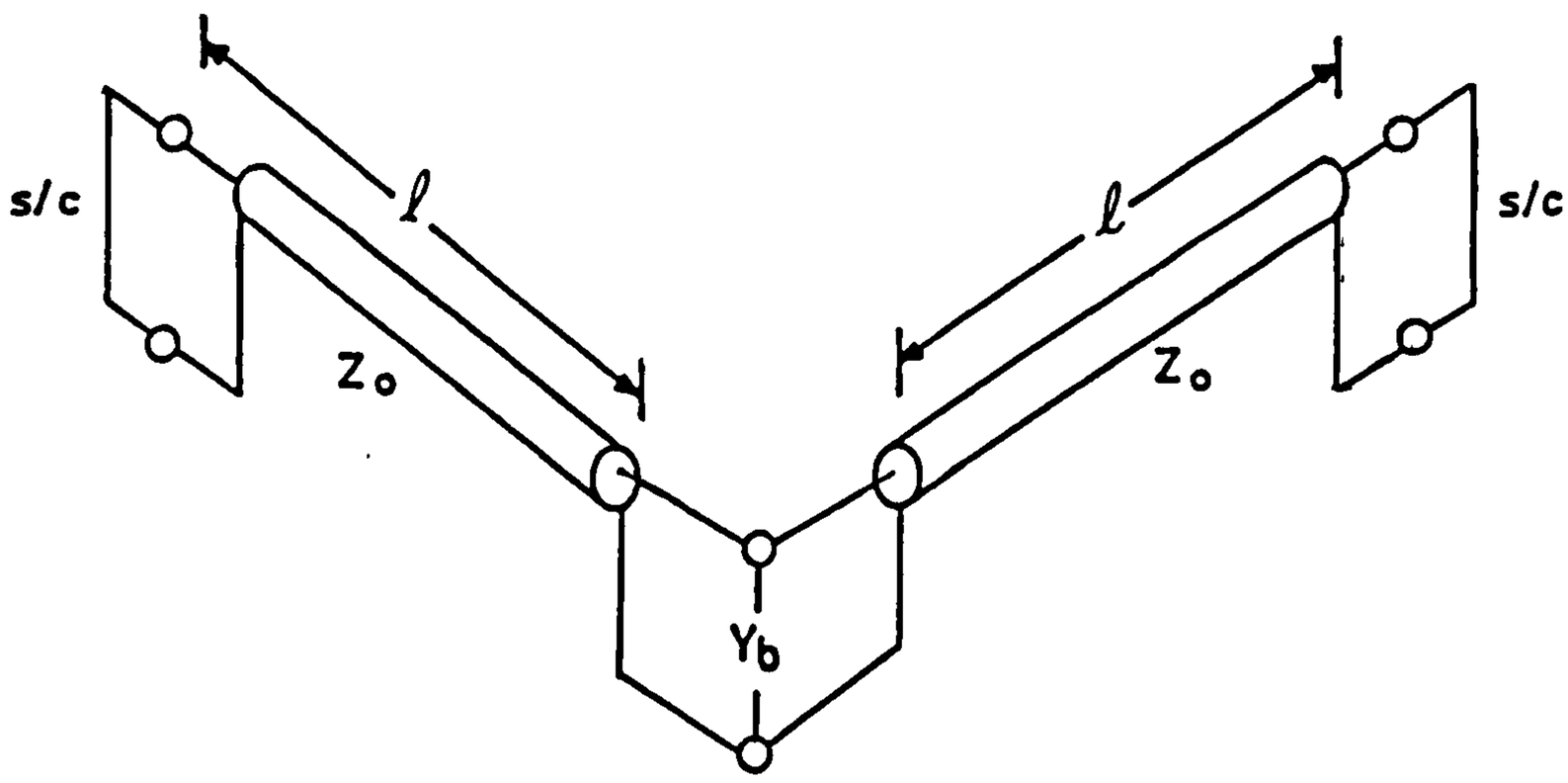

Figure 3.10 Equivalent circuit of the resonator for the analysis.

For each half of the resonator the impedance at the junction is:

$$Z_e = Z_o \tanh(\gamma l) \qquad \langle 3.13 \rangle$$

and for both connected in parallel, and without loading by the capacitive coupling:

$$Z_b = 1/Y_b = (Z_o/2)\tanh(\gamma l) \qquad \langle 3.14 \rangle$$

where $\gamma = \alpha + j\beta$

α is the attenuation constant (nepers/metre)

β is the phase constant (radians/metre) and

l is the half length of the microstrip line (metres).

Thus, employing a standard identity:

$$Z_b = Z_o[\tanh(\alpha l) + \tanh(j\beta l)]/2[1 + \tanh(\alpha l)\tanh(j\beta l)] \qquad \langle 3.15 \rangle$$

Since low loss is essential to the usefulness of a resonator based method; $\alpha l \ll 1$, so a small angle approximation is applicable. Also:

$$\tanh(j\beta l) = j\tan(\beta l)$$

So:

$$Z_b = Z_o[\alpha l + j\tan(\beta l)]/2[1 + j\alpha l\tan(\beta l)]$$

or expressed as an admittance:

$$Y_b = 2[1-j\cot(\beta l)]/Z_o[1-j\alpha l\cot(\beta l)] \quad \langle 3.16 \rangle$$

Close to resonance (i.e $\beta l = \pi/2$)

$$\alpha l\cot(\beta l) \ll 1 \quad \langle 3.17 \rangle$$

So the admittance under this condition is given by the simple expression:

$$Y_b' = 2[1-j\cot(\beta l)]/Z_o \quad \langle 3.18 \rangle$$

Also, expressing the frequency in terms of a deviation from the angular resonant frequency, ω_o:

$$\beta = (\omega_o + \Delta\omega)/v$$

where v is the velocity of propagation

At resonance $l = \lambda/4$; so $\omega_o l/v = \pi/2$ $\langle 3.19 \rangle$

Thus:

$$Y_b' = 2[\alpha l - j\cot(\pi/2 + \Delta\omega l/v)]/Z_o \quad \langle 3.20 \rangle$$

or, substituting again from equation <3.19>:

$$Y_b' = 2[\alpha l + j\tan(\pi\Delta\omega/2\omega_o)]/Z_o \quad \langle 3.21 \rangle$$

and finally, since the expression only applies close to resonance (i.e. $\Delta\omega/\omega_o \ll 1$)

$$Y_b' = (2\alpha l/Z_o)[1 + j(\pi/2\alpha l)(\Delta\omega/\omega_o)] \quad \langle 3.22 \rangle$$

The admittance of a lumped element parallel resonant circuit is given by the expression:

$$Y_p = G + j(\omega C - 1/\omega L) \quad \langle 3.23 \rangle$$

with the resonant frequency, ω_o, obtained from the condition:

$$1/\omega_o^2 LC = 1 \quad \langle 3.24 \rangle$$

Close to resonance, and substituting the expression for Q_U from equations <3.8>, the admittance can be expressed as:

$$Y_b' = G[1 + j2Q_U\Delta\omega/\omega_o] \qquad \text{<3.25>}$$

Comparing this equation with equation <3.22> it is evident that a lumped equivalent circuit for the half-wavelength transmission line resonator would have properties defined by the relationships:

$$G = 2\alpha l/Z_o \quad \text{(Siemens)} \qquad \text{<3.26>}$$

and

$$Q_U = \pi/4\alpha l \qquad \text{<3.27>}$$

3.3.2 The Effect of Capacitive Coupling

In order to make the measurement it is necessary to lightly couple the resonator to the reflectometer test port. With this resonator configuration the most convenient and effective method of coupling is via small capacitor at, or near, the centre of the resonant line. This may be formed by microstrip line, connected to the reflectometer, that terminates in an open circuit end close to the resonator. Coupling may be increased by means of a conducting foil overlay attached to the open end.

The effect of coupling is twofold; the Q of the resonator is reduced since energy is supplied to the measurement system and the resonant frequency is reduced because of the capacitive nature of the coupling mechanism. Figure 3.11 is a reflection coefficient plot typical of a capacitively coupled resonator. At resonance the magnitude of reflection coefficient is a minimum (ρ). From <3.12> and <3.7> it is evident that the unloaded Q may be determined from the minimum reflection coefficient and the unloaded, both of which may be measured, thus:

$$Q_U = Q_L\{1 + (1-\rho)/(1+\rho)\} \qquad \text{<3.28>}$$

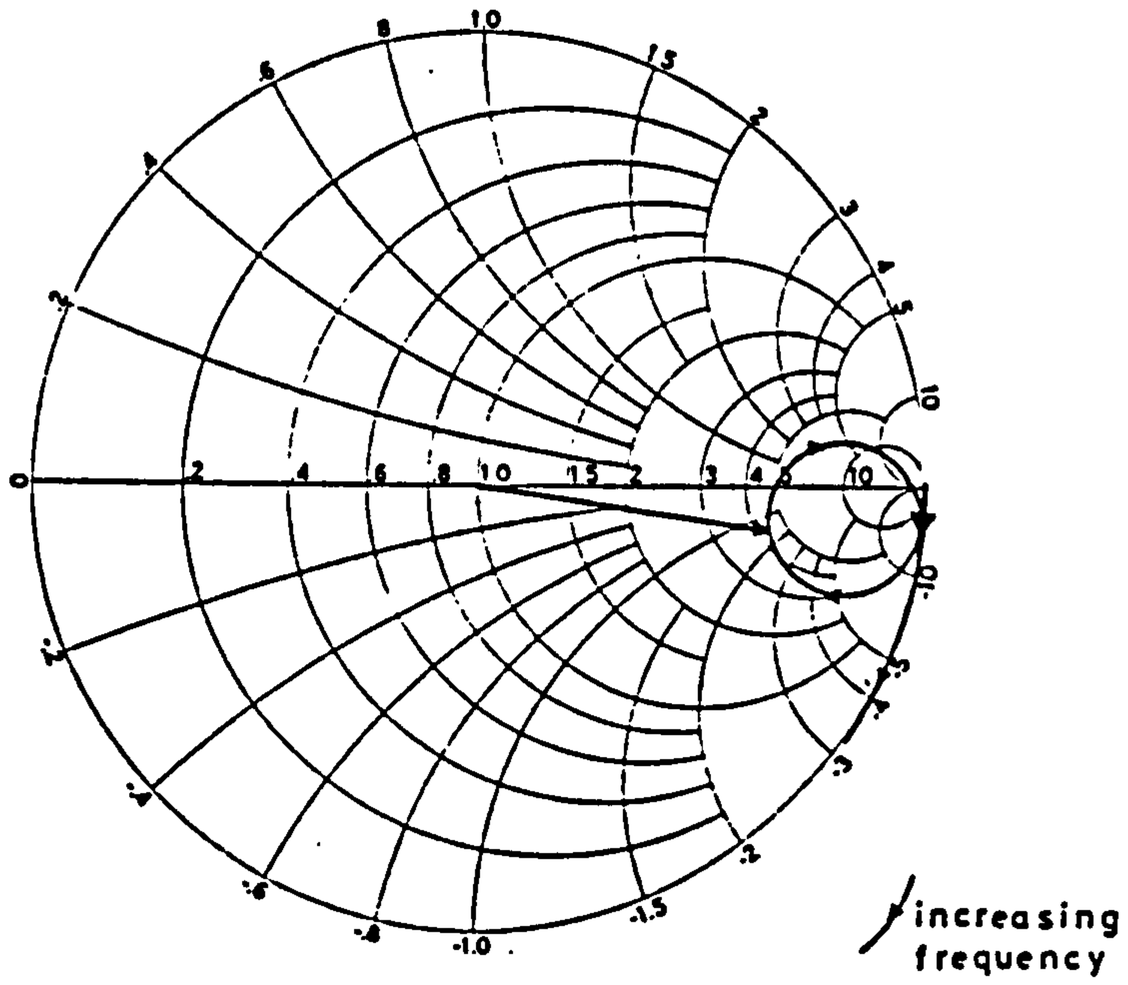

Figure 3.11 Typical reflection coefficient locus for capacitively coupled resonator.

The transmission line loss of the microstrip sample can therefore be obtained:

$$\alpha = \pi/41Q_U \text{ nepers/m}$$

$$\text{or} \qquad \alpha' = 8.6859/41Q_U \text{ dB/m} \qquad \langle 3.29 \rangle$$

The graphs of figure 3.12 illustrate these relationships for some representative cases. Unfortunately the measurement of Q for a lightly coupled resonator from reflection coefficient is not trivial. Certainly the simple direct method of determining the frequencies at which the locus cuts the Q contours on Smith Chart (cf. figure 3.6) is highly imprecise for the small 'loop' observed. The lossy characteristics of the transmission line are, however, a secondary issue and therefore this approach is not pursued here. Furthermore an alternative method for the determination of loss emerges from the following analysis.

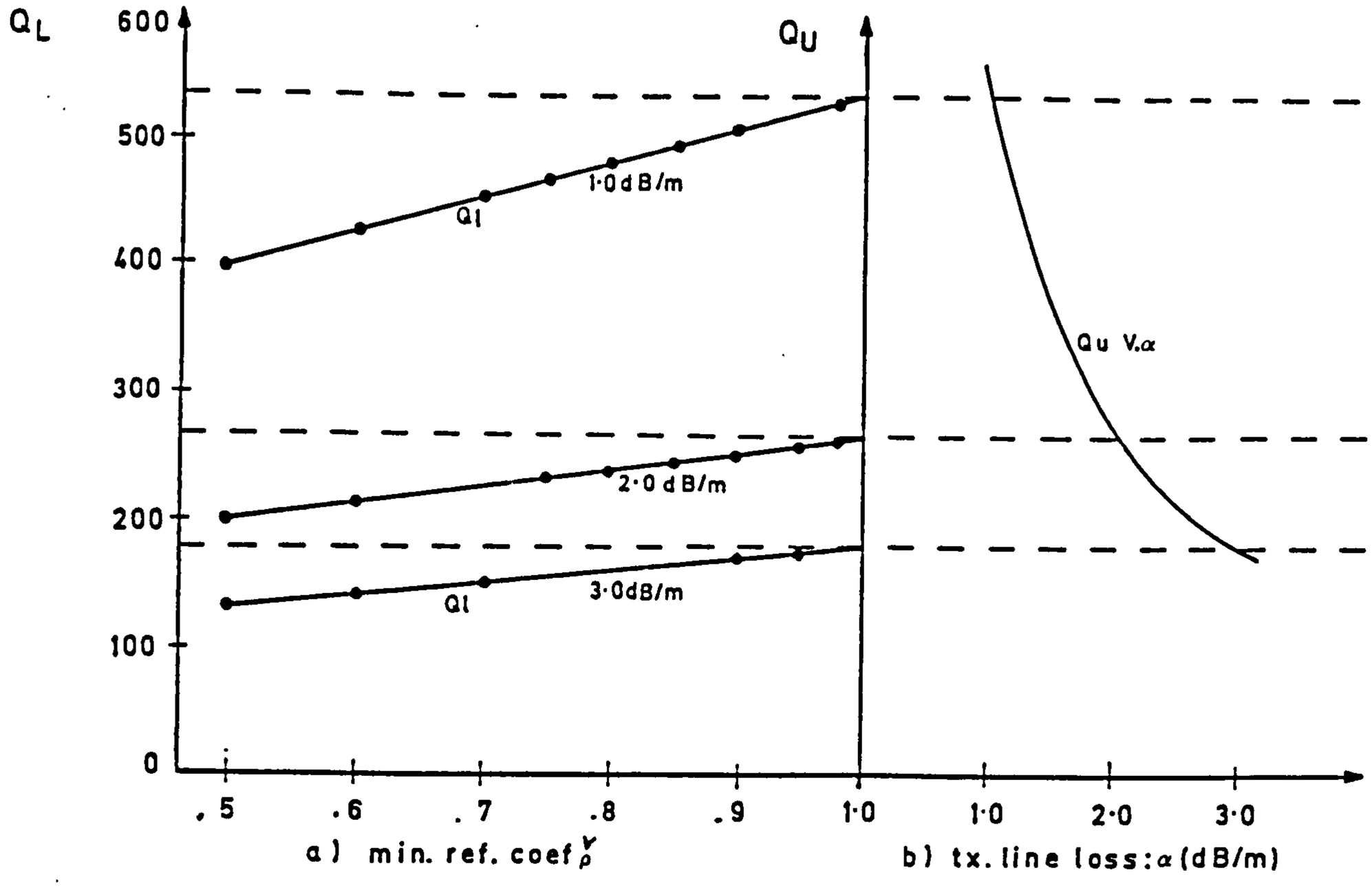

Figure 3.12 Graphs illustrating the relationships between

a) loaded Q and minimum reflection coefficient, and

b) loaded Q and transmission line loss

(note: these graphs could be developed to provide a useful nomograph for relating the three quantities).

To obtain an understanding of the effect on resonant frequency of the coupling capacitor it is necessary to consider an equivalent circuit (applicable close to resonance). The transmission line resonator is represented by the equivalent parallel tuned circuit already discussed, whilst the coupling circuit, assuming the coupling capacitor to be connected to the reflectometer by a transmission line of characteristic impedance equal to its reference impedance (typically 50 Ohm), is represented by a series R-C. The resulting equivalent circuit is illustrated in figure 3.13a. At a single frequency the shunt equivalent for the coupling circuit can be replaced producing the more convenient representation of figure 3.13b. This can be regarded as applicable over

the region close to resonance as the rate of change of the load admittance, Y_L will be much lower than the rate of change of the resonator admittance, Y_R.

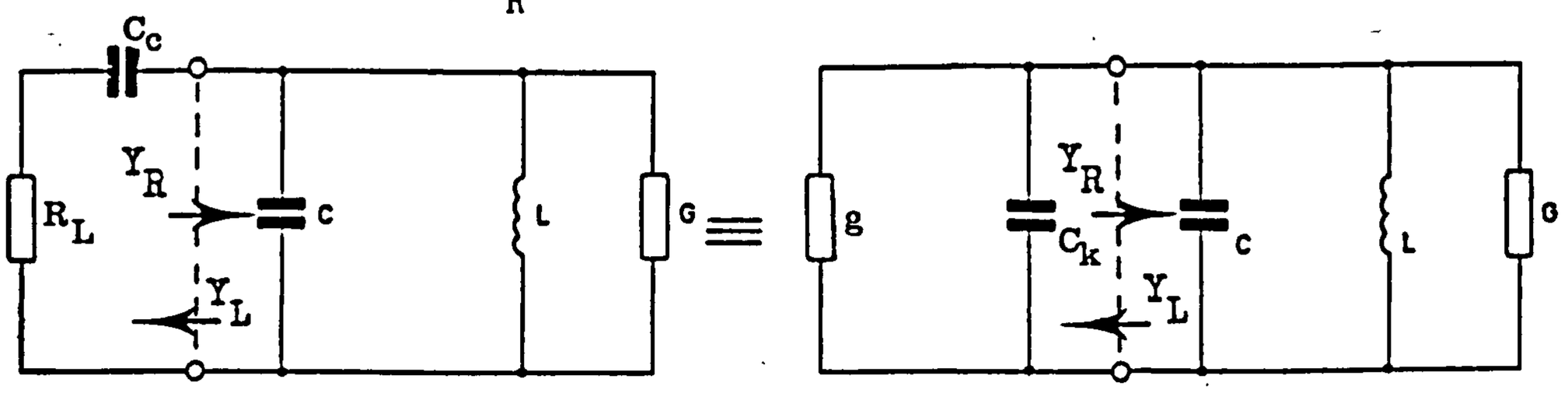

Figure 3.13 Equivalent circuits for the capacitively coupled resonator (close to resonance).

The component values for the equivalent circuit are related to the physical circuit by the following expressions:

$$Y_L = g + jb_k = \omega_o^2 C_c^2 R_L^2/\{(\omega_o C_c R_L)^2+1\}+j\omega_o C_c/\{(\omega_o C_c R_L)^2+1\} \quad \langle 3.30\rangle$$

$$G = 2\alpha l/Z_o \quad \langle 3.31\rangle$$

$$C = Q_U G/\omega_o = \pi/2Z_o\omega_o \quad \langle 3.32\rangle$$

$$L = 1/\omega_o Q_U G = 2Z_o/\pi\omega_o \quad \langle 3.33\rangle$$

and $$\omega_o = 1/\sqrt{LC} \quad \langle 3.34\rangle$$

[Note that Z_o is the characteristic impedance of the resonant line, the characteristic impedance of the coupling line being equal to R_L (usually 50 Ohm)]

Since the coupling is light (i.e. $\omega C_c \ll 1$) equation <3.30> may be simplified thus:

$$Y_L = \omega_o^2 C_c^2 R_L + j\omega C_c$$

So that $$C_k = C_c \quad \langle 3.35\rangle$$

and $$g = \omega_o^2 C_c^2 R_L = \omega_o^2 C_k^2 R_L \quad \langle 3.36\rangle$$

Including the coupling capacitor in the resonant circuit:

$$Y_R' = G + j\{\omega(C + C_k) - 1/\omega L\}$$

The modified resonant frequency ω', is therefore:

$$\omega' = 1/\sqrt{L(C+C_k)} \quad \langle 3.37\rangle$$

or $$\omega' = \{LC(1 + C_k/C)\}^{-1/2} \quad \langle 3.38 \rangle$$

By substitution of equation <3.34> this modified resonant frequency can be related to the unperturbed condition thus:

$$\omega'/\omega_o = f'/f_o = (1 + C_k/C)^{-1/2} \quad \langle 3.39 \rangle$$

Since the coupling is light, $C_k << C$ and using the binominal approximation:

$$f_o = f'(1 + C_k/2C) \quad \langle 3.40 \rangle$$

So the true resonant frequency may, at least in principle, be deduced from the measured resonant frequency. Thus the observed resonant frequency is a linear function of the coupling capacitance and, with reference to equation <3.32>, independent of the loss of the resonator. The relationship is illustrated in figure 3.14a.

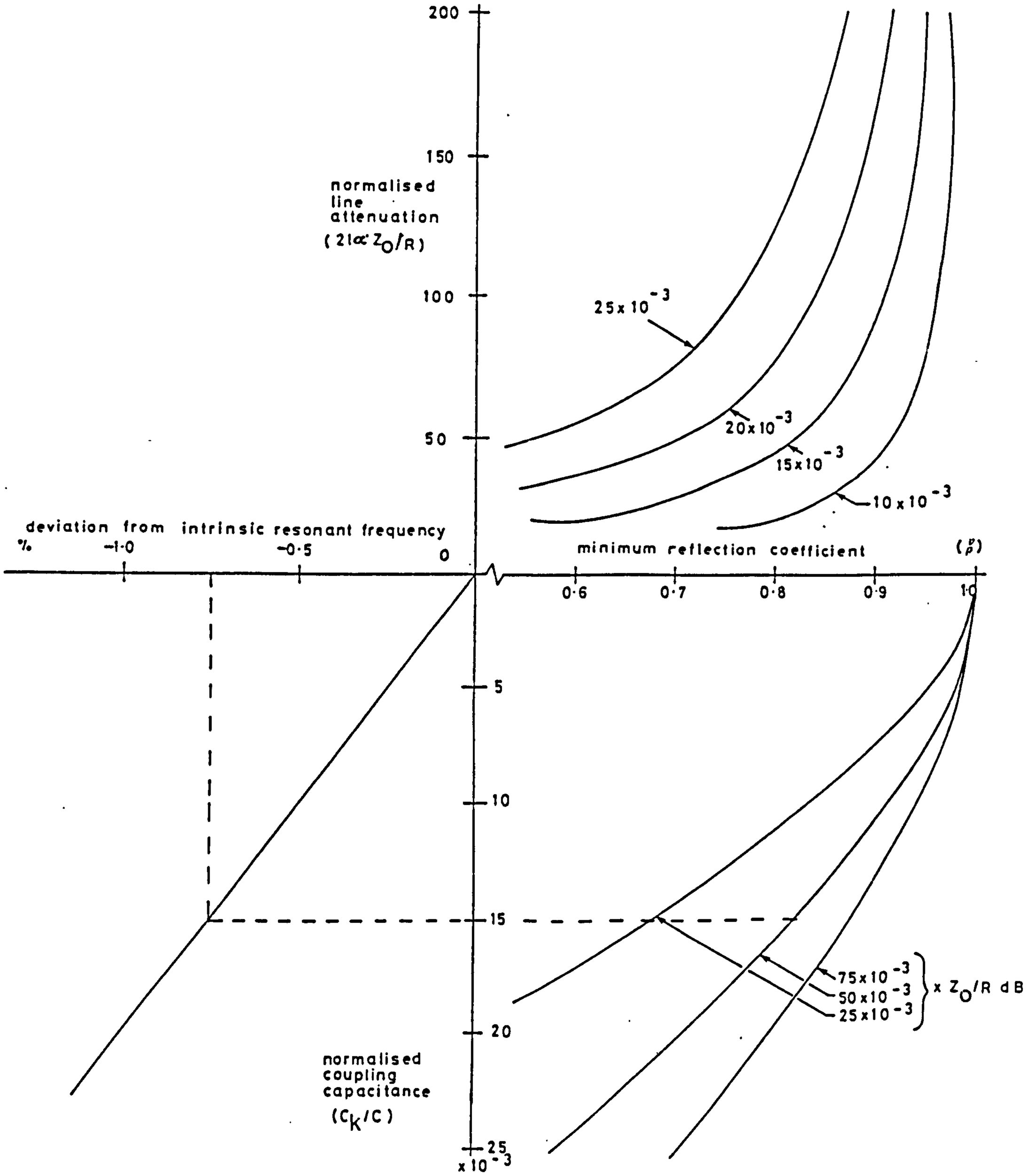

Figure 3.14 Graphs illustrating the relationship between resonant frequency, coupling capacitance, minimum reflection coefficient and transmission line loss for representative cases.

Neither C nor C_k can be directly obtained by measurement so it is necessary to relate their ratio to known or measurable quantities. From equations <3.36> and <3.6>:

$$C_k = (1/\omega_o)/(Gk/R_L)^{1/2} \qquad \text{<3.42>}$$

and substituting for G from equation <3.31>:

$$C_k = (1/\omega_o)/(2\alpha lk/Z_o R_L)^{1/2} \qquad \text{<3.43>}$$

Therefore, from equation <3.32>:

$$C_k/2C = (A.k)^{1/2} \qquad \text{<3.44>}$$

where $A = 2\alpha l Z_o/2R_L$

The coupling factor, k, can be obtained from the measurement of minimum reflection coefficient by equation <3.7>. The minimum reflection coefficient, $\check{\rho}$, can be related to the normalised coupling capacitor thus:

$$\check{\rho} = \{4A - (C_k/C)^2\}/\{4A + (C_k/C)^2\} \qquad \text{<3.45>}$$

This relationship is explored for some representative cases in figure 3.14 b and c. The graphs of figure 3.14 have been constructed with coincident axes to permit their use as a nomograph for equations <3.40> and <3.45>.

The product of the attenuation constant and the characteristic impedance, αZ_o, remains undetermined. Substituting back into <3.40> it is evident that the expression:

$$f_o = f' \{1 + (A.k)^{1/2}\} \qquad \text{<3.46>}$$

contains two terms that may be conveniently ascertained by measurement (viz. f_o and k) and two unknown terms (viz f′ and A). This suggests that measurements for two values of coupling factor will provide sufficient information to facilitate the determination of the true (unloaded) resonant frequency. The coupling factor can be varied by changing the value of coupling capacitor, the resonant frequency and minimum reflection coefficient being recorded for each condition, such that:

$$f_0 = f_1'\{1 + (A.k_1)^{1/2}) = f_2'\{1 + (A.k_2)^{1/2}\} \qquad \text{<3.47>}$$

Thus:

$$A = \{(f_2' - f_1')/(f_1'/k_1 - f_2'/k_2)\}^2 \qquad \langle 3.48 \rangle$$

and the true resonant frequency can be found by substitution into <3.47>.

For this analysis to be valid, A must be unchanged between the two measured resonant frequencies. Since the method is applicable only to relatively high-Q structures it may be assumed that the difference between these frequencies is relatively small, i.e.:

$$2(f_2' - f_1')/(f_2' + f_1') \ll 1 \qquad \langle 3.49 \rangle$$

Clearly, under this condition, the properties of the microstrip line (α and Z_o) will not vary perceptably. The value of the source/load impedance presented by the reflectometer (R_L) should be treated with a little caution. The VSWR at the test port may be no better than 1.2:1 and will be further degraded by the coax-microstrip transition to, say, 1.5:1. The load resistance is, therefore, likely to be frequency dependant. Nevertheless, it is highly improbable that it could possess a rate of change of admittance comparable to that produced by the resonator. Thus R_L is assumed invariant but uncertain in value (ranging between 33 and 75 Ohm for the VSWR suggested). Bearing this in mind the line microstrip transmission line attenuation can be determined from the measurement, albeit with substantial uncertainty.

$$\alpha = 8.6859\ (\pi^2 R_L/21 Z_o)A \qquad \langle 3.50 \rangle$$

[Note: Z_o, the characteristic impedance of the rsonant line is supplied by the microstrip analysis of Chapter 2 and, although un-confirmed by measurement, will be known much more precisely than R_L].

This algorithm for the determination of the true resonant frequency, embodying equations <3.48>, <3.49> and <3.50>, has been implemented as a program for a CBM PR100 pocket calculator in Appendix B. The velocity of propagation is simply ascertained using the expression:

$$v = 2f_o(21) \quad m/s$$

3.4 MEASUREMENT METHODOLOGY

As stated previously the determination of the frequency of resonance by amplitude measurement is imprecise because of the zero first derivative of reflection coefficient magnitude with frequency at resonance. Phase measurement is therefore to be preferred; the first derivative of reflection coefficient phase with frequency being a maximum at resonance. Two questions need to be answered; how does one establish a phase reference and does the resonant frequency so determined correspond to the definition used in the analysis of section 3.3.2 ?

3.4.1 Establishing the Phase Reference

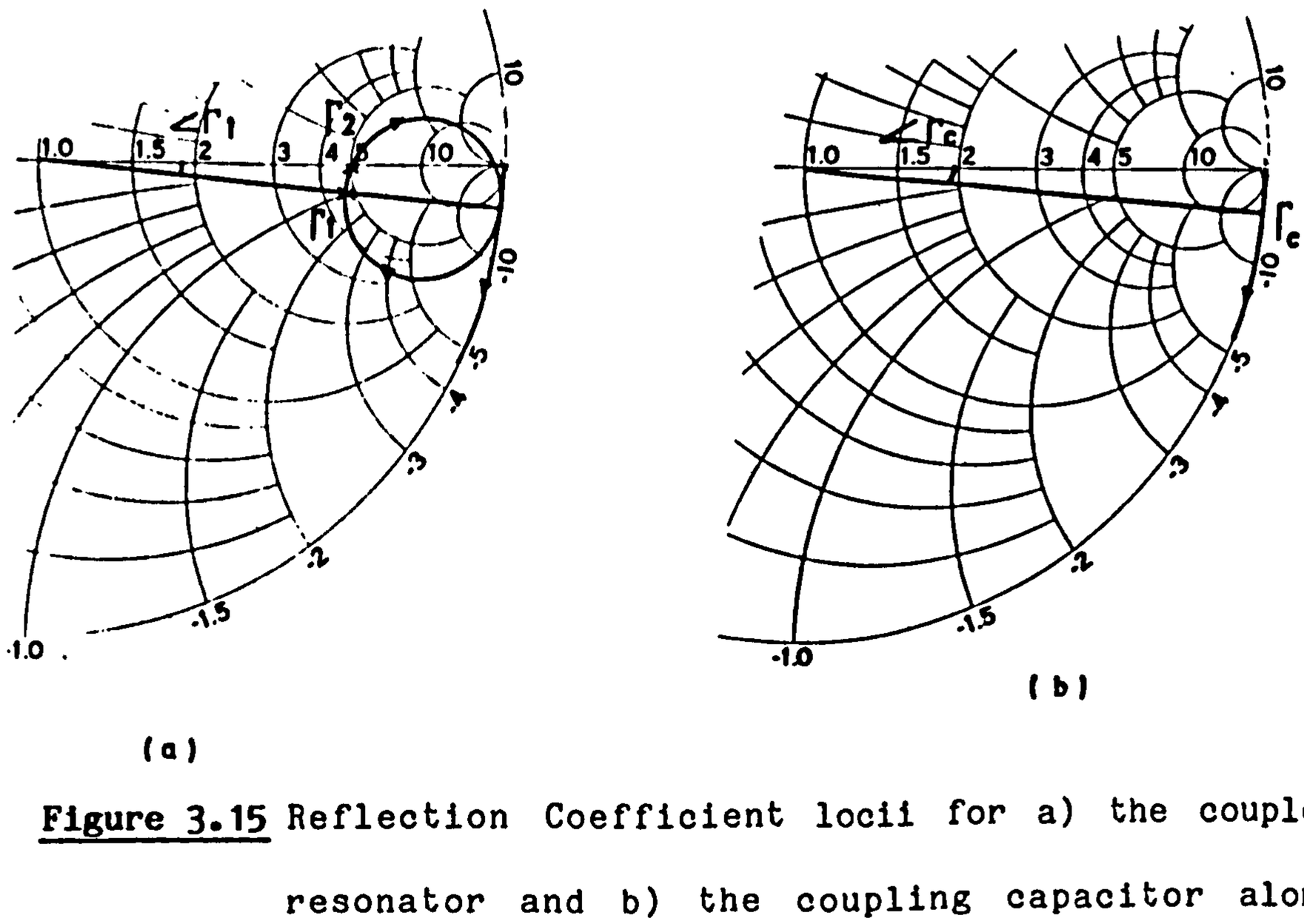

Figure 3.15 Reflection Coefficient locii for a) the coupled resonator and b) the coupling capacitor alone (arrows indicate increasing frequency)

Figure 3.15 illustrates the behaviour of the coupled resonator. Clearly there are potentially two situations where a convenient datum for resonant frequency which facilitate the use of phase measurement. The first corresponds to the amplitude condition of minimum reflection

coefficient (i.e. $|\Gamma_1| = \breve{\rho}$). The angle of reflection coefficient at this point will correspond to that subtended by a radial line bisecting the loop. The second case is defined by the point at which the locus cuts the real axis (i.e. $\angle\Gamma_2 = 0$).

Thus, for this latter case a suitable phase reference would be an open circuit at the plane of the coupling capacitors external terminal. Unfortunately, this apparently simple requirement is difficult to achieve since the plane of connection and the parasitics of the open circuit are difficult to define, especially when foil overlays are used to enhance the coupling. Figure 3.15b illustrates an alternative way of obtaining a phase reference.

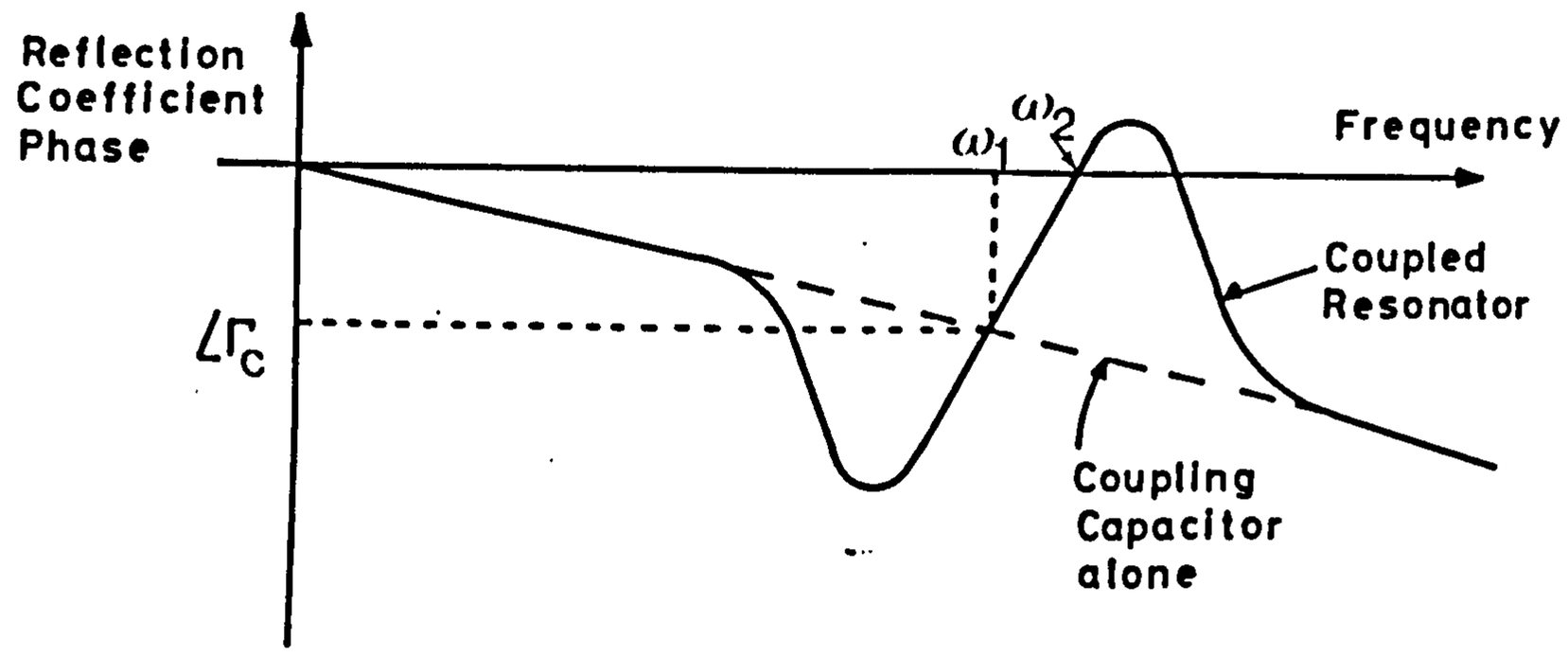

Figure 3.16 Plot a reflection coefficient phase versus frequency

If the coupling capacitor were to be shorted to the ground plane the simple locus shown would be produced. At the resonant frequency it will have a reflection coefficient, Γ_C, having unit magnitude and an angle increasing (negatively) with frequency at a rate much slower than that associated with the coupled resonator (figure 3.16). Thus, knowing the resonant frequency approximately from an initial measurement, a phase reference may be established.

In principle, a structure duplicating the test assembly but having a substrate on which the resonator is replaced by a conducting path to the

ground plane, could be used. It would, however, be impracticable to duplicate the variable value of coupling capacitor formed by the foil overlay. The solution lies in the "detuned-short" method described by Sucher [7]. Whilst the high Q resonator presents a high impedance at, or very close to, the resonant frequency, at a frequency a little removed from resonance it presents a relatively low impedance. Quantatively, the condition for a low impedance at the point of coupling can be expressed thus:

$$|\omega_{lo-Z} - \omega_o| >> \omega_o/Q \qquad \langle 3.51 \rangle$$

Under this condition the reactance of the coupling capacitor dominates and thus the measured reflection coefficient will tend to that of the coupling capacitor alone. So, if the tuning of the resonator can be changed, by placing the metallic items on the microstrip, the angle of reflection coefficient of the coupling component can be determined. This result can then be used after removing the detuning elements, as the phase reference for a more accurate measurement of resonant frequency. After a couple of iterations the frequency at which the same phase angle is measured both with and without the detuning elements can be determined. Convergence is rapid, since the rate of change of phase for the detuned case is very much lower than that due to the high-Q tuned circuit at resonance. Thus, referring to figure 3.15, the measured resonant frequency is given by the condition:

$$\angle\Gamma_1(\omega_1) = \angle\Gamma_C(\omega_1) \qquad \langle 3.52 \rangle$$

3.4.2 Defining the Resonant Frequency

From figure 3.15 it is apparent that there are two alternative phase datums for the measurement of the resonant frequency, one

corresponding the condition of equation <3.51> and the other to the condition:

$$\angle\Gamma_2(\omega_2) = 0 \qquad \text{<3.53>}$$

Although it is known that the behaviour of the transmission line resonator is analagous to a parallel resonant circuit the locus is that of a series circuit resonant at f_2 (cf. figure 3.16). This is a consequence of the small value of the coupling capacitor; the action of which approximates the immittance inverter of filter theory. Alternatively, and equivalently, the series resonance is that resulting from the interaction of the small value coupling capacitor with the large net inductance of the intrinsic resonator, below the resonant frequency. This situation is illustrated by the equivalent circuit of figure 3.17b and from the condition of equation <3.53> the imaginary part of impedance at resonance is:

$$I\{Z_s(\omega_2)\} = -\{(1/\omega_2 C_c)+(\omega_2 C-1/\omega_2 L)/[G^2+(\omega_2 C-1/\omega_2 L)^2]\} \qquad \text{<3.54>}$$

The definition of resonance used for the analysis of section 3.3.2 was based on the equivalent circuit of figure 3.17c for which the resonant frequency, ω', is defined by the condition:

$$I\{Y_R'(\omega')\} = \omega'(C + C_k) - 1/\omega' L = 0 \qquad \text{<3.55>}$$

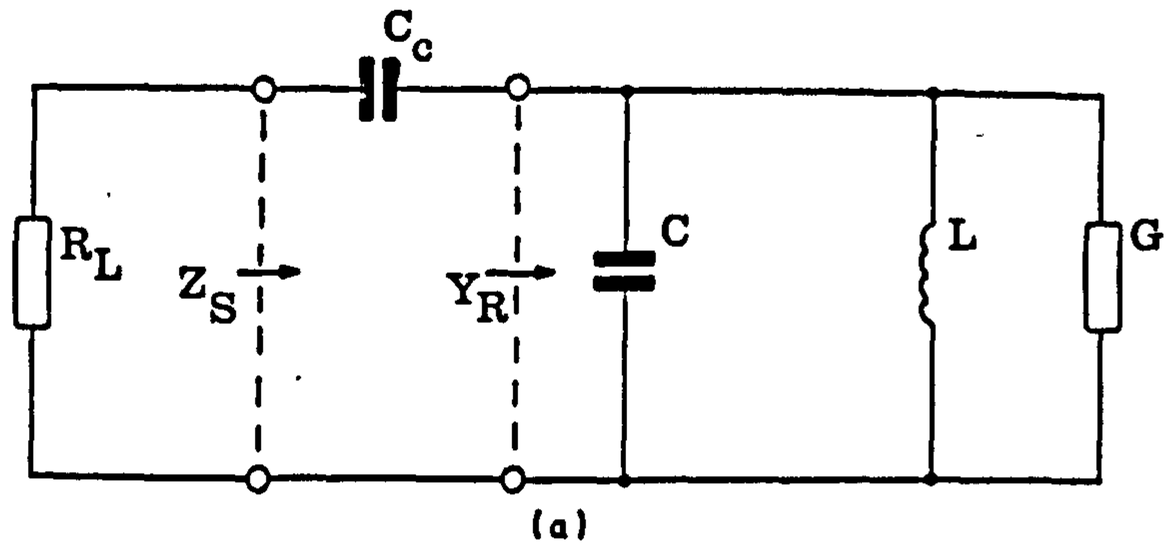

Figure 3.17 Various equivalent circuits for the coupled resonator: a) physical lumped, b) effective series, c) effective parallel, d) detuned

and it was established that, for light coupling:

$$\omega C_k = \omega C_s / \{\omega C_s R_s)^2 + 1\} \qquad \langle 3.56 \rangle$$

For the convenience of measurement, however, the definition of resonance

is given by <3.52> or, at ω_1:

$$b_1/a_1 = b_c/a_c \qquad \text{<3.57>}$$

where $\rho_1 = a_1 + jb_1$ and $\rho_c = a_c + jb_c$

Now, the reflection coefficients are related to the impedances thus:

$$\rho_1 = (Z_1/R_L - 1)/(Z_1/R_L + 1) \qquad \text{<3.58>}$$

where $Z_1 = r_1 + jx_1 = -j/\omega_1 C_c + 1/\{G_p + j(\omega_1 C - 1/\omega_1 L)\}$

and
$$\rho_c = (Z_c/R_L - 1)/(Z_c/R_L + 1) \qquad \text{<3.59>}$$

where $Z_c = jx_c = -j/\omega_1 C_c$

$$b_1/a_1 = 2x_1/R_L\{(r_1/R_L)^2 + (x_1/R_L)^2 - 1\} \qquad \text{<3.60>}$$

and similarly for b_c/a_c.

Substituting in <3.57>, and after some manipulation:

$$(r_1/R_L)^2 = (x_c/R_L - x_1 R_L)(x_1/R_L + R_L/x_c) \qquad \text{<3.61>}$$

where $r_1 = G/\{G^2 + (\omega_1 C - 1/\omega_1 L)^2\}$

and $x_1 = -1/\omega_1 C_c - (\omega_1 C - 1/\omega_1 L)/\{G^2 + (\omega_1 C - 1/\omega_1 L)\}$

After some rearrangement the relationship can be reduced to:

$$\omega_1 C_c/\{1 + (\omega_1 C_c \ R_L)^2\} + \omega_1 C - 1/\omega_1 L = 0 \qquad \text{<3.63>}$$

Substituting into this expression the result of <3.56>:

$$\omega_1(C_k + C) - 1/\omega_1 L = 0 \qquad \text{<3.64>}$$

and comparing with the resonance definition used for the analysis; restated as <3.55> it is evident that

$$\omega_1 = \omega_o \qquad \text{<3.65>}$$

Thus it is established that the definition for resonance used for measurement and analysis are compatible.

3.4.3 Substrate Preparation

The substrates were attached to a brass base plate with shorting blocks at each end of the resonator. An APC-7 to microstrip transition was employed for the connection to the reflectometer; a network analyser,

with only one of its two test ports in use. The base plate and shorting blocks were lightly gold plated to ensure high conductivity and to minimise leaching of the gold ground plane and edge plated short circuits from the substrate during solder attachment. Soldering was accomplished on a hot plate using LMP alloy (lead-tin with 2% loading for leach retardation) in paste form. The assembly was removed from the hot plate as soon as the solder had wetted the surfaces. The substrate was aligned using the shorting blocks and all three items were soldered simultaneously; capilliary action carrying solder up the interface between the substrate edge plating and the vertical surfaces of the shorting blocks. The completed assembly is illustrated in figure 3.18.

Also shown is the foil overlay which both enhances the coupling and provides a means of adjusting the coupling factor. The gold plated copper foil strip is connected at one end to the microstrip spur from the coaxial transition by solder or conducting epoxy. The coupling capacitance is controlled by adjustment of the proximity of the free end to the resonant line.

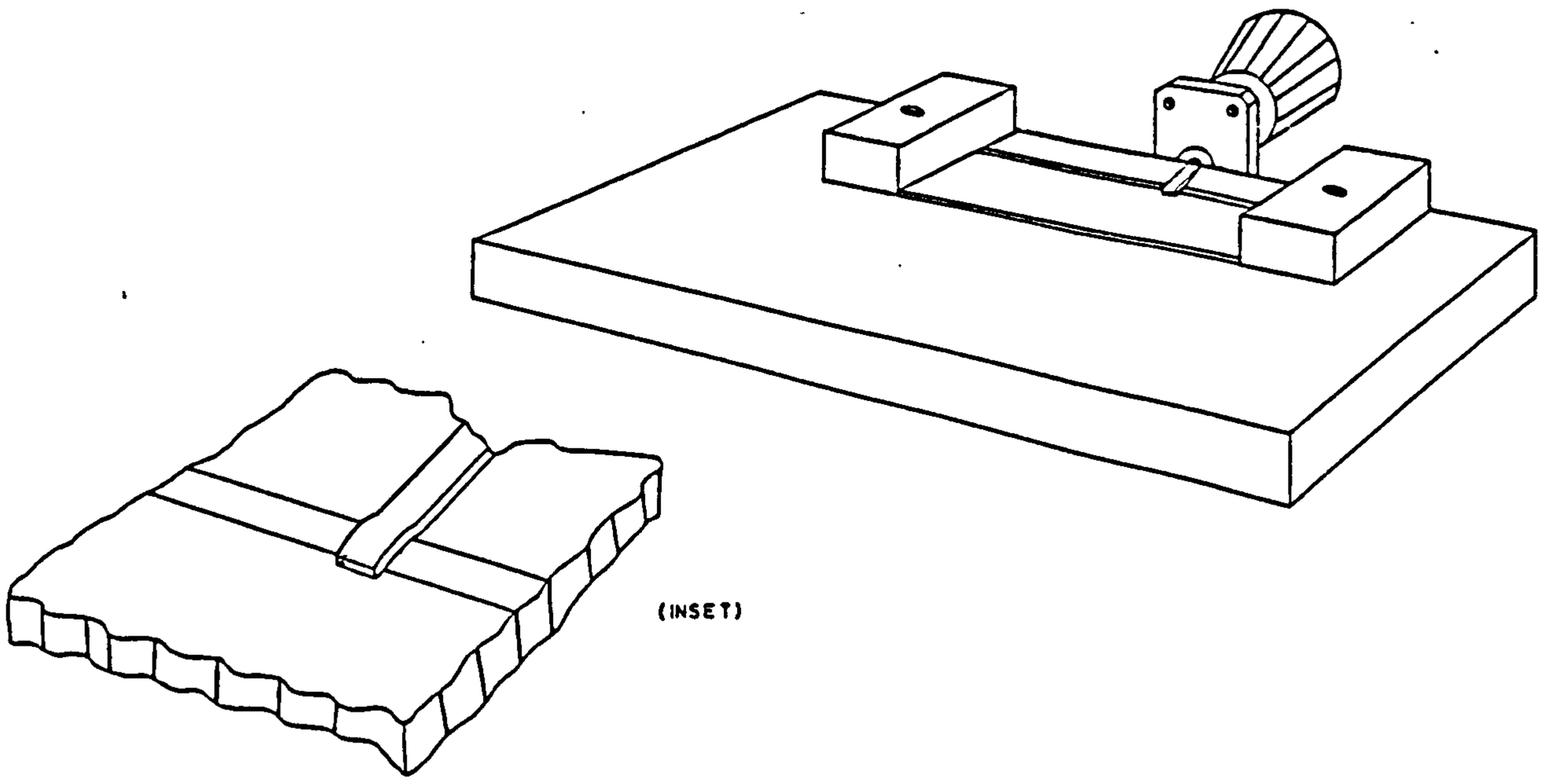

Figure 3.18 A view of the assembled test jig with insert showing the foil overlay to enhance coupling.

3.4.4 The Measurement Procedure

Measurement of resonant frequency and minimum return loss must be made for, at least, two values of coupling. Data for more than two cases can prove useful in establishing a level of confidence in the results, as will be demonstrated in section 3.6. In all cases coupling must be light for the algorithm used to determine the unperturbed resonant frequency to be accurate. Nevertheless the coupling values, set by manipulating the foil strip, should be sufficiently different to avoid degradation of the accuracy due to undue exaggeration of the instrument's limited discrimination.

Detuning is achieved using a couple of small gold plated brass blocks that were placed either side of the coupling point on the resonant microstrip line. Care must be exercised to avoid deflecting the foil overlay and thereby altering the coupling factor. The detuning blocks must not be placed so close to the coupling point that the coupling capacitance could be affected, but their effectivity is diminished as they are moved towards the short circuits. Difficulty is sometimes encountered when the Q of the resonator is relatively low (as it is for high impedance lines) since the resonator must be detuned by a greater amount. Cleanliness of the contacting surfaces is found to be of importance.

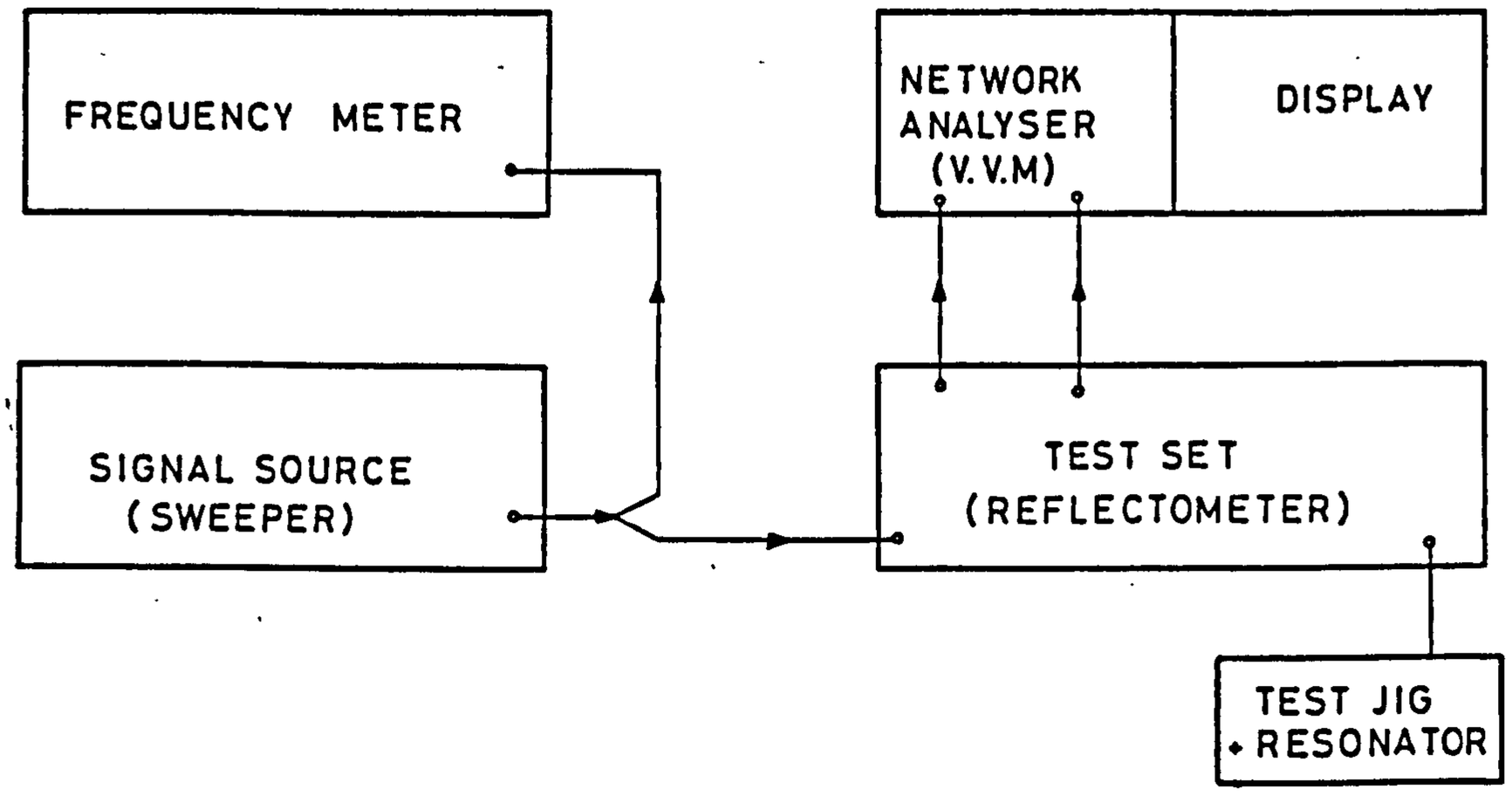

Figure 3.19 Apparatus for the measurement of singly coupled resonators.

Figure 3.19 illustrates the apparatus used for the measurements on the microstrip resonators. The vector voltmeter/network analyser should be fitted with a phase magnitude display or phase-gain meter (HP 8412 or 8413 for the HP 8410) rather than the polar display (HP 8414) which does not permit expansion of high reflection coefficient readings.

The measurement procedure is set out below.

i) Using standard techniques the reflectometer reference plane is set in the vicinity of the coupling point.

ii) Locate the resonance (using a swept signal source if the phase-magnitude display is in employed).

iii) Check reference plane position on wide sweep: phase should be substantially independent of frequency either side of the resonance.

iv) Manipulate the foil coupling strip to produce a suitable dip in the magnitude response.

v) Set the signal source (CW mode) to the frequency at which

reflection coefficient is a minimum.

vi) Detune the resonator and set the phase reading to zero (on the high discrimination range of the display device) using the phase adjust on the vector voltmeter (network analyser).

vii) Remove the detuning elements and return the phase reading to zero by making a small adjustment to the frequency of the source.

viii) Repeat steps (vi) and (vii) until the phase reading remains unchanged when the detuning elements are removed and replaced.

ix) Record the frequency (f_1).

x) Detune the resonator once more and zero the magnitude reading, using the highest resolution range of the display.

xi) Remove the detuning elements and using the i.f. step attenuator of the network analyser as necessary read the return loss value (i.e. $20\log_{10}\rho_1$) without making any adjustment to the frequency.

xii) Repeat steps (iv) to (xi) inclusive for a differing value of minimum reflection coefficient to obtain f_2 and ρ_2.

xiii) Using the calculator program of Appendix B complete the true resonant frequency (f_o) and transmission line loss (o).

xiv) Preferably repeat steps (iv) to (xi) to obtain several sets of values of f and ρ and calculate values of f_o and α for all permutations to improve confidence in the results.

3.5 ACCURACY OF MEASUREMENT

The accuracy of the measurement is limited by a number of factors. These include approximations in the analysis, the resolution of the phase meter/display and the accuracy of the measurements of frequency and reflection coefficient. In addition, when relating the results back

to the parameters of the microstrip line, the effects of finite metallization thickness and dispersion must be taken into account. All these considerations are discussed below and estimates of the error for the representative case of a 25mm long, 50 Ohm microstrip line having an attenuation of 3dB/m and measured with a 50 Ohm test set.

3.5.1 Approximations in the Analysis

Since the analysis of sections 3.3.1 and 3.3.2 is used as the basis of the algorithm to find the true (unloaded) resonant frequency the approximations made must be assessed in terms of their impact on the result.

The first of these approximations relates to the value of x, the alternative constant and is the small angle approximation for the hyperbolic tangent used in equation <3.16>, i.e.

$$\alpha l \simeq \tanh(\alpha l)$$

In the example suggested:

$$\alpha l = 4.3173*10^{-3} \text{ nepers}$$

$$\{\alpha l - \tanh(\alpha l)\}/\alpha l = 6.2*10^{-5} \text{ or } 0.0006\%$$

which is not of significance and only affects the accuracy of frequency determination in as much as it enters into the next approximation, that of equation <3.17>, i.e.

$$\alpha l \cot(\beta l) \ll 1 \text{ for } \beta l \simeq \pi/2$$

From an inspection of the graphs in figure 3.14 it is evident that the perturbed resonant frequency should never differ by more than 1% from the true resonance. In such an extreme case:

$$\alpha l \cot(\beta l) = 6.782*10^{-5}$$

giving an error of 0.014% in the expression for the resonant circuit admittance. Since, however, it applies to both the real and imaginary

part it only affects the term equivalent to the shunt conductance in the final expression. Nevertheless it is assumed that this quantity remains constant for the two measurements used to find the true resonant frequency. But the error is acceptably small.

The remaining approximation is the expression for the resonant line admittance (equation <3.22>) is that, close to resonance:

$$\theta \simeq \tan(\theta)$$

where $\theta = (\Delta\omega/\omega_o)\pi/2$

and for the same extreme 1% offset:

$$\{\theta-\tan(\theta)\}/\theta = 8.227*10^{-5} \text{ or } 0.0082\%$$

again of little consequence when the target accuracy for the measurement is 0.1%.

For the analysis of the capacitively coupled resonator the assumption that the effective shunting capacitor, C_k, is equivalent to the actual coupling capacitor, C_c is an approximation to the true relationship, viz:

$$C_k = C_c/\{(\omega_o C_c R_L)^2 + 1\}$$

applicable when coupling is light. From <3.40> and <3.32>

$$\omega_o C_c \simeq (1-\omega/\omega_o)$$

So, for the example given and a 1% offset; $\omega_o C_c = 6.28*10^{-4}$

and so $(\omega_o C_c R_L)^2 = 9.87*10^{-4}$

Thus the assumption that $C_k = C_c$ is in error by less than 0.1% for all likely situations.

The remaining approximation is that employed in arriving at the expression <3.40> and involves the binominal expansion. The next term in the series is:

$$3/8(C_k/C)^2 = 1.5*10^{-4} \text{ or } 0.015\%$$

for the example given.

3.5.2 Measurement Errors

Two quantities are measured; resonant frequency and minimum reflection coefficient. The frequency meter itself, with better than 1 part in 10^7 measurement accuracy will make a negligible contribution to the error budget. But the resonant condition is found, as discussed in section 3.4.4, by the comparison of two phase measurements. The vector voltmeter/network analyser with suitable display module is capable of resolving phase difference to 0.1 degrees. The comparative measurement of phase is conducted at a constant frequency and is, therefore, not susceptible to instrument error. Clearly the accuracy of the frequency measurement is crucially dependant on the rate of change of phase observed at resonance. A rough, but conservative, estimate of the accuracy can be obtained in the following manner.

Consider the locus of the coupled resonator referred to the detuned phase measurement plotted on the Smith Chart in figure 3.19.

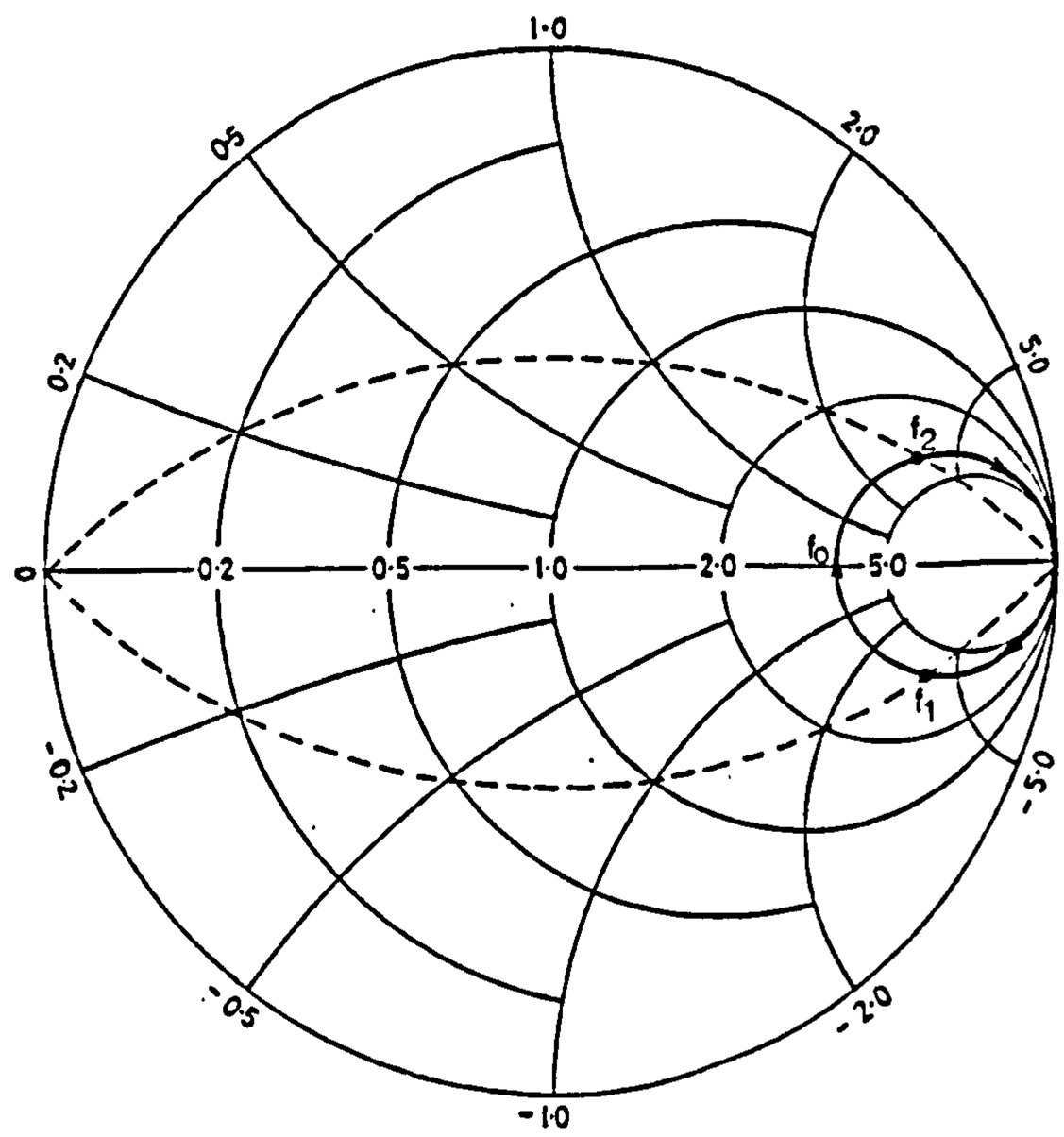

Figure 3.19 Locus of the coupled resonator shown with Q-Measurement contours.

Also, plotted are the Q measurement contours. These contours are defined by the impedance condition.

$$r = |x| \qquad \text{<3.70>}$$

$$\text{for } Z = r + jx$$

The resonant loop cuts both the contours at frequencies separated by:

$$\Delta f = f_o/Q_L$$

The loaded Q (Q_L) can be obtained from a knowledge of the unloaded Q (Q_U) and the minimum reflection coefficient by <3.7> and <3.12>, thus:

$$Q_L = Q_U/\{1+(1-\rho)/(1+\rho)\} \qquad \text{<3.71>}$$

The angle of reflection coefficient (θ) is related to impedance (from <3.60>) by the expression:

$$\theta = \tan^{-1}(2x/R_L/\{(r/R_L)^2 + (x/R_L)^2 - 1\}) \qquad \text{<3.72>}$$

Now the locus of the coupled resonator follows a constant resistance circle of a value, r_o related to the minimum reflection coefficient thus:

$$r_o/R_L = (1 + \rho)/(1 - \rho) \qquad \text{<3.73>}$$

The angle subtended between the two points of coincidence of the locus and the contours is, therefore:

$$\Delta\theta = 2\tan^{-1}([2r_o/R_L]/\{2(r_o/R_L)^2-1\}) \qquad \text{<3.74>}$$

For light coupling the angle is small and the value of r_o high, so:

$$\Delta\theta = 114\ R_L/r_o \text{ degrees} \qquad \text{<3.75>}$$

The approximate rate of change of phase with frequency at resonance is then:

$$\Delta\theta/\Delta f = 114\ R_L Q_L/r_o f_o \text{ deg/Hz} \qquad \text{<3.76>}$$

In fact the rate of change of phase is not uniform over the frequency interval, but rather greater at the 'zero phase' point: i.e.

$$\Delta\theta/\Delta f < d\theta/df \quad \text{at } f_o \qquad \text{<3.77>}$$

Since there are two phase measurements involved in the determination of resonant frequency the worst case phase error, θ_e = 0.2 degrees. The

peak frequency is, then:

$$f_e < 0.2\,\Delta f/\Delta\theta \qquad \langle 3.78\rangle$$

Normalising and making the obvious substitution:-

$$f_e/f_o < r_o/570Q_LR_L \qquad \langle 3.79\rangle$$

For the example of a 25mm long, 50 Ohm line with a loss of 3dB/m, with the coupling set to give a minimum reflection coefficient of 0.8:

$$Q_U = 182, \quad Q_L = 164, \quad r_o/R_L = 9$$

therefore $$f_e/f_o < 0.96*10^{-4} \text{ or } 0.0096\%$$

The effect on the computed true resonant frequency could, in unfavourable circumstances, be an error of twice this value, i.e. 0.02%. Nevertheless the error is still small compared to the accuracy target of 0.1%.

The measurement of minimum reflection coefficient is made relative to the unity reflection datum provided by the measurement of the detuned resonator. Both measurements are made at the same frequency and the only instrument errors to consider are those due to non-linearity (or deviation from logarithmic law, when a return loss display is employed) i.f. attenuator step accuracy (if used) and display resolution.

The typical resolution available, denoted here by Δ, is 0.1% (~0.01 dB). The worst case error for the difference measurement can be obtained from the following expression:

$$1 - \rho' = 1 - \rho + (1 + \rho)\Delta \qquad \langle 3.80\rangle$$

and clearly approaches $2\Delta(0.02)$ for the lightly coupled case.

On the contrary the scale related error denoted by e, declines with a decreasing difference as indicated by the following expression:

$$1 - \rho' = 1 - \rho + (1 - \rho)e \qquad \langle 3.81\rangle$$

where a typical value for e would be 0.005 (0.5%).

Combining these two effects in a single expression for coupling factor yields, after some manipulation, the relationship:

$$k' = k(1 - e - \Delta/k)/(1 + k_e + \Delta) \qquad \langle 3.82\rangle$$

and for light coupling:

$$k' = k(1 - \delta) \qquad \langle 3.83 \rangle$$

where $\delta = e + \Delta/k$

Table 3-1 contains values for the error in coupling factor for a representative set of values.

TABLE 3-1 COUPLING FACTOR AND RELATED FREQUENCY ERRORS

Min. refl. coef.	Coupling factor	Total error	Error in frequency
γ	k	δ	$\delta/2\sqrt{2Ak}$
0.98	0.0101	0.104	0.015%
0.95	0.0256	0.044	0.010%
0.90	0.0526	0.024	0.008%
0.80	0.1111	0.014	0.007%
0.70	0.1764	0.011	0.007%

The error in the coupling factor is of concern in as much as it perturbs the determination of true resonant frequency. The observed resonant frequency is related to the coupling factor by the expression (from <3.47>):

$$f_1 = f_o/(1 + \sqrt{Ak_1}) \qquad \langle 3.84 \rangle$$

where f_o and A may be regarded as constants of the particular coupled resonator. For small error in coupling factor the effect on the observed resonant frequency is given by the relationship:

$$f_1' = f_1/\{1 - \{\delta/2\}\sqrt{Ak_1}/(1 - \sqrt{Ak_1})\} \qquad \langle 3.85 \rangle$$

and since, for lightly coupled high-Q resonator, the value of Ak_1 is small:

$$f_1' = f_1(1 + \{\delta/2\}\sqrt{Ak_1}) \qquad \langle 3.86 \rangle$$

In the case of the example cited previously $A = 8.75*10^{-4}$ and the errors

for a number of cases have been computed and are included in table 3-1. Since two observations of resonant frequency are involved in the determination of the true resonant frequency these insignificant errors will be exaggerated somewhat, especially if the two measured frequencies are closely spaced relative to their displacement from the true resonant frequency.

Inevitably, the accuracy of the determination of resonant frequency is impaired when the Q is low. The rate of change of phase with frequency at resonance is reduced and the large frequency offsets, caused by coupling capacitance necessary to obtain a useful reflection coefficient dip, call into question the assumed invariance of A. The consequence is that the uncertainty in the measurement is likely to be greatest for the high impedance (narrow) microstrip lines. A representative case is assessed in Table 3-4.

Clearly the potential for error in the determination of the line loss, α , is much greater than for the resonant frequency, since it depends on the knowledge of the unmeasured absolute values. Whilst all the sources of error so far discussed affect α in that they contribute to uncertainty in the value of A (equation <3.48>), by far the most detrimental aspect is the calculation of α from A by equation <3.50>. The characteristic impedance of the microstrip line, Z_o, is known only from the theoretically based computation that is to be verified by these requirements. But this uncertainty pales into insignificance when compared to that associated with resistive part of the load impedance presented by the reflectometer, R_L, which with a modest enough VSWR of 1.5:1 at the point of coupling has error bounds of +50%,-33%! Given that the determination of line loss is secondary to the purpose of the experiment, no effort was directed at the reduction of this uncertainty. The principle benefit afforded by the extraction of line loss data from

the measurements is that it provides an indicator to the degree of uncertainty in the resonant frequency determination.

3.5.3 Metallization Thickness Effects

The finite thickness of the track metallization results in a deviation from the theoretical analysis, which assumed infinitely thin conductors, that increases as the microstrip width is reduced. It must therefore be taken into account when comparing measured and calculated data, particularly for lines of high characteristic impedance. For this purpose the expression of Bahl and Garg [10]; which operate as the width to height ration, producing an effective width increased to accommodate the additional contribution of the strip edges (figure 3.20).

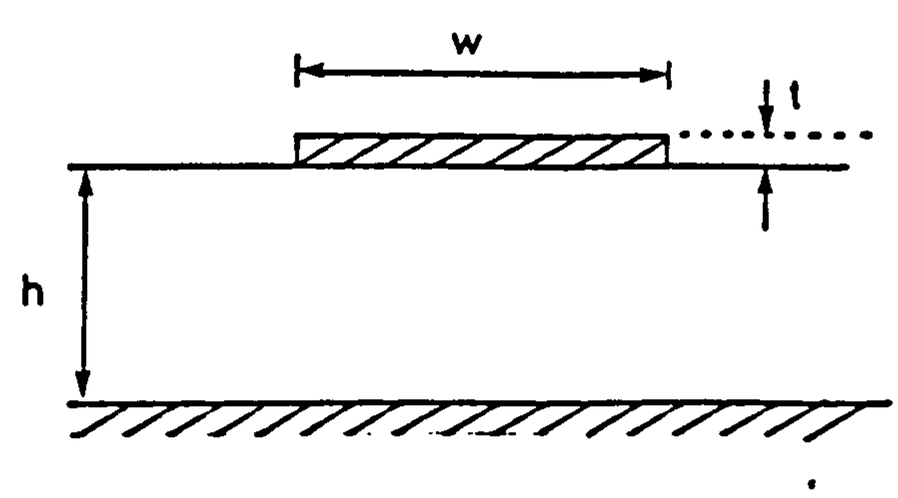

Figure 3.20 Microstrip with finite metallization thickness

The expressions are quoted below:

$$w'/h = w/h + (1.25\ t/\pi h)\{1 + \ln(x)\} \qquad \langle 3.87 \rangle$$

where $x = 4\pi w/t$; for $w/h \leqslant 1/2\pi$

or $x = 2h/t$; for $w/h \geqslant 1/2\pi$

It is assumed that the error in the assessment of this second order effect due to the modest substrate anisotropy has insignificant impact on the overall uncertainty.

From <3.87> the change in width to height ratio for a 0.05mm wide line on a 0.635mm thick substrate with $4\mu m$ thick metallization is:

$$(w' - w)/h = 0.015$$

and for w/h > 1.6 the offset, which is then independent of width, is:

$$(w' - w)/h = 0.017$$

and is, therefore, of reducing consequence as w/h increases. In order to simplify the presentation of the results this correction has been applied (negatively) to the measured velocity producing results that are effectively those of a zero thickness microstrip. This is indicated in the results graphs by an arrow wherever the offset is significant.

3.5.4 Dispersion Effects

Due to the ability of the mixed dielectric structure of microstrip to support higher order modes with differing velocity factors, the velocity of propagation along the micrstrip is frequency dependent. The analysis of chapter 2 was quasi-static, based on the assumption of TEM mode propagation, which becomes progressively inadequate as frequency increases. For frequencies at which the wavelength is small compared to the lateral dimensions of the microstrip structure, the deviation from TEM conditions is, however, small and easily accommodated by a correction factor.

Getsinger's [11] work' based on a longditudinal-section electric (LSE) mode on a transmission line model representing microstrip, is summarised in the simple expressions included below.

$$\epsilon_{eff} = \epsilon_r - [\epsilon_r - \epsilon_{effo}]/[1 + G(f/f_p)^2] \qquad \langle 3.88 \rangle$$

where $f_p = Z_o/2\mu_o h$, $\mu_o = 4\pi * 10^{-7}$ H/m

$G = 0.6 + 0.009Z_o$

ϵ_{effo} = effective relative permittivity from quasi-static analysis

ϵ_r = relative permittivity of substrate.

For an isotropic alumina (ϵ_r=9.8) substrate this yields the figures of

table 3.2, expressed also terms of velocity via the relationship:

$$v = v_o/\sqrt{\epsilon_{eff}}\ , \quad v_o = 2.998*10^8\ \text{m/s} \qquad \langle 3.89 \rangle$$

TABLE 3.2 DISPERSION FOR 50.0HM MICROSTRIP ON ALUMINA (h = 0.635mm)

Frequency (GHz)	Effective Permittivity	Velocity of Propagation
0	6.5514	$1.1713*10^8$
1	6.5549	$1.1709*10^8$
2	6.5652	$1.1701*10^8$
3	6.5824	$1.1685*10^8$
4	6.6061	$1.1664*10^8$
5	6.6360	$1.1638*10^8$

Edwards and Owens [12] have adapted Getsinger's work to cover microstrip on a sapphire substrate. Their empirical expression for G in <3.88> is quoted here:

$$G = [(Z_o - 5)/60]^{1/2} + 0.004Z_o \qquad \langle 3.90 \rangle$$

The parameter, ϵ_r in <3.88> is replaced by an equivalent isotropic relative permittivity obtained from a companion paper [2]. This expression can be rearranged to give a result in terms of relative velocity decrease, thus:

$$v'/v = \sqrt{\epsilon_{effo}/\epsilon_{eff}} = \{G(f/f_p)^2\epsilon_r/\epsilon_{effo}+1\}^{-1/2}\{1+G(f/fp)^2\}^{1/2}$$

Table 3.3 records some values for a frequency of 2.5GHz, being the approximate resonant frequency of the microstrip lines on 0.635mm thick sapphire with the C-axis normal to the substrate face.

TABLE 3.3 DISPERSION FOR MICROSTRIP ON SAPPHIRE (h=0.635mm,f=2.5GHz)

w/h	ϵ_{effo}	ϵ_{req}	Z_o (Ohm)	ϵ_{eff}	v' ($*10^8$ m/s)	v'/v (%)
0.125	6.522	10.80	97.76	6.534	1.1728	-0.088
0.5	6.965	10.96	63.26	6.985	1.1344	-0.140
1.0	7.391	11.10	46.60	7.419	1.1007	-0.186
4.0	8.806	11.40	19.51	8.866	1.0068	-0.342
10.0	9.718	11.50	10.17	9.805	0.9574	-0.447

3.5.5. Microstrip Geometry

Since the property of the microstrip being measured is a function of the physical cross sectional geometry (w/h) it is imperative that tolerances in the dimensions be taken into account. Furthermore, since the velocity of propagation is related to the resonant frequency by the physical length of the microstrip it must also be accurately determined. Measurement of the length is easily achieved using a travelling microscope with an estimated accuracy of +0.02mm, giving rise to an error of 0.086% in velocity determined from a 23.35mm long resonator.

Width (w) and thickness of the substrate (h) may vary along the line. Width of the strip can be controlled to a 5μm tolerance by normal thin film processing techniques. Thickness variations across the substrate, usually referred to as camber, were estimated at 10μm. The average of three micrometer readings was used as the value of h. The worst case error in w/h is then:

$$E_{woh} = w + \Delta w/w + h + \Delta h/h \qquad \langle 3.91 \rangle$$

Orientation of the substrate with respect to the sapphire crystal is considered ideal.

3.5.6. Summary

The error contributions discussed above are summarised for two cases in Table 3.4. Errors in the value of strip width and metallization thickness are best accommodated by offsets in the x-axis of results graph (figure 3.23). For the purpose of comparison, however, they are expressed in the table as velocity error. Values of slope of velocity with w/h were estimated as 0.14 for $0.1 < w/h < 0.2$ and 0.52 for $0.5 < w/h < 2.0$.

TABLE 3.4a CONTRIBUTIONS TO ERROR IN VELOCITY DETERMINATION
(expressed as a percentage of true velocity)

CASE	APPROXIMATIONS				MEASUREMENT		MICROSTRIP			
	$\tanh\alpha l = \alpha l$	$\alpha l \cot\beta 1 = 0$	$\tan\theta = \theta$	$(\omega CR)^2 = 0$	Phase	Ampl.	Metal Thick	Disp.	w/h	length
1	0.0006	0.007	0.0082	0.099	.0096	0.007	0.09	0.19	0.08	0.08
2	0.006	0.20	0.074	0.27	0.034	0.24	0.24	0.09	0.99	0.08

TABLE 3.4b DESCRIPTION OF CASES IN TABLE 3.4a

CASE	Z_o	w/h	l	α	f/f_o	$\check{\rho}$	h
	Ohm		mm	dB/m	%		mm
1	50	1.0	25	3	-1.0	0.8	0.635
2	90	0.1	25	30	-3.0	0.89	0.635

The two cases assessed are intended to be representative of 'wide'

and 'narrow' lines respectively. Even with an extremely severe line loss of 30dB/m (Q_U = 18.2) the accuracy should be better than 1%, except for the factor relating to the cross-sectional uniformity of very narrow microstrip. Most error contributions and could be compensated. With the exception of thickness and dispersion effects, this has not been considered worthwhile.

In case 1 the objective of 0.2% accuracy seems to be broadly attainable. For case 2 the accuracy is just acceptable for the purpose of assessing the quality of the anisotropic microstrip analysis.

3.6 RESULTS

3.6.1 Isotropic (Alumina) Substrates

Initial experiments with the short circuit resonator method were conducted using alumina substrates, thus excluding anisotropy considerations from the assessment of the technique. Measurements were made for a number of values of coupling to give increased confidence in the results. A typical set of results is presented in Table 3.5a. Table 3.5b records the unloaded (true) resonant frequency and loss for all combinations of the measurements

.

TABLE 3.5a MEASUREMENTS OF 50OHM MICROSTRIP RESONATOR ON ALUMINA

Ident	Meas. Res. Freq. (GHz)	Max R.L. (dB)	Min Rho
I	2.29518	1.45	0.8463
J	2.29246	1.92	0.8017
K	2.30001	0.80	0.9120
L	2.30334	0.43	0.9517

TABLE 3.5b RESULTS COMPUTED FROM TABLE 3.5a

Ident	Loss (dB/m)	Corr. Res. Freq. (GHz)
J & I	2.498	2.31334
I & K	2.686	2.31402
K & L	2.137	2.31249
J & K	2.616	2.31383
J & L	2.454	2.31315
I & L	2.440	2.31312
Mean	2.472	2.31333
Stand.Dev	0.174	0.5×10^{-3}

From these result for a 25.4mm long resonator the velocity of propagation is $1.1752*10^{8}$m/s with a variability (3σ) of 0.065%. This compares well with the analysis that yields a value of $1.171*10^{8}$m/s.

Other alumina samples bearing strips of two different widths (0.1 and 0.61mm) have been made. In all these cases the measured loss was considerably higher and, as may be expected, the standard deviation of the frequency measurements was somewhat greater. The results obtained are recorded in Table 3.6 and plotted on the graph of figure 3.21, which also displays curves obtained from the program GREEN for a nominal dielectric constant of 9.8 and ±2% deviation from nominal.

TABLE 3.6 RESULTS FOR MICROSTRIP ON ALUMINA

MICROSTRIP			CALCULATED		MEASURED			
Ident.	Width (mm)	w/h	Z_o Ohms	Vel. $*10^8$m/s	Vel. $*10^8$m/s	3σ Vel.	loss dB/m	3σ Loss
1	0.61	0.961	50.46	1.171	1.1752	0.07%	2.47	22.1%
2	0.61	0.961	50.46	1.171	1.1596	0.19%	30.07	16.3%
3	0.61	0.961	50.46	1.171	1.1618	0.33%	22.34	29.0%
4	0.10	0.157	96.18	1.225	1.2434	0.26%	61.70	15.3%
5	0.10	0.157	96.18	1.225	1.2196	0.16%	56.53	10.2%

$\epsilon_r = 9.8 \pm 2\%$, h = 0.635

These excessively high losses suggest that an error occurred in processing, whereby the plating thickness was much less than the 3um minimum specified.

Since the method of Bianco and Parodi [6], involving the reflection coefficient measurement of 4 open circuit lines, was incorporated in the microstrip network analyser calibration scheme of Chapter 6, results were also obtained by this method. Using two sets of open circuit lines, results were collected over the frequency range 1 to 5 GHz, and are presented in figure 3.22. Also plotted is a dispersion curve after Getsinger [11]. Whilst some evidence of a trend associated with dispersion is apparent, the dominant feature is an offset of ~2% between the results obtained from the two substrates. This indicates that the dielectric constants of the substrate must be near the extremes of the tolerance band. A measurement of an additional substrate similar to "B" was then conducted using the same technique (although over a reduced band of frequencies) and the results obtained showed a reduced offset compared with those of figure 3.22. Results recorded for each

substrate at 2.5 GHz are plotted on figure 3.21 and demonstrate acceptable correlation with those obtained by the half-wavelength short circuit resonator technique. The measurements of line loss are presented, along with those from sapphire substrates, in figure 3.24.

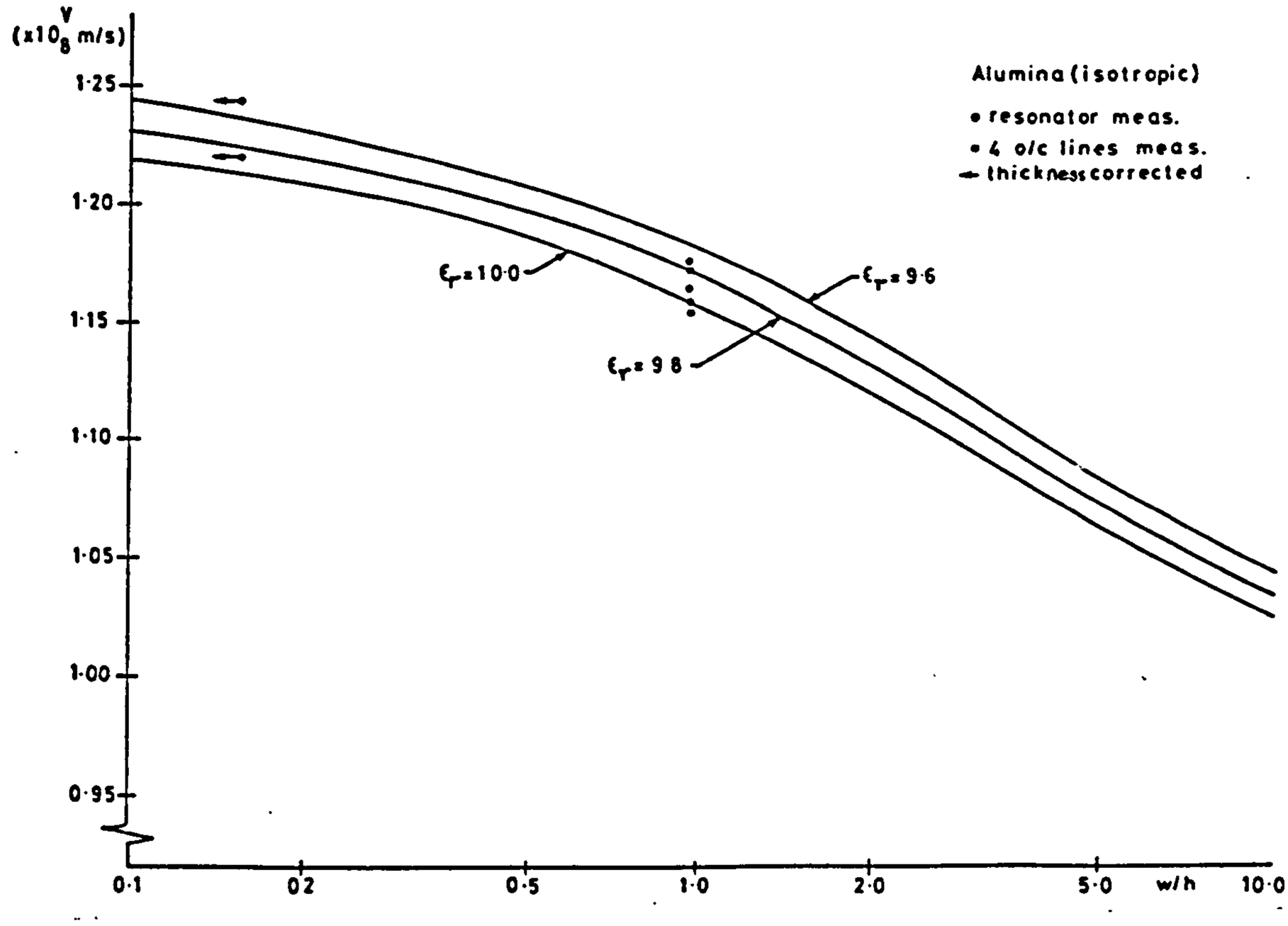

Figure 3.21 Results of microstrip velocity measurements on an Alumina substrate compared with analysis

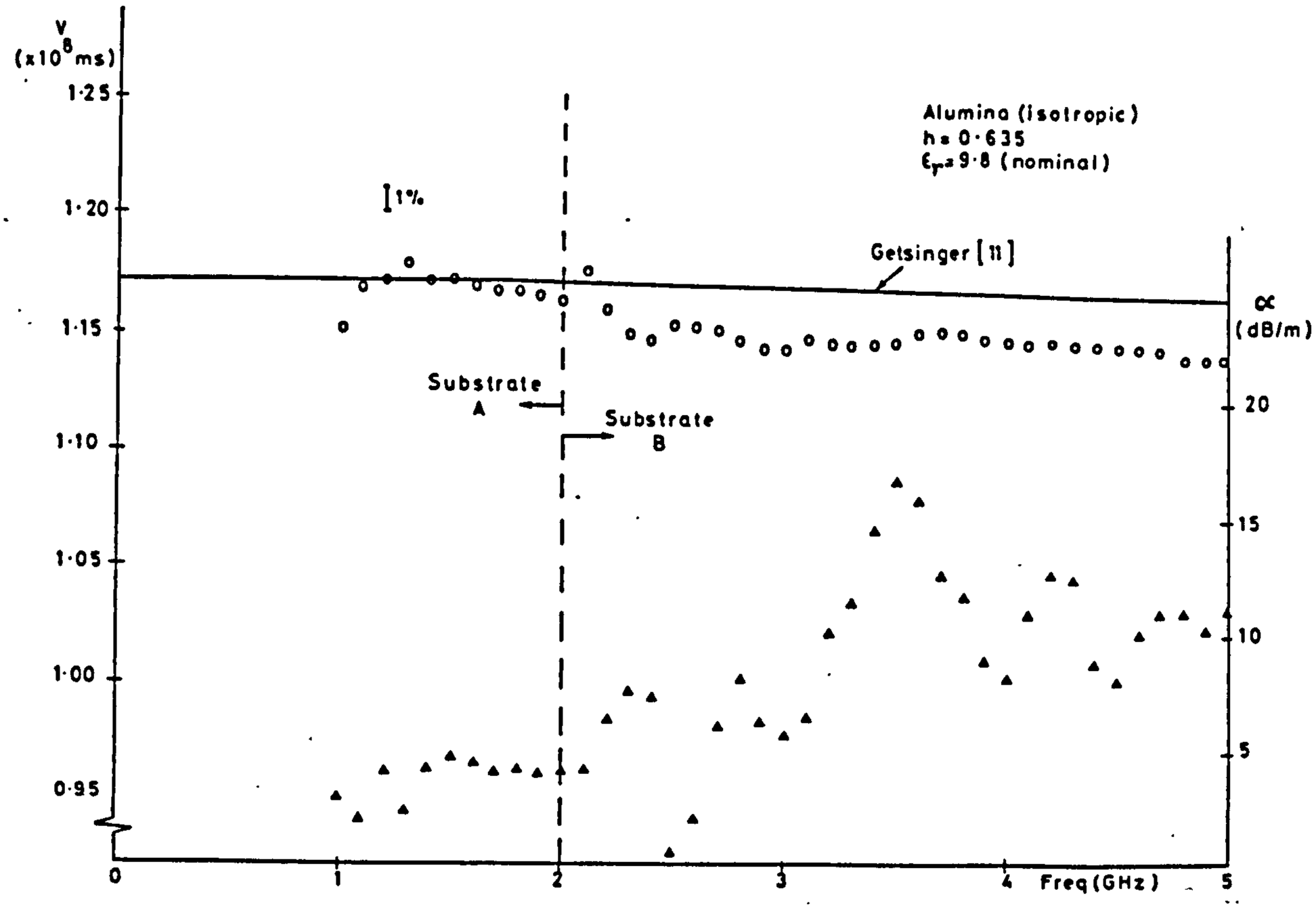

Figure 3.22 Results from microstrip velocity measurements on an alumina substrate by the 4 open circuit lines technique

3.6.2 Anisotropic (Sapphire) Substrates

A set of resonators, having various strip widths were prepared on the 0.635mm nominal thickness sapphire samples cut with the substrate face perpendicular to the C-axis. The results are recorded alongside values obtained from the analysis of Chapter 2 in table 3.7 and plotted on the graph of figure 3.23. Two results obtained from resonators on 0.254mm (0.010") nominal thickness sapphire substrates, similarly prepared, are also presented, identified by Greek characters.

A few samples of sapphire substrates, cut with the C-axis parallel to the substrate face, were acquired, courtesy of the Hewlett-Packard company. Referring to figure 3.1 the orthogonal relative permittivities are $\epsilon_n = \epsilon_y = \epsilon_z = 9.4$, $\epsilon_t = \epsilon_x = 11.6$. Measurement of resonators,

patterned on these precoated (including a Tantalum Nitride resistive layer), 0.635mm thick substrates, are also recorded, identified by lower case characters. Corrections for metallization thickness (referred to the zero thickness conductor case) are indicated, where significant, by small arrows in figure 3.23. Measurements of the line attenuation are presented in figure 3.24, where the bars signify the 3σ spread in the results obtained from all combinations of five coupling conditions.

TABLE 3.7 RESULTS FOR MICROSTRIP ON SAPPHIRE

MICROSTRIP				CALCULATED		MEASURED			
Ident.	h mm	w mm	w/h	Z_o Ohms	Vel $*10^8$ m/s	Vel. $*10^8$ m/s	3σ Vel	Loss dB/m	3σ Loss
A	0.686	0.15	0.219	84.04	1.1636	1.1847	0.26	26.45	21.66
B	0.648	0.18	0.278	78.06	1.1571	1.1742	0.24	21.60	21.22
C	0.635	0.21	0.331	73.71	1.1518	1.1674	0.27	17.62	28.82
D	0.640	0.43	0.672	56.23	1.1243	1.1376	0.27	13.10	29.10
E	0.648	0.74	1.143	43.85	1.0962	1.0988	0.20	10.36	24.32
F	0.655	2.03	3.098	23.61	1.0282	1.0226	0.134	4.457	22.28
G	0.660	3.52	5.330	15.68	0.9918	0.9851	0.129	3.917	24.43
H	0.635*	1.03	1.622	36.03	1.0736	1.0598	0.29	19.93	25.8
I	0.635*	1.03	1.622	76.03	1.0736	1.0717	0.170	2.70	39.9
o	0.254*	1.03	4.016	19.28	1.0097	1.0086	0.236	16.70	27.0
B	0.254*	3.52	13.85	-	-	0.9344	0.136	2.313	33.6
a	0.635*	0.43	0.677	58.79	1.1791	1.2058	0.137	41.92	9.11
b	0.635*	1.03	1.622	38.49	1.1470	1.1524	0.196	31.56	14.35
c	0.635*	3.52	5.543	16.62	1.0812	1.0240	0.337	16.65	33.69

* nominal (unmeasured) substrate thickness

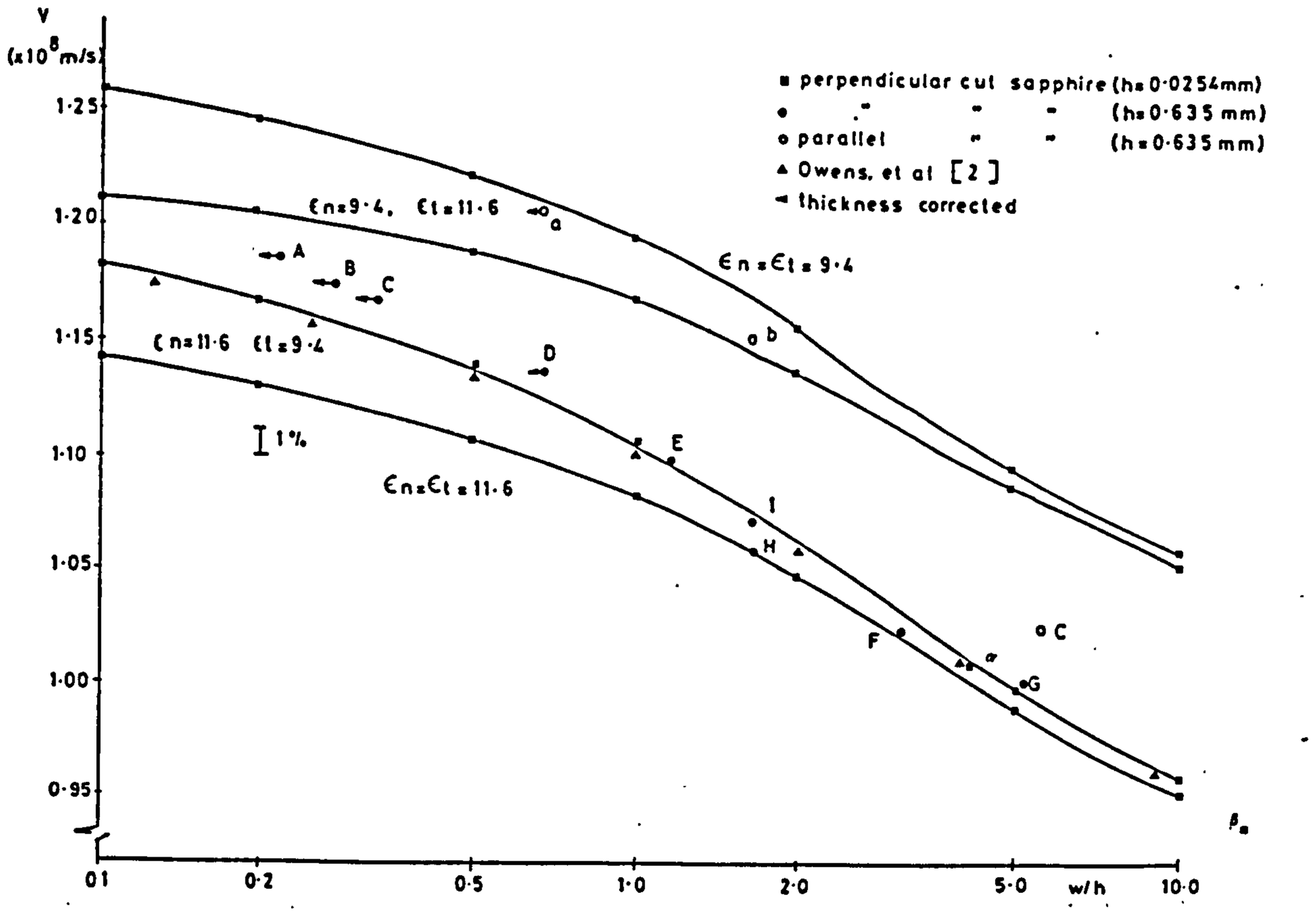

Figure 3.23 Results of microstrip velocity measurements on a Sapphire substrate compared with analysis

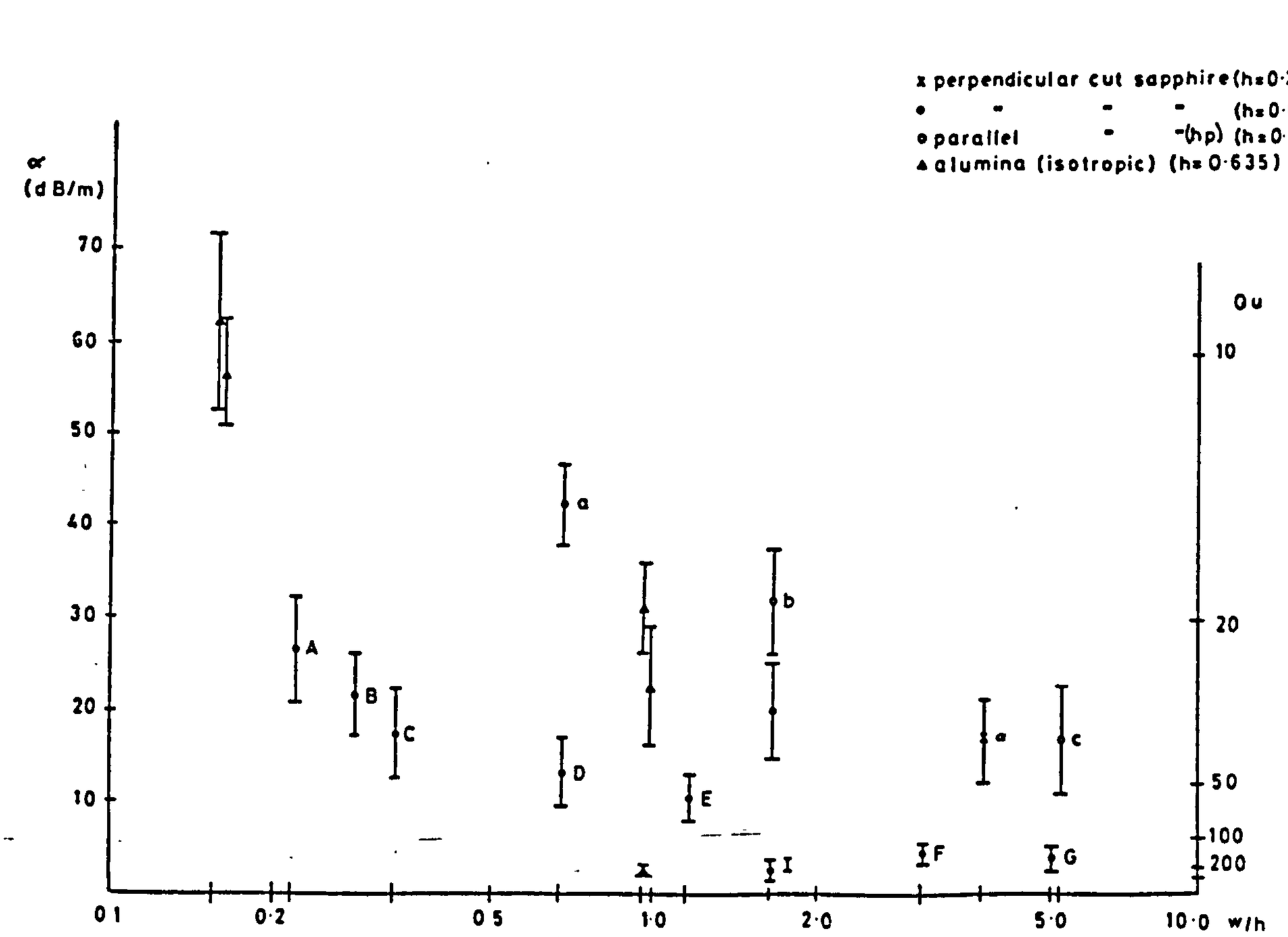

Figure 3.24 Measured microstrip loss of resonators on alumina and sapphire substrates

3.6.3 Discussion of Results

The results for the perpendicular cut sapphire show broad agreement with the analysis of chapter 2 and the work of Owen, et al [2]. Indeed for width to height ratios greater than unity the agreement is excellent, with the exception of point "H". Compared with the other measurements on 0.635mm sapphire the loss of resonator "H" was anomalously high; hence an additional resonator labelled "I" was introduced with a consequent improvement in both attenuation and velocity results.

For lower width to height ratios, the agreement deteriorates with a deviation of up to 1.5%. It has already been indicated that results for narrow lines would be more in error than for wide, related in part to the high line attenuation; confirmed by the results in figure 3.24. The discrepancies do, however, appear consistent and marginally significant when assessed against the error budget of section 3.5.

Whilst the greatest weakness in the analysis is surely the lack of a rigorous treatment for the finite conductor thickness on the anisotropic substrates, it does seem unlikely that this source of error alone could account for the deviation observed. Nevertheless the sense of the discrepancy and its dependance on track width is consistant with an underestimate of this effect. No other physical explanation is offered. The modest deviation outside the predicted error bounds did not merit the substantial additional work involved in attempting to isolate the effect.

But for the parallel cut sapphire substrates the outcome is less satisfactory. Only point "b" is within 1% of the theoretical curve and the result for resonator "c" approaches the prediction for perpendicular cut sapphire substrates. This fact suggests that the orientation may be in doubt. The proximity of point "a" to the isotropic $\epsilon_r = 9.4$ case

could also be explained if the C-axis were aligned with the strip.

Accepting uncertainty in the sapphire crystallographic orientation any result within the bounds defined by the isotropic $\epsilon_r = 9.4$ and the anisotropic $\epsilon_n = 11.6$, $\epsilon_t = 9.4$ cases, could be regarded as valid. Unfortunately, it is difficult to verify the crystal orientation in a thin sheet sample and no further samples were available.

Note the higher loss associated with these resonators which may be attributed to the resistive TaN layer of the nominal 50 Ohm/square value. As observced previously the potential for error is increased by loss and therefore these results must be less reliable than those for the perpendicular cut sapphire.

In conclusion the results from the measurement for the most part confirm the theory of chapter 2 with an error of less than 1% except for narrow strips. There is some evidence that the effect of strip metallization thickness may be more substantial than published work on the isotropic case suggests, and could account for the greater discrepancies associated with the narrower strips.

3.7 REFERENCES

[1] OLYPHANT,M., DEMENY, D.D. & NOWICKI,T.E.: "Epsilam-10: A new high dielectric constant conformable copper-clad laminate" CU-tips No. 6, 3M Company. 1976.

[2] OWENS,R.P., AITKEN,J.E. & EDWARDS,T.C.: "Quasi-static characteristics of microstrip on an anisotropic sapphire substrate". IEEE Trans **MTT-24**, No. 8, August 1976, pp 499-505.

[3] FONTANELLA,J., ANDEEN,C. & SCHUELE,D.: "Low-frequency dielectric constants of o -quartz, sapphire, MgF2 and MgO" Jnl. Appl. Phys., 45, No.7, July 1974, pp 2852-4.

[4] ROYAL SIGNALS: "Handbook of Line Communication". Vol.1, HMSO, 1947, p 718.

[5] MIDDLETON,J. & DAWE, C.: Private Communication. (Marconi Instruments Limited.)

[6] BIANCO, B. PARODI, M., RIDELLA, S. & SELVAGGI, F.: "Launcher and Microstrip characterisation", IEEE Trans IM-25, 1976, pp 320-3.

[7] SUCHER,M. & FOX,J.: "Handbook of Microwave Measurements". 3rd Ed. Vol.II., Wiley. 1963, New York. pp 417-493.

[8] RICHINGS,J.G.: "An accuracte experimental method for determining the important properties of microstrip transmission lines", Marconi Review, 4th Qtr., 1974, pp 209-215.

[9] MEHMET, K., McPHUN, M.K. & MICHIE, D.F.: "Simple resonator method for measuring dispersion of microstrip", IEE Electron. Lett. 8, 1972, pp 165-6.

[10] BAHL,I.J. & GARG, R.: " Simple and accurate formulas for a microstrip with finite strip thickness", Proc IEEE, 65, No.11, Nov 1977, pp 1611-2.

[11] GETSINGER, W.J.: "Microstrip dispersion model", IEEE Trans. MTT-21, No.1, Jan 1973, pp 34-9.

[12] EDWARD,T.C. & OWENS,R.P.: "2-18GHz dispersion measurements on 10-100Ohm Microstrip lines on sapphire", IEEE Trans. MTT-24, No.8, August 1976, pp 506-13.

[13] MARCHENT, B.G.: "Interactive computer programs for the computer aided design of linear microwave circuits", Ph.D. Thesis, University of Warwick, 1973.

CHAPTER 4

MICROSTRIP DISCONTINUITIES

4. MICROSTRIP DISCONTINUITIES

In chapter 2 the analysis of microstrip transmission lines was based on the assumption of uniformity: the lateral dimensions of the structure were assumed constant with displacement along this line. Whilst the principle application of most transmission lines is the conveying of microwave energy from one point in space to another, microstrip is frequently used as a circuit element. It may be used to form reactive elements or impedance transformers in filters or matching circuits. In such applications the uniformity of the microstrip is limited in extent. Junctions between two or more microstrip lines of differing characteristic impedance, abrupt open circuit ends and rectangular lands for component attachment are commonly encountered. In each case the substantially 2-dimensional field pattern of the uniform microstrip acquires a third dimension.

At least initially, microwave circuit design is conducted in terms of nodally connected, well defined lengths of uniform transmission lines. If the effects associated with the non-ideal behaviour of discontinuities in the transmission structure are not taken into account, significant discrepancies between the design and achieved performance are likely to occur [1].

Full and general electro-magnetic analysis of such structures would involve far too much computational resource to be appropriate for most design tasks, particularly if circuit optimisation techniques are to be employed. For this purpose lumped equivalent circuit models are usually employed. A volume of work on the derivation of suitable models for microstrip discontinuities has been presented [2-23]. None of these results pertains directly to microstrip on an anisotropic substrate.

This chapter presents a pragmatic approach to the assessment of some discontinuities in a manner that is applicable to the anisotropic substrate case. The quasi-static assumption of chapter 2 will continue to prevail in the following discussion.

4.1 EQUIVALENT CIRCUITS FOR ISOTROPIC DIELECTRIC SUBSTRATES

Since, in general, the distribution of both electric and magnetic fields are perturbed at a discontinuity any comprehensive equivalent circuit must include both capacitive and inductive elements. Figure 4.1 illustrates a small set of microstrip discontinuities together with their corresponding equivalent circuits.

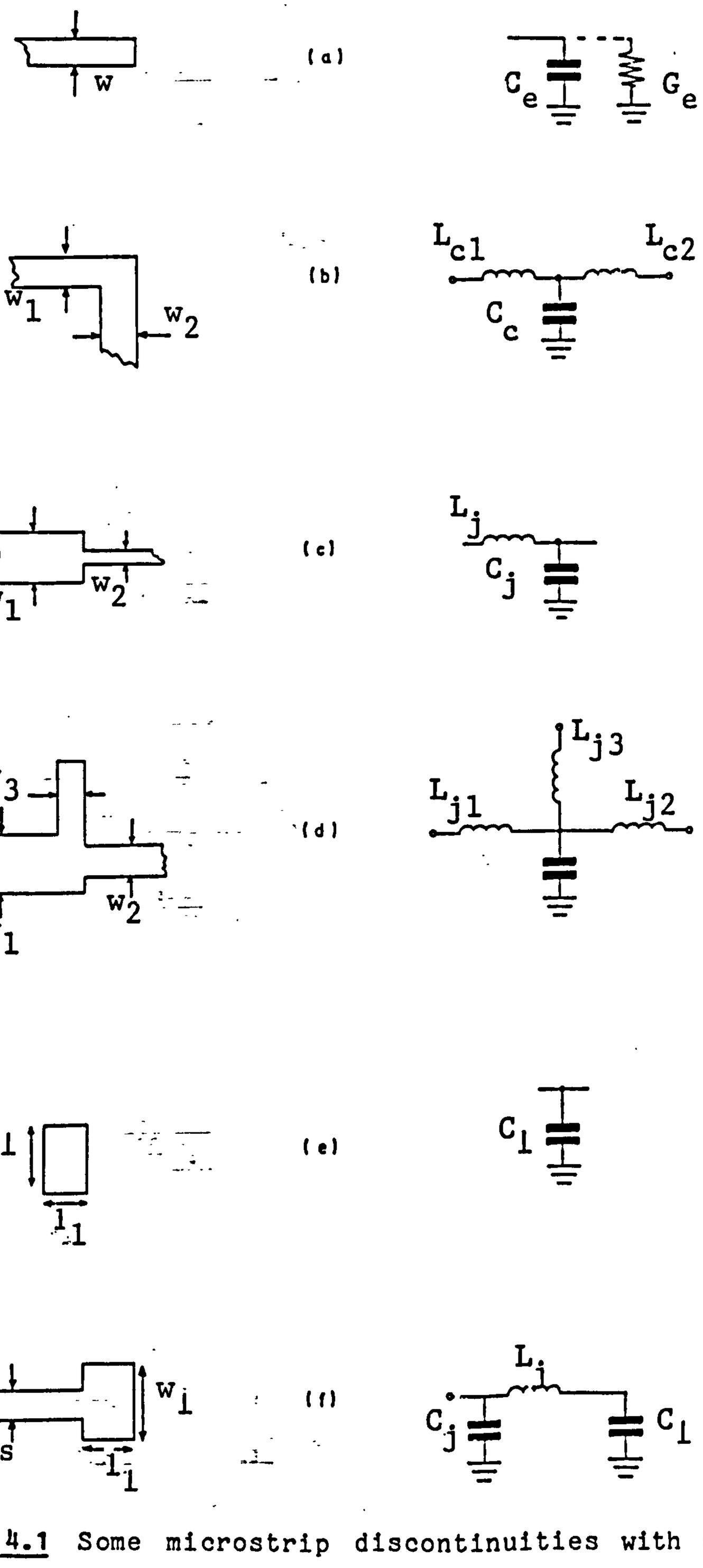

Figure 4.1 Some microstrip discontinuities with equivalent circuits: a) open circuit, b) corner, c) step junction, d) 3-way junction, e) isolated land, f) connected land

4.1.1 Open Circuit End

The open circuit end (figure 4.1a) has a simple capacitive equivalent circuit. Since no current can flow in an open circuit, there exists no magnetic field for the discontinuity to affect. The end effect capacitance represents the electric fringing field at the abrupt end of the microstrip line.

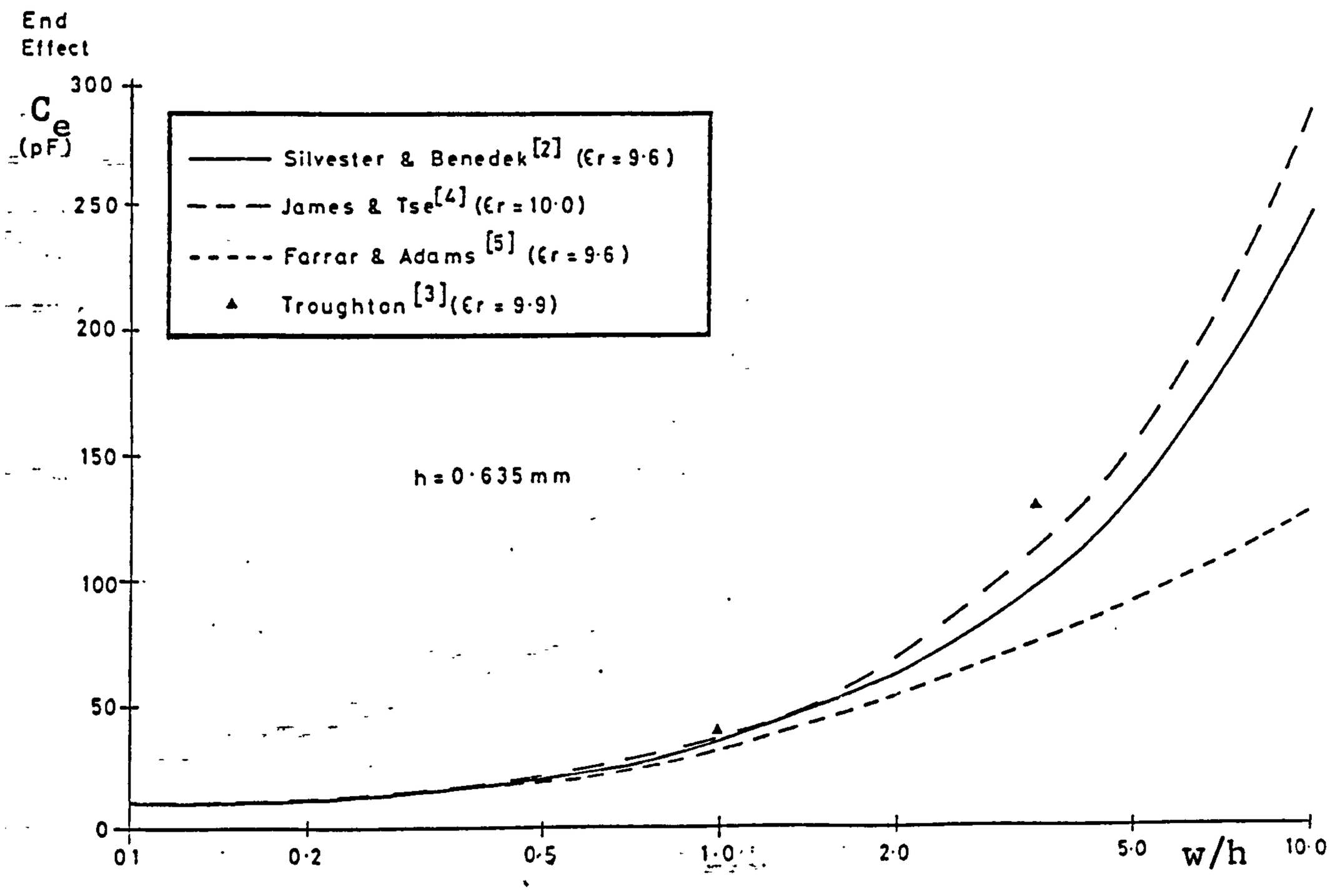

Figure 4.2 Published results for open circuit end effect

Figure 4.2 illustrates the results from a number of contributions to the literature. It can be seen that with one exception there is broad agreement in the data for microstrip lines of characteristic impedance close to 50 Ohm. Clearly the end effect capacitance would be expected to increase with track width and thus with a fall in characteristic impedance.

This variation is so pronounced it is convenient to normalise the data by defining an equivalent line extension as shown in figure 4.3.

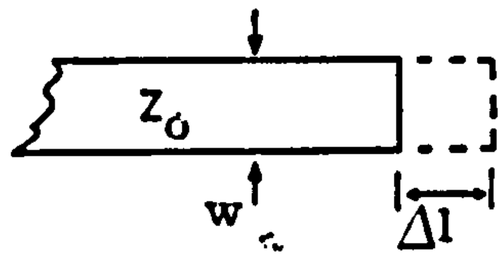

Figure 4.3 Equivalent end extension to account for open circuit end effect.

This end extension is given by:

$$\Delta l = \{v/w\}\tan^{-1}(wC_e/Y_o) \qquad \langle 4.1a \rangle$$

and, if $wC_e << Y_o$

$$\Delta l = vC_e/Y_o \quad \text{or} \quad \Delta l \simeq C_e/C \qquad \langle 4.1b \rangle$$

where v is velocity of propagation of the microstrip

Y_o is the characteristic admittance of the microstrip

C is the capacitance/unit length of the microstrip.

Expressing the end effect in this manner allows the effect to be accommodated in circuit design simply by foreshortening open circuit lines by Δl. Some of the results from figure 4.2 have been transformed to this form and are presented in figure 4.4. These results indicate a "rule-of-thumb" figure for open end effect could be h/3. This figure holds reasonable well for all widths within a 2:1 range of the 50 ohm characteristic impedance and for relative dielectric contents above 4.0.

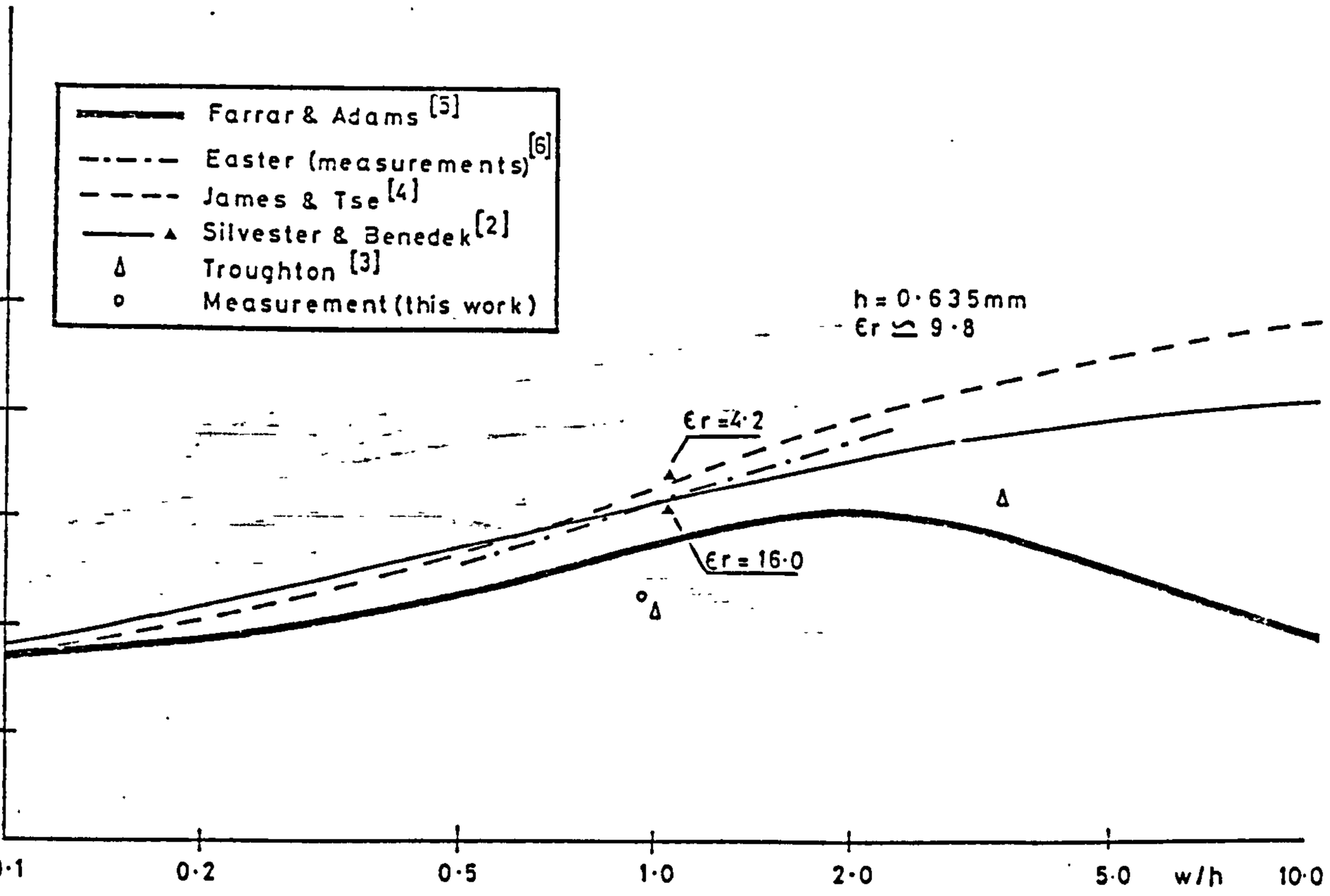

Figure 4.4 End effect results expressed as effective line extension.

A simple computer program to evaluate the curve fitted polynomial expressions of Silvester and Benedek named ENDEFFECT, has been written and is included in Appendix C.

Of these results the most convincing are those of James and Tse [4] and of Silvester & Benedek [2] are most convincing. The later work is adopted as the standard of reference in the following discussion.

Measurements of open end effect on an alumina substrate were made using a development of the resonator technique of chapter 3. In addition to the half-wavelength short circuit resonator, an open circuit microstrip line of twice the length was fabricated. With the coupling

point at the centre of the line the resonance occurs at a frequency for which the open circuit line is one wavelength long. In the absence of end effect the resonant frequency would be identical to that of the short circuit resonator. The end effect equivalent line extention can, therefore, be related to the difference between the two resonant frequencies.

$$\Delta l = l_{s/c}(f_{s/c}/f_{o/c}) - l_{o/c}/2 \qquad \langle 4.2 \rangle$$

The experiment was conducted for microstrip of two widths correponding to characteristic impedances of 50 (0.61mm) and 96 ohms (0.1mm). To obtain the unloaded resonant frequencies of the resonators the method of chapter 3 was applied. The pair of short and open circuit resonators were prepared from the same substrate and two sets for each strip width were produced. The results presented in Table 4.1 are the mean values from the duplicate measurements and have been plotted on the graph of figure 4.4.

For the reasons discussed in Chapter 3 the degree of uncertainty is much greater for the narrow microstrip. Given the differential nature of the technique the confidence level associated with the results for equivalent end extention is not great.

TABLE 4.1 END EFFECT MEASUREMENTS ON ALUMINA

w(mm)	w/h	$\Delta l/h$
0.1	0.157	0.31
0.61	0.961	0.22

4.1.2 Corners

A right-angle junction of two microstrips (figure 4.1b) is often necessary and introduces discontinuity effects. Both the electric and magnetic fields are perturbed by the abrupt change in the direction of propagation. Consequently inductive, as well as capacitive elements are necessary for complete characterisation of this discontinuity [7,13].

In design it is often desirable to minimise the effect of this discontinuity. Freqently the corner is necessary in a microwave hybrid circuit for topological reasons alone. Thus the right-angle junction is introduced into an otherwise matched, uniform transmission line.

Since the corner has a surfeit of capacitance [11,12] due to the extra periphery on the outside edge a simple expedient to compensate the discontinuity effect is to chamfer or mitre the corner. Various views on how much of the corner to remove have been expressed. [8,9] Most chamfers employed lie between two limiting cases, illustrated in figure 4.5.

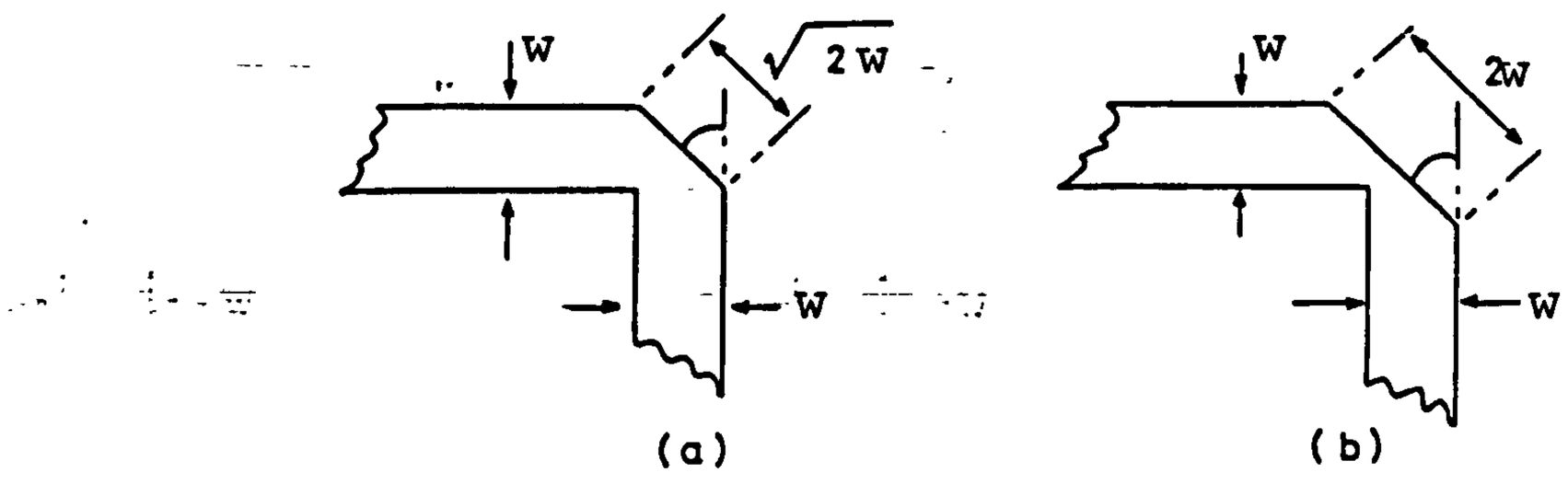

Figure 4.5 Frequently used mitres for compensated corners

It should be bourne in mind that removal of an area sufficient to cancel the discontinuity capacitance of the uncompensated corner would not result in optimum electrical compensation of the corner. The chamfering of the corner has little effect on the inductive component which results

from the current crowding on the inside of the corner. A residual excess capacitance, ΔC_c, such that the characteristic impedance of the lumped equivalent circuit, defined thus:

$$Z_c = \sqrt{2L_c/\Delta C_c} \qquad \langle 4.4 \rangle$$

where $L_c = L_{c1} = L_{c2}$

equals that of the microstrip line, will result in better compensation [19]

To be completely general any solution for the elements of the equivalent circuit must cope with a range of characteristic impedances (widths) for both lines entering the junction and with varying degrees of chamfering. Very little of the published material is that general. Anders and Arndt [19] have produced a useful set of graphs for arbitrary angle mitred bends and for uncompensated right angle junctions between dissimilar lines. Techniques for fully general frequency dependent analysis have been developed [8,14] and are supported by a suite of computer programs.

TABLE 4.2 EQUIVALENT CIRCUIT VALUES FOR UNCOMPENSATED RIGHT ANGLE CORNERS

w/h	L_c (pH)	C_c (fF)	Source
0.5	40.5	41.5	[6]
1.0	2.7	102.5	[6]
2.0	100.2	343.9	[6]
0.5	- 8.8	31.7	[7] & [12]
1.0	-13.4	99.9	[7] & [12]
2.0	92.7	322.5	[7] & [12]

$h = 0.635$, $\epsilon_r = 9.8$

4.1.3 Step Junctions

In matching circuit it is frequently necessary to join two lines of differing characteristic impedance (figure 4.1c). Again both magnetic and electric fields are perturbed by the abrupt change of microstrip width. Clearly, the edges perpendicular to the direction of propagation ($(w_1-w_2)/2$ on each side) contribute surplus fringing capacitance. Inductance results from the crowding of the current in the wider microstrip at the junction with the narrower line. On a uniform line the current distribution is approximately exponential in form being a minimum at the centre and rising to a peak value at each edge.

Table 4.3 lists some typical values for the equivalent circuit elements taken from the literature.

TABLE 4.3 EQUIVALENT CIRCUIT VALUES FOR A STEP JUNCTION DISCONTINUITY

h(mm)	ϵ_r	w_1/h	w_2/h	C_j(fF)	L_j(pH)	Source
1.5	2.3	2.93	8.8	-	290	[15]
1.5	2.3	2.0	9.0	1.21	-	[16]
1.5	2.3	2.0	0.1	24.1	-	[16]
0.635	9.6	1.0	0.1	13.2	-	[16]
0.635	9.6	1.0	3.0	27.7	72	[15]-[17]
0.635	9.6	1.0	5.0	71.4	140	[15]-[17]
0.635	9.6	2.0	0.1	33.5	-	[16]
0.635	9.6	2.0	0.5	19.7	20	[16]&[18]
0.635	9.6	0.5	2.0	38.9	49	[16]&[18]
0.635	9.6	0.5	10.0	218.7	-	[16]

It is interesting to compare the discontinuity capacitance of the step junction, C_j, with the open circuit end effect capacitance, C_e. The end effect capacitance for a microstrip line of width equal to the wider of the two lines entering the junction should represent a lower bound on the discontinuity capacitance for a large change in width.

4.1.4 Multi-Way Junction

The behaviour of a junction of three or more microstrip lines (figure 4.1d) is more complex. Before a useful equivalent circuit can be evaluated it is necessary to define the plane of connection for each line entering the junction. The simplest option is to define the connection planes at the first point of contact of each line with any of the others [20]. This leaves a residual area of conductor not part of any transmission lines which must be included in the discontinuity model. The equivalent circuit must account for the multi-port transmission behaviour of this "island". For design purposes it is often more convenient to absorb some of the discontinuity effects by moving the notional connection plane some way into the central island in a manner similar to the accommodation of open circuit end effect by foreshortening of the microstrip line (cf. Section 4.1.1).

The combination and permutations of the widths and disposition of the microstrip lines at the junction are almost limitless. Comprehensive analysis of multi-way junctions is outside the scope of this work and the reader is referred to the work of Wolff [14] and Menzel [21] which is supported by computer programs.

4.1.5 Isolated Lands

Although not truly a discontinuity, this feature, commonly encountered in microwave hybrid circuits, requires analysis techniques similar to those applied to the assessment of discontinuity effects [22]. Such a land (figure 4.1e) may be used to mount a chip component, the land being oversize on the component to allow bond wire attachment, or to realise a small value capacitance to ground. It could also be used as a capacitively coupled resonant element. For this discussion, however, only the case where the land may be regarded as a simple lumped capacitor (i.e. maximum dimension less than $\lambda/10$ at the highest frequency of interest) will be considered.

The capacitance of the land comprises two parts: the "parallel-plate" capacitance of the area of the land itself and the fringing field capacitance of the periphery. For structures meeting the "lumped" criterion at microwave frequencies the fringing field is invariably of significance and can, in some cases, account for the major part of the capacitance.

In many cases the land will be connected to a microstrip line as illustrated in figure 4.1f. The equivalent circuit will then include the elements of the step junction model but with values that may be somewhat different as a consequence of the small dimensions of the land. Depending largely on the nature of the component attached to the land, the inductive element may or may not be of importance. It is often acceptable to consider only the capacitive effects which can be estimated readily for an evaluation of the capacitance of the isolated land.

4.2 THE EFFECT OF SUBSTRATE DIELECTRIC ANISOTROPY

Just as dielectric anisotropy of the substrate affects the properties of uniform microstrip it will also modify the behaviour of discontinuities. A fully comprehensive analysis of arbitrary junctions on an anisotropic substrate would be rather intractable and the end result so computationally intensive or cumbersome to apply that it would find little favour with MIC designers. It is therefore desirable to find a method of relating the properties of the discontinuities for the anisotropic case to those of the isotropic situation for which much data already exists.

Since only the dielectric properties of the region have been affected by the change of substrate, the magnetic effects of the discontinuities are unchanged. Thus it is permissible to carry over the values for inductive elements of the equivalent circuits providing the conductor geometries are comparable. Only the capacitive elements need modification to take account of the generalisation to include dielectric anisotropy.

A further simplification stems from the restriction to a special case of dielectric orientation. The principle axes of the tensor permittivity are simply aligned with the substrate. For the case of a monocrystalline substrate, like sapphire, this corresponds to the cutting of the substrate with its major faces perpendicular to the principle crystalline axis (C-axis). This situation, illustrated in figure 4.6, is commonly adopted since it results in a dielectric constant in the plane of the substrate that is independent of direction ($\epsilon_x = \epsilon_z \neq \epsilon_y$)

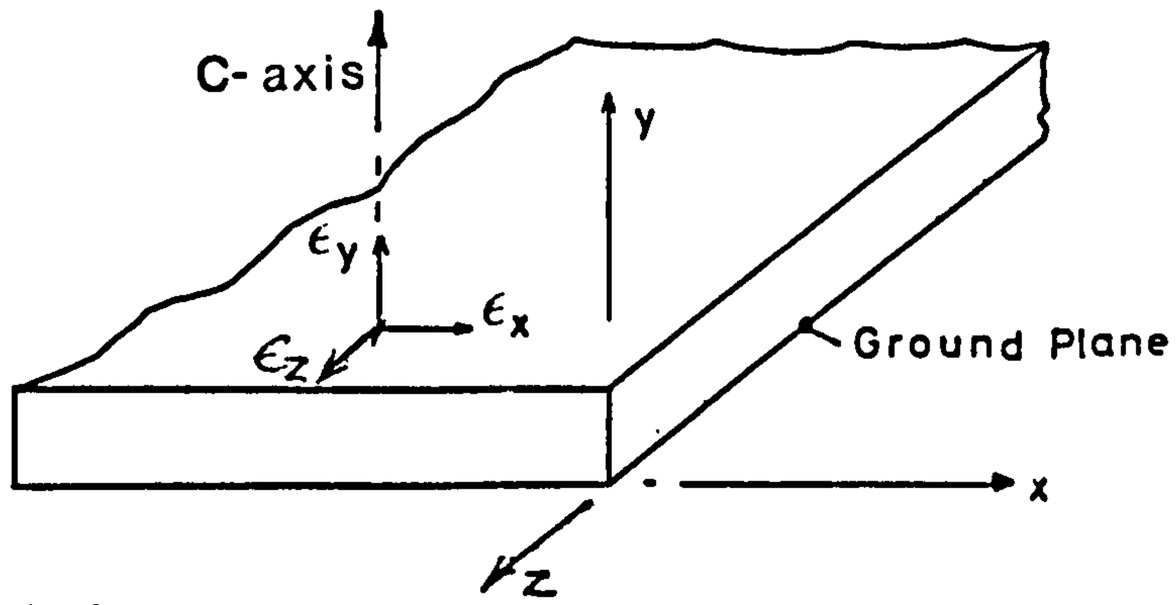

Figure 4.6 Assumed substrate dielectric orientation

With this assumption in force it is possible to establish a relationship between the isotropic and anisotropic situation. Consider the disposition of the electric field in the vicinity of a metallized area above a continuous ground plane (figure 4.7).

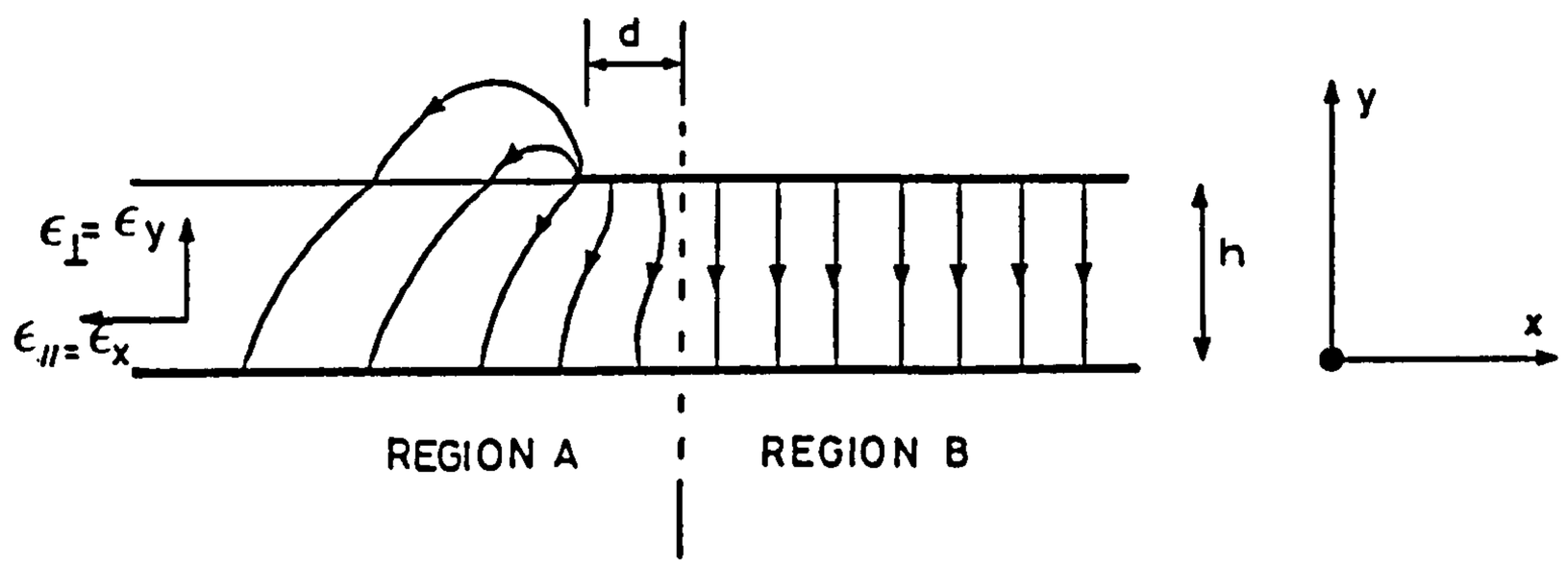

Figure 4.7 Electric field near the edge of a conducting area above a ground plane

Two regions can be identified: region A; near the edge of the metallized area where a complex fringing field exists, and region B; under the body of the metallized area, where a simple uniform field distribution prevails. The division between these two regions occurs a distance, d, from the edge of the metallized area, where d is of the same order as h, the substrate thickness. Consideration of this static field distribution is relevant to the microwave behaviour if h is small compared to the wavelength with the substrate dielectric (the quasi-static assumption).

Since the field under the conducting area (region B) is perpendicular to the substrate face only one component of the permittivity tensor is of

significance, i.e.:

$$D_B = \epsilon_o \epsilon_{||} E_B = \epsilon_o \epsilon_y E_B \qquad \langle 4.5 \rangle$$

Thus the capacitance per unit area is identical to that with an isotropic substrate of relative dielectric constant equal to ϵ_y. The difference between the anisotropic and isotrcpic situations is therefore confined to the fringing field at the periphery (region A). In the assessment of discontinuity capacitances one is largely concerned with the evaluation of fringing field.

The fringing field at the periphery of a metallized area is no different from that along one edge of a microstrip providing the line is wide enough to prevent the fringing fields on opposite edges interacting. This condition has been explained in section 2.4.1 and can be expressed thus:

$$w/h > 1$$

except possibly in cases of gross anisotropy.

In Chapter 2 the analysis of microstrip on an anisotropic substrate was discussed and the computer program, GREEN, described. This analysis can be used to quantify the capacitance per unit length relating to the fringing field along a straight edge

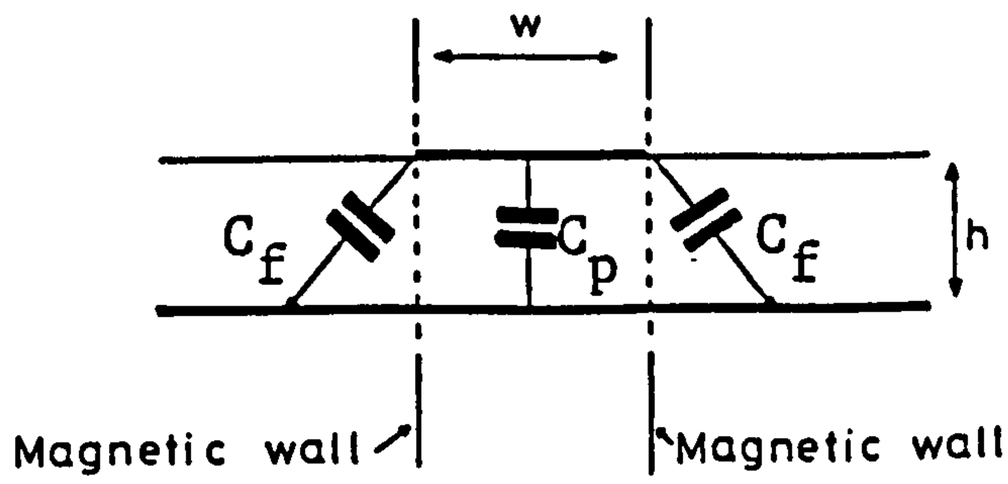

Figure 4.8 Notional model of microstrip for the evaluation of "fringing capacitance"

The capacitance per unit length of the microstrip is considered to comprise two components. The first is the "parallel-plate" capacitance of the strip, C_p, assuming perpendicular magnetic walls at its edges,

which is proportional to the strip width, w. The other component is that due to fringing field, $2C_f$ which is substantially independent of the strip width. Since the field is not ideally uniform within a distance, d, of the edge of strip as assumed for the definition of C_p, the "fringing capacitance", C_f, actually represents the deviation from uniformity occurring at the edge of the conductor. Using GREEN the total capacitance (per unit length) of the strip, C_μ, can be computed, enabling the "fringing capacitance" to be determined.

$$C_f = (C_\mu - C_p)/2 \qquad \langle 4.6 \rangle$$

$$\text{where} \quad C_p = \epsilon_y \epsilon_o w/h$$

The fringing capacitance can be evaluated for both the anisotropic situation, C_{fA}, and for a related isotropic case, C_{fI}, where the substrate permittivity equals ϵ_y, and the thickness, h, is consistent. The ratio, C_{fA}/C_{fI}, represents an adjustment factor that can be useful in the determination of discontinuity capacitances for the anisotropic case, given values obtained from work using isotropic substrate materials. Use of this factor does, however, involve identifying the portion of the discontinuity capacitance attributable to the fringing at the edges of the conductors. Capacitance due to the body of conductors can, of course, be carried over directly from the comparable isotropic case. Although strictly only applicable to straight edges, given the substrate-dielectric orientation specified, this adjustment factor should hold reasonable well for corners also.

One small problem arises: the fact that, due to computational inaccuracies, the value of the fringing field obtained from the modified version of GREEN is not constant above unity width to height ratio. This was discussed in Chapter 2 and it was demonstrated that the performance of GREEN was better than another comparable program. Nevertheless, it is not immediately obvious how to define a value for the interaction free

fringing capacitances. The dependance of fringing capacitance on w/h for 0.025" (0.635mm) alumina is plotted in figure 4.9 using a logarithmic scale. It is evident that there are two adjoining regions where the behaviour conforms to straight line relationships. In the lower region, the fringing capacitance is affected by interaction between the opposite edges of the microstrip whilst in the upper region it is supposed that variation is due to inadequate quantisation of the strip in the computation. The breakpoint is at w/h=0.6 and the value of the fringing capacitance at the intersection of the straight line is 41.5pF/m. This value is used as C_{fI} for alumina and values of C_f for other substrates, determined in a similar manner, are included in Table 4.4. Note how close are the values for the alternative orientations of sapphire

TABLE 4.4 VALUE OF FRINGING CAPACITANCE

ϵ_n ($=\epsilon_y$)	ϵ_t ($=\epsilon_x$)	C_{fI} (fF)	C_{fA} (fF)
9.4	9.4	40.7	-
9.4	11.6	-	44.4
9.6	9.6	41.5	-
9.8	9.8	42.3	-
10.0	10.0	43.0	-
11.6	9.4	-	44.8
11.6	11.6	48.9	-

h=0.635mm

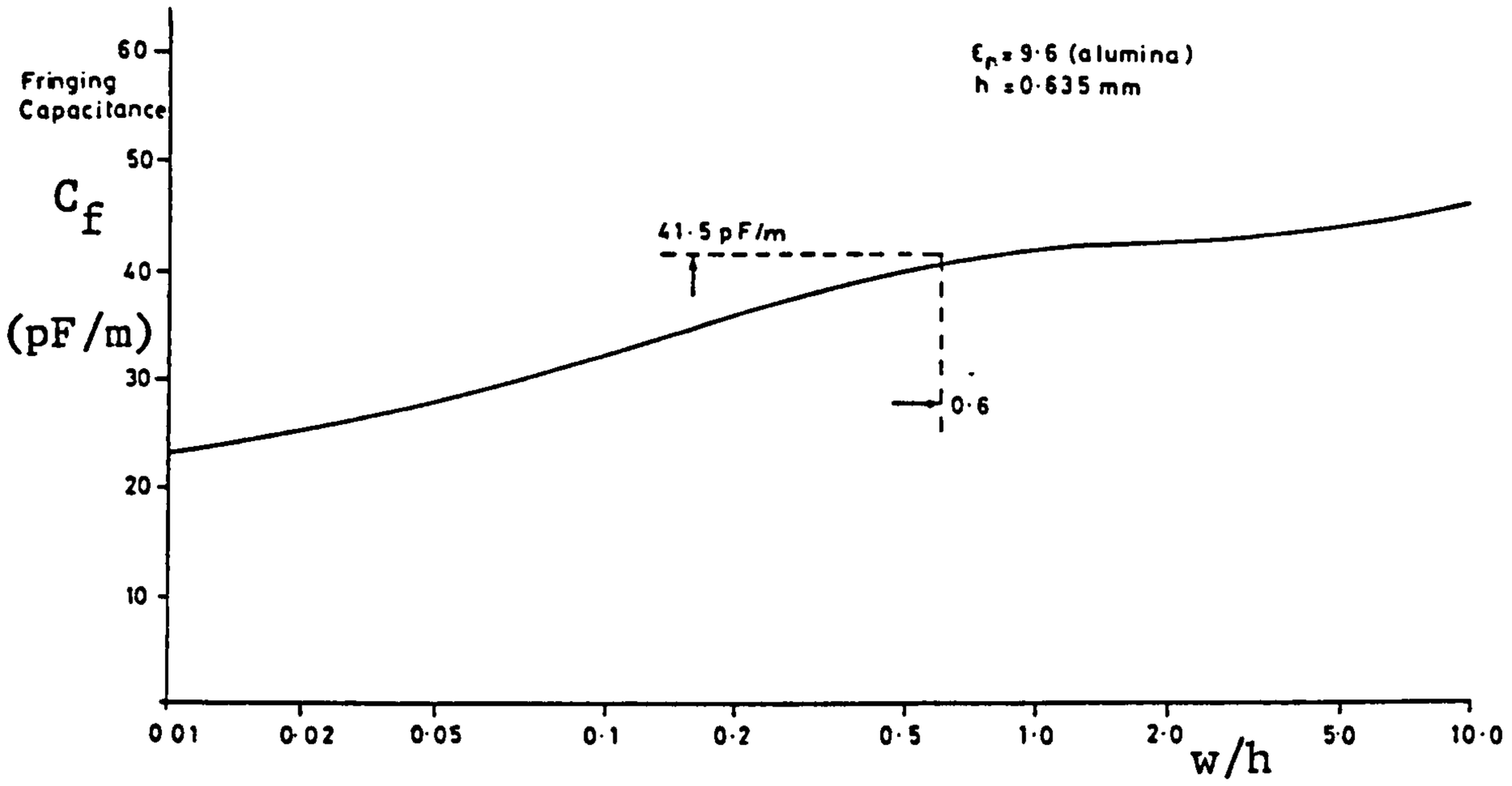

Figure 4.9 Fringing Capacitance (calculated by GREEN) against log(w/h)

The anisotropic adjustment factor has been evaluated for single crystal sapphire with the C-axis normal to the substrate face.

$$\frac{C_{fA}}{C_{fI}} = 0.915 \qquad \text{<4.7>}$$

for $\epsilon_x = \epsilon_z = 9.4$

$\epsilon_y = 11.6$

4.3 EVALUATION OF DISCONTINUITY CAPACITANCES FOR SOME SIMPLE STRUCTURES

The heuristic principles of the preceding discussion have been applied to a limited range of structures with both isotropic and anisotropic substrate dielectrics. The structures studied were those that required attention during the author's work on MIC amplifiers. They are presented here as examples of the pragmatic approach to discontinuity

evaluation presented in this chapter.

4.3.1 Open Circuit End

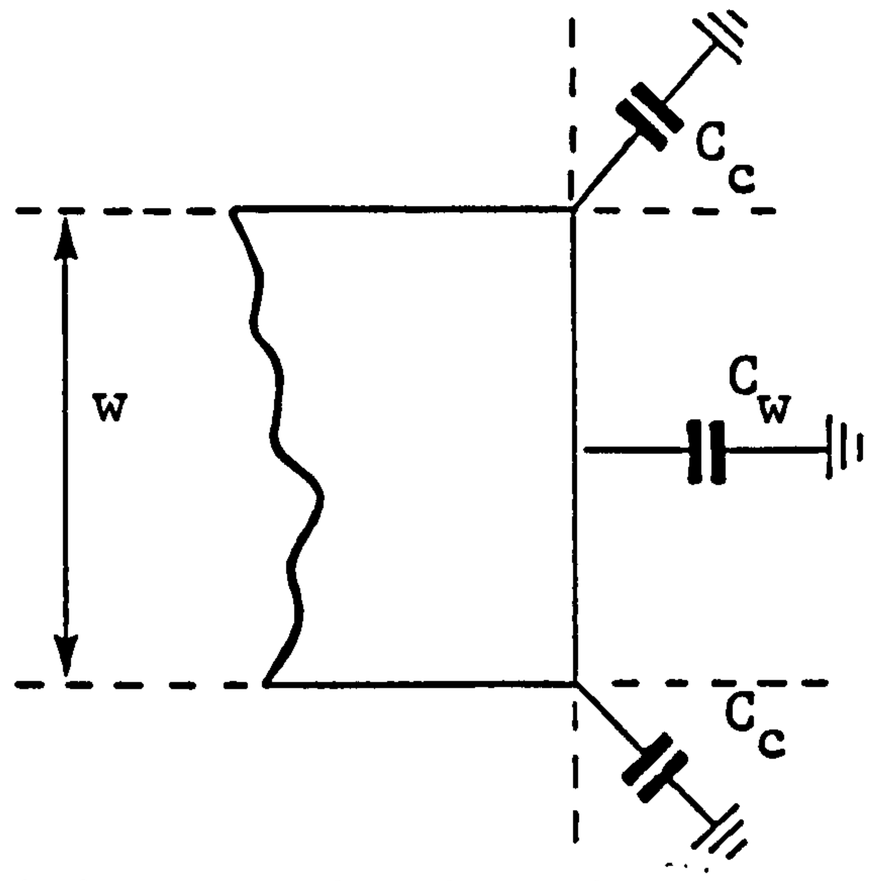

Figure 4.10 Microstrip open circuit end detail showing notional magnetic walls partitioning capacitance contributions.

The area at the end of the microstrip line is divided into three regions as illustrated in figure 4.10. The boundaries cannot be rigorously defined as magnetic walls since the concentration of charge at the corners will disturb the uniformity of the field distribution across the end of the strip. Nevertheless this notional division is tenable for the purpose of the following analysis provided the fields in the two corner regions do not significantly interact; a condition similar to that for non-interaction between opposite edges of the microstrip line: i.e. w/h > 1. With this stipulation the end effect capacitance is given by:

$$C_e = C_w + 2C_c \qquad \langle 4.8 \rangle$$

Using values obtained for fringing field at a straight edge expressed as capacitance per unit length, C_w can be evaluated.

$$C_{wI} = wC_{fI} \text{ (isotropic)} \qquad \langle 4.9a \rangle$$

$$C_{wA} = wC_{fA} \text{ (anisotropic)} \qquad \langle 4.9b \rangle$$

Figure 4.10 is a graph comparing C_{wI} with end effect capacitance computed

by the program ENDEFFECT (after Silvester and Benedek [2]) for a range of normalised microstrip widths, w/h, on a isotropic (ϵ_r=9.6) dielectric substrate. Clearly, the nearly constant offset corresponds to the sum of the corner effects, $2C_c'$. The accuracy does not appear significantly degraded even well below the supposed validity limit of unity width to height ratio.

The value of the end effect capacitance can then be computed for the anisotropic case. Using GREEN to evaluate C_{fA} and C_{fI}, the end effect capacitance is given by the expression:

$$C_{eA} = C_{fA} + 2C_c'(C_{fA}/C_{fI}) \qquad \langle 4.10 \rangle$$

where the corner capacitance C_c' is obtained from evaluation of the end effect with an isotropic substrate with dielectric constant equal to ϵ_y for the anisotropic substrate.

All the data obtained in terms of end effect capacitance can be converted to the quasi-normalised form of effective line extention using equation <4.1>.

It is evident from figure 4.11 that either the data for wide strips obtained from ENDEFFECT is in error, or the value of C_{fI} obtained by GREEN is slightly too large. It is supposed that the former is the case and that the work of James and Tse [4] is superior to that of Silvester and Benedek as their value of C_{eI} is never less than $w.C_{fI}$. The difference between these quantities (using the program ENDEFFECT) is plotted in figure 4.11b and the average value in the region $0.2 \leq w/h \leq 2$ yields a corner capacitance C_c=3.8fF. It would appear that, contrary to expectation, useful accuracy maintained to values of w/h as low as 0.1.

The corner capacitance has been obtained for a permittivity of 9.6 and must be transformed to produce a value of C_c' for an isotropic permittivity of 11.6 before equation <4.10> can be applied:

$$C_c' = (C_{fI}/C'_{fI})C_c = 1.178\ C_c \qquad \langle 4.11 \rangle$$

where C'_{fI} is the fringing capacitance for ϵ_r=9.6.

Clearly both transformations can be conducted simultaneously by letting C'_{fI} in equation <4.11> take the value of C'_{fI}, thus:

$$C_e = 44.8w + 1.08 * 2C_c \quad fF \qquad \langle 4.12 \rangle$$

Results from the application of this expression are plotted in figure 4.11a.

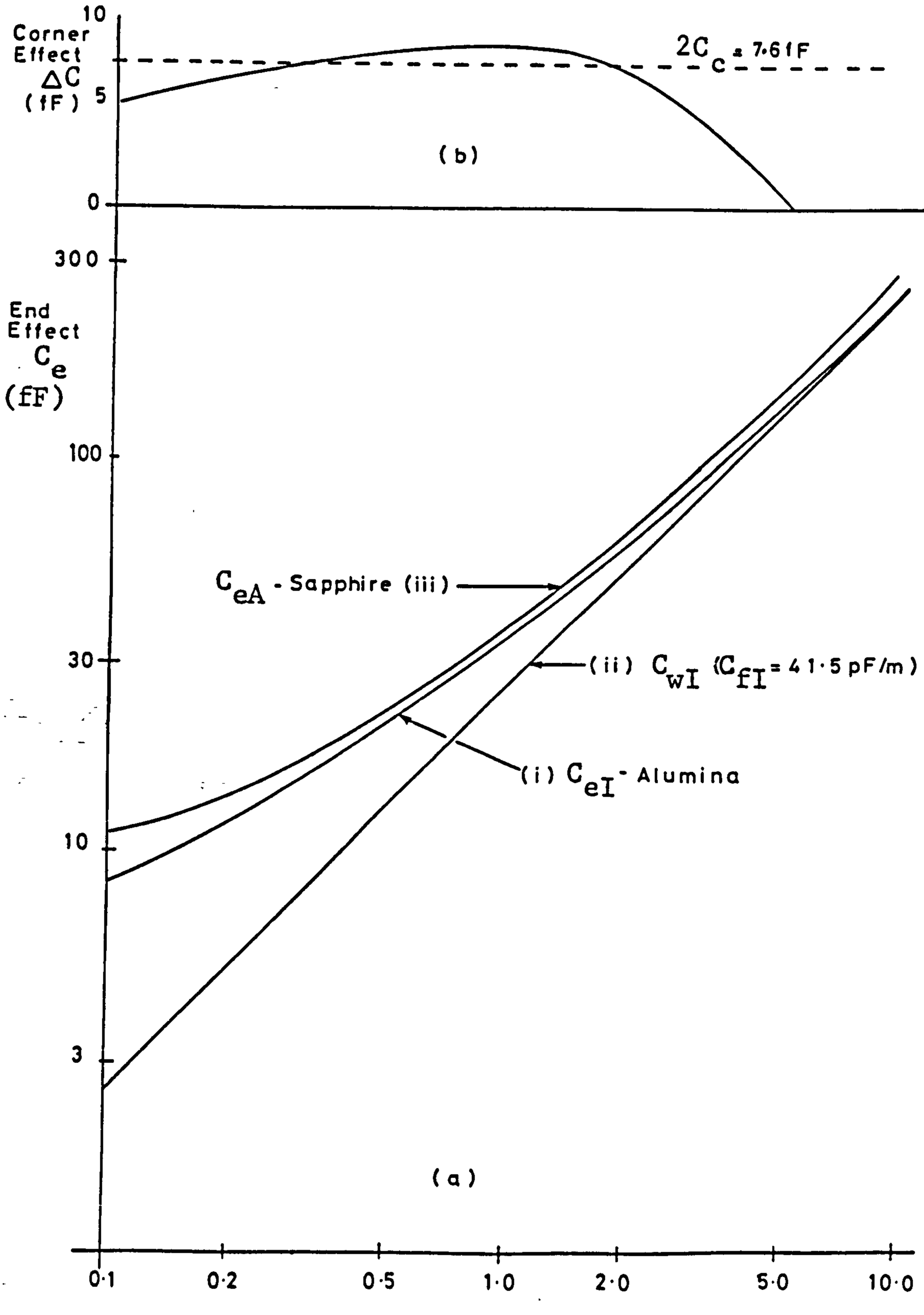

Figure 4.11 a) End effect capacitance versus normalised microstrip width from, (i) ENDEFFECT program (C_{eI}), (ii) straight edge fringing only (wC_{fI}) and (iii) conversion for sapphire (C_{eA}).

b) Difference between curves (i) and (ii) being the corner effect capacitance.

4.3.2 Step Junction

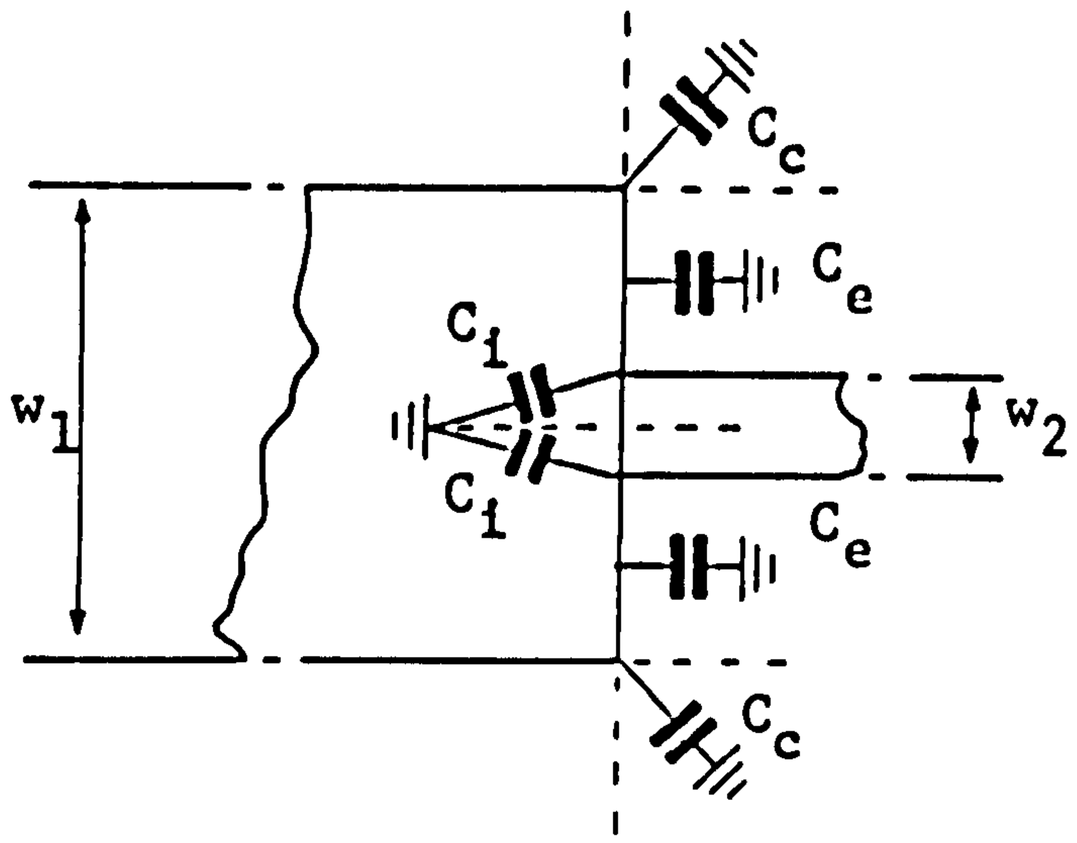

Figure 4.12 Step junction detail showing components of discontinuity capacitance.

The step junction between two microstrip lines can be treated in a similar manner to the open circuit end. In addition to the edge and external contributions to the discontinuity capacitance already discussed there is the effect of the internal corner to consider. The capacitance associated with this feature (C_i in figure 4.12) is negative in value. The total discontinuity capacitance of the junction is given by the expression:

$$C_j = (w_1 - w_2)C_f + 2C_c + 2C_i \qquad \langle 4.11 \rangle$$

Accuracy can only be expected for large steps and for $w_1/h > 1$ where insignificant interaction between various components can be guaranteed. In practice, this restriction is of little consequence as it is for such situations that the discontinuity capacitance is of most significance.

Data from the work of Gupta & Gopinath [17] has been used to generate the curves of figure 4.13a for an isotropic (ϵ_r=9.6) substrate. Also plotted (figure 4.13b), is the difference between these results and an estimate computed from equation <4.11> neglecting the contribution from the internal corner. The mean value of the offset (in the range $3.0 \leq w1/h \leq 6.0$) yields the value of C_i as -19.4fF, a value that holds

reasonably well over a range of parameters, providing the conditions set out above are observed.

The evaluation of the step discontinuity capacitance, where the substrate is anisotropic, can then be conducted using the anisotropy adjustment factor in two ways. Using equation <4.13> adapted for the anisotropic case, thus:

$$C_{jA} = (w_1 - w_2)C_{fA} + 2\{C_{fA}/C'_{fI}\}(C_c + C_i) \qquad \langle 4.14 \rangle$$

the total junction capacitance can be calculated from the knowledge of the individual contributions. Alternatively, the anisotropy transformation can be applied directly to the published (isotropic) values of the junction capacitance, viz:

$$C_{jA} = \{C_{fA}/C'_{fI}\}C_{jI} \qquad \langle 4.15 \rangle$$

From the curves of figure 4.13 it is apparent that the latter approach yields the most convincing results whilst the former method has the advantage that, once C_c and C_i are known, a wide range of structures may be evaluated simply and quickly. As expectd, the accuracy of equation 4.14 is poor when the step is small, due to the interaction of the field between nearby regions. For results of useful accuracy, the smallest lateral dimensions should not be less than the substrate thickness, h.

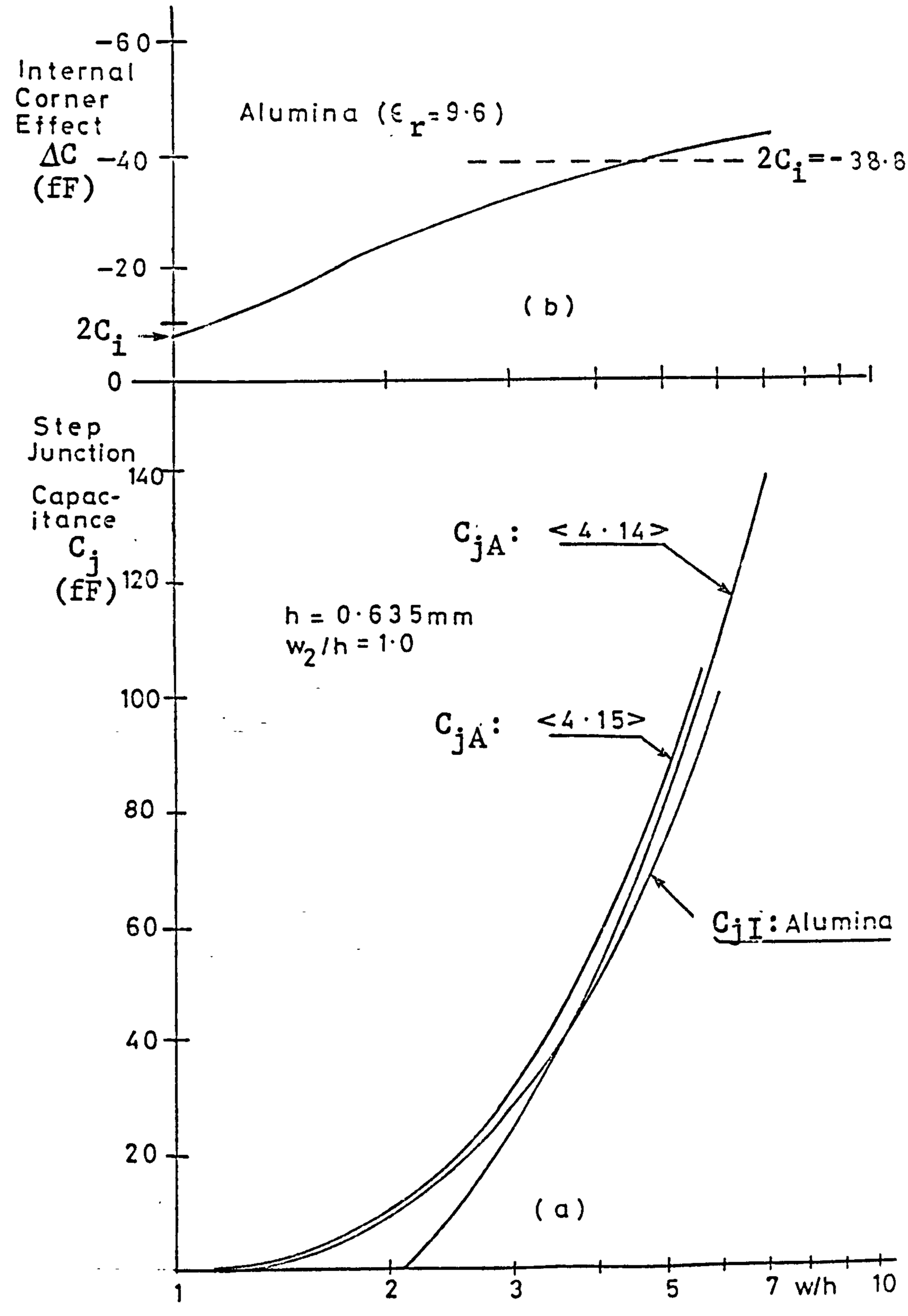

Figure 4.13 a) Step junction capacitance for Sapphire and Alumina

b) Internal corner effect on Alumina

4.3.3 Isolated Lands

In accordance with the discussion of the section 4.1.5 the lands discussed will be considered small enough ($<\lambda/10$) in linear dimensions to be regarded as lumped. If this stipulation is invalid the land should be modelled a transmission line with associated end effects. Figure 4.14 illustrates the components of the lumped model; the total capacitance being:

$$C_l = 2C_w + 2C_s + 4C_c + C_a \qquad \langle 4.16 \rangle$$

where C_a = parallel plate capacitance of the land

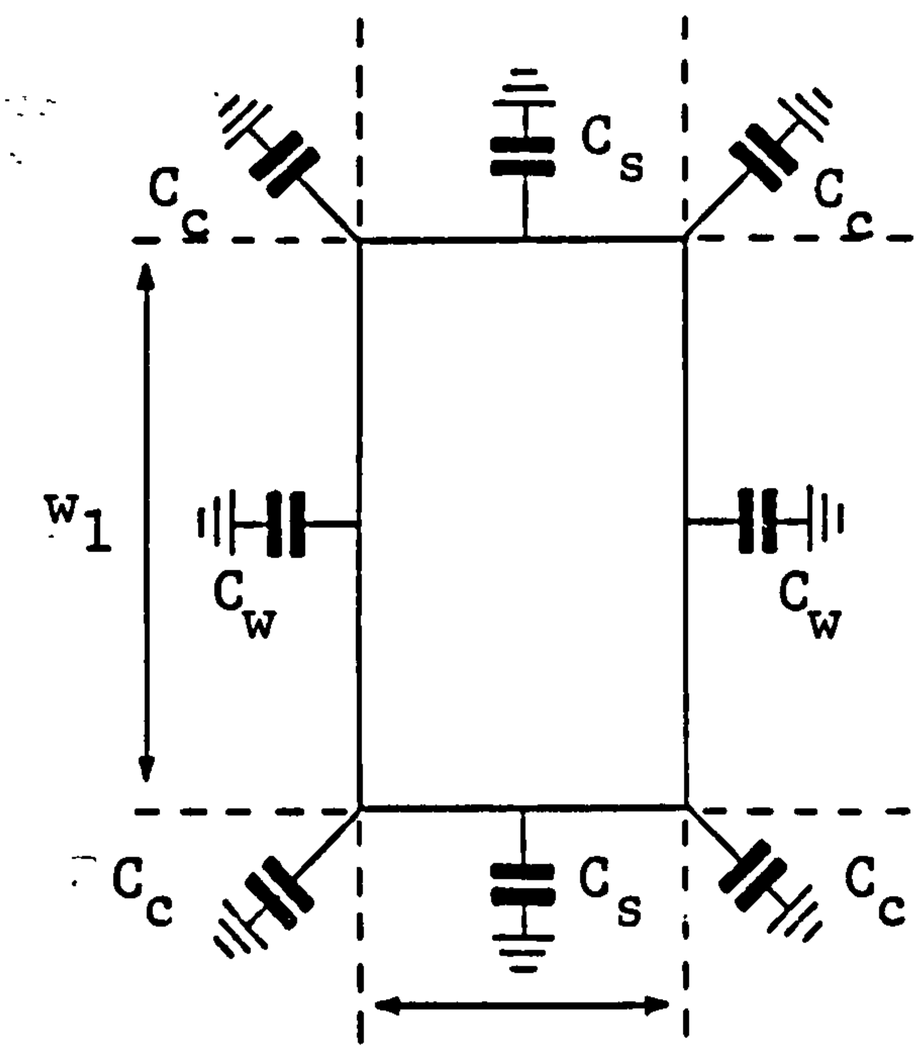

Figure 4.14 Isolated land detail showing fringing capacitance model

Making appropriate substitutions, the capacitance of the land can be computed for both the isotropic and anisotropic case using data previously obtained;

$$C_{lI} = 2C_{fI}(w_1 + l_1) + \epsilon_r \epsilon_o w_1 l_1/h + 4C_c \qquad \langle 4.17a \rangle$$

$$C_{lA} = 2C_{fA}(w_1 + l_1) + \epsilon_n \epsilon_o w_1 l_1/h + 4C_c\{C_{fA}/C_{fI}\} \qquad \langle 4.17b \rangle$$

subject to w_1/h and l_1/h being greater than unity.

An arguably more accurate approach which allows the smaller of the

dimensions to be reduced below this limit is proposed. The land may be regarded as a microstrip line having a width equal to the smaller dimension of land ($w=L_e$), for which the capacitance (per unit length) C_μ may be computed using the program GREEN. Thus the interaction between the fringing field on opposite edges is taken into account. Curves for the microstrip capacitance of alumina and sapphire are presented in figure 4.15.

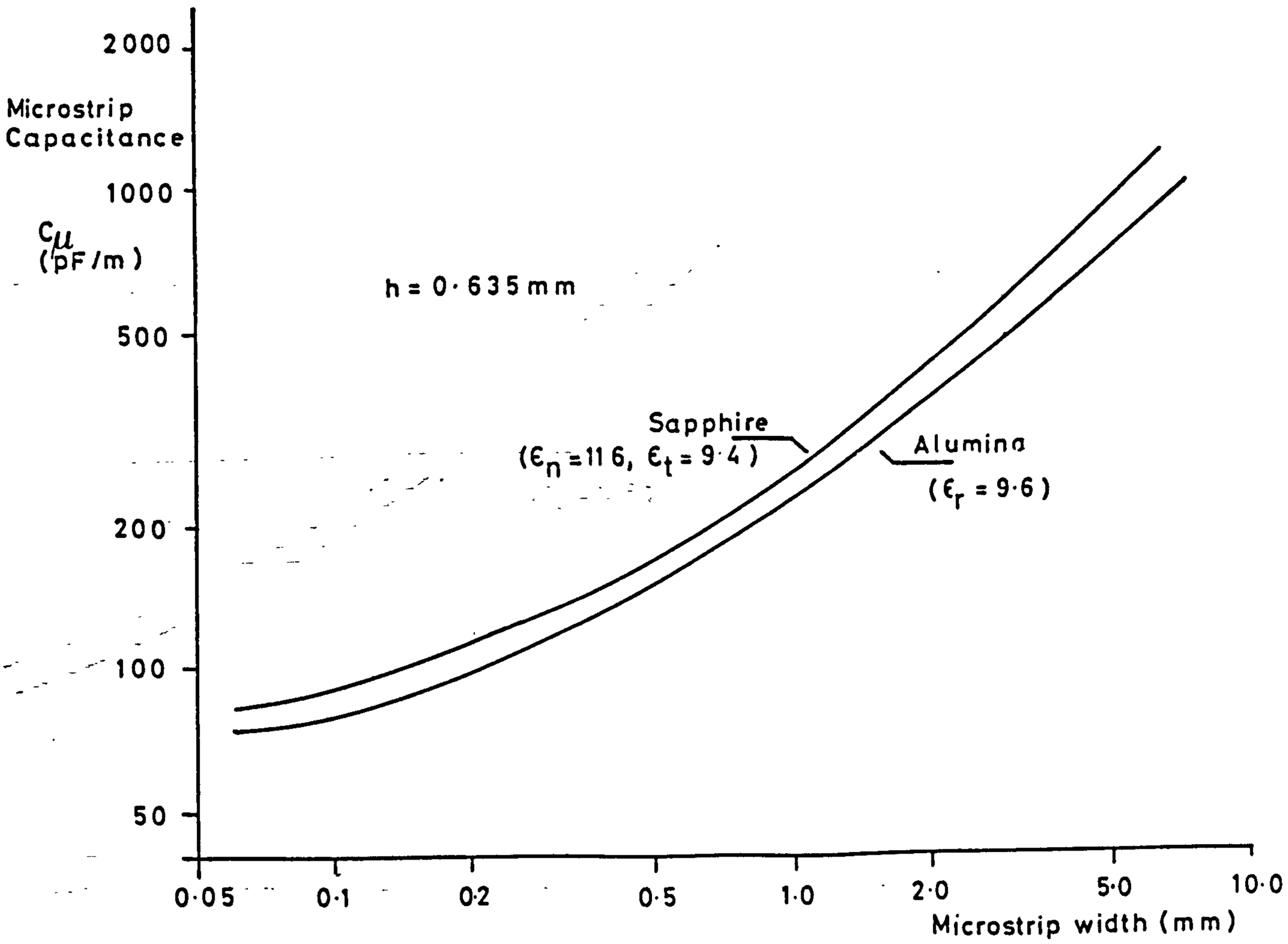

Figure 4.15 Microstrip line capacitance for alumina and perpendicular cut sapphire.

The capacitance of land is then obtained by adding the open circuit end effect values of section 4.3.1, thus:

$$C_l = w_l C_\mu(l_l) + 2C_e \qquad \langle 4.18 \rangle$$

By this means the representative curves of figure 4.16 have been generated.

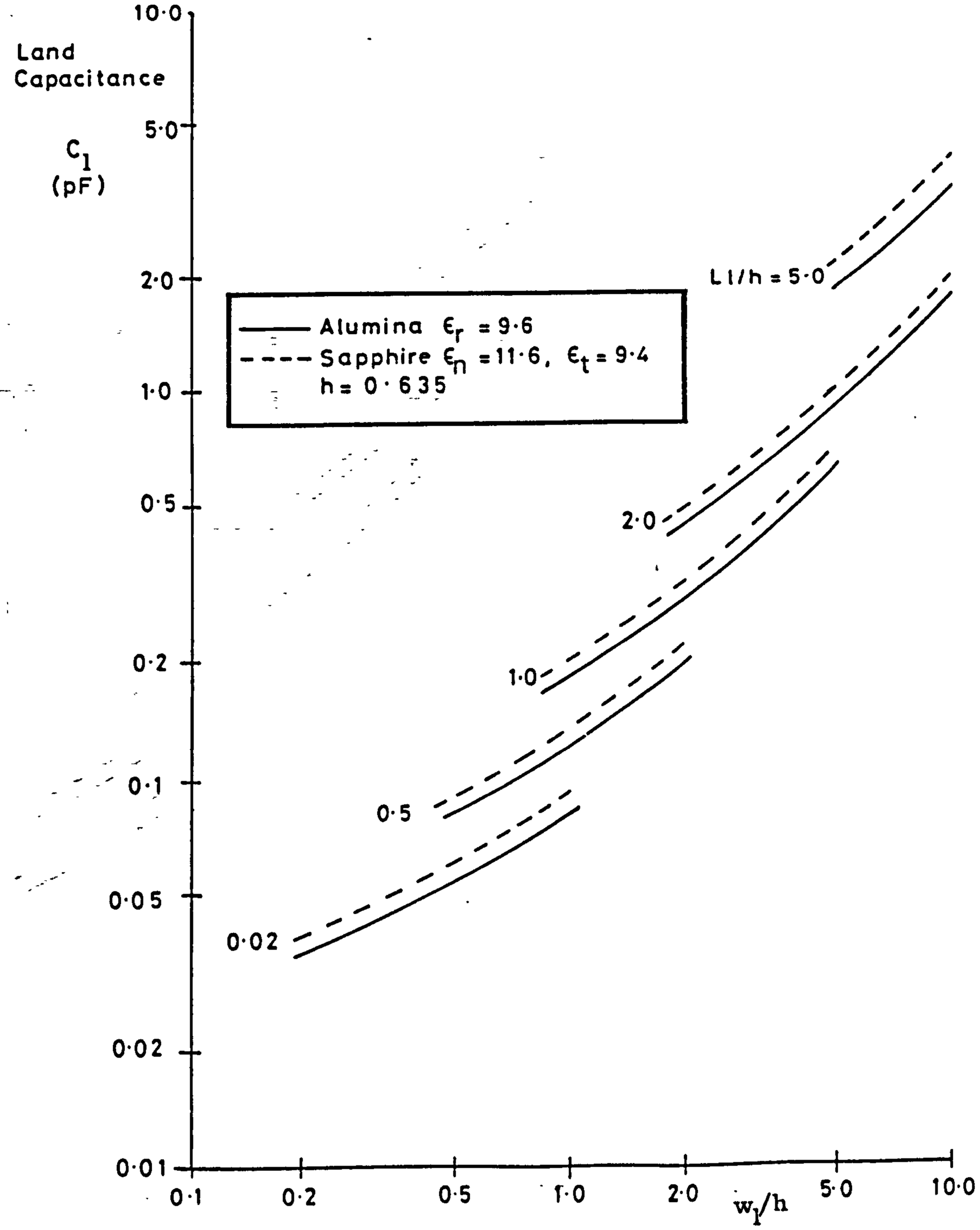

Figure 4.16 Isolated land capacitances for 0.635mm thick alumina and sapphire substrates.

4.3.4 Connected Lands

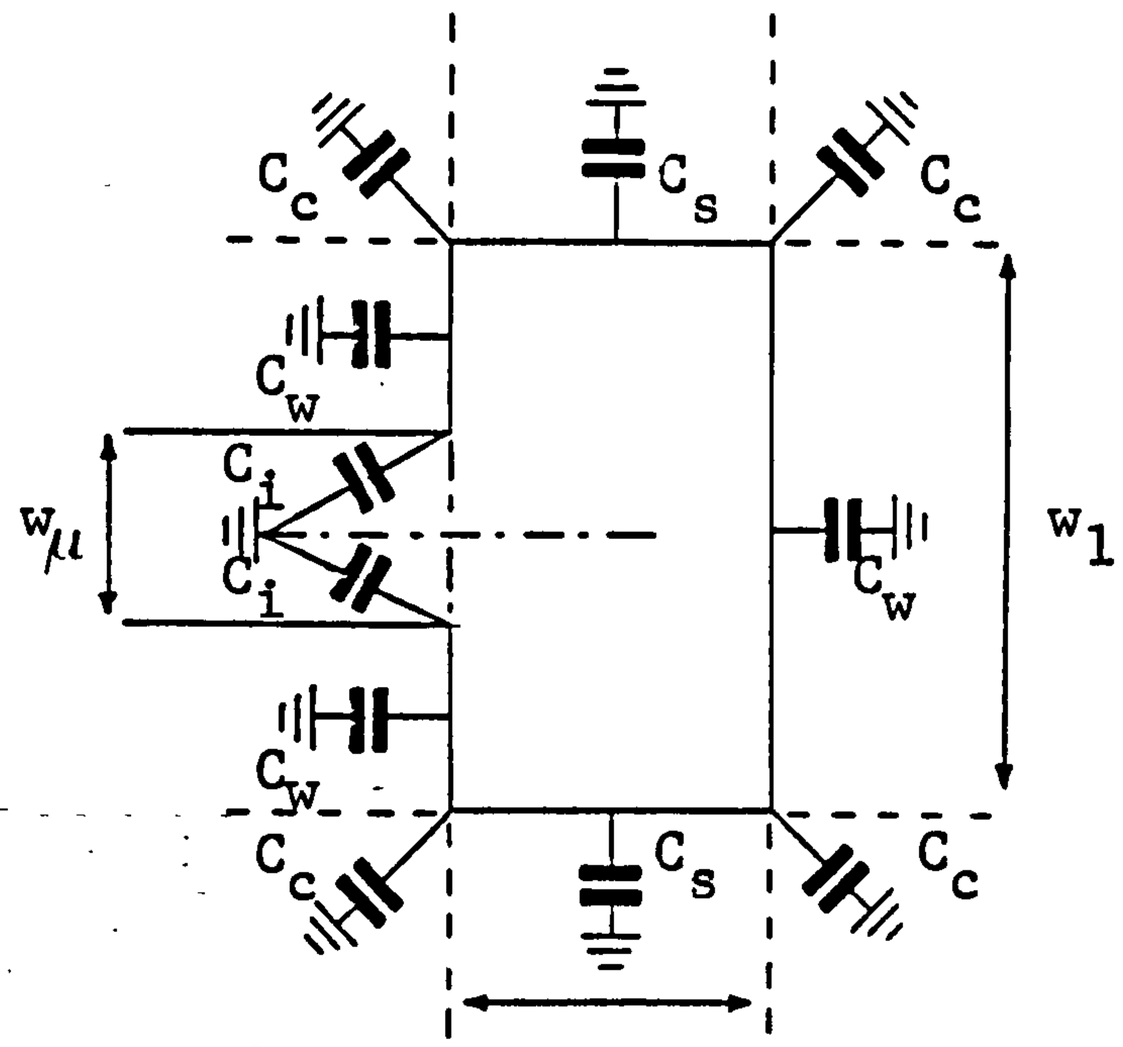

Figure 4.17 Connected land detail showing fringing capacitance model.

Often the land will be connected by a microstrip line. For example, lands are often necessary when mounting a chip capacitor in the circuit. This structure having the appearance of a "hammer-head" is illustrated in figure 4.17 which indicates the way in which the fringing field is modelled. The total capacitance can then be expressed:

$$C_l = C_w + 2C_w' + 2C_s + 4C_c + 2C_i + C_a \qquad \langle 4.19 \rangle$$

which may be re-written in the now familiar fashion

$$C_{lI} = C_{fI}(2w_1 - w_\mu + 2l_1) + \epsilon_r\epsilon_o w_1 l_1/h + 4C_c + 2C_i \qquad \langle 4.20a \rangle$$

$$C_{lA} = C_{fA}(2w_1 - w_\mu + 2l_1) + \epsilon_r\epsilon_o w_1 l_1/h + 2(2C_c + C_i)\{C_{fA}/C_{fI}\} \qquad \langle 4.20b \rangle$$

for isotropic and anisotropic substrates respectively. Obviously there are alternative ways of constructing the model. The land may be viewed as a microstrip line of width, w_1, joined to the connecting line by a step junction at one end with the opposite end open circuit, such that:

$$C_l = l_1 C_\mu(w_1) + C_s(w_1, w_\mu) + C_e(w_1) \qquad \langle 4.21 \rangle$$

where $C_\mu(w)$ is the appropriate capacitance as a function of the relevant physical dimensions

In another alternative approach the connected land may be treated as a variation of the isolated land of the previous section, viz:

$$C_l = w_l C_\mu(l_l) + 2C_e(l_l) - w_\mu C_f - 2C_i \qquad \langle 4.22 \rangle$$

with values chosen, as before, to suit the type of substrate.

A typical example of a land with w_l = 2.0mm, l_l = 1.5mm connected by a microstrip line of w_μ = 0.635mm on a sapphire substrate 0.635mm thick, has been evaluated by the three alternative expressions:

TABLE 4.5 CAPACITANCE OF A CONNECTED LAND ON SAPPHIRE

Equation	C_{eA} (pF)
<4.20>	0.744
<4.21>	0.761
<4.22>	0.835

The spread in the results (~12% overall) is indicative of the certainty of the value and is considered acceptable for amplifier design purposes. Equation <4.21> is to be preferred as it is the most direct and fortuitously delivers the median of the three results in the example above.

4.4 CONCLUSIONS

A simple but effective way to model the capacitive component of commonly encountered microstrip discontinuities, on both isoptropic and anisotropic substrates, has been presented. Based on the partitioning of the region around the discontinuity the method can be applied to a large range of structures. In particular, the open circuit end, the step junction and isolated and connected lands have been studied and results

compare favourably with those in the literature for a useful range of parameters. The complexity involved in the calculation of fringing fields is ameliorated by using a modified version of a program originally prepared for the calculation of microstrip parameters. Since this program had previously been extended to cope with substrate anisotropy, this permitted the application of the technique to sapphire MICs. An anisotropy adjustment factor has been defined to allow values obtained for 3-dimensional structures on isotropic substrates to be applied to anisotropic substrates.

Whilst a restriction to structures with smallest linear feature dimension comparable to the substrate thickness was envisaged it appears that, with some reservations, the accuracy remains at a useful level for simple structures much smaller than suggested. The accuracy of the open circuit end model appears excellent and the uncertainty associated with wide strips that was noted is insignificant when expressed as an equivalent line extention. No coroborative data for the discontinuities on sapphire substrates in available but adequate confidence can be established by reference to data for alumina.

Some results for the inductive component, which is unchanged by the dielectric anisotropy of the substrate, have been extracted from the referenced literature and included for completeness.

4.5 REFERENCES

[1] AKELLO, R.J., EASTER, B & STEPHENSON, I.M.: "Effects on Microstrip discontinuities on GaAs - MESFET - Amplifier Gain Performance", IEE Electron Lett, 13, pp. 160-2, 1977

[2] SILVESTER, P & RENEDEK, P.: "Equivalent capacitances of microstrip open circuits," IEEE Trans MTT-20, pp. 511-5, 1972

[3] TROUGHTON, P.: "Design of complex microstrip circuits by measurement and computer modelling", Proc. IEE, 118, pp. 469-74, 1971

[4] JAMES, D.S & Tse, S.H.: "Microstrip end effects", IEE Electron Lett. 8, pp. 46-6, 1972

[5] FARRAR, A. & ADAMS, A.T.: "Computation of lumped microstrip capacities by matrix methods - rectangular sections and end effect", IEEE Trans, MTT-19, pp. 495-7, 1971

[6] EASTER, B.: "The equivalent circuit of some Microstrip discontinuities", IEEE Trans. MTT-23 pp. 655-60, 1975

[7] THOMSON, A.F. & GOPINATH, A.: "Calculation of microstrip discontinuity inductances", IEEE Trans. MTT-23, pp. 648-55, 1975

[8] STEPHENSON, I.M. & EASTER, B.: "Resonant techniques for establishing the equivalent circuits of small discontinuities in microstrip", IEE Electron Lett. 7, pp. 582-4, 1971

[9] HOWE, H.: "Stripline circuit design", Artech House, Dedham MA, 1974, pp. 47-52

[10] MENZEL, W.: "Frequency-dependent transmission properties of truncated microstrip right-angle bends", IEE Electron Lett. 12, pp. 641, 1976

[11] HORTON, R.: "Electrical characterisation of a right-angled bend in microstrip line", IEEE Trans. MTT-21, pp. 427-29, 1973

[12] SILVESTER, P & BENEDIK, P.: "Microstrip discontinuity capacitances for right-angle bends, T-junctions, and crossings", IEEE Trans. MTT-21, pp. 341-6, 1973

[13] RUEHLI, A.E., KULASZA, N. & PIVNICHNY, J.: "Inductance of nonstraight conductors close to a ground return plane", IEEE Trans MTT-23, pp. 706-8, 1975

[14] MENZEL, W. & WOLFF, I.: "A method for calculating the frequency dependent properties of microstrip discontinuities", IEEE Trans MTT-25, pp. 107-112, 1977

[15] KOMPA, G.: "Design of Stepped Microstrip Components", IERE Rad & Electron Eng. 48, pp. 63-63, 1978

[16] EASTER, B., GOPINATH, A. & STEPHENSON, I.M.: "Theoretical and experimental methods for evaluating discontinuities in microstrip", IERE Rad & Electron Eng. 48, pp. 73-84, 1978

[17] GUPTA, C. & GOPINATH, A.: "Equivalent circuit capacitance of microstrip step change in width", IEEE Trans. MTT-25, pp. 819-22, 1977

[18] THOMPSON, A.F. & GOPINATH, A.: "Calculation of microstrip discontinuity inductances", IEEE Trans. MTT-23, pp. 648-55, 1975

[19] ANDERS, P. & ARNDT, F.: "Microstrip discontinuity capacitance and inductances for double steps, mitred bends with arbitrary angle, and asymmetric right angle bends", IEEE Trans. MTT-28, pp. 1213-7, 1980

[20] AKELLO, R.J., EASTER, B. & STEPHENSON, I.M.: "Equivalent circuit of the asymmetric crossover junction", IEE Electron Lett. 13, pp. 117-8, 1977

[21] MENZEL, W.: "Calculation of the S-parameter of an unsymmetric microstrip T-junction", Computer Program Descriptions, IEEE Trans. MTT-26, pp. 217, 1978

[22] CHAO, C.L.: "A network reduction technique for microstrip three-dimensioned problems", IEEE MTT Syposium Digest, pp. 73-5, 1978

[23] NAPOLI, L.S. & HUGHES, J.J.: "Foreshortening of microstrip open circuits on alumina substrates", IEEE Trans. MTT-19, pp. 559-61, 1971.

CHAPTER 5

THE

COMPUTER CORRECTED

NETWORK ANALYSER

5. THE COMPUTER CORRECTED NETWORK ANALYSER

In recent years the Network Analyser has displaced the slotted line as the microwave engineer's principal measurement tool. Its major benefit is that it can characterise a two-port network over a wide range of frequencies quickly and provide an immediate display of the measured parameters. The data is presented in the form of small-signal scattering (s-)parameters (complex reflection and tranmission coefficients) and consequently is directly useful for design purposes.

The network analyser does, however, have some severe limitations: its accuracy is rather poor and it is tedious to record the large amount of data that it is capable of collecting. To overcome these restrictions the ubiquitous digital computer has been applied in a dual role. The computer is used to control and collect data from the intruments and then to correct for the systematic errors. Since the first Computer Corrected Network Analyser system (CCNA) was reported [1] advances in computing technology have reduced the cost and physical size of the computer required to perform these tasks. As a result the number of CCNAs employed in design and calibration laboratories has increased markedly in the last few years.

5.1 COMPUTER ASSISTED S-PARAMETER MEASUREMENT SYSTEMS

The work presented here is concerned with computer corrected network analysers of the type based on the conventional manual, direct reading, harmonic conversion, super-heterodyne network analyser. The introduction of a computer does, however, present a number of possible alternative approaches for s-parameter measurement.

One such approach involves the making of time-domain measurements

which are then converted into s-parameters using the Fast Fourier Transform (FFT) technique. The principal piece of hardware is a sampling oscilloscope which is used to produce a short rise-time step function and to measure the response of the Device Under Test (DUT). Transition errors can conveniently be removed by time 'windowing' the reflected or transmitted step response and conducting the FFT on the portion of the step response relating to the DUT itself. Work already conducted elsewhere[2] on such systems shows promising results but the resolution of the system is limited at higher microwave frequencies due to the difficulty of developing adequate high frequency energy in the step funtion stimulus, without compromising small-signal conditions.

Another approach which is attracting considerable attention[3-5] is the use of 6- (or more) port couplers. In a system based on the use of multi-port couplers the vector reflection or transmission measurements are obtained using only scalar power measurement. Three or four power meters are attached to each of the two multi-port couplers required for a 2-port network analyser. By computation, vector reflection and tranmission coefficents may be deduced. The couplers may be realised either as a combination of 4-port hybrids[4] or directly as a 6-port stucture formed by coupling three transmission lines or waveguides [5]. Such a system does not require the relatively elaborate harmonic conversion vector voltmeter but has the disadvantage of utilising more elaborate microwave components which have yet to demonstrate truly wide-band capability. In addition it does require a large number of stable, high dynamic range power meters. Both of these alternative systems are incapable of yielding manual direct readings; requiring the services of a computer to derive the s-parameter data.

The conventional approach under discussion is the most popular for a number of reasons. Firstly, the hardware is readily available; the

manual network analyser being commonplace in microwave laboratories, and it remains capable of direct s-parameter measurement when the computer is unavailable or when an operation involving tuning of the DUT requires immediate display. Secondly, the microwave hardware is capable of operation over a very wide frequency range, typically covering .5-18GHz, and, whilst an improvement would be desirable, a relatively large dynamic range (>60dB) is obtained across this band.

During the course of his research the author has had access to two CCNA systems of the conventional type: those in the Engineering Department of the University of Warwick and at Marconi Instruments Ltd., St.Albans site. The first of these was amoung the earliest CCNA systems in this country and has been described in a number of works[6-8]. The second of these systems was developed by some of the author's colleagues at Marconi Instruments during the period of his research. Many of the developments decribed in this and the following chapter were initially applied to the Warwick University system and subsequently implemented on the Marconi Instuments CCNA.

Although the material presented here is directly applicable only to the conventional, harmonic converter type of network analyser, many of the principles and techniques could be carried over to work on the other forms of CCNA decribed above.

5.2 THE CCNA HARDWARE

The hardware that constitutes a computer corrected network analyser comprises three major items; the microwave instruments, the computer and its peripherals, and the interface between the computer and the instruments.

5.2.1 The Microwave Instruments

The microwave hardware required for a CCNA system is very similar to that used in a manual network analyser. There are three basic elements; a signal source, an s-parameter test set (or a reflection/transmission test set) and the network analyser itself. The term 'network analyser' is applied to both the system as a whole and to the principal instrument which is described below.

5.2.1.1 The Signal Source

The source of the microwave signal required to act as the stimulus for the measurements conducted with the network analyser is usually a microwave sweeper with facilities for remote control. The remote control of frequency may be simply achieved either by providing analogue voltage control or, more elaboratly, by digital programming using a bus system (e.g. GP-IB = General Purpose Instrument Bus = IEEE 488 Bus). Due to the wide frequency coverage desirable for a CCNA system it is usually necessary to use more than one sweeper, or sweeper 'plug-in', and to provide coaxial switches to select the frequency band under computer control. The maximum frequency range of current CCNAs is 100 MHz to 18 GHz, being determined primarily by the limitations of the network analyser instrument.

5.2.1.2 The Test Set

The test set is the collection of microwave coaxial components, such as directional couplers, switches and attenuators, required to facilitate reflection and transmission measurements. If a reflection/transmission test set is used the DUT must be reversed during measurement to obtain the 2-port s-parameters. The s-parameter test set

includes switching which relieves the operator of this chore and allows the computer control over the complete measurement. The line-stretcher, included in most test sets to enable the user to equalise the reference and test channel path lengths, is redundant when the test set is used as part of a CCNA.

5.2.1.3 The Network Analyser

The network analyser is an instrument capable of making measurements of the relative amplitude and phase of two microwave signals: it is a sophisticated vector voltmeter having a variety of display facilities. The polar display option is normally used in a CCNA system as use of the X and Y outputs overcomes the problem, encountered with other display options, of an ambiguity when the relative phase has the value of 180 degrees. Figure 5.2 is a simplified block diagram of the instrument with the polar display and the associated harmonic converter [9]. At the heart of the instrument is a vector voltmeter operating at frequency of 278kHz. The microwave input signals enter a sampling mixer, with a local oscillator frequency in the range 60-120MHz, to produce IF outputs at 20.278MHz. The reference channel signal is compared with a crystal oscillator output at the IF frequency in a phase sensitive detector to produce a control signal to the voltage-controlled local oscillator. Thus a phase locked loop is formed which tunes the sampling system to produce a constant IF frequency regardless of the frequency of the microwave input signal. The network analyser has a variable gain IF amplifier which in most CCNA systems, can be controlled by the computer.

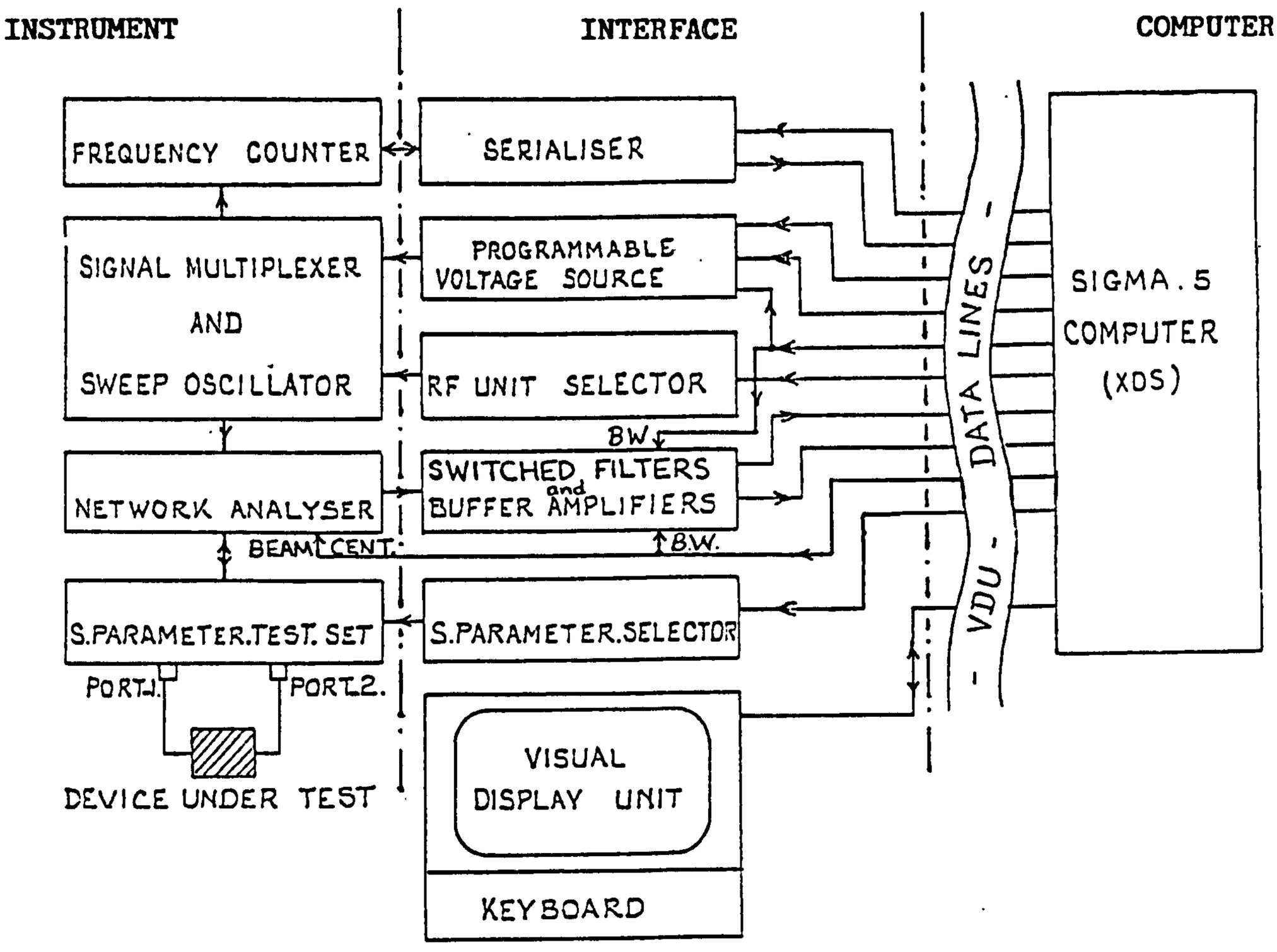

Figure 5.1 Elements of a CCNA System

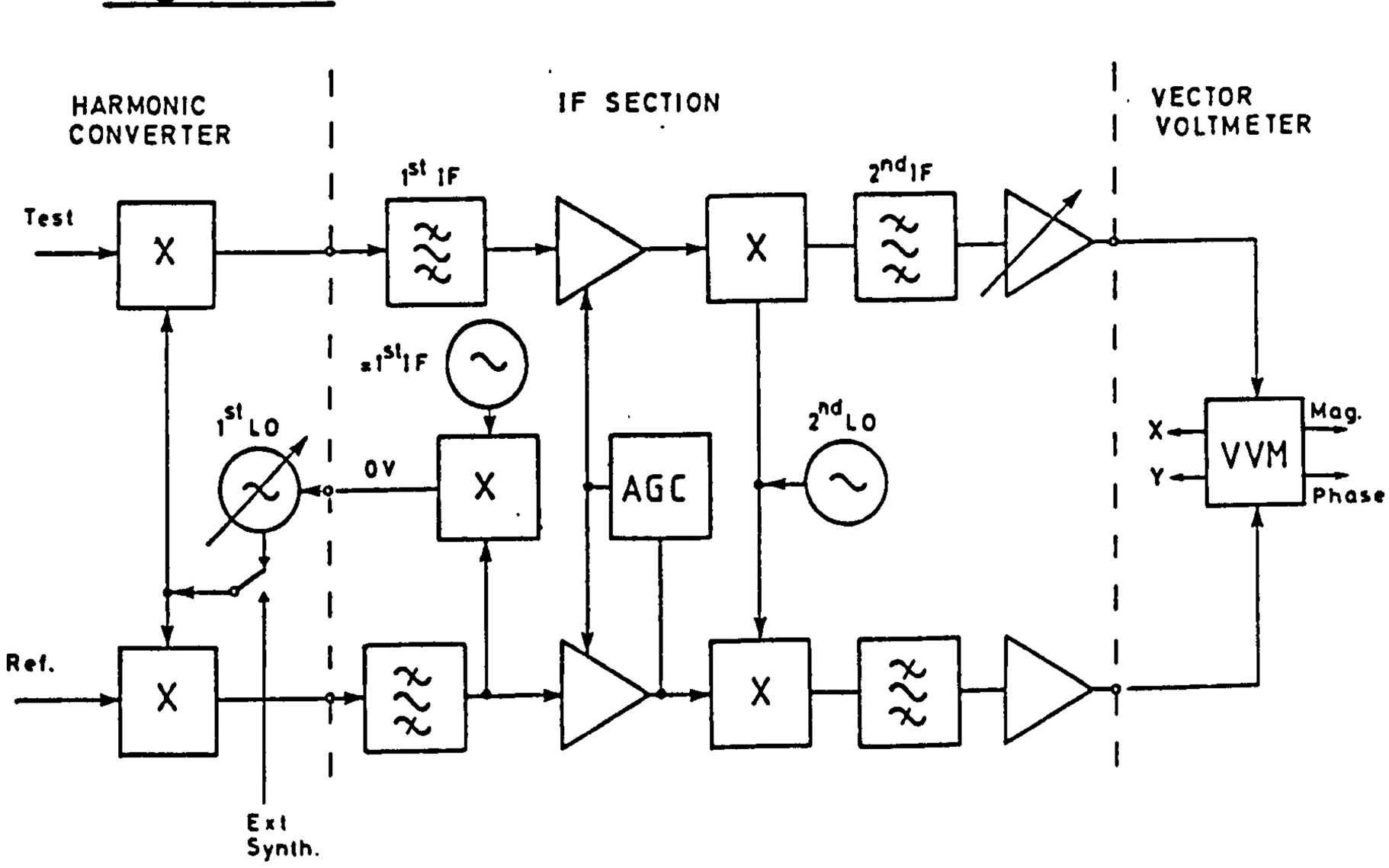

Figure 5.2 Simplified block diagram of a network analyser

5.2.2 The Computer and Peripherals

Two basic approaches to the use of a computer with a Network Analyser exist. One is to use a small computer (a mini- or "desk top") which is sited local to the instruments. The other is to utilise a time-shared computer which is usually some distance from the intruments. The system that uses a small local computer has the advantage of being under the control of the user and dedicated to the operation of the CCNA. Also in its favour is the relative ease of interfacing (discussed below) and sometimes, when compared to a heavily loaded time-sharing system, a speed advantage. The use of a small machine does usually limit the size of the CCNA program and consequently the number of options, say, of output formats or calibration schemes, that can be provided is severely curtailed. In addition the number of periperals available with a dedicated small computer is often limited. In contrast most time-sharing computer systems will provide facilities for mass storage on disc or tape, high speed printing, interactive and hard-copy graphics as well as access to a body of general purpose software.

The computer peripherals required for a basic CCNA are a keyboard and display, a printer and some method of program and data storage. Facilities for computer graphics are a highly desirable extra as they provide a presentation of the corrected measurements in a similar form to the results displayed by the manual system.

5.2.3 The Instrument-Computer Interface

The most important factor affecting the interfacing of the computer to the microwave instruments is the type of computer system used. If the computer is a dedicated local machine there is no incentive

to minimise the number of connections; a separate wire could be used for each controlled function. In recent years the availability of "desk top" computers with GP-IB input/output and of instruments designed to operate on this bus has presented a simpler solution for those users content with a small local processor.

Where a remotely sited time-sharing system is involved it is impractiable to use a bus system because of the long signal path and the large number of connections required. Alternative solutions have to be found, such as the one adopted at Warwick University. The Xerox Sigma-5 computer has an analogue input/output capability and 10 coaxial lines, in addition to the one required for the graphics terminal, connect the instruments to the computer. Specially designed interface circuits and a precision voltage source are required to connect the instruments to the lines on to which some control information is coded as multiple voltage levels. Figure 5.1 illustrates this arrangement.

A more modern and elegant approach to the problem of interfacing to a remote computer system, (adopted for the CCNA at Marconi Instruments) involves only one connection made to the computer as for any ordinary time-sharing user. Instead of the usual terminal the connection is made to a specially built microprocessor Controller. Attached to the Controller are the intruments and the terminal. Terminal input/output procedes as normal. If, however, the processor recognises a command addressed to the instruments it decodes first the function designation and then the parameter value. A command to make a reading prompts the processor to check the instrument conditions and take a large number of measurements of the X and Y outputs of the network analyser via the multiplexer and A-D converter. The results are averaged and transmitted to the remote computer.

5.3 PRINCIPLES OF ERROR CORRECTION

The primary incentive for the use of a CCNA system is the greatly enhanced measurement accuracy that it offers. The errors that limit the accuracy of the manual (uncorrected) network analyser may be divided into two catagories: systematic and non-systematic. Action required to reduce these errors is distinctly different in the two cases.

5.3.1 Systematic Errors

Systematic errors are those which effect the measurements in a repeatable fashion. Examples are coupler directivity, test port mismatch and intrument gain and phase errors. Most of the material published on CCNA's[10-13] has been concerned with this catagory of error. In outline the procedure adopted is as follows:

(i) An error model, based on the known physical imperfections of the instrument is constucted.

(ii) Calibration pieces having known reflection or transmission characteristics are connected to the CCNA and measured.

(iii) Results from the calibration measurements are used to ascribe values to the elements of the error model.

(iv) The DUT is connected to the CCNA and measured.

(v) The true parameters of the DUT are de-embedded from the measured data using the information contained in the error model.

It should be noted that the prime requirement for the calibration pieces is that their parameters can be independently established, either from their physical properties or by electrical measurement.

5.3.2 Non-systematic Errors

Non-systematic errors are those that are attributable to unpredictable or random effects. Examples of such effects are electrical noise, poor connector or switch repeatability and frequency drift. Whilst sytematic errors can, in principle, be totally eliminated this type of error cannot. Two approaches to minimising non-systematic errors are available; both are usually exploited in a CCNA system. The first is to select, design or modify the system hardware to reduce the effect to the lowest realistic level. The second, applicable only when the effect is random in nature, is to take make multiple measurements and average the results. In this area trade-offs between complexity and cost of the hardware, the time taken to do the measurements, and the reduction of the errors are evident.

If it were not for the inevitable presence of non-systematic errors in the system it would ultimately be possible to eliminate systematic errors from the measurement process altogether. Woods[12] has queried the merit of using hardware of the quality necessary for a manual network analyser, as once correction is applied the systematic imperfections are irrelevant. However, due to non-systematic effects the accuracy of corrected results deteriorates as the systematic errors to be eliminated grow larger.

5.3.3 A Simple Example

The principles of error correction and reduction outlined above apply, of course, to virtually all measurement problems. Consider the situation where the problem is to obtain an accurate measurement of a potential difference with an electronic voltmeter. Firstly the error

model is deduced from the physical properties of the instrument: it has zero offset and gain errors but it is known to be highly linear. Consquently two calibration measurements are made; one with the input short circuit to establish the zero offset, and the second with a reference voltage applied. The results of the two measurements are used to fix points on the straight line error model. The potential difference in the circuit under test is then measured and the actual (corrected) voltage computed from the reading using the error model. In most practical cases these corrections could be made by setting up preset controls in the voltmeter.

The problem of noise still remains. In order to reduce its effect, each reading would be repeated a number of times (say ten).

5.4 SOURCES OF ERROR IN THE NETWORK ANALYSER SYSTEM

There are four major sources of systematic error that must be corrected by the CCNA system. These are; the gain and phase errors of the network analyser, the directivity errors of the directional couplers in the test set, the mismatches associated with the test ports to which the DUT is connected and the signal leakage between various points in the system. All these error contributions are frequency dependant by are assumed independant of absolute signal amplitude (i.e. linear)

5.4.1 Gain and Phase Errors

At the heart of the network analyser system is the vector voltmeter, the readings from which are subject to instrument errors. (Of these aberrations, the most significant is quadrature error, the subject of section 5.10.) In addition, loss, coupling and reflection effects in the

associated test set, via which the DUT is connected, contribute to errors in the measurement of the relative amplitude and phase of the signal being considered. Errors of this type have the same effect on all measurements regardless of the DUT parameters. In non-automated systems errors of this type are frequently compensated using a storage normaliser to display the results relative to those obtained for a short circuit or through line calibration piece. This can, of course, be done manually by recording the values obtained at several frequencies, with the calibration piece connected, and subtracting them from the measured parameter of the device. Not only is this procedure tedious it may also be positively misleading as the measurements will also be affected by the sources of error discussed below, which are dependant on the DUT parameters. Consequently the DUT measurements will be corrupted in quite a different way to those of the calibration pieces.

5.4.2 Directivity Error

The s-parameter test set contains a number of directional couplers or bridges for the purpose of separating incident and reflected waves when measuring reflection coefficients. In a practical context these components have limited directivity; a measure of the discrimination between forward and reverse travelling waves. Thus, even when the DUT is perfectly matched some output from the coupler or bridge would be observed and the network analyser would indicate a degree of mismatch. Conversely, if the DUT had a return loss of the same order as the coupler directivity, at some frequency it is likely that the components of the incident and reflected waves appearing at the coupler output will interfere distructively, causing the instument to falsely indicate that the DUT was perfectly matched. This source of error is of most

significance when the reflection coefficient to be measured is low. Figure 5.3 illustrates how the measurement uncertainty varies with the DUT reflection coefficient.

The effective (system) directivity is further degraded by any mismatches occuring between the directional coupler or bridge and the DUT. The effect is similar to directivity error. Particular offenders in this respect are the between series adapters frequently required to cope with the large variety of connectors currently in general use. The effective directivity of an adaptor is equal to its return loss.

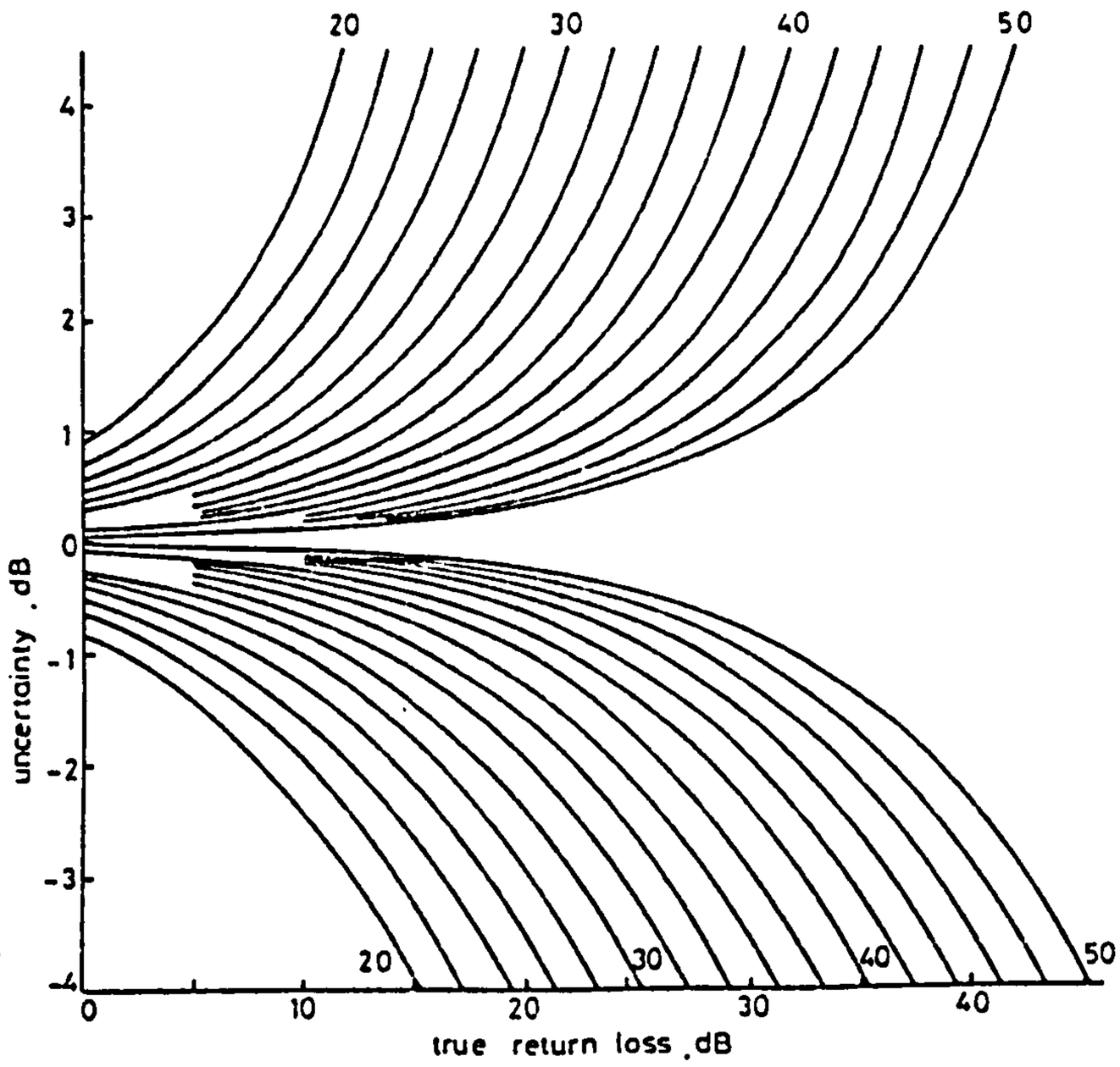

Figure 5.3 Measurement uncertainty for various values of coupler directivity

5.4.3 Test Port Mismatch

Imperfections in the microwave hardware result in mismatched terminations being presented to the DUT. This source of error contributes most to the measurement uncertainity when measuring devices with high reflection coefficient. Figure 5.4 indicates the effect on

the accuracy of reflection coefficient measurements. When a 2-port device is being measured the mismatch at both test ports contributes, in general, to the measurment uncertainty for all four s-parameters. S-parameters are defined with no incident wave on the undriven port, but for a DUT with finite insertion loss and a test set with non-zero port reflection coefficient this is not the case. Once again the use of adapters to connect the DUT can degrade the measurement accuracy significantly.

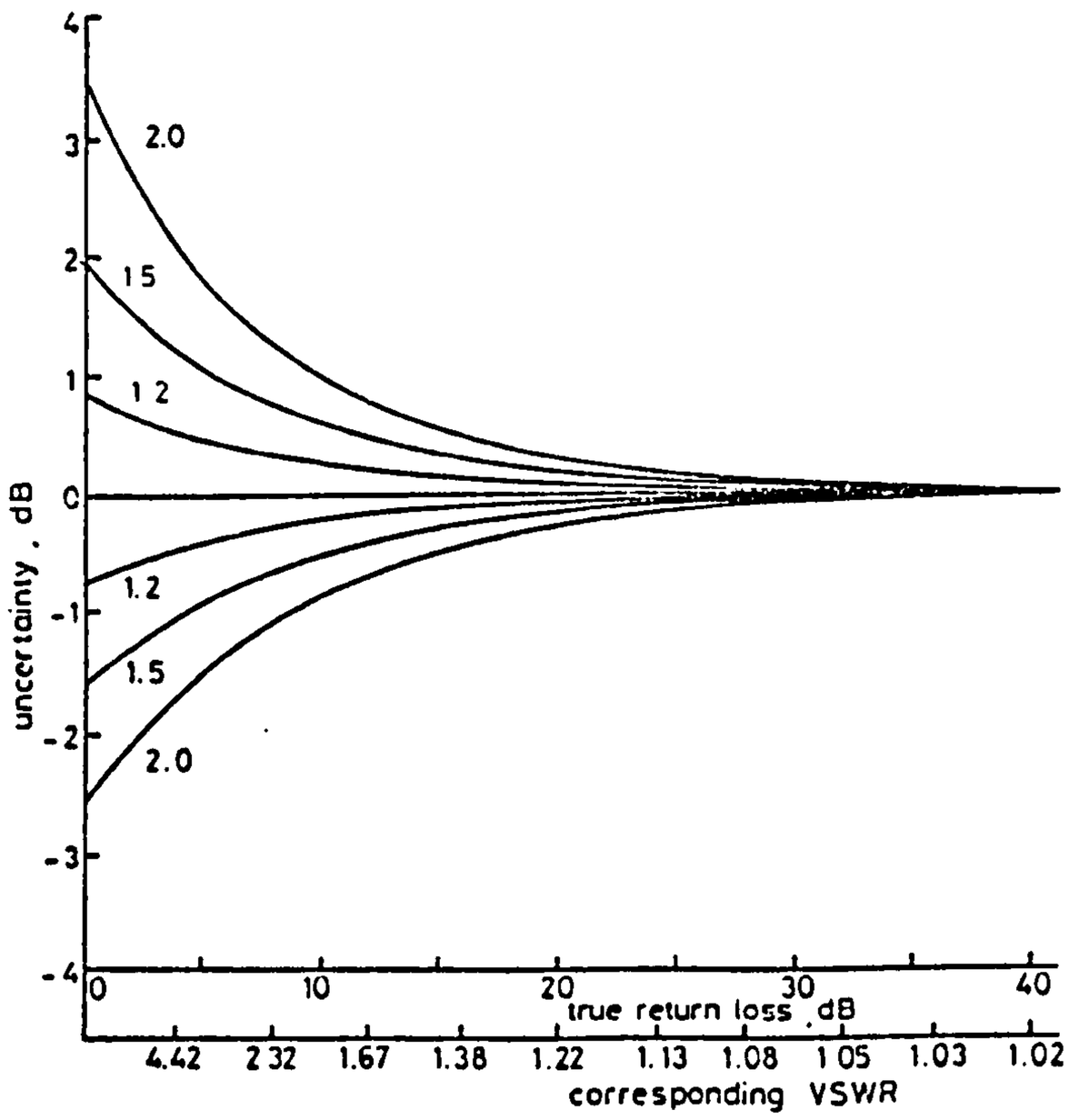

Figure 5.4 Measurement uncertainty due to various test port VSWRs

5.4.4 Leakage

In general, signal leakage or crosstalk can exist between any two points in the measurement system. In most network analyser systems the dominant leakage path is that via the common local oscillator feed to the reference and test channel sampling mixers. The crosstalk is, of course, bi-directional and resultant error is most pronounced when the

signal differentials are greatest. When measuring reflection coefficient, the contribution to the measurement uncertainty due to signal leakage is similar to that due to directivity error, having the most detrimental effect on the measurement of low reflection coefficients. In the case of transmission measurement, the effect of leakage is only significant when the DUT has high insertion loss. Because of the multiplicity of potential leakage paths completely rigorous calibration, especially where 2-port measurements are involved, is impracticable, even though the effect is systematic in nature [14].

Any crosstalk that occurs after the IF gain control contributes a variable amount to the total leakage error. This contribution is best treated as an aberration of the vector voltmeter along with quadrature error, an effect with which it shares some common features (c.f. section 5.10). Magnitude and phase deviations caused will display a phase dependence with a periodicity of 360° (twice that of quadrature error effects), and may be regarded as an equivalent to an origin offset (figure 5.5) and corrected accordingly.

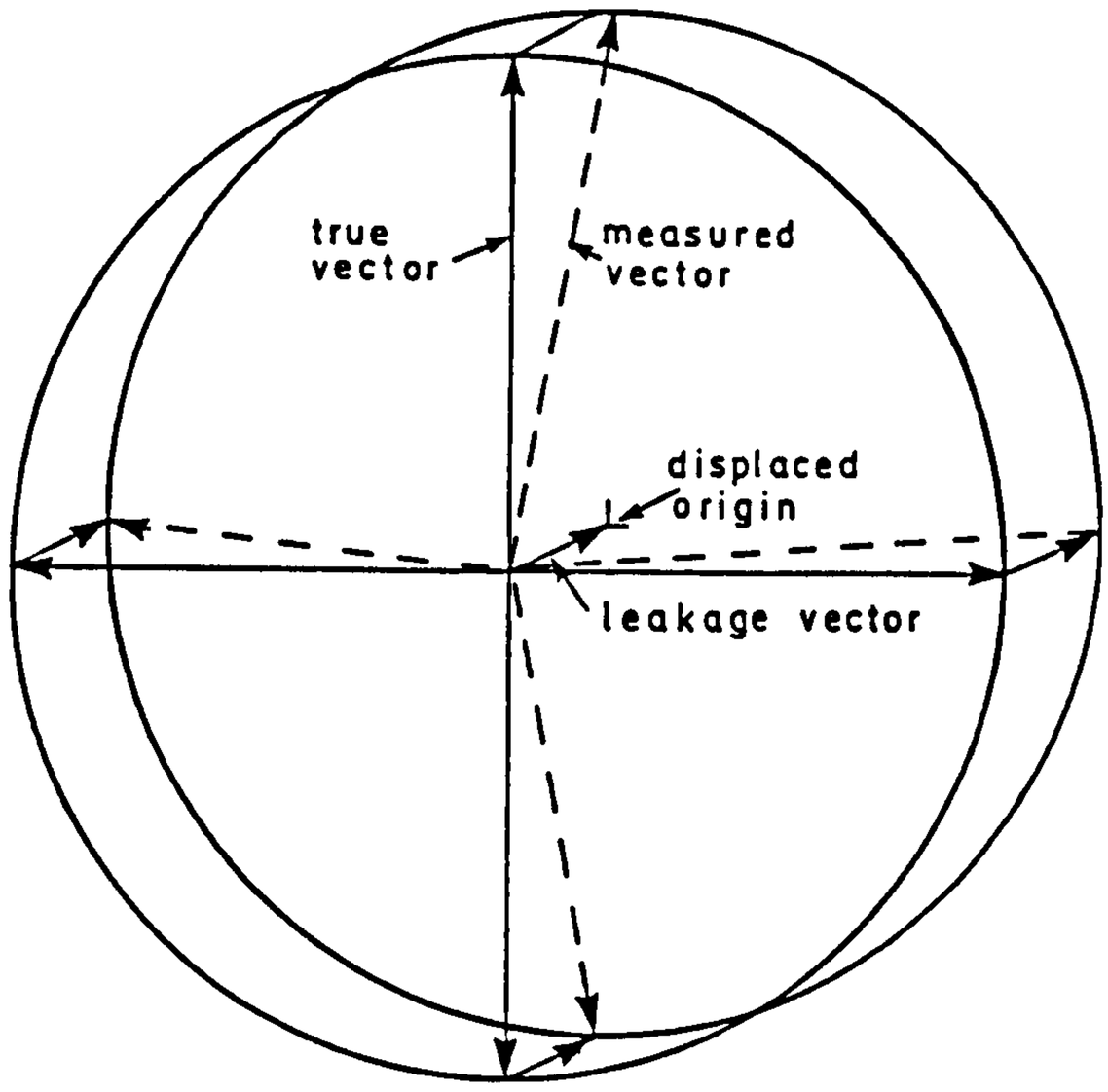

Figure 5.5 The effect of leakage, illustrating equivalence to an origin shift

Whilst there are many other possible sources of error that can degrade the accuracy of a network analyser system the above are usually dominant and are almost impossible to reduce sufficiently by hardware changes alone. They will serve as a basis for the development of an error model for the system; other sources of error will be considered as they arise.

5.5 GENERATING ERROR MODELS

There are essentially two approaches to generating an error model for use with a CCNA system. The first is to consider the arrangement and electrical properties of the constituent components and to construct a model which takes into account all possible signal paths. Much simplification is then required to produce a manageable error model. The second is usually called the "error box" approach. The system is

considered to comprise of a perfect (error free) network analyser connected to the DUT via an error box or boxes. This approach is illustrated in figure 5.6 for a general N-port DUT; requiring a 2N-port error box or, neglecting crosstalk, N 2-port error boxes. It is not considered necessary to have any description of the error box(es) other than its network (e.g.s-) parameters. Both approaches will be used to develop error models in order that their strengths and weaknesses should become evident. The discussion will be restricted to error model for 1- and 2-port DUTs but many of the general points could be applied to the correction of 3- or more port measurements.

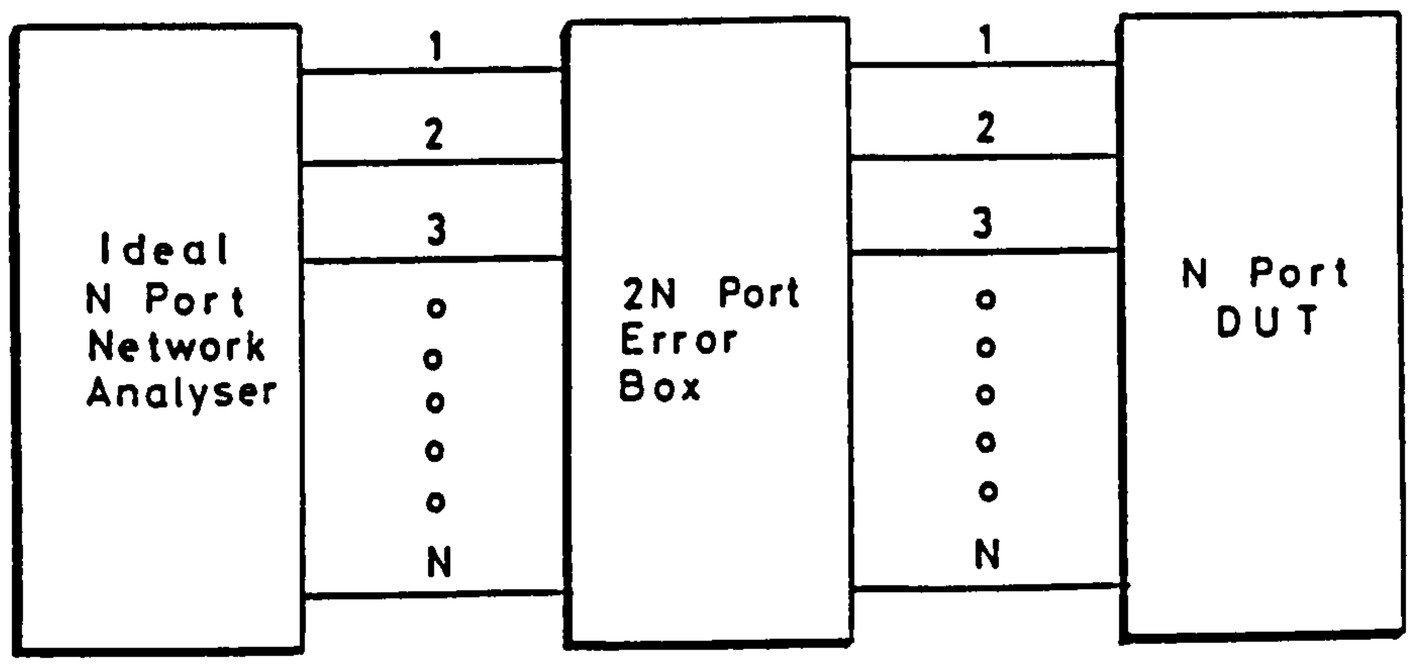

Figure 5.6 The 'Error Box' approach

5.5.1 Methods of Analysis

There are two principle mathematical tools for the constuction and exploitation of the error model: flowgraph analysis and matrix renormalisation. Flowgraph analysis[16] has the advantage of providing a close correspondance between the mathematical model and the physical system. Flowgraph manipulation and reduction allow the user to simplify the model whilst maintaining a 'feel' for the signal flow. It does however become cumbersome when an attempt to include all possible factors

is made. It is in this circumstance where complex voltage wave s-parameter matrix renormalisation[15] is of most value; facilitating a rigorous analysis of the complete system [14]. Because of it's clearer representation of the physical factors affecting the measurement problem the flowgraph technique will be applied to the following discussion of error models.

5.6 1-PORT ERROR MODELS

5.6.1 The Error Box Approach

The basic assumption made is that the system is that described in figure 5.6 where N=1. The error box is completely characterised by its 2-port s-parameters (denoted e_{xy}) and can therefore be represented by the flowgraph of figure 5.7.

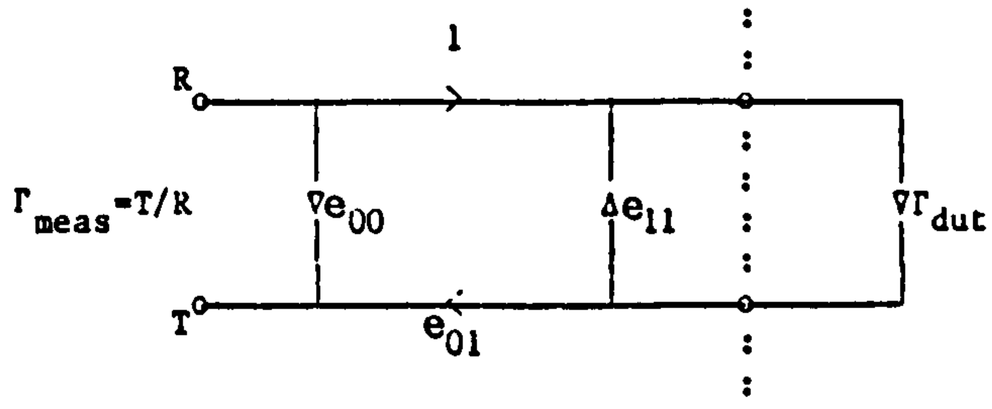

Figure 5.7 Flowgraph Representation of figure 5.6 for 1-port measurement

From this we obtain the well known result for the measured reflection coefficient:

$$\Gamma_{meas} = e_{00} + e_{01}\Gamma_{DUT}/(1-e_{11}\Gamma_{DUT}) \qquad \langle 5.1 \rangle$$

This expression demonstrates that there are only three independant complex error parameters involved in the reflection coefficient correction problem.

Shurmer[17] has applied a bilinear transform to the same problem with the proviso that the error box is assumed lossless. The transform

$$w = (az + b)(cz + d) \qquad \langle 5.2 \rangle$$

maps complex numbers in the z-plane to complex numbers in the w-plane. It has the significant property that a set of circles within circles in the z-plane are transformed to a similar set in the w-plane. If we allow the z-plane to be the relection coefficient plane of the DUT, which is bounded by the unit circle, we know that the w-plane is also a circularly bounded region. Letting the w-plane become the measured reflection coefficient plane, it can be shown that the general transform degenerates to the particular form:

$$\Gamma_{meas} = (a\Gamma_{DUT} + b)(c\Gamma_{DUT} + 1) \qquad \langle 5.3 \rangle$$

for this situation.

Now, rearranging <5.1> we have:

$$\Gamma_{meas} = (e_{00} - \Delta\Gamma_{DUT})/(1 - e_{11}\Gamma_{DUT}) \qquad \langle 5.4 \rangle$$

where $\Delta = e_{00}e_{11} - e_{01}$

Clearly, these two statements are equivalent where:

$$a = \Delta\ ,\ b = e_{00},\ c = -e_{11}$$

We observe, therefore that the stipulation concerning losslessness it unnecessary and that the two approaches yield identical results. The bilinear tranform technique will be developed in the following chapter in connection with microstrip calibration.

5.6.2 The Physical Approach

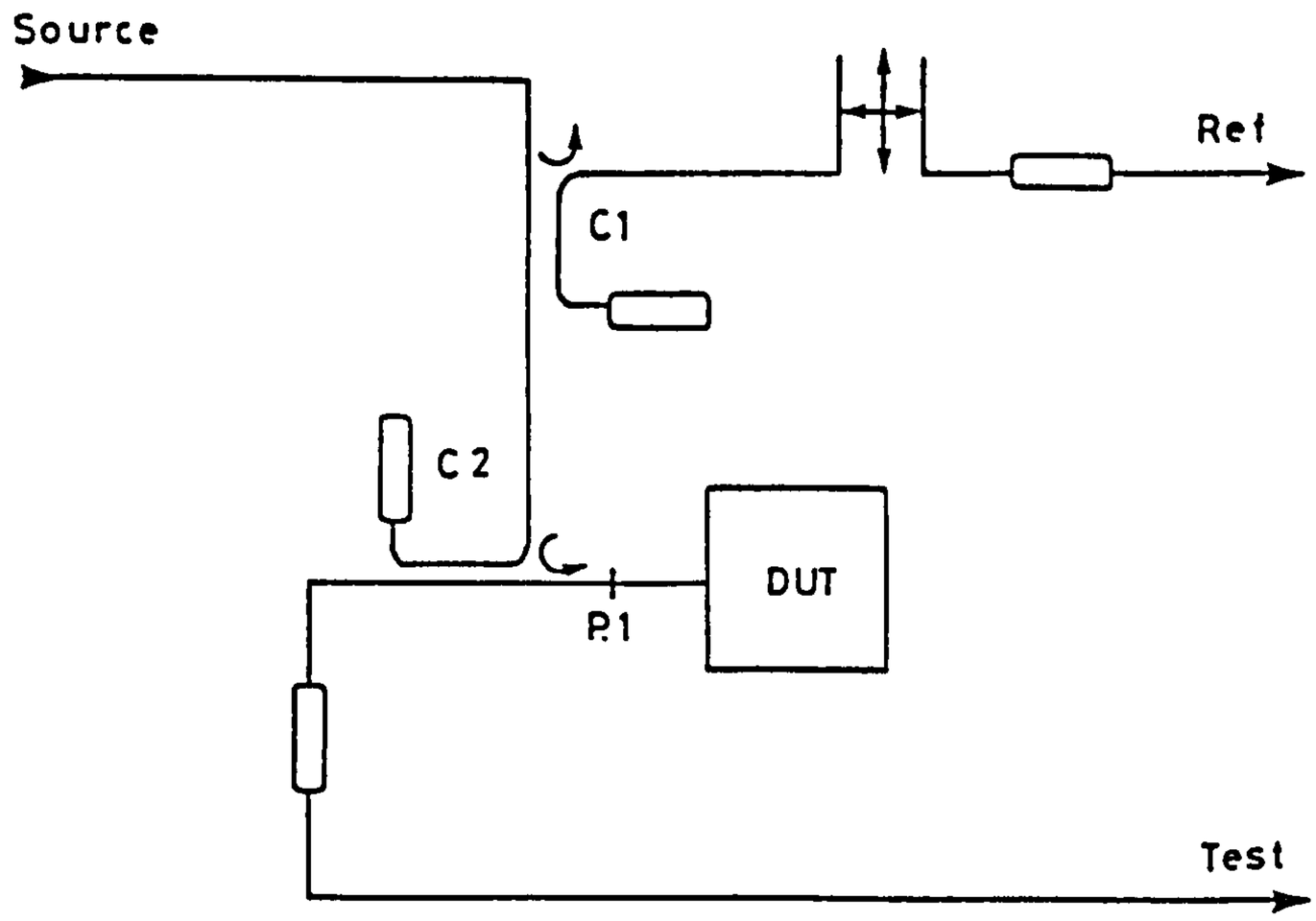

Figure 5.8 The Configuration of Microwave Hardware in a Typical Reflectometer System

A typical configuration for the reflectometer, or 1-port network analyser is illustrated in figure 5.8. The test coupler C2 is arranged so as to minimise the signal level incident on the DUT, whilst maintaining the dynamic range of the system, in order to ensure small signal conditions apply. When all possible component imperfections and their interactions are taken into account the flowgraph reprsentation becomes unwieldy. Application of the rules of flowgraph manipulation could ultimately produce an equivalent but grossly simplified flowgraph, but the task would be a mammoth one. Woods[14] has analysed this situation using the complex renormalised s-parameter method but it is here considered to be more instructive to treat the problem in terms of a number of elementary flowgraph error models. Each model need only accommodate one or two of the manifold error sources. Subsequently the effects described in each model can be superposed with the others on the basis of the linear assumption. Whilst this treatment is not completely exhaustive or rigorous it does, in the view of the author, yield a

greater insight to the problem.

Figure 5.9 is the flowgraph corresponding to the basic hardware of figure 5.8 assuming that the components are ideal.

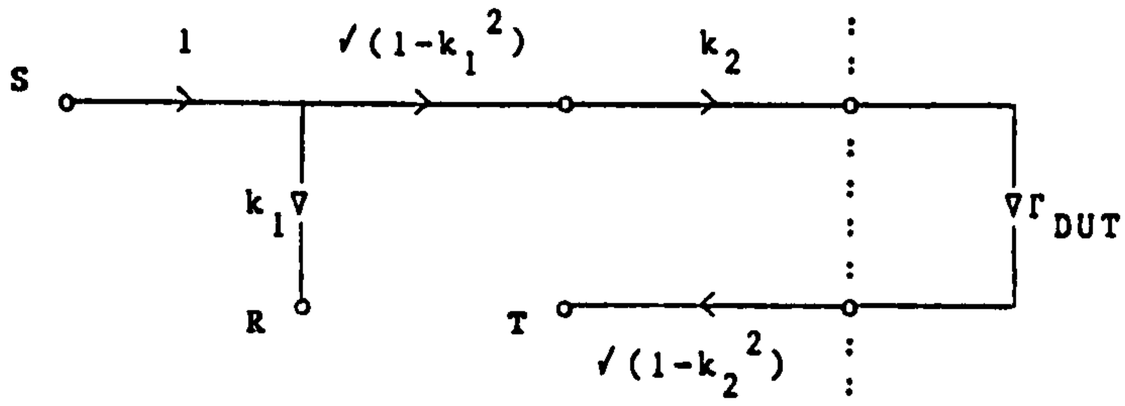

Figure 5.9 Reflectometer flowgraph assuming ideal components

The measured reflection coefficient is:

$$\Gamma_{meas} = T/R = \Gamma_{DUT}\sqrt{1-k_1^2}.k_2\sqrt{1-k_2^2}/k_1 = K\Gamma_{DUT} \qquad \langle 5.5 \rangle$$

where k_i is the coupling factor of the ith coupler.

The flowgraph can, by application of the rules of flowgraph analysis, be rearranged to eliminate the common generator, resulting in the simplified flowgraphs of figure 5.10, in which the reference port becomes the effective source.

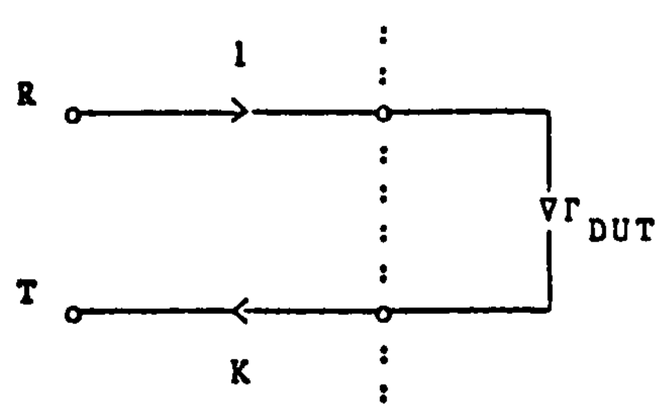

Figure 5.10 Simplified flowgraph after elimination of common generator

The ideal reflectometer uses a matched pair of couplers having small, identical coupling factors, such that:

$$k_1 = k_2 = k \quad , \quad 1 - k^2 = 1 \quad \text{and} \quad \Gamma_{meas} = \Gamma_{DUT}$$

If a larger coupling factor is required the coupling coefficients should not only be identical but also independent of frequency so that the term $1-k^2$ can be compensated using the analyser gain and phase offset controls. When, as is usually the case, the coupling factors are neither indentical nor independent of frequency the gain and phase deviations may

be recorded from measurements on a high reflection coefficient standard (e.g. a short circuit) and subtracted from the results for the DUT. Thus the flowgraph of figure 5.10 represents the assumed error model behind the use of the storage normaliser discussed in section 5.4.1.

Now re-introducing the directivity (d_j) and test port mismatch (r_t) effects the flowgraph of figure 5.9 becomes:

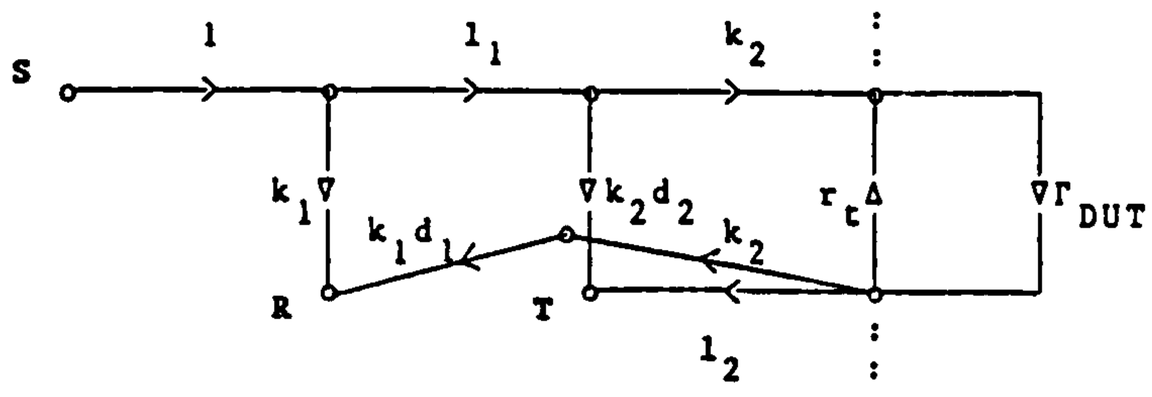

Figure 5.11 Flowgraph of Reflectometer including Directivity and Test Port Mismatch effects

Applying the rules of flowgraph manipulation this situation may be rearranged to the form of figure 5.7 yielding the following equivalences:

$$e_{00} = l_1 d_2 k_2 / k_1$$

$$e_{01} = (l_2 - l_1 k_2 d_1 d_2) l_1 k_2 / k_1$$

$$e_{11} = r_t - d_1 l_1 k_2$$

where $l_i \geq \sqrt{1-k_i^2}$ is the transmission loss of the couplers.

In a similar manner the effects of leakage, and source and detector mismatches can be accommodated and in all cases the minimised flowgraph conforms to the three term error model of figure 5.7.

5.7 2-PORT ERROR MODELS

Two approaches to the construction of an error model for a 2-port parameter measurement system will be considered.

5.7.1 The Error Box Approach

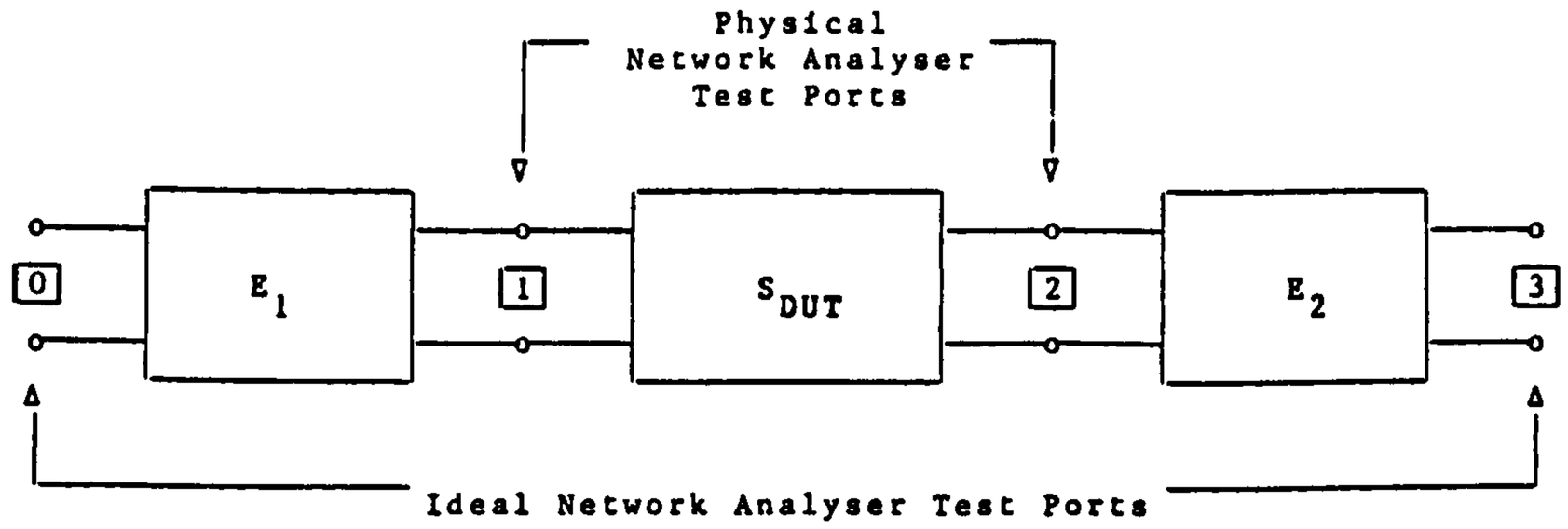

Figure 5.12 The 2-port error box model

Figure 5.12 illustrates the basic assumption made when adopting the error box approach. Note the simplification from the general situation of figure 5.6, there being no cross-coupling between the two error boxes. These boxes; 'E_1' and 'E_2', are completely characterised by their 2-port s-parameters. Using the flowgraph technique this situation may be represented by figure 5.13.

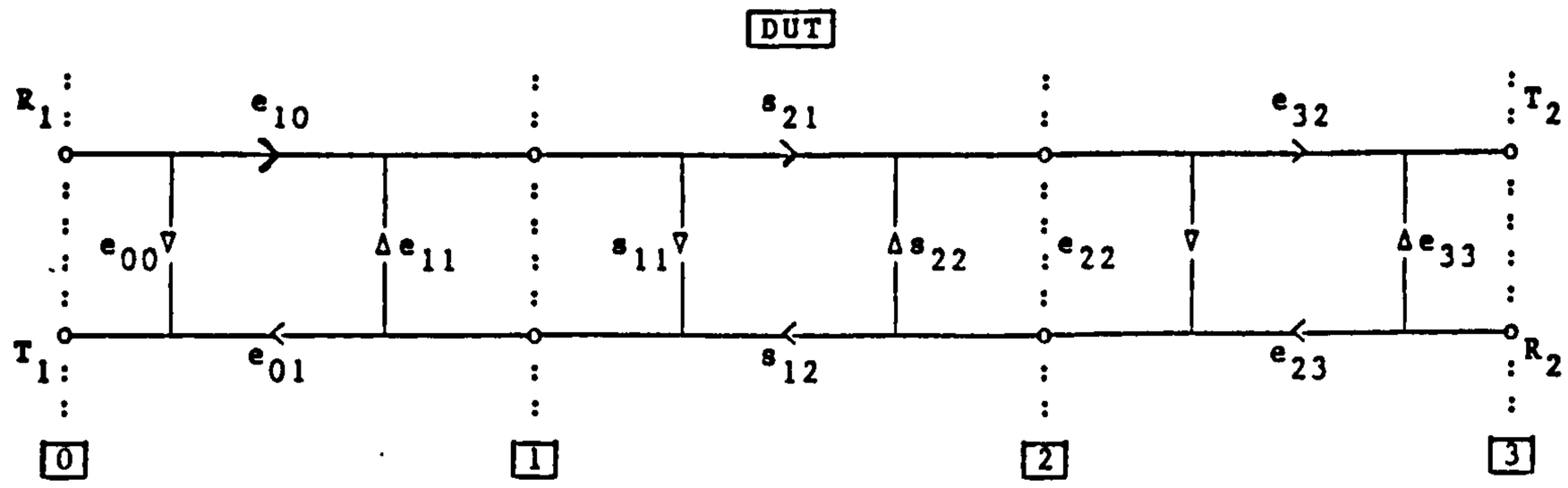

Figure 5.13 Flowgraph representation of the 2-port error box model for an s-parameter test set

The four measured s-parameters (denoted U_{jk}) are, therefore;

$$U_{jk} = T_j/R_k \; ; \quad j = 1,2; \quad k = 1,2 \qquad \langle 5.7 \rangle$$

where R_1 and R_2 are the alternative reference generators and T_1 and T_2 are the two test channel connections. These are related to the true s-parameters of the device by the following equations:-

$$U_{11} = e_{00} + e_{10}e_{01}\{s_{11}(1-s_{22}e_{22}) + s_{21}s_{12}e_{22}\}/D \qquad \langle 5.8a \rangle$$

$$U_{21} = s_{21}e_{10}e_{32}/D \qquad \langle 5.8b \rangle$$

$$U_{12} = s_{12}e_{23}e_{01}/D \qquad \langle 5.8c \rangle$$

$$U_{22} = e_{33} + e_{23}e_{32}\{s_{22}(1-s_{11}e_{11}) + s_{21}s_{12}e_{11}\}/D \qquad \langle 5.8d \rangle$$

where $D = 1 - s_{11}e_{11} - s_{22}e_{22} + \Delta e_{11}s_{22}$

and $\Delta = \det_{[S]} = s_{11}s_{22} - s_{12}s_{21}$

or $D = (1 - s_{11}e_{11})(1 - s_{2}e_{22}) - s_{12}s_{21}$

Note the pairing of the terms $e_{10}e_{01}$, $e_{23}e_{32}$, $e_{10}e_{32}$, $e_{23}e_{01}$. Using this feature we may rearrange the flowgraph as illustrated in figure 5.14.

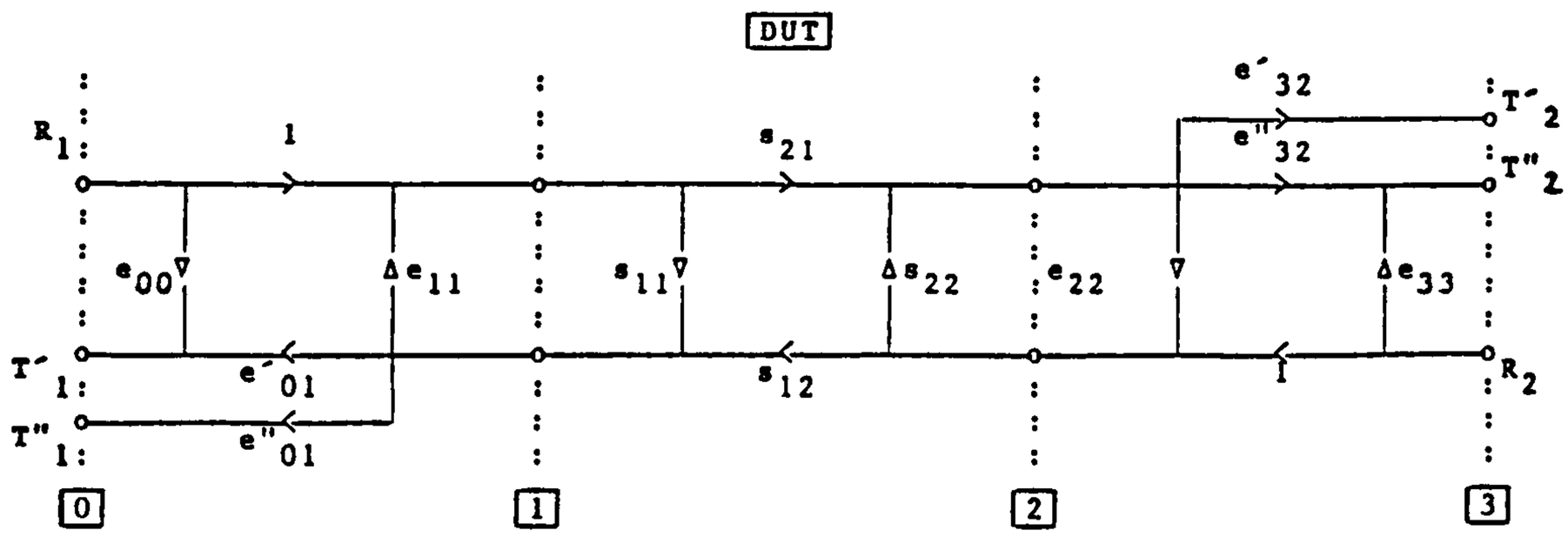

Figure 5.14 Flowgraph of 2-port Network Analyser using the pairing of the terms to separate transmission and reflection paths,

where the following equivalences apply:-

$$e'_{01} = e_{10}e_{01} \qquad e''_{01} = e_{23}e_{01}$$

$$e'_{32} = e_{10}e_{32} \qquad e''_{32} = e_{23}e_{32}$$

This highlights the fact that this approach produces an error model equivalent to the one-port error model of figure 5.7, duplicated for the two ports of the test set, plus two additional complex error parameters related to the transmission measurements. The total number of independant error parameters is, in either case, eight; the minimum number required for correction of 2-port s-parameter measurements. As will be demonstrated by consideration of the physical approach, this

error model is not comprehensive enough for many applications.

5.7.2 The Physical Approach

5.7.2.1 The Reflection/Transmission Test Set

Many network analyser systems incorporate a reflection/ transmission test set, so requiring the operator to reverse the DUT when it is not electrically symmetrical. Whilst this can be inconvenient, this test set has the virtue of being somewhat simpler than the s-parameter test set as it includes fewer coax switches. It is for this reason that the error model for the reflection/ transmission test set will be considered first; that for s-parameter test set will be developed subsequently.

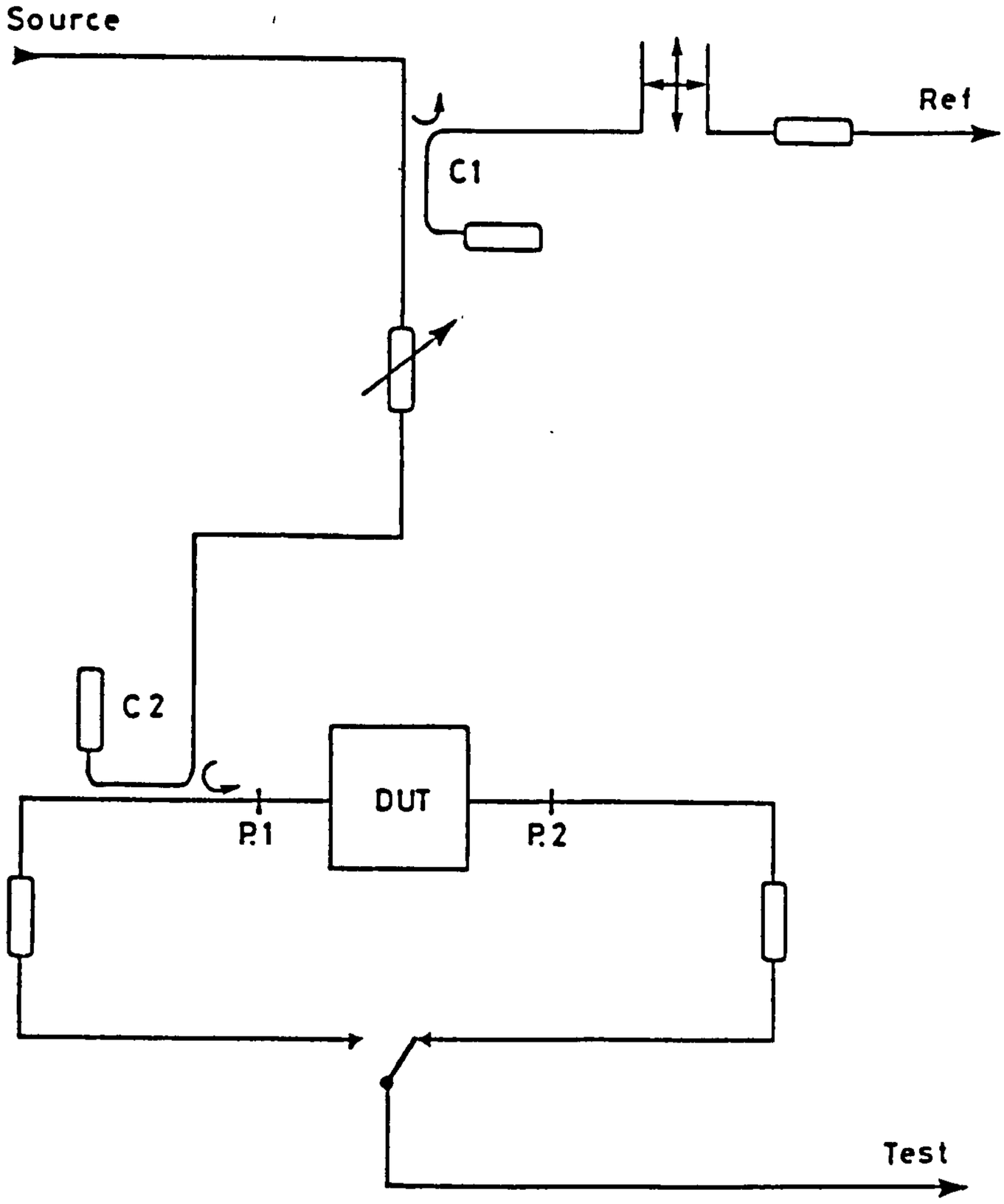

Figure 5.15 Simplified diagram of the Reflection/ Transmission Test Set

An attempt to construct a complete flowgraph representation reaches an impass when the switch is encountered. By assuming that the network analyser instrument has two test ports it is possible to produce the flowgraph of figure 5.16

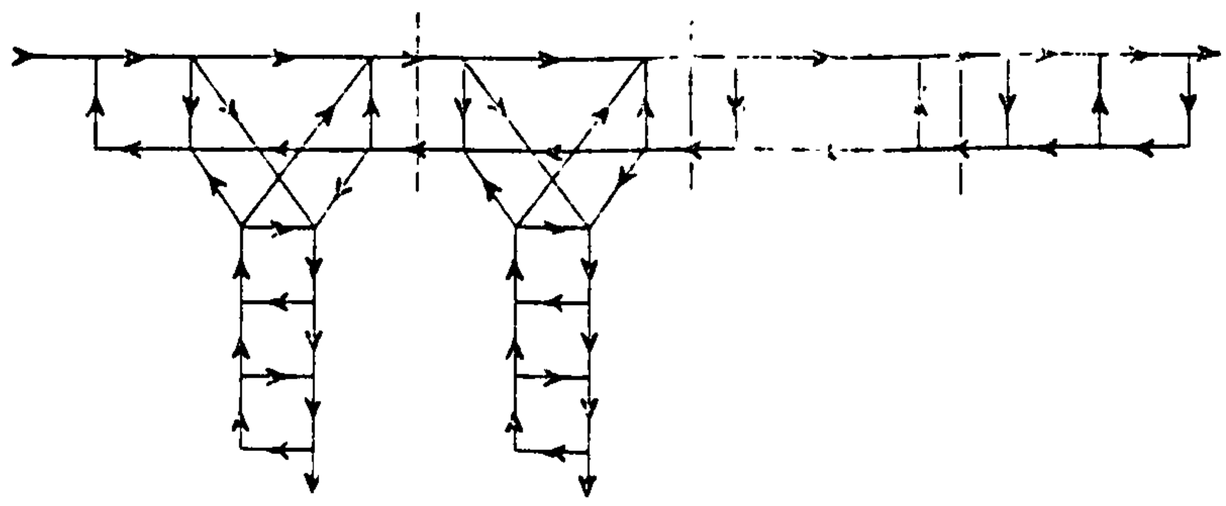

Figure 5.16 Complete (?) flowgraph of the Reflection/ Transmission Test Set (with dual test port network analyser)

Unfortunately at the present time no commercial microwave network analysers fulfil this requirement. Consequently there is an obstacle to the construction of a rigorous error model for the commercial microwave network analyser [12]. Given that, in general, the test port of the network analyser instrument presents a different terminating impedance from the internal loads, the switching of the test port results in a change of the test port mismatches. Usually the elements of the error model are considered invariant when changing between the transmission and reflection modes. This additional source of systematic error will be called "switching error" and should not be confused with the non-systematic effect of switch repeatability. Further consideration will be given to the problem of switching error later in this chapter, but for the present we shall consider the error model to be unaffected by the switching error. In the test set 10dB attenuator pads are included to moderate this effect by providing a 10:1 (20dB reduction in mismatch variation.

As for the case of the reflectometer, direct application of the techniques of flowgraph reduction to the complete flowgraph of figure 5.16 would be rather cumberscme. Woods [14] has applied voltage-wave s-parameter complex renormalisation (a technique utilised elsewhere in this thesis) to this problem. Once more, however, the approach adopted here, because of its evident links with the physical effects concerned, will be to consider the individual error contributions, subsequently aggragating their effect to produce the complete error model. Refering to figure 5.15 it is apparent that the reflection/transmission test set is an extension of the reflectometer of figure 5.8. The addition of the second (transmission) test port and the associated hardware introduces further sources of systematic error: transmission gain and phase error, opposite test port mismatch and transmission leakage or crosstalk. These

error sources have been fully discussed in sections 5.4.1, 3 & 4 respectively.

Using the results for the reflectometer described in section 5.6 and applying similar flowgraph manipulation techniques to the new elements the error model becomes that of figure 5.17. The elements shown dotted are irrelevant to the error model as they contribute to neither the transmission nor reflection paths.

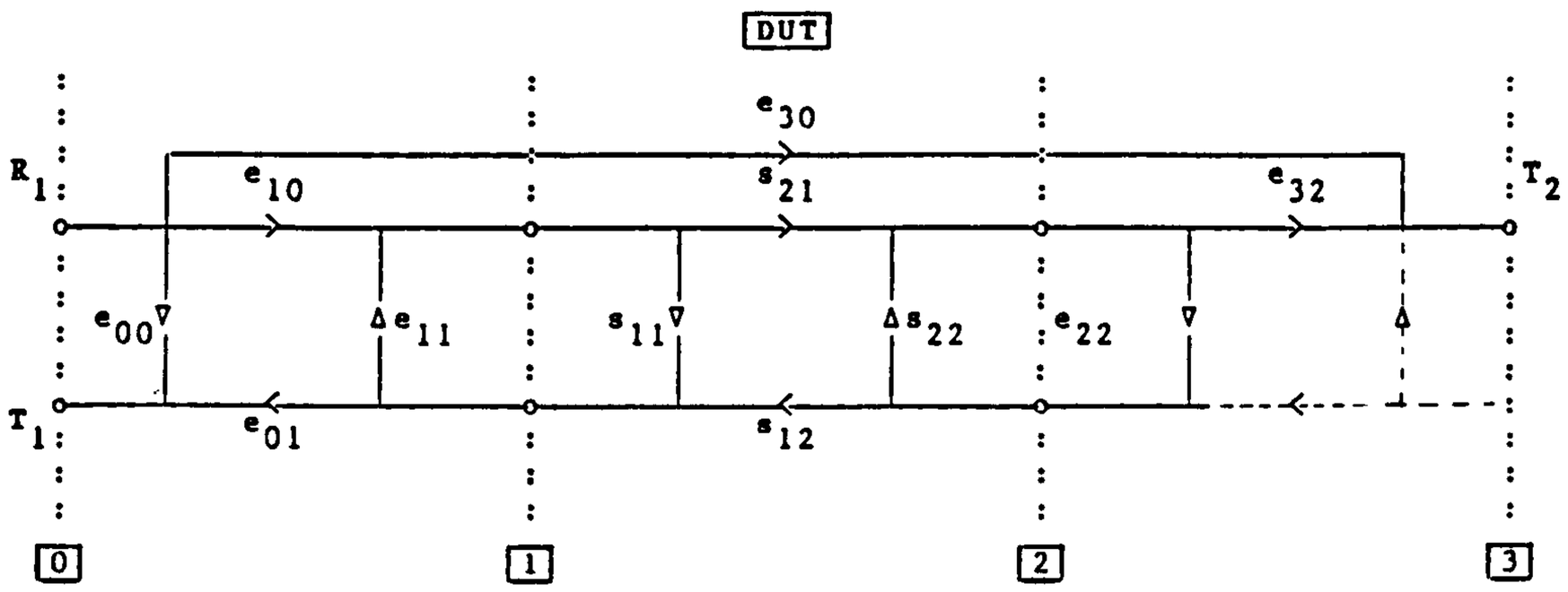

Figure 5.17 Flowgraph error model for reflection/transmission test set

The corresponding equations for the reflection/transmission test set are:-

$$U_r = T_r/R = e_{00} + e_{01}\{s_{11}(1-s_{22}e_{22})-s_{12}s_{21}e_{22}\}/D \qquad \langle 5.9a \rangle$$

$$U_t = T_t/R = e_{30} + s_{21}e_{32}/D \qquad \langle 5.9b \rangle$$

where $D = 1 - s_{11}e_{11} + s_{22}e_{22} + \Delta e_{11}e_{22}$

In the error model above it has been assumed that the dominant crosstalk occurs between the reference and test sampling mixers and that it is undirectional (i.e. from reference to test only) as it is most common for test signal to be smaller than the reference. When an amplifier with high gain is to be measured it is usual to include attenuation between the reference coupler and the input of the DUT in order to avoid saturation of the sampling mixer or the DUT itself, thus reducing the test channel signal level to the same order as the reference. Unlike the 1-port situation the leakage results in the addition of the distinct

signal path to the flowgraph error model. This error model then has a total of six independent terms, possibly reducing to five if the leakage is substantially lower than the smallest s_{21} or s_{12} to be measured.

5.7.2.2 The S-Parameter Test Set

The s-parameter test set, as illustrated in figure 5.18, can be considered to be the reflection/transmission test set with the addition of a DUT reversing switch.

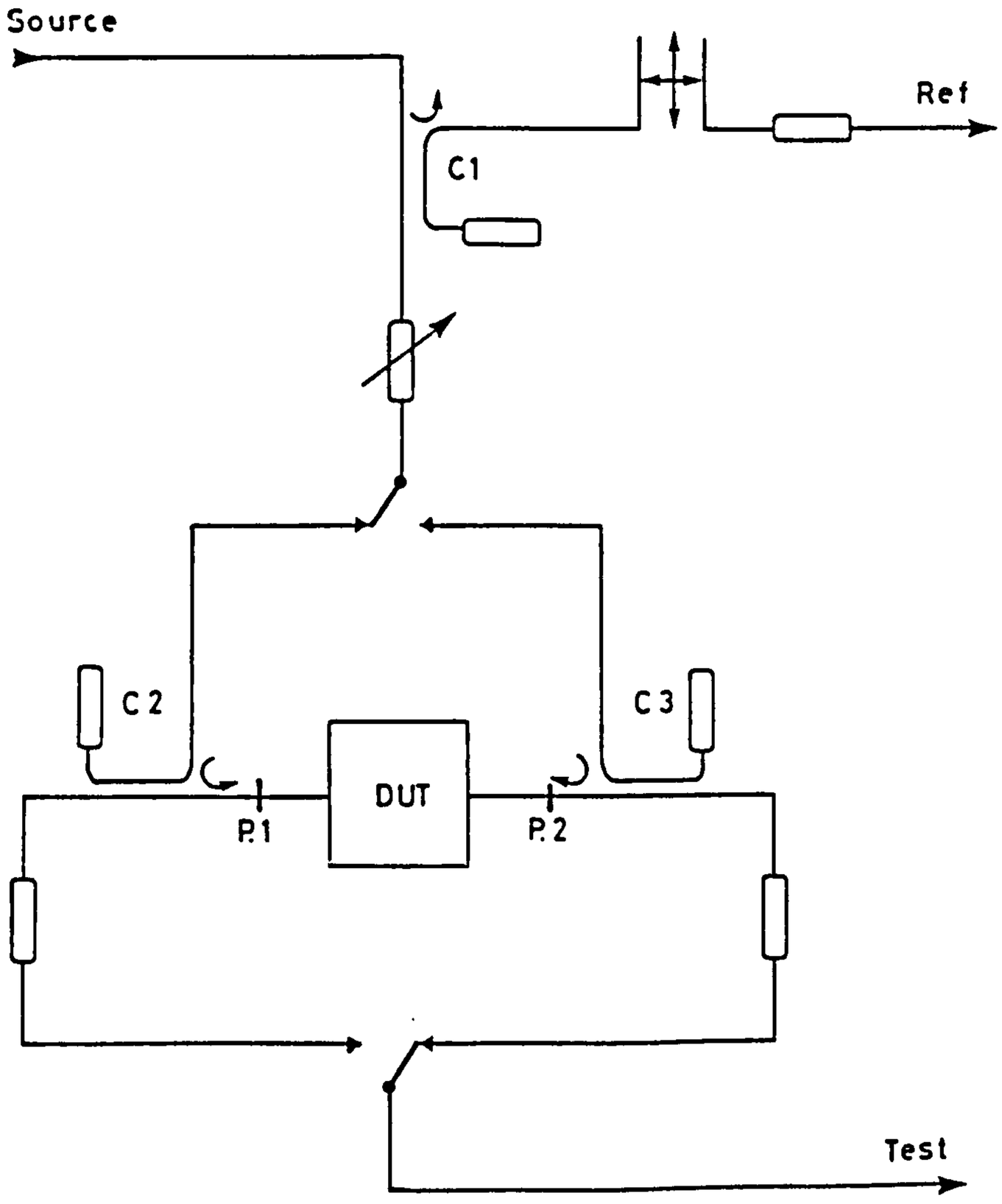

Figure 5.18 Diagram of S-Parameter Test Set

With this in mind, the best approach to the derivation of an error model for the s-parameter test set appears to be to use that for the reflection/transmission test set repeated and reversed for s_{22} and s_{12}. Thus the compound 12-term error model is that represented by the flowgraph of figure 5.19.

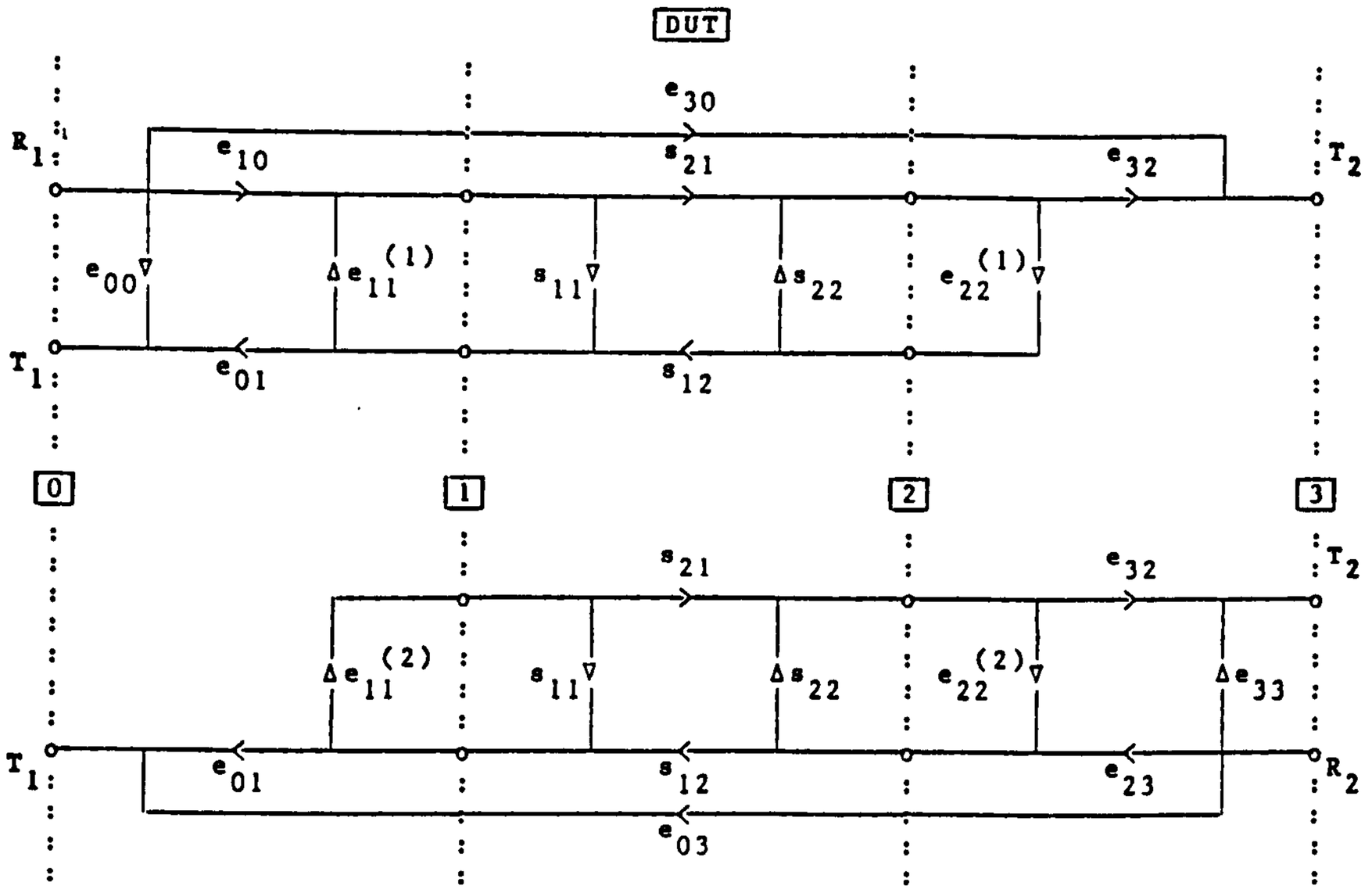

Figure 5.19 Bilateral 12-term error model for the S-Parameter Test Set

and described by the following equations:

$$U_{11} = e_{00} + e_{01}^{(1)}\{s_{11}(1-s_{22}e_{22}^{(1)}) + s_{21}s_{12}e_{22}^{(1)}\}/D^{(1)} \qquad \langle 5.10a \rangle$$

$$U_{21} = e_{30} + s_{21}e_{32}^{(1)}/D^{(1)} \qquad \langle 5.10b \rangle$$

$$U_{12} = e_{03} + s_{12}e_{01}^{(2)}/D^{(2)} \qquad \langle 5.10c \rangle$$

$$U_{22} = e_{33} + e_{32}^{(2)}\{s_{22}(1-s_{11}e_{11}^{(2)}) + s_{21}s_{12}e_{11}^{(2)}\}/D^{(2)} \qquad \langle 5.10d \rangle$$

where $D^{(1)} = 1 - s_{11}e_{11}^{(1)} - s_{22}e_{22}^{(1)} + \Delta e_{11}^{(1)}e_{22}^{(1)}$

$$D^{(2)} = 1 - s_{11}e_{11}^{(2)} - s_{22}e_{22}^{(2)} + \Delta e_{11}^{(2)}e_{22}^{(2)}$$

Comparing this result with figure 5.13 we observe that the physical approach produces an error model with four more terms than that obtained for the error box approach. What is the significance of the additional terms? Firstly, two are associated with crosstalk or leakage which, in the application of the error box approach, were assumed zero; permitting the 4-port error box to be divided into two 2-port boxes. The inclusion of the leakage terms may, or may not be of significance depending on the magnitude of the transmission coefficients to be measured. The other two additional terms result from the two values ascribed to each of the two

test port mismatch vectors (i.e. $e_{11}^{(1)}$, $e_{11}^{(2)}$ and $e_{22}^{(1)}$, $e_{22}^{(2)}$). Due to the effect of switching error these terms are, in general, different in magnitude and phase. Consequently the addition of these terms can result in a real improvement in calibration accuracy.

To be completely general, these test port mismatch vectors have four values; one for each s-parameter selection. Calibration for an error model which allows four values for each test port mismatch is difficult to achieve in the practical environment.

The construction of the error model of figure 5.19 makes the tacit assumption that:-

$$e_{11}^{(s_{11})} = e_{11}^{(s_{21})} = e_{11}^{(1)}, \quad e_{11}^{(s_{12})} = e_{11}^{(s_{22})} = e_{11}^{(2)}$$
$$e_{22}^{(s_{22})} = e_{22}^{(s_{12})} = e_{22}^{(1)}, \quad e_{22}^{(s_{21})} = e_{22}^{(s_{11})} = e_{22}^{(2)}$$

We should, however, attempt to justify this assumption by measurement of the values of e_{11} and e_{22} for all four modes. Using a second network analyser to perform the measurements Thomas [18] has produced the values recorded in table 5-1.

TABLE 5-1 MEASUREMENTS OF TEST PORT MISMATCH

FREQ	S_{11}		S_{21}		S_{12}		S_{22}	
(GHz)	Mag (dB)	Ang (deg)	Mag (dB)	Ang (deg)	Mag (dB)	Ang (deg)	Mag (dB)	Ang (deg
2.0	-28.8	-120	-35.6	0	-28.0	-120	-57.0	10
4.0	-28.8	-20	-26.3	40	-27.0	-30	-26.9	20
6.0	-31.1	-100	-31.6	170	-32.0	-100	-32.1	150
8.0	-40.8	160	-28.4	150	-39.0	130	-27.9	150
10.0	-25.3	-50	-30.5	-90	-25.0	-50	-30.3	-80
12.0	-22.6	40	-27.3	80	-25.0	30	-27.5	90

Note: Measured on port 1 of HP8746B S-Parameter Test Set

From the table it is evident that the pairing of the values used for the 12-term error model of figure 5.19 is inappropriate. Relating this to the hardware it is apparant that the switching of the signal to the test input of the network analyser instrument has a much greater effect than the switching of the source. Figure 5.20 is the composite error model, having in essence sixteen terms; because of the four possible values of each test port mismatch.

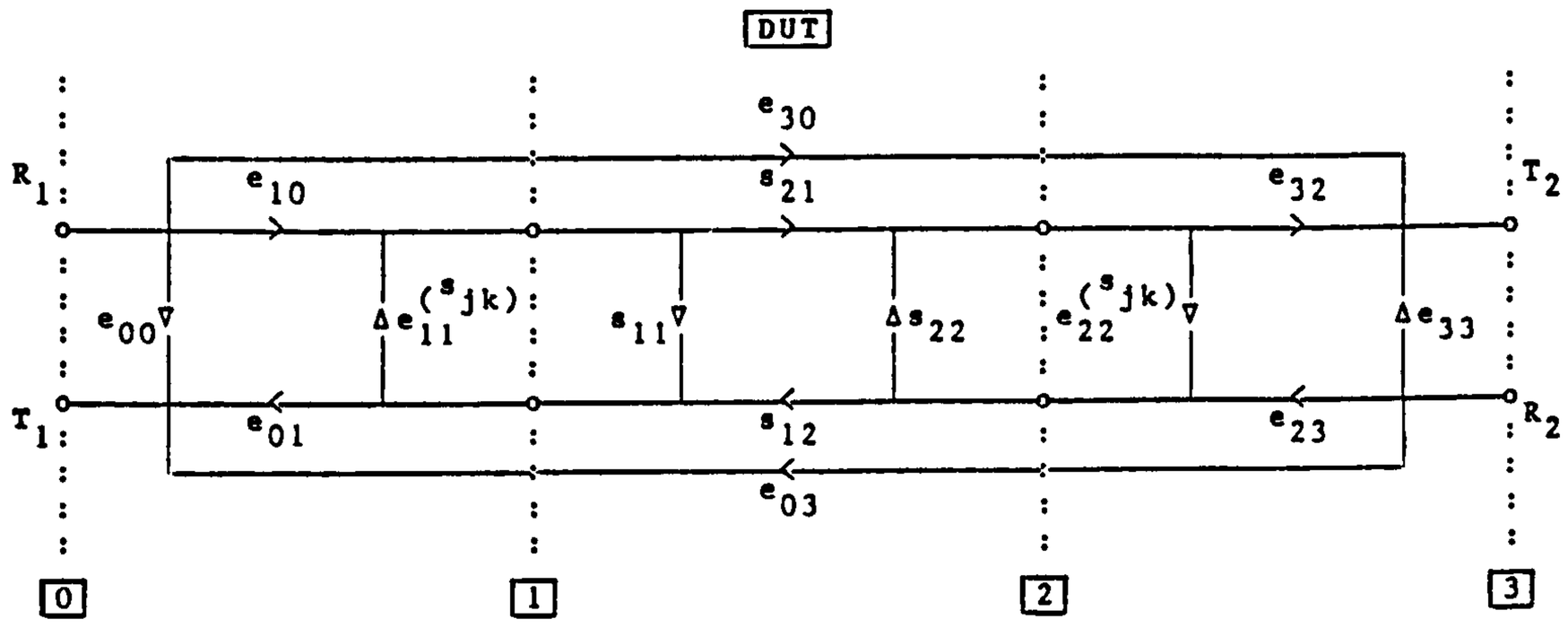

Figure 5.20 Composite 16-term error model for 2-port S-Parameter Test Set

If we now pair the terms in a way more appropriate to the results of the measurements recorded in table 1, we have:

$$e_{11}^{(s_{11})} = e_{11}^{(s_{12})} = e_{11}^{(1)}, \quad e_{11}^{(s_{22})} = e_{11}^{(s_{21})} = e_{11}^{(2)}$$

$$e_{22}^{(s_{11})} = e_{22}^{(s_{12})} = e_{22}^{(1)}, \quad e_{22}^{(s_{22})} = e_{22}^{(s_{21})} = e_{22}^{(2)}$$

We may now divide the composite error model of figure 5.20 in a manner similar to the bilateral model of figure 5.19, but with more appropriate pairing of the e_{11} and e_{22} terms, as illustrated in figure 5.21

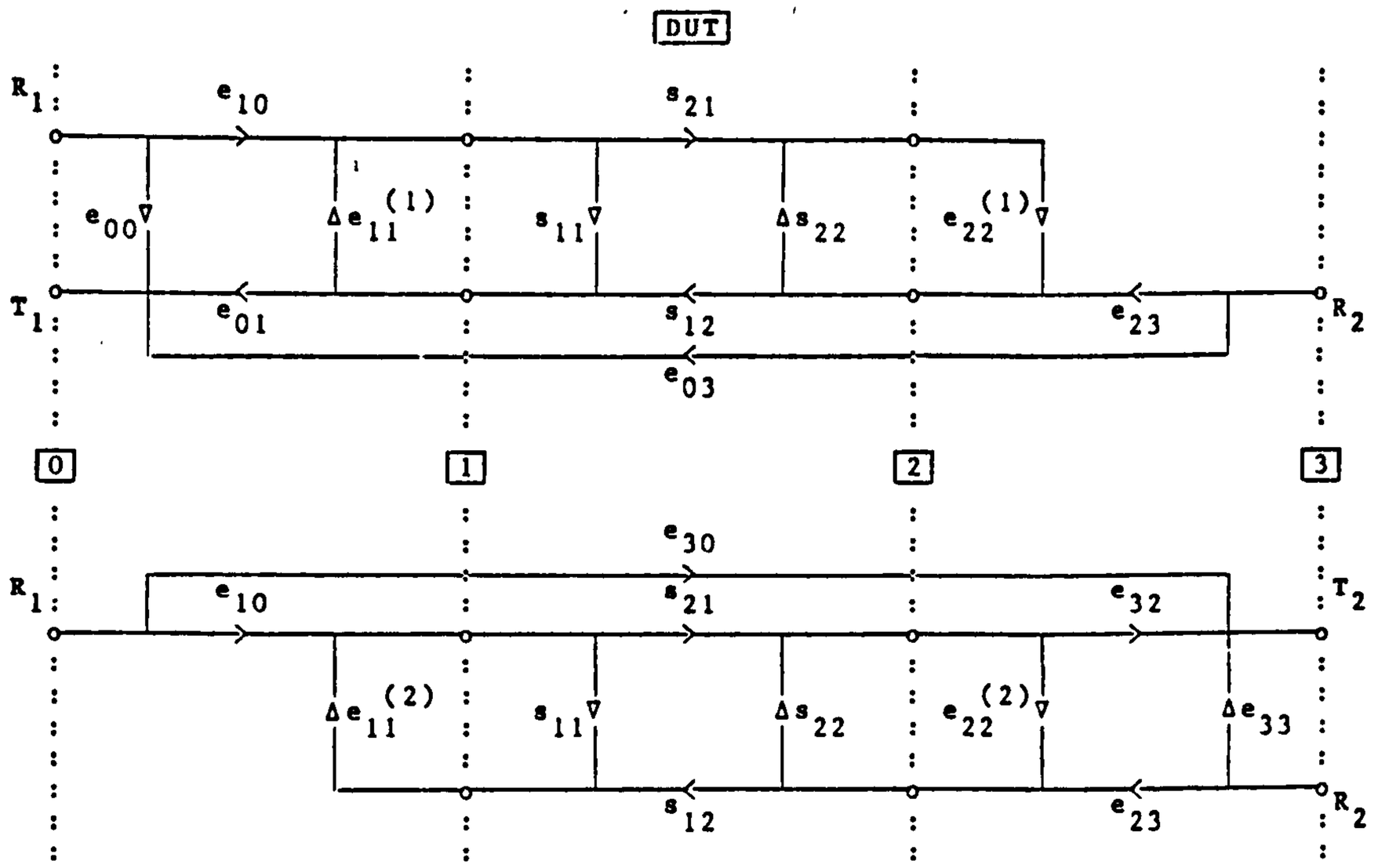

Figure 5.21 Modified bilateral 12-term error model of S-Parameter Test Set

Consequently we now have an improved 12-term error model where the pairing of the e_{11} and e_{22} terms for the four modes of the test set have been demonstrated, by measurement, to represent a closer conformance to the true situation than that most frequently applied. The significance of this revision is greatest when measuring DUT's with high reflection coefficients (s_{11},s_{22}). The additional error in the measurement of s_{21} (or s_{12}) for a DUT having s_{11} and s_{22} close to unity (e.g. a GaAs MESFET) could, from the results in Table 5-1, be of the order of 0.5dB when using the original pairing.

Saleh [19] identifies two classes of test set. This situation (exemplified by the HP8746B Test Set) corresponds to Type II, in which the directional couplers are arranged, in order to ensure small signal operation of the DUT, as illustrated in figure 5.22. A Type I test is configured to service large signal s-parameter measurement requirements and has couplers arranged as shown in figure 5.22. For such a test set (an example of which is the HP8746B Opt001 Test Set) the error model of

figure 5.19 is entirely suitable and the equations <5.10> should be applied.

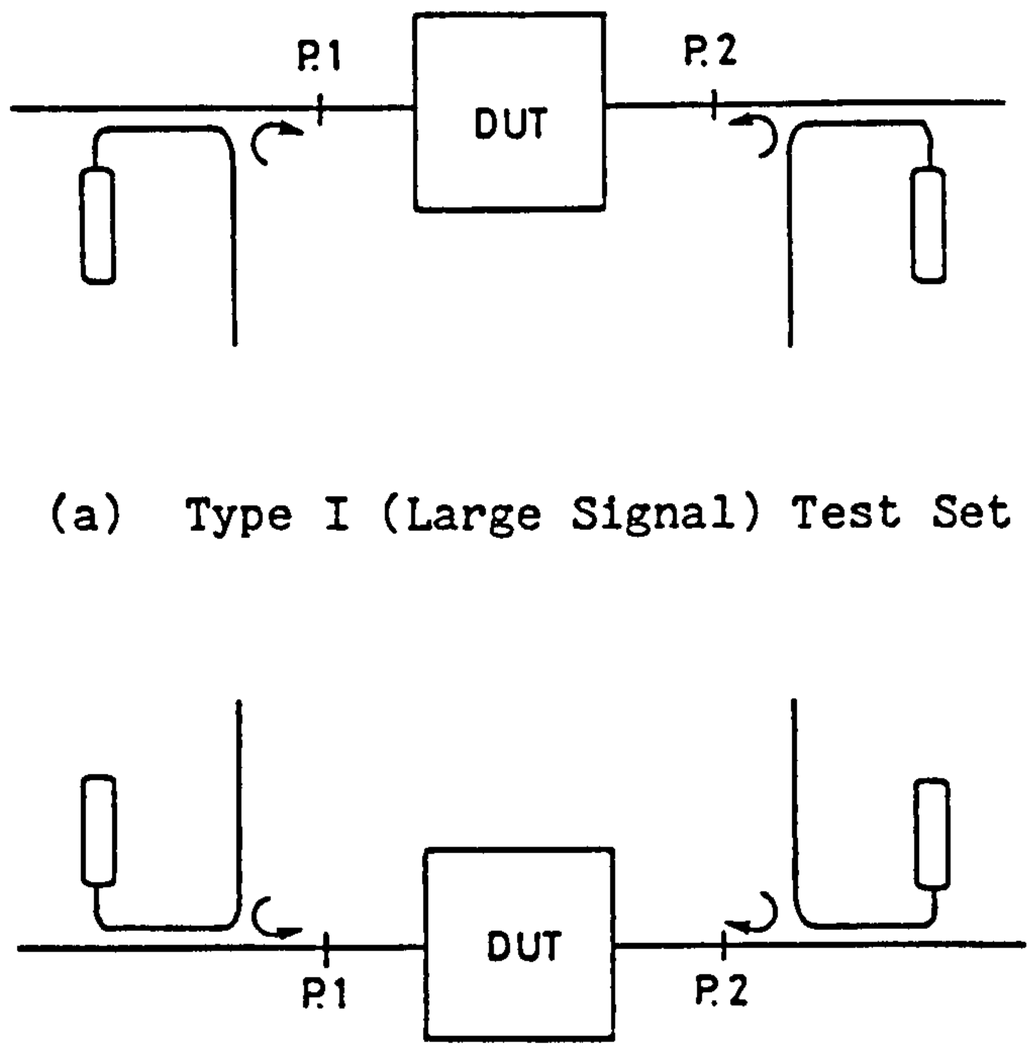

(a) Type I (Large Signal) Test Set

(b) Type II (Small Signal) Test Set

Figure 5.22 Alternative S-Parameter Test Set configurations

The equations for the flowgraph error model of figure 5.21, corresponding to the Type II test set are:

$$U_{11} = e_{00} + e_{10}^{(1)}\{s_{11}(1-s_{22}e_{22}^{(1)}) + s_{21}s_{12}e_{22}^{(1)}\}/D^{(1)} \qquad \text{<5.11a>}$$

$$U_{21} = e_{30} + s_{21}e_{10}^{(2)}/D^{(2)} \qquad \text{<5.11b>}$$

$$U_{12} = e_{03} + s_{12}e_{23}^{(2)}/D^{(2)} \qquad \text{<5.11c>}$$

$$U_{22} = e_{33} + e_{23}^{(2)}\{s_{22}(1-s_{11}e_{11}^{(2)}) + s_{21}s_{12}e_{11}^{(2)}\}/D^{(2)} \qquad \text{<5.11d>}$$

where $D^{(1)} = 1 - s_{22}e_{11}^{(1)} - s_{22}e_{22}^{(1)} + \Delta e_{11}^{(1)}e_{22}^{(1)}$

$D^{(2)} = 1 - s_{11}e_{11}^{(2)} - s_{22}e_{22}^{(2)} + \Delta e_{11}^{(2)}e_{22}^{(2)}$

The error model resulting from the application of the physical approach is superior to that obtained from the error box approach, as it is usually applied, in two respects; the inclusion of leakage paths and the variation of test port mismatch with s-parameter mode switching. The most comprehensive error model is the 16-term model of figure 5.20, but

no practical method of calibration exists for this situation. Thus an uncertainty remains. The real solution to this remaining inadequacy in the error model lies with the hardware design. The elimination of one set of switches, most appropriately the test channel switching, would result in a test set that, aside from the issues affecting leakage already be discussed, could be rigorously modelled by the original bilateral 12-term error model of figure 5.19. This would require, however, a network analyser having three channels (reference and two test channels).

5.8 1-PORT CALIBRATION SCHEMES

The purpose of the calibration process is to ascribe values to the chosen error model by measurement of a number of calibration standards. The most elementary calibration scheme involves the use of a short circuit termination and, when 2-ports are to be measured, a through line. This calibration is required to set up the uncorrected manual network analyser. The application of the storage normaliser to this case has already been discussed (cf. section 5.41). The most fundamental requirements are that the scheme should use calibration pieces that can be independently assessed (or are inherently self checking) and that they result in well ordered solutions for error terms. Other factors affecting the choice of calibration schemes are the frequency range and bandwidth under consideration, and the characteristics of the DUT. Ideally any calibration scheme should be as accurate for any DUT as any other but, in practise because of the limited dynamic range of the instrumentation and other non-systematic effects the best results are obtained when at least one of the calibration pieces has a reflection coefficient similar to that of the DUT. We shall initially consider the

calibration of 1-port or reflectometer systems and subsequently the full 2-port calibration problem will be discussed.

From the dicussion of section 5.6 we observe that three dissimilar calibration standards must be used to determine the three unknowns in the error model.

5.8.1 Three General Standards

Using the one port calibration equation (equation <5.1>) for each of the three known standards with complex reflection coefficients $\Gamma_{s1},\Gamma_{s2},\Gamma_{s3}$, we have:

$$\Gamma_{m1} = e_{00} + e_{01}\Gamma_{s1}/(1-e_{11}\Gamma_{s1}) \qquad \langle 5.12 \rangle$$

$$\Gamma_{m2} = e_{00} + e_{01}\Gamma_{s2}/(1-e_{11}\Gamma_{s2}) \qquad \langle 5.13 \rangle$$

$$\Gamma_{m3} = e_{00} + e_{01}\Gamma_{s3}/(1-e_{11}\Gamma_{s3}) \qquad \langle 5.14 \rangle$$

Solution of these three simultaneous equations yields values for the three error vectors. A matrix formulation can be applied to this system of equations [18], see also [20] thus:

$$[\Gamma_m] = [\Gamma_s].[E] \qquad \langle 5.15 \rangle$$

where

$$[\Gamma_m] = \begin{bmatrix} \Gamma_{m1} \\ \Gamma_{m2} \\ \Gamma_{ms} \end{bmatrix}$$

$$[\Gamma_s] = \begin{bmatrix} 1 & \Gamma_{s1} & \Gamma_{s1}\Gamma_{m1} \\ 1 & \Gamma_{s2} & \Gamma_{s2}\Gamma_{m2} \\ 1 & \Gamma_{s3} & \Gamma_{s2}\Gamma_{m3} \end{bmatrix}$$

$$[E] = \begin{bmatrix} e_{00} \\ e_{01}-e_{00}e_{11} \\ e_{11} \end{bmatrix}$$

Solving for the elements of [E] is then an elementary matrix problem easily handled by standard techniques.

Some particular choices of calibration standards will now be considered.

To produce the best conditioned solution of the calibration equations it is necessary to select the standards to ensure the minimum interdependance of the three complex error parameters. In practical terms this can be considered in terms of the disposition of the the reflection coefficients of the standards on the reflection coefficient plane (the Smith chart).

5.8.2 Load, Short, Open Calibration

An ideal load has the reflection coefficient; $\Gamma_{s1} = 0$

thus equation <5.14> becomes:

$$\Gamma_{m1} = e_{00} \qquad \text{<5.16>}$$

A short circuit has the reflection coefficient; $\Gamma_{s2} = -1$

so:

$$\Gamma_{m2} = e_{00} - e_{01}/(1 + e_{11}) \qquad \text{<5.17>}$$

An ideal open circuit has the reflection coefficient; $\Gamma_{s3} = +1$

so:

$$\Gamma_{m3} = e_{00} + e_{01}/(1-e_{11}) \qquad \text{<5.18>}$$

or $$\Gamma_{m2} - \Gamma_{m1} = - e_{01}/(1 + e_{11}) \qquad \text{<5.19>}$$

and $$\Gamma_{m3} - \Gamma_{m1} = e_{01}/(1 - e_{11}) \qquad \text{<5.20>}$$

This calibration scheme is so well conditioned that the problem reduces to that of finding the solution to a pair of simultaeous equations, which in themselves, (due to the sign change) are well ordered. Moreover, as the reflection coefficients are (ideally) invariant with frequency, the calibration scheme can be used over the whole frequency range of the hardware (e.g. .1 - 18 GHz).

There are, however, some practical problems with the realisation of the calibration pieces. A short circuit, having properties very close to

ideal, is readily constructed, at least in coaxial systems, by simply terminating the transmission line in a conducting plane perpendicular to the axis of the structure. In contrast, the open circuit can never be ideal due to the fringing field at the abrupt end of the line. Loss due to propagation effects is usually minimised by extending the outer (ground) conductor to form a cylindrical waveguide below cut-off. The end effect capacitance, for simple coaxial structures, can be calculated from electrostatic theory, and results in a reflection coefficient for the open:

$$\Gamma_{s3} = (Y_o - j\omega C_e)/(Y_o + j\omega C_e) \qquad \langle 5.21 \rangle$$

where $Y_o = 1/Z_o$ = the characteristic admittance of the measurement system.

The result is useful at frequencies well below the cut-off frequency of the lowest non-TEM mode that the structure will support, but as the cut-off is approached, the apparant value will change. Expressing the end effect as an equivalent length of transmission line having the same static capacitance thus:

$$\Delta l = \{v/\omega\} \tan^{-1}(\omega C_e/Y_o) \qquad \langle 5.22 \rangle$$

where v is the velocity of propagation

goes some way to simulating this frequency dependance of the end effect Particular difficuties are presented by sexed connector systems (e.g. Type-N,SMA) where the centre conductor pin and socket have differing external diameters when open circuit and where the necessary mechanical tolerances of the sliding parts make the position of the reference plane imprecise. This means that for connector systems other than the hermaphrodite styles (APC-7,GR900), having a single plane of cleavage, this calibration scheme is difficult to implement much above 2 GHz.

It is quite impossible to produce anything approaching an ideal load over a wide band of frequency. Two solutions are possible: the load may

be measured to the best available accuracy in a standards laboratory at a large number of frequencies and the results used in the computation of the error parameters, or a sliding load may be used. The sliding load, which is the most commonly adopted solution, consists of a tapered lossy material load, free to slide along a length of uniform coaxial air-line. The center conductor has no supports apart from the mating connector and the lossy material load itself. Consequently, the only reflection coefficient presented to the test port is that of the sliding part. Sliding the load causes the reflection coefficient vector to trace out a circle on the reflection coefficient plane, the centre of which corresponds to the reflection coefficient of an ideal load. This facilitates the determination of the error vector e_{11}, which is principally identified with the directivity of the system. Three points, corresponding to three positions of the sliding load, are required to uniquely define the circle; the use of additional points and a least squares fitting algorithm[21] enhances the accuracy by reducing the susceptability to non-systematic effects..

5.8.3 Load,Short,Offset Short Calibration

In view of the limitation on accuracy in the scheme discussed above, due to the use of the open circuit, an offset short circuit may be substituted for the open. The offset short circuit is simply a length of unsupported uniform coaxial airline, having the same characteristic impedance as the load, terminated in the same way as the short circuit. The accuracy is as high as the mechanical integrity of the structure allows. Thus the three standards have the reflection coefficients:

$$\Gamma_{s1} = 0$$

$$\Gamma_{s2} = -1$$

$$\Gamma_{s3} = -1.\exp(-2\gamma l)$$

where $\gamma = \alpha + j\beta$

and α is the attenuation const. of the tx. line

$\beta = 2\pi f/v_o$: the phase constant

f is the frequency of calibration

$v_o = 2.998*10^8$ m/s : the velocity of light in free space

l is the offset length.

Equations <5.19> and <5.20> become

$$\Gamma_{m2} - \Gamma_{m1} = -e_{01}/(1+e_{11}) \qquad \text{<5.23>}$$

$$\Gamma_{m3} - \Gamma_{m1} = -e_{01}\exp(-2\alpha l)/[1 - e_{11}\exp(-2\alpha l)] \qquad \text{<5.24>}$$

In most practical situations the loss of the short length of coaxial air-line associated with the offset short can be neglected. At the frequency at which the offset is a quarter-wavelength long, it appears to be an ideal open, (ie. Γ_{s3}=1) resulting in a well ordered solution of the calibration equations. However, at twice the frequency, $\Gamma_{s3} = -1 = \Gamma_{s2}$, and again at low frequencies, $\Gamma_{m3} \rightarrow -1$, causing the system to become ill conditioned, thus limiting the useful bandwidth of the scheme. In practice, to ensure adequate angular separation between Γ_{s2} and Γ_{s3}; the short and offset short reflection coefficients respectively, this scheme is restricted to a frequency range of 3:1 with offset chosen to be close to $\lambda/4$ at the geometric mean frequency.

5.8.4 Three Short Circuits

An alternative scheme, useful when it is inconvenient to employ a sliding load, utilises a short and two offset shorts of identical characteristic impedance but dissimilar length. The reflection

coefficients, neglecting transmission line loss, are then:-

$$\Gamma_{s1} = -1$$

$$\Gamma_{s2} = -1.e^{-2j\beta l_1}$$

$$\Gamma_{s3} = -1.e^{-2j\beta l_2} \text{ , respectively.}$$

These may simply be substituted in the matrix formulation of equation <5.15> to evaluate the error parameters.

The exclusive use of high reflection coefficient calibration standards makes this scheme particularly appropriate to the measurement of DUTs which are grossly mismatched. Nevertheless, it has been demonstrated [10,26] that this and similar schemes are capable of producing adequate accuracy when measuring low reflection coefficient items like a load (cf. section 5.12). Because of the need to ensure sufficient angular separation of the reflection coefficients of the standards, so as not to compromise the conditioning of the calibration equations, the useful frequency span for this scheme is little more than 2:1 (i.e. an octave). The optimum relationship between the two offset lengths; l_1 and l_2, is:

$$l_2 = 2.l_1$$

where l_1 is approximately $\lambda/_7$ at the band centre.

Schemes using other combinations of the above mentioned calibration standards may readily be devised (e.g. short,offset short, open) and, providing the factors already discussed are considered, they should give satisfactory results. The matrix formulation will be most useful in implementing such schemes.

5.9 2-PORT CALIBRATION SCHEMES

There are two alternative approaches to the development of a 2-port calibration scheme. One is to extend one of the schemes devised

for the 1-port or reflectometer case, adding extra calibration measurements to determine the values of the additional unknowns. The other approach is to devise a scheme, from first principles, applicable only to the 2-port (or multi-port) situation. Several such schemes have been described [22,23,24], the most publisised being the Through-Short-Delay (TSD) method of Speciale and Franzen [22].

The former is the approach pursued here, although some consideration will be given to the TSD method later.

5.9.1 Extending 1-Port Calibration Schemes

The first step in ascribing values to the 2-port error model, is to conduct a 1-port calibration of both test ports using one of the schemes described in section 5.1. The four calibration equations for the bilateral 12.term error model are repeated below:

$$U_{11} = e_{00} + e_{R1}\{s_{11}(1-s_{22}e_{22}^{(1)}) + s_{21}s_{12}e_{22}^{(1)}\}/D^{(1)} \quad \text{<5.25a>}$$

$$U_{21} = e_{30} + s_{21}e_{TF}/D^{(n)} \quad \text{<5.25b>}$$

$$U_{12} = e_{03} + s_{12}e_{TR}/D^{(3-n)} \quad \text{<5.25c>}$$

$$U_{22} = e_{33} + e_{R2}\{s_{22}(1 - s_{11}e_{11}^{(2)}) + s_{21}s_{12}e_{11}^{(2)}\}/D^{(2)} \quad \text{<5.25d>}$$

where $D^{(k)} = 1 - s_{11}e_{11}^{(k)} - s_{22}e_{22}^{(k)} + \Delta e_{11}^{(k)}e_{22}^{(k)}$

and $\Delta = \det[S] = s_{11}s_{22} - s_{12}s_{21}$

or $D^{(k)} = (1 - s_{11}e_{11}^{(k)})(1 - s_{22}e_{22}^{(k)}) - s_{21}s_{12}e_{11}^{(k)}e_{22}^{(k)}$

These equations have been generalised to permit their application to either the conventional bilateral error model of figure 5.19 or the modified bilateral error model of figure 5.21, depending on which of these error models best suits the test set employed. The relationship between the terms in these equations and those of the equations quoted in section 5.7 are stated in Table 5.2. The 8-term model of figure 5.13 and that of reflection/transmission test set (figure 5.17) constitute trivial

degenerate cases and they will not, therefore, be treated separately in this discussion.

TABLE 5.2.1 LOOK-UP TABLE FOR EQUATION <5.25>

Model	Conventional	Modified
n	1	2
Type of Test Set	I	II
Figure	5.19	5.21
Equation	<5.10>	<5.11>
e_{R1}	$e_{01}^{(1)}$	$e_{10}^{(1)}$
e_{TF}	$e_{32}^{(1)}$	$e_{10}^{(2)}$
e_{TR}	$e_{01}^{(2)}$	$e_{23}^{(1)}$
e_{R2}	$e_{32}^{(2)}$	$e_{23}^{(2)}$

As none of the 1-port calibration pieces provides any transmission between the test ports, s_{21} and s_{12} in <5.25a & d)> are zero, viz:

$$[S_r] = \begin{bmatrix} \Gamma_s^{(1)} & 0 \\ 0 & \Gamma_s^{(2)} \end{bmatrix} \qquad \text{<5.26>}$$

yielding the following equations:

$$U_{11}^{(r)} = e_{00} + e_{R1}\Gamma_s^{(1)}/(1 + e_{11}^{(1)}\Gamma_s^{(1)}) \quad \{= \Gamma_m^{(1)}\} \qquad \text{<5.27a>}$$

$$U_{22}^{(r)} = e_{33} + e_{R2}\Gamma_s^{(2)}/(1 + e_{22}^{(2)}\Gamma_s^{(2)}) \quad \{= \Gamma_m^{(2)}\} \qquad \text{<5.27d>}$$

These are identical in form to the 1-port calibration equation <5.1> so, by applying the same manipulation we may obtain values for six of the error vectors, viz: $e_{00}, e_{R1}, e_{11}, e_{22}, e_{R2}, e_{33}$.

The principle additional calibration standard is a through line; a length of uniform transmission having the same characteristic impedance as the relection coefficient standards and connected between the test

ports.

Such a component has the s-matrix:

$$[S_t] = \begin{bmatrix} 0 & \exp(\gamma l_t) \\ \exp(-\gamma l_t) & 0 \end{bmatrix} \qquad \langle 5.28 \rangle$$

where $\gamma = \alpha + j\beta$

and l_t = length of line

for a lossless air-line:

$$\alpha = 0 \ , \quad \beta = 2\pi f / v_o$$

where $v_o = 2.998 * 10^8 m.s^{-1}$, velocity of light in free space.

Substituting in <5.25a & d> results in the following expressions:

$$U_{11}^{(t)} = e_{00} + e_{R1}e_{22}^{(1)}\exp(-2\gamma l_t)/[1-e_{11}^{(1)}e_{22}^{(1)}\exp(-2\gamma l_t)] \qquad \langle 5.29a \rangle$$

$$U_{22}^{(t)} = e_{33} + e_{R2}e_{11}^{(2)}\exp(-2\gamma l_t)/[1-e_{22}^{(2)}e_{11}^{(2)}\exp(-2\gamma lt)] \qquad \langle 5.29d \rangle$$

There is, with most systems, a topological problem with the use of a straight through line, so it is normal to use a flexible cable or 'flexible arm' on at least one test port. The 1-port calibration standards should then be connected to the free end of the cable or arm so that its imperfections are calibrated out along with those of the network analyser. When hermaphodite connectors are in use the two test ports can be connected together to form a zero length through line, which has the s-matrix:

$$[S_{to}] = \begin{bmatrix} 0 & 1 \\ 1 & 0 \end{bmatrix}$$

Equations <5.29a & d> may then be simplified apppropriately.

After measurement of U_{11} and U_{22}, all the terms are known except $e_{22}^{(1)}$ and $e_{11}^{(2)}$, which may be readily calculated by rearranging the expressions. In essence the two ports of the network analyser, having been independantly calibrated, have been used to make a corrected

measurement of the mismatch of the opposite port. Had the error model resulting form the error box approach (figure 5.13) been adopted, these measurements would have been redundant, as it would be assumed that e_{11} and e_{22} had only a single value; that already determined from the 1-port calibration (cf <5.27a & d>). With the through line connected the transmission coefficients U_{21} and U_{12} are also measured. Substituting in equations <5.25b & c> the s-parameters of the finite length through line we obtain:

$$U_{21}^{(t)} = e_{30} + e_{TF}\exp(-\gamma l_t)/[1-e_{11}^{(n)}e_{22}^{(n)}\exp(-2\gamma l_t)] \qquad \text{<5.30b>}$$

$$U_{12}^{(t)} = e_{03} + e_{TR}\exp(-\gamma l_t)/[1-e_{11}^{(3-n)}e_{22}^{(3-n)}\exp(-2\gamma l_t)] \qquad \text{<5.30c>}$$

Thus we arrive at solutions for e_{22} and e_{11} where the only remaining unknowns are the leakage terms.

Calibration for leakage effects is basically a matter of disconnecting the test ports and making bi-directional transmission measurements. Under these conditions the equations <5.25b & c> reduce to:-

$$U_{21} = e_{30} \qquad \text{<5.31b>}$$

$$U_{12} = e_{03} \qquad \text{<5.31c>}$$

To ensure that the leakage between the test port connectors is negligible (i.e. s_{12} and s_{21} really are zero) during this measurement, it is advisable to terminate them. It is apparent, from the error model and the equations that the reflection coefficients of the terminations (s_{11} and s_{22}) are irrelevant to the determination of the leakage parameters. In practice however, the termination used does effect the calibration. This is due to the fact that, as already discussed in section 5.4.4, the error model is not rigorous in this respect. The leakage path in the flowgraph error model in representative only, and there are, in fact, many other leakage paths unaccounted for, some of which are termination dependant. The best choice of termination for leakage calibration would

be one having a reflection coefficient similar to that of the DUT but, as this is seldom practicable, the most convenient termination is a load connected to each port.

5.2.2 The Through-Short-Delay Method

The Through-Short-Delay (TSD) calibration scheme requires only three calibration pieces for full 2-port correction. It is generally associated with the error box approach to modelling the system imperfections [22] and the corresponding eight term error model of figure 5.13.

The procedure is as follows. Short circuits are connected to both ports and the reflection coefficients are measured. A through line, often of zero length, and a delay; a transmission line of appropriate characteristic impedance, are connected in turn and the four s-parameters measured in both cases. Thus ten vector measurements are made to ascribe values to only eight complex error terms. By manipulation of the calibration equations it is possible to use this additional information to determine the loss and velocity of propagation of the 'delay' transmission line (twice over) which, therefore, need not be specified. After having determined these parameters the eight error terms can be computed. Crosstalk can be accounted for by conducting two extra calibration measurements; transmission coefficients with both ports terminated, preferably with matched loads, but, most conveniently, with the short circuitss. In this case it is not possible to accommodate the two values of each test port mismatch, necessary to adequately calibrate the reversing (s-parameter) test set.

Speciale [25] has demonstrated excellent results using an interesting technique to verify the performance of the scheme. Error boxes having

filter-like characteristics are connected to both ports in a computer model of a CCNA system. The connection of the calibration standards is simulated and the error model evaluated at each frequency specified. The results are compared to the computed s-parameters of the filter-like error boxes.

5.9.3 Non-standard Measurement Impedances

Most network analyser systems are constructed to operate for only one characteristic or measurement impedance and that is usually 50 ohms. As a result the instrument produces s-parameters normalised to this single impedance and is calibrated using standards involving transmission lines and loads of the same impedance. In discussing the computer correction of network analyser measurements it is implicit that the measurement impedance is not in fact identical to the nominal impedance of the instrument. The normalising impedance of the corrected s-parameters is, therefore, defined by the characteristic impedance of the standards used in the calibration process. Consequently, it is possible to calibrate a CCNA based on a 50 ohm network analyser instrument to other impedances be constructing a set of standards in the new impedance. Also, since the normal standards will never be of precisely the correct impedance and will, in fact, due to transmission line losses have a complex characteristic impedance, may not be precisely that intended. Providing the standards are self consistent and fully characterised any resulting error may be eliminated by subsequent renormalisation[15] (cf. Appendix D) of the corrected DUT s-parameter.

5.10 DE-EMBEDDING

After having obtained a set of values for the error parameters from the calibration measurments at each frequency of interest the DUT is connected and measured. The remaining activity is the computation of the corrected or true s-parameters of the DUT from the measured parameters and the error model.

5.10.1 1-Port Dembedding

Obtaining the corrected reflection coefficient is simply a matter of rearranging the calibration equation <5.1> to present the true reflection coefficient in terms of the measured reflection coefficient and the known error parameters, thus:-

$$\Gamma_{DUT} = (\Gamma_{meas} - e_{oo})/(e_{11}\Gamma_{meas} - e_{oo}e_{11} + e_{01}) \qquad \langle 5.32 \rangle$$

Da Silva and McPhun[26] have combined the calibration and de-embedding processes in expressions where the independant variables are the measurements of the three general calibration standards; $\Gamma_{m1}, \Gamma_{m2}, \Gamma_{m3}$, and the measurement of the DUT; Γ_{dut}.

5.10.2 2-Port De-embedding

With reference to the error box model, illustrated in figure 5.12, the essence of the process may be simply demonstrated.

The calibration equation <5.25> can be expressed in transmission (t-) parameters thus:

$$[T_U] = [T_{E1}].[T_S].[T_{E2}] \qquad \langle 5.33 \rangle$$

where T_U, T_S, T_{E1}, T_{E2} are the 2-port transmission matrices describing the measured parameters, the actual parameters and the system errors,

respectively. The de-embedded (corrected) t-parameters of the device under test may, therefore, be found from the matrix expression:

$$[T_S] = [T_{E1}]^{-1}.[T_U].[T_{E2}]^{-1} \qquad \langle 5.34 \rangle$$

where the index '-1' indicates matrix inversion.

If the effect of crosstalk or leakage is incorporated in the error model (a total of ten terms) the matrix of measured or uncorrected s-parameters is first adjusted thus:

$$[U] + \begin{bmatrix} 0 & -e_{03} \\ -e_{30} & 0 \end{bmatrix} \text{--> } [U]$$

Expansion of the matrix equations results in cumbersome expressions. The alternative approach; rearranging the 2-port calibration equations (i.e. <5.25>) to present s_{11},s_{22},s_{21} and s_{12} as the dependant variables is somewhat more difficult. Indeed in early systems [11] the solution was arrived at via the interactive process as, at that time, no explicit solution had been formulated.

A number of explicit solutions for the calibration equations relating to both the 8-term and bilateral 12-term error models of figures 5.13 and 5.19 have since been published [27,28]. As a result of the addition of the modified 12-term error model of figure 5.21 it is, however, necessary to develop a more general solution. The required solution is readily obtained by using the work of Rehnmark [28]. Rehnmark's equations for the 8-term model (relating to <5.8>) are repeated here with appropriate changes to the nomenclature.

$$s_{11} = [X_{11}(1 + e_{22}X_{22}) - e_{22}X_{12}X_{21}]Y \qquad \langle 5.35a \rangle$$

$$s_{21} = X_{21}/Y \qquad \langle 5.35b \rangle$$

$$s_{12} = X_{12}/Y \qquad \langle 5.35c \rangle$$

$$s_{22} = [X_{22}(1 + e_{11}X_{11}) - e_{11}X_{12}X_{21}]Y \qquad \langle 5.35d \rangle$$

where $Y = (1 + e_{11}X_{11})(1 + e_{22}X_{22}) - e_{11}e_{22}X_{12}X_{21}$

and $X_{11} = (U_{11} - e_{00})/e_{R1}$, $X_{12} = (U_{12} - e_{03})/e_{TR}$

$X_{21} = (U_{21} - e_{30}/e_{TF}$, $X_{22} = (U_{22} - e_{33})/e_{R2}$

Referring to the discussion of section 5.9.1 it is apparent that the 12-term error model can be obtained by partitioning the 10-term (8-term model with the addition of the leakage terms) model in a way appropriate to the s-parameter switching. Thus the test port mismatch terms take on two independant values each. The equations <5.35> may now be rewritten with the selection of the relevant test port mismatch terms. This results in the need for two expressions for the denominator, and although it would be possible to manipulate the expression into a form analageous to Rehnmark's equations for the conventional 12-term model, it is such a trifling inconvenience when writing the computer program there is little point in pursuing the matter.

$$s_{11} = \{X_{11}(1 + e_{22}^{(1)}X_{22}) - e_{22}^{(1)}X_{12}X_{21}\}/Y^{(1)} \quad \text{<5.36a>}$$

$$s_{21} = X_{21}/Y^{(n)} \quad \text{<5.36b>}$$

$$s_{12} = X_{12}/Y^{(3-n)} \quad \text{<5.36c>}$$

$$s_{22} = \{X_{22}(1 + e_{11}^{(2)}X_{11}) - e_{11}^{(2)}X_{12}X_{21}\}/Y^{(2)} \quad \text{<5.36d>}$$

where $Y^{(k)} = (1 + e_{11}^{(k)}X_{11})(1 + e_{22}^{(k)}X_{22}) - e_{11}^{(k)}e_{22}^{(k)}X_{12}X_{21}$

and $X_{11}, X_{22}, X_{12}, X_{21}$ defined as above.

Observe the similarity in form of these expressions to the calibration equations from which they are derived.

5.10.3 Reference Plane Shifting

Ideally the network analyser should be calibrated complete with cables, flexible arms and adaptors by standards that establish the reference planes at the DUT terminal. This ideal is, however, not always achievable. The need to compromise this stipulation might be a

consequence of the non-insertable nature of the DUT (e.g. a DUT with female connectors on both ports), the lack of calibration set in a particular connector style or simply the use of a calibration set that does not allow the desired displacement of the reference plane from the connection plane. Where the parameters of the additional items are known the principle of de-embedding discussed in the previous section can be applied to 'stripping' the DUT parameters out of the results for the composite structure. With reference to figure 5.23a the matrix expression in terms of t-parameters is:

$$[T_{DUT}] = [T_A]^{-1}.[T_{comp}].[T_B]^{-1} \qquad \langle 5.37 \rangle$$

In the situation where movement of the reference plane along a uniform transmission line is all that is required (or a pragmatic approach to the effect of adaptors is to be adopted) the solution may be greatly simplified.

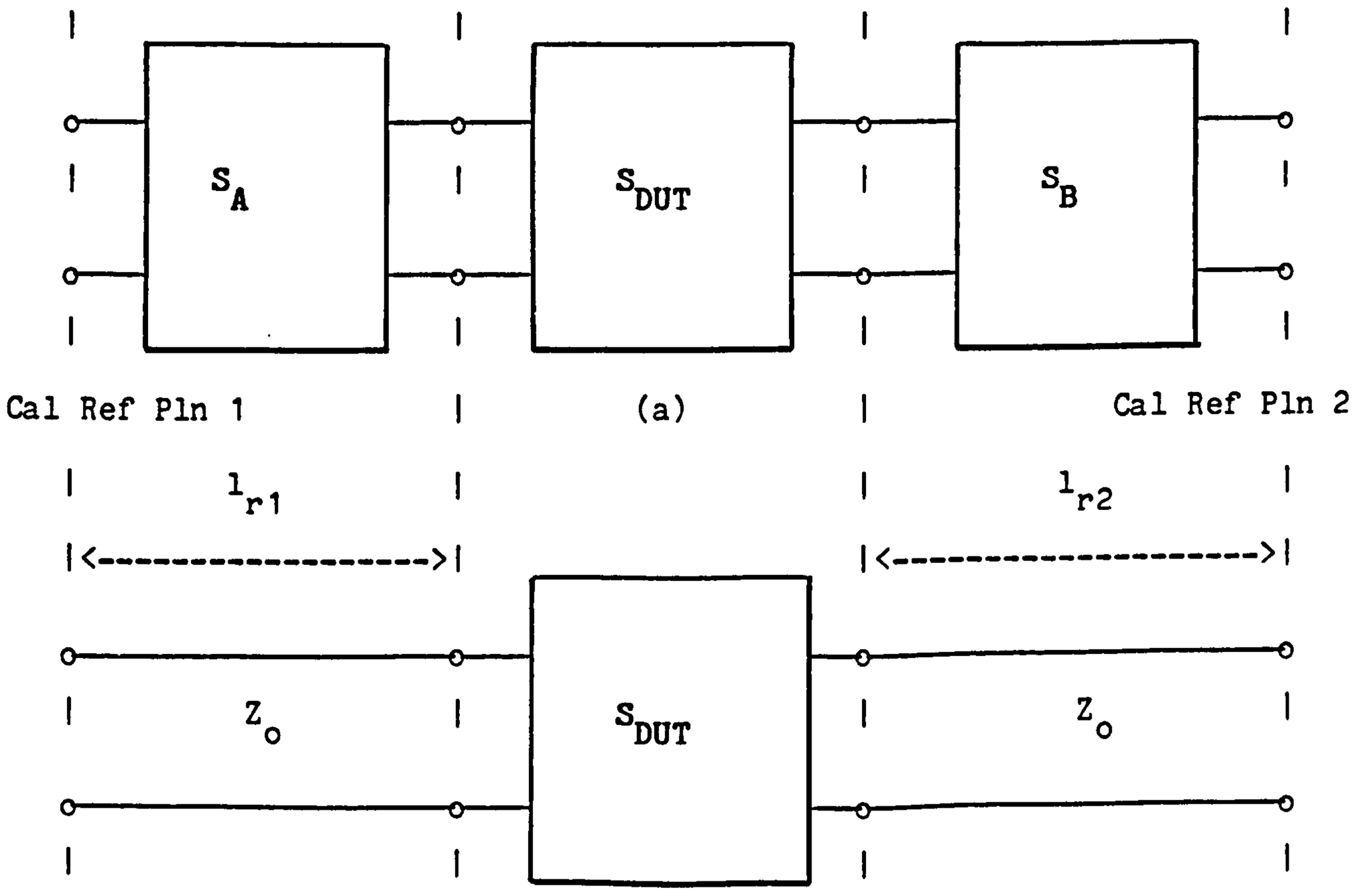

Figure 5.23 The DUT measured in conjunction with (a) additional items and (b) and with uniform transmission lines

The T-matrix for a lossless line having a characteristic impedance identical to the system normalising (calibration) impedance and an electrical length (i.e. equivalent airline length) l_{ri}, is

$$[T_{lri}] = \begin{bmatrix} \exp(-2\pi l_{ri}/\lambda_o) & 0 \\ 0 & \exp(2\pi l_{ri}/\lambda_o) \end{bmatrix} \quad \langle 5.38 \rangle$$

where λ_o is the free space wavelength.

Note that the inverted t-matrix for the uniform transmission line is equivalent to that for a negative length line. Thus moving the reference planes in a positive direction, (i.e. extension towards the DUT) is equivalent to adding negative length transmission lines to the measured results referred to the calibration reference planes, thus:

$$[S_{DUT}] = \begin{bmatrix} \exp\{4\pi l_{r1}/\lambda_o\}s_{11} & \exp\{2\pi(l_{r1}+l_{r2})/\lambda_o\}s_{12} \\ \exp\{2\pi(l_{r1}+l_{r2})/\lambda_o\}s_{21} & \exp\{4\pi l_{r2}/\lambda_o\}s_{22} \end{bmatrix} \quad \langle 5.39 \rangle$$

5.11 RESIDUAL ERROR SOURCES

The correction algorithm having been implemented, with due regard to the matters discussed earlier in this chapter, there a number of residual error sources that can significantly degrade the performance of CCNA system. It is difficult to do anything about some non-systematic errors, for example; switch and connector repeatability, other than to use harware of the highest quality. Some other recognised sources of non-systematic error, such as electrical noise, instrument drift, frequency setting accuracy and stability can be ameliorated by good system design. In some cases statisical techniques may be applicable to the reduction of the error introduced by these effects. There also remains at least one systematic error source; namely the so called

'quadrature error' of the vector voltmeter.

5.11.1 Electrical Noise

There are two types of noise that impinge upon network analyser measurements; noise in the conversion and vector voltmeter systems of the network analyser instrument itself, and phase noise on the signal form the microwave generator. The effect of the latter is minimised by ensuring test and reference paths are near identical. The use of phase locked or synthesized sources can dramatically reduce the phase noise present. The former, which, in the typical system limits the dynamic range to approximately 60dB, is susceptible to improvment by the application of filtering and averaging of the vector voltmeter outputs.

The Warwick University system has the additional disadvantage that the A-D converters are situated with the computer, remote from the network analyser and the long cables involved are susceptable to electrical interference. The video bandwidth of the X and Y outputs is restricted to 10kHz within the polar display plug-in. Measurements of the noise spectrum, at the computer end of the lines, using both a conventional super-heterodyne spectrum analyser and a digital fourier transform analyser were made. Interference picked up by the cables includes coherent signals; principally at line and radio frequencies. The anti-aliasing filters effectively remove the RF interference. Sample rates and filter bandwidths were adjusted to minimise the deleterious effects of interference.

5.11.2 Quadrature Error and Correction

Throughout the discussion of error models it has been tacitly assumed

that the network analyser instrument itself; the microwave vector voltmeter, is free of systematic error. In fact it may suffer from a number of imperfections such as non-linearity, IF step attenuator inaccuracy and quadrature error. In CCNA system where the polar display plug-in (HP8414) is used as the analogue part of the vector voltmeter for both magnitude and phase measurements, quadrature error is usually the most severe of those mentioned. Even in systems where the Polar Display is used only for phase measurement quadrature error is still often dominant. Since digital output is required the complete vector voltmeter includes A-D converters which will aggravate these inadequacies.

Quadrature error may be succinctly defined as the dependence of the amplitude and phase measurements upon the value of the phase difference between the two signal inputs to the vector voltmeter. The effect can be demonstrated by connecting a length of airline, terminated in a short, to one port of a calibrated network analyser and making measurements over a band of frequency sufficient to include at least one complete rotation of the reflection coefficient vector with respect to the reference short circuit. A plot of the amplitude results (e.g. figure 5.24) will show a cyclic variation repeating at a interval of $v_o/21$ Hz, (where v_o is the velocity of light and l the length of the line). Corruption of the phase information will be evidenced by a similar cyclic deviation from the linear phase curve.

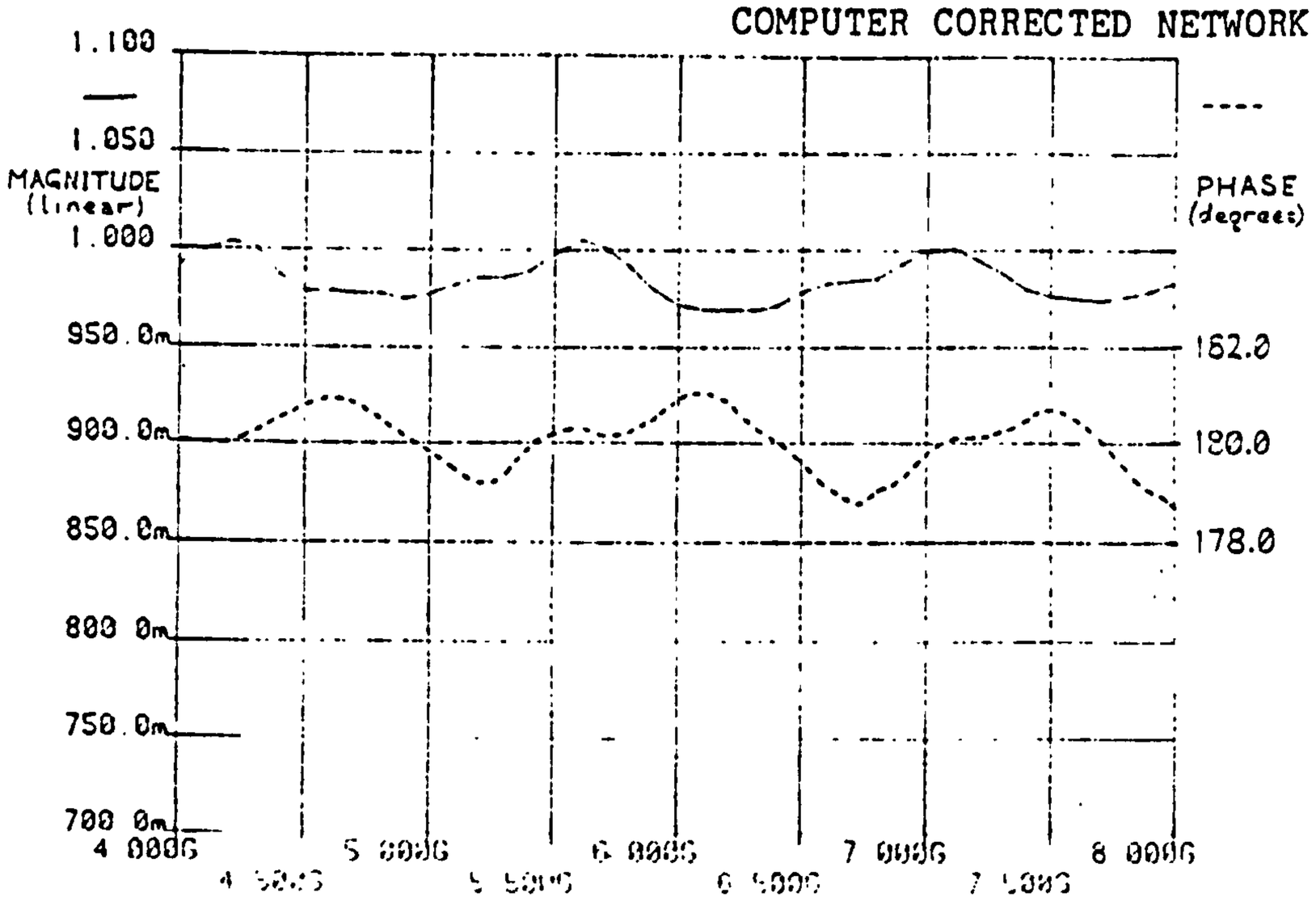

Note: Phase results after shifting reference plane

Figure 5.24 Measured effect of quadrature error (10.21cm line)

(10.21cm Line: repetition interval 1.468GHz

Expressed algebraically the measured vector can be related to the true vector thus:

$$A' = A(1 + f(\theta)) \qquad \langle 5.40a \rangle$$

$$\theta' = \theta + \emptyset(\theta) \qquad \langle 5.40b \rangle$$

where f and $\emptyset$ are functions of θ

Consider the operation of the relevant parts of the polar display plug-in and the A-D converters that comprise the vector voltmeter as illustrated below.

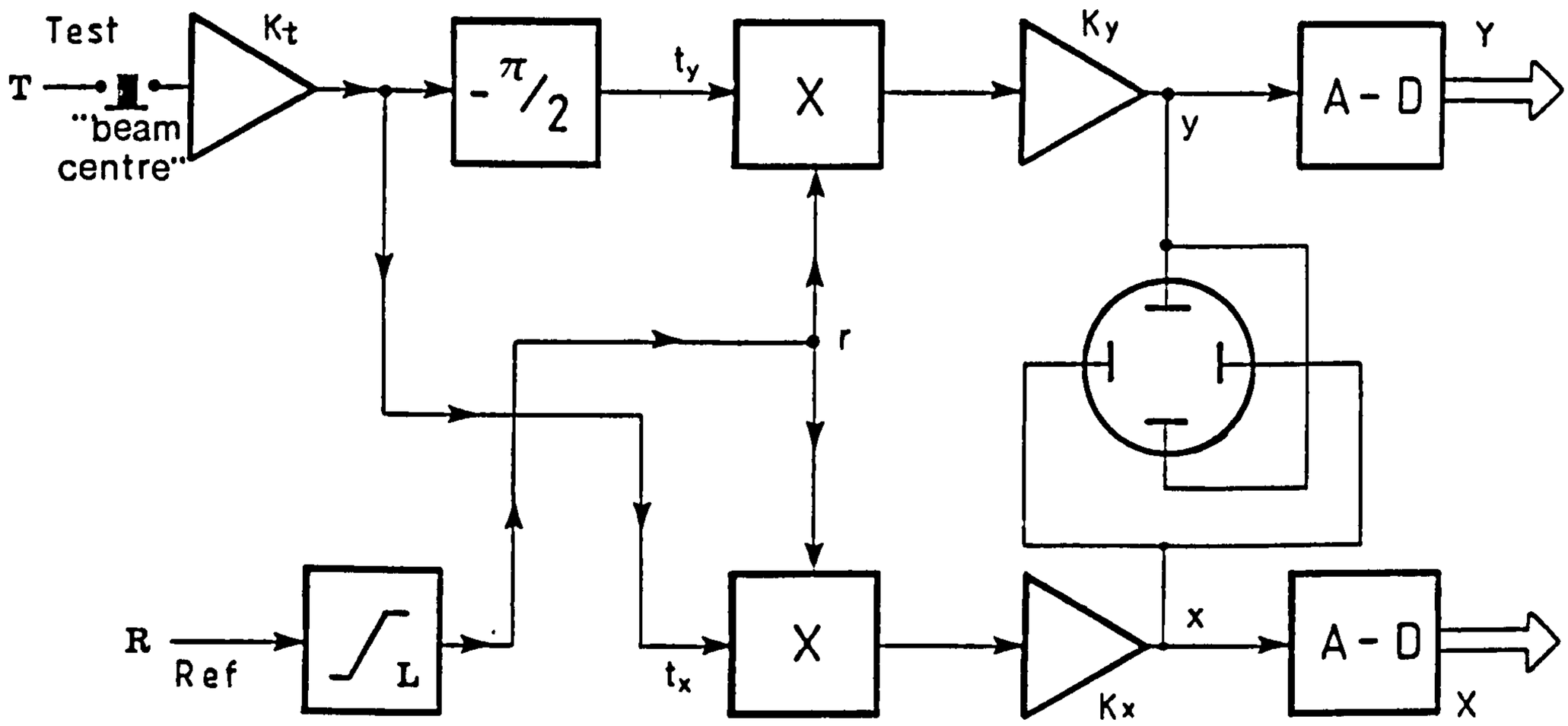

Figure 5.25 The quadrature vector voltmeter (polar display)

In the following analysis it will be assumed that the amplifiers preceding the product demodulators have identical, negligible phase shift.

The reference and test waves incident on the sub-system at a 2nd i.f. are, respectively;

$$R = A_r \cos(\omega t) \qquad \text{<5.41a>}$$

$$T = A_t \cos(\omega t + \theta) \qquad \text{<5.41b>}$$

The operation of the network analyser AGC is such that the amplitude of the test signal is related to the amplitude ratio of the two microwave inputs and any residual amplitude fluctuations in the reference signal are removed by the action of the limiter. The inputs to the X product demodulator are, therefore:

$$t_x = K_t A_t \cos(\omega t + \theta) \qquad \text{<5.42a>}$$

$$\text{and} \qquad r = L\cos(\omega t) \qquad \text{<5.42b>}$$

which results in d.c output, after filtering out the terms at twice the IF and higher:

$$x = K_x K_t L A_t \cos(\theta)/2 \qquad \text{<5.43>}$$

The test signal to the Y demodulator is first subjected to a phase shift of nominally 90 degrees.

Thus the inputs to this demodulator are:

$$t_y = K_t A_t \cos(\omega t + \theta - \theta_p) \quad \text{and} \quad r \qquad \langle 5.44 \rangle$$

resulting in an output:

$$y = K_y K_t L A_t \sin(\theta + \theta_e)/2$$

where $\theta_e = -\theta_p + \pi/2$, the deviation from the nominal phase shift

The digital outputs for the vector voltmeter may then be expressed as:

$$X = k_x K_t A_t \cos(\theta) \qquad \langle 5.45a \rangle$$

$$Y = k_y K_t A_t \sin(\theta + \theta_e) \qquad \langle 5.45b \rangle$$

where $k_x = K_x L/2$

and $k_y = K_y L/2$

Where reference signal level is maintained constant and the gains are assumed not to drift significantly.

Transforming the result into polar form:

$$A' = A_t K_t \sqrt{\{k_x^2 \cos^2(\theta) + k_y^2 \sin^2(\theta + \theta_e)\}} \qquad \langle 5.46a \rangle$$

$$\theta' = \tan^{-1}\{k_y \sin(\theta + \theta_e)/k_x \cos(\theta)\} \qquad \langle 5.46b \rangle$$

from which it is evident that the error in both amplitude and phase is a function of the phase angle itself. Applying standard triginometric identities these equations can be expressed in the form of <5.36> thus:

$$A' = A\{1 + [\delta/2] - [\delta/2]\cos(2\theta) + [\theta_e/2]\sin(2\theta)\} \qquad \langle 5.47a \rangle$$

$$\theta' = \theta + [\theta_e/2] + [\theta_e/2]\cos(2\theta) + [\delta/2]\sin(2\theta) \qquad \langle 5.47b \rangle$$

where $\delta = k_y/k_x - 1$ and $A = A_t K_t$

Making the assumptions that the channel gain mismatch is 2% and the phase shift error is 2^o, plots of these functions (figure 5.26) can be seen to faithfully reproduce the experimental results of figure 5.29 and conform to the general behaviour of those of figure 5.24.

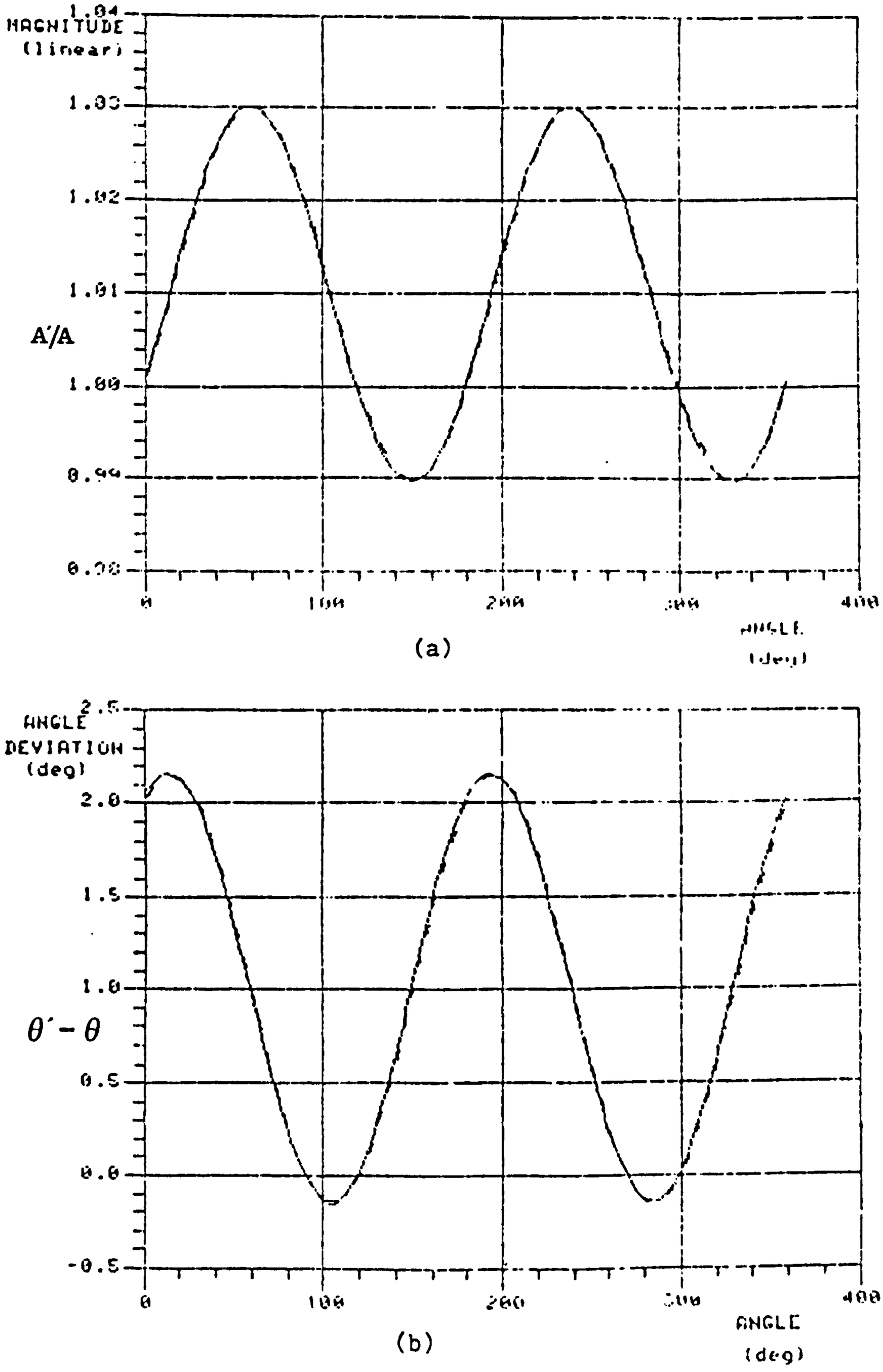

Figure 5.26 Plots of the magnitude and phase deviations from <5.47a & b> (dashed) compared to exact computation (solid)

The error in both the measured phase and magnitude are caused by two hardware shortcomings; dissimilar gains in the X and Y channels, and a

non-ideal 90^{o} phase shifter in the reference path. Although there is provision for adjustment of both factors, precise set-up is hindered by temperature changes when the unit case is replaced.

Since quadrature error is a systematic effect it must be possible to apply some correction strategy to eliminate, or at least moderate, its influence. In principle, since there are only two factors involved, it should be possible to determine the error functions from two normalised measurements. Since, however, the effect is small there is advantage in making a number of measurements and applying curve fitting or averaging to the results. Moreover, as the form of the error functions are known the curve fitting process will be highly efficient and risk free.

One that is frequently applied [29] makes use of the frequency dependence of transmission phase for a uniform transmission line. Figure 5.27 illustrates the quadrature error calibration procedure.

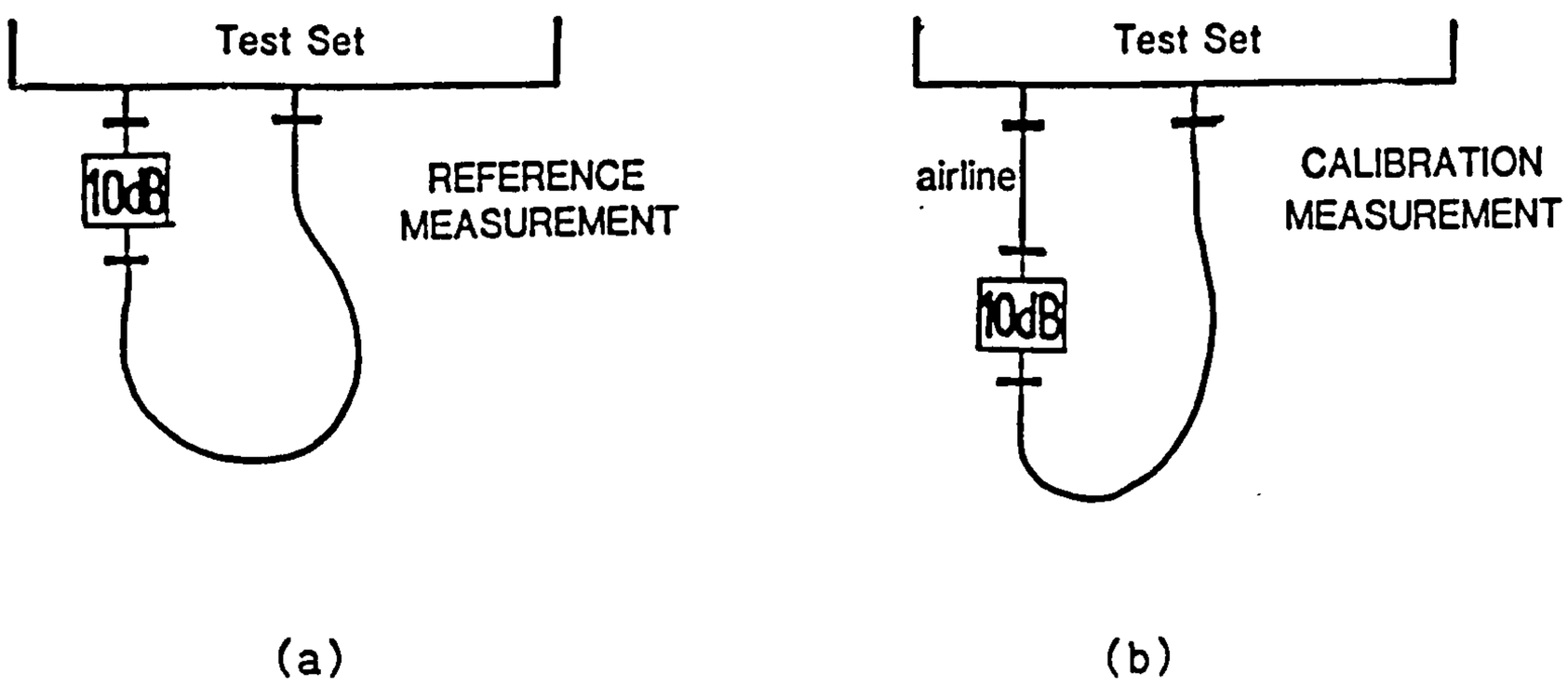

Figure 5.27 Quadrature error calibration procedure

The two test ports of the reflection/transmission or s-parameter test set are first connected together using a flexible arm or high stability cable. A cursory examination of the 2-port flowgraph error model of figure 5.17 will reveal that, for an ideal through line connection,

neglecting leakage, the only "loop" is that involving both test port mismatches (e_{11} and e_{22}). An attenuator (typically 10dB) is included at the free end of the arm or cable to minimise test port mismatch interaction, and the effective test port 2 is situated at the end of the attenuator connected to test port 1 by a "zero length" though line. Thus a transmission (s_{21} or s_{12}) measurement returns values that closely approximate the transmission gain and phase errors (error vectors $e_{10}.e_{32}$ or $e_{23}.e_{01}$). Inserting a known length of precision airline (figure 5.25(b)) introduces a defined phase shift at a given frequency with a minimum of loss. Neglecting again leakage and test port mismatch effects, the gain and phase errors obtained with the "zero length" through line can be subtracted from the new results to yeild the quadrature error for the defined phase angle.

A range of frequencies is selected in conjunction with the air-line length to allow sufficiently dense (35^{o}, say) and complete coverage of the circle. Clearly it is essential that the frequency can be set accurately enough to ensure adaquate certainty of phase shift along the air-line. In practice, leakage, and more significantly, test port mismatch interaction do influence the results to a discernable degree and so some "smoothing", by curve fitting techniques, is usually applied to the data. The quadrature error is then removed from all the subsequent measurements made on the CCNA system by subtracting the appropriate quadrature error vector, held in a look-up table and interpolated as necessary, from the raw measured data.

It is worth noting that interpolation is best conducted using magnitude and phase data rather than the complex number equivalent. The straight chords assumed when the latter is adopted introduce a new periodically varying phase dependant error!

A variation of this technique uses the line stretcher included in

most test sets instead of the air-line. The hardware is set up as in and the first set of readings taken. The line stretcher is then offset an appropriate amount (the same as the length of the alternative air-line) and the second set of readings taken. The only additional step necessary is the calibration of the offset length of the line stretcher as the scale accuracy of the front panel adjuster is usually inadequate. The frequency is set to a value for which the intended offset is $n\lambda/2$ and the phase reading on the display recorded. The line stretcher is extended by the desired amount as read from the front panel indicator and then trimmed by watching the displayed phase, whilst adjusting the line stretcher until the phase reading coincides with the starting value.

An alternative approach[18] involves additional hardware connected externally to the network analyser (HP8410). This quadrature error calibrator receives its input signal from the final IF reference channel output of the network analyser just prior to the polar display plug-in. The output is a fixed level signal at the same frequency as the input, but with a precisely defined phase difference set by a digital control word. It is connected to the test channel at a similar point in the system to that where the reference signal was extracted. When the Calibrator is in operation the test channel level is reduced below the noise level. The relative level of the Calibrator output is such that a near full scale deflection on the polar display is caused. With the phase shift set to zero, datum readings of magnitude and phase are recorded. The digital control word is then incremented and further values of magnitude and phase are taken, normalised to the datum and recorded for each phase step until the full circumference has been explored. This process is executed under program control and the results are written to a data file for subsequent application.

Figure 5.28 is a block diagram of such a quadrature error calibrator

having 5-bit word control of 32 phase shift values in 11.25° increments. An 8.896MHz ocillator is phase locked to the 32nd harmonic of the reference frequency using a 5-bit binary counter as a frequency divider and a digital phase detector. The data output of the counter is compared with the control word in a 5-bit comparator producing a result once every count cycle, offset from the reference signal by an amount;

$$\theta = N.360/32 \text{ degrees} \qquad \langle 5.48a \rangle$$

or $$t = N/8.896 \text{ micro-seconds} \qquad \langle 5.48b \rangle$$

where N is the value of the control word.

It is advisable to retime the divider and comparator outputs with the oscillator output to prevent logic propagation delays from contributing to the phase shift. The comparator is designed to produce an equal mark-space ratio output which is the passed through a filter to remove odd order harmonics and the DC component before connection to the network analyser test channel.

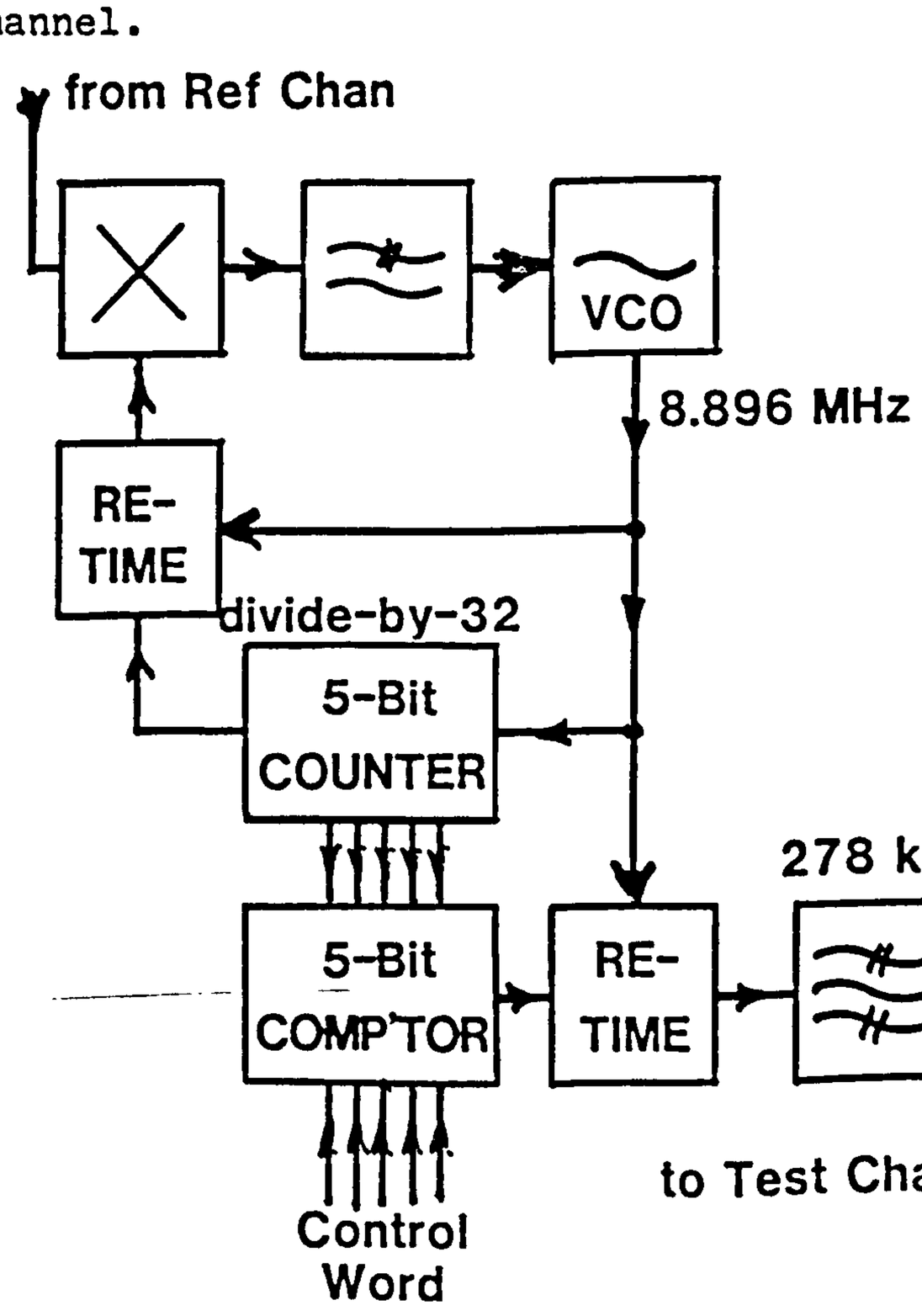

Figure 5.28 Quadrature Error Calibrator Block Diagram

Finally, and most directly, the vector voltmeter can be calibrated using a pair of synthesizers locked to a common reference and with the facility for setting phase offsets. Using this method Yeo[30] has produced results that confirm the postulated model for quadrature error (figure 5.29).

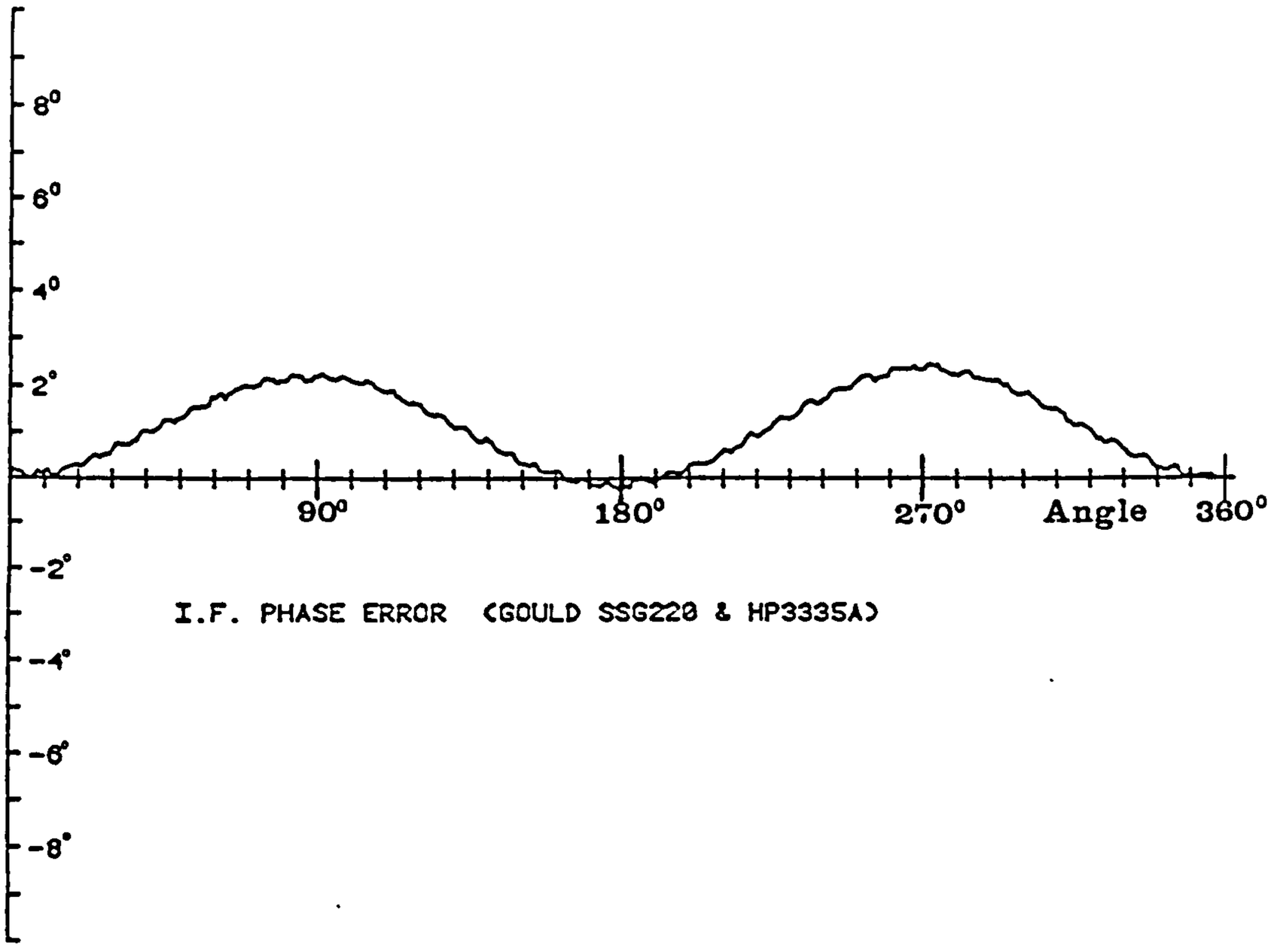

Figure 5.29 Measurement of phase quadrature error by two synthesizer method (after Yeo)

5.12 RESULTS AND DISCUSSION

Employing these techiques many measurements have been made in the course of this work. It is difficult to present results that confirm the accuracy in an independent and meaningful way. Frequently measurements of calibration standards are produced which, whilst not entirely without significance, can be very misleading.

A number of measurements of standard mismatches have been made at a frequency just beyond the specified upper frequency limit (12.4GHz) of the s-parameter test set used. The results are summarized in Table

5.3. Also recorded are measurements of the effective directivity of the system; obtained by finding the centre of the circle fitting the results of a series of measurements of a sliding load.

TABLE 5.3 MEASUREMENTS OF MATCHED AND MISMATCHED TERMINATIONS

12.645GHz	CALIBRATION 1		CALIBRATION 2		CALIBRATION 3	
ITEM	VSWR	deg	VSWR	deg	VSWR	deg
Weinschel 2.0:1	2.11	-83.4	2.11	-84.5	2.07	-84.3
Maury 2.0:1	1.94	-43.8	1.94	-43.8	1.92	-43.4
Weinschel 1.5:1	1.52	-119.0	1.51	-119.1	1.51	-121.8
Maury 1.5:1	1.45	-45.7	1.45	-43.4	1.42	-45.4
Weinschel 1.2:1	1.21	-163.2	1.21	-162.0	1.23	-167.6
Maury 1.1:1	1.090	-56.8	1.090	-55.1	1.068	-55.1
Maury 1.05:1	1.009	165.7	-	-	-	-
HP Load	1.022	63.8	1.021	63.9	1.034	102.7
Maury Load	1.019	154.6	-	-	-	-
S/Load Centre	1.0004	-60	-		1.021	144

Calibration 1 was conducted using a sliding load together with short and offset short circuits. The sliding load centre measurement is therefore incestuous and represents the repeatability of measurement rather than an effective directivity (of -74.0dB). In both Calibration 2 and 3, the sliding load was substituted by an additional offset short circuit. These two calibration and measurement sequences were conducted on separate occasions. By comparison with the results obtained using Calibration 1 it appears that measurements based on Calibration 2 are superior to those from Calibration 3. No effective directivity measurement was conducted but the vector differences between Calibrations

1 and 2 indicates an effective directivity of the same order as the short term repeatability of the system (i.e. ~75dB). The effective directivity obtained using Calibration 3 was ~-40dB. This confirms that, for many purposes, adequate calibration can be obtained using high reflection coefficient standards alone, right up to the upper frequency limit of the test set, at least.

Graphs of VSWR versus frequency for two interesting cases are presented in figure 5.30. Both measurements were made using Calibration 1. The 1.1:1 mismatch produces a result, in table 5.3, that is very close to its nominal value. From the graph (fig. 5.30a) this appears fortuitous. In contrast, the 12.645GHz result for the 1.05:1 mismatch deviates significantly from its nominal value. From the graph of figure 5.30b it is evident that this frequency was an unfortunate choice! There is every reason to believe this result is as accurate as the supplied calibration certificate indicates a value of 1.02:1. is to be expected at 12GHz. Note also that, in both graphs, the curve formed by the corrected results is smooth and progressive in stark contrast to the behaviour of the raw measured data.

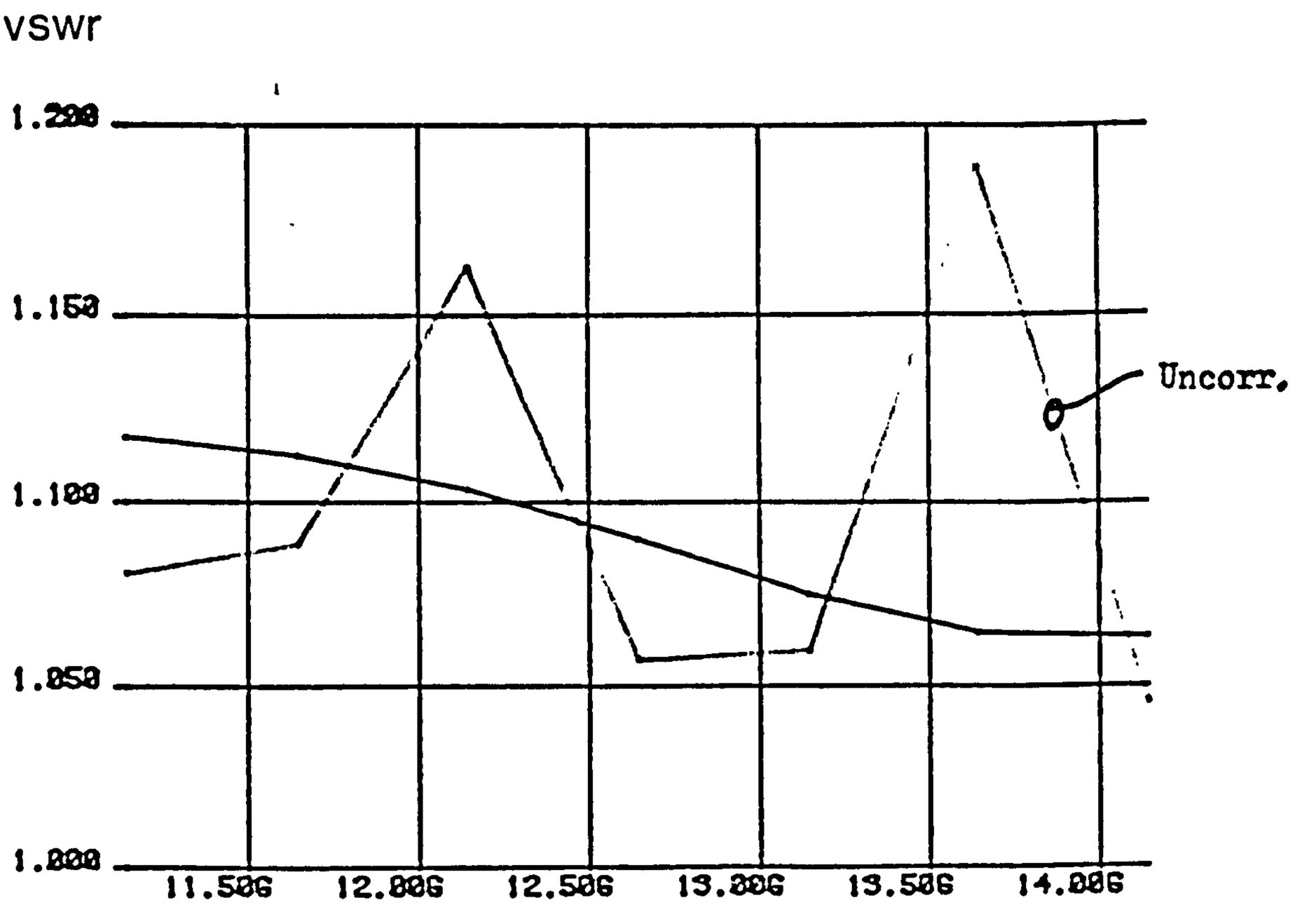

(a) 1.1:1 nominal

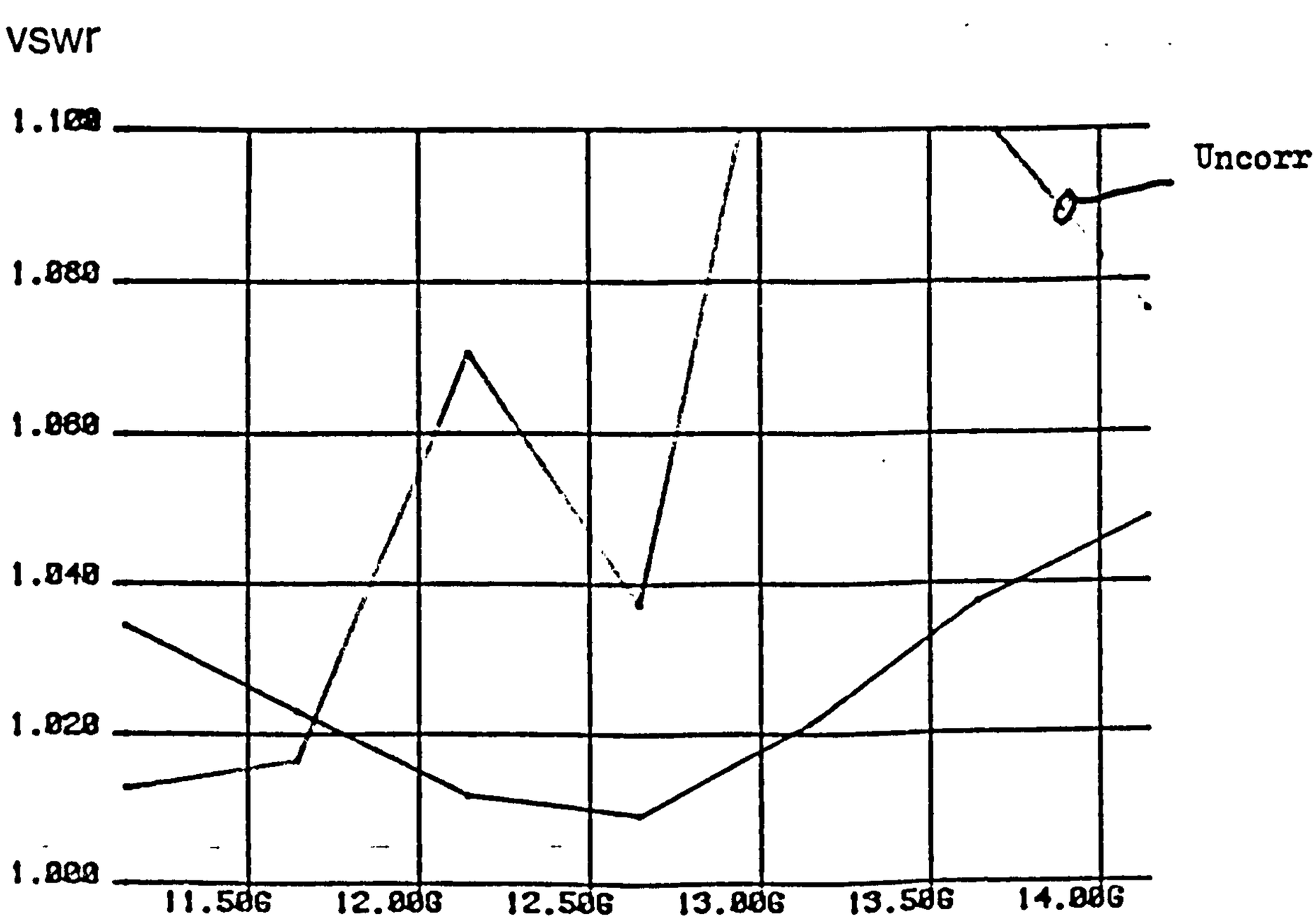

(b) 1.05:1 nominal

Figure 5.30 CCNA measurements of standard mismatches

5.13 REFERENCES

[1] RYTTING, D.K. & SANDERS, S.N.: "A system for automatic network analysis", Hewlett-Packard Jnl., Vol. 21 (6), Feb. 1970, pp.1-10.

[2] LOEB, H.W.: "Automatic time domain spectrometry methods as an alternative to automatic network analysers:, IEE Colloquium on "Automatic systems and RF microwave measurements", London, 1/3/77, Digest No. 1977/15/

[3] ENGEN, G.F. "Calibration of an arbitrary six-port junction for the measurement of active and passive circuit parameters "IEEE Trans. IM-22, 1975, pp.295-9.

[4] ENGEN, G.F.: "An improved circuit for implementing the six-port technique of microwave measurements", IEEE Trans. MTT-25, 1977, pp.1080-3.

[5] CULLLEN, A.L., JUDAH, S.K., & NIKRAVESH, F.: "Impedance measurement using a 6-port directional coupler", Proc. IEE, Vol. 127, Part H, 1980, pp.92-8.

[6] SHURMER, H.V., LUXTON, H.E.G., HOSSEINI< N>M> & STONEMAN< K>A.: "The application of an on-line computer to microwave measurement", Proc. ACTA IMEKO, Budapest, Hungary, 1976, pp.67-80.

[7] HOSSEINI, N.M.: "Application of computer-aided design to microstrip circuits," Ph.D. Thesis, University of Warwick, 1977.

[8] SHURMER, H.V.: "A flexible microwave automatic network analyser," IERE Rad. & Electron. Eng., Vol. 51, 1981, pp.287-98.

[9] HEWLETT-PACKARD Co.: "Microwave Network analyser applications, Application Note 117-1.

[10] DA SILVA, E.F. & McPHUN, M.K.: "Calibration of microwave network analyser for computer connected s-parameter measurements", IEE Electron. Lett., Vol.9, pp.126-8.

[11] HACKBORN, R.A.: "An automatic network analyser system", Microwave Jnl., Vol.11, May 1968, pp.45-52.

[12] WOODS, D.: "Rigorous deviation of computer-connected network-analyser calibration equations", Electron. Lett., Vol.11, 1975, pp.403-4.

[13] FITZPATRICK, J.: "Error models for systems measurement", Microwave Jnl., Vol.21(5), May 1978, pp.63-6.

[14] WOODS, D.: "Reappraisal of computer-connected network analyser design and calibration", Proc. IEE, Vol.124, 1977, pp.205-11.

[15] ————————: "Multiport network analysis by matrix renormalisation employing voltage-wave s-parameters with complex normalisation", ibid, pp.198-204.

[16] HUNTON, J.K.: "Analysis of microwave measurement techniques by means of signal flow graphs. IRE Trans. MTT-8(2), Mar. 1980.

[17] SHURMER, H.V.: "Correction of a Smith-chart display through bilinear transformations", IEE Electron. Lett., Vol.5, 1969, pp.209.

[18] THOMAS, N.E.: Private Communications, Marconi Instruments Ltd., 1978.

[19] SALEH, A.A.M.: "Expliicit formulas for error correction in microwave measuring sets with switching dependent port mismatches", IEEE Trans. IM-28, 1979, pp..67-71.

[20] SWANSON, D.: "Ferret out fixture errors with careful calibration", Microwaves, Jan. 1980, pp.79-85.

[21] KASA, I.: "A curve fitting procedure and its error analysis", IEEE Trans. IM-25, 1976, pp.8-14.

[22] FRANZEN, N.R. & SPECIALE,R.A.: A new procedure for system calibration and error removed in automated s-parameter measurements", Proc. 5th European Microwave Conf., Sept. 1975, pp.67-73.

[23] WATERS, J.D.: "The computer correction of s-parameter measurements using microstrip references for calibration", GEC HIRST RESEARCH CENTRE, REPORT TRL/710, FEB. 1978.

[24] BIANCO, B. et a.: "Launcher and microstrip characterisation", IEEE Trans. IM-25, 1976. pp.320-3.

[25] SPECIALIE, R.A., GROBOWSKI, R.E., FRANZEN, N.R.: "Accurate scattering parameter measurements on non-connectable microwave networks". Proc. 6th European Microwave Conf., Sept. 1976, pp.210-4.

[26] DA SILVA, E.F. & McPHUN, M.K.: "Calibration technques for one-port measurement,", Microwave Jnl., June 1978, pp.97-100.

[27] DAVIES, O.J., DOSHI, R.B. & NAGENTHIRAM B.: "Correction of microwave-network-analyser measurements of 2-port devices", IEE Electron Lett., Vol.9, 1973, pp.543-4.

[28] REHNMARK, S.: "On the calibration of automatic network analyser systems", IEEE Trans. MT-22, 1974, pp.457-8.

[29] HEWLETT-PACKARD Co.: Software manual for 9409B ANA.

[30] YEO, M.: IEE Colloquium on "Advances in s-parameter measurements micro-wavelengths", London, 23 May 1983.

CHAPTER 6

S-PARAMETER MEASUREMENTS OF MICROSTRIP MOUNTED COMPONENTS

6. S-PARAMETER MEASUREMENTS OF MICROSTRIP MOUNTED COMPONENTS

The general theory and practice of Computer Corrected Network Analysis and the application, principally to the measurement of components having coaxial connectors were considered in Chapter 5. Naturally the concepts are applicable to all transmission structures, including waveguides and strip transmission lines, but some present special problems. Coaxial structures (coax) have the particular advantages that several well established precision connector systems exist and that calibration standards are readily constructed and their electrical properties easily verified. In many situations the constraint of establishing calibration only in a selection of coaxial connector systems is satisfactory. Indeed, even when making measurements on complete Microwave hybrid Integrated Circuit (MIC) modules, the s-parameters are often referred to the coax connector interface. When, however, the design of an MIC module is undertaken it is highly desirable to characterise the components and devices used at their point(s) of connection to the microstrip transmission line(s). As it is impossible to realise a perfect transition from coax to microstrip over a broad frequency band a further source of error is introduced. Moreover, as the components to be measured often have high reflection coefficients the effects of test port mismatch (cf. Section 5.4.3) are emphasised. Thus it is unsatisfactory to use the CCNA calibrated in a coax system to measure a component mounted in microstrip, simply by using the reference plane shift facility to accommodate the electrical length of the transitions.

There are two obstacles to the successful calibration of the CCNA to measurement planes in microstrip: the difficulty of obtaining calibration standard, realised in microstrip form, having sufficient integrity, and

the need for a repeatable system of connection both for the coax-microstrip transitions and the device under test (DUT).

6.1 MICROSTRIP CALIBRATION STANDARDS

Other workers[1,4,5] have endeavoured to produce microstrip equivalents of the commonly used coax calibration standards so enabling them to use the established calibration schemes (e.g. those of Sections 5.8 & 9) to include the effects of the transitions in the error model. Many of the necessary structures are technologically difficult to realise with sufficient accuracy and the integrity of the resulting calibration pieces is hard to establish.

6.1.1 Microstrip Loads

The foregoing is particularly pertinent to microstrip loads or matched terminations. Kwesah[4] used a 50 Ohm chip resistor which, due to its physical size, exhibits a number of parasitic effects at microwave frequencies. The problem, is then, to establish its true reflection coefficient which returns us to the problem of making accurate measurements of components mounted in microstrip. Hossieni[5] attempted to construct a microstrip sliding load using a wedge of lossy material resting across a microstrip line on a 4" long alumina substrate. The operation of a sliding load is dependent upon the transmission line having negligible loss and more crucially upon the reflection coefficient of the load remaining constant, thus placing great demands on the mechanical stability of all the constituent parts.

The author's original proposal was to produce a 'quasi-sliding load' using a chip resistor mounted in a stud package which could be inserted, in turn, in holes at the end of each of a set microstrip lines of

differing lengths. This proposal suffers from two drawbacks: the connection of the resistor has to be both robust and highly consistent, and, the requirement for a large number of lines; typically, a set of three lines for each octave band of interest.

The problems associated with microstrip calibration loads induce one to consider calibration schemes that do not require their use.

6.1.2 Microstrip Short Circuits

It is possible, with some care, to produce an almost perfect microstrip short circuit. The cardinal rule, to be observed when designing one, is to ensure that all the electric field is bounded by a highly conductive plane perpendicular to the direction of propagation. This must include the field in the region above the dielectric substrate as well as within it. The short cicuit so constructed is unaffected by microstrip dispersion as it acts also upon the non-TEM modes of propagation as well as on the dominant (TEM) mode (cp. the waveguide short).

The short circuits made for this work were constructed around an alumina substrate (0.635mm thick) bearing a 50 Ohm microstrip line connected to the ground plane at one end by the edge plating. The substrate is attached, by soldering, to a gold plated brass block having a step against which the plated edge of the substrate is butted. It has been found experimentally that the perpendicular conducting surface should extend at least 6mm above, and to the side of, the microstrip line (cf. Section 3.2.3 and figure 3.18).

The preparation of an offset short circuit presents an additional problem; the need to establish the electrical length of the offset. To obtain this information from the physical dimensions it is necessary to know the velocity of propagation along the microstrip line. It may also

be desirable to know the line attenuation; as the loss of the offset length of line can be significant. Providing the substrate relative dielectric constant is accurately known computational techniques described in Chapter 2 may be applied, yielding values with an uncertainty of a fraction of a percent. The variations between samples of alumina substrates from a single manufacturer are not, however, negligible being typically ± 0.2 from a nominal value of dielectric constant of 9.8. (This corresponds to an uncertainty of $\pm 1\%$: equivalent to $\pm 1.8^{\circ}$ for a $\lambda/4$ offset length.). Microstrip resonator patterns (cf. Chapter 3) can be included on the same substrate as that from which both the short and offset short circuits are made, but this is somewhat inconvenient and fails to take account the effects of dispersion (dependence of velocity of propagation on frequency).

6.1.3 Microstrip Open Circuits

Fabricating microstrip open circuits is comparatively trivial: merely requiring the application of standard photolithographic techniques to produce a specified length of 50 Ohm microstrip line. Unfortunately, due to the fringing field, the open end does not possess ideal properties. The open end effect has been discussed in Chapter 4. For frequencies at which dispersion on the microstrip line is insignificant, a quasi-static solution, in terms of an equivalent end capacitance or line extension, is acceptable. Values may be obtained from the computer program of Appendix C. Experimental determination of the open end effect is also possible (cf. section 4.1.1). The fringing field does give rise to some loss due to radiation, which may be accounted for in terms of an equivalent shunt resistance.

Offset opens suffer from the same additional problems as offset short circuits.

6.1.4 Microstrip Though lines

Microstrip through lines sre seldom of zero length, often being similar in physical length to the device under test. Realised as a straight uniform microstrip line having a characteristic impedance equal to the system calibration impedance, it is necessary to know the propagation constants in order to compute the electrical length and attenuation of the through line. As for the offset short and open circuits, dispersive effects aggravate this problem.

6.2 MICROSTRIP 1-PORT CALIBRATION SCHEMES

Given the evident problems associated with attempts to construct microstrip calibration standards to suit existing calibration schemes, it is necessary to develop a calibration strategy using only standards that are readily fabricated and attested in microstrip form.

Aitchison's[6] method is to carefully characterise a coax to microstrip transition in terms of z-parameters, and measure the DUT through it. The s-parameters of the composite structure, including the transition(s), the DUT, and interconnecting microstrip line(s) of known electrical length, are determined using a CCNA calibrated in the connector system suitable for the transition. By matrix manipulation, or application of de-embedding techniques described in section 5.10, the true s-parameters of the DUT can be extracted.

Superficially this approach seems to obviate the need for microstrip calibration pieces, but it is still necessary to connect microstrip structures of particular properties (i.e. four open circuit lines) to the transition in order to deduce its properties. Thus in essence, a single calibration is replaced by two; the coax calibration of the CCNA and the

microstrip calibration of the transition. The latter need only be done occasionally. The method then relies on the stability of the transition which is frequently mounted and demounted or on the consistency between samples of the same type of transition.

The method proposed here employs four open (or short) circuit lines of differing lengths for reflectometer calibration. The principle virtue of this scheme is that it uses an additional calibration measurement (three complex results are sufficient for 1-port calibration) in order to obtain the propagation constants of the transmission line used. This additional capability is of significant advantage when microstrip, with its mixed dielectric (resulting in dispersion) and dielectric tolerance problems, is to be employed.

The above method which, although developed independently, is essentially similar to that of DA Silva & McPhun [7,8], has also been extended to include 2-port calibration (section 6.3) and demonstrates improved broad-band accuracy attributable to a better conditioned algorithm (cf. Appendix E).

6.2.1 The Four-Opens Calibration Scheme

The open circuit line is the simplest structure to produce in microstrip form (cf. Section 6.1) and consequently it is adopted in preference to short circuit lines. There are two stages in the process of determining the error model element values from the measurement of the four opens (i.e. an open circuit line and three different offset open circuit lines). The first is the computation of the microstrip propagation velocity and line attenuation at each frequency of measurement. Three of the four measurements are then selected, at each frequency, and used, in conjunction with the microstrip parameters previously obtained, to calibrate the reflectometer.

6.2.1.1 Determining the Microstrip Parameters

The method adopted for this process is due to Bianco and Parodi[9], originally applied to the measurement of microstrip dispersion through an imperfect transition. Their work is based on the principle of the invariance of the complex cross-ratio under bilinear transformation [10].

As discussed in Section 5.5.1 the reflectometer calibration equation is a particular form of the bilinear transformation which is restated here:

$$\Gamma_{meas} = (e_{11} - \Delta\Gamma_{DUT})/(1 - e_{22}\Gamma_{DUT}) \qquad \langle 6.1 \rangle$$

where $\Delta = e_{11}e_{22} - e_{12}e_{21}$

The complex cross-ratio is formulated from four complex numbers A, B, C & D thus:

$$Z = (A - C)(B - D)/(A - B)(C - D) \qquad \langle 6.2 \rangle$$

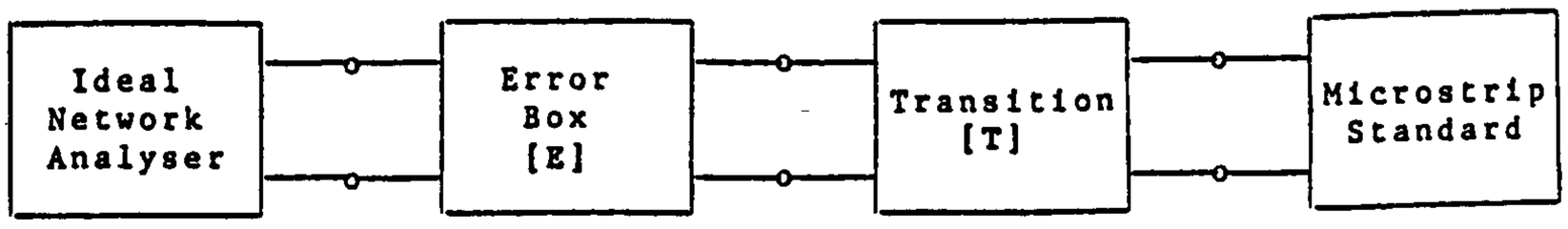

Figure 6.1 The conceptual configuration of the microstrip reflectometer undergoing calibration.

Figure 6.1 sets out the arrangement for calibration of the microstrip reflectometer to which the standards, having reflection coefficients Γ_{sk}, k=0 →4, are connected in turn, resulting in corresponding measured coefficients Γ_{mk}. Both the network analyser and the transition errors are described as s-parameter black boxes. So the system can still be defined by the bilinear transformation of equation <6.1>. It is therefore possible to relate the true and measured reflection coefficients of the four standards by the equivalence of the complex

cross-ratios, viz:

$$\frac{(\Gamma_{m0} - \Gamma_{m2})(\Gamma_{m1} - \Gamma_{m3})}{(\Gamma_{m0} - \Gamma_{m1})(\Gamma_{m2} - \Gamma_{m3})} = Z = \frac{(\Gamma_{s0} - \Gamma_{s2})(\Gamma_{s1} - \Gamma_{s3})}{(\Gamma_{s0} - \Gamma_{s1})(\Gamma_{s2} - \Gamma_{s3})} \qquad \langle 6.3 \rangle$$

The four open circuit microstrip lines are illustrated in figure 6.6. Three of the opens are offset from the first by differing lengths of uniform microstrip linxe. Each line may be considered, therefore, as comprising three regions: 1. a transition region, where the microstrip line is perturbed by the structure of the transition, 2. a central region, where propagation along the uniform line is essentially unperturbed, and 3. an end region, where the fields associated with the propagation along the line are perturbed by the open end effects. The lines differ from each other in only one respect, the length of the central region (2).

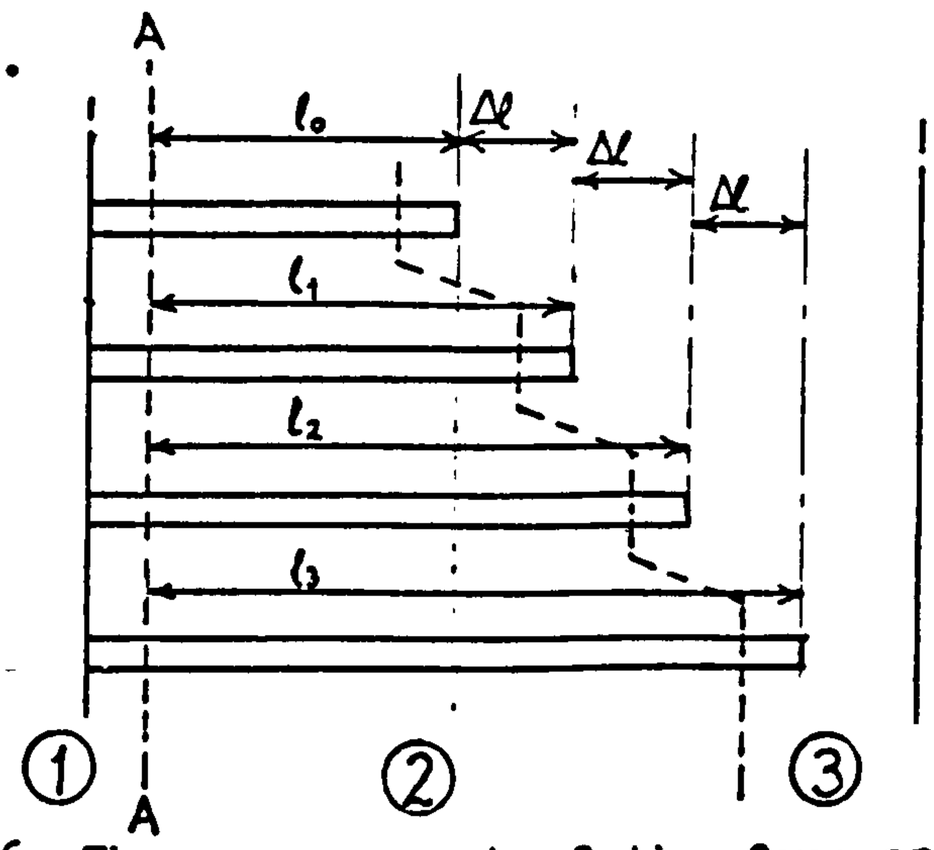

Figure 6.6 The arrangement of the four open circuit microstrip lines.

If Γ_e is the reflection coefficient of the open end; region 3, the reflection coefficients of the lines at the reference plane A-A are:

$$\Gamma_{sk} = e^{-2\gamma l_k}\Gamma_e \quad ; \quad k = 0,1,2,3 \qquad \langle 6.4 \rangle$$

Substituting these values into the complex cross-ratio, equation <6.3>, dividing through by $e^{-2\gamma l_o}$ and making the substitutions:

$$l_j - l_o = \Delta l_j \quad ; \quad j = 1,2,3$$

$$Z = \frac{(1 - e^{-2\gamma\Delta l_2})(e^{-2\gamma\Delta l_1} - e^{-2\gamma\Delta l_3})}{(1 - e^{-2\gamma\Delta l_1})(e^{-2\gamma\Delta l_2} - e^{-2\gamma\Delta l_3})} \qquad \langle 6.5 \rangle$$

where the physical lengths and the reflection coefficients can be measured in order to determine the value of $\gamma = \alpha + j\beta$; the propagation constants of the microstrip line.

If a further condition is placed on the disposition of the four open circuit lines: that they should have equal relative offsets, Δl; i.e.

$$\Delta l_1 = \Delta l, \quad \Delta l_2 = 2\Delta l, \quad \Delta l_3 = 3\Delta l \qquad \langle 6.6 \rangle$$

then <6.5> simplifies thus:

$$Z = \frac{(1 - e^{-4\gamma\Delta l})(e^{-2\gamma\Delta l} - e^{-6\gamma\Delta l})}{(1 - e^{-2\gamma\Delta l})(e^{-4\gamma\Delta l} - e^{-6\gamma\Delta l})} \qquad \langle 6.7 \rangle$$

$$Z = 4.\cosh^2(\gamma\Delta l) \qquad \langle 6.8 \rangle$$

or $$2\gamma\Delta l = \pm\ln\{(Z - 2)/2 + /[Z - 2)^2/4 - 1]\} \qquad \langle 6.9 \rangle$$

where from <6.3> Z can be determined from four measurements.

Equation <6.9> is more convenient for computer program application, where complex inverse hyperbolic cosine may not always be available. Thus the velocity of propagation and the line loss may be obtained for the microstrip line by measurement assuming substrate uniformity, equal width track, and equal relative displacement of the open ends.

Whilst it is possible to apply an iterative solution for the general case where the relative offset lengths are not all equal (cf. <6.5>), it has not been found necessary in practice. To ensure uniformity of dielectric constant and loss tangent, the four opens are produced on a single substrate, by standard microelectronic photolithographic techniques. Using a single substrate, any misalignment of the photographic mask, although resulting in line lengths different from the design lengths, cannot cause the relative displacements of the open ends to vary. Thus the condition of <6.6> is likely to be met accurately without difficulty. As the propagation constants are computed from measurements at each frequency, the effects of dispersion will be taken into account.

6.2.1.2 Selecting the Three Calibration Open Circuits

Having used the measurements of the four open circuit lines to determine the microstrip transmission line constants, in a manner unperturbed by the vagaries of the network analyser, it is then possible to use any three of the measurements (the data having been retained by the computer) to calibrate the CCNA. Thus there is a degree of freedom in the selection of the three out of four open ended lines to be used a microstrip calibration standards at each frequency. It is desirable to make the choice in a way that maximises the useful frequency range of calibration that can be obtained with a single set open circuit lines. In any case the reference open; the shortest line, is included in order to define a consistant reference plane. At the high frequency end of the band of calibration, the shortest offset lengths; the first and second offset opens are most appropriate. Conversely, at the low end of the band, it is desirable to include the longest (the third) offset open. In this case, the selection of the first or second offset open for inclusion in the calibration is arbitrary; the second having been chosen for the work presented here. The breakpoint between these two states has been defined in terms of the angular separation of the measured reflection coefficients of adjacent open-ended lines (i.e. the offset angle $\theta=\beta\Delta l$), the condition chosen being: $\theta=\pi/2$.

6.2.1.3 Calibration with Three Open Circuits

The calibration process is conducted in a similar manner to that described in Section 5. First, however, the true reflection coefficients must be deduced from the measurements of the microstrip line propagation constants and the physical offset lengths of the open-ended lines for the two cases defined in the last section, viz:

TABLE 6.1 TRUE REFLECTION COEFFICIENTS OF MICROSTRIP STANDARDS

	CASE 1 ($\beta\Delta l > \pi/2$)	CASE 2 ($\beta\Delta l < \pi/2$)
Γ_1	Γ_e	Γ_e
Γ_2	$\exp(-2\gamma\Delta l).\Gamma_e$	$\exp(-4\gamma\Delta l).\Gamma_e$
Γ_3	$\exp(-2\gamma\Delta l).\Gamma_e$	$\exp(-4\gamma\Delta l).\Gamma_e$

where $\gamma = \alpha + j\beta$

At this stage, Γ_e, the microstrip open end reflection coefficient is not defined, a matter that will be discussed in the next section. The shortest line, after allowing for the open end reflection coefficient defines the calibration reference plane. Substitution of the true reflection coefficients given in the table above into the matrix formulation of the calibration equations <5.15> will facilitate complete calibration of the network analyser including the effects of the coax-microstrip transition. Expanding the equation with the error model terms as dependant variables yeilds <6.10> to <6.12> where the values of c and Γ_{ci} corresponding to the cases defined above can be found in Table 6.1.

$$e_{00} = \frac{\Gamma_{c1}\Gamma_{c2}(e^{-2c\gamma\Delta l}-1)-\Gamma_{c2}\Gamma_{c3}(e^{2\gamma\Delta l}-1)-\Gamma_{c3}\Gamma_{c1}(e^{-2c\gamma\Delta l}-e^{2\gamma\Delta l})}{\Gamma_{c1}(e^{2\gamma\Delta l}-1)+\Gamma_{c2}(e^{-2\gamma\Delta l}-e^{2\gamma\Delta l})+\Gamma_{c3}(1-e^{2c\gamma\Delta l})} \quad \text{<6.10>}$$

$$e_{11} = \Gamma_e\{e^{2c\gamma\Delta l}(\Gamma_{c2}-e_{00})-(\Gamma_{c2}-e_{00})\} = \Gamma_e e'_{11} \quad \text{<6.11>}$$

$$e_{01} = \Gamma_e(\Gamma_{c1}-e_{00})(1-e_{11}) = \Gamma_e e'_{01} \quad \text{<6.12>}$$

TABLE 6.2 SELECTION OF TERMS IN EQUATIONS <6.10> to <6.12>

	CASE 1	CASE 2
Γ_{c1}	Γ_{mo}	Γ_{mo}
Γ_{c2}	Γ_{m1}	Γ_{m1}
Γ_{c3}	Γ_{m2}	Γ_{m2}
c	1	2

6.2.1.4 Allowing for the Open-End Effect.

In section 6.1.3 the effects of fringing fields and radiation associated with an open circuit microstrip line were discussed. These effects may be represented in equivalent circuit form by a lumped capacitor, C_e, (or short length (dl) of transmission line) and a shunt resistor (conductance).

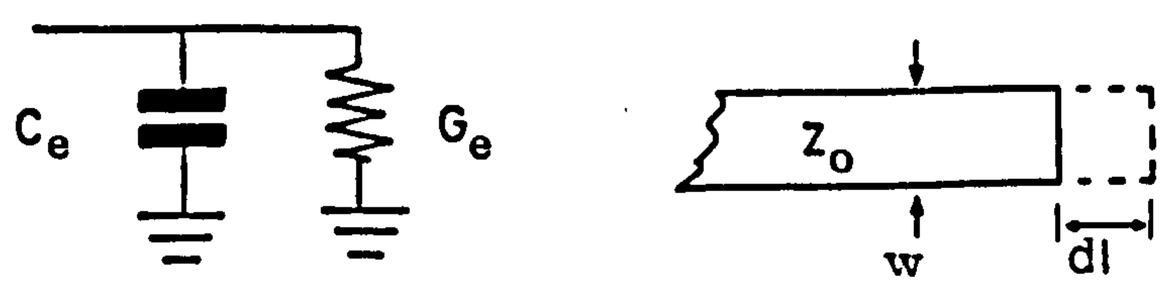

(a) (b)

Figure 6.2 Microstrip Open-End Models.

If the model of figure 6.2(a) is used then the open end reflection coefficient is:

$$\Gamma_e = \frac{(1 - Z_o G_e) - j2\pi f C_e Z_o}{(1 + Z_o G_e) - j2\pi f C_e Z_o} \qquad \text{<6.13>}$$

where f is the frequency of interest.

At frequencies for which the equivalent line extention, dl, is small compared to a wavelength, <6.14> relates the equivalent circuits of figure 6.2.

$$C_e = 1/2\pi f Z_o \cot(\beta dl) \qquad \text{<6.14>}$$

The end effect can then be accommodated merely by allowing a notional shift in the calibration reference plane of dl. Expressing the open end effect as a line extension has the advantage that the value of the extension, dl, is very much less dependent on characteristic impedance (line width), substrate thickness and dielectric constant than is the equivalent capacitance, C_e. It is worth noting that most published results (cf. Section 4.1.1), both computed and empirical, concur, at least, on the value of the open-end effect for 50 ohm microstrip lines on alumina, viz: $C_e \simeq 33fF$, $dl \simeq 0.2mm$. A useful rule of thumb applicable to all microstrip lines on medium and high permittivity substrates (cf. figure 4.4) is:

$$dl \sim h/3 \qquad \langle 6.17 \rangle$$

where h is the substrate thickness.

An alternative approach is to include a short circuit microstrip line as an additional calibration standard.

6.2.2 Including a Short Circuit in the Calibration Process

In Section 6.1.2 microstrip short circuits were considered and it was concluded that they could be almost ideal in their electrical properties, provided the perpendicular conducting boundary extended beyond the influence of the field in all directions. The requirement of the calibration scheme, described in the preceding section, for a set of lines terminated by identical high reflection coefficient, with precisely equal relative spacing, made on a single substrate (to ensure dielectric uniformity) is, however, incompatible with the construction of such short circuits.

The four opens calibration, as described so far, can enable complete calibration of the network analyser system, in an system of characteristic impedance equal to that of the microstrip lines used, with

only one remaining uncertinty; the open-end effect. Thus, if the microstrip open circuit were assumed ideal (Γ_e = 1 + j0), any measurement of an unknown impedance would yield a corrected reflection coefficient relative to that of the open end. If, however, structure with a known reflection coefficient were to be measured by the system this remaining complex factor could be determined. The microstrip short circuit fills this role most conveniently as its simple reflection coefficient (Γ_s = -1 + j0) generates a 'corrected' reflection coefficient (Γ_s') that is merely the reciprocal negation of the open circuit reflection coefficient, i.e:

$$\Gamma_e = -1/\Gamma_s' = -1/\{e'_{11} + e'_{01}(\Gamma_{ms} - e_{00})\} \qquad \langle 6.16 \rangle$$

Or, equivalently, if the open circuit has negliable loss:

$$\Gamma_e = -\Gamma_s'^{*} \qquad \langle 6.17 \rangle$$

Consequently the error model may be adjusted by substituting Γ_o in <6.11> and <6.12> to obtain the new values of e_{11} and e_{01}. For confirmation of accuracy and future use when calibration without the use of a short circuit is most appropriate, the equivalent circuit parameters of Section 6.2.1.4 may be found:

$$G_e = R\{Y_e\}\ , \quad C_e = I\{Y_e\}/2\pi f \qquad \langle 6.18 \rangle$$

$$\text{where } Y_e = (1 - \Gamma_o)/Z_o(1 + \Gamma_o)$$

The foregoing has been based on the assumption that the short is placed at precisely the same position as the reference open end, but removal of the short from this position presents no additional problem as the factor obtained; Γ_o', will then include the effect of length of transmission line as well as the open end effect. Thus, the short circuit may be used as a device for shifting the reference plane to a position appropriate to the intended DUT; facilitating the use of a single set of offset open circuit lines in a wide range of applications.

Ideally the short circuit is made from the same piece of substrate material as the offset opens (by scribing and cracking in the case of

ceramics). Since, however, a single microstrip short can be used at all frequencies, whereas each set of offset open covers, at best, a 3:1 band of frequencies, it is convenient to compromise; using substrates from the same batch of material to produce a complete set of calibration pieces covering the whole frequency range of interest (e.g. 1-16GHz). Furthermore, the use of a single short circuit tends to improve the continuity at the overlap between frequency bands calibrated with different sets of offset opens.

6.2.3 Reference Plane Shifting.

Since it would be tiresome to make a new set of microstrip open circuits and/or a new short circuit for every DUT of differing goemetry a facility to adjust the reference plance, to which corrected results are referred, is desirable. To allow the reference plane to be shifted to the correct physical position a knowledge of the microstrip propagation velocity (and, when significant, the line loss) is required, so that the electrical effect of the shift may be computed. As the microstrip parameters have already been determined as part of the calibration process, the data is available in the program. The user is therefore able to express the reference plane shift in terms of the physical separation between the calibration reference plane and the required DUT reference plane.

As already discussed (Section 5.10.3) it is possible to accommodate the reference plane shift, either as part of the calibration data, including its effect in the error model, viz:

$$e_{00}{}^{r} = e_{00} \qquad \text{<6.19a>}$$

$$e_{01}{}^{r} = \exp(-2\delta l_r).e_{01} \qquad \text{<6.19b>}$$

$$e_{11}{}^{r} = \exp(-2\delta l_r).e_{11} \qquad \text{<6.19c>}$$

or, as a transformation upon the corrected result, viz:

$$\Gamma^{r}_{corr} = \exp(2\gamma l_r).\Gamma_{corr} \qquad \text{<6.20>}$$

where l_r is the shift length (+ve for extension)

6.3 MICROSTRIP 2-PORT CALIBRATION SCHEMES

In a similar manner to coaxial calibration, microstrip 2-port calibration can be approached in one of two fundamentally different ways. The first is to extend a suitable 1-port calibration scheme with the additional calibration pieces necessary for the determination of the additional error model terms. The alternative approach is to use a calibration scheme exclusively applicable to 2-ports (or, possibly, multi-ports) utilising the interaction between the test ports as an essential part of the calibration process. Such are the schemes proposed by Waters and Bianco, et al.

Waters [11] proposes a particularly efficient scheme using only a microstrip open circuit, a (negative) offset open, connected alternately to each port, and a through line connected between them. A knowledge of the microstrip propagation constants and the open end effect is required so Waters has included an open circuit half-wavelength resonator on the substrate bearing the calibration pieces in order to monitor their values. Bianco, et al [12] have described a technique akin to the Thru-Short-Delay scheme for coax calibration described in Section 5.9.2, where microstrip open circuits, in lieu of the shorts, and microstrip through lines of differing length constitute the calibration set. This method utilises the redundant calibration data to determine the microstrip propagation parameters. The extended through line or delay can, however, be inconvenient to realise on a standard width substrate, as the extra length can only be accommodated by meandering the microstrip

line. The corners or bends introduce additional uncertainties.

Although these schemes operate with minimum redundancy of calibration data they suffer from disadvantages similar to those discussed in connection with the TSD scheme. In particular, the poor ordering of the solution for the error model, which is restricted to the 8-term configuration, makes the results unnecessarily susceptible to noise, quantization error and numerical inaccuracies.

As already set out in Section 5.9 the principle benefit of extending a 1-port calibration scheme to suit the 2-port situation is that the redundancy of calibration data obtained facilitates the generation of the 12-term error model. This more comprehensive error model allows us to take into account some of the errors associated with the s-parameter selection switches necessary in most test sets, as well as providing a well-ordered solution of the calibration equations that reduces the susceptibility to non-systematic errors.

6.3.1 Extending the Four Opens and Optional Short Scheme for 2-Ports

To extend the 1-port calibration scheme of Section 6.2 to the 2-port case necessitates the introduction of at least one additional calibration piece; a through line. If the calibration were to take account of leakage effects a pair of matched terminated lines (loads) would also be required (cf. Sections 5.4.4 and 5.9.2). Although the analysis to follow will, for completeness, include the leakage terms, no provision for obtaining their values from calibration measurements will be made. Factors relating to this decision are; (a) the difficulty of providing suitable calibration pieces in microstrip form, and, (b) the small benefit in potential accuracy improvement when characterising typical microstrip circuits and devices. The respective justifications are then:

a) Given that, in respect of the leakage terms, the error model is inexact and, in practise, the leakage or crosstalk is dependent upon the test port termination impedances, the optimum terminations for leakage calibration are matched loads. For effective leakage calibration the coupling or crosstalk between the two terminations must be significantly less than the system leakage terms (i.e. <<-60dB). Clearly this presents real practical problems when working at microwave frequencies using a single, unenclosed substrate.

b) As the primary aim of the work described in this thesis is to further the "state of the art" in the area of microwave amplifier design the microstrip calibration scheme is being developed in order to characterise active devices, passive components and structures used in such amplifiers with sufficient accuracy for design purposes. In few cases do the transmission coefficients of the DUT fall much below 0.1 (-20dB). Thus the error arising, if a worst case network analyser system leakage of -60dB is ignored, will be 1% (0.1dB) which, for the s_{12} parameter, is not of practical significance.

The following analysis relates to the modified bilateral 12-term error model of figure 5.21 and the corresponding calibration equations (<5.25>,where n=2); chosen in preference to the conventional 12-term model since a small-signal (Type II) s-parameter test set was employed throughout.

The application of the reflection coefficient calibration scheme to port 1 and port 2 independently, yields values for e_{00}, e_{10}, $e_{11}^{(1)}$ and e_{33}, e_{23}, $e_{22}^{(2)}$, respectively. A microstrip through line of physical length, l_t defined relative to the reflection coefficient calibration planes is then connected.

The values of the microstrip line attenuation and phase constants are available twice over from the reflection coefficient calibration. It might be expected that, since the same calibration pieces would be used on each port, the two results should be the same. In practise, however, non-systematic errors in the system give rise to small differences, particularly towards the edges of the useful frequency band of the calibration. This redundancy may be used to good effect by averaging the two pairs of results, at each frequency, for use in the 2-port calibration.

Values; $U_{11}^{(t)}$, $U_{21}^{(t)}$, $U_{12}^{(t)}$, $U_{22}^{(t)}$, corresponding the measurements of the four s-parameters of the through line are obtained at each calibration frequency. Then, by manipulation of the calibration equations and substitution of the through line s-parameters of the remaining error model terms may be found.

$$e_{11}^{(2)} = X_{22}\exp(2\gamma l_t)/\{1 + X_{22}e_{22}^{(2)}\} \quad \text{<6.21>}$$

$$e_{22}^{(1)} = X_{11}\exp(2\gamma l_t)/\{1 + X_{11}e_{11}^{(1)}\} \quad \text{<6.22>}$$

$$e_{TF} = (U_{21}^{(t)} - e_{30})\{\exp(\gamma l_t) - e_{11}^{(2)}e_{22}^{(2)}\exp(-\gamma l_t)\} \quad \text{<6.23>}$$

$$e_{TR} = (U_{12}^{(t)} - e_{03})\{\exp(\gamma l_t) - e_{11}^{(2)}e_{22}^{(2)}\exp(-\gamma l_t)\} \quad \text{<6.24>}$$

where $X_{11} = (U_{11}^{(t)} - e_{00})/e_{R1}$, $X_{22} = (U_{22}^{(t)} - e_{33})/e_{R2}$

and $e_{03} = e_{30} = 0$ (negligable leakage)

Thus the 2-port calibration is complete and de-embedding may procede in a manner identical to that described in Section 5.10.2.

6.3.2 Through Lines & Reference Plane Shifting

A typical 2-port calibration and test substrate appears as illustrated in figure 6.3.

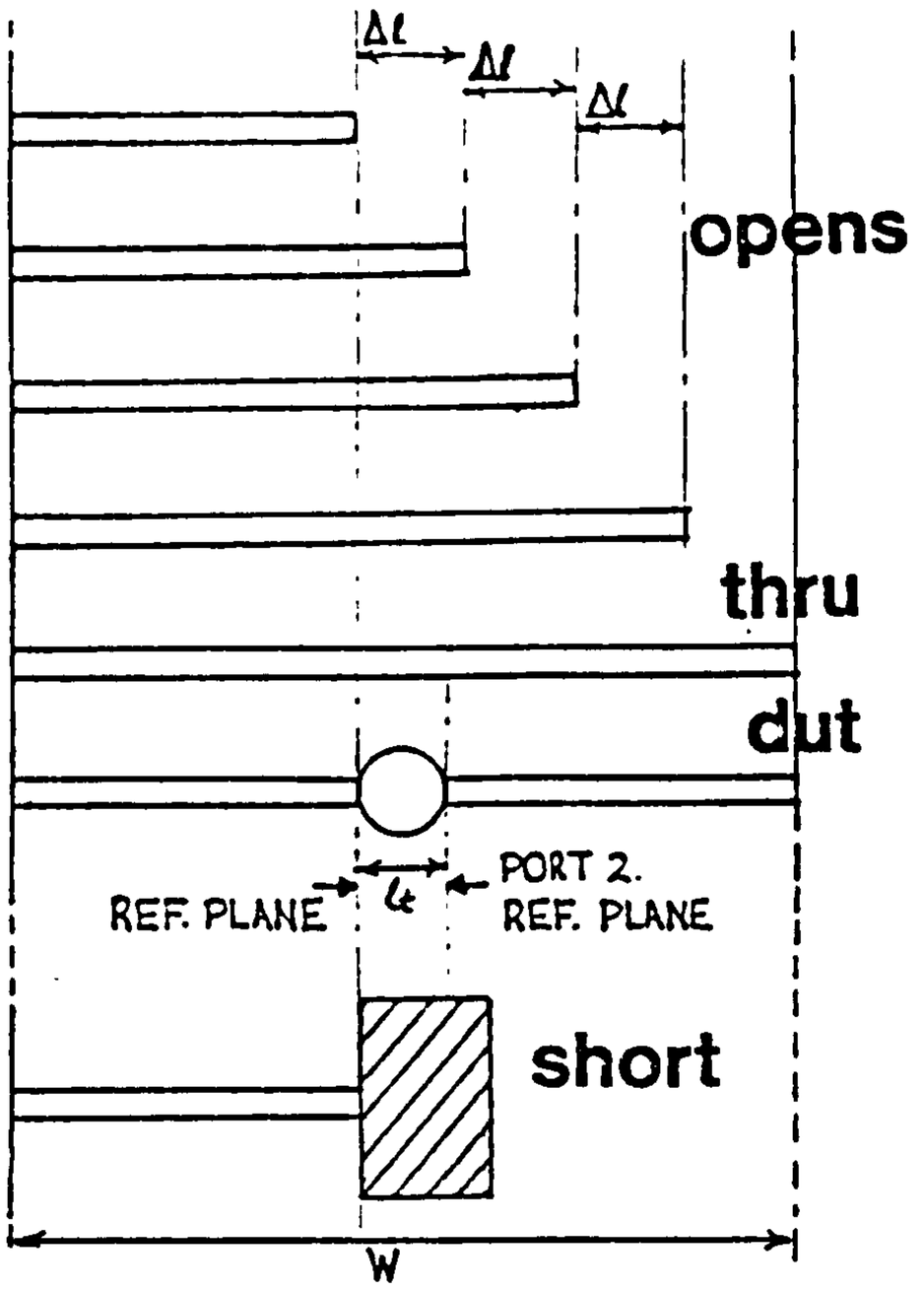

Figure 6.3 A typical calibration and test substrate

In an ideal situation

$$l_{d1} = l_{d2} = l_o + dl = l_s \qquad \langle 6.25 \rangle$$

$$\text{and} \quad W = l_{d1} + l_{d2} + l_t \,, \quad \text{i.e. } l_t = l_{DUT} \qquad \langle 6.26 \rangle$$

where dl is the amount by which the open end line is foreshortened to allow for the end effect and so obviate specification of the end effect capacitance. The microstrip short circuit is made by severing the short circuit line by scribing and attaching it to a metal block in accordance with the recommendations of section 6.1.2. In this ideal situation the calibration reference planes coincide with the terminals of the DUT and, because of the use of a substrate of configured to fit a jig of fixed port separation, the through line length is equal to the length of the DUT. Consequently four opens and optional short circuit calibration can be applied to measurement of the 2-port DUT with prior knowledge of only two physical lengths; Δl, the offset length and l_{DUT}, the length of the DUT. The measured microstrip propagation parameters are applied directly

to the computation of the electrical length of the through line.

Often, however, additional complications arise. The DUT may not be mounted centrally in the substrate, the short circuit microstrip line may not have been cut to the correct length, or it may be desirable to use the calibration set for measurement on a DUT of differing length. Consequently, there is a need to move the reference planes from the default calibration position to accommodate these variations. As observed in Section 5.10.3 reference plance shifting can be accomplished by applying a transformation either to the error model, or to the corrected s-parameters. In the application to coax measurements the latter seemed most appropriate. Since, in the microstrip case, the reference phase shift is most frequently applied to accommodate the inadequacies of the calibration pieces it is considered apposite to include the effect of reference plane shifts in the error model. Thus the corrected s-parameters may be read directly without further regard to this consideration. An incidental advantage is that there is no need for the computer to hold values for the propagation constants at each frequency (desirable principally to allow for dispersive effects) for latter use in translating the physical reference plane shifts into electrical lengths. With reference to figure 6.2 consider now the non-ideal case where:

$$l_{d1} \# l_{d2} \# l_s \# l_o + dl \qquad \langle 6.27 \rangle$$

Then when the 4-opens calibration is used; the port 1 and port 2 reference plane shifts are, respectively;

$$l_{r1} = l_{d1} - (l_o + dl) \ , \ l_{r2} = l_{d2} - (l_o + dl) \qquad \langle 6.28 \rangle$$

and, similarly, when the optional short circuit is included:

$$l_{r1} = l_{d1} - l_s \ , \ l_{r2} = l_{d2} - l_s \qquad \langle 6.29 \rangle$$

The resulting transformation of the error vectors is then:

$$e_{00s} = e_{00} \qquad \text{<6.30a>}$$

$$e_{R1s} = e_{R1} \cdot \exp(-2\gamma l_{r1}) \qquad \text{<6.30b>}$$

$$e_{11s}^{(j)} = e_{11}^{(j)} \cdot \exp(-2\gamma l_{r1}) \qquad \text{<6.30c>}$$

$$e_{TFs} = e_{TF} \cdot \exp(-\gamma\{l_{r1} + l_{r2}\}) \qquad \text{<6.30d>}$$

$$e_{TRs} = e_{TR} \cdot \exp(-\gamma\{l_{r2} + l_{r1}\}) \qquad \text{<6.30e>}$$

$$e_{22s}^{(j)} = e_{22}^{(j)} \cdot \exp(-2\gamma l_{r2}) \qquad \text{<6.30f>}$$

$$e_{R2s} = e_{R2} \cdot \exp(-2\gamma l_{r2}) \qquad \text{<6.30g>}$$

$$e_{33s} = e_{33} \qquad \text{<6.30h>}$$

where $j = 1,2$

and $\gamma = \alpha + j\beta$ the mean of the propagation constants obtained from the measurements of the four open circuits on both test ports.

Having included the reference plane shifting with the calibration data it is convenient to continue to express the effective through line length (l'_t) as equal to the physical length of the DUT, that is; the distance between the reference planes <u>after</u> shifting:

$$l_t = W - l_{d1} - l_{d2} = l_{DUT} \qquad \text{<6.31>}$$

But the calibration equations are formulated using a through line length (l_t) equivalent to the separation of the reference planes <u>before</u> shifting.

$$l_t = W - 2(l_o + d1) \quad \text{[4 opens]} \qquad \text{<6.32a>}$$

or $$l_t = W - 2l_s \quad \text{[4 opens + short]} \qquad \text{<6.32b>}$$

therefore, by substitution of <6.28> or <6.29> in <6.31>

$$l_t = l'_t + l_{r1} + l_{r2} \qquad \text{<6.33>}$$

6.4 MICROSTRIP TEST FIXTURE DESIGN

Crucial to the successful application of any microstrip calibration scheme is a method of successively connecting the calibration pieces and DUT. Whilst the actual electrical quality of the microstrip transition is, in principle, unimportant it should be highly repeatable so that the error associated with both the network analyser system and the transition may be accurately determined and eliminated. In practise, however, it is advisable to make the transition reasonably well matched, in order to minimise the dependence of calibration quality upon non-systematic effects in the system as a whole, including any lack of repeatability in the transition. The fixture must permit swift and easy changes of calibration and test items, eliminating unnecessary tedium and human error as far as reasonably possible. Some adaptability may also be required to accommodate substrates of differing widths, if only to cater for mechanical tolerances, and, possibly, lateral offset between test ports.

There are two distinct approaches to the construction of the microstrip test fixture. The first is to use a separate, similar coax-microstrip transition for each microstrip line associated with the calibration pieces and DUT. Changing between items is then simply a matter of disconnecting and reconnecting coaxial connectors. The second method involves only a single pair of transitions to which the microstrip lines are connected by a clamp mechanism. This mechanism must include a release device that will allow the substrate to slide between the two transitions, moving from one microstrip line to the next, or to be removed and replaced.

The simpler mechanical structure, which affords great flexibility in choice of substrate size and microstrip configuration, when used in conjunction with flexible coaxial cbles, is an advantage of the former

method. This method does, however, depend on the doubtful assumption that the electrical characteristics of all the transitions are identical. Furthermore, suitable high quality transitions are expensive and their bulk severely restricts the number of connections to substrates of typical dimensions.

The latter approach, whilst confining points of connection to opposite edges of the substrate, does permit much closer spacing, limited only by the considerations of electrical interaction between adjacent lines. The principle advantage of this approach is, however, that the same transitions are used throughout the calibration and test process which, provided consistent clamp force and good contact surfaces are ensured, guarantees that uniformity of the transition's electrical properties is maintained. It is worthy of note that, as the microstrip lines not in use are terminated by open circuits at both ends and thus may behave as high-Q resonators, there may be significant interaction even though the electromagnetic coupling is minute. To circumvent this problem, without resorting to excessive separation of the lines, pieces of proprietary ferrous loaded rubber, having high magnetic losses at microwave frequencies, are placed across adjacent lines. A separation of at least five substrate thicknesses is then satisfactory for most situations.

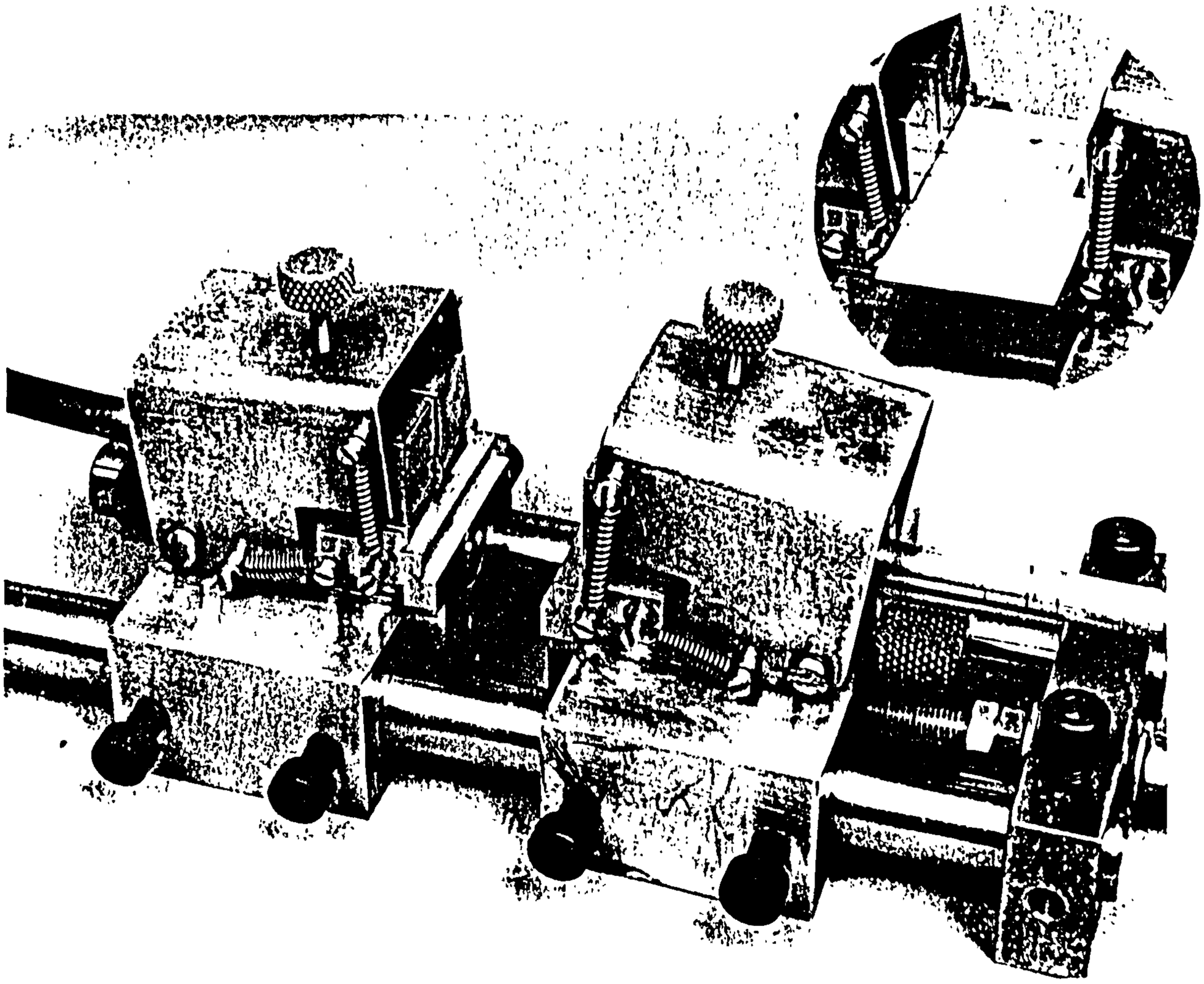

Figure 6.4 Microstrip Test Fixture (Inset shows calibration substrate in position)

Figures 6.4 shows the microstrip test fixture; of the style using a single pair of transitions with clamp connection to the microstrip lines. Initially, a fixture, available as an outcome of previous work [13], was modified by the author to improve the connection repeatability in accordance with the recommendations set out below. As a result of experience gained with this fixture the the improved fixture illustrated above was designed and built in collaboration with Marconi Instruments Limited. The transitions used in both are essentially similar in concept; although rather different in implementation.

6.4.1 The Coax-Microstrip Transition

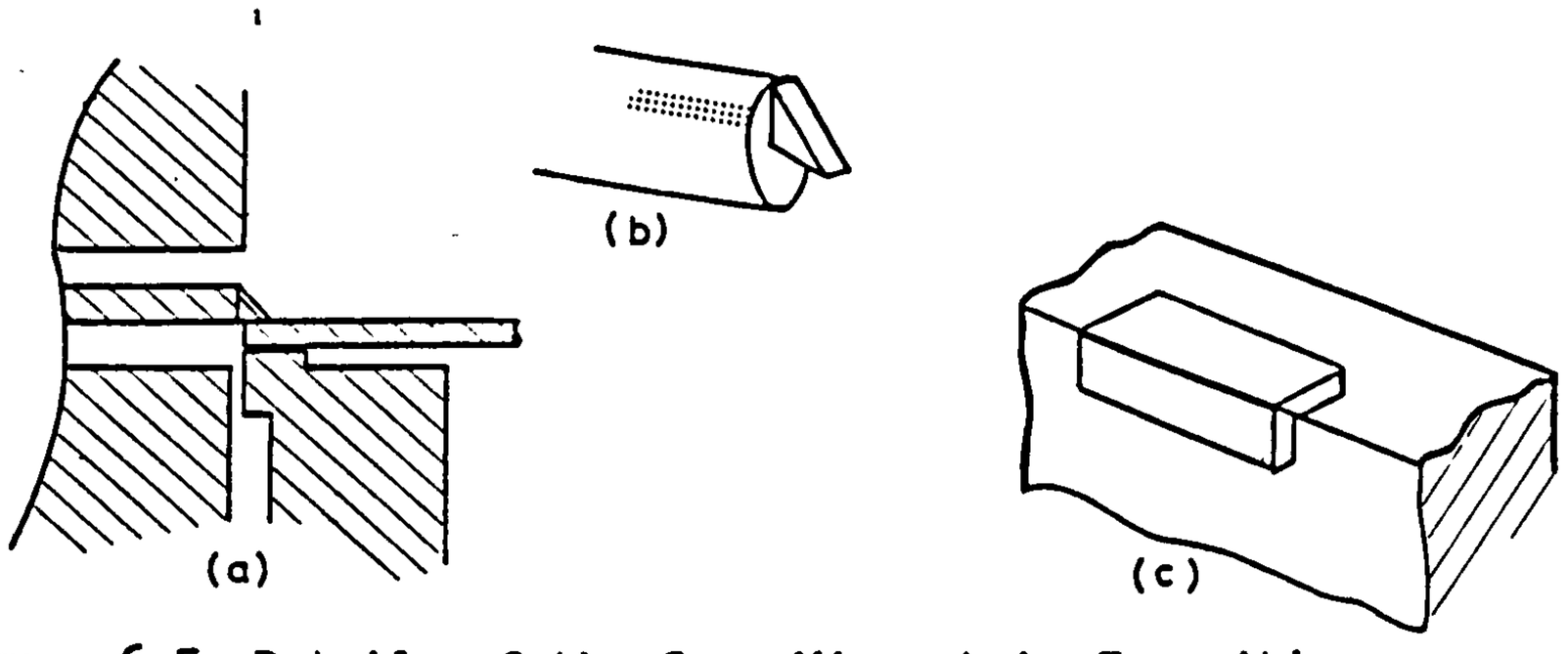

Figure 6.5 Details of the Coax-Microstrip Transition.

The basic elements of the transition are illustrated in figure 6.5. A securely mounted rigid air-line centre conductor emerges from a gold plated vertical face. A "wedge" shape at the end of the centre conductor, which is also gold plated, makes contact with the microstrip line on the substrate. A slight rake on the underside of the "wedge" guarantees a consistant point of connection even if the substrate suffers from warp, camber or surface irregularities. The substrate is supported by a gold plated block which has raised lands on the faces that make the ground connection of the transition. These lands ensure that a minimum path length ground connection is obtained repeatably. Contact pressure on both connecting faces is maintained by spring tension in the vertical and horizontal directions. An arrangement for presetting the force applied is included so as to ensure that any deflection of the centre conductor is precisely repeated on each connection. The block is constrained to resist the turning moment and maintain the contact faces parallel to the substrate ground plane and the coax ground face. The fixture allows the separation of the two transitions to be adjusted whilst keeping their axes coincident. The fixture of figure 6.4 has a cam operated substrate release mechanism and the preset tension may be adjusted using the thumb screws above the transitions. The transition

involves no connectors as direct connection is made to a length of 0.25" precision semi-rigid (solid copper) cable shaped to attach directly to the test set, with enough free length to allow a reasonable range of substrate width adjustment to be obtained.

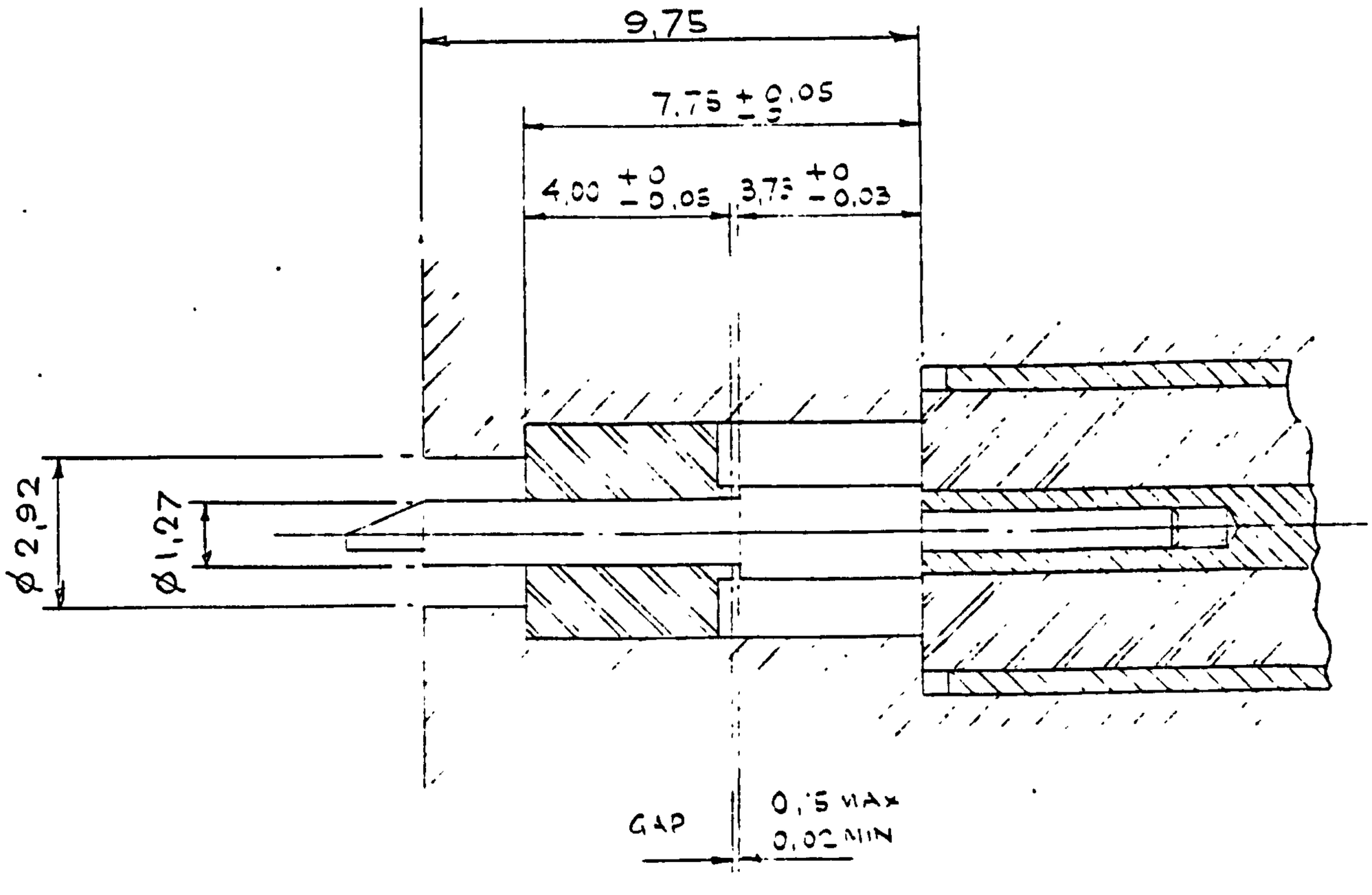

Figure 6.6 Details of the transition between 0.25" semi-rigid cable and the coax-microstrip interface

The centre conductor of the transition is formed by a gold plated steel pin that is force fitted to a drilling in the centre conductor of the semi-rigid cable. A PTFE bead acts as a cantilever support to give mechanical rigidity to the structure. The transition from the relatively large diameter dielectric filled coaxial line to the much smaller air-line at the microstrip interface comprises three sections as illustrated in figure 6.6. In order to minimise discontinuities [and simplify their compensation] the diameter of only one of the conductors is altered at each interface. Within each section the characteristic impedance, which

is maintained at 50 ohms, conforms to the expression:

$$Z_o = \{120\pi/\sqrt{\epsilon_r}\}.\ln(b/a) \qquad \text{<6.34>}$$

where a is the exterior diameter of the inner conductor

and b is the interior diameter of the outer conductor.

The test fixture described allows independent use of the two coax-microstrip transitions. This feature is particularly useful when calibrating at lower frequencies (say <4GHz) when the overall length of the open ended calibration line set exceeds the standard width (1") adopted for most of the substrates. In such a situation the opens calibration is conducted on each port in turn with the jig split.

6.4.2 Device (GaAs MESFET) Fixture Considerations.

The principle application of the 2-port microstrip calibration scheme envisaged, for the purposes of this research, was the measurement of packaged GaAs MESFETs. Consequently it was necessary to devise a microstrip test fixture suitable for the package style adopted. Indeed the requirement to characterise the devices was a factor that influenced the choice of package, the one selected being the P103 style.

It is essential that the package can be removed and replaced non-destructively so that the fixture may be used for many devices and allow the measured device to be incorporated in the amplifier modelled around its s-parameters. Furthermore, it is important to ensure that the test fixture is closely representative of the intended application of the DUT. A low inductance ground path for the source contributes significantly to the broad-band performance of a GaAs FET and the stud source connection which also provides mechanical location and fixing of the P103 package is an advantage in this respect. The device manufacturers intention is that the source connection be made by securing the shoulder on the package stud against a counterbore in a carrier plate

to which the drilled substrate is attached.

The gate and drain tabs would then be soldered to the microstrip lines. The application of the test fixture requires that the device connections be by pressure contact at all three terminals. The mechanical structure of the package poses a problem in this respect as the three terminals are in two separate planes. Some method of accommodating tolerances between these planes, other than solder attachment is therefore necessary. The solution adopted is shown in figure 6.7.

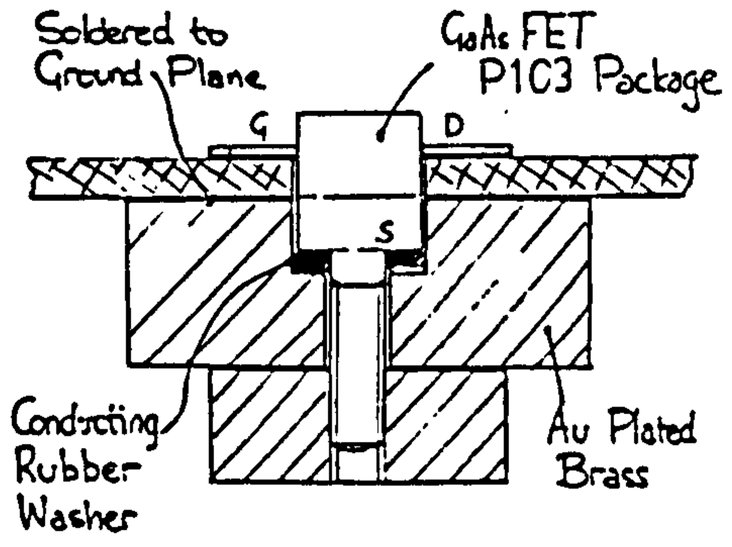

Figure 6.7 The P103 package mount

Using a specially made tool, washers were punched from a sheet of conducting (silver loaded) silicone rubber sheet. One such washer is slipped over the threaded part of the stud and, when the device is inserted in the fixture, is compressed between the shoulder on the stud and a counterbore in a gold flashed brass ring soldered to the ground plane. The soldering process, for which silver loaded solder cream (LMP) with reduced leaching properties is used, is facilitated by use of a stainless steel "dummy" package which aligns and clamps the parts together, while heat is applied from a hot plate.

Avoidance of the use of a carrier plate under the whole area of the substrate obviates the need for matched temperature coefficient of expansion materials and reduces ground plane discontinuities at the transitions.

In use the FET to be measured is inserted into the fixture with the

stud through the conducting rubber washer and a specially made enlarged "nut" is screwed onto the protuding stud. The "nut" is then tightened gradually by hand until the gate and drain tabs register against the microstrip lines. Incidentally, the rubber washer assists in the mounting procedure by resisting the rotation of the device package as the tightening is completed.

Experiments, concerned with clamping the gate and drain tab contacts from above, were conducted. The clamp was constructed from a proprietry radome material; a foam posessing a very low relative dielectric constant (<1.1) and good structural properties.

A FET, previously characterised while retained only by the package stud from the underside, was released with above-substrate clamp in position. The results collected revealed no detectable difference up to 12 GHz. Thus, although the above-substrate dielectric clamp is clearly a useful and successful structure, its application is irrelevant with the package style selected, mounted in the manner originally proposed. Consequently it was not adopted.

6.5 ACCURACY CONSIDERATIONS

Assessment of the accuracy of CCNA's is a complex problem. Assuming that the error model correctly represents the systematic inadequacies of the test set the residual errors depend upon the integrity of the calibration pieces, vector voltmeter inaccuracies (e.g. quadrature error, cf. Section 5.11.2) connector and switch repeatibility, noise and other non-systematic effects. Some workers [14] have estimated the size of each effect and its contribution to the corruption of the results from the CCNA, taking the RMS sum as an indication the likely uncertainty of the measurements. Of course, no single accuracy figure emerges, as the

uncertainty depends on the error model, calibration scheme and connector system in use, as well as on the absolute values of the parameters of the DUT. Meritorious as this approach is, the acid test is the measurement of a range of items which have been independently characterisited using standards laboratory facilities or have parameters that may be accurately computed from their physical properties. This option does not exist when directly calibrating the CCNA to reference plane(s) in microstrip. Hence, it is appropriate to establish the accuracy of those parts of the calibration process that can be quantitatively assessed.

The discussion that follows is concerned with factors not discussed elsewhere that are relevant to the microstrip calibration system proposed in this chapter. Primarily these are associated with the determination of microstrip propagation parameters since the remainder of the calibration process is essentially similar to that for a short and two offset short circuits, the performance of which is adequately attested in Section 5.12.

The two factors that impinge upon the accuracy of the determination of the microstrip parameters from reflection coefficient measurements on 4 open cicuit lines are the numerical precision of the arithmetic and the measurement accuracy of the vector voltmeter part of the system.

6.5.1 Numerical Problem

DASilva [15] encountered problems computing the microstrip parameters, due to the limited word length of the computer that had the effect of restricting the useful bandwidth of calibration. In this work the complex cross-ratio formulation of Section 6.2.1 was applied thus:

$$(\alpha + j\beta) = \pm \{\ln([Z - 2]/2 + /[Z - 2]^2/4 - 1\}/2\Delta l \qquad \langle 6.35 \rangle$$

$$\text{where } Z = \frac{(\Gamma_{m0} - \Gamma_{m2})(\Gamma_{m1} - \Gamma_{m3})}{(\Gamma_{m0} - \Gamma_{m1})(\Gamma_{m2} - \Gamma_{m3})}$$

and Δl is the offset length of the uniformly spaced microstrip open ended lines,

using a standard Fortran complex natural logarithm function. Clearly a numerical risk occurs when any of the factors, $|\Gamma_{mx} - \Gamma_{my}|$ becomes small, representing the difference between two much larger quantities. This situation arises under two conditions:

a) $\Delta l \ll \lambda$ <6.36a>

or

b) $k\Delta l \simeq n\lambda/2$, k=1,2,3; n=1,2,3,4,..... <6.36b)

at the measurement frequency; i.e. whenever the angular separation between any two of the reflection coefficients measurements becomes small, the accuracy of the values of Z and hence ($\alpha + j\beta$) obtained is suspect. The computer word length, for single precision arithmetic is 4 bytes (32 bits) which is equivalent to 6-1/2 decimal digits. As the system is potentially capable of measurement to accuracies of the order of 0.1%, the margin for numerical corruption, though reasonable, is not generous. Incidentally, had the stipulation concerning uniformity of the offset lengths not been made (cf. Section 6.2.1.1 the iterative solution that would have been necessary could aggravate the problem considerably. The test program, primarily designed to test the computational performance of the alogrithm used is described in Section 6.5.3 below.

6.5.2 Measurement Problems

Since the determination of the microstrip propagation parameters is unaffected by the systematic errors of the system except for those associated with the network analyser vector voltmeter itself, it is these that must be investigated. Linearity and IF attenuator accuracy are possible considerations but, in practice, there is one dominant source of error: quadrature error. Quadrature error, that is the dependence of the

amplitude and phase measurements on the value of the phase, and its correction has been discussed in Section 5.11.2.

Naturally, in an automated system the analogue to digital converters contribute errors to the vector voltmeter sub-system. Quantization error, which arises because of the limited number of bits used, can be a consideration but if a minimum of 12-bit conversion is provided the resultant 0.025% resolution is usually adequate. Other imperfections of the A-D converters contribute error effects similar to shortcomings of the vector voltmeter itself that have already received consideration. Non-linearity of the converters will add to the non-linearity of the analogue circuits of the vector voltmeter. Gain mismatch, and lack of tracking, between the converters will aggravate the vector voltmeter accuracy problem.

Particularly sensitive to these inadequacies is the determination of of the microstrip line attenuation constant. Because of the short offset lengths (Δl) of the microstrip lines used in the calibration, the effect of the normally quite low line attenuation on the magnitude of the reflection coefficients is minimal. Since α is crucially dependent on the differences in the magnitudes of the measured reflection coefficients, any of the error mechanisms described above can seriously disturb the result.

Clearly, as the angular displacement of the reflection coefficients is a function of frequency the measurement accuracy is frequency dependent in a similar way to the numerical accuracy of the algorithm discussed previously. From a consideration of the frequency dependence it is possible to deduce the limits on the useful range of calibration. The discussion of the numerical problem indicated that points of risk arise under the conditions of <6.36>. Given that three independent points are required for 1-port calibration the scheme must fail under the

condition:

$$\Delta l << \lambda \quad \underline{\text{or}} \quad \Delta l \simeq n\lambda/4 \qquad \text{<6.37>}$$

since the four measurements will deliver only two sufficiently independent results. Expressing these results in terms of frequency the spectrum is divided thus:

$$f \simeq 0,\ v/6\Delta l,\ v/4\Delta l,\ v/3\Delta l,\ v/2\Delta l,\ nv/6\Delta l,\ ,\ \text{etc.} \qquad \text{<6.38>}$$

where the frequencies in bold type are those where the calibration is bound to fail, the remaining points being those where there is increased risk of numerical errors.

Note that the geometric nature of the progression means that the ratio between adjacent points decreases with increasing frequency. Since it is desirable to calibrate the CCNA over at least one octave the only acceptable region of operation is:

$$0 < f < v/4\Delta l \qquad \text{<6.39>}$$

Since this restriction was assumed when the algortihm was coded into the CCNA program the calibration will in practise fail at all frequencies above this range as the necessary sign changes have not been provisioned.

It still remains to ascertain how far below $f=v/4\Delta l$ the calibration will perform satisfactorily with the known numerical and measurement problems, and what will happen at $f=v/6\Delta l$, the point of numerical risk.

6.5.3 Test Program Simulation

In order to discover how tolerant the calibration process is to the errors discussed above and to determine the useful frequency range of calibration a test program was written. This program is designed to simulate the most critical part of the microstrip calibration process; the determination of the microstrip propagation constants. Given the microstrip parameters, the open end effect and the offset lengths of the calibration set of open circuit lines, the program first computes the

reflection coefficients of these lines, at the common reference plane for a range of frequencies. This data is then applied to the algorithm used in the CCNA software to determine the "measured values" of the propagation constants. The results obtained at each frequency are compared to the given values and the deviations are tabulated. Single precision arithmetic was used and the results indicated that numerical inadequacies do not unduly restrict the useful band of application.

In order to simulate the effect of the measurement errors; quantization and quadrature error, and noise, some perturbation of the reflection coefficient data, derived in the first part of the program, is required. This was simply achieved, in a psuedo-random manner, by truncating both the real and imaginary parts of the four reflection coefficients to a specified number of digits. The numbers are multiplied by the appropriate factor (u), the fractional part is removed and the mantissas are divided by the same factor. The resulting maximum perturbation is one half the reciprocal of the factor. Thus if the original reflection coefficient, $\Gamma = a + jb$ then the modified reflection coefficient is:

$$\Gamma' = (a - 1/2u \pm \{<1/2u\}) + j(b - 1/2u \pm \{<1/2u\}) \qquad <6.41>$$

Two points should be noted. The error is not proportional to the signal magnitude but independent of it as, in fact, is the case for noise and quantization error in the practical vector voltmeter. Secondly, the method of simulating the perturbation introduces a mean magnitude offset of:

$$-1/\sqrt{2}u$$

which is of no consequence since the magitudes of the reflection coefficients are very similar and the algorithm is sensitive to their relative values only.

Some results from the test program and associated documentation is

included in Appendix E. It was found that for a 0.1% measurement accuracy (u = 500) a useful bandwidth of 3:1 can be expected. With a poorly set-up polar display section used as the vector voltmeter, 0.5% errors (u = 100) could arise which would restrict the bandwidth of calibration to an octave. The application of a quadrature error correction scheme should ensure that satisfactory results are obtained over rather more than an octave.

6.5.4 Air-Line Simulation

A practical test of the accuracy to confirm the findings of the test program is desirable. The CCNA software that supports the microstrip calibration scheme includes a facility for tabulating the microstrip propagation parameters. Conducting an effective test with calibration sets of microstrip open-ended lines does present some problems. A series of resonator tests (cf. Chapter 3), ideally using the same piece of substrate material, is necessary in order to determine the propagation constants over the frequency range concerned. Connection repeatibility is inevitably worse for microstrip than for precision coaxial connectors and can confuse the issue.

A simple expedient was to use a set of offset open circuits constructed around the precision APC-7 connector in 7mm air-line. Four alternative centre conductors made from standard precision ground 7mm air-line centre conductor, tapped out one end and finished to a precisely defined length can be fixed, in turn, to the APC-7 connector pin. This arrangement conforms to the requirements set out in Section 6.1.2.1. The outer conductor extends beyond the longest centre conductor, as a circular waveguide below cut-off, sufficient to isolate the open end of the line from external influences.

The offset length, Δl used was 10mm. The expected value of velocity

for the air-line is, of course, 2.998 * 10^8 m/s; the velocity of light in free space. The attenuation constant cannot be precisely defined but is probably of the order of 1 → 2dB/m. This represents a negligible attenuation in a line length of 10mm and the experimental results are thus likely to be extremely sensitive to measurement error. Any value below 5dB/m would be regarded as acceptable. The results are plotted below:

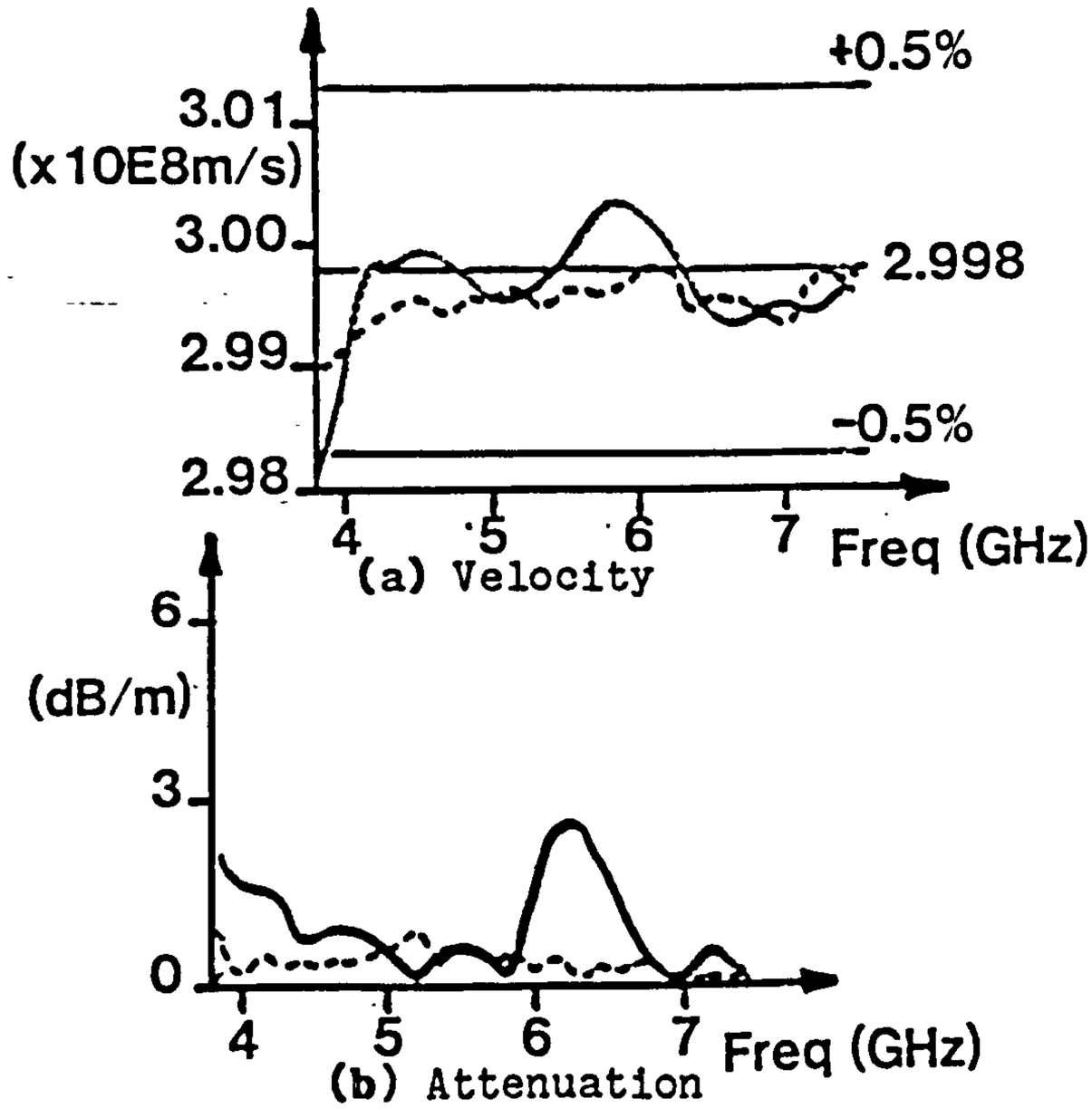

Figure 6.8 Air-line propagation parameters determined by measurements of 4 open circuits (solid line: without quadrature error correction; dashed line: with quadrature error correction)

An examination of the figure reveals that the results are satisfactory without quadrature error correction over an octave band. The upper frequency limit of 7.5 GHz corresponds to the frequency at which the offset length is a quarter wavelength. The lower band edge is defined by the steadily rising errors in the results. With quadrature error correction applied an improvement is evident.

6.6 IMPLEMENTATION AND RESULTS

6.6.1 Software Implementation

The 4 open circuits and optional short circuit calibration scheme described in this chapter was initially implemented by modification of 1- and 2-port network analyser control and correction programs. Figure 6.9(a) is a VDU display typical of the interactive dialogue specifying the calibration condition. The calibration and DUT measurement sequence procedes as shown in figure 6.9(b).

```
THIS CALIBRATION REQUIRES 4 OPENS, AN OPTIONAL SHORT & A THRU LINE
PHYSICAL OFFSET LENGTH OF OPEN CIRCUITS (MM) = 2.64
IS SHORT CIRCUIT TO BE USED ? (TYPE Y OR N)  NO
SPECIFY OPEN CIRCUIT END EFFECT EQUIVALENT CIRCUIT
SHUNT RESISTANCE (KOHMS) = 25.0
SHUNT CAPACITANCE (PF) = 0.78
IS REFERENCE PLANE SHIFTING REQUIRED ? (TYPE Y OR N)  YES
PORT 1 PHYSICAL REF PLANE SHIFT (+VE=EXTENSION) (MM) = 3.55
PORT 2 PHYSICAL REF PLANE SHIFT (+VE=EXTENSION) (MM) = -2.78
THRU LINE LENGTH IS DEFINED AS PHYSICAL LINE LENGTH BETWEEN REF PLANES
AFTER REFERENCE PLANE SHIFTING
LENGTH OF THROUGH LINE (MM) = 2.04
CHARACTERISTIC IMPEDANCE OF LINES (OHMS) = 50.
```

(a) Calibration specification

```
K=1   CONNECT OPEN CIRCUIT ON PORT 1>YES
K=2   CONNECT OFFSET O/C 1 ON PORT 1>YES
K=3   CONNECT OFFSET O/C 2 ON PORT 1>YES
K=4   CONNECT OFFSET O/C 3 ON PORT 1>YES
K=5   CONNECT SHORT CCT ON PORT 1   >YES
K=6   CONNECT OPEN CIRCUIT ON PORT 2>YES
K=7   CONNECT OFFSET O/C 1 ON PORT 2>YES
K=8   CONNECT OFFSET O/C 2 ON PORT 2>YES
K=9   CONNECT OFFSET O/C 3 ON PORT 2>YES
K=10  CONNECT SHORT CCT ON PORT 2   >YES
K=11  CONNECT THROUGH LINE          >YES

NEW DEVICE ? >YES
TYPE DEVICE IDENTIFICATION & TERMINATE WITH CR
THIS IS A DEMONTRATION
K=19  CONNECT DEVICE (AND SWITCH ON)>>YES
```

(b) Calibration and measurement procedure

Figure 6.9 VDU displays associated with the operation of the microstrip calibration scheme

6.6.2 GaAs MESFET Measurements

The primary task conducted using this microstrip calibration scheme was the measurement of the GaAs MESFETs used for the amplifier design work. Ten FETs, from three manufacturing batches, were measured

At 250MHz intervals from 2.0 to 12.0 GHz. Calibration and measurement were conducted in three bands: (i) 2 to 4GHz, (ii) 4 to 8GHz and (iii) 8 to 12GHz. The optional short circuit was employed in the calibration for measurements in band (iii) except for the measurement of s_{22} where the 4 open circuits calibration was used throughout. FET bias conditions were V_{DS} = 5 volts, with a drain current, $I_D = I_{DSS}/2$.

A summary of the results obtained is contained in table 6-3. The average values of each of the eight parameters is given together with the standard deviations for the sample of ten. This data was used for the design of the prototype amplifier of chapter 8.

TABLE 6.3 Mean Values (and Standard Deviations) Measured GaAs MESFET S-parameters

Freq	$\|s_{11}\|$	$\angle s_{11}$	$\|s_{21}\|$	$\angle s_{21}$	$\|s_{12}\|$	$\angle s_{12}$	$\|s_{22}\|$	$\angle s_{22}$
2.0	0.967	- 31.98	2.020	143.9	0.044	64.93	0.800	- 18.22
	(.0043)	(1.12)	(0.105)	(0.68)	(.0018)	(0.70)	(0.017)	(0.66)
3.0	0.922	- 49.57	1.938	126.5	0.062	53.20	0.780	- 29.53
	(.0082)	(1.45)	(0.101)	(1.00)	(.0029)	(0.78)	(0.016)	(1.01)
4.0	0.817	- 65.82	1.870	111.0	0.072	45.21	0.780	- 38.89
	(.0124)	(2.16)	(0.105)	(1.35)	(.0035)	(0.92)	(0.020)	(1.07)
5.0	0.832	- 81.99	1.841	95.7	0.083	38.24	0.764	- 49.17
	(.018)	(2.72)	(0.109)	(1.83)	(.0035)	(1.36)	(0.017)	(1.22)
6.0	0.740	-100.69	1.797	77.8	0.098	26.06	0.679	- 56.83
	(.020)	(4.10)	(0.110)	(2.16)	(.0046)	(1.30)	(0.023)	(1.41)
7.0	0.694	-122.80	1.775	63.4	0.111	16.36	0.657	- 67.06
	(.022)	(4.10)	(0.098)	(2.22)	(.0055)	(1.35)	(0.020)	(1.78)
8.0	0.693	-137.49	1.775	46.8	0.116	10.17	0.665	- 76.79
	(.027)	(5.74)	(0.102)	(2.53)	(.0059)	(2.01)	(0.025)	(2.76)
9.0	0.635	-155.83	1.713	33.4	0.116	6.39	0.658	- 86.73
	(.028)	(6.27)	(0.097)	(2.20)	(.0068)	(4.20)	(0.023)	(3.08)
10.0	0.571	-171.94	1.631	19.8	0.120	- 2.66	0.610	- 91.00
	(.027)	(8.38)	(0.089)	(2.99)	(.0069)	(3.11)	(0.030)	(3.22)
11.0	0.530	166.05	1.624	3.6	0.124	-11.2	0.539	-105.97
	(.025)	(8.42)	(0.093)	(2.25)	(.0069)	(3.99)	(0.035)	(3.80)
12.0	0.522	149.70	1.573	- 12.4	0.125	-12.29	0.511	-119.35
	(.030)	(10.22)	(0.107)	(4.32)	(.0064)	(4.86)	(0.037)	(3.93)

Results for a particular device are presented in figure 6.10 and 11. Both raw measured data and corrected results are displayed. The generally progressive nature of the corrected result traces inspires some confidence in the integrity of the results.

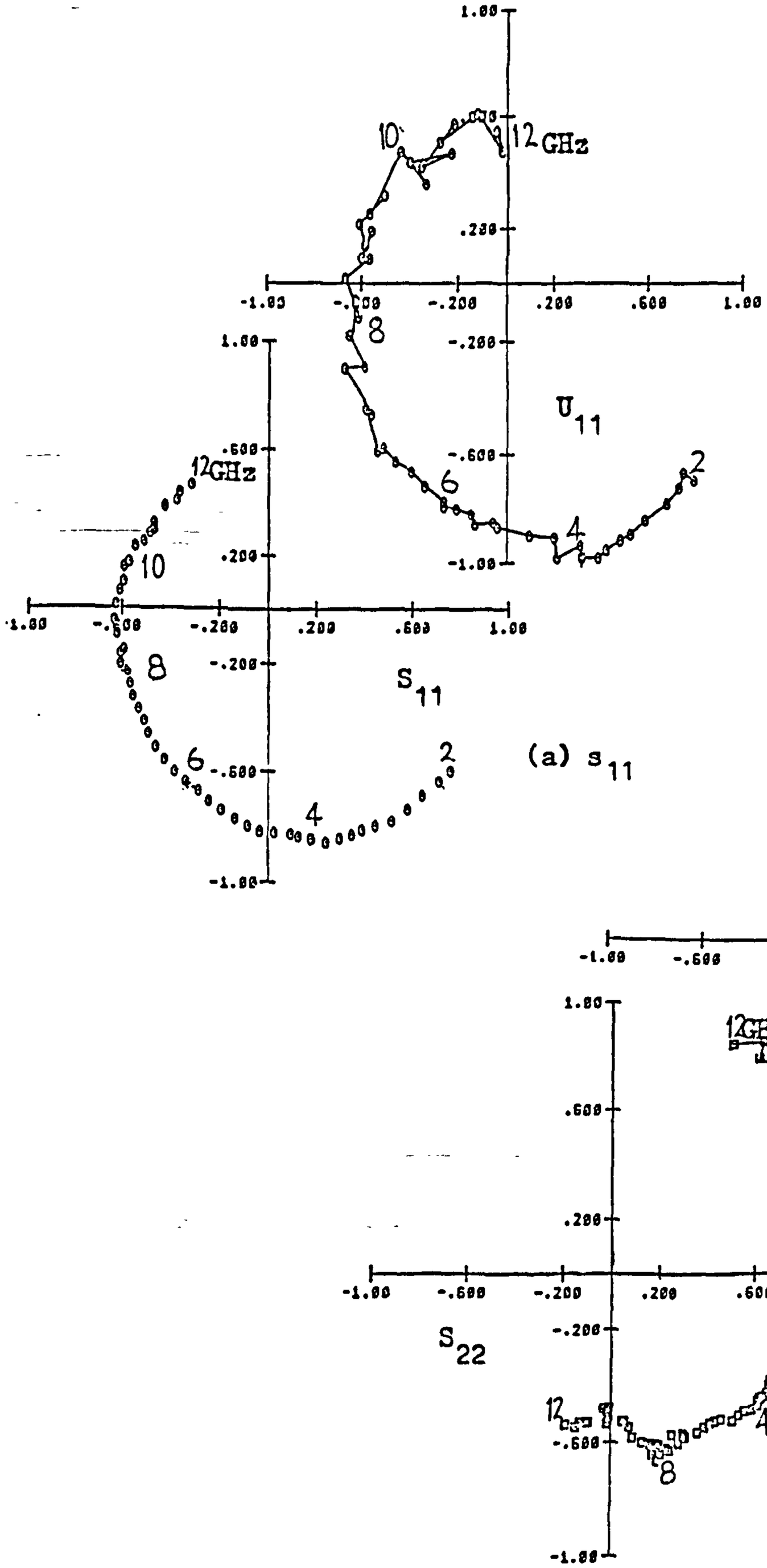

Figure 6.10 Measurements of s_{11} and s_{22} of a GAT4, P103 GaAs MESFET (Bias: V_{DS}=5V, I_D=50mA) [U_{xy}: uncorrected measurements, S_{xy}: corrected results.]

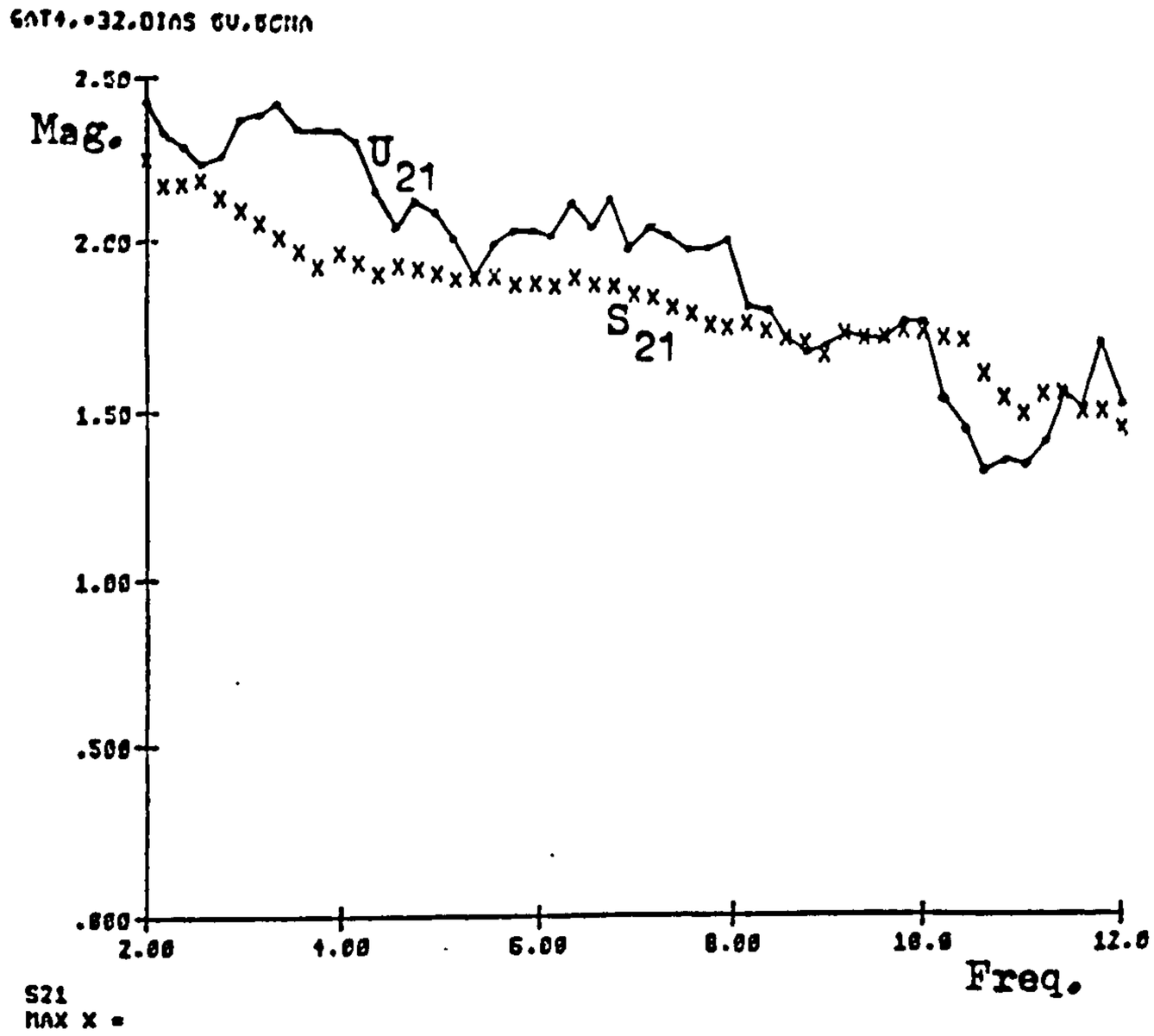

(a) s_{21}

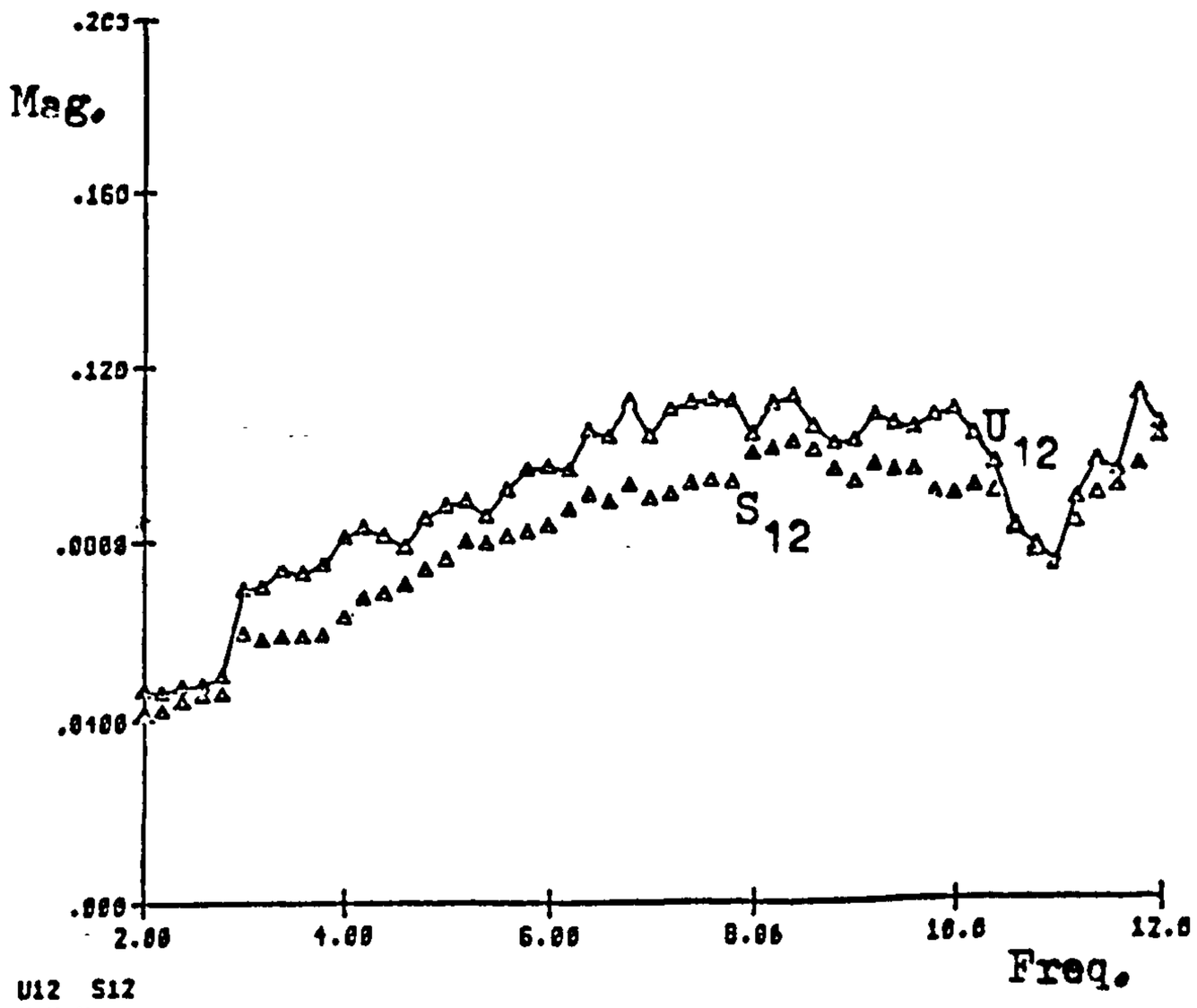

(b) s_{12}

Figure 6.11 Measurement of s_{21} and s_{12} of a GaAs MESFET (see figure 6.10 for details)

6.6.3 Conclusions

The 4 open circuits and optional short circuit calibration scheme has also been used for the measurement of many passive components and microwave circuit structures. Employing 4 short circuit standards in place of the open circuits the technique has also be successfully applied to co-planar waveguide measurement.

Whilst it is impossible to refer to some traceable calibration cross check as a measure of system accuracy the consistency and credibility of the results has been generally satisfactory and encourages confidence in the measurements obtained.

6.7 REFERENCES

[1] REICH, VON VOLKER.: "Microstrip - messungen mit netzwerk - analysator", Nachr Tech. Z., Vol.5, 1971, pp.255-9

[2] SHURMER, H.V.: "Calibration procedure for computer-corrected s-parameter characterisation of devices mounted in microstrip", IEE Electron. Lett., Vol.9, 1973, pp.323-4

[3] DA SILVA, E.F. & McPHUN, M.K.: "Calibration of microwave network analyser for computer-corrected s-parameter measurements", IEE Electron. Lett., Vol.9, 1973, pp.126-8

[4] KWESAH, A.: "Characterisation of integrated bipolar transistors using computer aided measurements and optimization" Ph.D. Thesis, University of Warwick, 1976

[5] HOSSEINI , N.M.: "Application of computer-aided design to microstrip circuits", PH.D. Thesis, University of Warwick, Jul. 1977

[6] AJOSE, S.O., MATTHEWS, N.A. & AITCHISON, C.D.: "Characterisation of coaxial-to-microstrip connector suitable for evaluation of microstrip 2-ports", IEE Electron. Lett., Vol.12

[7] DA SILVA, E.F. & McPHUN, M.K.: "Calibration of an automatic network analyser using transmission lines of unknown characteristic impedance, loss and dispersion", IERE Rad. & Electron. Eng. Vol.48, 1978, pp.227-34

[8] ---------- : "Calibration techniques for one port measurement", Microwave Jnl., June 1978, pp.97-100..

[9] BIANCO, B. & PARODI, M.: " Measurement of the effective relative permittivities of microstrip", IEE Electron. Lett., Vol.11, 1975, pp.71-2

[10] DESCHAMPS, G.A.: "Determination of reflection coefficients and insertion loss of a wave-guide junction", Jnl. Appl. Phys., Vol.24, 1953, pp.1046-50

[11] WATERS, J.D.: "The computer correction of s-parameter measurements using microstrip references for calibration", GEC Hirst Research Centre, Internal Report; TRL/710, FEB, 1978

[12] BIANCO, B., PARODI, M., RIDELLA, S. & SEVAGGI, F.: "Launcher and microstrip calibration", IEEE IH-25, 1976, pp.320-3

[13] HOSSEINI, N.M., "Application of computer aided design to microwave circuits", PH.D. Thesis, University of Warwick, July 1977, pp.81-3

[14] HAND, B.P., "Developing accuracy specifications for automatic network analyser systems", Hewlett Packard Jnl., Vol.21(6), Feb 1970

[15] DA SILVA, E.F., "New calibration techniques for one-port measurements using a computer corrected network analyser", Ph.D. Thesis, University of Warwick, 1978

CHAPTER 7

MICROWAVE BROAD-BAND

AMPLIFIER DESIGN

7. MICROWAVE BROAD-BAND AMPLIFIER DESIGN

7.1 APPLICATIONS OF MICROWAVE AMPLIFIERS

In any electronic system the amplifier is a fundamental building block. At low frequencies it is possible to conceive a "universal" amplifier suitable for a variety of applications. Such is the ubiquitous integrated circuit operational amplifier, the precise characteristics of which can be defined by external feedback and compensation components. At microwave frequencies, however, amplifiers tend to be tailored to the particular application in mind. Amplifiers for receiver applications usually have an emphasis on low noise operation whilst those used in transmitters have output power as the primary specification. Multi-channel communications systems place stringent requirements on linearity of signal path components. Electronic counter measures (ECM) applications demand, however, broad-band operation as a prime requirement. A further area of application that shares this requirement is in the instrumentation that supports these major industries. Optical communications is a growing field where wide-band microwave amplifiers will increasingly find application in modulation sub systems.

7.1.1 General Purpose Microwave Amplifiers

The increasing complexity of all these systems and their associated local oscillator and signal processing sub-systems is generating a great demand for broad-band general purpose microwave amplifiers. Such amplifiers are required to have a flat gain response over a broad frequency band and to perform sufficiently well in other respects to allow their use in a variety of applications. As well as the usual stipulations concerning noise figure, power output, intermodulation

distortion and VSWR's, other criterea, such as unconditional stability reverse isolation, size, manufacturability and cost, are important considerations for these amplifiers. A typical specification might be:-

TABLE 7.1 A TYPICAL GENERAL PURPOSE MICROWAVE AMPLIFIER SPECIFICATION

FREQ. RANGE:	**4.3 - 8.6 GHz**
GAIN:	**~14 dB**
GAIN FLATNESS:	**±1 dB**
INPUT VSWR:	**<2.5:1**
OUTPUT VSWR:	**<3.0:1**
REV. ISOLATION:	**>50 dB**
	(>65 dB at 4.5 GHz)
POWER OUTPUT:	**+11 dBm (+17 dBm)**
NOISE FIGURE:	**<10 dB**

Amplifiers conforming to this specification would be suitable for use as signal distribution amplifiers, isolation buffers, mixer local oscillator drivers and post low noise amplifier gain stages. The specification of Table 7-1 has, however, been formulated with a particular (cf. section 7.3) instrument application in view.

7.1.2 Manufacturing and Cost Considerations

Designing a microwave amplifier for manufacture within a budget is not simply a matter of choosing the cheapest components and using a minimum quantity of them. The use of chip transistors, for example, saves the cost of device packaging but adds the cost of hermetically packaging the complete amplifier. Furthermore, no screening of the microwave parameters of the chip devices is practicable and their subsequent removal from an inadequate amplifier is difficult, probably resulting in the loss of the amplifier with its full complement of components.

The performance of commercially available amplifiers is often adjusted during production, usually by wire bonding between tracks and small adjacent 'lands'. This task involves skilled personnel and an expensive capital equipment and consequently adds considerably to the cost of the finished amplifier. The need for trimming arises from circuit geometry tolerances and component variations, predominantly, transistor parameter spreads. A worthwhile objective for the design of low-cost amplifiers, even if some additional components need be included, is then, the elimination of a production trimming requirement. This can only be achieved by painstaking measurement of statistically significant numbers of devices early in the design process, and using the results in design to cater for the variations wherever possible. This approach may have a significant effect on the form of the amplifier.

The general requirements placed upon such an amplifier are summarised in the table

TABLE 7.2 GENERAL REQUIREMENTS

- LOW COST
- SMALL ACTIVE AREA
- USE PACKAGED DEVICES
- NO DEMANDING GEOMETRIES
- NO CIRCUIT TRIMMING

7.2 AMPLIFIER DESIGN CONSIDERATIONS

7.2.1 Device Properties

In the context of this work three terminal active devices, bipolar or field-effect transistors, are to be considered exclusively. The small-signal properties of such a device can be completely described

by a 3 x 3 scattering matrix (i.e. 3-port s-parameters) by considering the device as a "floating" 3-port as illustrated in figure 7.1 [3]

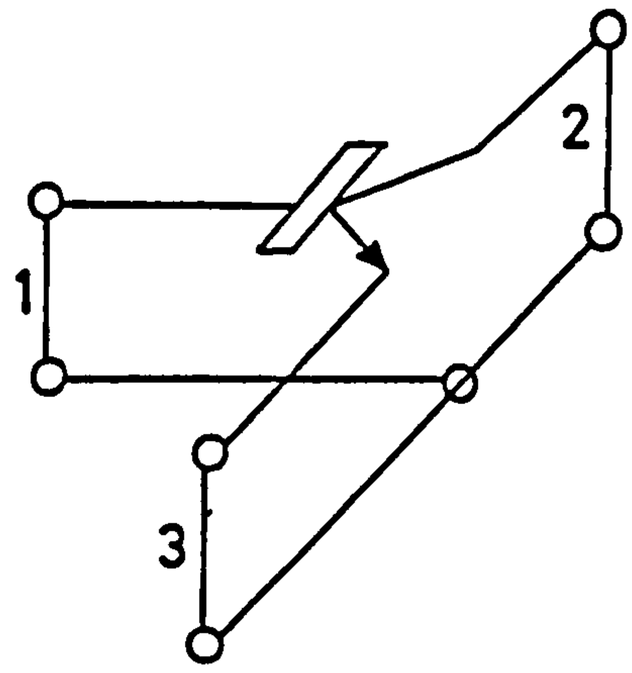

Figure 7.1 The transistor as a 3-Port.

This notion is analogous to that of the indefinite admittance matrix [1] of nodal circuit analysis. The particular configuration of the device in the application circuit can then be established by grounding the common terminal. In scattering terms this implies connecting a short circuit termination to the corresponding port. Given the 3-port s-parameters, the 2-port s-parameters can be derived by application of voltage wave renormalising transforms [4] (Appendix D), setting the appropriate port renormalising factor (reflection coefficient); $\Gamma = -1 + j0$. For the vast majority of microwave amplifiers, the common emitter or common source configurations are to be preferred, especially since almost all packaged devices are constructed for use in these configurations. The relevant transform is stated here: the more general case is dealt with in Appendix D.

$$\begin{bmatrix} s_{11} & s_{12} \\ s_{21} & s_{22} \end{bmatrix} = \frac{1}{1+s_{33}} \begin{bmatrix} s_{11}+\Delta_{33} & s_{12}-\Delta_{21} \\ s_{21}-\Delta_{12} & s_{22}+\Delta_{11} \end{bmatrix} \qquad \langle 7.1 \rangle$$

where Δ_{xy} are the co-factors of the 3-port matrix

viz: $\Delta_{33} = s_{11}s_{22} - s_{12}s_{21}$, $\Delta_{21} = s_{12}s_{33} - s_{13}s_{32}$

$\Delta_{12} = s_{21}s_{33} - s_{13}s_{31}$, $\Delta_{11} = s_{22}s_{33} - s_{23}s_{32}$

It is seldom convenient to measure the 3-port s-parameters of the device and given the almost universal adoption of the common emitter/source

configuration the discussion will proceed assuming the appropriate 2-port description is adequate.

Three definitions of useful gain may be applied to derive values that are, in general, dissimilar.

7.2.1.1 Insertion Power Gain

Insertion power gain is the gain measured when the device is inserted between 50Ohm source and load and consequently is simply:

$$G_I = |s_{21}|^2 \qquad \text{<7.2>}$$

The insertion power gain of a bipolar device would typically fall with increasing frequency, in the microwave region, at a rate of approximately 6dB/Octave whilst FET's have an almost flat response across most of their useful band.

7.2.1.2 Maximum Unilateral Power Gain

If the device is terminated in arbitrary impedances at each port, the power gain that would be obtained is known as the Transducer Power Gain which is defined thus [5]:

$$G_T = \frac{|s_{21}|^2(1 - |r_1|^2)(1 - |r_2|^2)}{|1 - r_1 s_{11} - r_2 s_{22} + r_1 r_2 \Delta|^2} \qquad \text{<7.3>}$$

where $\Delta = \det[S] = s_{11} \cdot s_{22} - s_{21} \cdot s_{12}$

and r_1, r_2 are the reflection coefficients of the port impedances with respect to the s-parameter normalising impedance.

$$\text{i.e. } r_i = (Z_i - Z_o)/(Z_i + Z_o) \; ; \quad i = 1,2 \qquad \text{<7.4>}$$

assuming Z_o is real.

Now if the device is assumed to be unilateral (i.e. $s_{12} = 0$) the transducer power gain can be maximised by letting the terminating reflection coefficients equal the complex conjugate of the corresponding device port reflection coefficient (i.e $r_1 = s_{11}^*$, $r_2 = s_{22}^*$). The maximum unilateral power gain is, therefore:

$$G_{Umax} = |s_{21}|^2/(1 - |s_{11}|^2)(1 - |s_{22}|^2) \qquad \text{<7.6>}$$

This situation may be viewed as terminating the device for maximum power transfer at each port independently, although the actual gain achieved in practice would not equal G_{Umax}. The maximum unilateral power gain is the product of three terms; which allows us to conceptualise the device as a cascade of three 2-ports.

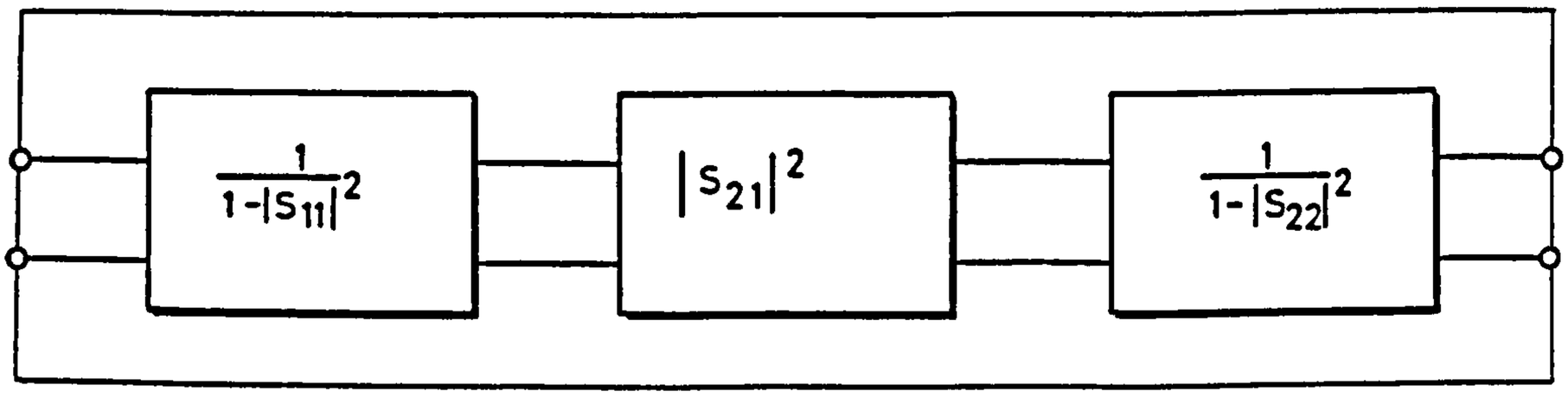

Figure 7.2 Conceptual Gain Breakdown for a Unilateral Device.

This indicates that the power gain is enhanced over the Insertion Power Gain by factors relating to the device port mismatch. These additional terms are in the form of "reflection loss" and so it may be considered that the extra gain results from recovering power previously lost by port mismatch. Both the bipolar and FET devices tend to exhibit a -6dB/Oct maximum unilateral gain slope with frequency, which, for the FET, is primarily attributable to the decreasing mismatch with increasing frequency.

Carson[2] has defined a unilateral figure-of-merit that more adequately describes the degree of unilaterality of device than $|s_{12}|$ alone.

$$U_{fom} = |s_{11}||s_{22}||s_{12}||s_{21}|/(1 - |s_{11}|^2)(1 - |s_{22}|^2) \qquad \langle 7.7 \rangle$$

7.2.1.3 Maximum Available Power Gain

Available (Power) Gain is defined as the ratio between the power available at the output of the device and the power available from the source. The following expression [2] for available gain:

$$G_A = |s_{21}|^2(1 - |r_1|^2)/(|1 - r_1 s_{11}|^2 - |s_{22} - r_1\Delta|^2) \qquad \langle 7.8 \rangle$$

has a maximum value for some source reflection coefficient, r_1. This

corresponds to the condition where the source is conjugately matched to the device . The maximum available gain, G_{Amax} is therefore realised when both the source and the load are simultaneously conjugately matched. To express this statement another way: a source and load reflection coefficients r_{1m} and r_{2m} are chosen such that when the s-parameters are (power wave) renormalised to their corresponding impedances; $s_{11}'=s_{22}'=0$

and $$G_{Amax} = |s_{21}'|^2 \qquad \langle 7.9 \rangle$$

The expression for G_{Amax}, derived [5] using the transforms of Appendix D, is

$$G_{Amax} = \left|K \pm \sqrt{K^2 - 1}\right| . |s_{21}|/|s_{12}| \qquad \langle 7.10 \rangle$$

where K = the stability factor: cf. <7.16>

$$\text{when } r_{im} = (B_i \pm \sqrt{B_i^2 - 4|C_i|^2})C_i^*/2|C_i|^2 \quad \begin{cases} + \text{ if } B_i \text{ -ve} \\ - \text{ if } B_i \text{ +ve} \end{cases} \qquad \langle 7.11 \rangle$$

$$\text{where } B_1 = 1 - |s_{11}|^2 - |s_{22}|^2 - |\Delta|^2 \text{ , } C_1 = s_{11} - \Delta s_{22}^*$$

$$\text{and } B_2 = 1 - |s_{22}|^2 - |s11|^2 - |\Delta|^2 \text{ , } C_2 = s_{22} - \Delta s_{11}^*$$

Figure 7.3 illustrates the gain-frequency behaviour of typical Si bipolar and GaAs FET devices.

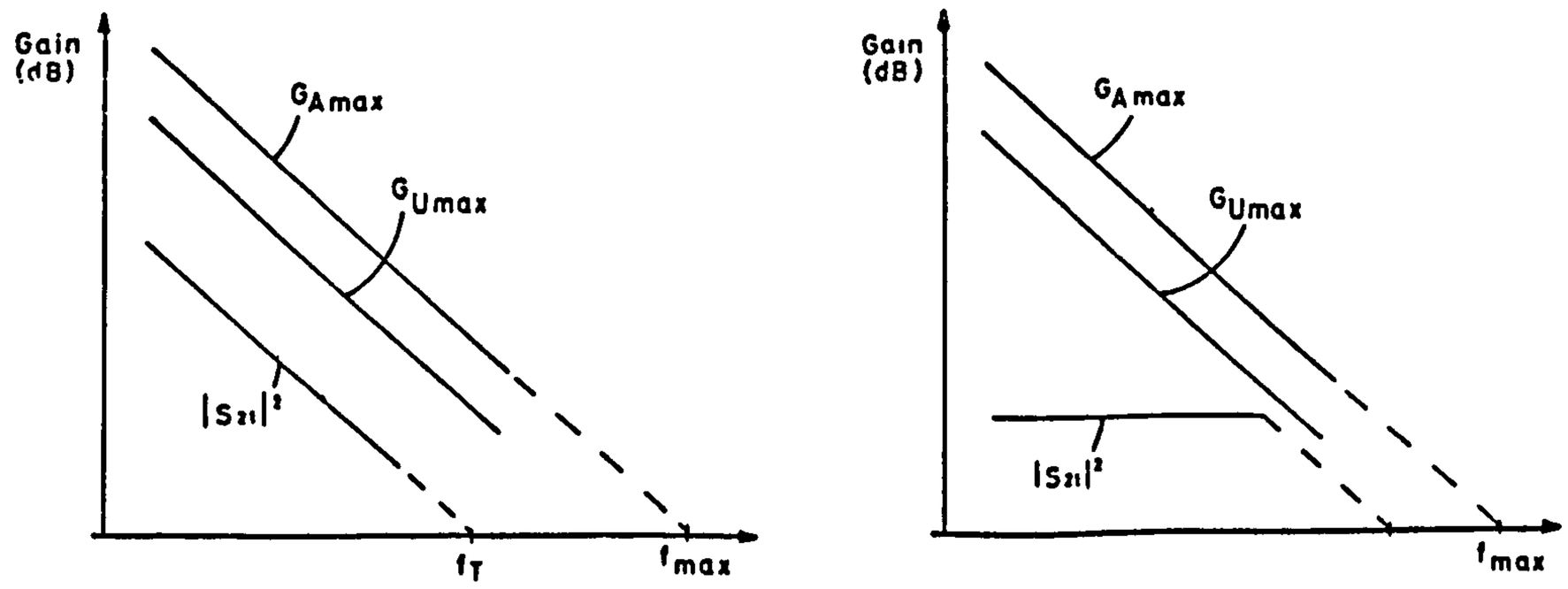

Figure 7.3 Typical device gain plots

The variation of maximum available gain with frequency for a microwave transistor invariably follows a -6dB/Oct (-20dB/decade) law from UHF almost up to the unity gain transition frequency. It is worth noting the maximum available gain transition frequency is the maximum frequency of

oscillation, f_{max}.

The three gains are related to each other, such that:

$$|s_{21}|^2 \leqslant G_{Umax} \leqslant G_{Amax} \qquad \text{<7.12>}$$

The insertion power gain, $|s_{21}|^2$, is equal to G_{Umax} and G_{Amax} when the device is inherently matched, viz:-

$$|s_{21}|^2 = G_{Umax} = G_{Amax} \Big|_{s_{11}=s_{22}=0} \qquad \text{<7.13>}$$

The maximum available gain, G_{Amax}, equals the maximum unilateral power gain, G_{Umax} if the device is totally unilateral, viz.

$$G_{Umax} = G_{Amax} \Big|_{s_{12}=0} \qquad \text{<7.14>}$$

7.2.2 Stability

A device is described as unconditionally stable, at a specified frequency, if it is stable (has no potential for oscillation) for all real source and load impedances. Inevitably few microwave transistors can claim this property over the whole spectrum and therefore the conditions under which stability is impaired must be considered. An unstable device is one that has no regions of stability on the left half of the input or output impedance planes (i.e $|r| < 1$). Fortunately, this property is more rare than the unconditionally stable situation! Over at least part of their useful frequency range most microwave transistors can be described as conditionally stable: they are potentially unstable for certain source and load impedances.

These regions of instability are bounded by circles, when plotted on the input or output coefficient plane. Where a region of instability encroaches within the unit circle the maximum available gain and the simultaneous conjugate match conditions become undefined. Under these conditions it is appropriate to define a maximum stable gain (MSG) such

that:

$$MSG = |s_{21}|/|s_{12}| \qquad \text{<7.15>}$$

A measure of the inherent stability of a device, or indeed any 2-port network, is given by the stability factor, K, which may be determined from the s-parameters, thus:

$$K = (1 - |\Delta|^2 - |s_{11}|^2 - |s_{22}|^2)/2|s_{12}|.|s_{21}| \qquad \text{<7.16>}$$

where $D = \det [S] = s_{11}\, s_{22} - s_{12}\, s_{21}$

For K>1 the device is unconditionally stable. Design using a conditionally stable device (K<1) requires more particular information about the potential instability to be obtained. Plotting of the stability circles on a Smith chart is a useful aid. Figure 7.4 shows plots of the input stability circles for a GaAs FET at three frequencies.

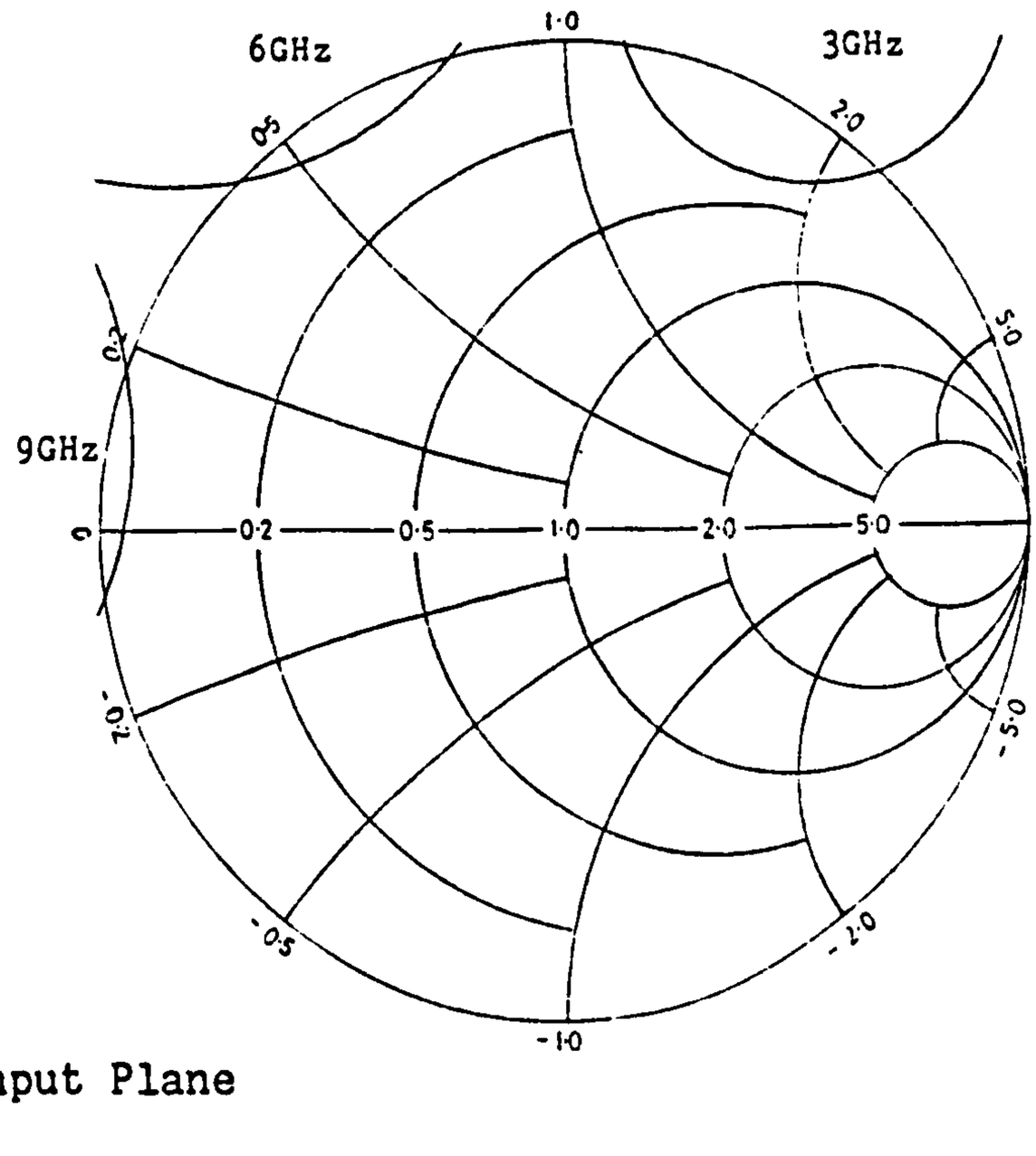

Figure 7.4 Stability Circles for a GaAs FET

(Plessey GAT4, P103 Package)

The circles for the i^{th} port (j = 3-i) are described by the following expressions [5]:

$$\text{Centre: } r_{ci} = (s_{ii} - \Delta s_{jj}^{*})^{*}/(|s_{ii}|^2 - |\Delta|^2) \qquad \langle 7.17 \rangle$$

$$\text{Radius: } R_i = |s_{12}s_{21}/(|s_{22}|^2 - |\Delta|^2)| \qquad \langle 7.18 \rangle$$

In the case illustrated the circle encloses the region of instability. It is possible for the region of stability to be enclosed instead but this situation is not common with common emmitter/source transistor configurations. A test can be applied to determine which situation prevails, thus:

$$\text{If } R_i < |r_{ci}| \text{ (i.e. origin not enclosed)} \qquad \langle 7.19 \rangle$$

then the circle encloses the region of instability

The region of instability on the reflection coefficient plane indicates the termination condition, either at the input or the output of the device, which provides a necessary condition for oscillation. Connecting lossless (reactive) networks to the device ports will move the stability circles but will not improve the value of the stability factor. As it is often desirable to make an amplifier unconditionally stable, it is necessary to devise a method of increasing the stability factor, K, to unity or greater. Furthermore, computer optimisation of amplifier circuits is much more likely to fail if the complete amplifier is only conditionally stable.

Two methods of increasing the stability factor are open to the circuit designer: the inclusion of feedback or the introduction of lossy terminating networks. Negative feedback is usually difficult to apply in a way that does not degrade the stability of the device somewhere in the spectrum. Topological constraints, particularly when packaged devices are used, and parasitic effects associated with the feedback circuit can result in a positive feedback situation. This condition is easily overlooked when it occurs outside the specified operational band of the

amplifier where it is aggravated by ill defined and highly reactive device terminations.

Introducing resistive loss into the matching network, while it does not guarantee unconditional stability at all frequencies, does tend to improve stability across the whole spectrum. At the most elementary level the device can be rendered unconditionally stable by series or shunt connecting a resistor to either or both of its ports. Lossless matching networks can then be designed; treating the device/resistor combination as a composite 2-port. The limiting values for the resistors can be read directly from the Smith chart with the stability circles superimposed. Using an impedance chart the minimum normalised series resistor value is given by the constant resistance circle that is tangential to the stability circle. For example; from figure 7.4 the minimum input series resistor at 6GHz would be 18Ohms. In an similar manner, using an admittance chart, the maximum value of an output shunt resistor can be determined, being in this case: 150Ohms. Clearly for this example, considering the frequency range 3 to 9GHz, the most appropriate choices would be a series resistor at the input or a shunt resistor at the output. Both can be used, the values being determined in the following manner. The input series resistor is set to half the value necessary to stabilise the device and the output stability circles, for this combination of the device and input resistor, is plotted. The new value of the output shunt resistor is then read from the Smith chart as before.

The inclusion of lossy stabilising networks will, naturally, reduce the useful gain of the device. Figure 7.5 is a plot of the maximum available gain of the composite "stabilised device" with the G_{Umax} of the transistor alone shown for reference.

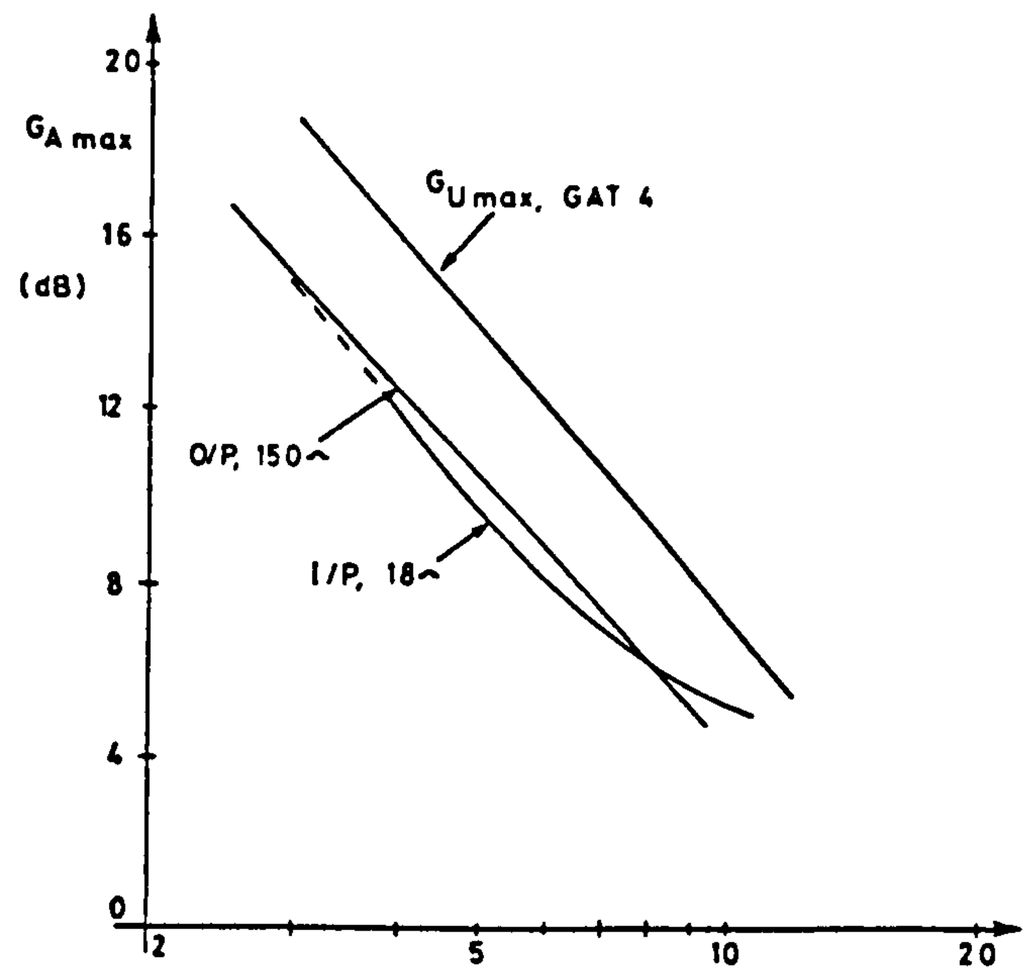

Figure 7.5 The effect of lossly stabilising networks on useful device gain

Ideally stability should be examined across the whole spectrum up to f_{max}. Initial evaluation of K across the microwave band helps focus attention on problem areas. Many instability problems do, however, occur below the microwave band at VHF or UHF. The problem arises because the device, in conjunction with bias decoupling capacitors and connecting lines, forms a Colpitt's oscillator as illustrated in figure 7.6.

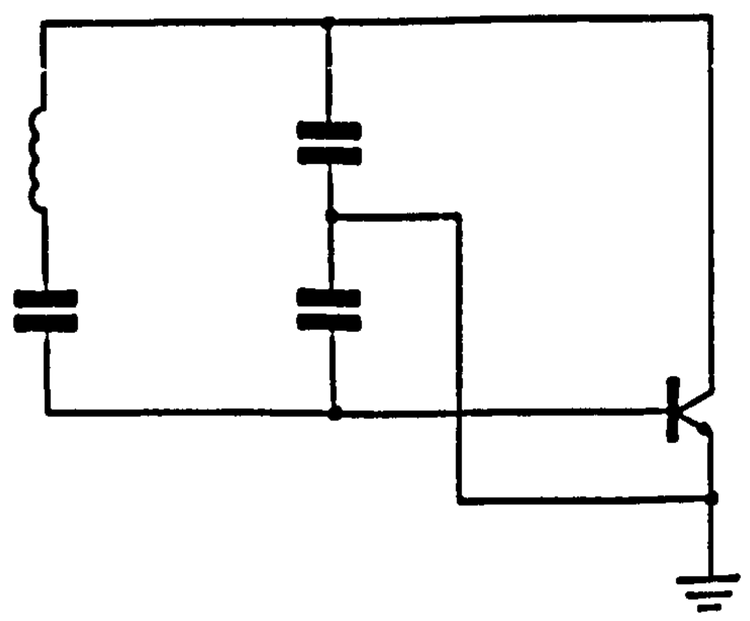

Figure 7.6 The Colpitt's oscillator illustrating the bias decoupling hazard

This phenomenon can be particularly troublesome when bipolar transistors, which characteristically possess a high transconductance (typical g_m=500mS), are involved. A modest amount of series resistance in the bias leads usually reduces the loop gain enough to quench the

oscillation.

Where GaAs FETs (typical $g_m \simeq 30mS$) are concerned it is found adequate to ensure that the gate terminal is shunted to ground by a relatively high value of resistance (> 500ohms) at low frequencies.

7.2.3 Gain Control

For simplicity, it will be assumed that stability considerations do not infringe upon the discussion of amplifier design that follows. In other words; read "device" as "composite device including any stabilising resistors".

The simplest amplifier (figure 7.7), intended for narrow-band operation, would comprise the device and lossless input and output matching networks.

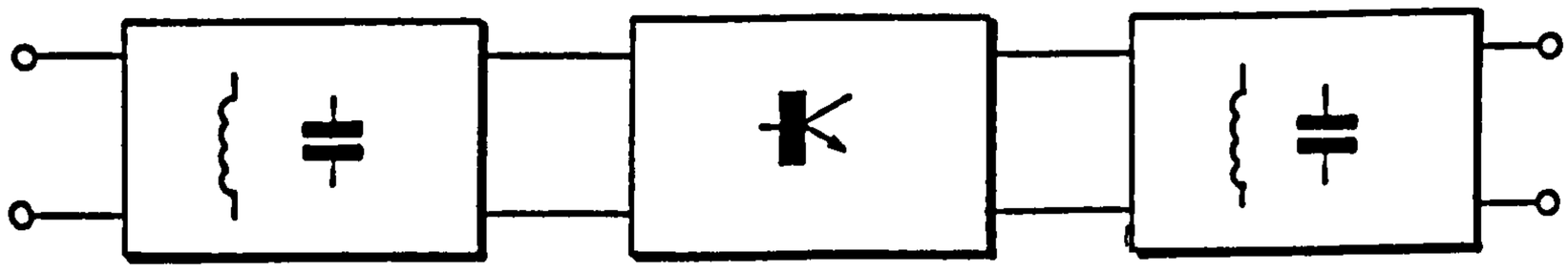

Figure 7.7 Elementary single stage amplifier

Designed at a single frequency, the input and output reactive networks provide simultaneous conjugate match conditions (r_{1m} and r_{2m}, respectively) to the device ports. Alternatively, and equivalently, the input and output network transform the matched device impedances ($s_{11}=r_{1m}^*$ and $s_{22}=r_{2m}^*$, respectively) to the external characteristic impedance (Z_o = 500hms). Neglecting circuit losses, the resultant amplifier would have gain, at the defined frequency, equal to the maximum available gain of the device and would be perfectly matched.

If the device were assumed unilateral and the networks designed to terminate each port independently in its conjugate impedance ($r_1=s_{11}^*$ and $r_2=s_{22}^*$) there would be some uncertainty about the amplifier gain. The

gain would not be equal to the maximum unilateral gain of the device for no device is, in practice, completely unilateral. The deviation of the amplifier gain from G_{Umax} may be termed the unilateralisation error, U_e, for which it is possible to compute upper and lower bounds, [2] thus:

$$(1 + U_{fom})^{-1} < U_e < (1 - U_{fom})^{-1} \qquad \langle 7.20 \rangle$$

where U_{fom}, the unilateral figure-of-merit for the device is defined by equation <7.7>.

Since the gain of this amplifier falls short of the G_{Amax} of the device and the matching networks are lossless, the amplifier must be mismatched at its terminals.

Mismatch does, however, facilitate control of the amplifier gain. Negative feedback is seldom used to control the gain, both because of the limited gain of the device at microwave frequencies and of the effect on device stability already discussed. Given the frequency dependence of the device gain it is particularly important to be able to regulate the gain when broad-band amplification is required. Frequency dependent mismatching, where the surplus signal power is reflected, is commonly applied to achieve a flat gain response over an octave or more. Such a single-stage reactively-compensated amplifier would consequently have progressively deteriorating VSWRs at its external ports as the frequency is decreased.

For design purposes, the relationship between the source and load reflection coefficients and the gain needs to be quantified. Constant Gain circles are a powerful graphical aid in this context. Conventionally, the constant gain circles which are plotted on the input and output reflection coefficient planes, are defined for condition where the opposite port is terminated as for the simultaneous conjugate match conditions (e.g. $\Gamma_L = r_{m2}$ for gain circles on the input plane). As the gain circles decrease in radius they converge on the point corresponding

to the simultaneous conjugate match condition at the port concerned. Each constant gain circle is the locus of reflection coefficients that will result in the specified gain. Figure 7.8 shows the constant gain contours for a resistor stabilised GaAs FET.

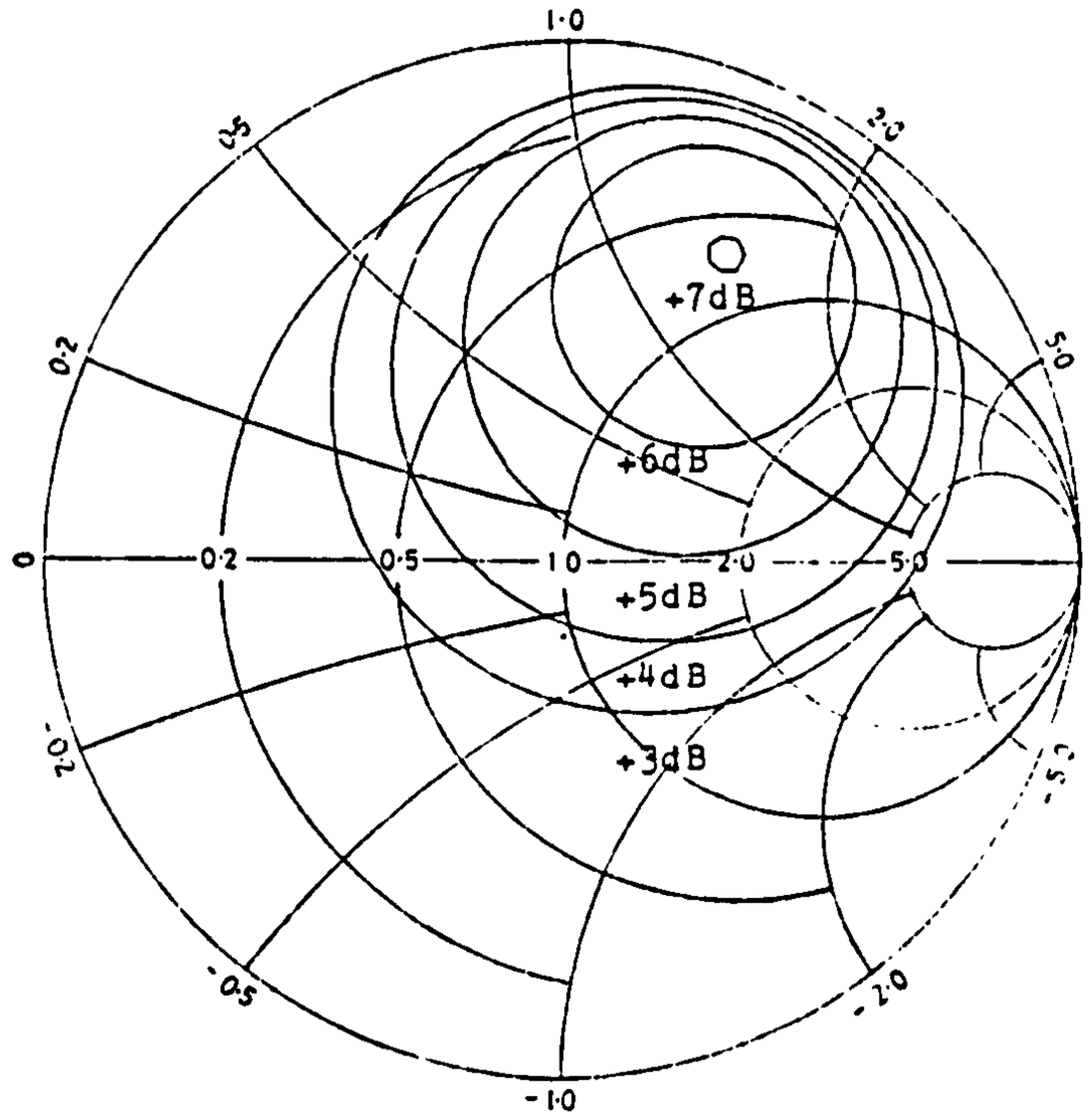

(a) Output Plane (Impedance Co-ordinates)

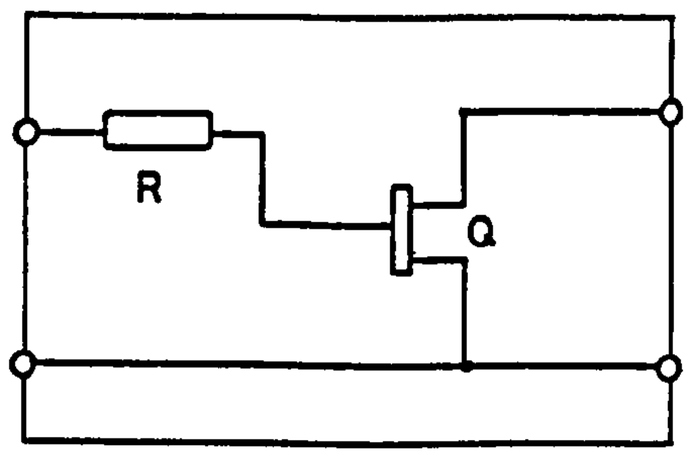

R = 18Ohm

Q = Plessey GAT4,P103

(Max. gain bias)

(c) Composite Device

Figure 7.8 Constant gain circles for the composite device.

The constant gain circles for the i^{th} port are described by the following expressions:

$$\text{Centre: } r_{ci} = \sqrt{1 - 2K|s_{12}s_{21}|g_i + |s_{12}s_{21}|^2 g_i^2}/(1+D_i g_i) \qquad \langle 7.21 \rangle$$

$$\text{Radius: } R_i = g_i C_i^*/(1 + D_i g_i) \qquad \langle 7.22 \rangle$$

where $D_i = |s_{ii}|^2 - |\Delta|^2$, $C_i = s_{ii} - \Delta s_{jj}^*$, $j=3-i$

and $g_i = G/|s_{21}|^2$; the normalised gain

$= 1 - |r_i|^2)/[(1-|s_{jj}|^2) + |r_i|^2(|s_{ii}|^2-|\Delta|^2) - 2R(r_i C_i)]$

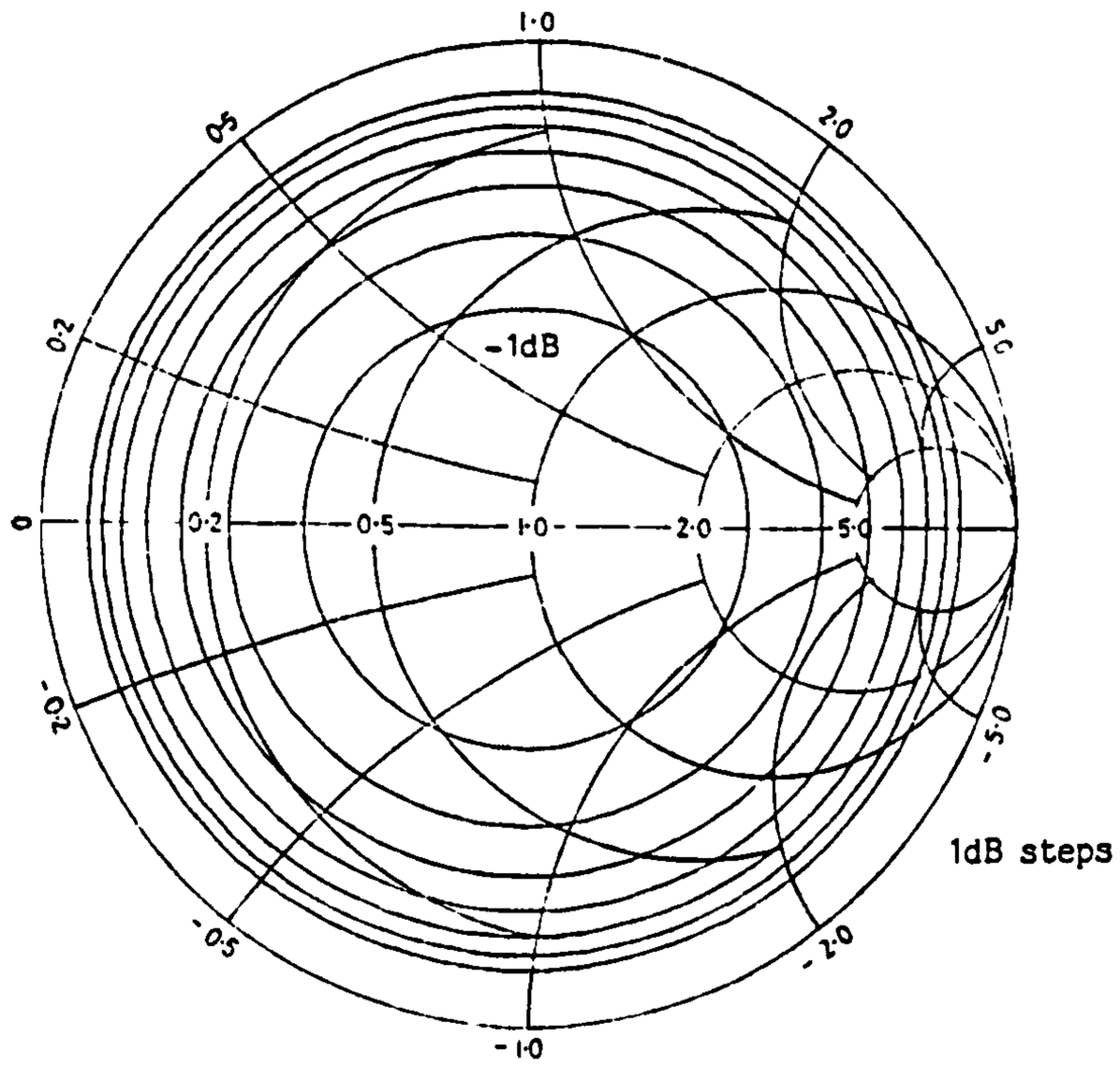

Figure 7.9 Reflection loss circles (normalised constant gain circles)

Constant gain circles can be more generally applied to any interface. If the reflection coefficients are (power wave) renormalised (cf. Appendix D) to the impedance on one side of the interface, a universal set of constant gain contours can be applied. These contours are concentric circles having their centre coincident with the centre of the reflection coefficient plane. They are therefore, constant VSWR circles, yet anotated in terms of lost gain. The lost gain is, of course, the conventional reflection loss associated with power

transmission through mismatched interfaces. Figure 7.9 is a Smith chart with the reflection loss circles over-printed. These contours are related to those of figure 7.8 by a bi-linear transform that can be associated with properties of the networks that would realise the simultaneous conjugate match conditions.

$$\Gamma_2 = (s_{11} - \Delta\Gamma_1)/(1 - s_{22}\Gamma_1) \qquad \text{<7.23>}$$

where [S] is the s-parameter matrix of the matching network and

$s_{11} = r_{mi}$

7.3 AMPLIFIER STRUCTURE

Prior to embarking upon the circuit design of the amplifier, its structure must be defined.

7.3.1 Single Ended Amplifiers

As previously discussed a single-stage single-ended reactively compensated amplifier that has a significant bandwidth will, necessarily exhibit a frequency dependent mismatch at either or both ports. Figure 7.10 is a graph of the relationship of VSWR to reflection loss described by the expression:

$$VSWR = (1 + \sqrt{1 - 10^{L/10}})/(1 - \sqrt{1 - 10^{L/10}}) \qquad \text{<7.24>}$$

where L is the reflection loss in dB

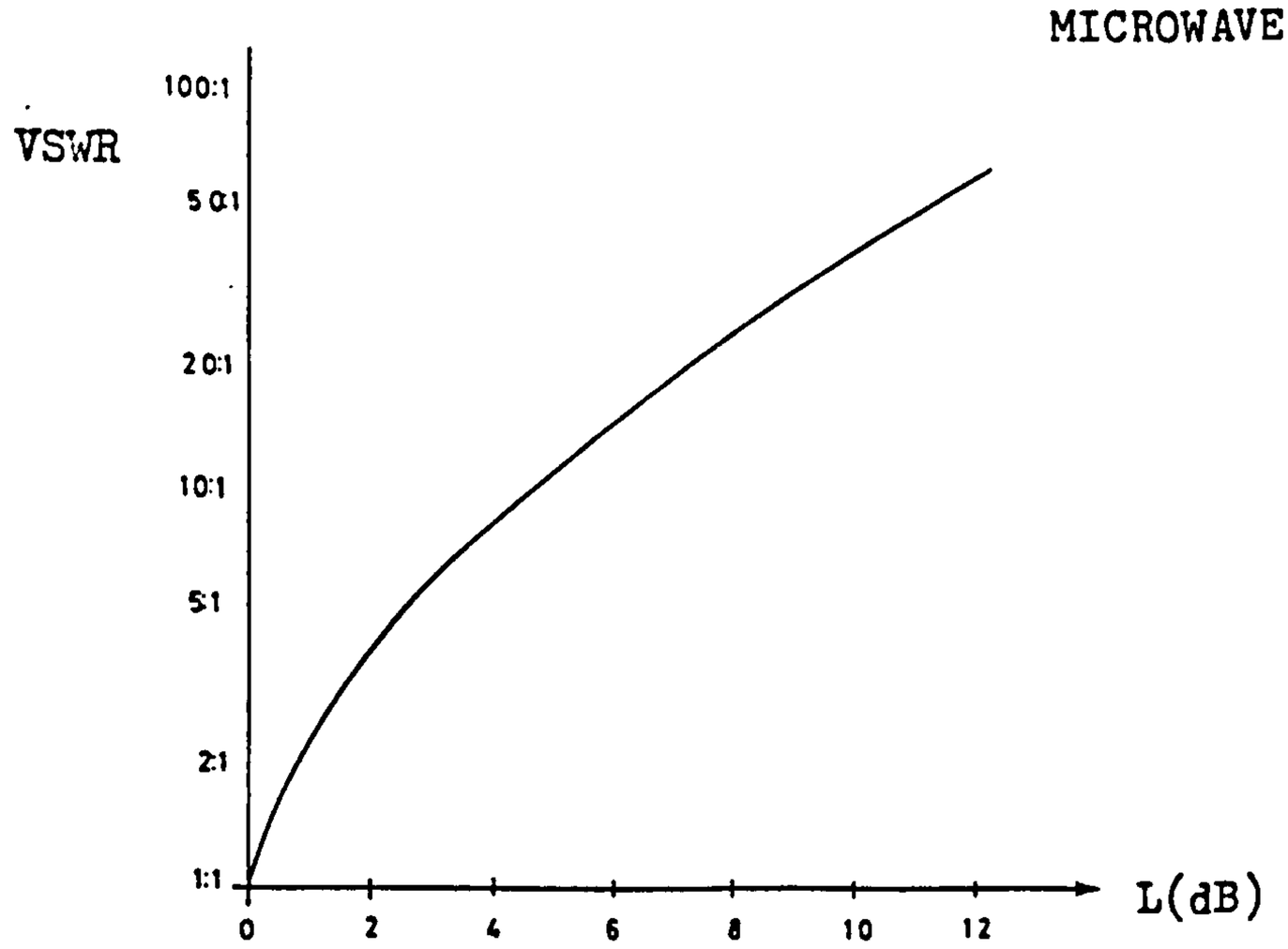

Figure 7.10 Relationship between port VSWR and Reflection Loss(L)

The gain of the amplifier would approach the maximum available gain of the device at the upper frequency and, if the gain compensation was divided equally between the two ports, the curves of figure 7.11 would typically approximate the amplifiers performance:

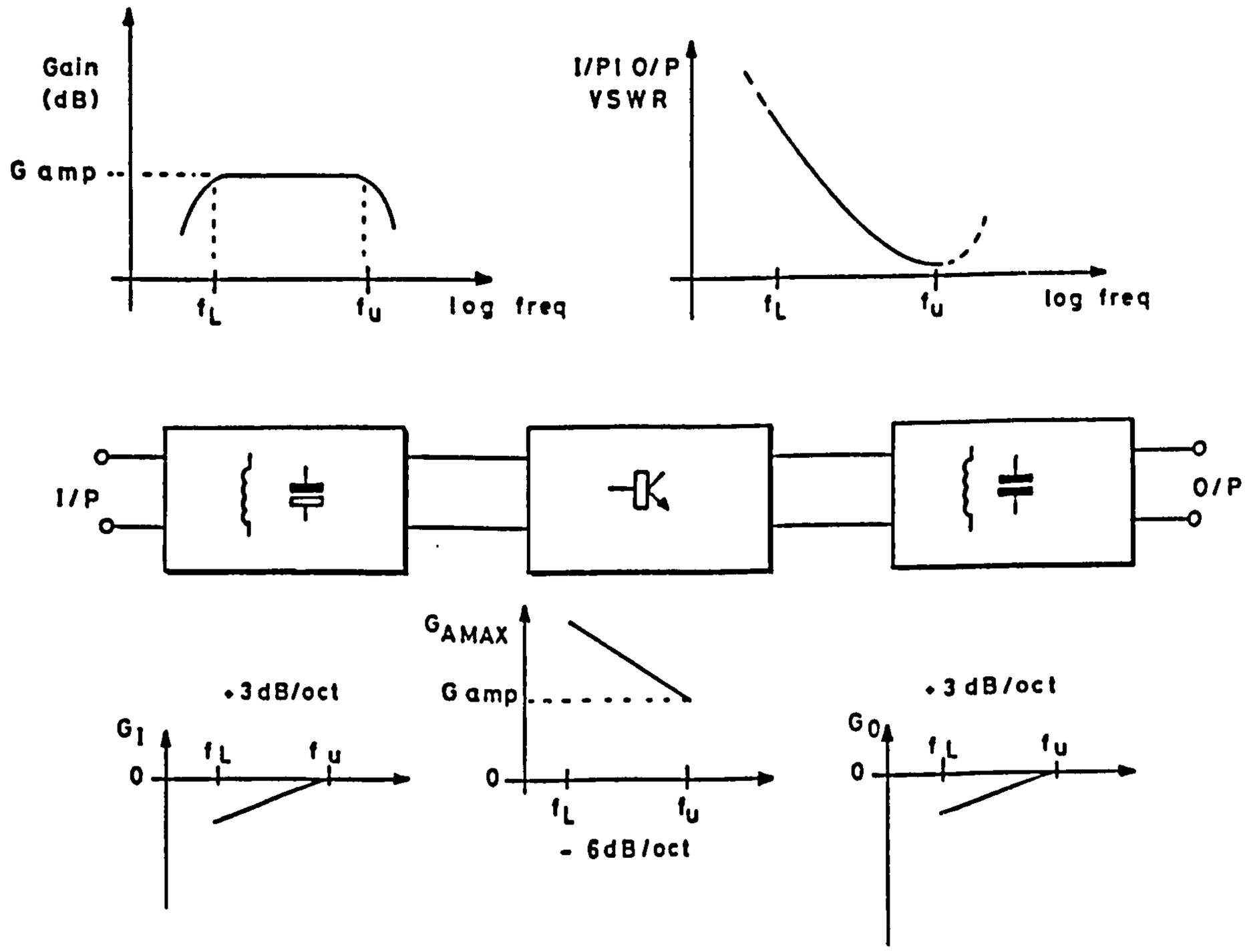

Figure 7.11 Typical structure and characteristics of a single-stage amplifier

When gain slope compensation is divided between input and output networks, the non-unilateral behaviour of the transistor adds a

complicating factor to the design process. The initial design of the network based on the constant gain circles, plotted at several points across the band, is done with the assumption that the opposite port remains matched. Since this is not the case there exists an interaction between the compensation circuits at each port. The effect on the design accuracy can be mitigated by designing the compensation networks sequentially; designing the second network against gain circles plotted for the device with the first network attached. Ultimately the only practical way to achieve the specifications is to apply computer optimization to the final circuit.

Because of the inevitable deterioration of the port matches as the frequency decreases, the single-stage single-ended reactively compensated amplifier is unattractive, where a relative bandwidth in excess of ~5% is required. One solution to this problem is to cascade two or more active devices so that the gain compensation can be confined to interstage networks thus allowing the input and output networks to be designed exclusively for the purpose of matching.

An architypal two-stage single-ended amplifier is illustrated in figure 7.12.

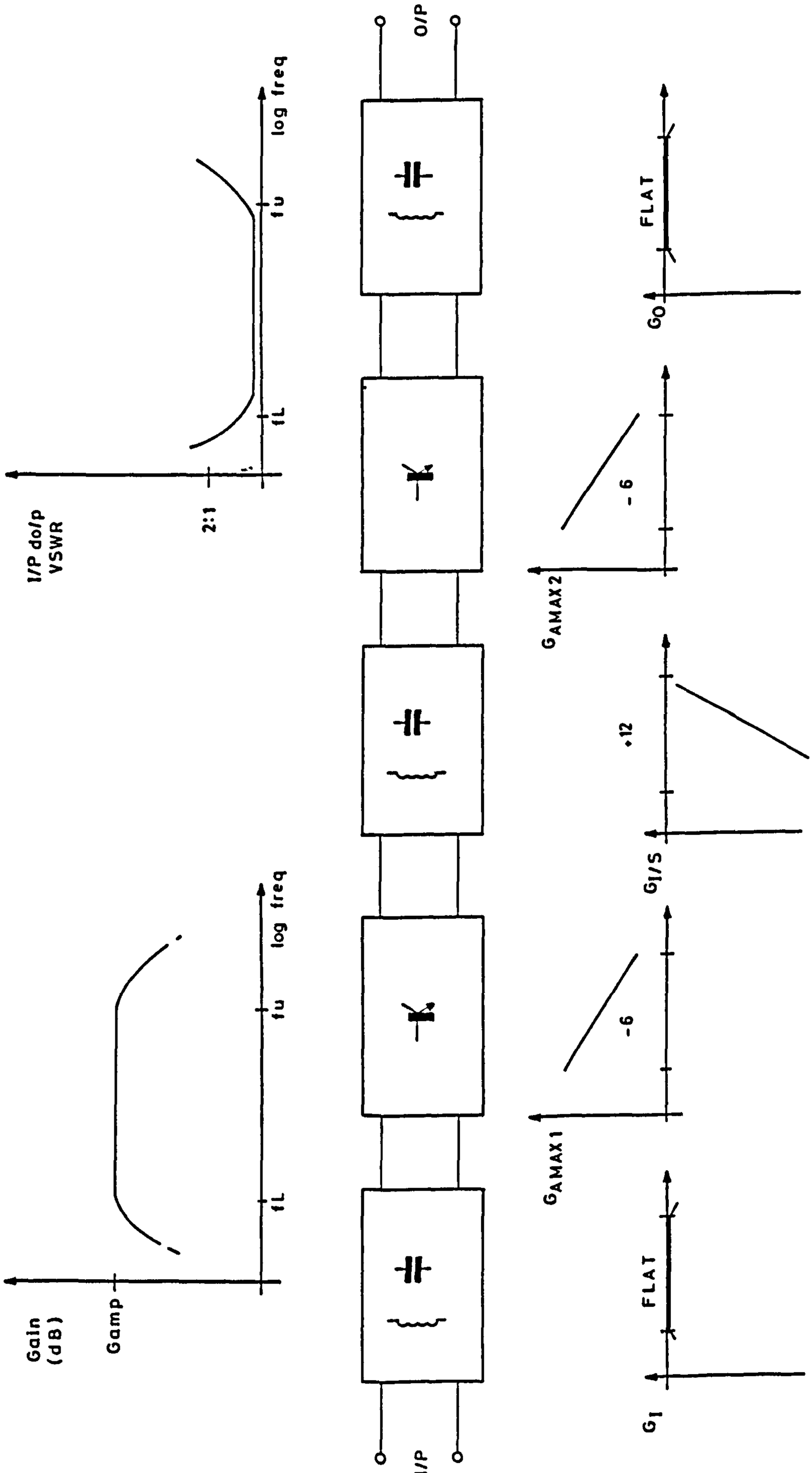

Figure 7.12 Typical single-ended two-stage reactively compensated amplifier

The penalty paid for the improved broad-band input and output match is that the interstage network, which must compensate the combined gain of the two transistors, must now provide 12dB/Oct gain slope by mismatching the interface between the devices. At the lower band edge of an octave band amplifier this corresponds to a 60:1 VSWR! Clearly the interaction between the networks through the non-unilateral devices is even more detrimental to design accuracy than for the single-stage configuration.

A useful design aid, when used in conjunction with constant gain circles, has been developed by Dawe [6]. "Dawe" circles are circles of opposite port constant VSWR: i.e. circles of constant input VSWR plotted on the output plane of the first device. The fact that they are circles is easily established. The contours of constant VSWR (constant ρ) at any reference plane are (concentric) circles. Refering them to some other plane through a 2-port is equivalent to applying bilinear transformation (as <7.23>). It is well known that, under bilinear transformation, circles map to circles. The "Dawe" circles of constant opposite port VSWR plotted on the i^{th} port plane are then described by the following equations:

$$\text{Centre: } r_{ci} = (\rho^2 s_{jj} - \Delta s_{ii}^{*})^{*} / (\rho^2 |s_{jj}|^2 - |\Delta|^2) \qquad \text{<7.25a>}$$

$$\text{Radius: } R_i = (\rho |s_{12}| . |s_{21}|) / (\rho^2 |s_{jj}|^2 - |\Delta|^2) \qquad \text{<7.25b>}$$

where the VSWR $= (1 + \rho)/(1 - \rho)$

and $\rho = |\Gamma|$, also $j = 3 - i$

In application, the "Dawe" circles, as well as the gain circles, for the transistor together with the input or output matching network, are plotted at the planes of the connection to the interstage network. Figure 7.13 illustrates an example for the output plane of the first device at a single frequency. From these mappings it is possible to choose its load impedance, not only fulfill the gain requirement but also

to cause the minimum degradation of the input match.

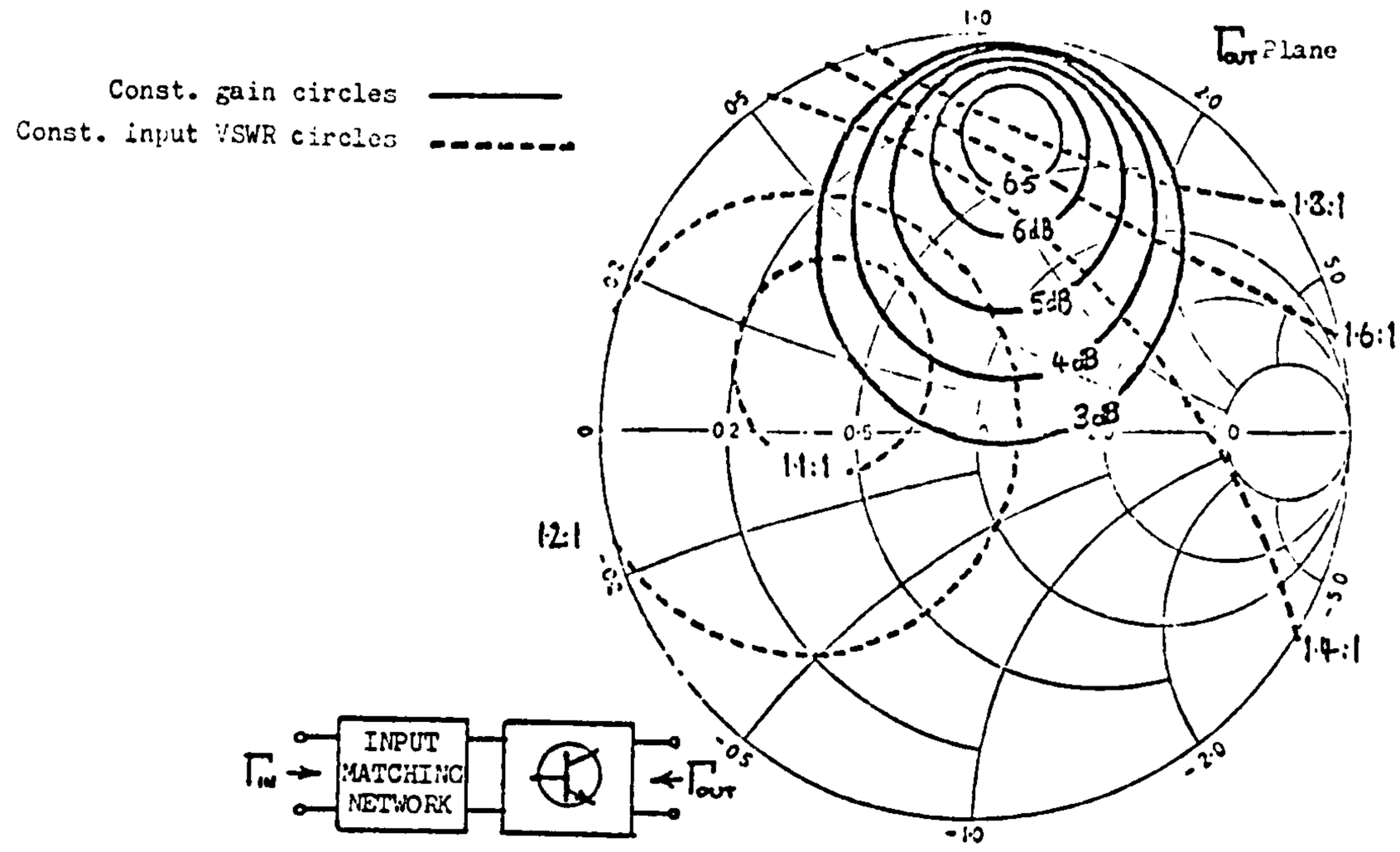

Figure 7.13 Circles of Constant Gain and Constant Input VSWR.

For the design of an interstage network, having the most suitable locus to simultaneously meet the gain and VSWR requirements of a broad-band amplifier, sets of circles at a minimum of three frequencies would be necessary. The reactive interstage network would be designed to provide the appropriate load impedance versus frequency contour, when terminated in the second device together with the output matching network. Having applied this technique, the designer can have confidence that only relatively minor charges to the input and output matching networks will be necessary to yield an amplifier design capable of achieving the specification. Consequently, the final process of computer optimization [13,14] although still necessary, is eased because of the accuracy of the initial design.

Although the two-stage single-ended amplifier configuration permits the design of broad-band flat, matched amplifiers, the interaction between match and frequency response dogs the design process. The high internal VSWRs aggravate loss mechanisms and sensitivity to circuit tolerances, and distorts the group delay response.

7.3.2 Balanced Amplifiers

Originally proposed by Engelbrecht [7], the balanced amplifier, comprising two identical single-ended amplifiers set between 90 degree, 3dB hybrids, releases the amplifier designer from the burden of simultaneously achieving port matches and a flat gain response. In order to appreciate the raison d'etre of this amplifier configuration, illustrated in figure 7.14, it is necessary to consider the properties of the hybrid.

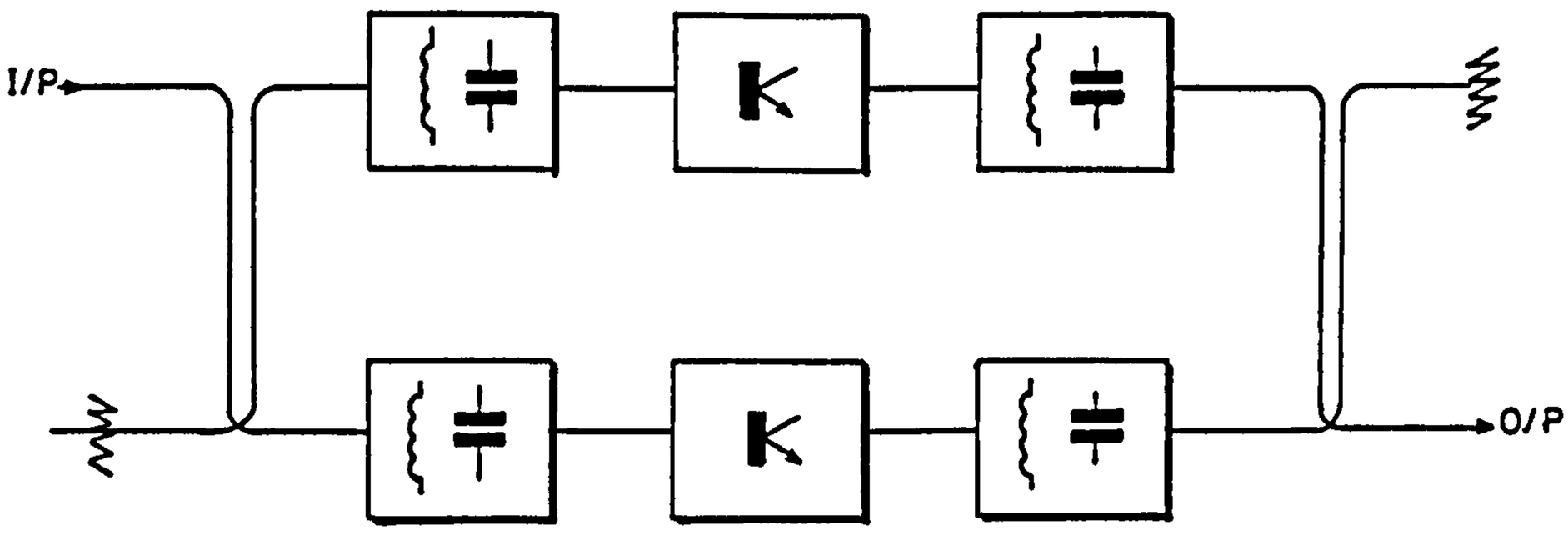

Figure 7.14 A Balanced Amplifier Stage

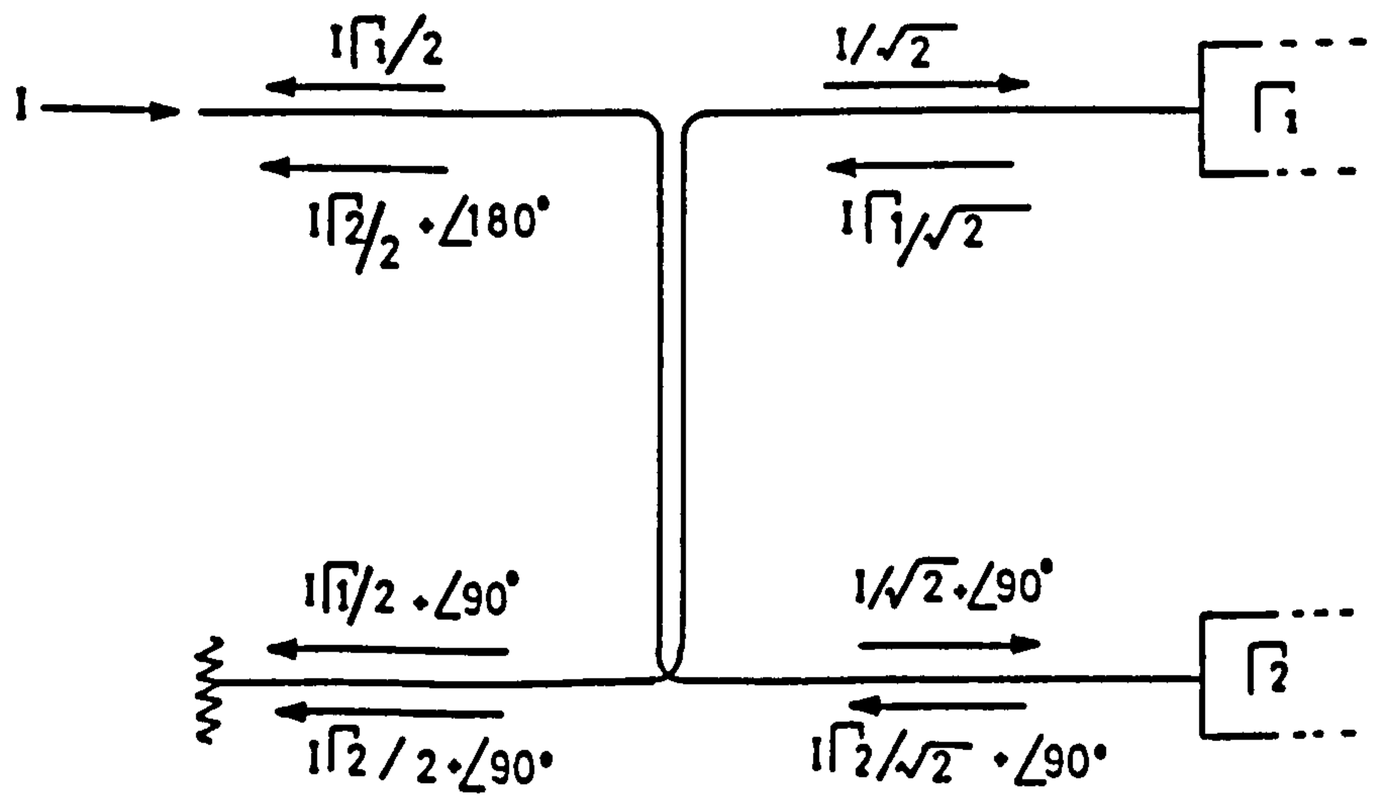

Figure 7.15 The 90 degree, 3dB Hybrid

From figure 7.15 it is apparent that, if the reflection coefficients are equal in both magnitude and phase, no signal is reflected at the driven port; the returned power being dissipated in the load termination. Thus, provided that the characteristics of the amplifiers

included between such hybrids are similar, a gain block having the same gain response as either single-ended amplifier but a good match substantially independant of their port impedances, is practicable. An additional bandwidth limiting factor is, however, introduced by the adoption of hybrids which possess sufficiently ideal properties typically over no more than an octave.

In principle, a pair of multi-stage amplifiers may be included between two hybrids, but this is not favoured because of the increased difficulty in ensuring adequate similarity in the characteristics of the amplifiers. It is, however, very attractive to employ the balanced amplifier approach using single-stage amplifiers to produce gain modules which, due to the excellent match ensured by the hybrids, can be cascaded with impunity. The design process is greatly simplified since the interactions between matching and gain compensation, and between stages have been eliminated.

The penalty paid for these benefits is not, however, insignificant. More components, notably the active devices, with their associated bias circuits are introduced. The circuit area is increased to include both the additional amplifier modules and the two hybrids for each stage. Because of the introduction of the coupled line structures the circuit geometries tend to become more demanding. The increased size of the enclosure militates against the achievement of high reverse isolation due to reduced "waveguide" attenuation. Furthermore, it is often found necessary to indulge in circuit trimming, in order to obtain close tracking between amplifiers, and thus the good input/output matches desirable for the cascading of stages.

Nevertheless, the design advantages cited above, the versatility permitted by the modular approach and performance advantages when low-noise or high-power operation are sought have made the balanced

amplifier the most popular structure in commercial microwave amplifier manufacture [8].

7.3.3 Output Power Considerations

Clearly, the primary factor in determining the output power capability of an amplifier is the choice of active device(s) employed in the final stage. The price of microwave transistors, particularly GaAs FETs, rises disproportionately with power specification and so it behoves the cost conscious designer to exploit the full potential of any suitable device. A further incentive to use a lower power device whenever possible is that the increased gate width of the higher power device reduces its potential matching gain-bandwidth.

Two additional factors must therefore receive consideration: the load impedance presented to the active device and the structure of the amplifier in which it is employed. The latter is of particular significance in broad-band amplifier design. The former, although outside the scope of this work, will be considered in as much as it effects the structure of the amplifier.

7.3.3.1 Load Impedance

In essence the power output of a microwave transistor operating in Class A is limited, like its low frequency counterpart by two constraints: the total power dissipation permitted in the mounted device and the current and voltage swing capability of the circuit. The temperature rise due to the power dissipation can be controlled by reduction of the thermal resistance of the mounting structure but is ultimately limited by the thermal resistance of the chip itself. For a typical 100mW GaAs FET, it is the current and voltage swing restrictions that dominate. In such a case, neglecting high frequency reactive effects, the optimum load resistance would be that for which current

swing and voltage swing limitations were reached simultaneously. Figure 7.16 illustrates this idealistic situation for a GaAs FET having a drain bias of 7V and I_{DSS} of 70mA.

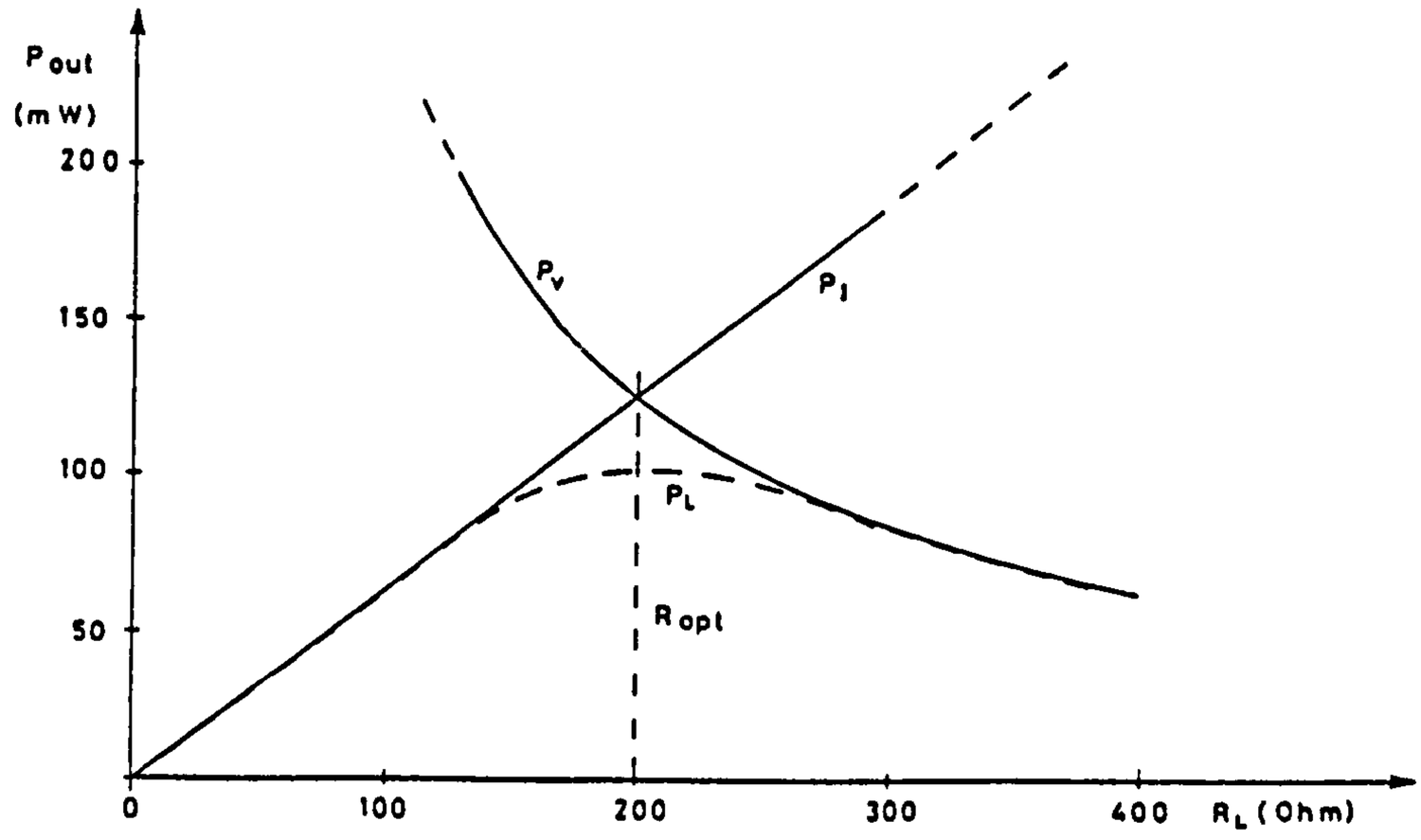

Figure 7.16 Determination of the optimum resistive load under ideal conditions.

This typical example indicates that an optimum load of 200Ohms would yield a "hard" limited output power of a little over 100mW. Since, however, the real situation is considerably more complex at microwave frequencies this simplistic approach is no more than a general indication of potential power output capability.

An output network designed for a small-signal conjugate match will, in general, present to the device a load impedance rather different from the optimum for large signal operation. It is, therefore, highly desirable that some additional characterisation of the device operating under large signal conditions be made.

Prior to considering the possible measurement techinques it is necessary to define a measure of the degree of non-linearity of the device. One possibility is the third-order intermodulation distortion

[12] but its measurement is rather complex. A more convenient measure for these purposes is "gain compression". As the signal power into a device, alone or within an amplifier, is raised so that saturation is approached, the gain appears to fall. As a result of the non-linearity a significant proportion of the signal energy is transferred to harmonics of the signal frequency. Thus, when making a measurement of gain compression, precautions, to avoid the harmonics degrading the power detection accuracy, should be taken. Commonly the value of gain compression is set at 1dB and the output power that results in this reduction from the small-signal gain is referred to as the 1dB compression point. Figure 7.17 illustrates a typical "power bench" test system. The compression point is determined by adjusting the input power until the desired reduction in the power meter reading occurs when the 20dB attenuation is moved from before to after the DUT.

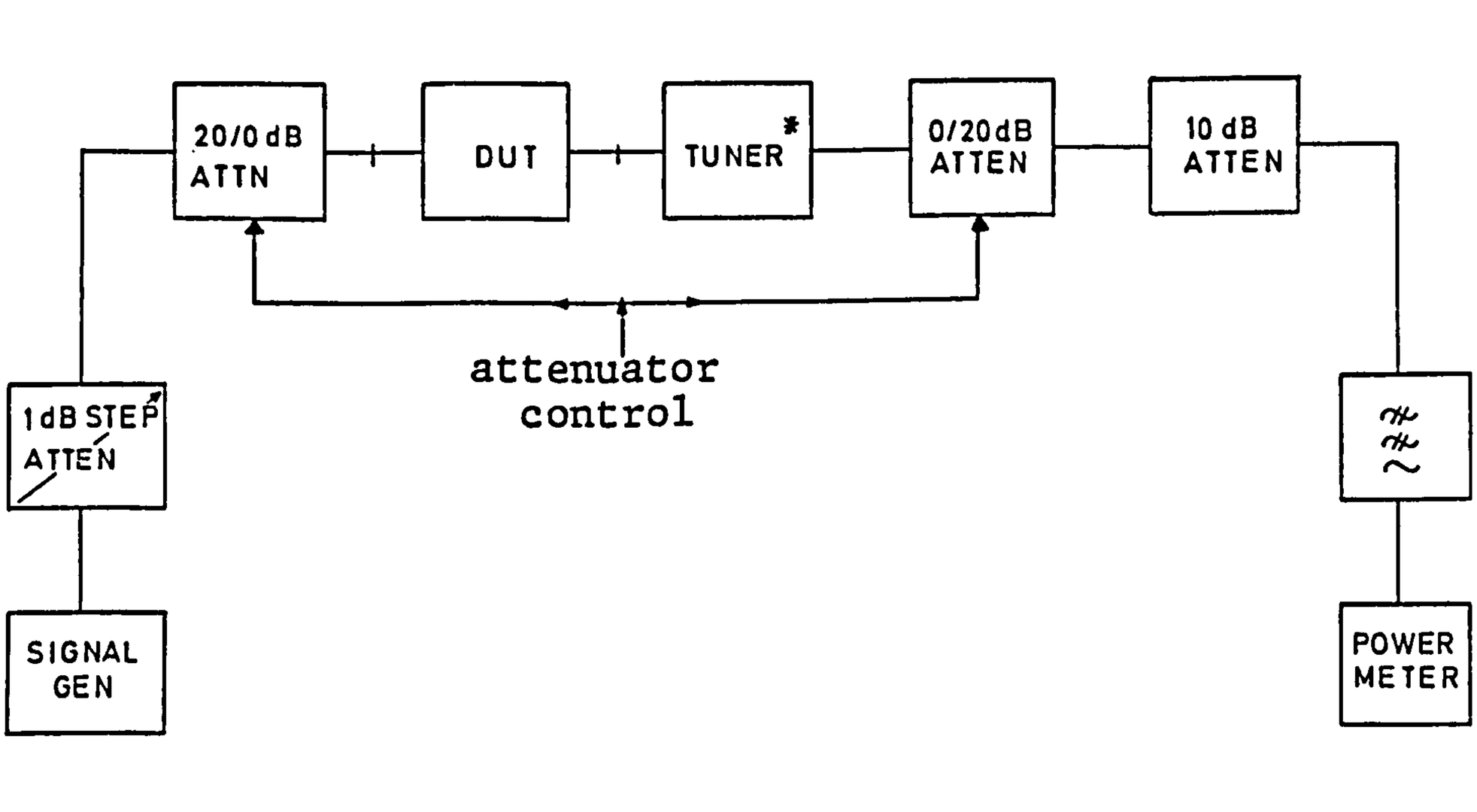

Figure 7.17 A "Power Bench" Test System

(* required for device characterisation - not needed for measurements on amplifiers)

Two methods for determination of the optimum large signal load impedance are available; large signal s-parameter characterisation [9]

and load pull measurements [10]. The output network can then be designed to present the optimum load impedance to the device [11] but only at the expense of small-signal matching performance.

7.3.3.2 Amplifier Structure

The high cost and limited capability of microwave power transistors indicates that the application of some ingenuity to their exploitation should yield dividends. Such is evident from the mass of literature on the subject. The total power output of an amplifier may be increased by combining the outputs of several amplifier modules. Combining in pairs using 3dB, 90 degree hybrids permits the design of output matching networks for optimum large signal operation without sacrificing small-signal output match. The general purpose amplifiers under discussion do not, however, merit such extravagant configurations. The required output power of >12mW in a single-ended configuration is, when circuit losses are taken into account, just within the capability of some small signal GaAs FETs (e.g. Plessey GAT 4). The use of small-signal FETs is imperative, given the broad band nature of the amplifier under discussion. Work on the 12mW amplifier was followed up using a 100mW version of the same device which retains the well conditioned s-parameter locii of the basic device, to realise an amplifier having greater than 50mW output over the same band.

Thus, the output power requirement, per se, does not represent a great challenge, but rather the achievement of the device output power potential across a broad band without jeopodising other aspects of the specification.

In such a multi-stage broad-band amplifier, the distribution of the gain slope compensation between the interstage networks is of significance in determining the limiting output power of the amplifier. Consider the two stage amplifier of figure 7.18(a). The input and output

networks contribute nothing to the compensation of the amplifier since they are required to establish good port matches. The interstage network then has, typically, to provide an insertion loss rising from zero at the top end of the band to 12dB an octave lower in frequency.

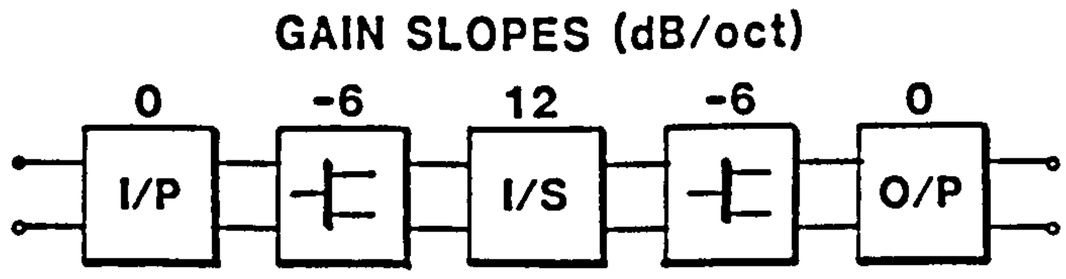

2-Stage Matched Amplifier

(a)

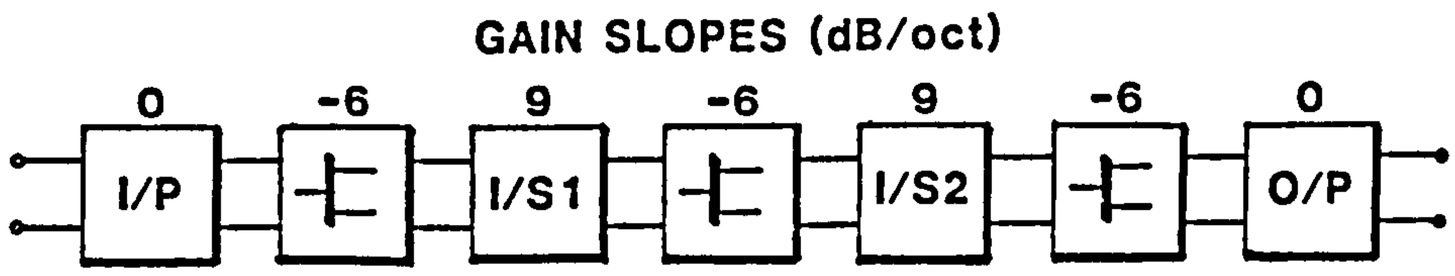

3-Stage Matched Amplifier

(b)

Figure 7.18 Multi-stage amplifier configurations for consideration of large-signal bandwidth.

In order to illustrate graphically the effect on large-signal bandwidth (figure 7.19) some more assumptions must be made. Typical values will be used. The device has a gain of 9dB at the upper frequency of 10GHz. The penultimate stage has a power output capability of only half (i.e. -3dB) that of the final stage. This assumption is justified on two counts. The load impedance seen by the penultimate device is, over the lower portion of the band, a gross mismatch (i.e. near purely reactive) and therefore far from ideal for achieving the output power potential of the device. Secondly, the common desire to economise on supply power often results in the earlier stages of an amplifier being biased less favourably than the output stage.

As can be seen from figure 7.19 the large-signal gain response of the amplifier has a break-point one octave below the upper frequency, below which the first device is limiting the output power of the amplifier. Thus, this representative amplifier would not exhibit a large-signal bandwidth of an octave.

Now, applying the same assumptions and techniques, consider a 3-stage amplifier (Figure 7.18b). The distribution of the gain slope compensation for the three transistors embracing two interstage networks results in a less severe 3dB/octave net gain slope following the penultimate device. The large-signal response break-point is now two octaves below the upper frequency and the roll-off below it is half the 6dB/oct of the 2-stage case. The 3-stage amplifier would then be capable of achieving its full output power objective over rather more than an octave.

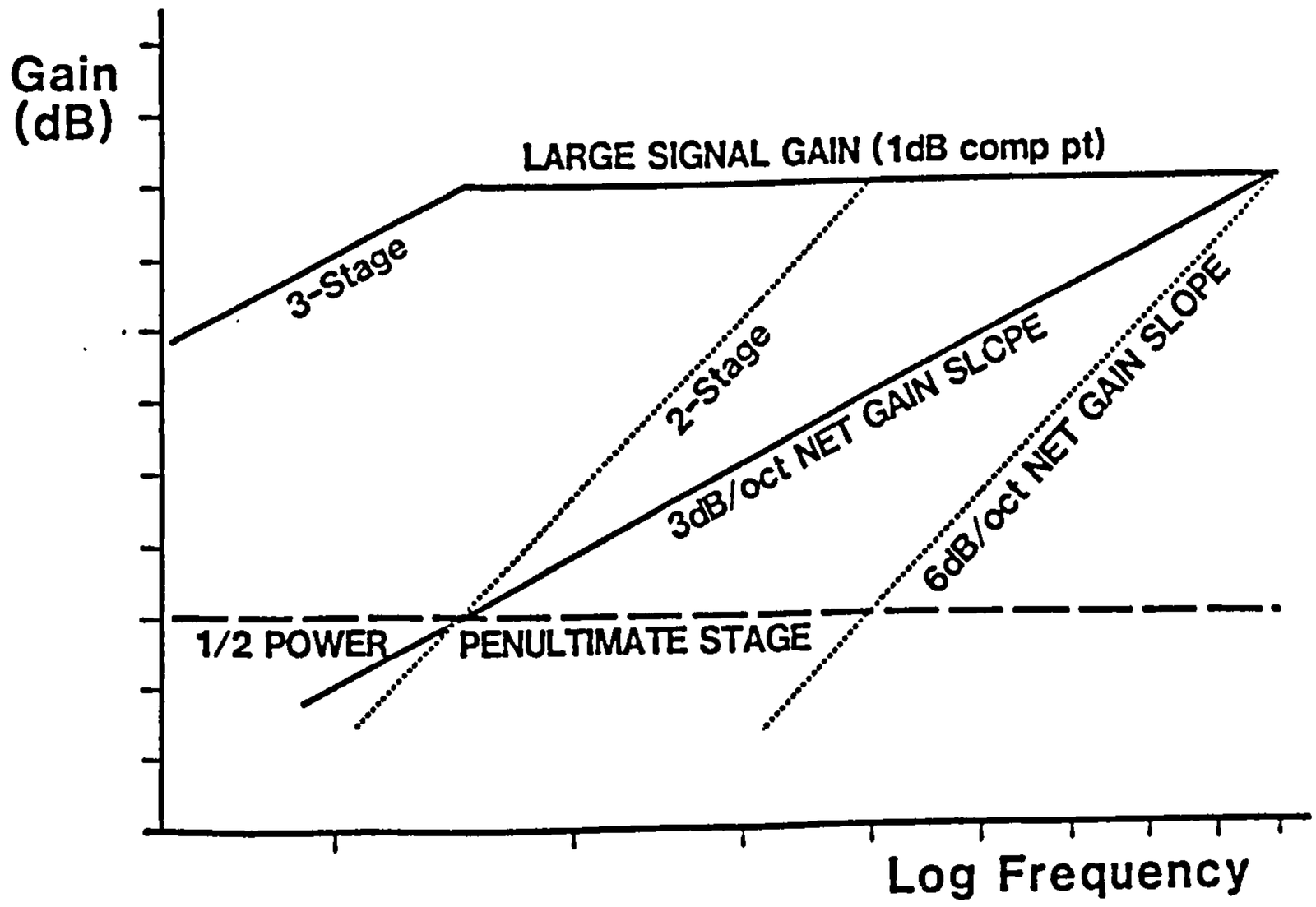

Figure 7.19 Penultimate stage power output limitation

Although the values used in the above example are specific the principle applies to all broad-band amplifiers where a flat large-signal response is required. · Whilst the hybrid connected balanced amplifier configuration does permit some extra freedom in determining the penultimate stage load impedance the same effect still occurs, but with

the break-point slightly lower in frequency. This principle indicates that the use of a higher power device, or the "parallelling" of two or more devices in the final stage of a broad-band amplifier, may be of little benefit unless the preceding stages are upgraded too.

7.3.4 Noise Considerations

The subject of design for low noise operation is outside the scope of this thesis. The noise specification of the general purpose amplifiers under consideration (10dB noise figure), unlike the output power requirements, does not direct any special attention to this aspect of the amplifier's performance. Some general observations are included, simply for completeness.

Design for low noise operation has substantial similarity with design for high output power. The noise properties device must first be established by measurement [15]. An optimum noise source impedance and contours of constant noise figure (Constant Noise Circles) plotted on the input reflection efficient plane are the outcome of such characterisation. The optimum noise source impedance and the conjugate match condition are seldom coincident [16]. Once more the use of 3dB, 90^{o} hybrids with a pair of amplifier modules permits two conditions to be simultaneously met, namely: a low input VSWR for the complete amplifier and optimum noise source impedances for the devices. Note that in the output (combining) hybrid the signal voltages add algebraically, whilst the uncorrelated noise voltages contribute to the total by the root-sum-of- squares rule. Alternatively, a low insertion loss isolator may precede a single-ended amplifier with similar advantage.

In a similar manner to the penultimate stage saturation problem of a broad-band power amplifier, the second (and subsequent) stages of a low noise broad-band amplifier can dominate the noise performance at the low

end of the band [17]. This effect occurs when the gain slope compensation in the first interstage network reduces the signal level incident on the second device to the same order as that incident on the first.

Friis formula (equation <7.26>) provides the means for computing the total noise factor of a cascade of two or more stages.

$$f = f_1 + \sum_{k=2}^{n} (f_n - 1) \Big/ \prod_{j=1}^{k-1} G_{aj} \qquad \langle 7.26 \rangle$$

where g_{ak} = available gain of stage k expressed as a ratio

f_k = noise factor of stage k

and the noise figure F is related to its noise factor thus: $F = 10\log_{10} f$

7.3.5 Reverse Isolation

The reverse isolation requirement set out in the specification of Table 7.1 is a stringent one. The reverse gain, s_{12}, of a suitable GaAs FET is typically -20dB. Since, at the top end of the band the devices are simultaneously conjugately matched, this figure is likely to be worsened slightly. This would suggest that, if a general specification of 50dB is to be achieved, a minimum of three stages will be necessary. At the low frequency end of the band the specification is yet more demanding; requiring an additional 15dB of isolation at 4GHz. The gain slope compensation included in the interstage networks should contribute some additional reverse signal attenuation.

Packaging and bias decoupling also merit special consideration if high reverse isolation is to be achieved. It is difficult to include these factors in any model of the amplifier and they should, therefore, be reduced to a level where the circuit performance is dominant. One simple precaution is to house the amplifier in an enclosure that behaves

as a waveguide below cut-off. Loosely this indicates that the greatest dimension of the enclosure perpendicular to the direction of propagation should be significantly less than a half wavelength at the highest frequency of operation. Figure 7.20 illustrates the situation.

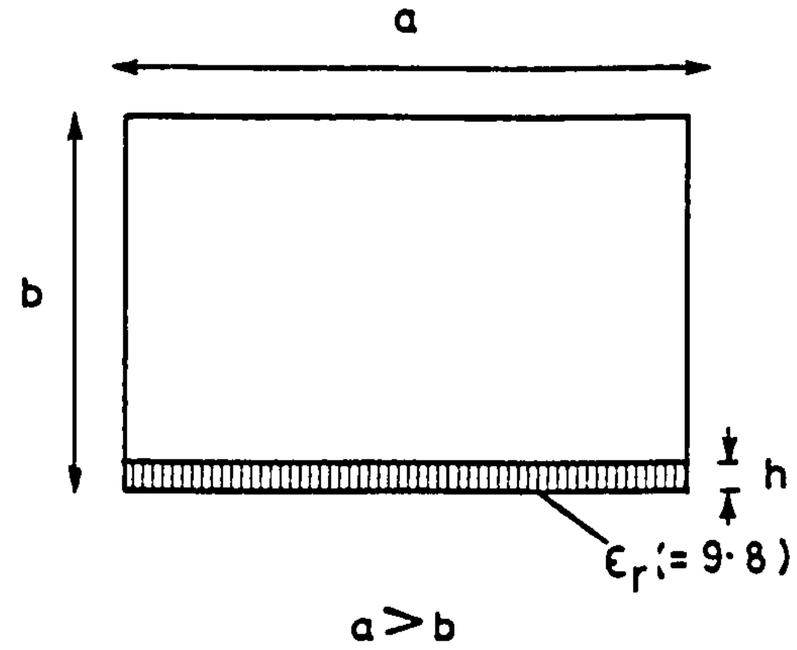

Figure 7.20 MIC Enclosure

In this example the width, being the largest of the lateral dimensions, is relevant when considering the lowest order (TE_{110}) mode. The presence of the dielectric adds considerable complexity if a rigorous approach is to be pursued [18]. For a working approximation, its effect can be seen as moving the bottom surface a little closer to the "roof" of the enclosure.

The cut-off wavelength: $\lambda_{c(TE10)} = 2a$ <7.27>

so the cut-off frequency: $f_c = v_o/\lambda_c = v_o/2a$ <7.28>

where v_o is the velocity of light in free space

For $f<f_c$, the propagation constant: $B = 0$ <7.29>

Thus the attentuation in the waveguide below cut-off is:

$$A = \exp[\alpha l] = \exp[(2\pi l/\lambda_c)\ /1 - (f/f_c)^2] \quad <7.30>$$

where L is the length of the waveguide

Taking logarithms and expressing the result in decibels:

$$L = 10\log_{10}A = 54.6\ l/\lambda_c\ /1-(f/f_c)^2 \text{ dB/unit length} \quad <7.31>$$

and for $f \ll f_c$:

$$L = 54.6l/\lambda_c = 27.3\ l/a \text{ dB/unit length} \quad <7.32>$$

i.e. 27.3 dB/width in length

Of course, with circuit constructed on a material of high permittivity, the launching of the TE_{10} mode is unlikely to be very efficient, so this relationship is, in practice, rather conservative. Nevertheless, the layout of the enclosure and circuit should be arranged to provide the minimum enclosure transmission across the active region of the amplifier substrate.

7.4 REACTIVE NETWORK DESIGN

Design of the reactive networks, used for impedance matching, or gain compensation by mismatch, forms the major task in the development of a microwave amplifier. Traditional techniques, employing quarter-wave transformers [19], stubs and L-section LC networks [20], are frequently inadequate for broad-band designs. At best these methods can manipulate 3 variables against the typical requirement for 4-6 terms necessary to achieve sufficient tracking of port impedances over an octave band. Seldom does human insight or inspiration alone extend to the design of adequately complex networks. A systematic methodology for the synthesis of these networks is therefore highly desirable. The technique of insertion loss synthesis, originally developed for filter design, has been developed by several workers [21,22] to facilitate its application to the design of amplifiers. The detail theory of the method is outside the scope of this work. But, since it has been used extensively by the author, and is an ingredient in the amplifier design methodology of chapter 8, the fundamental aspects will be reviewed. For a thorough treatment the reader is referred to the work of Mellor [26] and for details of the proprietary program used, to reference [24].

7.4.1 Gain-Bandwidth Restrictions

Matching between two purely real impedances can be achieved over an arbitrarily large bandwidth, using an unlimited number of reactive elements. If either impedance has an imaginary (reactive) component this state of affairs no longer prevails. There is a boundary to the bandwidth achievable for a given insertion loss or reflection coefficient which cannot be exceeded regardless of the complexity of an exclusively reactive network. This boundary can be quantified using the relationships given by Fano [25], which can be summarised (after [26]) thus:

$$\int_0^\infty \ln|1/\Gamma| \cdot dW \leqslant \pi/\tau \qquad \text{<7.33a>}$$

for low-pass terminations (i.e. capacitance, series inductance)

and:

$$\int_0^\infty W^{-2} \ln|1/\Gamma| \cdot dW \leqslant \pi/\tau \qquad \text{<7.33b>}$$

for high-pass terminations (i.e. series capacitance, shunt inductance), where all the zeros of the reflection coefficient function $\Gamma(W)$ are in the left hand half plane (the most favourable situation),

and: $\tau = \omega_U CR = \omega_U L/R$; terminating impedance time constant

$W = \omega/\omega_U$; normalised frequency

ω_U = upper band-edge (radian) frequency

For these conditions to apply accurately the port impedance function must conform to an RL or RC equivalent circuit, a stipulation that is frequently violated. Nevertheless these expressions can be used to give a reasonable guide to the achievability of a design and provide some insight into the design trade-offs.

It is apparent that, for the best possible match over the widest bandwidth for any given terminating impedance, the matching network

should be designed to mismatch totally everywhere outside the band of interest. Assuming a rectangular characteristic with uniform reflection coefficient between the band edges (figure 7.21), the integral equations can be simplified, thus:

Low-pass : $$(\omega_U - \omega_L).\ln\{1/\rho\} \lesssim \pi/\tau \qquad \langle 7.34a \rangle$$

High-pass : $$(\omega_U/\omega_L - 1).\ln\{1/\rho\} \lesssim \pi/\tau \qquad \langle 7.34b \rangle$$

where $\rho = |\Gamma|$

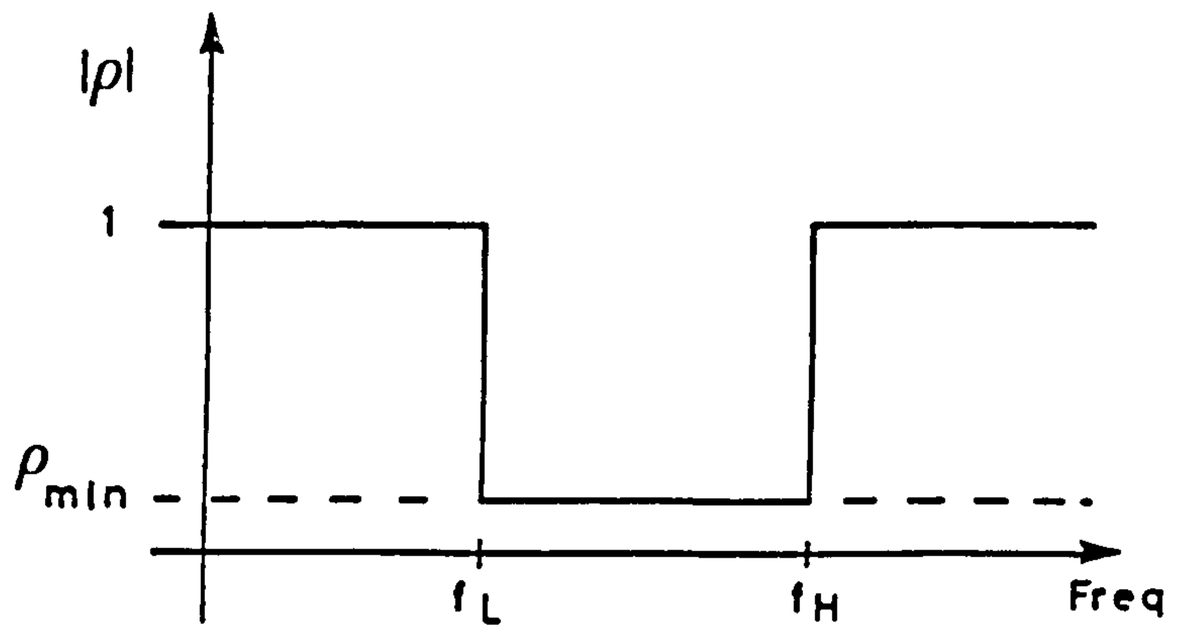

Figure 7.21 Rectangular matching characteristic for gain-bandwidth estimation

From these simple expressions it is possible to estimate the likely performance and complexity of a matching network in advance of designing it. Furthermore it is evident that filter-like behaviour is required of the network.

7.4.2 The Appproxima tion Step

The first step in reactive network synthesis is the definition of a rational function approximation to the frequency response required. Given the lossless nature of the network the transmission power gain, and reflection coefficient are related, at any frequency, by <7.35>

$$T(s) = 1 - |\Gamma(s)|^2 \qquad \langle 7.35 \rangle$$

and the insertion loss, $I = 10 \log_{10}(T)$, dB. Therefore, the behaviour of the matching network can be defined as a filter response. Considering

the class of filter network topologies known as trapless, having no transmission zeros other than a zero or infinitive frequency, the characteristic of figure <7.22> is representative.

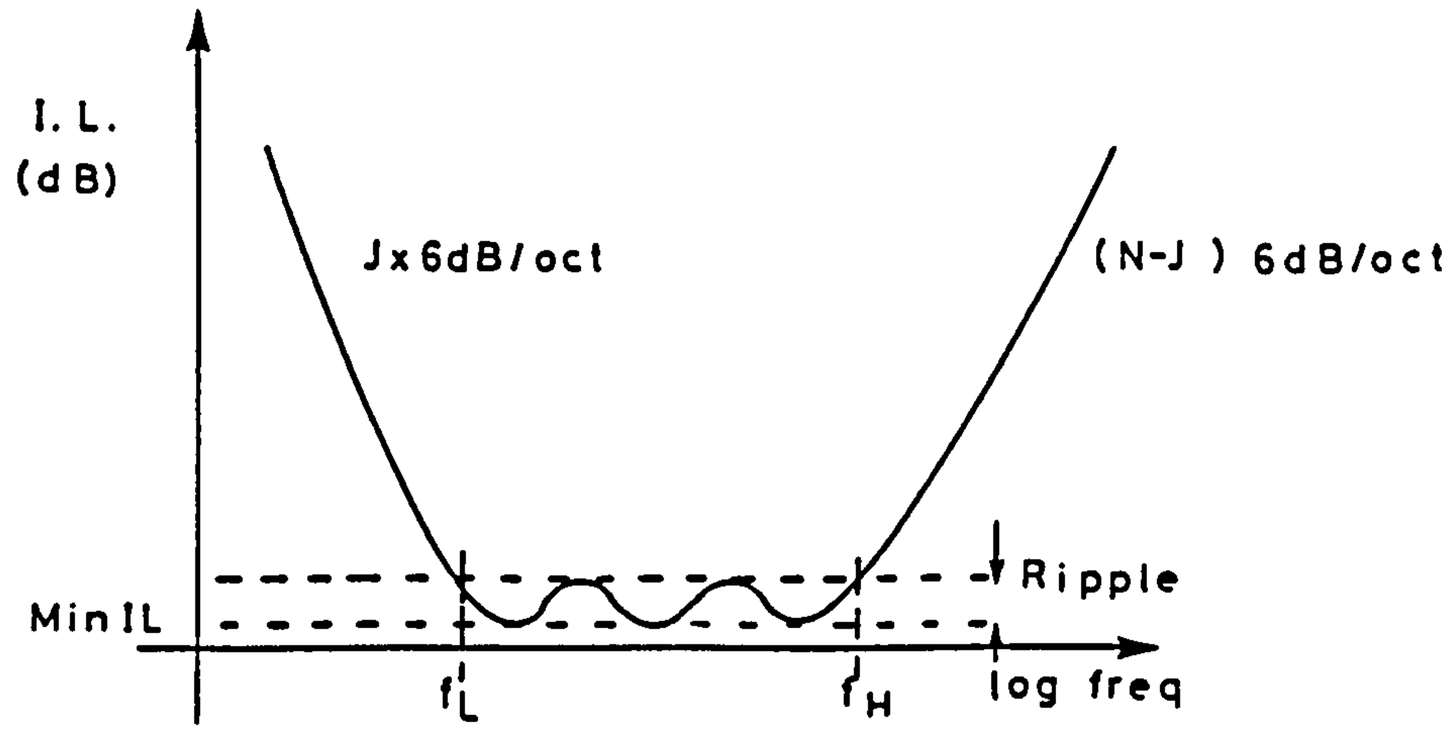

Figure 7.22 Typical trap-less filter response (N = order = no. of elements, J = no. of transmission zeros at d.c. = no. of high-pass elements)

Asymtotic behaviour above and below the band edges is determined by the number of low and high pass elements respectively. The degree of mismatch tolerable defines the minimum insertion loss and ripple. Mellor [21,26] describes how a specified insertion loss slope can be impressed on the pass band frequency response. This capability is not required for the design methodology developed in chapter 8.

From the specification of the response, and given the order of the network, a polynomial approximation to the required insertion loss characteristics can be generated. Frequently Butterworth and Chebyshev formulations are employed.

7.4.3 Topology Selection

For the simple synthesis technique described here the topology

is restricted to a cascade of single shunt or series connected elements. In lumped element synthesis these elements are either capacitors or inductors; making a selection of four element types in all. Distributed element synthesis adds a fifth element type to the catalogue. As well as the series and shunt connected open and short circuit stubs, there is the unit element; a section of transmission line inserted in the cascade.

Distributed element synthesis is conducted by the same methods as the lumped element but in a complex frequency plane transformed according to the Richard's [27] transform, viz:

$$\omega' = \tan(\omega) \qquad \langle 7.36 \rangle$$

The transformation distorts the frequency scale to compensate the tangent characteristic of a transmission line such that the elements display the same behaviour as the appropriate lumped component. Because of the use of this technique, distributed element synthesis is restricted to commensurate line lengths for all elements in any single network.

Several factors affect the choice of topology but ultimately the onus in topology selection lies with the design engineer. Certain combinations of elements are invalid [28]. The total number of elements (order of the network) is determined by the intrinsic difficulty of the matching problem: the magnitude of the ratio of source and load impedance, and the gain-bandwidth limitations discussed above. The proportion of high-pass (as opposed to low-pass) elements included is set to produce the assymtotic out-of-band response. The end element(s) must be of same type as the terminating reactance if parasitic absorption is to be applied. The sense of the impedance transformation also has an influence on the topology selected. Frequently it is necessary to synthesize networks of several alternative topologies before a satisfactory, realisable solution is found.

The advantage of distributed network synthesis is that, at least

ideally, the resultant network is direct implementable. Further, the terminating impedance(s) may be more aaccurately described by a transmission line element (with a resistor) than by the alternative lumped element. The singularity that occurs in the Richard's transformation <7.36> does, however, preclude the use of transmission lines of multiples of a quarter wavelength in length. In practice, given the commensurate nature of the element synthesized and the difficulty of reaslising transmission lines with characteristic impedances over a wider range than 4:1, some massageing of lengths and impedances is generally necessary. Realisability can often be improved, however, by the introduction of (additional) unit elements and the application of network transformations (such as those due to Kuroda; see [29]). Unfortunately this process usually aggravates the fundamental disadvantage of this method when applied to broad-band circuits: the excess rate of change of phase with frequency over and above that associated with the prototype lumped elements. When the bandwidth over which a matching network operates is substantial, especially when the gain-bandwidth limitation is to be closely approached, a lumped element approach is therefore to be prefered. Of course it will be necessary to realise many of the elements as transmission lines, but the lengths will be minimised to produce behaviour closely approaching the lumped element. Distributed element synthesis will not be discussed further, but the general principles of network synthesis described below do extend to the distributed case.

7.4.4 Symthesis

By equation <7.35> a polynomial expression for reflection coefficient can be obtained from that describing the insertion loss response. Similarly an admittance (or impedance) polynomial can be

derived thus:

$$Y(s) = 1/Z(s) = (1 - \Gamma(s))/(1 + \Gamma(s)) \qquad \langle 7.37 \rangle$$

The value of the first element is by removal of a transmission at zero or infinite frequency, depending on the element type.

TABLE 7.3 Chart for Zero Removal

CONNECTION	HIGH-PASS	LOW-PASS
Shunt	L = 1/Ys	C = Y/s
Series	C = 1/Zs	L = Z/s
CONDITION	S → 0	S → ∞

An immitance remainder is then formed by subtracting the element immitance (e.g. shunt capacitor: $Y'(s) = Y(s) - Cs$). This process is re-iterated until values are assigned to all element and the remainder is a number indicating the value of the resistive termination. This termination condition is an outcome of the synthesis procedure, not the specified value. In order to equate the two, network transformations, from L- to T-section [30], are invoked.

7.4.5 Parasitic Absorption

The networks synthesised, constructed entirely of reactive elements, form an impedance transformer designed to achieve optimum power transfer between purely resistive source and load. The reactance (parasitic) associated with either port impedance can be accommodated by a process termed parasitic absorption. Assuming the port impedance across the design pass-band can be effectively modelled by a single reactive element (in addition to the resistor) it can be included in the

first (or last) element of the network. Having chosen the extreme element types appropriate to the port characteristic, their values, generated by the synthesis procedure, need to be influenced to accommodate the port model reactive element. Changing any of the synthesis parameters can have such an influence, but there exists a degree of freedom that may be exercised without any effect on the transmission behaviour of the network. Because of the square in the relationship between reflection coefficient and insertion loss <7.35>, the reflection coefficient polynomial has arbitrary signs. This corresponds to an option on the position of reflection coefficient zeros on the s-plane. Parasitic absorption is optimised with all zeros located in the left half plane (LHP). But LHP zeros at one port correspond to RHP zeros at the opposite port. When parasitics are associated with both terminations, the zero positions must be manipulated to attempt accommodation of both. When the ciruit design is completed the end element(s) are adjusted to allow for the parasitic. It is often possible to influence the value of an extreme element to make it equal to the parasitic element. Thus the element count may be reduced by one.

7.6 DISCUSSION

In this chapter the tools and techniques of microwave circuit design, particularly in the context of broad-band amplifier development, have been expounded. Issues affecting secondary performance specifications and common pitfalls have been highlighted. In addition, an emphasis has been placed on techniques and methods that result in direct synthesis of the required circuits.

From this foundation, the novel approach described in the following chapter, is developed. Work presented in this chapter pertinent to the

structure and realisation of a representative amplifier is freely drawn upon.

7.6 REFERENCES

[1] MARCHENT, B.G.: "Interactive computer programs for the computer aided design of, linear microwave circuits", Ph.D. Thesis, University of Warwick, 1973.

[2] CARSON, R.S.: "High frequency amplifiers". J. Wiley & Sons, New York, 1975.

[3] BODWAY, G.E.: "Circuit design and characterisation of transistors by means of 3-port scattering parameters", Microwave Journal, Vol.11, 1968.

[4] WOODS, D.: "Multiport-Network Analysis by Matrix Renormalisation Employing Voltage Wave S-Parameters with Complex Normalisation", Proc. IEE, 1977, Vol.124, pp.198-204.

[5] BODWAY, G.E.: "Two Port Power Flow Analysis using Generalised Scattering Parameters", Microwave Jnl., 1967, Vol.10, No. 6.

[6] TEMPLE, G.J. & DAWE, C.: "Design & realisation of low-cost broad-band amplifiers", IEE Colloquium on "Design of RF Instruments", London 21/11/1980, Digest No.. 1980/68.

[7] ENGELBRECHT, R.S. & KUROKAWA, K..: "A Wide-Band Low Noise L-Band Balanced Transistor Amplifier", Proc. IEEE, 1965, pp..237-257.

[8] WALKER, M.G., MAUCH, F.T. & WILLIAMS, T.C.: "Cover X-Band with a FET Amplifier", Microwaves, 1975, Vol.8, pp.36-45.

[9] TUCKER, R.S.: "R.F. characterisation of microwave power FETs", IEEE Trans. MTT-29, 1981, pp.776-81.

[10] ABE, H. & AONO, Y.: "11-GHz GaAs power MESFET load-pull measurements utilising a new method of determining tuner Y-Parameters", IEEE Trans. MTT-29, 1979, pp.394-9.

[11] KELLY, W.M., et al.: "Design of Linear GaAs FET Amplifier, Proc. 7th European Microwave Conference, Copenhagen, 1977, pp.105-109.

[12] MARSHALL, N.: "Optimising Multi-stage Amplifiers for Linearity", Microwaves, 1974, Vol. 7, pp.60-64.

[13] HOSSEINI, N.M. & SHURMER, H.V.: "Computer-aided design of microwave integrated circuits", IERE Rad. & Electron Eng.., Vol. 48, 1978, pp.85-8.

[14] HOSSEINI, N.M.: "Application of computer-aided design to microstrip circuits", Ph.D. Thesis, University of Warwick, 1977.

[15] ABBOTT, D.A., SHURMER, H.V. & TEMPLE, G.J.: "Automatic characterisation of 2-port components and devices in microstrip", IEE Colloquium "Computer Controlled Microwave Measurements", 2/4/1979.

[16] EISENBERG, J.A.: "Design amplifiers for optimum noise figure", Microwaves, April 1974. pp.36-44.

[17] MARSHALL, N.: "Optimizing multi-stage amplifiers for low-noise", Microwaves, April 1974, pp.62-64

[18] ARMSTRONG, A.F. & COOPER, P.D.: "Techniques for investigating spurious propagation in enclosed microstrip", IERE Rad. & Electron Eng., Vol.48, 1978, pp.64-72.

[19] PRZEDPELSKI, A.B.:: "Bandwidth of transmission line matching circuits", Microwave Jnl., April 1978, pp.71-6.

[20] SMITH, P.H.: "Electronic applications of the Smith chart", McGraw-Hill, 1969.

[21] MELLOR, D.J. & LINVILL, J.G.: "Synthesis of Interstage Networks of Prescribed Gain versus Frequency Slopes", IEEE Trans., 1975, MTT-23, pp.1013-1020.

[22] BESSER, L. & SWENSON, S.: "Update Amplifier Design with Network Synthesis", Microwaves, 1977, Vol.10, pp.50-56.

[23] LEVY, R.: "Synthesis of mixed lumped and distributed impedance-transforming filters", IEEE Trans., MTT-20,, 1972, pp.223-33.

[24] AMPSYN User Manual, Compact Engineering Inc.

[25] FANO, R.M.: "Theoretical limitations on the broad-band matching of arbitrary impedances", Jnl.. Franklin Inst., Vol.249, 1950, pp.57-83 & 139-55.

[26] MELLOR, D.J.: "Computer aided synthesis of matching networks for microwave amplifiers", Ph.D. Thesis, Stanford University, 1975.

[27] RICHARDS, P.I.: "Resistor-transmission-line circuits", Proc. IRE, Vol.36, 1948, pp.217-20.

[28] SKWIRZYNSKI, J.F.: "On the synthesis of filters", IEEE Trans. CT-18, 1971, pp.152-63.

[29] WENZEL, R.J.: "Exact design of TEM Microwave circuits using quarter wave lines", IEEE Trans. MTT-12, 1964, pp.94-111.

[30] VINCENT, G.A.: "Impedance transformation without a transformer", Frequency Technology, Vol.7, No. 9, Sept. 1969. pp.15-21.

CHAPTER 8

DISSIPATIVELY COMPENSATED MICROWAVE AMPLIFIERS

8. DISSIPATIVELY COMPENSATED MICROWAVE AMPLIFIERS

8.1 INTRODUCTION

Chapter 7 was a review of the design procedures relevant to conventional reactively compensated amplifiers. That is to say; amplifiers in which the power gain slope with frequency of the active device is offset by frequency dependent mismatch provided by lossless networks. This, however, is not the only approach to broad-band microwave amplifier design. The alternative types are classified in figure 8.0. The merits and de-merits of each approach will be discussed.

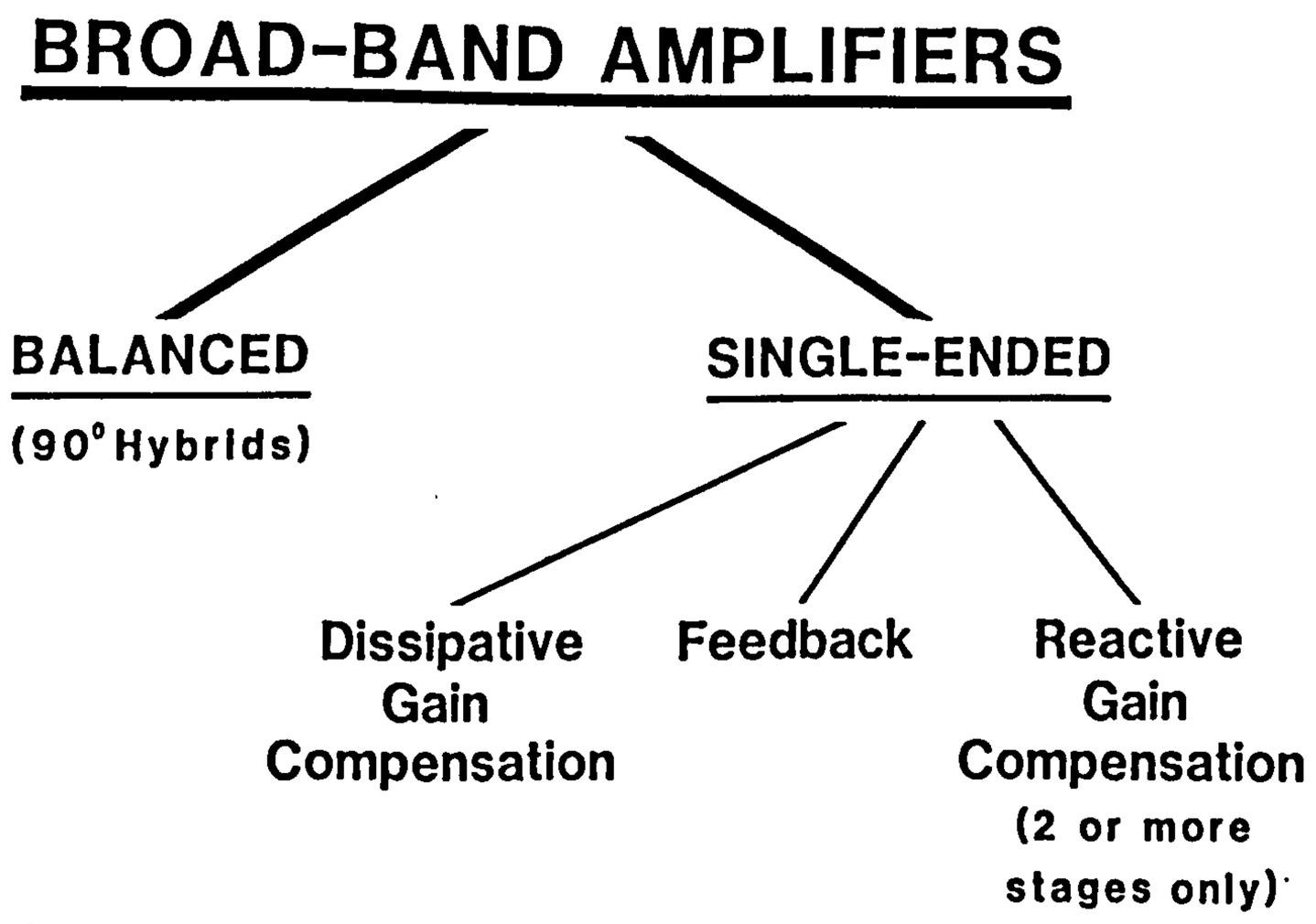

Figure 8.0 Microwave broad-band amplifier classification

8.1.1 Balanced Amplifiers

As already discussed in section 7.3.2., the balanced amplifier structure offers the substantial benefit of separating the input or output match requirements from the determination of device source or load impedance. Thus gain slope compensation by mismatch, optimum noise source matching and optimum output power load termination can be accommodated without compromising the external port mismatches. The

single-stage flat gain blocks that are, therefore, possible may be cascaded with impunity.

The penalties paid are increased circuit area and component count, the introduction of hybrids with their inherent band limiting and demanding geometries, and additional power consumption. The increased width of the circuit is, because of propagation through the enclosure, especially inconvenient where high reverse isolation is required.

In a cost conscious environment the benefits of design simplicity and versatility may not justify the greater unit cost.

8.1.2 Single-Ended, Reactively Compensated Amplifiers.

This class of amplifiers, representing the conventional approach to microwave amplifier design has been fully discussed in the previous chapter. Its advantages stem largely from the accumulated body of work that supports this design approach. The techniques of constant gain circle plotting and network synthesis are powerful tools for the designer. Furthermore, the exclusive use of reactive (ideally lossless) components offers the greatest potential performance in terms of gain, noise figure and power output.

Set against these advantages are a number of significant disadvantages. Although the design of such amplifiers is conceptually simple it is frequently excessively difficult to execute. The large mismatches involved, together with the limited reverse isolation of the active devices conspire to make the interaction between networks a major design problem. These excessive internal mismatches are accompanied by other problems, including anomalous exaggeration of circuit losses, sensitivity to device parameter, component and fabrication tolerances, radiation effects, large group delay variations [1], instability and premature output saturation of the transistors preceding the interstage

networks [2]. Single-stage amplifiers, matched at both ports having flat gain over any appreciable bandwidth are unrealisable and the input and output network matching bandwidth for all amplifiers using reactive components alone is ultimately limited by the gain-bandwidth restrictions discussed in section 7.4.1.

8.1.3 Single-Ended Feedback Amplifiers

The introduction of negative feedback has well known benefits in non-microwave amplifiers including the flattening of gain versus frequency response, the minimisation of the effect of device parameter variations and the reduction of non-linearity. Two factors hinder the application of negative feedback at microwave frequencies; the limited gain available from the active devices and the excess phase shift, due to delay, that can result in positive feedback and consequently instability. The latter carries the implication that, if useful at all, the application of feedback must be confined to single active devices so excluding the possibility of using feedback pairs with their increased loop gains. There are, then, three common-source (common-emitter) feedback configurations to be considered: those illustrated in figure 8.2.

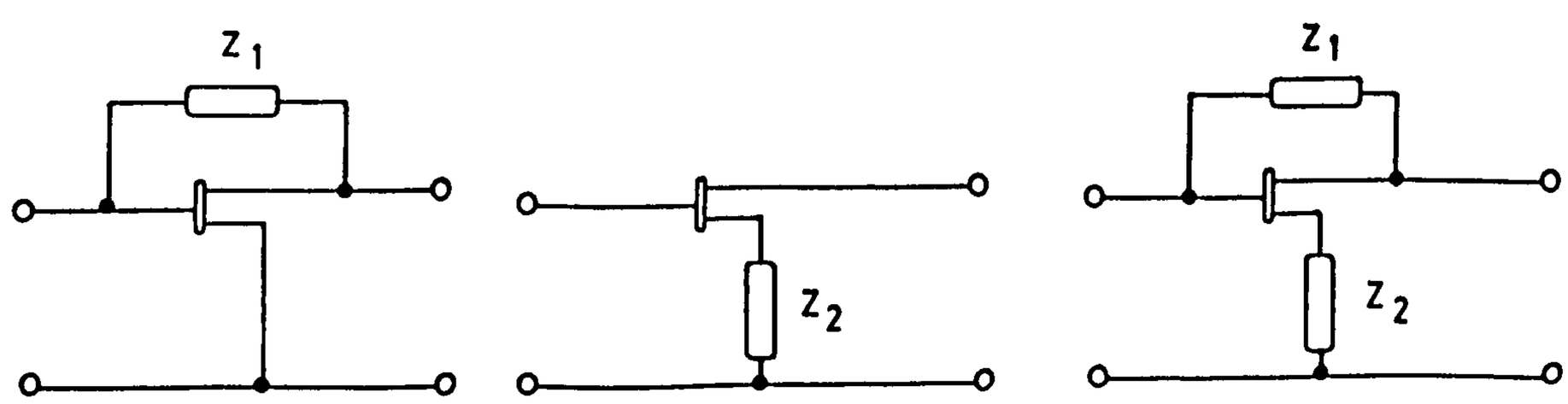

(a) Drain-Gate F/B (b) Source F/B (c) Composite F/B

Figure 8.2 Single-stage common-source feedback configurations

The feedback impedances, Z_1 and Z_2, may be purely resistive, purely

reactive or complex.

Drain-gate (collector-base) feedback, a case of voltage-shunt feedback (figure 8.2(a)), has the effect of reducing both the input and output impedances of the stage. This configuration is usually topologically inconvenient, especially with packaged devices, and path lengths involved are in practice too long to ensure wide-band stability. Using chip transistors both GaAs FET [3,4] and Si bipolar [5], excellent results have been obtained.

Source (emitter) degeneration, a manifestation of current-series feedback (figure 8.2(b)), raises the input and output impedances of the stage. Its inclusion is quite convenient when chip devices are employed, especially in self bias of an FET is also to be incorporated. Packaged devices do, however, present a problem. Since the ultimate performance of a common-source (common-emitter) device is obtained with the lowest intrinsic source (emitter) impedance the packages are usually constructed to minimise this parasitic element. In particular, the use of a stud (e.g. Plessey P103) precludes the inclusion of source networks.

Krowne [2] and Salmon [6] have studied this feedback configuration and demonstrated impressive results. Salmon's work demonstrates the use of an inductive feedback element to cause the conditions for optimum noise figure and input match to converge. The voltage wave renormalising transforms given in Appendix D are useful in obtaining the 2-port s-parameters from the 3-port description of the device with the third (source/emitter) port terminated in Z_2.

Finally, figure 8.2(c) represents a composite feedback configuration. From the foregoing remarks it is apparent that this configuration is topologically inconvenient and it is also unsuitable for low transconductance (g_m) devices like GaAs FETs. Nevertheless, it is described because, when using a high g_m device (e.g. a Si bipolar

transistor), the interaction of the two forms of feedback permits the designer to obtain 50 Ohm input and output impedances as well as flat gain [7]. In previous work the author has experience of this configuration in wide-band amplifiers operating up to 2GHz.

Feedback is a potentially useful technique at microwave frequencies. Flat gain response, greater immunity to device variation, a possible improvement in matching gain-bandwidth are among the benefits. On the other hand, the possibility of reduced out of band stability, the topological constraints, the substantial loss of the already minimal gain and the reduction of reverse isolation do constitute significant disadvantages. The preference for the use of packaged devices for this work on amplifiers in the 4-9 GHz range (cf. section 7.1.2) does, in practice, preclude the adoption of this approach.

8.1.4 Single Ended, Dissipatively Compensated Amplifiers

An alternative to the foregoing approaches involves the inclusion of frequency dependent dissipative networks. The rising dissipation with falling frequency characteristic of these networks would be designed to compensate the device gain slope. This approach has received comparatively little attention and, although resistors are often included for stability reasons, seldom are they included in the networks defining the frequency response of the amplifier. In cases where some dissipative compensation has been used [9,10], it has not been as a result of any coherent design process but rather as an adjunct to the conventional amplifier design process, introduced in an ad hoc manner.

Temple and Dawe [12] has described a method for the use of a resistor to improve broad-band match at the expense of a small degradation in gain. Figure 8.2 illustrates the effect on port immittances for shunt and series configurations and the expressions of <8.1> quantify the

associated gain loss.

$$\delta A = - \log_{10}(R_2/R_1) = - \log_{10}(G_2/G_1) \qquad \text{<8.1>}$$

where $R_2(G_1)$ is the initial value of the real part of impedance (admittance) at the port

and $R_2(G_2)$ is the final value of resistance (conductance) after adding series (shunt) resistor.

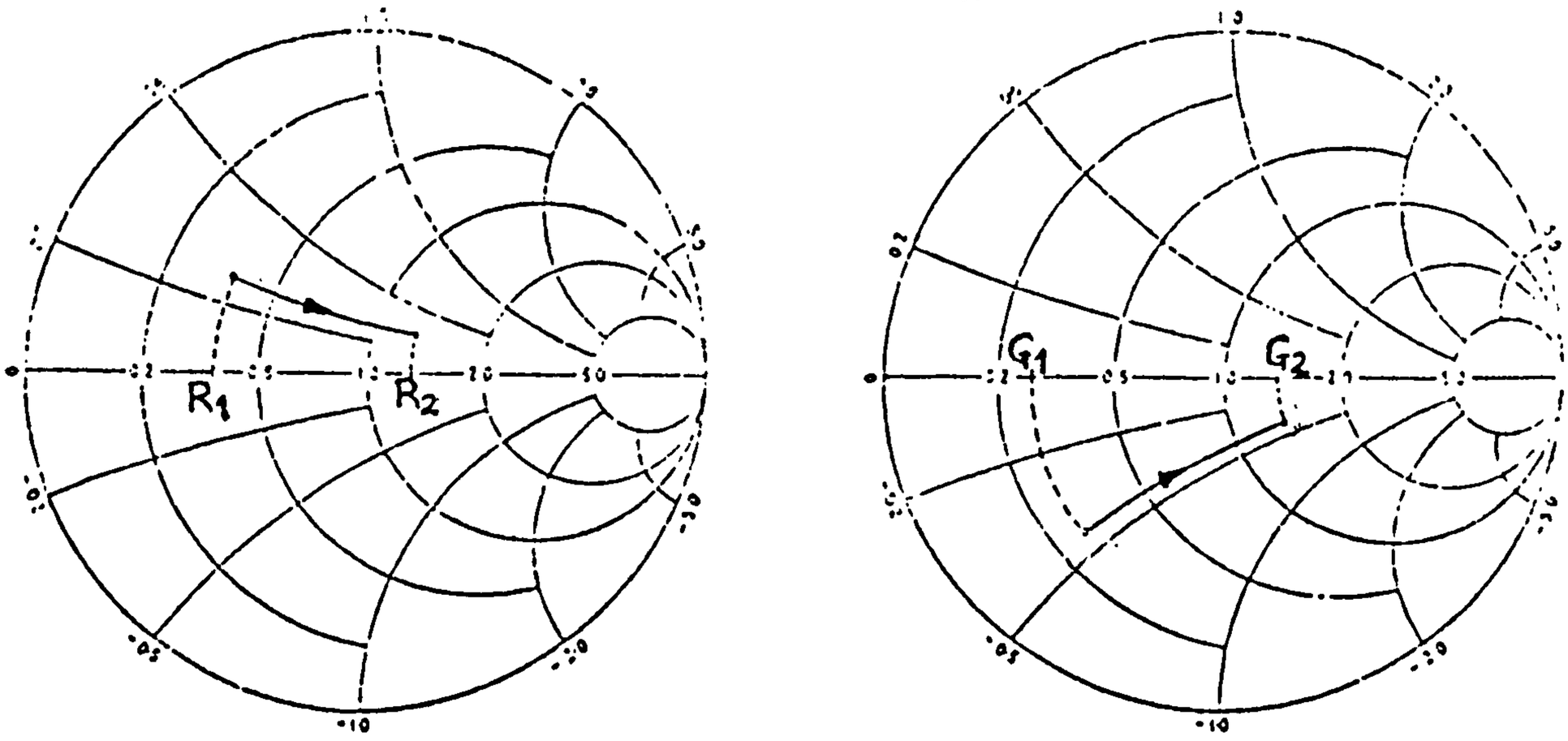

(a) DISSIPATIVE MATCHING -SERIES RESISTOR

(b) DISSIPATIVE MATCHING -SHUNT RESISTOR

Figure 8.2 The effect of a single resistor on port immittance.

The application of dissipative gain slope compensation has a number of evident advantages, principally as a consequence of the reduced internal mismatches. These include a reduction of the interaction between stages; potentially easing the design process and reducing sensitivity to device, component and circuit fabrication tolerances. Circuit losses should become more predictable, radiation effect less significant and group delay variations less severe. The inclusion of resistive elements will ease the matching gain-bandwidth restrictions permitting broader band amplifiers to be designed. The load impedances seen by devices driving interstage networks will be more favourable for large-signal operation. Furthermore stability, particularly out-of-band

stability, will be improved and reverse isolation, at the lower frequency end of the band, will be increased. An additional benefit is that, by including the frequency dependent dissipative networks, single-stage single-ended broad-band matched amplifiers become feasible.

There are, however, some handicaps associated with this approach. A principle problem is brought about by the requirement for resistors having good microwave properties. For amplifiers operating in C-band or above the only really satisfactory solution is to use photolithographically defined film resistors on the substrate. Clearly a likely penalty for the inclusion of dissipative elements is reduced dynamic range, as a result of a degraded noise figure and increased device output power capability requirement. In an appropriately configured multi-stage amplifier the deterioration can, however, be made insignificant [12].

A major disincentive to adoption of this otherwise attractive approach is that no design methodology currently exists. Whilst there is a great body of work covering the synthesis of lossless networks there is much less literature on the subject of mixed reactive-resistive network synthesis. That which is available (e.g. [11]) is difficult to relate to the general termination impedance, sloped insertion loss requirement of the microwave amplifier problem, and no relevant computer-aided-design (CAD) packages exist.

In this chapter the application of dissipative networks to microwave amplifier gain compensation is to be considered. A design methodology, with supporting CAD software, is developed and applied to the design of a 4-9GHz amplifier. Experimental results are assessed to establish design accuracy and the efficacy of the approach.

8.2 THE CONCEPT OF DISSIPATIVELY COMPENSATED AMPLIFIER DESIGN

Much information and software to facilitate the design of reactive matching networks of filter form already exists (cf. section 7.4). This suggests that the methodology for the design of amplifiers where the device gain slope is compensated by dissipative network should incorporate such established techniques.

8.2.1 The Compensated Device

Consider the configuration illustrated in figure 8.3.

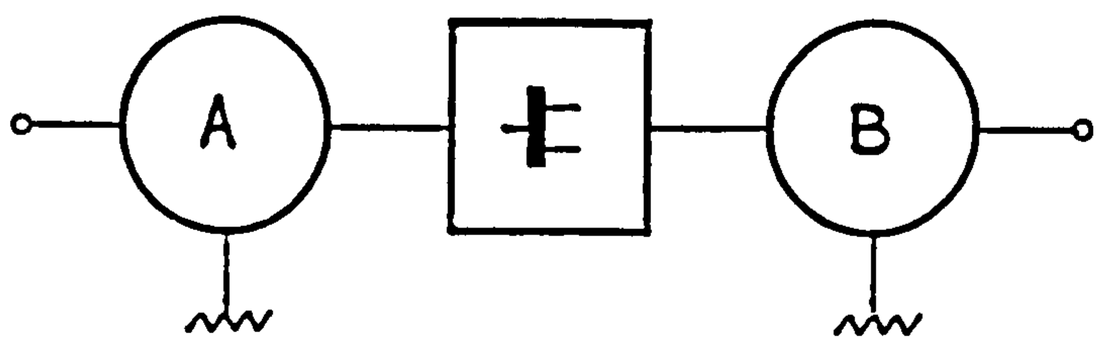

Figure 8.3 The Composite Device

'A' and 'B' are lossless networks that, with falling frequency, progressively divert the signal energy into the dissipative elements represented by resistive terminations. These networks may be regarded as a form of diplexor. Depending on the situation of the device within the amplifier such networks may be attached to either or both ports. The networks are intended to compensate the inherent device gain slope (typically 6dB/octave) so that the gain of the composite "device" so formed is, over the band of interest, substantially independent of frequency. Ideally, the compensation is achieved solely by the dissip•tion of the excess signal energy in the resistive elements. The definition of "gain" applied to the composite "device" is of great significance. Designing the networks to establish a flat maximum available gain (G_{Amax}) for the composite device would ensure that, when terminated in its simultaneous conjugate match conditions, a flat

frequency response is realised.

8.2.2 The "All-Matched" Amplifier

Consider the amplifier structure presented in figure 8.4.

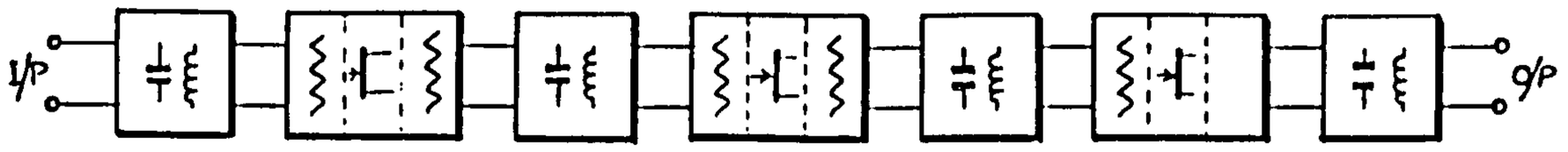

Figure 8.4 The "All-Matched" Amplifier structure

The flat gain composite devices are interconnected by reactive matching networks. The interstage networks are designed to present the simultaneous conjugate match load immittance to the output of the preceding composite device when terminated in the simultaneous conjugate match input immittance of the following device. Thus, over the design band, the interstage networks have a flat response. Input and output networks are designed to transform the external characteristic impedance (Z_o=50 Ohms) to the composite device simultaneous conjugate match input and output immittances respectively.

Thus, the maximum available gain of the composite devices is realised and no gain slope is contributed by the interconnecting reactive networks, the maximum available gain slope of the device having been compensated by the dissipative elements contained within the composite device. The amplifier may be described "all-matched" by virtue of the lack of mismatch at any of the block interfaces in figure 8.4.

This situation offers a number of significant benefits. The design process may be more structured, and therefore potentially less complex, because of the lack of interactions between the networks associated with each stage. Each composite device is terminated, at both ports by its simultaneous conjugate match conditions and is, therefore, accurately

described by its power-wave renormalised (generalised) s-parameters (cf. Appendix D) for that condition. The virtual elimination of internal mismatch will result in improvement of group delay response, reduction of the unpredictable circuit losses associated with high VSWR's, and reduction of the sensitivity to circuit component and device variations, when compared to the conventional reactively compensated design. The use of lossy compensating networks within the composite device increases the matching gain-bandwidth product and consequently the single-ended amplifier bandwidth achievable. In addition, out-of-band stability is improved and reverse isolation enhanced.

8.2.3 The Design Procedure

As indicated above, one of the merits of this amplifier concept is the structured nature of the design problem. That is; the lack of interaction between the networks included in the amplifier permits the design of the networks to proceed in a substantially independent manner. From a consideration of the amplifier specification and the active device properties the design may be compartmentalised into a set of specifications for the individual "blocks" within the amplifier. For example, gain and reverse isolation requirements would be the primary factors in deciding the number of stages necessary.

Dynamic range considerations would set the distribution of gain slope compensation between input, output and interstage dissipative networks, as well as influencing the number of stages employed. Device properties and realisability constraints may affect the division of the interstage compensation between the dissipative network at the output of the preceding device and the input network of the one following. From these deliberations the net maximum available gain slope for the compensated composite devices is determined.

Figure 8.5 illustrates a representative outcome of this process that forms the basis of the amplifier design to be described later. Note that, in order to avoid inclusion of compensation of the output of the amplifier first two devices are overcompensated by +1 and +2dB/octave respectively.

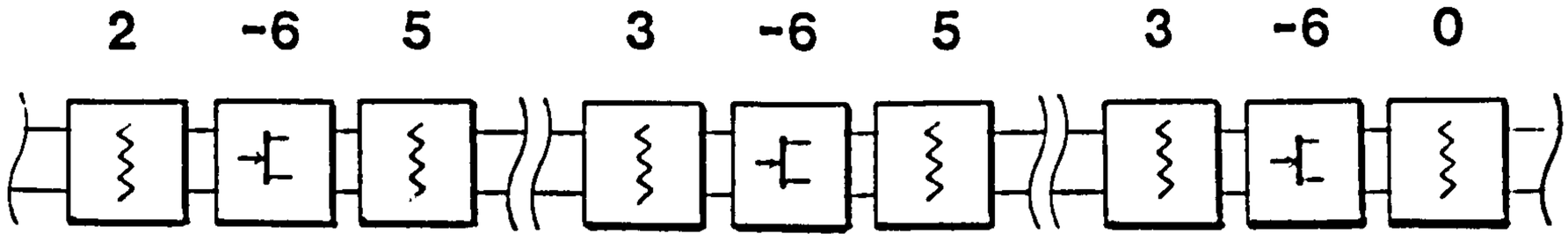

Figure 8.5 A typical amplifier gain slope breakdown (dB/oct.)

The design can then proceed, first by design of the gain slope compensating dissipative networks, and thereafter by design of the impedance transforming input, output and interstage matching networks. Since neither design process will be exact the final step will involve some interactive adjustment of element values. In practice, the procedure may need to be restarted several times before a satisfactory outcome is achieved. This is the inevitable penalty of such a structured approach since the low level realisation consequences of a high level selection cannot always be foreseen. The initial design is substantially more exact than that achievable by the conventional reactively compensated approach and computer circuit optimisation [13] is required only to deal with second order deviations from the desired response.

8.3 THE DESIGN OF FREQUENCY DEPENDENT DISSIPATIVE NETWORKS.

In general terms, the frequency dependent dissipative networks to be connected to either or both ports of the active devices may be regarded as contiguous diplexors with one port terminated by a resistor. Such an item, illustrated in figure 8.6a, would have the

property that would losslessly transfer all the signal energy incident at port 1 to ports 2 and 3 and with a ratio between them that has a prescribed relationship to the frequency (figure 8.6b). A conventional diplexor would comprise a number of reactive elements and would operate with simple resistive terminations on all ports. To provide a matching network between the diplexor and the active device would negate some of the advantages on the proposed configurations and the total component count for the diplexor and the matching network, which can recur twice for each active device, is prohibitive.

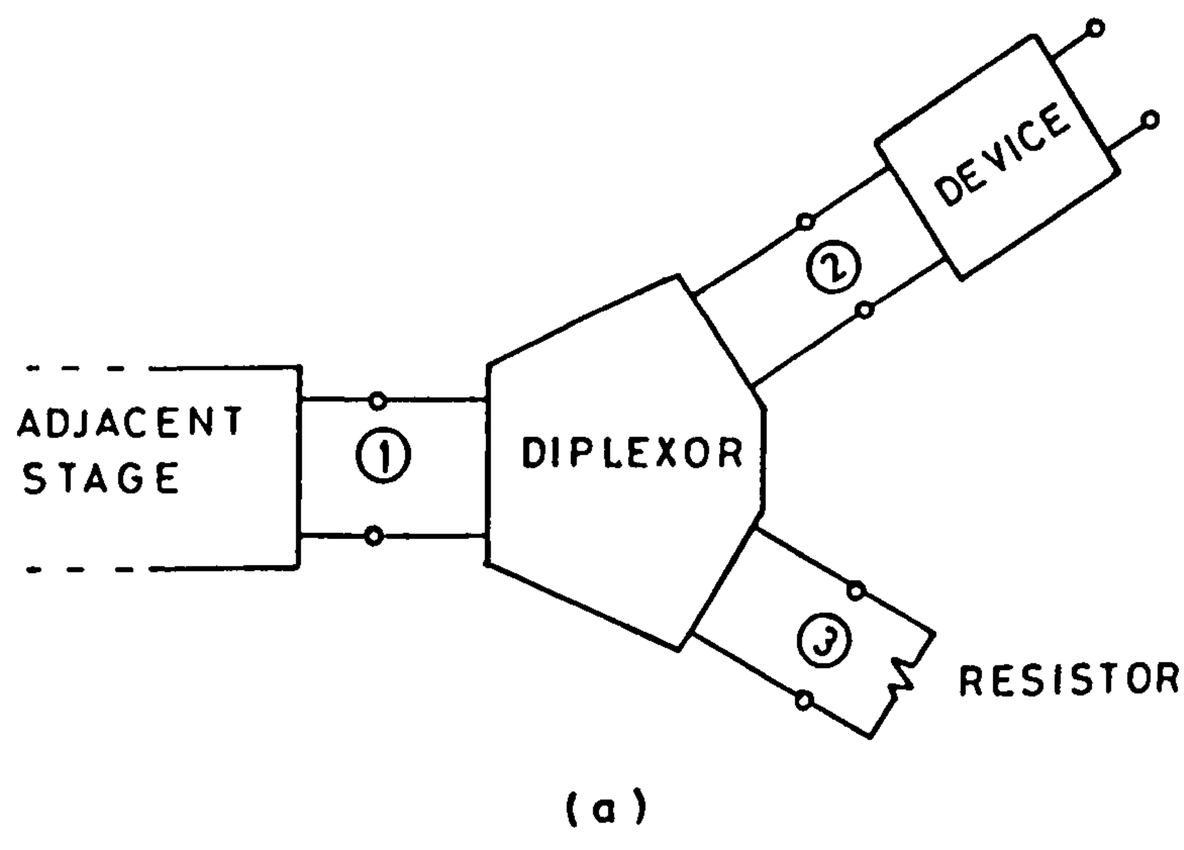

(a)

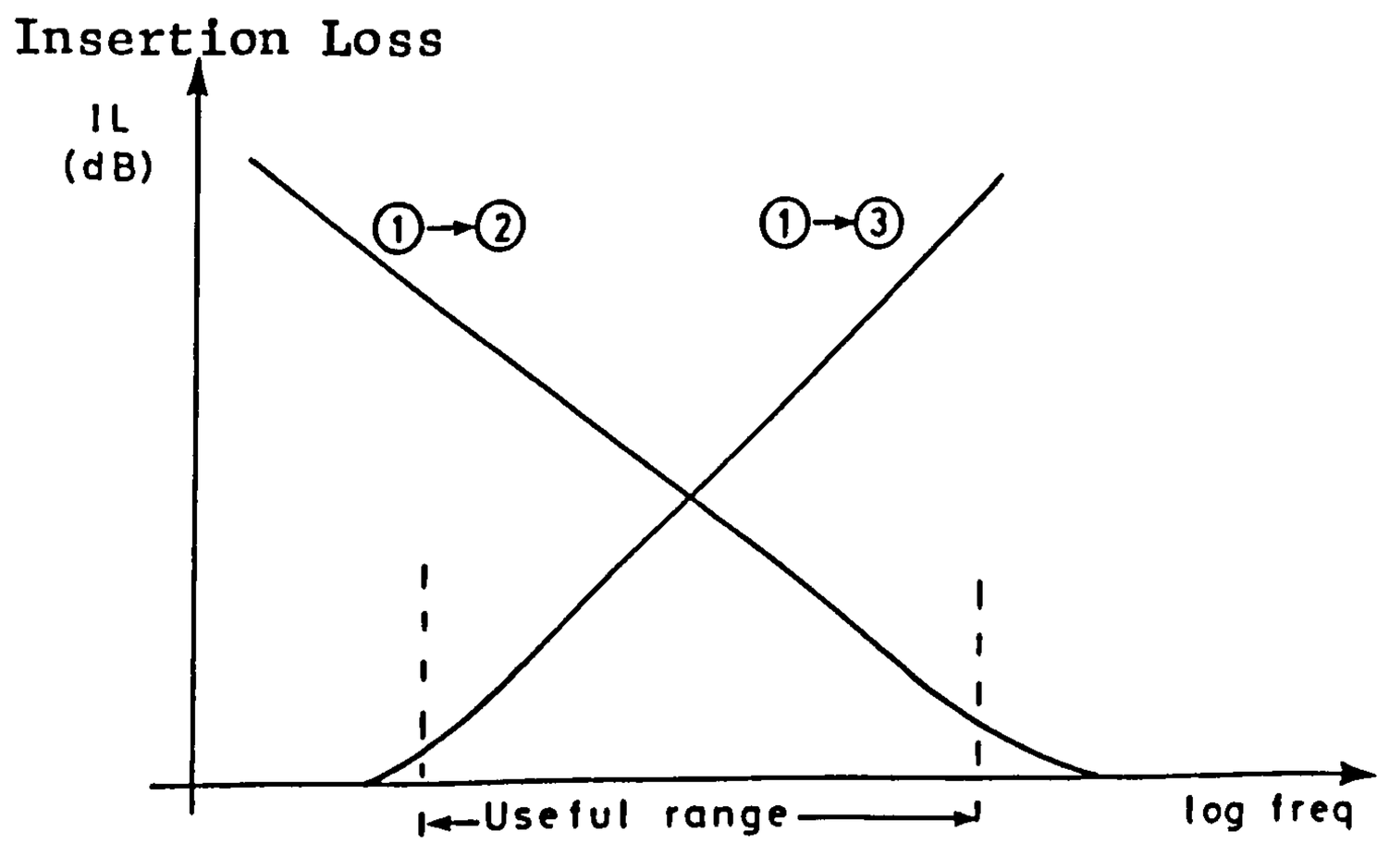

(b)

Figure 8.6 Employing a diplexor as a gain slope compensator; the configuration (a) and the frequency response (b).

Clearly simpler structures, designed in the context of more general

impedance interfaces, are required. Before discussing some appropriate circuit topologies, it will be necessary to establish useful definitions for the transfer functions of these networks.

8.3.1 Transfer Function Definitions

Since the dissipative network is to be inserted between arbitrary impedance source and load, the simple measure of insertion loss (cf. <7.2>) is inadequate.

Transducer (power) gain is convenient for specifying the gain of items connected to arbitrary source and load impedances. From the definition below it is apparent that its value depends upon both the degree of mismatch at both ports and hence the source and load impedances (cf. <7.3>).

$$\text{Transducer (Power) Gain} = \frac{\text{Power delivered to load}}{\text{Power available from source}} \qquad \langle 8.2 \rangle$$

From the structure of the "all-matched" amplifier (figure 8.4) it is known that one port of the dissipative network will always be terminated with its complex conjugate impedance.

Thus, the dissipative network connected to the input of the active device will always meet, at its input, the condition for optimum power transfer from the preceding input or interstage matching network. The measure of gain (or loss) employed should therefore reflect this situation and be independent of the source impedance. Such a measure is the ordinary or operating power gain.

$$\text{(Ordinary) Power Gain} = \frac{\text{Power delivered to load}}{\text{Power into 2-port}} \qquad \langle 8.3 \rangle$$

Similarly the appropriate measure of gain for the dissipative network at the output of the device is available (power) gain.

$$\text{Available (Power) Gain} = \frac{\text{Power available at output}}{\text{Power available from source}} \qquad \langle 8.4 \rangle$$

which may be computed from the expression <7.8>. Note that the available gain is independent of the load impedance but is a function of the source impedance.

Clearly, the definitions for available gain and ordinary power gain are identical except for orientation of the 2-port to which they relate. The relationship of <7.8> can, therefore, be generalised to express both gain measures for the network connected to the ith port of the device

$$G_{A/P} = |s_{21}|^2(1-|r_i|^2)/(|1-r_i s_{jj}|^2 - |s_{ii}-r_i^* \Delta|^2) \qquad \langle 8.5 \rangle$$

where [S] are the s-parameters of the dissipative network

r_{im} are the device source and load reflection coefficients

and $j = 3-i$; $i = 1,2$

(i.e. $i = 2$ for Available Gain of network at device output)

Note that if the network s-parameters are renormalised (cf. Appendix D) to the (complex) device port impedance this expression degenerates to

$$G_{A/P} = |s_{21}|^2/(1 - |s_{ii}|^2) \qquad \langle 8.6 \rangle$$

Given the condition that in the proposed amplifier structure one port of the network will always be, at least ideally, complex conjugately matched these gain definitions provide a convenient measure for use in the analysis and design of dissipative gain slope compensating networks having specified transfer functions.

Since the networks under discussion are for the particular application of device gain slope compensation the form of the transfer function is restricted to a limited type. The transfer function should exhibit a specified positive gain slope with frequency approaching a point of near zero minimum attenuation at a specified frequency

corresponding approximately to the upper band edge of the amplifier. This would indicate that any suitable network should have a minimum of two, ideally independent, variable elements, determining the slope and minimum attenuation frequency.

The discontinuous first derivative of the frequency response at f_H makes the ideal function unrealisable. A network with an arbitrarily large number of elements may produce an arbitrarily close approximation to the desired response but this would be contrary to the intention to minimise the number of components employed in the amplifier. Illustrated in figure 8.11 are representative responses of single resonant structure. Although it is a relatively poor approximation tc the ideal response it is still a useful one for bandwidths up to about two octaves. The modest deviations can be compensated for insertion loss ripple in the interstage reactive matching networks, without greatly compromising the target of an "all-matched" amplifier design.

The response of such a network can be fully characterised by gain values at three frequencies which may conveniently correspond to the extremities of the band of the amplifier (f_L and f_H) and the mid-band frequency (f_M). Specification of the response at three frequencies also permits some accommodation of deviation from the archtypical linear gain-frequency slope of the active device by introducing a "concave" or "convex" trend into the response of the network (figure 8.11). The design process must therefore produce values for a minimum of three element values.

8.3.2 Dissipative Network Topologies

The frequency dependent dissipative network has already been described as a diplexor (figure 8.6), a structure that can be represented as a pair of filters, either a high-pass, low-pass combination or two

band-pass filters dissimilarly tuned.

As previously stated the complexity of a fully matched contiguous diplexor is too great to permit its inclusion in several positions within a single amplifier. Hence it is necessary to examine some degenerate forms of such networks that will adequately service the particular application of device gain slope compensation. Clearly, two classes of network should be examined; (i) lumped element, and (ii) mixed lumped-distributed.

8.3.2.1 Lumped Element

The simplest manner in which the band-pass diplexor can be implemented is illustrated as figure 8.7a. The filters are realised as series resonant circuits giving the response of figure 8.7b. A similar result (figure 8.7d) can be obtained using the parallel resonant circuits of figure 8.7c as band-stop structures and reversing the order of the resonant frequencies.

Both of these circuits can be reduced in complexity by leaving out components; a process that may have little significant effect on the performance of the network in the context of device gain slope compensation. The band-pass/band-stop structures can be reduced to high/low pass elements or one of them omitted altogether. Figure 8.7e is an example of the latter. The removal of the series connected parallel resonant circuit simply removes the pole of infinite attenuation (figure 8.7f). In all these cases the dissipative loss is obtained by a shunt connected resistor. From the expression of <8.1> it is evident that series connected resistors are equally useful in gain control. Figure 8.7g is an example of the application of a series lossy element that is progressively bypassed by the series resonant circuit as the frequency rises towards resonance. This network is the dual of that of figure 8.7e and consequently has the same form of transfer function.

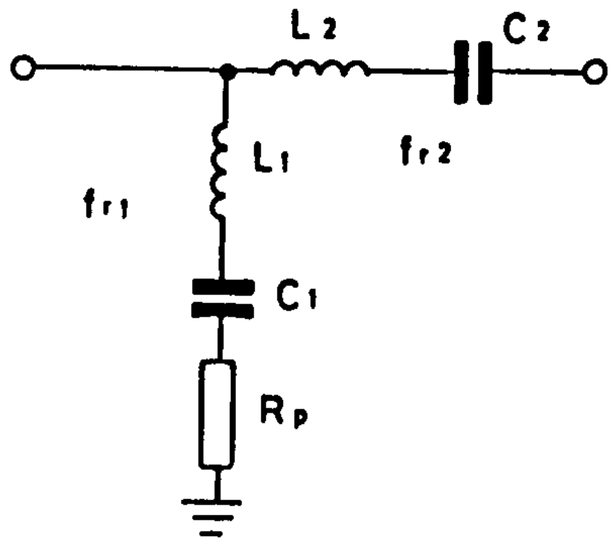

(a) employing series resonant circuits

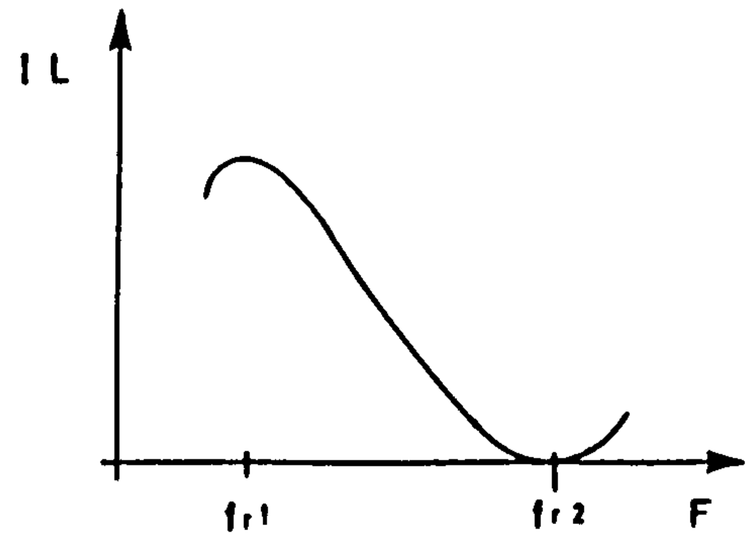

(b) transfer function of "a"

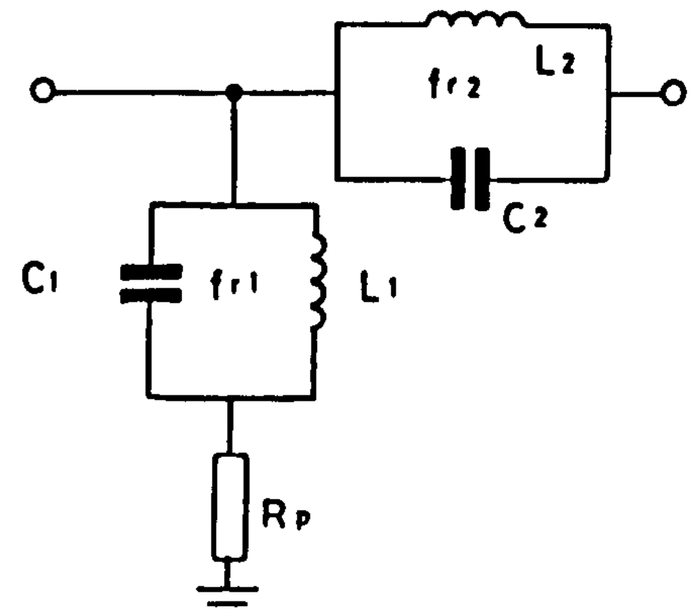

(c) employing parallel resonant lines

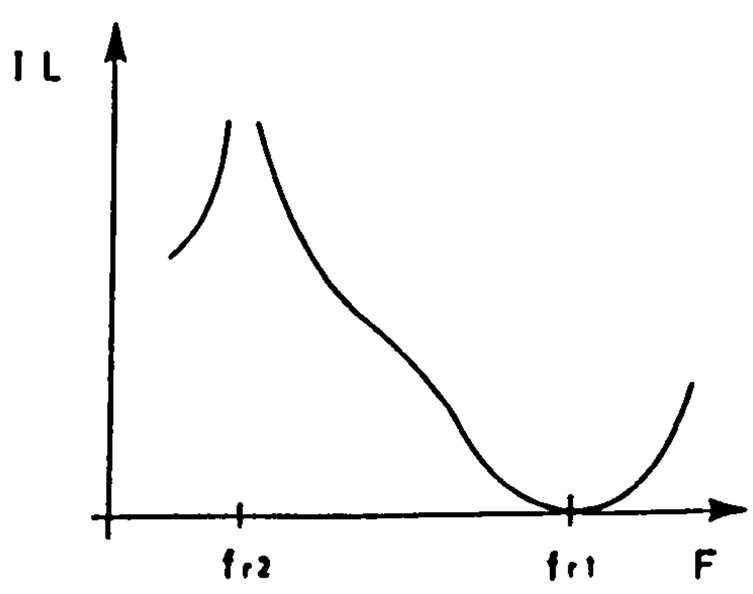

(d) transfer function of "c"

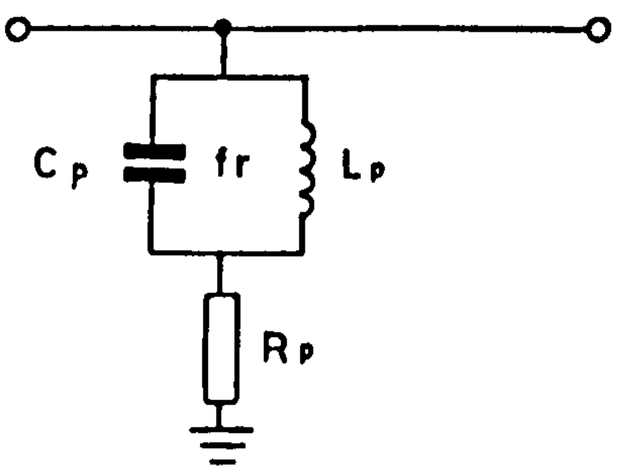

(e) as "c" but simplified

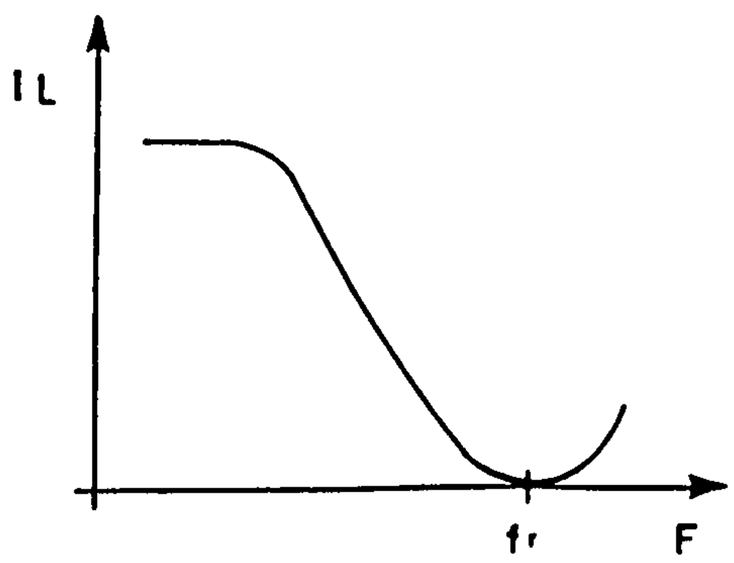

(f) transfer function of "e" & "g"

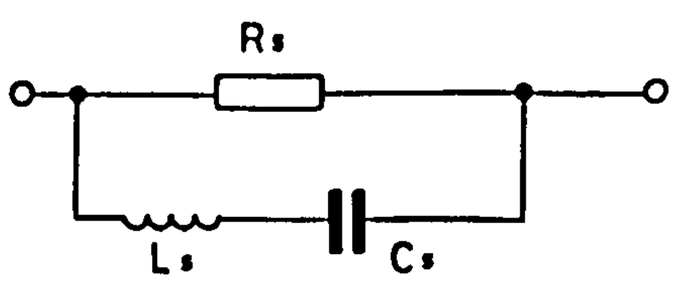

(g) dual of "e"

IL:= Insertion Loss (dB)

Figure 8.7 Lumped element frequency dependent dissipative networks (a,c,e,g) and their transfer functions (b,c,f)

These last two networks are of particular interest since they represent the minimum configuration meeting the requirement for three independent variables; L, C and R. A more meaningful expression of these variables is as the resonant frequency, f_r, the loaded Q and the "base-line" attenuation achieved far from resonance. These loosely correspond to stipulation that high, mid and low frequency points on the transfer function should be determined, preferably in a substantially independent manner.

A further simplification to the two element (lag-lead) networks of figure 8.8a and b produces a response of the form of figure 8.8c. Superficially, the response appears suitable for this application, and it can indeed be appropriate for some low gain slope situations, but the two variables; essentially the two time constants (formed with the load impedance Z_2), do not allow enough degrees of freedom for satisfactory design.

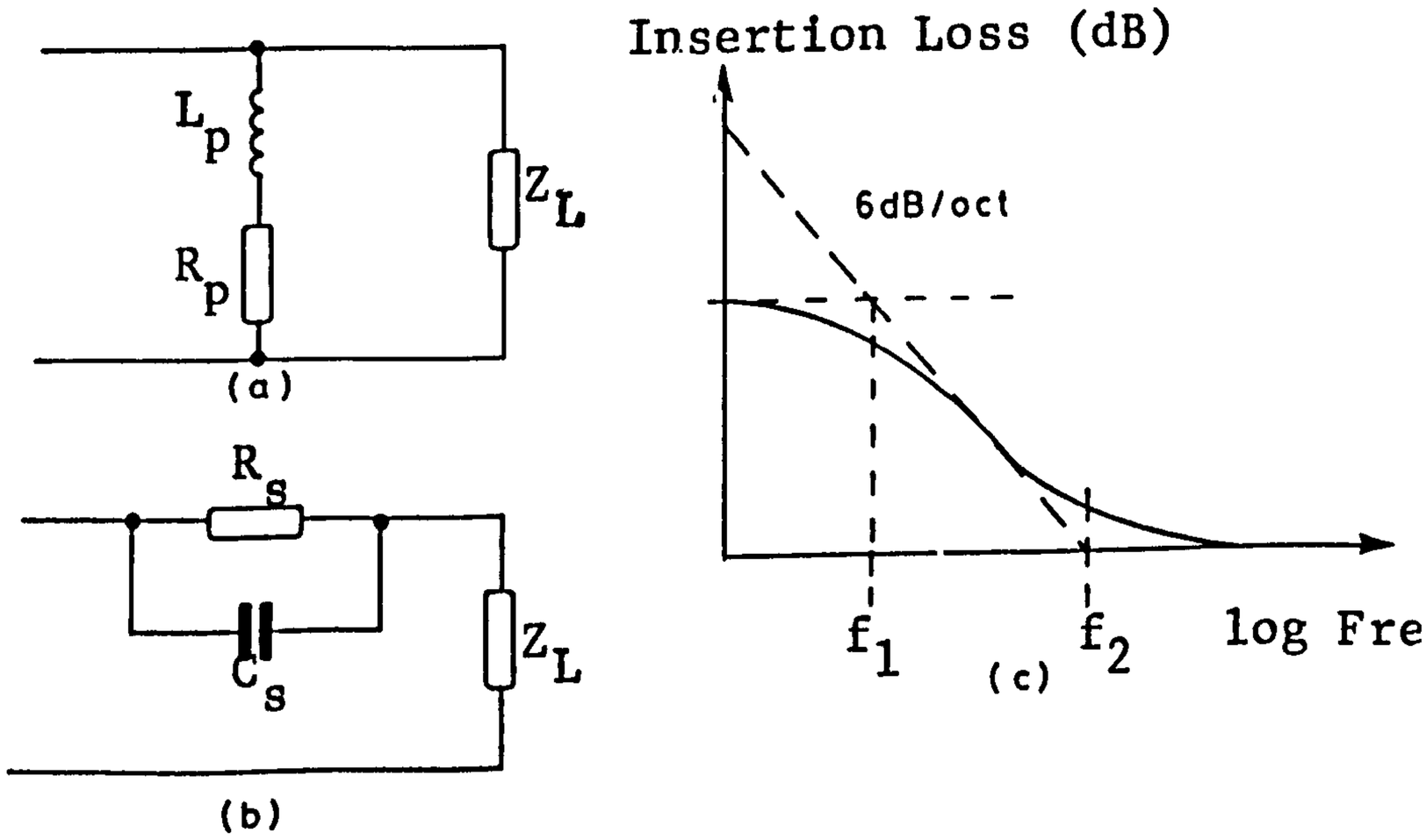

Figure 8.8 Two element networks.

A problem that can arise in practice can be illustrated using the circuit of figure 8.8a as an equivalent circuit for the network of figure 8.7e below resonance (i.e. within the amplifier pass-band). Typically, the active device, operating in its useful frequency range, will present predominantly capacitive load. Thus there is a parallel resonant circuit formed which may cause the impedance at the input of the network terminated by the device to rise dramatically within the useful band of the amplifier. This difficulty arises principally when the network is connected to the input of the device, because of the lower capacitive reactance and higher "Q" normally associated with this port. Naturally this would result in an unacceptable mismatch and a loss of gain. It is under such circumstances that the network's dual offers a potential benefit since the sign of reactance is reversed.

8.3.2.2. Distributed Element Networks

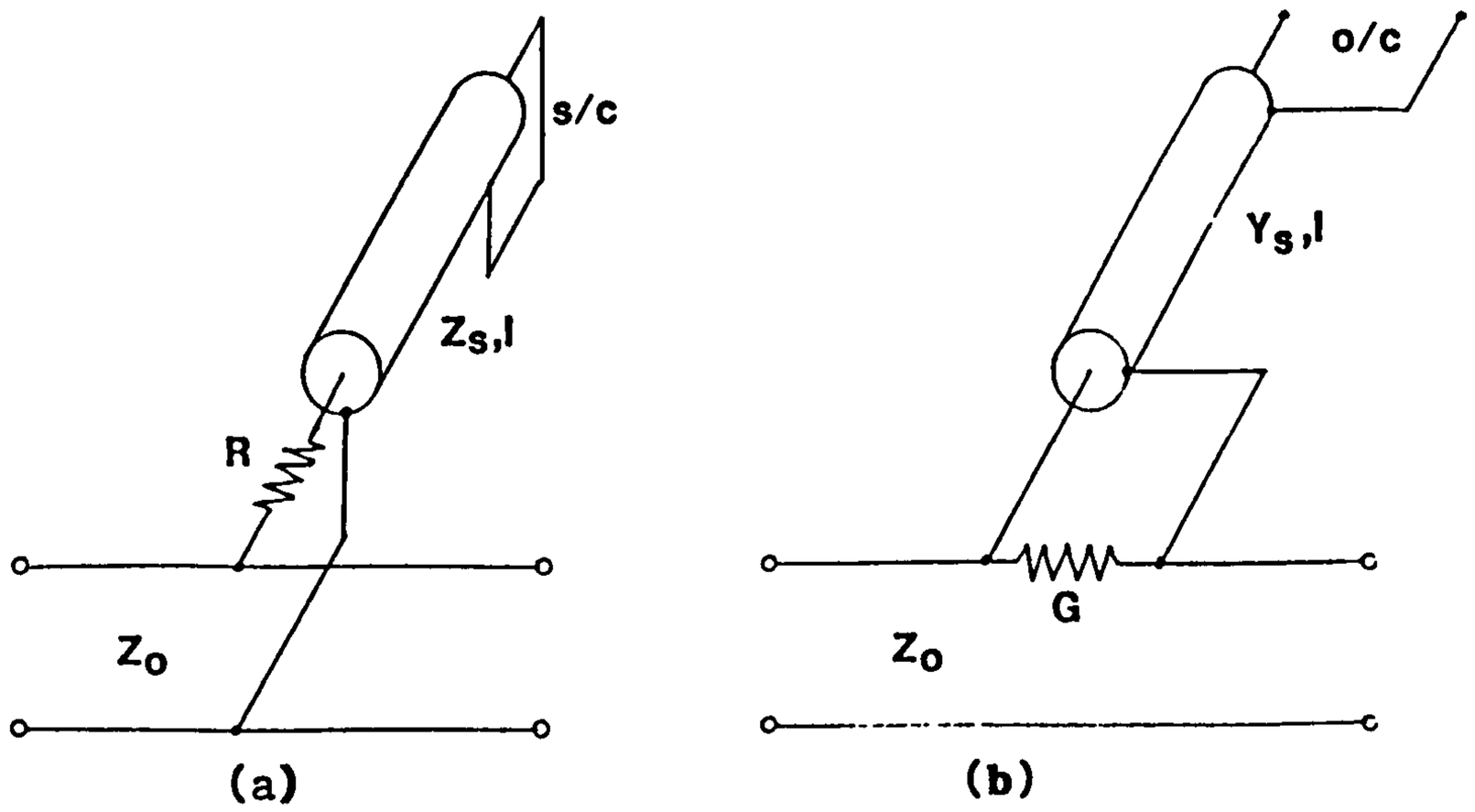

Figure 8.9 Distributed element dissipative networks

The transmission line based networks of figure 8.9a & b are effectively equivalent to the lumped element networks of figure 8.7e & g, respectively, when the line lengths are $\lambda/4$ at f_r. The short circuit shunt stub (figure 8.9a) can be introduced into an MIC amplifier circuit very conveniently, often combined with the bias insertion circuit. The series-connected stub is rather less useful; requiring edge coupled

structures which can be difficult to fabricate, have a limited range of reliable impedances and introduce inconvenient parasitic transmission line effects. In brief, a distributed element network is preferable where a shunt resistor is employed; when a series resistor is used a lumped element network has the advantage. The following discussion relates principally to the distributed element network of figure 8.9a.

8.3.3 Analysis of the Resistor-Stub Network

It is convenient to define a set of normalised parameters to describe the network:

- the normalised stub impedance:

$$r = (Z_s - Z_o)/(Z_s + Z_o) \qquad \langle 8.7 \rangle$$

- the normalised resistor value:

$$z = R/(Z_s + Z_o) \qquad \langle 8.8 \rangle$$

- the upper frequency offset

$$k = f_H/f_r \qquad \langle 8.9 \rangle$$

The normalising impedance, Z_o, may be chosen to suit the surrounding circuit conditions.

The stub and resistor combination are connected to the circuit by a 3-port junction, the resulting structure being included as a 2-port in the amplifier cascade. In practice, this ideally nodal junction has finite size and may be regarded as a microstrip T-junction.

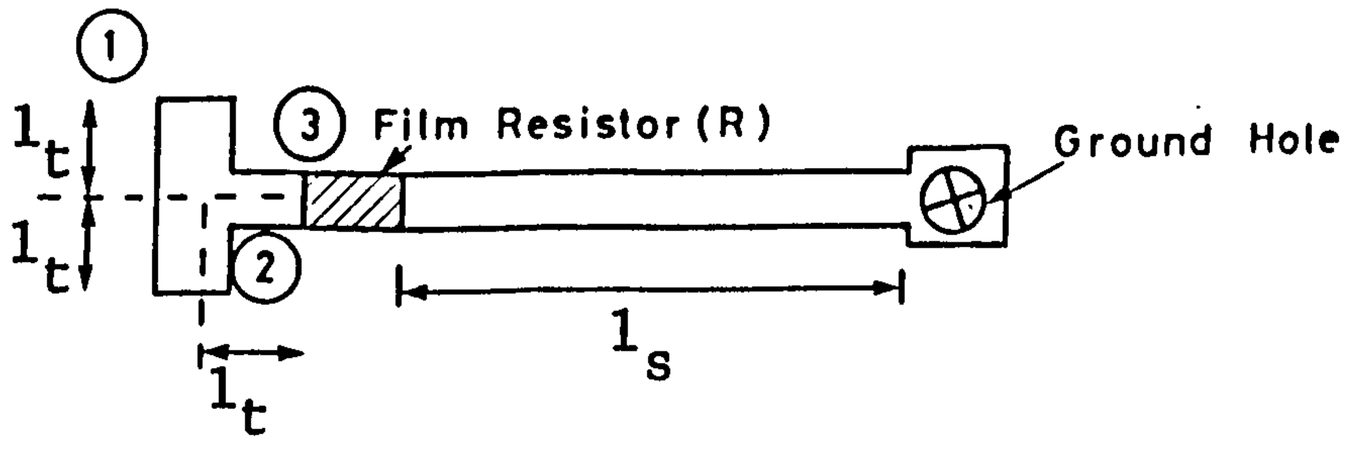

Figure 8.10 Typical microstrip layout of dissipative network of figure 8.9a.

The length of the T-junction arms, l_t, shown in figure 8.10 is representative only; the layout would be adjusted to accommodate discontinuity effects. With the effective length of all areas equal, the 3-port s-parameters of the junction are given by Woods [14] as:

$$[S]_{\{Zt\}} = e^{-2\gamma_t l_t} \begin{vmatrix} -1/3 & 2/3 & 2/3 \\ 2/3 & -1/3 & 2/3 \\ 2/3 & 2/3 & -1/3 \end{vmatrix} \qquad \langle 8.10 \rangle$$

where $\gamma_t = \alpha_t + j\beta_t$ = propagation constant of the tx. lines and Z_t the normalising impedance, equals the characteristic impedance of the tx. lines comprising the arms.

The 2-port s-parameters of the junction with the resistor and stub attached can be obtained by renormalising the s-parameter matrix of <8.10> to the impedance presented to port-3 Z_3, using the voltage wave transform of Appendix D:

$$[S]_{\{Zt\}} = \begin{vmatrix} (e^{-\gamma_t l_t}.r_3 - 1) & 2(e^{-\gamma_t l_t}.r_3 + 1) \\ (3e^{2\gamma_t l_t} + 1) & \\ & \\ 2(e^{\gamma_t l_t}.r_3 + 1) & (e^{-\gamma_t l_t}.r_3 - 1) \end{vmatrix} \qquad \langle 8.11 \rangle$$

where $r_3 = (Z_3 - Z_o)/(Z_3 + Z_o)$

If the normalising impedance of equations <8.7> and <8.8> is set equal to the T-junction line impedance (ie. Z_o+Z_t) then r_3 in <8.11> can be expressed in terms of the normalised network parameters, thus:

$$r_3 = [(r+z) + (z-1)e^{-2\gamma_s l_s}]/[(1+z) + (z-r)e^{-2\gamma_s l_s}] \qquad \langle 8.12 \rangle$$

S-parameters computed from <8.17> with <8.12> can be renormalised to any convenient impedance (say, 50 Ohms) differing from the T-junction line impedance, using the 2-port voltage-wave renormalising transforms (Appendix D).

From the expression of <8.6> the available/ordinary power gain frequency response were obtained for a matrix of values of r and z, with zero length T-junction and 50 Ohm normalising impedance. Figure 8.11

presents some typical curves. It was observed that the parameter z had a dominant effect on the linear slope bandwidth whilst r principally affected the slip magnitude.

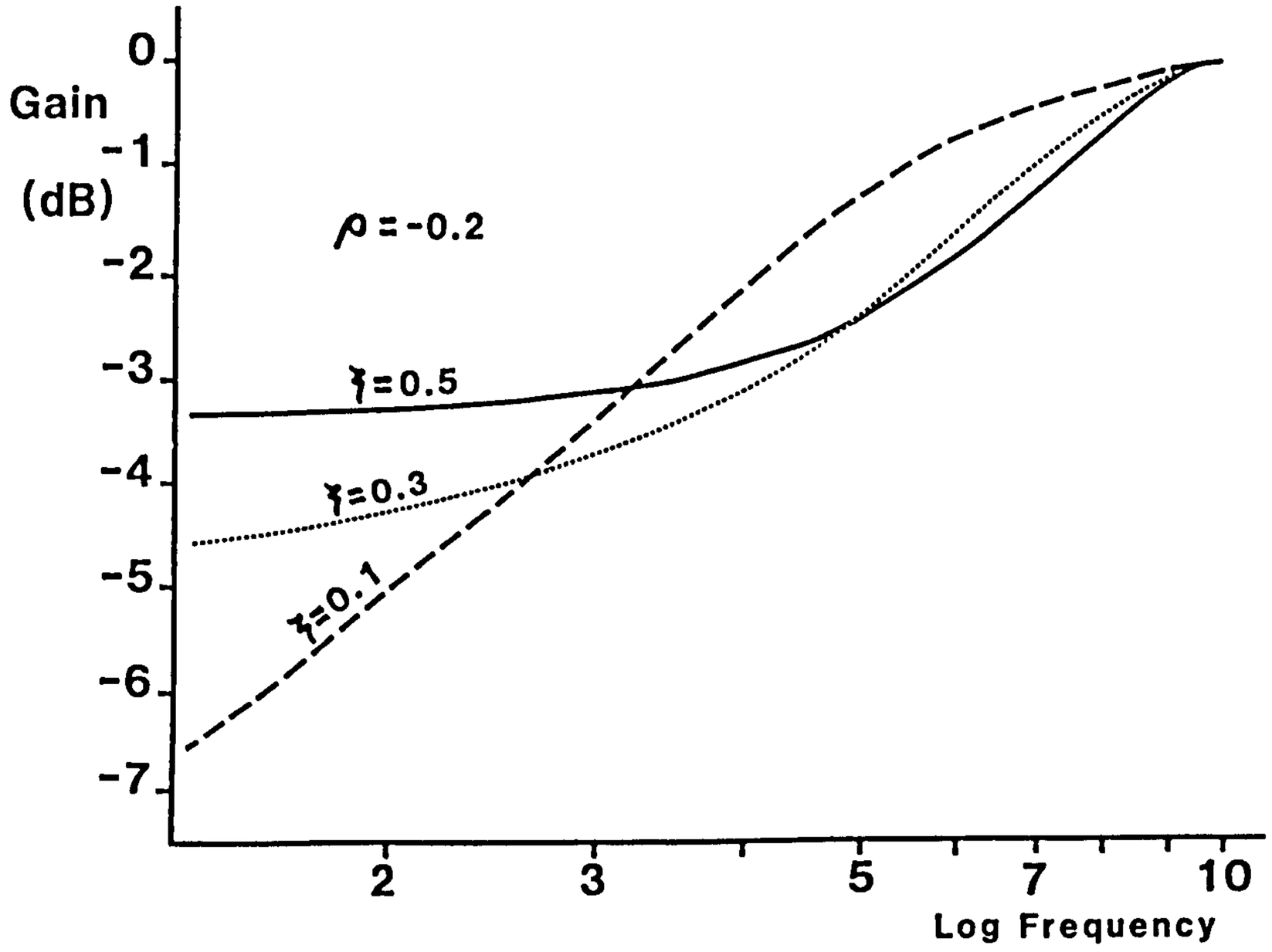

Figure 8.11 Typical available/ordinary power gain frequency responses of resistor/stub dissipative network

8.2.4 Synthesis of the Resistor-Stub Network

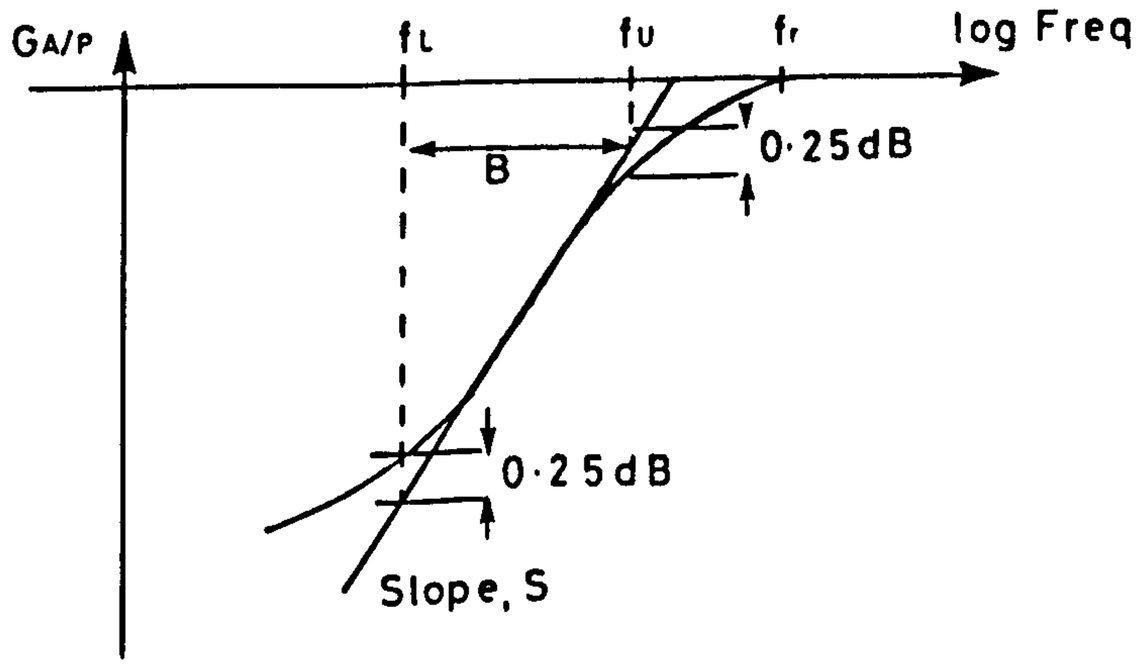

Figure 8.12 Definitions for the interpretation of available/operating power gain curves.

The available/operating power gain frequency response curves obtained for various values of the parameters z and r were quantitively assessed according to the definitions of figure 8.12, thus:

$$\text{Bandwidth} : B = f_U/f_L \qquad \langle 8.13 \rangle$$

$$\text{Slope} : S = dG/d(\log f) \qquad \langle 8.14 \rangle$$

$$\text{Frequency offset}: k = f_r/f_U \qquad \langle 8.15 \rangle$$

The results are plotted; r against slope, z and k against bandwidth in figures 8.23, 8.24 and 8.25 respectively*. Using simple regression curve fitting, empirical expressions for the network parameters; z and k, in terms of bandwidth and slope, were generated:

$$r = [0.838 - \ln(S)]/1.434 \qquad \langle 8.16 \rangle$$

$$z = \exp([1.28r - \ln(B)+0.17]/0.70) \qquad \langle 8.17 \rangle$$

$$k = 0.071B + 1.029 \qquad \langle 8.18a \rangle$$

(The latter expression has been modified subsequently for improved performance in the CAD program and now reads:

$$k = 0.035B + 1.1015 \qquad \langle 8.18b \rangle$$

These relationships may be used to find initial values for the network elements. But alone they are inadequate, primarily because the device port impedance to which they are connected is frequency dependent. The accuracy of initial values generated by <8.16> to <8.18> is improved by choosing the normalising impedance (Z_o in <8.7> to <8.9> as (the real part of) the device port immittance at the mid-band frequency, f_M. Further enhancement in the accuracy of determination of the element values for a specified gain slope requires the device port immittance at each frequency of interest to be taken into account. Complete analytic expression would be outrageously complex, so the following approach has been adopted.

Assuming the resonant frequency, f_r (i.e. length, l_s), is defined by the upper band edge of the required response (with a small offset, given

* Figures 8.23, 24, 25 are located on page 8.40

by k from <8.18b>), the mid-band and lower band edge gains can be expressed as functions of r and z;

$$G_M = F(r, z, f_M) \qquad \text{<8.19a>}$$

$$G_L = F(r, z, f_L) \qquad \text{<8.19b>}$$

respectively. Parameters r and z can then be determined by solving the pair of simultaneous equations. The available/ordinary power gains G_M, G_L can be computed from expression <8.5> with the device port reflection coefficient renormalised to the network normalising impedance, Z_o, or Z_t when a finite size T-junction is included (cf. Appendix F).

Because of the intractable nature of the expressions and the complex behaviour of the device port immittances, a standard non-linear equation solve routine was used to solve <8.19>. For this purpose the gains were expressed as deviations, thus:

$$\delta G_M = F(r,z,f_M) - G_U(f_U/f_L)^{-S/10\log 2} \qquad \text{<8.20a>}$$

$$\delta G_L = F(r,z,f_L) - G_U(f_U/f_L)^{-S/10\log 2} \qquad \text{<8.20b>}$$

where S, the gain slope, is expressed as db/oct and the upper band edge gain, G_U is close to unity. Using this approach resistor-stub networks, attached to either or both device ports, having specified gain clopes may be synthesized.

8.3.5 Alternative Networks

Only the shunt resistor-stub network has been discussed in detail. Its dual; the series resistor-stub network of figure 8.9b can be treated in a substantially identical manner but, for reasons discussed above, it has not been found useful to do so. Similar techniques can also be applied to the lumped element network equivalents of these distributed element structures shown in figures 8c and e. For modest degrees of gain slope only, the two element networks of figure 8.8 can be useful.

In practise, the shunt resistor-stub network is most appropriate but because of the device port immittance-network interactions that can sometimes be troublesome (cf. section 8.3.2.1), it has proved necessary to have an alternative available. For this purpose the simple series connected RLC combination (figure 8.7g) has been employed. The normalised network parameters used are:

$$g = Z_o/R \qquad \langle 8.21 \rangle$$

$$b = Z_o/(1/\omega_U C - \omega_U L) \qquad \langle 8.22 \rangle$$

where $\omega_U = 2\pi f_U$, the upper band-edge frequency

In an MIC amplifier the network will be inserted in a microstrip transmission line; as illustrated in the suggested configuration of figure 8.13.

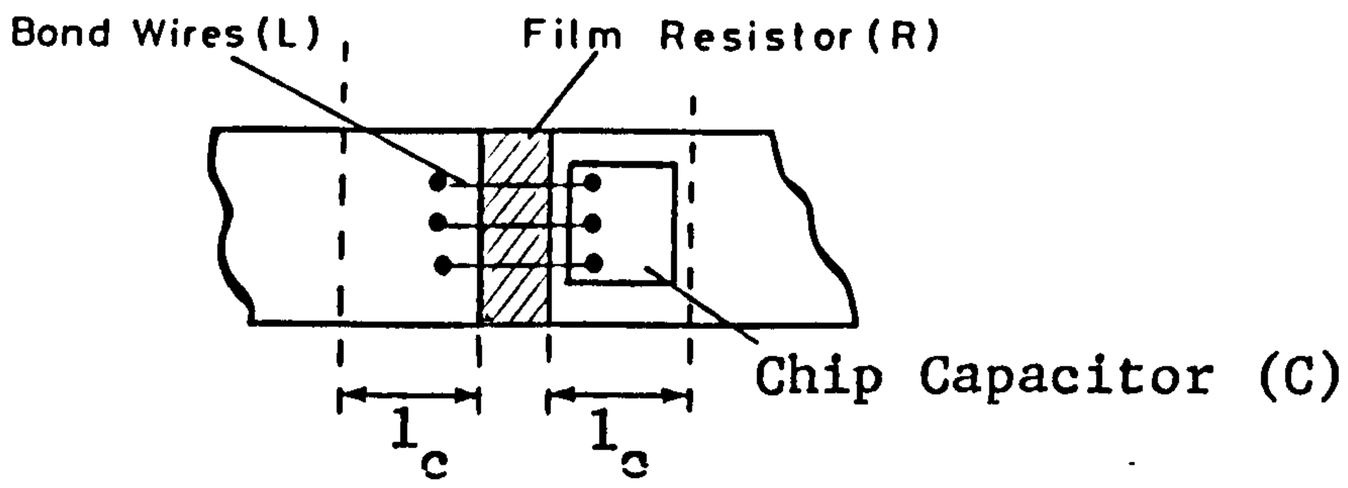

Figure 8.13 Typical MIC implementation of the series connected RLC network

It is convenient to make the normalising impedance Z_o, equal to the connecting line characteristic impedance, Z_c. Including a portion of the connecting line sufficient to attach the components, l_c, the s-parameter matrix of the network is:

$$[S]_{\{Z_c\}} = e^{-2\gamma l_c} \begin{bmatrix} z/(z+2) & 2/(z+2) \\ 2/(z+2) & z/(z+2) \end{bmatrix} \qquad \langle 8.23 \rangle$$

where $z = 1/(g + jb)$

If the inductance is small, such that the resonant frequency is much higher than the upper band edge this network degenerates to the series

connected parallel RC network of figure 8.8b. In either case synthesis can proceed as described in the previous section.

8.3.6 Review

In this section it has been shown how frequency dependent dissipative networks of specified gain slope can be synthesised. The gain measure has been chosen (the available/ordinary power gain) such that the gain slopes of the networks can be added to the slope of the device maximum available gain to produce the slope of the G_{Amax} of the composite "device". To obtain a composite "device" that has a flat frequency response when inserted between lossless matching network, it is simply necessary to synthesise dissipative network(s) having a (combined) gain slope numerically equal to the device G_{Amax} slope.

8.4 APPLICATION, RESULTS AND DISCUSSION

8.4.1 The Computer Program "DISSY"

A computer program, named "DISSY", has been developed. DISSY is an implementation of the approach to dissipative network design described in the foregoing section. A much simplified flow-chart is included below.

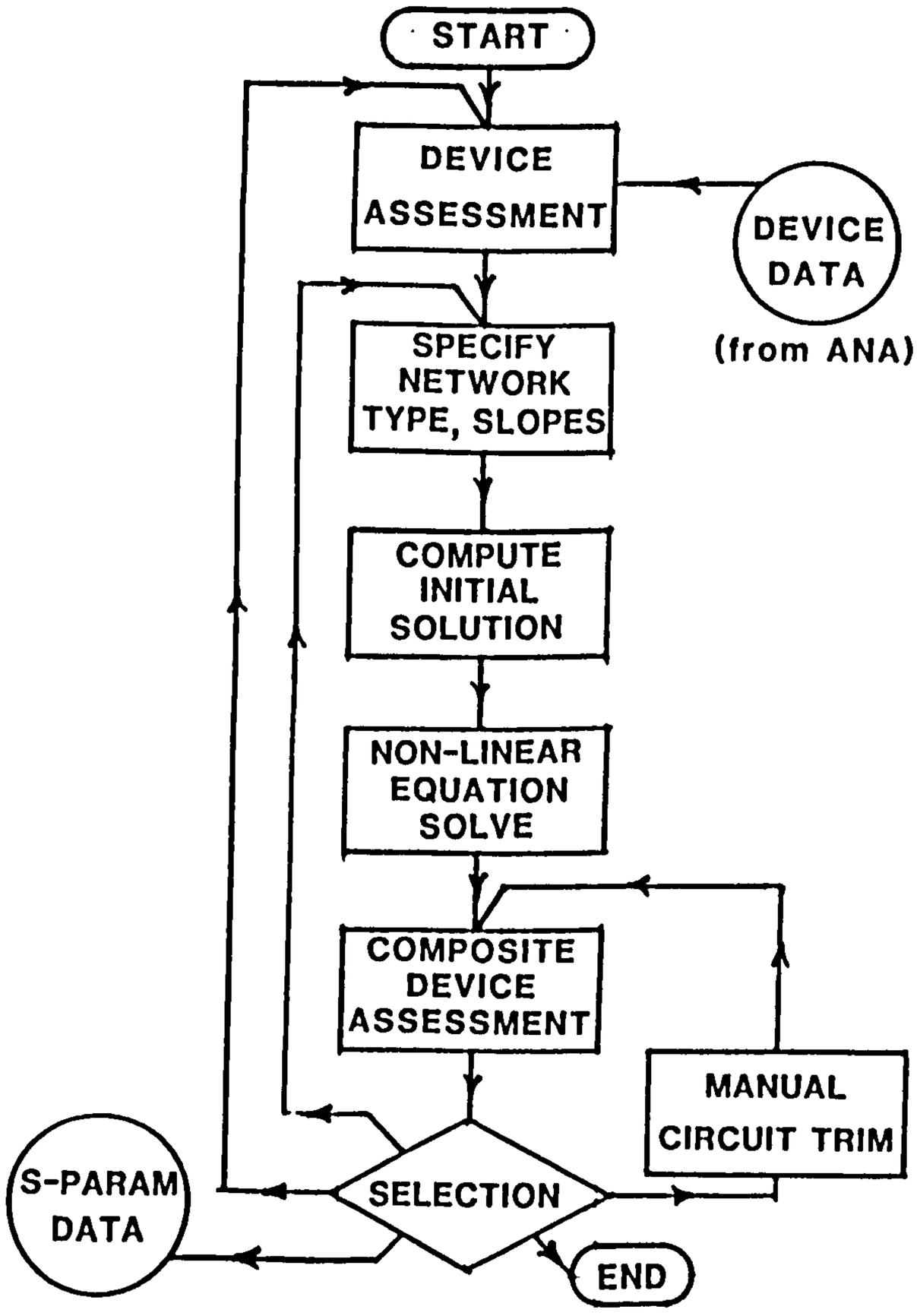

Figure 8.14 Flow-chart for program DISSY

DISSY has been designed to aid interaction between the design engineer and the program. Sensible default responses to most prompts are provided. Useful information relevant to the choices the designer must make is clearly presented. A module concerned with the assessment of device performance is used at the commencement of the program and again at its conclusion, where data related to the compensated "composite device" is presented. S-parameter data for up to 21 frequencies can be accommodated. Various stability factor, gain measures, simultaneous conjugate match conditions and gain slopes are tabulated.

To proceed with the design of a dissipative network(s) the user specifies network types, band-edge and mid-band frequencies, and gain slope(s). After computation of initial element values the non-linear equation solve routine is invoked; producing final element values that

take the device port characteristics into account. The sythesis procedure can be repeated with changes to any of the specifications. Connecting line (T-junction) details can be introduced at any stage.

A manual circuit trim facility allows any element value to be varied and the composite device re-assessed. An error function; being the r.m.s. sum of the deviations of G_{Amax} from the desired, frequency-independent value over the specified band, is computed on each occasion.

Finally an s-parameter data file, similar in format to that containing the device data and consistent with that used by measurement and circuit analysis software, describing the composite device is produced. A printed record of the interactive session can be produced and an example is presented in Appendix F, which also includes a technical description of DISSY. The outcome of a typical run of DISSY is illuustrated by the graph of figure 8.15. For the purpose of demonstration the device data used are the s-parameters of an FET together with a resistor chosen to make the device unconditionally stable. This allows the G_{Amax} of the device alone to be plotted across the frequency range shown. In practice, the dissipative networks would stabilise the FET except, possibly at lower frequencies. An RC network was used at the input with an R-stub network at the output of the device. The gain slopes were specified as for the middle composite device of the amplifier (cf. figure 8.4). The overall gain slope required across a 4 to 9GHz band was +2dB/octave a slope which the lower curve of figure 8.15 demonstrates admirably.

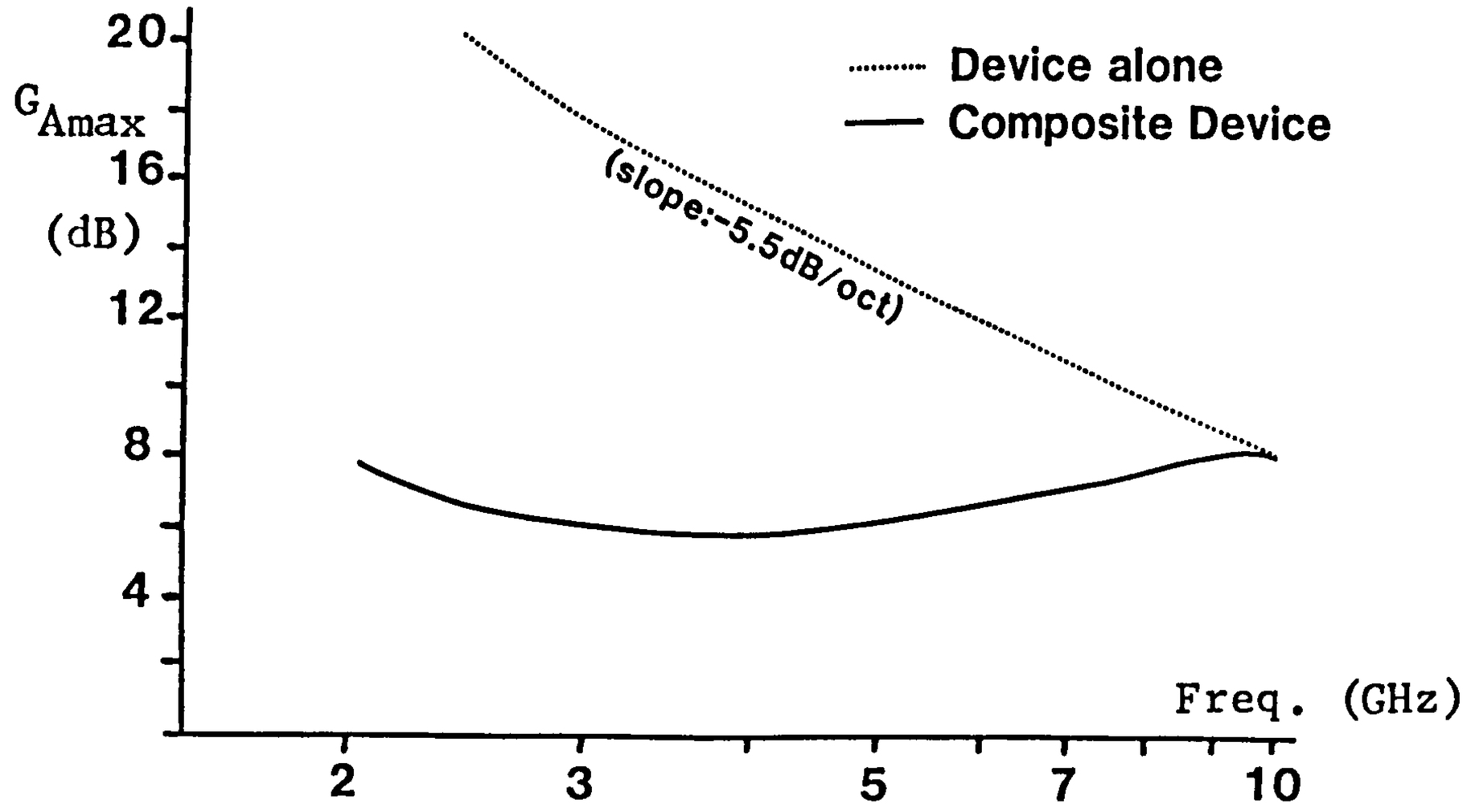

Figure 8.15 Sample results for a dissipatively compensated composite device designed using DISSY

8.4.2 The Prototype Amplifier

An amplifier, designed in accordance with the procedures described above, to the specification of figure 7.1, has been constructed. Three commercial stud packaged 1um gate length GaAs MESFETs (Plessey GAT4,P103) were used. Design was based on the measured results from 10 devices presented in chapter 6. Program DISSY was employed to facilitate design of the dissipative compensation networks according to the gain slope distribution of figure 8.4 Input, output and interstage matching networks were initially designed by lumped element network synthesis techniques (using a proprietary package) and converted to a mixed lumped-distributed realisation manually.

Discontinuities and parasitic effects were considered carefully and geometries adjusted accordingly. Finally, the design was trimmed using an optimisation program. Element value ranges were tightly constrained so as to preserve the prescribed gain distribution structure of the amplifier.

The circuit was fabricated by thin-film techniques on a high purity

alumina substrate. (Alumina was used in preference to sapphire for reasons of availability and ease of hole drilling). A tantalum-nitride layer was included so that photolithographically defined resistors could be used. Early attempts to design around chip resistors ultimately proved futile due to the gross parasitic reactance of such components. Conductors were formed by gold pattern plating on sputtered gold-chrome. Connections to the ground plane were made via holes, ultrasonically drilled prior to sputter coating. Subsequently clearance holes for the device packages were drilled and a metal block for securing the studs was soldered to the ground plae. Single layer chip capacitors were attached by use of solder preforms and connections were made by ultrasonic wire-bonding using multiple wires to reduce inductance in critical locations. The prototype amplifier is pictured in figure 8.16.

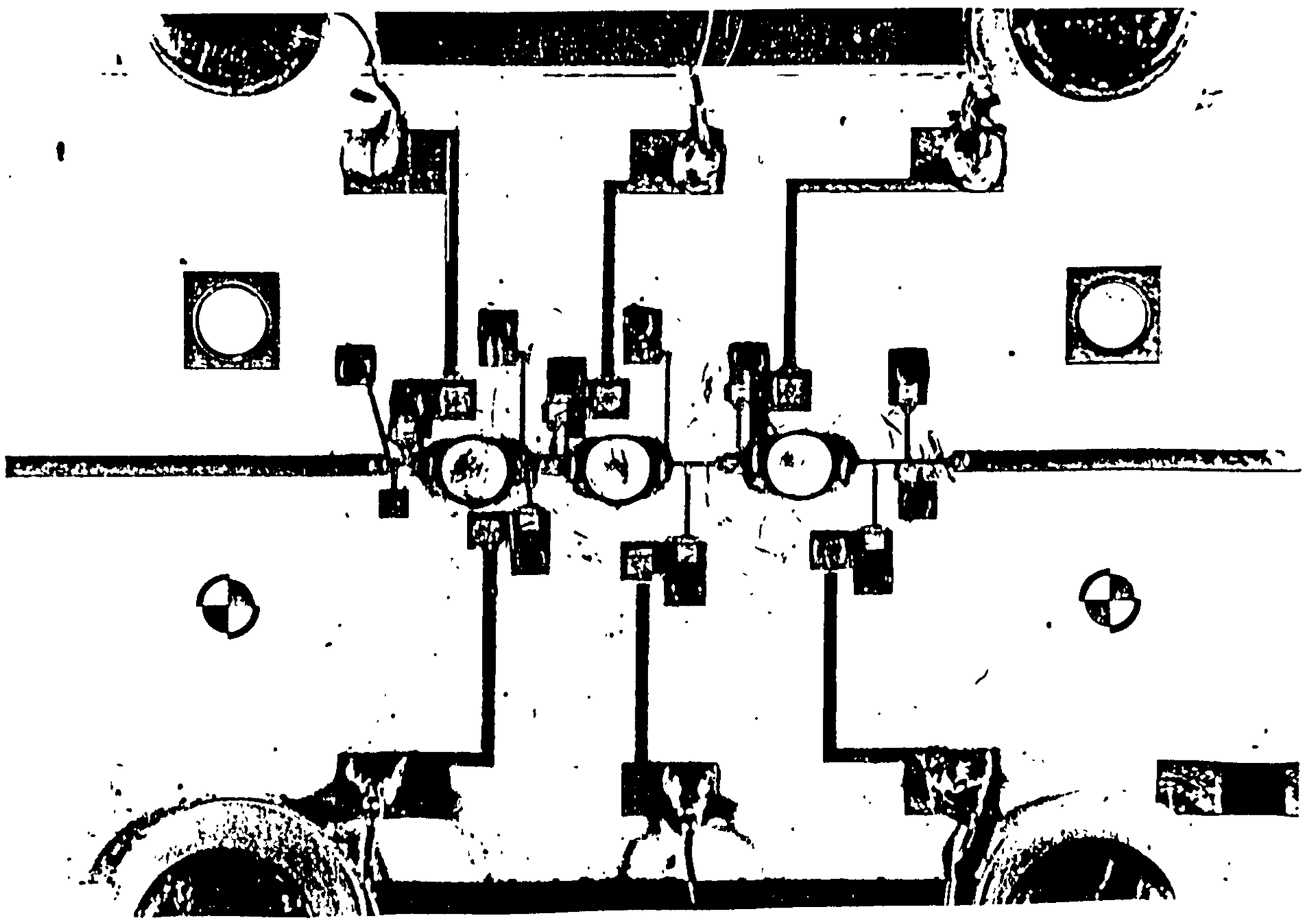

Figure 8.16 The prototype 4 to 9GHz amplifier

8.4.3 The Amplifier Performance

Figures 8.17 to 8.19 present the results of measurements, made using the CCNA, on the amplifier. Also plotted are the responses predicted by computer analysis of the circuit. The computed results were based on the average s-parameters, not the actual s-parameters of the devices fitted to the amplifier. Changing devices in the amplifier caused insignificant variation in the responses other than FET transconductance related charge in absolute gain. No adjustment or trimming of the circuit was done.

The original specification required only +11dBm output power and the FET was selected accordingly. After the design was completed it became desirable to increase the power output requirements to +17dBm (50mW). A variant of the FET type (GAT4-021) having a maximum power output capability of 100mW was substituted in the amplifier. No changes or adjustments were made to the circuit. Figure 8.19(b) shows the effect on both the computed and measured responses. The graph of figure 8.20 presents the results of 1dB compressed power output measurements using both transistor types

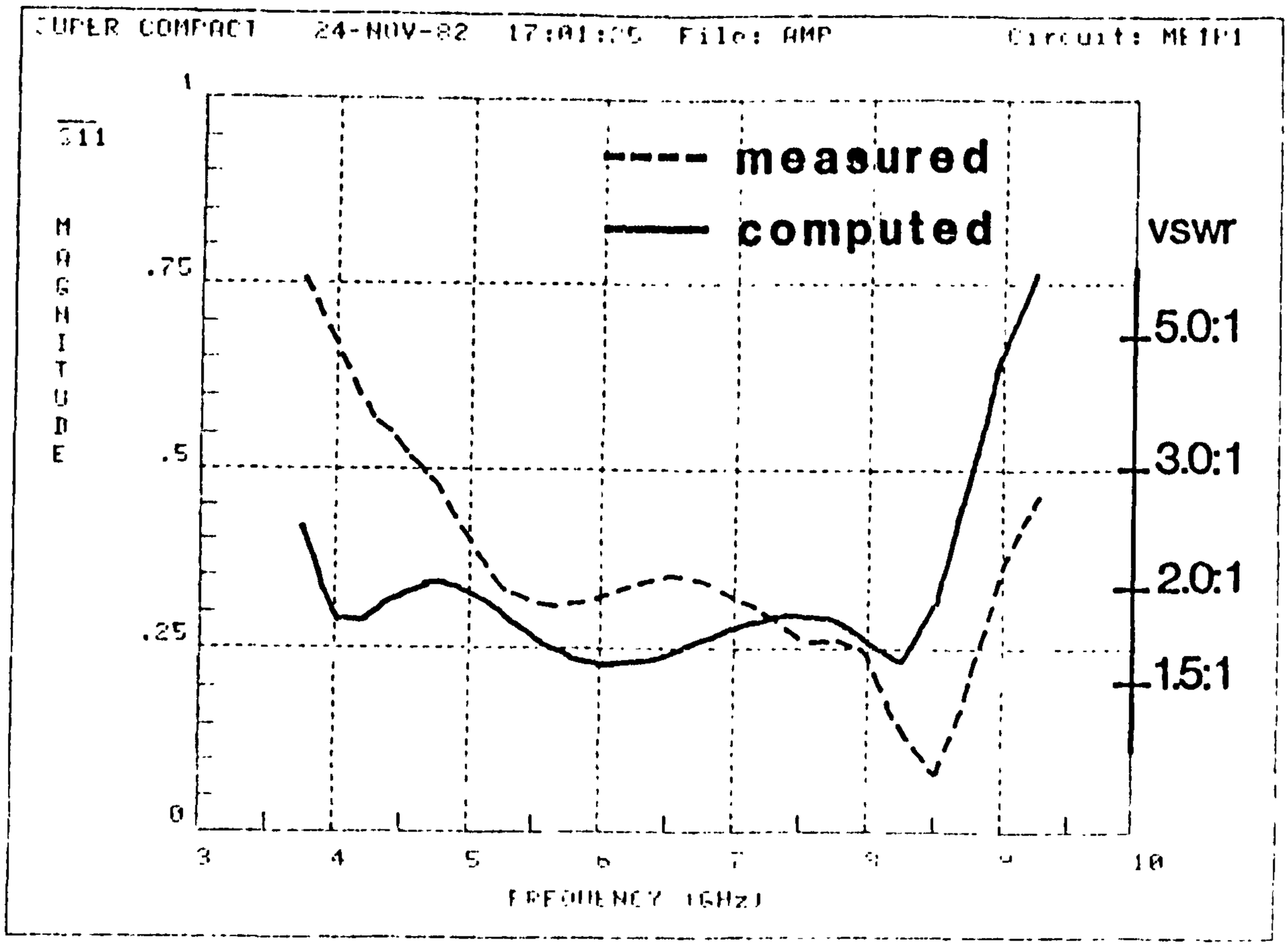

(a)

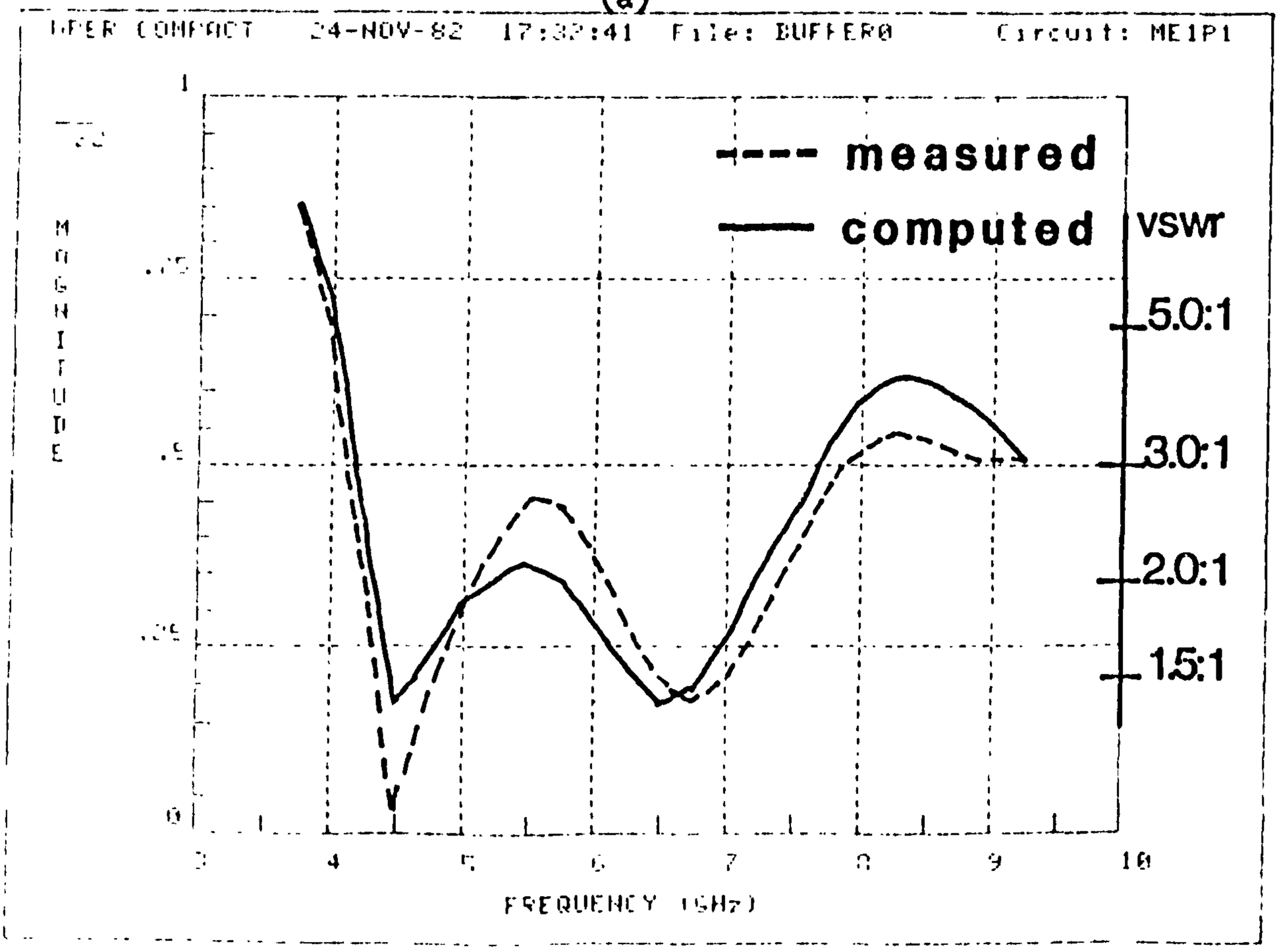

(b)

Figure 8.17 Input (a) and output (b) match

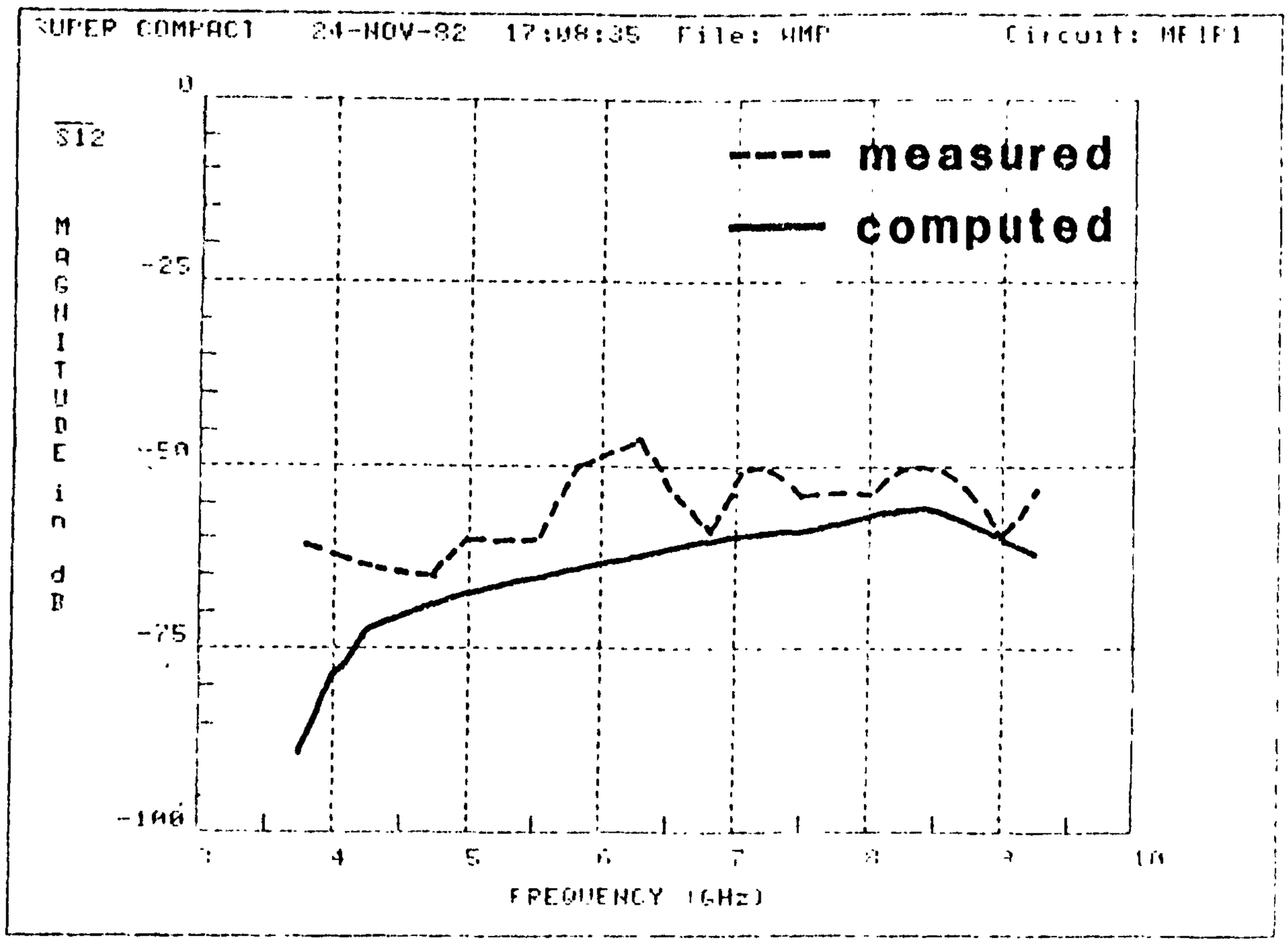

(a)

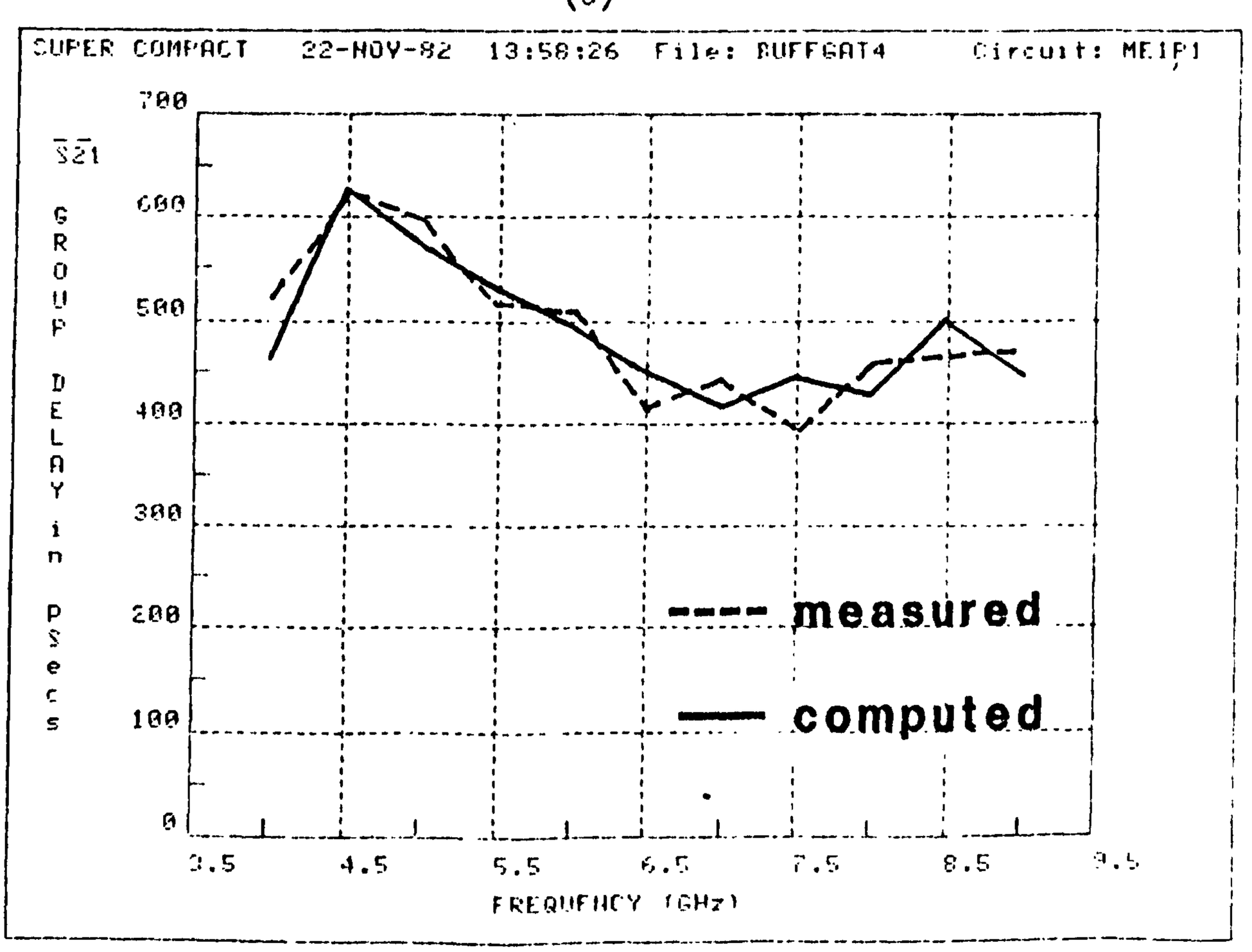

(b)

Figure 8.18 Reverse isolation (a) and group delay (b)

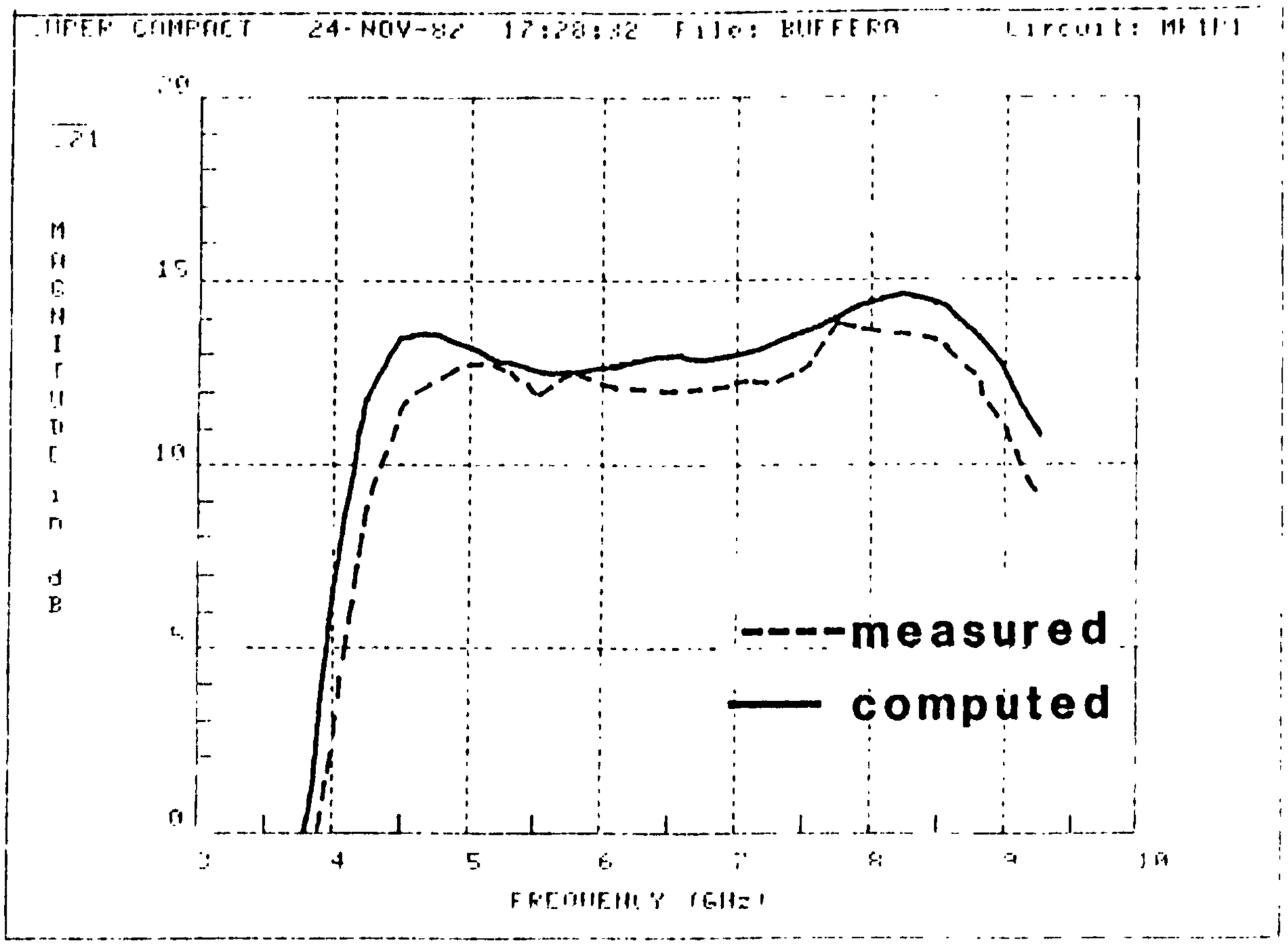

(a)

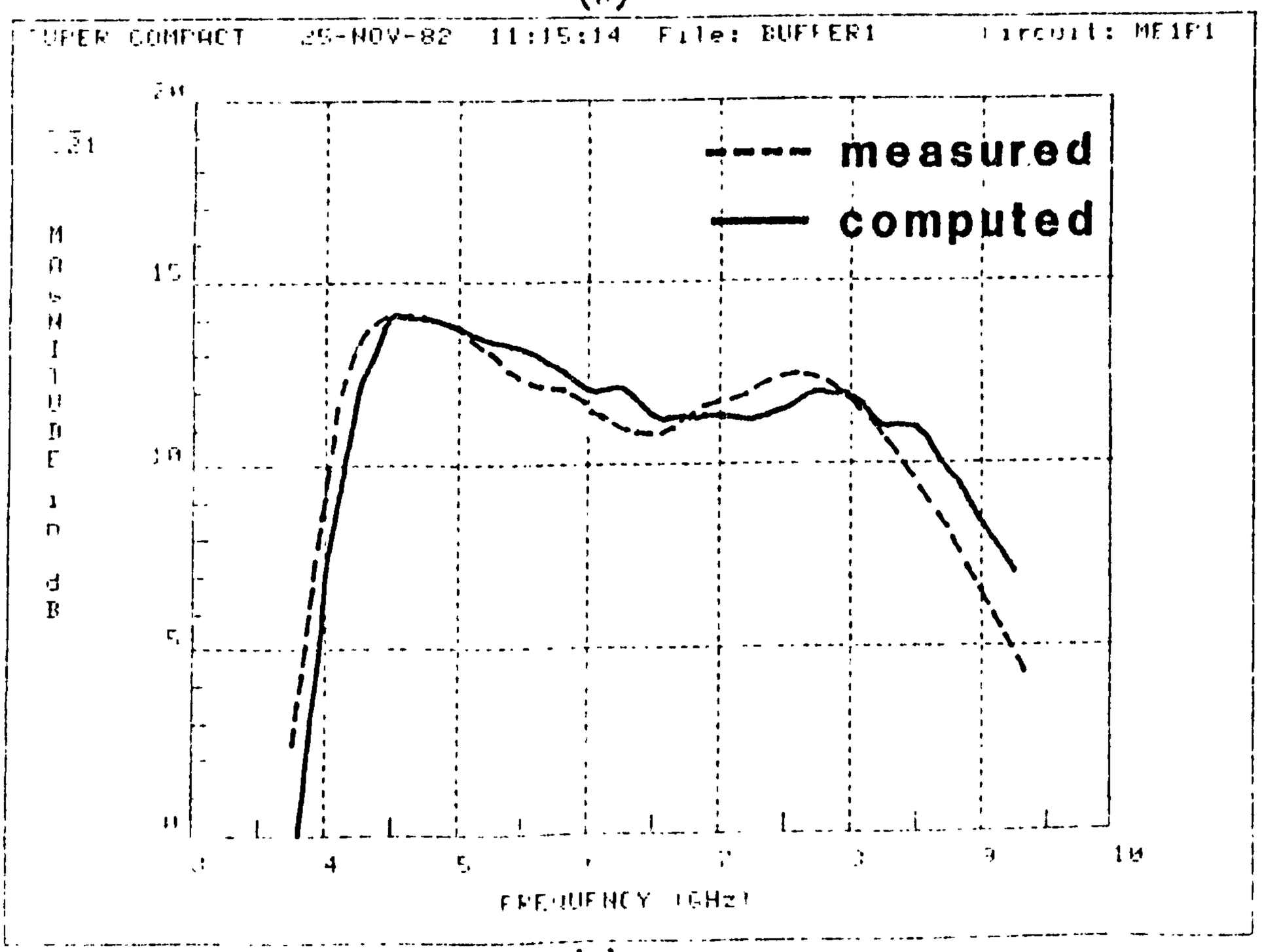

(b)

Figure 8.19 Forward small-signal gain with

(a) original GAT4 transistor and

(b) higher power GAT4-021 transistor

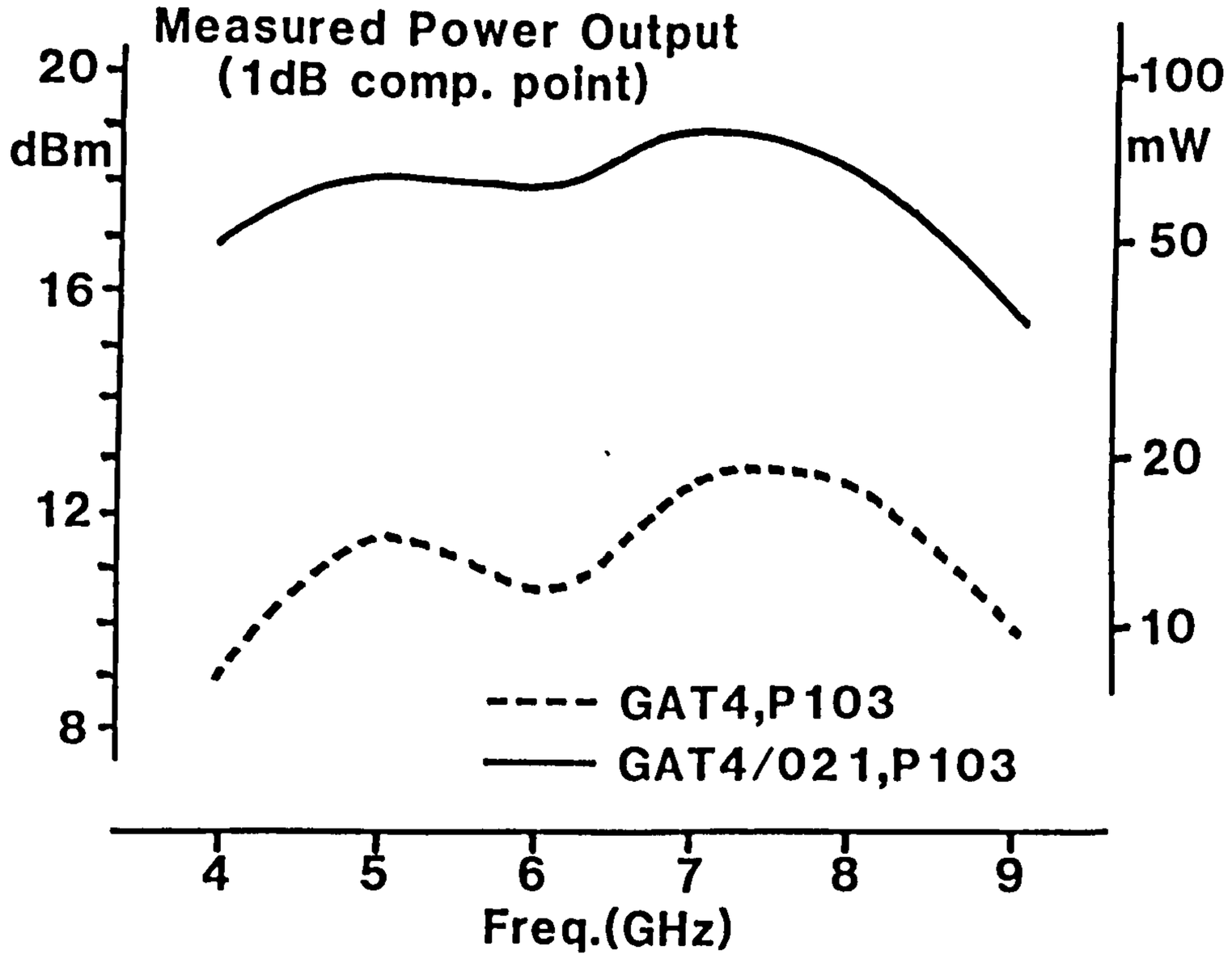

Figure 8.20 Output power measurements

Noise figure has been measured at two spot frequencies with the following results:

Noise Figure: @ 7.0 GHz : 7.6dB
@ 9.0 GHz : 7.4dB (single-sideband)

8.4.4 Discussion of Results

In most respects the amplifier meets the target specification. The output match is rather poorer than desirable towards the top end of the band but the agreement between measured and computed results is good. In fact, there are no major discrepancies between any measured and computed responses. The measurements of reverse isolation were corrupted by spurious crosstalk in the unenclosed measurement fixture; the peak at 6GHz is affected by any objects placed nearby!

The group delay response shows only modest variation across the band and conforms well with the model. The small variation of the gain responses with change of transistor type is indicative of the low sensitivity of the design to device parameter variations. The good

general agreement with the computer model, achieved without any circuit trimming, demonstrates both the low susceptibility to circuit tolerances of the dissipatively compensated amplifier and the benefits of careful design based on accurate measurements.

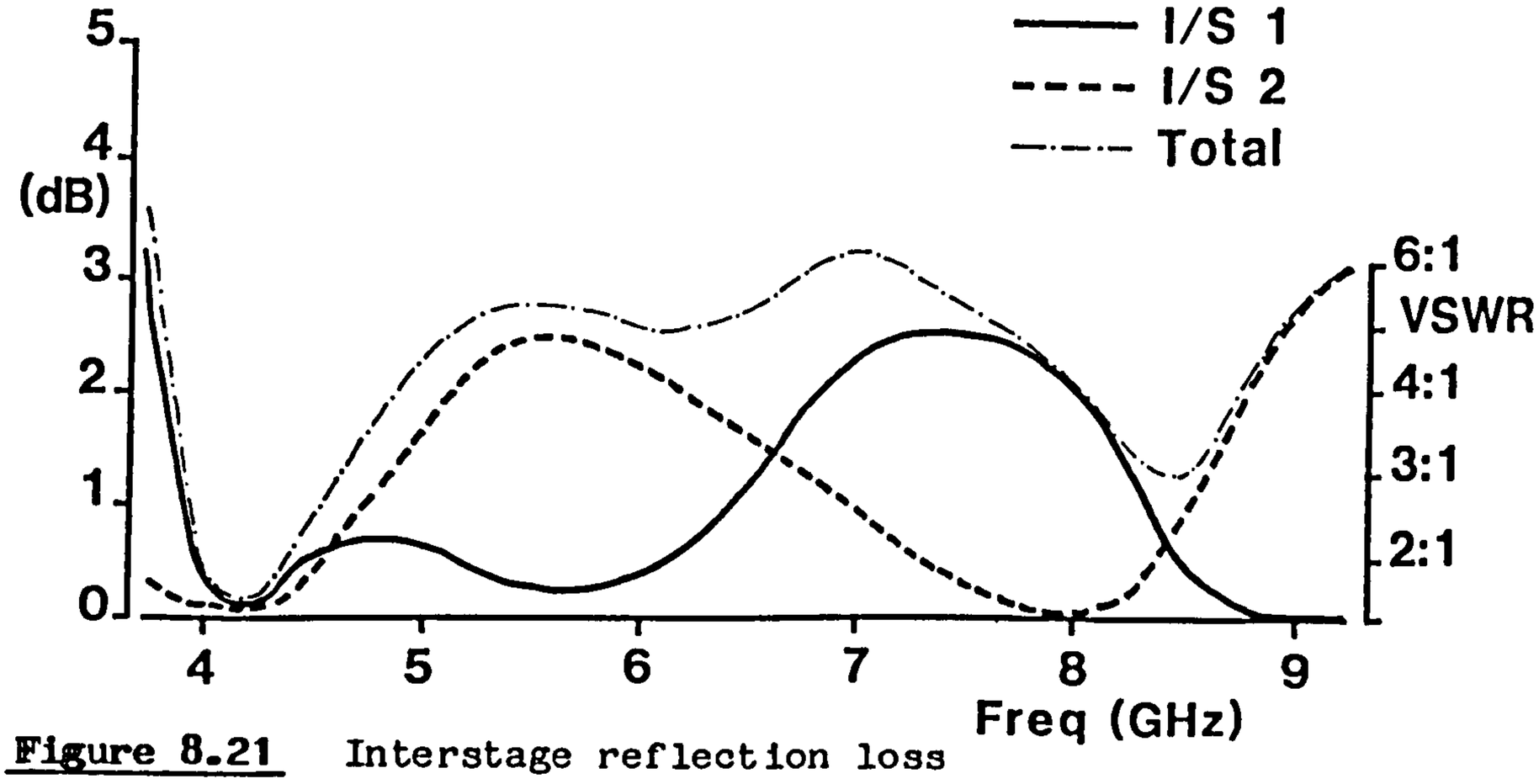

Figure 8.21 Interstage reflection loss

Figure 8.21 plots the reflection loss of both interstage networks computed from the model. This indicates the extent to which the reactive networks influence the response of the amplifier by mismatch effects. If the dissipative compensation functioned ideally no gain loss by mismatch would be necessary. But since the networks are simple and defined by a small number of parameters it is inevitable that fine tuning by the matching networks would be required. Note how the general characteristic is almost perfectly compensated by the dissipative networks; there being minima of total reflection loss at the extremes of the band. In fact, the slight over-compensation suggests that the overall gain could be increased by about 1.5dB. The reactive interstage networks have been adjusted by the optimisation package to offset errors in the mid-band gain. Nevetheless, when compared with total of ~18dB reflection loss that would be required to compensate a conventional octave band microwave amplifier of 3-stages, these results show a marked improvement. The worst case interstage VSWR of 5:1 contrasts with 30:1 for the reactively

compensated design.

Power output characteristics are free from the effects of penultimate stage limitations, again confirming that the proposed gain breakdown originally defined at the outset has been preserved through the design process. Noise figure is not impressive, but is much as expected since no attempt to optimise the noise performance has been made and a dissipative network has been included in the input stage. There is no evident reason why dissipative compensating networks should be used in low noise or high power designs providing they are introduced intelligently to the structure of the amplifier. The advantages of dissipative compensation in microwave amplifier design are ennumerated below.

BENEFITS of DISSIPATIVE GAIN COMPENSATION

- IMPROVES DESIGN ACCURACY
- EASES GAIN-BANDWIDTH LIMITATIONS
- ENSURES OUT-OF-BAND STABILITY
- INCREASES REVERSE ISOLATION
- REDUCES UNPREDICTABLE LOSSES
- MODERATES THE EFFECT OF VARIATIONS & TOLERANCES
- REDUCES GROUP DELAY VARIATIONS
- ELIMINATES DEMANDING CIRCUIT GEOMETRIES
- PHYSICALLY COMPACT
- APPLICABLE TO PACKAGED DEVICES
- SINGLE-STAGE BROAD-BAND AMPS ARE POSSIBLE

Finally, not only have the benefits of replacing reactive compensation with dissipative been clearly demonstrated, but also a coherent systematic and efficient methodology for the structured design of broad-band microwave amplifiers has been presented.

8.5 REFERENCES

[1] MARSHALL, N.: "Optimizing multi-stage amplifier for low-noise", Microwaves, April 1974, pp.62-4.

[2] ---------- : "Optimizing Multi-stage amplifiers for linearity", Microwaves, May 1974, pp .60-4.

[3] ULRICH, E.: "Use of negative feedback to slash wideband VSWR", Microwaves, October 1978, pp.66-70.

[4] NICLAS, K.B., WILSER, W.T., GOLD, R.B. & HITCHENS, W.R.: "The matched feedback amplifier: Ultrawide-band microwave amplification with GaAs MESFETs", IEEE Trans. MTT-28, 1980, pp.285-94.

[5] HSIEH, CC.C. & CHAN, S.P.: "Design of a 1.3-1.7GHz thin-film hybrid amplifier with optimum performance at low cost", Proc. of 8th ASIMOLAR Conference on Circuits, Systems and Computers.

[6] SALMON, S.K.: "A 1.1 to 2.4GHz transistor amplifier with low noise and good power match", IERE Rad. & Electron. Eng., Vol.49, 1979, pp.141-4.

[7] STURZU, P.: "Build a 12 octave hybrid amplifier", Microwaves, June 1974, pp.54-7

[8] KROWNE, C.M.: "Extending the low frequency range of GaAs FET broadband microwave amplifiers using microstrip transmission lines", IEE Electron. Lett., Vol.15, 1979, pp.197-8.

[9] HORNBUCKLE, D.P. & KUHLMAN, L.J.: "Broad-band medium-power amplification in the 2-12.4GHz range with GaAs MESFETs", IEEE Trans. MTT-24, 1976, pp.338-422.

[10] KRAMER, B., PARISOT, M. & COLLET, A.: "Modular construction of low-noise multi-stage FET amplifiers", IERE Rad. & Electron. Eng., Vol.48, 1978, pp.23-8.

[11] TIRTOPRODJO, S. & VAN BEERS, P.: "Multiple canonic RLC Ladder synthesis of biquadratic immittance functions with double poles and complex zeros", IEE Electron. Lett., Vol.14, 1978, pp.607-8.

[12] TEMPLE, G.J. & DAWE, C.: "Design & realisation of low-cost broadband amplifiers", IEE Colloquium on "The Design of RF Instruments", London, 21/11/1980, Digest No.: 1980/68.

[13] HOSSEINI, N.M. & SHURMER, H.V.: "Computer-aided design of microwave integrated circuits", IERE Rad. & Electron. Eng., Vol.48, 1978, pp.85-8.

[14] WOODS, D.: "Application of 3-port coaxial junction to RF immittance standardisation & measurements", Proc. IEE, Vol.119, 1972, pp.261-8.

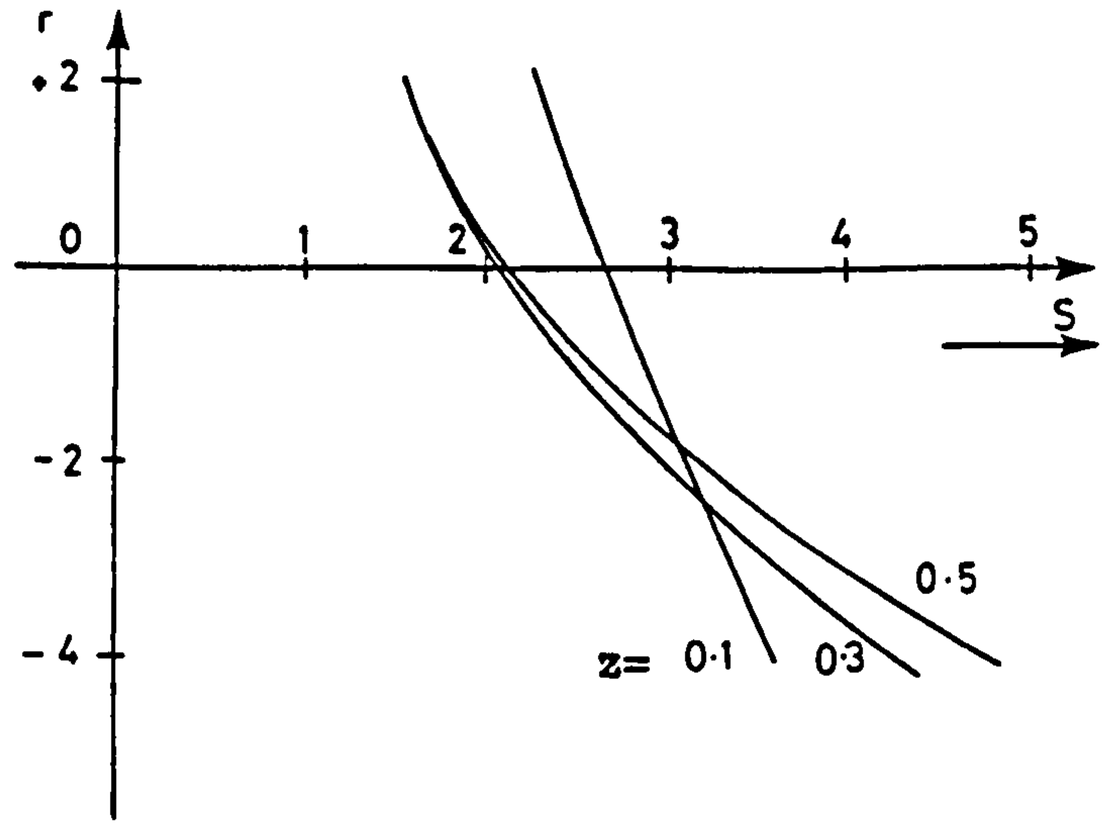

Figure 8.23 Normalised Stub Impedance, r, versus Gain Slope, S(dB), with z as a parameter, for Resistor-Stub network

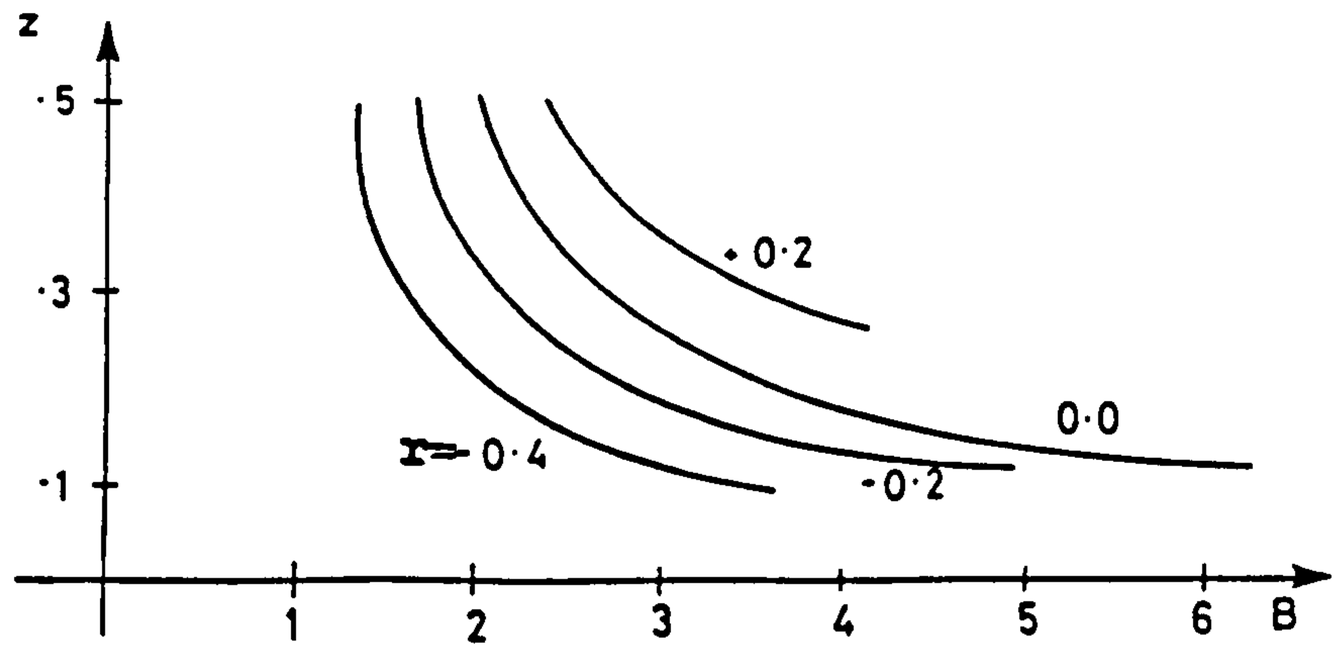

Figure 8.24 Normalised Resistor value, z, versus Bandwidth, B, with r as a parameter, for Resistor-Stub network

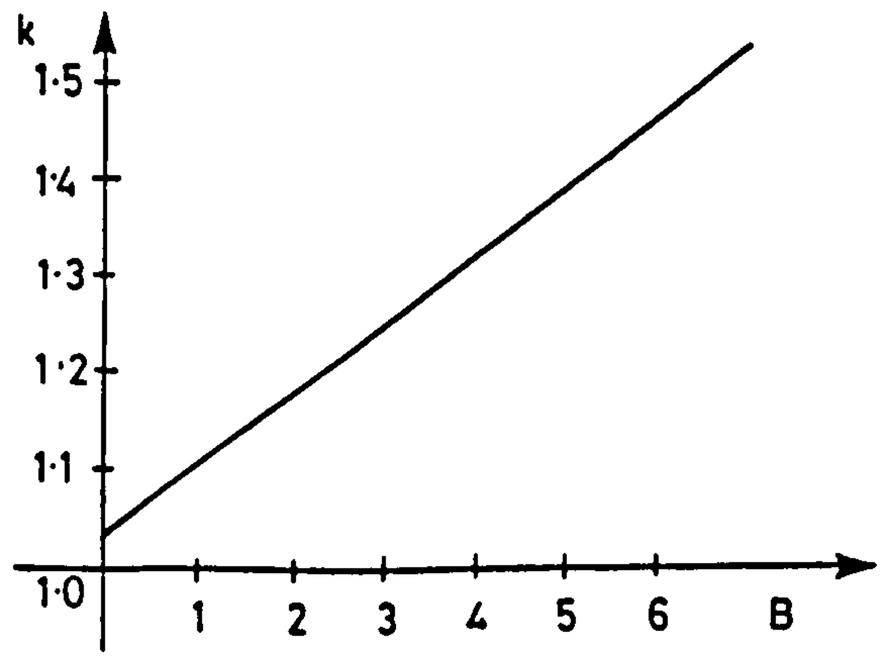

Figure 8.25 Upper Frequency Offset, k, versus Bandwidth, B, for Resistor-Stub network

A P P E N D I X A

A N I S O T R O P I C M I C R O S T R I P

C A L C U L A T I O N P R O G R A M

" G R E E N "

A. PROGRAM GREEN

A.1 Purpose Calculate capacitance, characteristic impedance and velocity of propagation of microstrip on an anisotropic substrate.

A.2 Method Calculates Green's function and solves Fredholm integral equation by the moment method.

A.3 Language Fortran IV+

A.4 Machine DEC PDP 11 and VAX 11 series (original version for Xerox Sigma 5) under IAS or VMS operating system

A.5 Input Data Free format file

each record: <NSEC,H,W,EN,ET>

NSEC: No. of sub-strips

H: Substrate thickness

W: Strip width

EN: Dielectric constant normal to substrate surface

ET: Dielectric constant tangential to substrate surface

A.6 Output Typical result file

ANISOTROPIC MICROSTRIP IMPEDANCE & VELOCITY PROGRAM BY SZENLUTI TRANSFORM
C J TEMPLE (U.M.H) 13-9-77

RATIO OF W/H	CHARACTERISTIC IMPEDANCE(OHMS)	LINE CAPACITANCE (F/M)	EFFECTIVE DIELECTRIC CONSTANT	PROPAGATION VELOCITY (1.0E8 M/S)	NORM ER	TANG ER	FRINGE CAPACITANCE
0.219	54.34	0.102E-09	6.639	1.1636	11.6	9.4	0.399E-10
0.278	78.06	0.111E-09	6.713	1.1571	11.6	9.4	0.411E-10
0.331	73.71	0.118E-09	6.774	1.1518	11.6	9.4	0.419E-10
0.672	56.23	0.178E-09	7.111	1.1243	11.6	9.4	0.446E-10
1.142	43.50	0.208E-09	7.460	1.0962	11.6	9.4	0.454E-10
2.099	23.61	0.417E-09	8.501	1.0282	11.6	9.4	0.468E-10
3.333	15.68	0.343E-09	9.136	0.9918	11.6	9.4	0.477E-10
1.222	34.02	0.259E-09	7.799	1.0736	11.6	9.4	0.460E-10
1.033	19.38	0.311E-09	8.617	1.0097	11.6	9.4	0.472E-10
[illegible]	58.79	0.144E-09	6.465	1.1791	9.4	11.6	0.439E-10
[illegible]	30.49	0.226E-09	6.632	1.1470	9.4	11.6	0.437E-10
[illegible]	[illegible]	0.357E-09	7.686	1.0812	9.4	11.6	0.476E-10

A P P E N D I X B

C A L C U L A T O R P R O G R A M F O R C O M P U T A T I O N

O F T R U E R E S O N A N T F R E Q U E N C Y

B. CALCULATOR PROGRAM FOR COMPUTATION OF TRUE RESONANT FREQUENCY

This program implements the algorithm described in chapter 3 for the computation of the true or unperturbed resonant frequency of a short circuit, half-wavelength transmission line resonator given measurements of apparent resonant frequencies and minimum return loss for two values of coupling capacitance. The relevant equations are summarised here:

$$k_1 = (1 - \check{\rho}_1)/(1 + \check{\rho}_1) \qquad \text{<B.1>}$$

$$k_2 = (1 - \check{\rho}_2)/(1 + \check{\rho}_2) \qquad \text{<B.2>}$$

$$A = (f_2 - f_1)/(f_1\sqrt{k_1} - f_2\sqrt{k_2}) \qquad \text{<B.3>}$$

$$f_o = f_2\,(1 + \sqrt{Ak_2}) \qquad \text{<B.4>}$$

$$\alpha = K.A/Z_o \qquad \text{<B.5>}$$

$$\text{where } K = 8.6859.n^2R_L/21 \qquad \text{<B.6>}$$

B.1 Machine

Programmable pocket calculator

Commodore (CBM) PR100

B.2 Input Data

From measurements with first value of coupling capacitor:

f_1 - apparent resonant frequency (GHz)

$\check{\rho}_1$ - minimum reflection coefficient (at f_1)

From measurements with second value of coupling capacitor:

f_2 - apparent resonant frequency (GHz)

$\check{\rho}_2$ - minimum reflection coefficient (at f_2)

Also:

Z_o - nominal characteristic impedance of resonant line (ohms)

K - constant for computation of line loss given by <B.6>

where the required parameters are:

l - half length of resonant line

R_L - nominal source/load impedance of reflectometer

B.3 Output Data

B.3.1 Displayed

α - transmission line loss (dB/m)

f_o - true resonant frequency (GHz)

B.3.1 In Memory

A - value of A from <B.3>

k_2 - coupling factor for second measurement

B.4 Memory Allocation

Memory	Variable
M_0	$Z_o(A)$
M_1	f_1
M_2	ρ_1
M_3	f_2
M_4	ρ_2
M_5	K
M_6	-
M_7	-
M_8	-
M_9	κ_2

B.5 Program Listing

Address	Key	Code	Symbol	Notes
00	MR	52		Compute A
01	3	83	f_2	
02	-	85		
03	MR	52		
04	1	81	f_1	
05	÷	75		Numerator of <B.2>
06	(	64		
07	(	64		
08	1	81		
09	-	85		
10	MR	52		
11	2	82	$\check{\rho}_1$	
12	÷	75		
13	(	64		
14	1	81		
15	+	84		
16	MR	52		
17	2	82	$\check{\rho}_1$	
18	)	65		
19	)	65	k_1	From <B.1>
20	√	35		
21	*	74		
22	MR	52		
23	1	81	f_1	
24	-	85		

Address	Key	Code	Symbol	Notes
25	(	64		
26	(	64		
27	1	81		
28	-	85		
29	MR	52		
30	4	71	$\check{\rho}_2$	
31	÷	75		
32	(	64		
33	1	81		
34	+	84		
35	MR	52		
36	4	71	$\check{\rho}_2$	
37	)	65		
38	)	65	k_2	From <B.2>
39	M	51		
40	9	63		Save k_2
41	√	35		
42	*	74		
43	MR	52		
44	3	83	f_2	
45	=	95	$\sqrt{A}$	
46	*	74		
47	=	95	A	From <B.2>
48	÷	75		Compute α
49	F	21		
50	M<->X	55		Swap A for Z_o

Address	Key	Code	Symbol	Notes
51	0	91	Z_o	
52	*	74		
53	MR	52		
54	5	72	K	From <B.6>
55	=	95	α	Display attn (dB/m)
56	R/S	13		Hit R/S to continue
57	MR	52		Compute f_o
58	3	83	f_2	
59	*	74		
60	(	64		
61	1	81		
62	+	84		
63	(	64		
64	MR	52		
65	0	91	A	
66	*	74		
67	MR	52		
68	9	63	k_2	
69	)	65		
70	$\sqrt{}$	35		
71	=	95	f_o	Display true resonant frequency
-	-	-		End (of memory)

A P P E N D I X C

M I C R O S T R I P O P E N E N D E F F E C T

C O M P U T A T I O N P R O G R A M

" E N D E F F E C T "

C. MICROSTRIP OPEN END EFFECT COMPUTATION PROGRAM "ENDEFFECT"

C.1 Purpose Calculate Microstrip open circuit end effect capacitance and equivalent line extention.

C.2 Method Calculated from polynomial expression with coefficients given for 6 discrete values of substrate permittivity, after Silvester and Benedek (Chapter 4, Reference [2]). Microstrip capacitance per unit length is computed by the curve fitted expression of Schneider (Chapter 2, Reference [12]).

C.3 Language Fortran IV+

C.4 Machine DEC PDP 11 and VAX 11 series under IAS or VMS operating systems, respectively. (Original version for Burroughs 6700 under CANDE interactive system.)

C.5 Input Data Interactive entry in free format

ERI: Substrate permittivity (desired)

H : Substrate thickness

WOH: Width to height ratio

(0 permits new ERI & H to be entered)

(-ve terminates session)

C.6 Output Data Displayed on terminal VDU (option session log file generated, name: RESULT.DAT)

ERI : Substrate permittivity (actual)

WOH : Width to height ratio

CAP : End effect capacitance (pF)

CAPL : Uniform line capacitance/unit length (pF/M)

DELTA: Equivalent end extention (MM)

C.7 Typical Interactive Session

```
$ ru end
  END EFFECT PROGRAM (SILVESTER & BENEDEK METHOD)
TYPE YES TO WRITE RESULTS :y
ENTER ER & H :2.3,.5
NO COEFFICIENTS FOR THIS DIELECTRIC; USE  1.0  2.5  4.2  9.6 16.0 51.0
RE-ENTER EF :2.5
ENTER W/H (0 TO ENTER NEW ER & H,-VE TO STOP) :0.1
 DIELECTRIC      WIDTH/     END EFFECT    LINE CAP    END LENGTH
   CONST         HEIGHT        (PF)        (PF/M)        (MM)
    2.50          0.10      0.00251       23.15         0.108

ENTER W/H (0 TO ENTER NEW ER & H,-VE TO STOP) :0.2
 DIELECTRIC      WIDTH/     END EFFECT    LINE CAP    END LENGTH
   CONST         HEIGHT        (PF)        (PF/M)        (MM)
    2.50          0.20      0.00360       27.95         0.129

ENTER W/H (0 TO ENTER NEW ER & H,-VE TO STOP) :0.5
 DIELECTRIC      WIDTH/     END EFFECT    LINE CAP    END LENGTH
   CONST         HEIGHT        (PF)        (PF/M)        (MM)
    2.50          0.50      0.00617       38.26         0.161

ENTER W/H (0 TO ENTER NEW ER & H,-VE TO STOP) :1.0
 DIELECTRIC      WIDTH/     END EFFECT    LINE CAP    END LENGTH
   CONST         HEIGHT        (PF)        (PF/M)        (MM)
    2.50          1.00      0.00986       52.06         0.189

ENTER W/H (0 TO ENTER NEW ER & H,-VE TO STOP) :2.0
 DIELECTRIC      WIDTH/     END EFFECT    LINE CAP    END LENGTH
   CONST         HEIGHT        (PF)        (PF/M)        (MM)
    2.50          2.00      0.01667       76.69         0.217

ENTER W/H (0 TO ENTER NEW ER & H,-VE TO STOP) :5.0
 DIELECTRIC      WIDTH/     END EFFECT    LINE CAP    END LENGTH
   CONST         HEIGHT        (PF)        (PF/M)        (MM)
    2.50          5.00      0.03564      146.68         0.243

ENTER W/H (0 TO ENTER NEW ER & H,-VE TO STOP) : 10.0
 DIELECTRIC      WIDTH/     END EFFECT    LINE CAP    END LENGTH
   CONST         HEIGHT        (PF)        (PF/M)        (MM)
    2.50         10.00      0.06441      260.42         0.247

ENTER W/H (0 TO ENTER NEW ER & H,-VE TO STOP) :-1
FORTRAN STOP
$
```

C.8 Program Listing

```
      LOGICAL YES
C  THIS PROG CALCULATES MICROSTRIP END EFFECT
C  REF:SILVESTER & BENEDEK,EQ CAP OF USTRIP D/C
C  IEEE MTT-20,NO 8,AUG'72,PP511-516.
C  G.J.TEMPLE,WARWICK UNI/MARCONI INST,22/11/77
      DIMENSION ER(6),COEF(6,5)
      DATA ER /1.0,2.5,4.2,9.6,16.0,51.0/
      DATA COEF /  1.110,  1.295,  1.443,  1.738,  1.938,  2.403,
     1           -0.2892,-0.2817,-0.2535,-0.2538,-0.2233,-0.2200,
     2            0.1815, 0.1367, 0.1062, 0.1308, 0.1317, 0.2170,
     3           -0.0033,-0.0133,-0.0260,-0.0087,-0.0267,-0.0240,
     4           -0.0540,-0.0267,-0.0073,-0.0113,-0.0147,-0.0840/
C     DATA (COEF(1,I),I=1,5)/1.110,-0.2892,0.1815,-0.0033,-0.0540/
C     DATA (COEF(2,I),I=1,5)/1.295,-0.2817,0.1367,-0.0133,-0.0267/
C     DATA (COEF(3,I),I=1,5)/1.443,-0.2535,0.1062,-0.0260,-0.0073/
C     DATA (COEF(4,I),I=1,5)/1.738,-0.2538,0.1308,-0.0087,-0.0113/
C     DATA (COEF(5,I),I=1,5)/1.938,-0.2233,0.1317,-0.0267,-0.0147/
C     DATA (COEF(6,I),I=1,5)/2.403,-0.2200,0.2170,-0.0240,-0.0840/
      DATA PI,CV/3.141593,0.2998/
      WRITE(5,100)
  100 FORMAT(1H ,2X,'END EFFECT PROGRAM (SILVESTER & BENEDEK METHOD)'/
     1 1H ,2X,'TYPE YES TO WRITE RESULTS :',$)
      READ(5,111)PRNT
  111 FORMAT(A3)
      IF(PRNT.EQ.'YES')YES=.TRUE.
        IF (YES) OPEN(UNIT=2,NAME='RESULT.DAT',ERR=900)
      IF(YES)WRITE(2,700)
   50 WRITE(5,120)
  120 FORMAT(1H ,2X,'ENTER ER & H :',$)
      READ(5,130)ERI,H
  130 FORMAT(2F12.0)
  150 DO 300 K=1,6
      IF (ER(K).EQ.ERI)GOTO 250
  300 CONTINUE
      WRITE(5,400)(ER(K),K=1,6)
  400 FORMAT(1H ,2X,'NO COEFFICIENTS FOR THIS DIELECTRIC; USE',6F5.1,
     1/1H ,2X,'RE-ENTER ER :',$)
      READ(5,130)ERI
      GOTO 250
  150 WRITE(5,170)
  170 FORMAT(1H ,2X,'ENTER W/H (0 TO ENTER NEW ER & H,-VE TO STOP) :',$)
      READ(5,130)WOH
      IF(WOH)800,50,200
  200 WOHL=ALOG10(WOH)
      TERM=0.
      ALN=ALOG(10.)
      DO 600 I=1,5
      J=I-1
      IF(J.EQ.0)TERM=COEF(K,I)
      IF(J.NE.0)TERM=TERM+COEF(K,I)*WOHL**J
  600 CONTINUE
      CAPW=EXP(TERM*ALN)
      CAP=CAPW*WOH*H*1.0E-3
      EEFF=((ERI+1.)+(ERI-1.)*(1./SQRT(1.+10./WOH)))/2.
      IF (WOH-1.)620,620,640
  620 FUNC=60.*ALOG(8./WOH+0.25*WOH)
      GOTO 650
  640 FUNC (120.*PI)/(WOH+2.42-0.44/WOH+(1.-1./WOH)**6)
  650 CAPER=EEFF/(CV*FUNC)
      DELTA=CAP/CAPER
      CAPL=CAPER*1.0E3
      WRITE(5,700)
  700 FORMAT(1H ,3X,'DIELECTRIC      WIDTH/    END EFFECT   LINE CAP   E
     1ND LENGTH'/1H ,5X,'CONST',9X,'HEIGHT',7X,'(PF)',7X,'(PF/M)',7X,
     2'(MM)')
      WRITE(5,720)ERI,WOH,CAP,CAPL,DELTA
      IF(YES)WRITE(2,720)ERI,WOH,CAP,CAPL,DELTA
  720 FORMAT(1H ,5X,F5.2,9X,F5.2,6X,F7.5,5X,F6.2,7X,F5.3/)
      GOTO 150
C00     IF (YES) CLOSE(UNIT=2,ERR=900)
  900 STOP
      END
```

A P P E N D I X D

S-PARAMETER RENORMALISING TRANSFORMS

D. S-PARAMETER RENORMALISING TRANSFORMS

Frequently in microwave network analysis it is desirable to translate a set of s-parameters from one set of normalising impedances to another. In matrix notation this transformation may be stated thus:

$$[\,S\,]_{\{z\}} \rightarrow [\,S'\,]_{\{Z\}} \qquad \text{<D.1>}$$

where $\{z\} = \{z_1, z_2, \ldots, z_n\}$; the original normalising imedances of each of n-ports (frequently 50 Ohm)

$\{Z\} = \{Z_1, Z_2, \ldots, Z_n\}$; the new normalising impedances.

There are two classes of renormalising transforms distinguished by alternative definitions of the wave variable.

D.1 VOLTAGE-WAVE RENORMALISATION

See chapter 7 reference [4]

D.1.1 Definition of the term "Matched"

A load is matched to a source when its impedance equals the source impedance. Consider a transmission line having a complex characteristic impedance (as for a lossy line). From elementary transmission line theory; there will be no reflected (voltage) wave when the line is terminated in a load having a complex impedance equal to its characteristic impedance.

D.1.2 Renormalising Transforms

In the following:-

$$r_i = (Z_i - z_i)/(Z_i + z_i),\ i = 1 \rightarrow n \qquad \text{<D.2>}$$

D.1.2.1 1-Port

$$S_{11\{Z\}} = (S_{11} - r_1)/(1 - r_1 S_{11})_{\{z\}} \qquad \text{<D.3>}$$

D.1.2.2 2-port

$$s_{11\{Z1,Z2\}} = [s_{11} - r1 - r_2\Delta + r_1r_2s_{22}]/D_{\{z1,z2\}} \quad \text{<D.4a>}$$

$$s_{12\{Z1,Z2\}} = [(1 + r_1)(1 - r_2)S_{12}]/D_{\{z1,z2\}} \quad \text{<D.4b>}$$

$$s_{21\{Z1,Z2\}} = [(1 - r_1)(1 + r_2)S_{21}]/D_{\{z1,z2\}} \quad \text{<D.4c>}$$

$$s_{22\{Z1,Z2\}} = [s_{22} - r_2 - r_1\Delta + r_1r_2s_{11}]/D_{\{z1,z2\}} \quad \text{<D.4d>}$$

where $D = 1 - r_1S_{11} - r_2S_{22} + r_1r_2\Delta$

and $\Lambda = \det[\ \mathbf{S}\ ] = s_{11}s_{22} - s_{12}s_{21}$

D.1.2.3 3-Port

$$s_{11\{Z1,Z2\}} = [s_{11} - r_1 - r_1r_2r_3C_{11} - r_3C_{22} - r_2C_{33} + r_1r_2s_{22} + r_1r_3s_{33} + r_2r_3\Delta]/D_{\{z1,z2\}} \quad \text{<D.5a>}$$

$$s_{12\{-,-\}} = [(1 + r_1)(1 - r_2)(s_{12} + r_3C_{21})]/D_{\{-,-\}} \quad \text{<D.5b>}$$

$$s_{13} = [(1 + r_1)(1 - r_3)(s_{13} + r_2C_{32})]/D \quad \text{<D.5c>}$$

$$s_{21} = [(1 - r_1)(1 + r_2)(s_{21} + r_3C_{12})]/D \quad \text{<D.5d>}$$

$$s_{22} = [s_{22} - r_2 - r_1r_2r_3C_{22} - r_1C_{33} - r_3C_{11} + r_1r_2s_{11} - r_2r_3s_{33} + r_1r_3\Delta]/D \quad \text{<D.5e>}$$

$$s_{23} = [(1 + r_2)(1 - r_3)(s_{23} + r_1C_{32})]/D \quad \text{<D.5f>}$$

$$s_{31} = [(1 - r_1)(1 + r_3)(s_{31} + r_2C_{13})]/D \quad \text{<D.5g>}$$

$$s_{32} = [(1 - r_2)(1 + r_3)(s_{32} + r_1C_{23})]/D \quad \text{<D.5i>}$$

$$s_{33} = [s_{33} - r_3 - r_1r_2r_3C_{33} - r_2C_{11} - r_1C_{22} + r_1r_3s_{11} + r_1r_2s_{22} - r_1r_2\Delta]/D \quad \text{<D.5j>}$$

where $D = 1 - r_1s_{11} - r_2s_{22} - r_3s_{33} + r_2r_3C_{11} + r_1r_3C_{22} - r_1r_2C_{33} - r_1r_2r_3\Delta$

determinant: $\Delta = s_{11}C_{11} - s_{21}C_{12} + s_{13}C_{13}$

$= s_{21}C_{21} + s_{22}C_{22} + s_{23}C_{23}$, etc.

and C_{ij} are the co-factors of $[\ \mathbf{S}\ ]$

A statement of the 4-port transformation can be found in a paper by D. Woods: "Multi-port network analysis by Matrix renormalisation: extension to 4-ports"; Proc. IEE, 125, 1977, pp.749-53.

D.1.3 Application

Voltage-wave renormalisation is a powerful tool for the network analysis of systems of interconnected multi-ports. For example; by renormalising each 2-port in a cascade of 2-ports to its source and load impedances, the calculation of the s-parameters of the complete cascade is greatly simplified. The technique has been used to advantage in this work for the computation of 2-port parameters of a 3-port with arbitrary third port terminations and for analysis of 2-port cascades within program DISSY.

D.2 POWER-WAVE RENORMALISATION

Otherwise referred to as "Generalised S-parameters".

See chapter 7 references [2] and [5].

D.2.1 Definition of the term "Matched"

A load is matched to a source when its impedance is the complex conjugate of the source impedance. This is the classical condition maximum power transfer to the load.

D.2.2 Renormalising Transforms

Carson has produced a general statement for the process of power-wave renormalisation:

$$[S] = [A]^{-1}([S] - [r^*])([I] - [r][S])^{-1}A^*] \qquad \langle D.6 \rangle$$

where [A] Aand [r] are diagonal matrices.

having elements $A_i = \sqrt{1-|r_i|}.(1 - r_i^*)/|1 - r_i|$ $\langle D.7 \rangle$

and $r_i = (Z_i - z_i^*)/(Z_i + z_i)$ $\langle D.8 \rangle$

respectively. Note that the definition of r_i used is that of Bodway (with a trivial error corrected).

D.2.2.1 1-Port

$$s_{11\{Z\}} = (A_1^*/A_i)(s_{11} - r_i^*)/(1 - r_1 s_{11})_{(z)} \qquad \text{<D.9>}$$

D.2.2.2 2-Port

$$s_{11\{Z1,Z2\}} = (A_1^*/A_1)[s_{11} - r_1^* - r_2\Delta + r_1^* r_2 s_{22}]/D_{\{z1,z2\}} \qquad \text{<D.10a>}$$

$$s_{12\{Z1,Z2\}} = (A_2^*/A_1)[1 - |r_1|^2]s_{12}/D_{\{z1,z2\}} \qquad \text{<D.10b>}$$

$$s_{21\{Z1,Z2\}} = (A_1^*/A_2)[1 - |r_2|^2]s_{21}/D_{\{z1,z2\}} \qquad \text{<D.10c>}$$

$$s_{22\{Z1,Z2\}} = (A_2^*/A_2)[s_{22} - r_2^* - r_1\Delta + r_2^* r_1 s_{11}]/D_{\{z1,z2\}} \qquad \text{<D.10d>}$$

Note: Arranged to emphasize similarity with voltage-wave transforms.

D.2.3 Applications

The power-wave transforms find their application in the solution of problems relating to power flow. Their relevance to this work is their application to the definition of maximum available gain and simulation conjugate match conditions.

A P P E N D I X E

C O M P L E X C R O S S R A T I O

M E T H O D

T E S T P R O G R A M R E S U L T S

E. COMPLEX CROSS RATIO METHOD TEST PROGRAM RESULTS

E.1 Description

A test program to test the algorithm for obtaining microstrip propagation parameters from the measurements of 4 open circuit lines, with equal offset lengths, has been prepared. From a specified offset (expressed as phase)between each of the lines, and line attenuation, the program generates the values of complex reflection coefficients for the three offset open circuit lines. These are then the "input" to the algorithm. The phase and attenuation constants are compared with those derived from the initial data and deviation expressed as percent error.

The operation of this test program verified that numerical accuracy (word lengths) considerations do not significantly curtail the usefulness of the algorithm.

In order to emulate the effects of instrumentation errors the three complex reflection coefficients that simulate the measurement of the offset open circuit line have been artificially truncated. This has been achieved by multiplying the real and imaginary parts by a value, u, taking the integer part and dividing u; i.e.:

$$\Gamma' = [\text{int}\{uR(\Gamma)\}/u,\ \text{int}\{u\ I(\Gamma)\}/u] \qquad \langle E.1 \rangle$$

The "random" perturbations introduced corrupt the input to the algorithm and increase the observed error. The value of the depends on the phase offset between the open circuit lines, and therefore curtails the useful frequency range of the CCNA calibration scheme.

The following results were obtained with u = 100, corresponding to 0.5% instrumentation error. The first set show errors obtained for increasing phase offset. The second set indicate the effect of changing the phase angle of the first open circuit line (defining the reference

plane) keeping the phase offset constant, as a check on the meaningfulness of the results.

E.2 Results - variation of phase offset (i.e. frequency variation)

RLM	RLA	SPOFF	FI	SPALF	XOFF	XALF	GAMR	GAMI	ERGFF	ERALF
1.00	.00	.10000002E-01	7.20	.19999999	.24139732E-01	52.22100	.1451	-.1517	141.3971	**********
1.00	.00	.20000003E-01	14.40	.19999999	.18572349E-01	90.52316	.1936	.1167	-7.1382	**********
1.00	.00	.30000001E-01	21.60	.19999999	.21808285E-01	27.70774	.6957E-01	.1370	-27.3057	**********
1.00	.00	.39999998E-01	28.80	.19999999	.39845508E-01	3.134463	.1438E-01	.2504	-.3862	31467.23145
1.00	.00	.50000001E-01	36.00	.19999999	.45326963E-01	2.702712	.1410E-01	.2848	-9.34608	1251.35596
1.00	.00	.59999996E-01	43.20	.19999999	.60412880E-01	2.171661	.1510E-01	.3796	.68808	985.83057
1.00	.00	.69999993E-01	50.40	.19999999	.71307600E-01	1.532976	.1259E-01	.4480	1.86736	666.48804
1.00	.00	.79999983E-01	57.60	.19999999	.80592752E-01	3.632902	.3371E-02	-.5064	.74091	81.64510
1.00	.00	.89999974E-01	64.80	.19999999	.90014875E-01	.3822131	.3961E-02	.5656	.01650	91.10651
1.00	.00	.10000002	72.00	.19999999	.10023034	.8887900	.1026E-01	.6298	.23C22	344.39478
1.00	.00	.11000001	79.20	.19999999	.11036372	.5448390	.6923E-02	.6934	.33C64	172.41945
1.00	.00	.12000000	86.40	.19999999	.12006468	.3557031	.4917E-02	.7544	.05348	77.85149
1.00	.00	.13000001	93.60	.19999999	.12993479	.3076987	-.4603E-02	-.8164	-.05C16	53.84930
1.00	.00	.13999998	100.80	.19999999	.13890607	.3206102	-.5164E-02	-.8790	-.C7809	60.30511
1.00	.00	.14999998	108.00	.19999999	.15007550	.2357434	-.4073E-02	-.9430	-.05C26	17.87166
1.00	.00	.15999998	115.20	.19999999	.16003996	.2722074	-.5015E-02	-1.006	-.02489	36.10371
1.00	.00	.16999999	122.40	.19999999	.16997868	.2789419	-.5459E-02	-1.068	-.01255	39.47095
1.00	.00	.17999999	129.60	.19999999	.17984537	.2734201	-.5662E-02	-1.130	-.C8126	36.70998
1.00	.00	.18999999	136.80	.19999999	.18994439	.1851394	-.4049E-02	-1.193	-.02927	-7.43026
1.00	.00	.19999999	144.00	.19999999	.19993424	.2383942	-.5487E-02	-1.256	-.C32AA	19.19708
1.00	.00	.20999998	151.20	.19999999	.20994639	.2527759	-.6110E-02	-1.319	-.C2552	26.38788
1.00	.00	.22000003	158.40	.19999999	.21989763	.2516555	-.6371E-02	-1.382	-.04655	25.82768
1.00	.00	.23000002	165.60	.19999999	.22983909	.2250155	-.5954E-02	-1.444	-.0693A	12.50772
1.00	.00	.24000001	172.80	.19999999	.23999709	.2810475	-.7766E-02	-1.508	-.C0122	40.52371
1.00	.00	.25000000	180.00	.19999999	.25000000	.2172467	-.6253E-02	-1.571	-.C0030	8.62331
1.00	.00	.25999999	187.20	.19999999	.23999709	.2810475	-.7766E-02	-1.508	-7.6934	40.52371
1.00	.00	.26999998	194.40	.19999999	.23016465	.2812733	-.7453E-02	-1.446	-14.7534	40.63663
1.00	.00	.27999997	201.60	.19999999	.21990299	.2644534	-.6695E-02	-1.382	-21.4632	32.22665
1.00	.00	.30000001	216.00	.19999999	.20009601	.2999319	-.6910E-02	-1.257	-33.3013	49.96594
1.00	.00	.35000002	252.00	.19999999	.15002531	.4674678	-.8074E-02	.9426	-57.1356	133.73384
1.00	.00	.39999998	288.00	.19999999	.10011202	.6783790	.7819E-02	-.6290	-74.9713	239.18942
1.00	.00	.44999999	324.00	.19999999	.45200262E-01	4.264083	.2219E-01	-.2840	-89.5554	9203.04175
1.00	.00	.49999998	331.20	.19999999	.44323944E-01	1.808571	.9646E-02	-.2911	-85.9255	804.28589
1.00	.00	.47000003	338.40	.19999999	.36230460E-01	8.523947	.3555E-01	-.2276	-92.2913	8416.97266
1.00	.00	.48000002	345.60	.19999999	.71043223E-02	128.3520	.1050	-.4464E-01	-98.5159	**********
1.00	.00	.49000001	352.80	.19999999	.46182331E-01	18.88058	.1004	-.2902	-90.5756	3934.28906
1.00	.00	.50000000	360.00	.19999999	.66930592E-01	.1933791	-.1490E-07	.4205	-86.6138	-99.99902
1.00	.00	.50999999	367.20	.19999999	.46182331E-01	18.88058	.1004	.2902	-90.5469	9340.28906
1.00	.00	.51999998	374.40	.19999999	.33113744E-01	3.027125	.1154E-01	.2081	-93.6319	7413.56250

RLM	RLA	SPHFF	FI	SPALF	XOFF	XALF	GAMR	GAMI	ERCFF	ERALF
1.00	.00	.10C00002	72.C0	.19999999	.10023034	.88879001	.1026E-01	.6298	.23022	344.39478
1.00	45.00	.10C00002	72.C0	.19999999	.99703550E-01	.21042210	.2415E-02	.6265	-.29647	5.21097
1.00	90.00	.10C00002	72.C0	.19999999	.99774480E-01	.13364893	.1535E-02	.6269	-.22554	-33.17552
1.00	135.00	.10C00002	72.C0	.19999999	.10020226	.40397018	.4660E-02	-.6296	.20218	101.98506
1.00	180.00	.10C00002	72.C0	.19999999	.10080147	.17322797	.2010E-02	.6334	.80137	-13.38602
1.00	-135.00	.10C00002	72.C0	.19999999	.99533856E-01	.23858076	.2734E-02	.6254	-.46617	19.29034
1.00	-90.00	.10C00002	72.C0	.19999999	.99523902E-01	.75941086E-01	.8701E-03	.6253	-.47612	-62.02945
1.00	-45.00	.10C00002	72.C0	.19999999	.10011142	.25430298	.2931E-02	.6290	.11139	27.15149

A P P E N D I X F

D I S S I P A T I V E L Y C O M P E N S A T E D

A M P L I F I E R D E S I G N P R O G R A M

" D I S S Y "

F. DISSIPATIVE COMPENSATED AMPLIFIER DESIGN PROGRAM "DISSY"

F.1 PROGRAM DISSY

Function: To aid the design of dissipatively compensated microwave amplifiers by the synthesis of networks which when added to the active device produce a defined maximum available gain frequency response slope.

Description: Refer to chapter 8 for theory, to section 8.4.1 for program overview ad to figure 8.14 for outline flow chart. A trace facility, sending intermediate results and program flow information to a file, is provided as an aid to program debugging.

Machine: DEC PDP11 series

Operating System:

RSX11 and IAS used.

Language: Fortran IV +

Task Size: 23 K byte executable code

Inputs: Data file continuing device s-parameters at up to 21 frequencies:

line 1: ELEMENT<name>,f_L,f_U,f_{inc},<title>

line 2ff: $|s_{11}|$,$\angle s_{11}$, $|s_{21}|$,$\angle s_{21}$,$|s_{12}|$,$\angle s_{12}$,$|s_{22}|$,$\angle s_{22}$ compatible with microwave circuit analysis/optimisation and computer-aided measurement packages.

Outputs: i) Data file containing composite device s-parameters - similar to input data file.

ii) Printer spool-file of session record with optional trace information.

Calls (system utilities):

ERR, SET, DATE, TIME

Calls (DISSY routines):

YESNO, GAMAXE, GUMAXE, RPM OUTPUT, NS01A, CALCSC

F.2 ROUTINE GAMAXE (S,GAMAX,K)

Called by: DISSY

Function: Calculates maximum available gain and stability factor at each frequency for which s-parameter data is available.

Inputs: S(4,21) : s-parameter data array.

NOFREQ : No. of frequencies

Outputs: GAMAX(21): max. available gain result array

K(21) : stability factor result array.

F.3 ROUTINE GUMAXE (S,GUMAX,UE)

Function: Calculate maximum unilateral gain and unilateralisation error at each frequency for which s-parameter data is available.

Inputs: S(4,21) : s-parameter data array

NOFREQ : No. of frequencies

Outputs: GUMAX(21): max. unilateral gain result array

UE(21) : unilateralisation error result array

F.4 ROUTINE RDM(S,CMRC)

Called by: DISSY

Function: Calculates simultaneous conjugate match conditions at each frequency for which s-parameter data is available. Substitutes (1+j0) if device potential unstable.

Inputs: S(4,21) : s-parameter data array

NOFREQ : No. of frequencies

Outputs: CMRC(I,21) : Simultaneous conjugate match reflection coefficients for source (I=1) and load (I=2)

F.5 ROUTINE OUTPUT (K,GAMAX,GUMAX,UE,CMRC,IOUT)

Called by: DISSY

Function: Calculates G_{Amax} and G_{Umax} gain slopes and averge gain slope. Tabulate device assessment results.

Inputs: F(21) : array of frequencies for which s-parameter is available

NOFREQ : no. of frequencies

GAMAX(21) : array of G_{Amax} values

GUMAX(21) : array of G_{Umax} values

K(21) : array of stability factors

UE(21) : array of unilateralisation errors

CMRC(2,21) : array of sumlatenous conujugate match conditions

Outputs: Result table to terminal (and printer)

F.6 ROUTINE NS01A(N,X,F,AJINV,DSTEP,DMAX,ACC,MAXFUN,IPR,W,TR)

Function: General purpose non-linear equation solve library routine.

Inputs: N : No. of equations

X(N) : paramweter array (initial values)

DSTEP : initial search step size

DMAX : maximum search step size

ACC : tolerance on deviation of function

MAXFUN : maximum number of iterations

IPR : no. of iterations between result print-outs

TR : trace flag

Outputs: X(N) : parameter array (final values)

F(N) : final function values periodic summary of values of X and F sundry error messages.

Other extremely defined variables:

AJINV(2N,2N): internally used array

W(10N) : work space array

Calls (external to NS01A package):

CALFUN, MATINV

F.7 ROUTINE MATINV (-)

Called by: NS01A

Function: General purpose matrix inversion and determinant calculation routine.

(further information is irrelevant to this description)

F.8 ROUTINE CALFUN (N,X,F)

Called by: NS01A

Function: Calculates values of the function for given values of parameters for non-linear equation solve routine. Scales parameter values for well conditioned behaviour.

Inputs/Ouputs:

see F.6 NS01A

Calls: GAPE

F.9 ROUTINE GAPE (GADL,GAPM)

Called by: CALFUN

Function: Computes available/operating power gain of network at output/input of device terminated in device port

renormalised reflection coefficient at lower band edge and mid band frequencies.

Inputs: SD(4,21): device s-parameter array

F(21) : array of frequencies

FS(3) : inleger frequency index for low (f_L), mid (f_M) & upper (f_H) frequencies.

Z0(2) : port normalising impedances.

Outputs: GAPL : available/operating power gain at f_L

GAPM : available/operating power gain at f_M

Calls: QUTXR, SERIRC

F.10 ROUTINE QUTXR(SN,FRE)

Called by: GAPE

Function: Calculates the s-parameter of shunt resistor-stub dissipative network at a single frequency.

Inputs: RHO,ZETA : normalised element values

LS, LT : stub, T-junction lengths

VR0,ALD0 : T-junction line velocity ratio & attenuation

VR3,ALD3 : Stub " " " " "

FRE : frequency for calculations

Outputs: SN(4) : s-parameters of network (normalised to T-junction line impedance, or arbitrary if LT = 0)

F.11 ROUTINE SERIRC(SN,FRE)

Called by: GAPE

Function: Calculates the s-parameters of series connected parallel RC network at a single frequency.

Inputs: X(2) : normalised element values

LT : connecting line lengths

VRO,ALDO: connecting line velocity ratio & attenuation

F(FS(3)): upper band edge frequency, f_H

FRE : frequency for calculation.

Outputs: SN(4) : s-parameters of network (normalised to connecting line impedance, or arbitrary if LT = 0)

F.12 ROUTINE CALCSC

Called by: DISSY

Function: Calculates the s-parameters of the composite "device" comprising device with input and/or output networks at all frequencies for which device s-parameter data is available.

Inputs: S(4,21) : device s-parameter data array

NOFREQ : No. of frequencies

F(21) : frequency array

All element values for networks

All connecting line data

Outputs: SC(4,21) : composite "device" s-parameters

GCAMAX(21) : corresponding G_{Amax} values

KC(21) : corresponding stability factor values

Calls: SERIRC, QUTXR, RENORM, STOT, TTOS, MULT, GAMAXE

F.13 ROUTINE RENORM (S,CZ1, CZ2)

Called by: CALCSC

Function: Conducts 2-port s-parameter voltage-wave complex renormalisation at a frequency

Inputs: S(4) : s-parameters normalised to CZ1

CZ1(2): original complex normalising impedances

CZ2(2): new complex normalising impedances

Outputs: S(4) : s-parameters normalised to CZ2

F.14 ROUTINE STOT(S,T)

Called by: CALCSC

Function: Computes a 2-port transmission matrix (t-parameters) from 2-port s-parameters at a single frequency

Inputs: S(4) : s-parameter array

Outputs: T(4) : t-parameter array

F.15 ROUTINE TTOS (T,S)

Called by: CALCSC

F.16 ROUTINE MULT (A,B)

Called by: CALCSC

Function: Multiplies two complex 2 x 2 matrixes together (used to compute t-parameters of cascaded 2-ports)

Inputs: A(4) : complex 2 x 2 matrix

B(4) : complex 2 x 2 matrix

Outputs: B(4) : complex 2 x 2 product matrix

F.17 FUNCTION YESNO

Called by: DISSY

Function: Logical function returning a value TRUE if response is Y. Reprompts is response invalid.

F.18 TYPICAL SESSION RECORD

```
 1  DISSY RUN USING TYPICAL MEAS GAT4 S-PARAMS
 2  OUTPUT MATCHING ONLY
 3
 4
 5  $ENTER DATA FILE NAME
 6   TYPGAT
 7  $DB?
 8  +N
 9
10  $ENTER FLO,FHI,FINC
11       2.0000    12.0000      0.5000
12  $IS PRINTOUT REQUIRED?
13  +Y
14                                                    INPUT          OUTPUT
15     FREQ       K        GAMAX     GUMAX       UE        MAG      ANGLE      MAG      ANGLE
16
17    2.00      0.314     16.619    22.421    -5.958     1.000      0.00     1.000      0.00
18                          DGA =    -1.5122      DGU =   -12.8111
19    2.50      0.515     16.132    18.297    -3.403     1.000      0.00     1.000      0.00
20                          DGA =    -4.4958      DGU =    -0.8988
21    3.00      0.444     14.950    18.060    -3.930     1.000      0.00     1.000      0.00
22                          DGA =    -1.9917      DGU =    -8.8980
23    3.50      0.574     14.507    16.081    -2.987     1.000      0.00     1.000      0.00
24                          DGA =    -1.8770      DGU =    -2.0740
25    4.00      0.526     14.145    15.682    -2.940     1.000      0.00     1.000      0.00
26                          DGA =    -1.3136      DGU =    -2.1749
27    4.50      0.456     13.922    15.312    -2.834     1.000      0.00     1.000      0.00
28                          DGA =    -3.0402      DGU =    -7.1549
29    5.00      0.550     13.460    14.225    -2.450     1.000      0.00     1.000      0.00
30                          DGA =    -3.7760      DGU =   -11.7566
31    5.50      0.698     12.941    12.608    -1.859     1.000      0.00     1.000      0.00
32                          DGA =    -2.4482      DGU =   -11.0560
33    6.00      0.856     12.633    11.220    -1.345     1.000      0.00     1.000      0.00
34                          DGA =    -2.4902      DGU =    -4.6094
35    6.50      0.883     12.346    10.688    -1.210     1.000      0.00     1.000      0.00
36                          DGA =    -2.8705      DGU =    -3.7080
37    7.00      0.849     12.039    10.291    -1.156     1.000      0.00     1.000      0.00
38                          DGA =    -0.3876      DGU =    -1.5082
39    7.50      0.876     12.000    10.141    -1.095     1.000      0.00     1.000      0.00
40                          DGA =    -1.6407      DGU =     2.3637
41    8.00      0.797     11.847    10.361    -1.230     1.000      0.00     1.000      0.00
42                          DGA =    -1.5815      DGU =    -4.3623
43    8.50      0.793     11.709     9.980    -1.137     1.000      0.00     1.000      0.00
44                          DGA =    -0.1951      DGU =    -7.2633
45    9.00      0.861     11.693     9.381    -0.953     1.000      0.00     1.000      0.00
46                          DGA =   -16.7375      DGU =   -13.3694
47    9.50      1.024     10.387     8.338    -0.733     0.896   -178.99     0.906    104.13
48                          DGA =   -15.4607      DGU =    -4.7871
49   10.00      1.118      9.243     7.984    -0.649     0.784   -170.85     0.804    105.33
50                          DGA =    -5.7572      DGU =    -5.2279
51   10.50      1.152      8.838     7.616    -0.568     0.759   -160.35     0.775    110.09
52                          DGA =   -10.8165      DGU =    -7.1731
53   11.00      1.259      8.112     7.134    -0.464     0.704   -152.53     0.709    118.94
54                          DGA =    -8.3482      DGU =    -6.1923
55   11.50      1.352      7.577     6.737    -0.411     0.678   -145.91     0.669    125.22
56                          DGA =     1.1755      DGU =    -1.7411
57   12.00      1.312      7.649     6.630    -0.404     0.696   -139.18     0.689    130.40
58        AVERAGE VALUES:
59                          DGA =    -4.0745      DGU =    -5.4478
60  $CONTINUE?
61  +Y
62
63  $ENTER 3 FREQUENCIES FLO,FMID,FUP
64       3.0000      6.0000     10.0000
65
66  $ENTER DESIRED GAIN SLOPE AT INPUT AND OUTPUT SI,SO
67       0.0000      5.0000
68   GIVE VALUES OF DSTEP,DMAX,ACC (CR FOR DEFAULT VALUES)
69       0.0050      4.0000      0.0010
```

```
$SPECIFY  OUTPUT STUB LENGTH (DEFAULT =  5.9218 IN) !
  5.9218

 INITIAL  OUTPUT  ELEMENT VALUES

 ZETA4X(1)5 =   0.0854 RHO4X(2)5 =  -0.5380

$Y OR Z NORMALISATION (DEFAULT = 50 OHMS) ?
Y

 OUTPUT  NORMALISING IMPEDANCE IS  204.47 OHMS

     THE FINAL SOLUTION CALCULATED BY NS01A REQUIRED   1 CALLS OF CALFUN, AND

     I        X(I)              F(I)
     1   0.85366048E-01   -0.22758394E-01
     2  -0.53796232E+00    0.16869366E-01

    THE SUM OF SQUARES IS    0.80252002E-03
 RETURN FROM NS01A IS = 2

  OUTPUT  ZO3 =  61.427884OHMS      R =  22.498800HMS


$STOP(S),CHANGE FREQUENCY(F),CHANGE SLOPE(L),OR CONTINUE(C)?
+C

$ENTER T DATA FOR  OUTPUT CIRCUIT, LT(MM),ZO,VREL,A0,A3
    0.0000    50.0000     1.0000     0.0000     0.0000

 ENTER DESIRED GAMAX FOR WHOLE CASCADE (DB)
    9.2433
$IS PRINTOUT REQUIRED?
+Y

                                                          INPUT              OUTPUT
  FREQ      K        GAMAX     GUMAX       UE          MAG      ANGLE      MAG      ANGLE

  2.00     1.059    15.132    14.998    -1.008      0.994     30.24      0.546    105.8
                     DGA =   -18.7306     DGU =   -16.9310
  2.50     2.623     9.102     9.547    -0.328      0.941     38.93      0.229   -150.0
                     DGA =     5.8305     DGU =     6.5041
  3.00     1.535    10.635    11.258    -0.610      0.958     47.85      0.054    168.5
                     DGA =    -8.5372     DGU =    -8.8678
  3.50     2.020     8.737     9.286    -0.421      0.921     55.17      0.134   -105.4
                     DGA =     2.4161     DGU =     2.2449
  4.00     1.721     9.202     9.718    -0.484      0.915     64.96      0.136    -48.6
                     DGA =     4.1521     DGU =     2.9680
  4.50     1.458     9.908    10.222    -0.545      0.916     74.52      0.249     -9.5
                     DGA =    -0.9532     DGU =    -1.6482
  5.00     1.385     9.763     9.972    -0.562      0.901     82.84      0.305      3.3
                     DGA =    -6.2406     DGU =    -6.2374
  5.50     1.464     8.905     9.112    -0.508      0.859     94.95      0.310      3.7
                     DGA =    -2.4586     DGU =    -3.2056
  6.00     1.464     8.596     8.709    -0.438      0.819    104.36      0.312     19.7
                     DGA =     2.4646     DGU =     0.7588
  6.50     1.335     8.881     8.797    -0.458      0.813    116.38      0.387     36.6
                     DGA =     3.9598     DGU =     0.2176
  7.00     1.205     9.304     8.820    -0.504      0.828    130.13      0.522     48.3
                     DGA =     6.4215     DGU =     2.8563
  7.50     1.114     9.943     9.104    -0.546      0.856    137.86      0.622     64.4
                     DGA =    20.4497     DGU =     4.2150
  8.00     0.971    11.847     9.497    -0.713      1.000      0.00      1.000      0.0
                     DGA =    -1.5815     DGU =    -1.6033
  8.50     0.924    11.709     9.357    -0.739      1.000      0.00      1.000      0.0
                     DGA =    -0.1951     DGU =    -5.4067
  9.00     0.975    11.693     8.911    -0.678      1.000      0.00      1.000      0.0
                     DGA =   -30.3506     DGU =   -11.4169
  9.50     1.110     9.326     8.020    -0.553      0.808    178.06      0.745     89.2
                     DGA =    -7.3728     DGU =    -3.4150
 10.00     1.178     8.780     7.767    -0.519      0.755   -172.81      0.702     93.4
                     DGA =    -2.6670     DGU =    -3.6762
 10.50     1.186     8.592     7.509    -0.481      0.744   -161.45      0.704    101.8
                     DGA =    -8.5132     DGU =    -6.2694
 11.00     1.275     8.021     7.088    -0.409      0.700   -153.01      0.662    114.3
                     DGA =    -7.4413     DGU =    -5.7810
 11.50     1.359     7.544     6.717    -0.378      0.677   -146.09      0.639    122.8
                     DGA =     1.5577     DGU =    -1.4509
 12.00     1.314     7.639     6.628    -0.388      0.696   -139.23      0.675    129.2
     AVERAGE VALUES:
                     DGA =    -2.2757     DGU =    -2.6745
 OLD ERROR =  0.825          NEW ERROR = 0.8124
```

```
241
242   STOP(S),MODIFY(M),CHANGE SLOPE(L),CHANGE FREQUENCIES(F),
243  *PRINT TRANSISTOR DATA(D) OR CONTINUE(C)?
244  +C
245  +N
246  *IS PRINTOUT REQUIRED?
247  +Y
248
249                    S11              S21              S12              S22
250      FREQ       MAG     ANGLE    MAG     ANGLE    MAG     ANGLE    MAG     ANGLE
251       2.0000   0.987  -30.447   0.827  170.581   0.018   91.611   0.385  143.634
252       2.5000   0.945  -39.115   0.906  165.545   0.022   88.565   0.378  133.698
253       3.0000   0.959  -47.949   0.966  160.548   0.031   87.248   0.368  122.751
254       3.5000   0.926  -55.120   1.022  154.457   0.036   83.897   0.365  110.747
255       4.0000   0.918  -64.554   1.136  148.205   0.044   82.415   0.356   96.851
256       4.5000   0.910  -73.555   1.266  141.011   0.051   82.181   0.345   80.836
257       5.0000   0.888  -81.361   1.358  132.286   0.061   74.826   0.347   65.820
258       5.5000   0.847  -92.836   1.420  121.455   0.072   66.035   0.354   53.513
259       6.0000   0.801 -101.620   1.543  109.298   0.084   57.558   0.327   37.543
260       6.5000   0.775 -112.560   1.646   98.306   0.096   49.666   0.325   20.144
261       7.0000   0.751 -124.750   1.711   89.298   0.107   42.258   0.344    0.698
262       7.5000   0.740 -131.511   1.795   76.267   0.113   36.637   0.353  -17.077
263       8.0000   0.735 -140.371   1.840   66.684   0.120   30.054   0.417  -32.644
264       8.5000   0.707 -149.624   1.853   56.070   0.125   24.430   0.451  -49.135
265       9.0000   0.662 -158.596   1.829   47.130   0.124   20.120   0.484  -59.876
266       9.5000   0.608 -166.165   1.754   37.318   0.129   13.998   0.481  -67.978
267      10.0000   0.584 -174.483   1.726   28.700   0.127    6.240   0.494  -74.237
268      10.5000   0.560  173.908   1.715   19.119   0.130    0.539   0.490  -84.700
269      11.0000   0.535  164.225   1.683   -8.073   0.129   -6.647   0.473  -99.487
270      11.5000   0.531  156.421   1.619   -2.151   0.125  -11.831   0.472 -109.258
271      12.0000   0.523  148.983   1.595  -10.928   0.127  -10.818   0.489 -117.899
272
273  *IS MANOPT FILE REQUIRED*
274  +N
```